UNIVERSIDAD POLITÉCNICA DE MADRID
Escuela Técnica Superior de Ingenieros Industriales

Development of an in-vitro optical diagnostic system for the detection of different pathologies. Case studies of Coronavirus Disease 2019 and Alzheimer's Disease.

DOCTORAL THESIS

Submitted for the degree of Doctor by:

Ana María Martín Murillo
Máster en Investigación en Inmunología

Madrid, 2024

UNIVERSIDAD POLITÉCNICA DE MADRID
Escuela Técnica Superior de Ingenieros Industriales

Doctoral Degree in Mechanical Engineering

Development of an in-vitro optical diagnostic system for the detection of different pathologies. Case studies of Coronavirus Disease 2019 and Alzheimer's Disease.

DOCTORAL THESIS

Submitted for the degree of Doctor by:

Ana María Martín Murillo
Máster en Investigación en Inmunología

Under the supervision of:
Dr. Miguel Holgado Bolaños
Dr. María Fe Laguna Heras

Madrid, 2024

Title: Development of an in-vitro optical diagnostic system for the detection of different pathologies. Case studies of Coronavirus Disease 2019 and Alzheimer's Disease.

Author: Ana María Martín Murillo

Doctoral Programme: Mechanical Engineering

Thesis Supervision:

Dr. María Fe Laguna Heras, Profesor titular en el Departamento de Física Aplicada e Ingeniería de Materiales de la Escuela Técnica Superior de Ingenieros Industriales de la Universidad Politécnica de Madrid (Supervisor).

Dr. Miguel Holgado Bolaños, Catedrático en el Departamento de Física Aplicada e Ingeniería de Materiales de la Escuela Técnica Superior de Ingenieros Industriales de la Universidad Politécnica de Madrid.

External Reviewers:

Thesis Defense Committee:

Thesis Defense Date:

This thesis has been partially supported by Grants for Industrial Doctorates in the Madrid Regional Research Program IND2019/IND-17207, the HERON project with reference TEC2017-84846-R supported by the Spanish Ministry of Economy and Competitiveness, the Center for the Development of Industrial Technology (CDTI) under the project ADMARKERS with reference IDI-20190800, by the Research and Innovation program of Universidad Politécnica de Madrid under the project with reference: VIMPACTO20MHB and within the framework of the project COVIDTECH-CM of the Regional Government of Madrid (Spain).

Mira dentro de ti. Eres más de lo que te has convertido.

Mufasa.

Acknowledgment

Y por fin ha llegado el momento. El momento de terminar esta etapa de tesis doctoral y empezar otra nueva. A veces parecía que el camino era eterno y que este momento no iba a llegar nunca, pero de repente te ves terminando de escribir y preparando la defensa del trabajo que has realizado durante años, aunque sea un pequeño salto al vacío.

Estos cuatro años de tesis han sido posibles gracias a muchas personas que me han acompañado, ayudado, comprendido, respaldado y animado a luchar durante todo el camino.

En primer lugar, doy las gracias a mis directores de tesis, Miguel y Marifé, que me dieron la oportunidad de empezar esta tesis y de formar parte del GOFB hace ya camino de cinco años. También a la Universidad Politécnica de Madrid y al Centro de Tecnología Biomédica que han sido mi casa durante esta aventura.

Por otro lado, quiero dar las gracias a mis padres, que han sido siempre el apoyo más incondicional, tanto para seguir como para abandonar. Gracias por querer siempre lo mejor para mí y acompañarme en todas las decisiones, buenas y malas.

Y por supuesto, gracias a mi hermano, al mejor hermano que se puede tener. Por todos los malos momentos que hemos arreglado jugando al Mario y por hacer que esté siempre bien cuando estoy contigo. A ti y a Jacquie, por estar, por ayudarme y apoyarme.

Gracias a la familia que elegí (Patri, Sara, Tomi y Nerea). Gracias por ser esos amigos que una vez llegan ya nunca se van, por aguantar durante todo este tiempo mis quejas, mis malos momentos y mi forma tan larga de contar todas las historias que han pasado. Gracias por acompañarme hasta aquí y apoyarme tanto.

Gracias a los chicos del GOFB, a Luis, Luca, Alberto, Pedro y Juanpa. Gracias por todo lo que me habéis aguantado y por escucharme siempre (que no han sido pocas veces). Y gracias por hacer que todos los días fueran mejores. Creo que nunca imaginé que iba a tener a los mejores compañeros que se convirtieron en amigos.

Y claro está, gracias a las chicas del GOFB. A Yoli, que cuando empezamos a trabajar juntas en 2018, creo que ninguna de las dos imaginábamos las horas que íbamos a pasar juntas en el laboratorio unos años después. Y cómo lo he echado de menos en el final de este camino. Gracias por estar cuando todo se venía abajo. A Ana, que a contrarreloj se encargó de todo el doctorado industrial y las reuniones desde EEUU para explicarme la silanización. Gracias por formar parte de todo esto. Y a Betxu, por todo. Me has ayudado en tantas cosas, que no podría ni numerarlas, hasta el tener que coger un avión. Gracias por empujarme siempre.

Gracias también a la persona más especial que me dio la biología. Gracias Lola por todos los años, por estar aun desde lejos y por las tardes arreglando el mundo. Hemos podido, podemos y podremos.

A Raquel, que es de esas personas que aparecen de repente y te das cuenta que es de las que quieres tener siempre. Gracias por todo lo que has hecho por mí siempre, por los desayunos, las meriendas, por avisarme de la lluvia, por las horas hablando…Gracias de corazón.

Gracias a la Universidade de Aveiro y Ana Gabriela por darme la oportunidad de realizar allí la estancia y poder aprender durante los meses que estuve que allí. Y gracias por supuesto a Tania y Margarida que me acogieron y enseñaron.

Y ha llegado el momento de dar las gracias a una de las personas más importantes. Al que ha sido un compañero incondicional durante todo este tiempo y desde hace cinco años. Gracias Alberto, por aguantar todo este tiempo con las subidas y bajadas que ha conllevado todo esto. Gracias por creer en mí más que yo misma e incluso cuando yo no lo hacía. Gracias por no rendirte nunca, por la paciencia que has tenido y quererme como lo has hecho. No sé cómo hubiera llegado hasta aquí si no hubieras estado tu viniendo conmigo. Mil gracias siempre.

Y, por último, gracias a todas las personas que han pasado por el GOFB que han estado conmigo en esos momentos. Gracias a todos los amigos que me han apoyado y comprendido, a todos los que me han escuchado y animado siempre.

Gracias a todos, porque al final esta tesis doctoral lleva un pedacito de todos los que habéis estado ahí durante estos cuatro años.

Abstract

The area of clinical diagnostics and increasingly specific and sensitive detection systems has acquired great relevance in recent decades, in particular, the field of biosensors, as they are a powerful tool for the diagnosis of diseases. This is because they allow the analysis and measurement of a great variety of biomarkers specific to each pathology in a multitude of human samples such as blood, urine, saliva, etc.

This added to the advantages they provide, such as the possibility of obtaining results quickly, their high sensitivity and specificity, their portability, versatility, and easy handling, make them a great alternative in the diagnostic field, allowing in many occasions the early detection of diseases and consequently the improvement of treatments, as well as monitoring chronic diseases. In this way, it is possible to offer a more personalized and efficient medicine.

In recent years the growth in the use of biosensors has seen a large increase mainly due to the pandemic caused by Severe Acute Respiratory Syndrome Coronavirus 2 (SARS-CoV-2) in March 2020, responsible for Coronavirus Disease 2019 (COVID-19). At that time, biosensors were crucial for the detection and control of the disease. This was one of the motivations in the work of this thesis, since, when the beginning of the pandemic was decreed, the development of an *in-vitro* diagnostic system based on an optical biosensor for the detection of specific antibodies (Abs) against SARS-CoV-2, both in serum and saliva, was prioritized as an objective. In addition to detecting other biomarkers related to the disease.

On the other hand, among the increasingly widespread pathologies worldwide are Neurodegenerative Diseases (NDD), with Alzheimer's Disease (AD) being the leading cause of dementia. One of the major problems related to this disease is that it has no cure and that the symptoms appear once it is very advanced. It has been demonstrated that the first changes that occur are at the biochemical level, changing the expression profile of certain biomarkers such as tau protein, among others, in addition to the appearance of pathological structures in the brain. This is why it is of the utmost importance to have a system capable of detecting these variations that are difficult to detect.

This is the motivation for the second main objective of this thesis, which is the development of an *in-vitro* diagnostic system using the same type of biosensor for the detection of biomarkers related to AD in different types of human samples.

During the development of this thesis, it was possible to detect specific Abs against SARS-CoV-2 in serum samples of patients who had suffered from the disease (severe, moderate, and mild) and to perform a study of Ab detection in the saliva of volunteers over time.

Thanks to these experiments, it was possible to develop a mathematical model to determine the severity of the disease based on the different biomarkers measured in the patient's samples.

In the case of AD, a system based on the use of nanoparticles (NPs) was developed to reach very

low detection levels of tau protein in serum samples. In addition, we were able to determine other markers such as lactoferrin in saliva samples or the phosphorylation of tau protein (which is increased in the progression of the disease).

So, in conclusion, we were able to develop a diagnostic KIT valid for different pathologies and that is extrapolable thanks to its versatility to any other pathology. Thanks also to the use of NPs it is possible to use samples with more complex matrices and to reach much lower detection limits, making the use of this type of biosensor with NPs a great tool for the early diagnosis of diseases.

Resumen

El área del diagnóstico clínico y los sistemas de detección cada vez más específicos y sensibles ha tomado una gran relevancia en las últimas décadas, en concreto, el campo de los biosensores, ya que son una gran herramienta para el diagnóstico de enfermedades. Esto se debe a que permiten el análisis y la medición de una gran variedad de biomarcadores específicos de cada patología en multitud de muestras humanas como la sangre, la orina, la saliva, etc.

Esto sumado a las ventajas que proporcionan, como la posibilidad de obtener resultados de forma rápida, su alta sensibilidad y especificidad, su portabilidad, la versatilidad y su fácil manejo, hacen que sean una gran alternativa en el campo diagnóstico, permitiendo en muchas ocasiones la detección temprana de enfermedades y consecuentemente la mejora de tratamientos, así como el seguimiento de enfermedades crónicas. De esta forma es posible ofrecer una medicina más personalizada y eficiente.

En los últimos años el crecimiento del uso de los biosensores ha sufrido un gran aumento sobre todo debido a la pandemia causada por el Coronavirus del Síndrome Respiratorio Agudo Grave de tipo 2 (SARS-CoV-2) en marzo de 2020, responsable de la Enfermedad por Coronavirus 2019 (COVID-19). Momento en el que los biosensores fueron cruciales para la detección y control de la enfermedad. Esto fue una de las motivaciones en el trabajo de esta tesis, ya que, al decretarse el inicio de la pandemia, se priorizó como objetivo el desarrollo de un sistema de diagnóstico *in-vitro* basado en un biosensor óptico para la detección de anticuerpos específicos frente al SARS-CoV-2, tanto en suero como en saliva. Además de detectar otros biomarcadores referentes a la enfermedad.

Por otro lado, dentro de las patologías cada vez más extendidas a nivel mundial, se encuentran las enfermedades neurodegenerativas, siendo la enfermedad de Alzheimer (EA) la primordial causa de demencia. Uno de los mayores problemas relativos a esta enfermedad es que no tiene cura, y que los síntomas aparecen una vez se encuentra muy avanzada. Está demostrado que los primeros cambios que ocurren se dan a nivel bioquímico, cambiando el perfil de expresión de determinados biomarcadores como la proteína tau, entre otras, además de la aparición de estructuras patológicas a nivel cerebral. Es por esto que es de relevada importancia contar con un sistema capaz de detectar dichas variaciones que son difícilmente perceptibles.

Es aquí donde se encuentra la motivación para el segundo gran objetivo de esta tesis que es el desarrollo de un sistema de diagnóstico *in-vitro* utilizando el mismo tipo de biosensor para la detección de biomarcadores relacionados con la EA en diferentes tipos de muestras humanas.

Durante el desarrollo de esta tesis se consiguieron detectar anticuerpos específicos frente al SARS-CoV-2 en muestras de suero de pacientes que habían sufrido la enfermedad (graves, moderados y leves) y realizar un estudio de detección de anticuerpos en saliva de voluntarios a lo largo del tiempo.

Gracias a estos experimentos se pudo desarrollar un modelo matemático para determinar la gravedad de la enfermedad en base a los diferentes biomarcadores medidos en las muestras de

los pacientes.

Para el caso de la EA, se consiguió desarrollar un sistema basado en el uso de nanopartículas para llegar a niveles de detección muy bajos de la proteína tau en muestras de suero. Además, se pudieron determinar otros marcadores como la lactoferrina en muestras de saliva o la fosforilación de la proteína tau (la cual se encuentra aumentada en el progreso de la enfermedad).

Por lo que, en conclusión, fuimos capaces de desarrollar un KIT de diagnóstico válido para diferentes patologías y que es extrapolable gracias a su versatilidad a cualquier otra patología. Gracias también al uso de las nanopartículas se pueden emplear muestras con matrices más complejas y llegar a límites de detección mucho más bajos, haciendo que el uso de este tipo de biosensor con las nanopartículas sea una gran herramienta para el diagnóstico temprano de enfermedades.

Table of Contents

List of Figures

List of Tables

Abbreviations and Acronyms

3P-Tau	Triphosphorylated-Tau
aa	amino acids
Abs	Antibodies
ACE2	Angiotensin-Converting Enzyme 2
aCSF	artificial Cerebrospinal Fluid
AD	Alzheimer's Disease
AF4	Asymmetrical Flow Field-Flow Fractionation
AFM	Atomic Force Microscopy
Ag*	Labeled Antigen
Ags	Antigens
ALT	Alanine AminoTransferase
APCs	Antigen-Presenting Cells
APLP1	Amyloid Precursor-Like Protein 1
APLP2	Amyloid Precursor-Like Protein 2
APOE4	Apolipoprotein E4
APP	Amyloid Precursor Protein
ARDS	Acute Respiratory Distress Syndrome
AST	Aspartate AminoTransferase
Au	Gold
Aβ	Amyloid-beta
BC	Baltimore Classification
BCA	Bicinchoninic Acid Test
BCR	B Cell Receptor
BICELLs	Biophotonic Sensing Cells
BiMW	Bimodal Waveguides
BIOD S. L.	Bio Optical Detection S.L.
BSA	Bovine Serum Albumin

C	Constant
CBGP	Centro de Biotecnología y Genómica de Plantas
CD	Cluster of Differentiation
cDNA	Complementary DNA
CDRs	Complementarity-Determining Regions
CFR	Case Fatality Rate
CLIA	Chemiluminiscence Immunoassay
CMP	Common Myeloid Progenitor
CNB	Centro Nacional de Biotecnología
CNS	Central Nervous System
COVID-19	Coronavirus Disease 2019
CRISPR	Clustered Regularly Interspaced Short Palindromic Repeats
CRP	C-Reactive Protein
CSF	Cerebrospinal Fluid
CSIC	Consejo Superior de Investigaciones Científicas
CTB	Centro de Tecnologia Biomédica
CTD	C-Terminal Domain
CTLs	Cytotoxic T cells
DAS	Double Antibody Sandwich
DCs	Dendritic Cells
DEA	Diethanolamine
D_h	Hydrodynamic Diameter
DLS	Dynamic Light Scattering
DNA	Deoxyribonucleic Acid
DPI	Dual-Polarization Interferometer
E	Envelope protein
EA	Enfermedad de Alzheimer
EDC	Ethyl(dimethylaminopropyl) carbodiimide
EIA	Enzyme Immuno Assay
ELISA	Enzyme-Linked ImmunoSorbent Assay

Equation	Eq
EVs	Extracellular Vesicles
Fc	Fraction Crystallizable
FDA	Food and Drug Administration
FIA	Fluoroimmunoassay
FP	Fusion Peptide
FPI	Fabry-Perot Interferometer
FTH1	Ferritin
FTIR	Fourier-Transform Infrared Spectroscopy
f_{trans}	Transfer Function
GOFB	Group of Optics, Photonics, and Biophotonics
H	Heptad Domain
H_2O_2	Hydrogen peroxide
H_2OmQ	MiliQ water
H_2SO_4	Sulfuric acid
HABA	4´-hydroxyazobenzene-2-carboxylic acid
HADAS	Heterologous Antiglobulin Double Antibody Sandwich
HCoV	Human Coronavirus
HCoV-229E	Human Coronavirus 229E
HCoV-HKU1	Human Coronavirus HKU1
HCoV-NL63	Human Coronavirus NL63
HCoV-OC43	Human Coronavirus OC43
HE	Hemagglutinin-Esterase dimer
HI	Hartman Interferometer
HIV	Human Immunodeficiency Virus
HRP	Horseradish Peroxidase
HSP70	Heat Shock Protein 70
ICU	Intensive Care Unit
IFNγ	Interferon-gamma
IgA	Immunoglobulin A

IgD	Immunoglobulin D
IgE	Immunoglobulin E
IgG	Immunoglobulin G
IgM	Immunoglobulin M
Igs	Immunoglobulins
IL-12	Interleukin-12
IL-1β	Interleukin-1 beta
IL-21	Interleukin-21
IL-23	Interleukin-23
IL-2	Interleukin-2
IL-4	Interleukin-4
IL-6	Interleukin-6
IL-8	Interleukin-8
ILVs	Intraluminal Vesicles
IML	Instituto de Medicina de Laboratorio
IODM	Interferometric Optical Detection Method
I_{ref}	Reference signal
IROP	Increased Relative Optical Power
ISEV	International Society for Extracellular Vesicles
I_{sig}	Measurement signal
K_d	Dissociation constant
L1CAM	L1 Cell Adhesion Molecule
LoD	Limit of Detection
LSC	Level of Severity of COVID-19
M	Membrane protein
MALDI-TOF	Matrix-Assisted Laser Desorption/Ionization Time-Of-Flight
MAPT	Microtubule-Associated Protein Tau
MCI	Mild Cognitive Impairment
MERS-CoV	Middle East Respiratory Syndrome Coronavirus
MES	2-Morpholinoethanesulphonic acid

MHC	Major Histocompatibility Complex
min	minutes
miRNAs	micro RNAs
MLRM	Multiple Linear Regression Model
mRNA	messenger RNA
MVBs	Multivesicular Bodies
MWCO	Molecular Weight Cut-Off
MZI	Mach-Zehnder Interferometer
N	Nucleocapsid protein
Na_2CO_3	Sodium carbonate buffer
NC	Negative Control
NDD	Neurodegenerative Diseases
NFTs	Neurofibrillary Tangles
NGS	Next-Generation Sequencing
NHS	N-Hydroxysuccinimide
NIA-AA	National Institute on Aging-Alzheimer's Association
NK	Natural Killer
NLRs	NOD-like Receptors
NMDA	Methyl-D-aspartic acid
NPs	Nanoparticles
NTA	Nanoparticle Tracking Analysis
OD	Optical Density
ON	Overnight
OP	Optical Power
PAMPs	Pathogen-Associated Molecular Patterns
PBS	Phosphate Buffer Saline
PBS-T	Phosphate Buffer Saline-Tween
PC	Positive Control
PC1	Positive Control 1
PC2	Positive Control 2

PC3	Positive Control 3
PCR	Polymerase Chain Reaction
PDI	Polydispersity Index
PET	Positron Emission Tomography
PFA	Paraformaldehyde
PoC	Point-of-Care
PRRs	Pattern Recognition Receptors
pTau181	Threonine-phosphorylated tau protein 181
PVC	Polyvinyl Chloride
PVP	Polyvinylpyrrolidone
RBD	Receptor-Binding Domain
RI	Refractive Index
RIA	Radioimmunoassay
RIG-I	Retinoic acid-Inducible Gene
RLRs	Retinoic acid-Inducible Gene I (RIG-I)-like Receptors
rN	recombinant N protein
RNA	Ribonucleic Acid
rpm	revolutions per minute
rRBD	recombinant RBD protein
rS1	recombinant Spike protein 1
rS1	recombinant Spike protein 2
RT	Room Temperature
RT-LAMP	Reverse Transcription Loop-Mediated Isothermal Amplification
RT-PCR	Real Time-PCR
s	seconds
S	Spike protein
SARS-CoV	Severe Acute Respiratory Syndrome Coronavirus
SARS-CoV-2	Severe Acute Respiratory Syndrome Coronavirus 2
SEM	Scanning Electron Microscopy
sEVs	small Extracellular Vesicles

Si	Silica
sIgA	specific IgA
sIgG	specific IgG
sIgM	specific IgM
sIgT	Total specific Immunoglobulins
SiO_2	Silicon oxide
S-NTD	N-Terminal galectin-like Domain
SPR	Surface Plasmon Resonance
SPs	Senile Plaques
STV	Streptavidin
TBS	Tris-Buffered Saline
TBS-T	TBS-Tween
TCR	T Cell Receptor
TEM	Transmission Electron Microscopy
TGF-β	Transforming Growth Factor-beta
Th	Helper T cell
TIR	Total Internal Reflection
TLRs	Toll-like Receptors
TMB	3,3',5,5' Tetrametilbenzidina
TNF-α	Tumor Necrosis Factor alpha
Treg	Regulatory T cells
UPM	Universidad Politécnica de Madrid
UV	Ultraviolet
V	Variable
WB	Western Blot
WHO	World Health Organization
YI	Young interferometer
αAb	anti-Ab
$\alpha A\beta_{16}$-biotin	anti-$A\beta_{16}$-biotin
$\alpha A\beta_{40}$	anti-$A\beta_{40}$

αAβ_{42}	anti-Aβ_{42}
αBSA	anti-BSA
αHuman-CRP	anti-Human-CRP
αHuman-FTH1	anti-Human-FTH1
αHuman-IgA	anti-Human-IgA
αHuman-IgG	anti-Human-IgG
αHuman-IgM	anti-Human-IgM
αL1CAM	anti- L1CAM
αLactoferrin	anti-Lactoferrin
αMouse-IgG-HRP	anti-Mouse-IgG Ab labeled with HRP
αp24	anti-p24
αRabbit-IgG-HRP	anti-Rabbit-IgG Ab labellet with HRP
αSARS-CoV-2	anti-SARS-CoV-2
αTau	anti-tau
ζ-potential	Zeta potential

1. Introduction

Biosensors are becoming increasingly important in clinical diagnostics because of the growing need for detection systems that **are reliable, with high specificity and sensitivity, that are easy to use and that reduce costs and time** in clinical determinations.

These are some of the characteristics of biosensors that make them a great tool for the diagnosis and monitoring of multiple diseases. On the one hand, they are systems that **can reach very low detection limits**, improving established conventional systems. On the other hand, this detection becomes very specific, regardless of the type of sample being measured, since they have the possibility of **reducing the matrix effect**.

In the case of the biosensor used during this thesis, in addition to these advantages, it also has many others:

- The **simplicity in the manufacture process** of the biosensor allows it to be scaled up, being able to manufacture a large number of these in a short time, greatly reducing costs during the manufacturing process.
- The **versatility** in designing what we want to determine in the biosensor. A **multiplexed design** can be performed to determine multiple biomarkers in a few samples, or a single biomarker can be determined in a large number of samples. In addition, this versatility allows on the other hand to use this biosensor in the determination of multiple pathologies.
- The **sample volume** is also an important factor to consider, as there are cases where the sample is poor or difficult to obtain. In addition, if less volume is needed to determine one marker, multiple biomarkers can be determined with the same amount of sample. In this case, the biosensor used is capable of determining the biomarker of interest with **only 1 µL of sample.**
- Decrease the **number of steps** during assays to allow faster determinations. In the case of some biomarkers, these can be determined directly or label-free, without the need for secondary antibodies (Abs) or a chemical developer. It is also possible in some cases to eliminate the surface blocking step. Therefore, thanks to the lack of these steps, faster protocols can be carried out.
- Obtain **quantitative as well as qualitative results**. In addition to being able to determine the presence or absence of the biomarker, it is possible to quantify the biomarker of interest with a calibration curve.
- **Easy handling** by laboratory operators also simplifies the work. It does not require complicated steps during use and some processes can be automated, such as the dispensing of drops for incubations. This also reduces human error and achieves greater

repeatability in the assay and between assays performed by the same or different people.

- The **readout system** of this biosensor is also easy to use, with a **user-friendly** interface that allows in real time to see if the readout is being performed correctly. In addition, being able to obtain data at each step of the protocol is also very important, as it allows to **control the experiment at each step** and to know at what point the assay may be failing without having to wait for the final step of developing the assay.

So due to all these advantages, the optical biosensor employed during this thesis is a great candidate to be used in clinical practice.

All this became more evident in March 2020 when the pandemic caused by **Severe Acute Respiratory Syndrome Coronavirus 2 (SARS-CoV-2)** started. This is a Ribonucleic Acid (RNA) virus that first appeared in Wuhan, China, at the end of 2019 and quickly spread around the world causing **Coronavirus Disease 2019 (COVID-19),** which is a respiratory disease that causes fever, cough, and respiratory distress (in addition to other symptoms) leading to death.

At this time, international collaboration at multiple levels was very important, among them in research in order to have effective and rapid diagnostic systems that would allow a large population screening. It is for this reason that the **first objective of this thesis** was decided at this time as:

- To **develop an optical *in-vitro* diagnostic system for the detection of specific Abs against SARS-CoV-2**. In order to develop this objective, also different biomarkers characteristic of the disease will be determined in human serum and saliva samples.
    - A mathematical model will then be developed to determine the severity of the disease based on the biomarkers measured.

But, in addition to this emerging disease, we must keep in mind that there are thousands of other pathologies in the world. A very widespread case is **Neurodegenerative Diseases (NDD),** which increasingly affect millions of people worldwide. Among these diseases is **Alzheimer's Disease (AD),** which causes 60% of cases of dementia worldwide, with more and more people suffering from this pathology. The importance of the diagnosis of AD is due to the fact that it is a disease that has no cure and whose treatments are only to alleviate the symptoms and try to slow its progression. However, once these treatments begin, it seems too late, since the symptoms appear when the neuronal damage is high and it is very difficult to stop it.

Therefore, it is necessary to think of an alternative, and this is **the determination of different proteins involved in the pathology of the disease.** The first changes that occur between 15-20 years before symptoms appear are at the biochemical level, as the expression patterns of some proteins that can act as biomarkers change. However, it must be considered that these first changes are difficult to perceive since although some proteins increase or decrease, **they do so in very small concentrations.**

This was the motivation for the **second objective** of this thesis:

- **To develop an optical *in-vitro* diagnostic system for NDD**. In this case, the model disease used was AD.

Another factor to consider is that at present, the sample used for these determinations is **Cerebrospinal Fluid (CSF)**, which is very invasive and makes monitoring the disease very complicated. Therefore, the aim would be to be able to **measure these proteins in serum**, adding the difficulty that **serum concentrations are even lower**. For this reason, it is necessary to develop a system capable of having very low detection limits in order to be able to determine very low concentrations of the biomarkers of interest. To this end, as a complement to the optical biosensor, we use **Nanoparticles (NPs) that can act as refractometric amplifiers**. These can be manufactured with different materials, in this case, the **NPs used are of Silicon oxide (SiO_2)** that after a biofunctionalization process, in which the surface of the NP is modified, can be used as biomarker collectors in the samples and after this step, they can be incubated in the biosensor increasing the sensitivity of the system and can **detect the concentration of pg/mL**.

The need to use NPs in the detection system sets the **third objective** of this thesis:

- **Develop a protocol for the biofunctionalization of NPs to modify their surface and coat them with specific Abs against the biomarkers of interest**. In this way, thanks to its use, competitive assays will be performed in order to quantify the biomarkers in the different types of samples used, increasing the sensitivity of the sensor.

It is important to consider that for a biosensor to be competitive in the market, among other characteristics, it is important that it has a **very low Limit of Detection (LoD)** in order to improve the currently established detection systems. For this reason, in order to improve this point, the **fourth objective** of this work was determined as follows:

- **To develop a system that increases the detection sensitivity of the biosensor and thus obtain a lower LoD for direct detection**. Among the available systems, the biotin-streptavidin (STV) system was chosen.

Of all the proposed objectives, promising results have been achieved that open up new ways to detect other pathologies or help in their follow-up. In addition, sensitivity has been significantly improved and its possible use with different types of samples, including serum and saliva, has been corroborated, opening up the possibility of its use in future clinical diagnosis.

2. State of the art

2.1. Introduction to biosensors

A **biosensor** is defined as a device capable of converting a chemical or biological interaction into a measurable signal. These reactions are **specific** and can be mediated by Abs, enzymes, cells, and nucleic acids, among others, generating signals that can be optical, electrical, etc. (IUPAC, 2012). Among the main characteristics of biosensors, noteworthy are their ease of handling and use, speed, reduced costs, and the significantly lower sample quantity required (Ziegler & Göpel, 1998).

A typical biosensor comprises the following elements: the **bioreceptor**, the **transducer**, and the **detector** (Bhalla et al., 2016; IUPAC, 2012; Wild, 2013).

- The **bioreceptor** is a molecule capable of specifically recognizing the analyte of interest. This recognition triggers a biological interaction that generates a measurable signal, known as the recognition signal, which can manifest as a change in pH, light emission, etc.
- The **transducer** is responsible for converting this biological interaction into a measurable signal. Its mechanism can be of various types, including electrochemical, optical, magnetic, etc.
- The **detector** processes the signals sent from the transducer, enabling their analysis. Utilizing both hardware and software, it facilitates the presentation of data.

Figure 1 illustrates the schematic of a biosensor where the bioreceptor, typically a specific biomolecule, is anchored to the transducer's surface and interacts with the analyte. This interaction, facilitated by the transducer (a physical element), is transduced, and sent to the reading device for processing. This system converts the signal emitted by the transducer into a digital format, which may or may not be quantifiable, and presents it in a user-friendly manner.

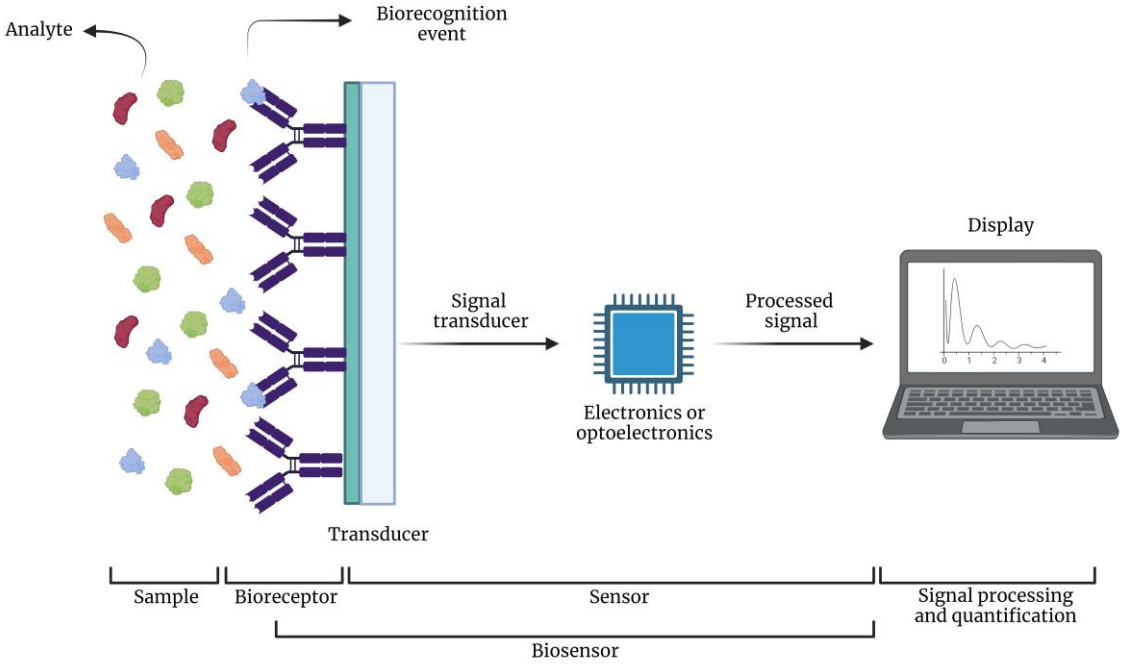

Figure 1. Depiction of the parts of a biosensor. Created with Biorender.com.

Each type of transducer operates on a different principle. Focusing on the biosensors used in this thesis, which are **optical biosensors, the transduced signal is the light**. The recognition interaction between the bioreceptor and the analyte of interest generates an optical response, altering the properties of light based on the optical characteristics of the transducer.

The biosensor market has experienced exponential growth in recent years, primarily driven by the emergence of nanotechnology-based biosensors and significant technological advancements. Additionally, the demand surged during the SARS-CoV-2 pandemic, further propelling advancements in this sector (A. Kumar et al., 2022).

These biosensors find widespread and routine applications in various fields, including disease diagnosis, water quality control, and food composition analysis, among many others. However, their viability for a particular bioapplication depends on specific characteristics outlined by the World Health Organization's (WHO's) **ASSURED criteria** (Affordable, Sensitive, Specific, User-friendly, Rapid and robust, Equipment-free, and Deliverable to end-users). These characteristics are described in Table 1.

Table 1. Characteristics of the biosensors.

Characteristic	*Definition*	*Source*
Selectivity	It refers to the method's capacity to **determine specific analytes** under the conditions of the sample matrix (simple or complex) without interference from other components. In the case of biosensors, it relates to ensuring that the bioreceptor used will exclusively interact with the analyte of interest present in the sample, while avoiding interactions with other substances. This specificity is crucial to accurately detect and measure the target analyte in the presence of various compounds or elements in the sample. **Diagnostic selectivity** is defined as the probability that the test result will be negative in a person who does not have the disease (**true negatives**).	(Akobeng, 2007; Vessman et al., 2001)
Precision	It refers to the **equality among results** obtained through repeated measurements in independent assays that have followed the same experimental procedure. Therefore, when measuring the same sample in the biosensor, it provides similar results in terms of dispersion or variability. This reliability ensures consistency and reproducibility in the measurements, allowing for confidence in the obtained data and its interpretation.	(Vessman et al., 2001)
Sensitivity	**Analytical sensitivity** is defined as the **slope of the dose-response curve**, or the change in response per unit concentration. If the slope of the straight line is very steep, it will have a higher sensitivity, if it is not very steep the method will have a lower sensitivity. **Diagnostic sensitivity** is defined as the probability of a positive diagnostic test result in a person affected by the disease (**true positives**).	(Akobeng, 2007; Lavín et al., 2018)
Resolution	It is the **smallest change in magnitude that a device can perceive significantly**. In other words, it represents the minimum change that the device can detect in the measured magnitude.	(Bhalla et al., 2016)
Accuracy	This refers to how close the measurements taken by a device are to the true value of the measured magnitude. In essence, it represents the **instrument's ability to provide values close to the actual or true value** when the sample is measured multiple times. This characteristic reflects the precision and accuracy of the instrument in obtaining reliable and close-to-real values across repeated measurements.	(Vessman et al., 2001)

Characteristic	*Definition*	*Source*
Stability	It assumes that the **measured values are not influenced by external factors** during their measurement or throughout their lifespan. For a biosensor, this characteristic is related to susceptibility to environmental disturbances within the biosensor system's surroundings, which can lead to signal drift during readings and errors in the measured concentration. Factors affecting stability include temperature variations, affinity between the analyte of interest and the bioreceptor, degradation of the bioreceptor, and storage conditions. These factors play a crucial role in maintaining the biosensor's stability and accuracy by minimizing signal fluctuations or errors caused by environmental influences.	(Naresh & Lee, 2021)
Reproducibility	This refers to obtaining **consistent results in experiments conducted independently** but following the same protocol and using the same materials under different conditions. It signifies achieving results that align, even when conducted by different individuals or in different laboratories. This reproducibility validates the reliability and robustness of the experimental method, ensuring that the outcomes are consistent and in agreement across various settings or operators.	(Bhalla et al., 2016; Vessman et al., 2001)
LoD	The LoD is typically defined as the **minimum quantity or concentration of a substance reliably detectable by a specific analytical method**. Intuitively, the LoD would be the minimum concentration obtained from measuring a sample (containing the analyte) that we can distinguish from the concentration obtained by measuring a blank sample, one without the analyte present. The primary issue regarding LoD lies in its calculation, as there is no consensus on its determination. This complicates the comparison between different biosensors on the market since various methods or criteria are used, making it challenging to establish a universal standard for LoD determination.	(Currie, 1995; Lavín et al., 2018)
Linearity	This attribute **correlates the measured responses from a set of measurements taken at different analyte concentrations in a proportional manner**, resembling results plotted on a straight line represented mathematically by the calibration curve as y = mx + c, where "c" is the intercept, "x" is the concentration of the analyte, "y" is the output signal, and "m" (the slope of the line) represents the biosensor's sensitivity. In essence, it signifies the proportionality of the biosensor's	(Bhalla et al., 2016)

Characteristic	*Definition*	*Source*
	response concerning the analyte concentration. This proportionality is especially crucial in biosensors that not only detect the presence of an analyte but also quantify it accurately. The linear relationship depicted by the calibration curve helps in quantifying the analyte concentration based on the biosensor's response signal.	

2.1.1. Types of biosensors

The number of biosensors today has experienced a significant increase, presenting numerous variabilities in the molecules employed (both as receptors and analytes to be determined), as well as the types of transducers that can be utilized in manufacturing different biosensors.

The primary aim of this thesis is **the development of technology capable of detecting multiple pathologies** using a biosensing system based on an interference-based optical transducer without labeling, coupled with an optical detection system that measures changes in Refractive Index (RI). Depending on the pathology to be detected, **NPs have also been employed as a method of refractometric amplification** to detect very low concentrations in the samples used.

To comprehend the employed system, an introduction and description of this type of biosensor will be provided.

2.1.2. Classification

There are various classification types in the literature, but the most established ones are based on **biochemical interaction**, the type of **detection interaction** (direct or indirect), the **bioreceptor** used, and finally, based on the **transducer** upon which the biosensor relies. Figure 2 represents this classification based on the literature found (Karunakaran et al., 2015; Kaur et al., 2018; J. V. Kumar et al., 2022; Monošík et al., 2012).

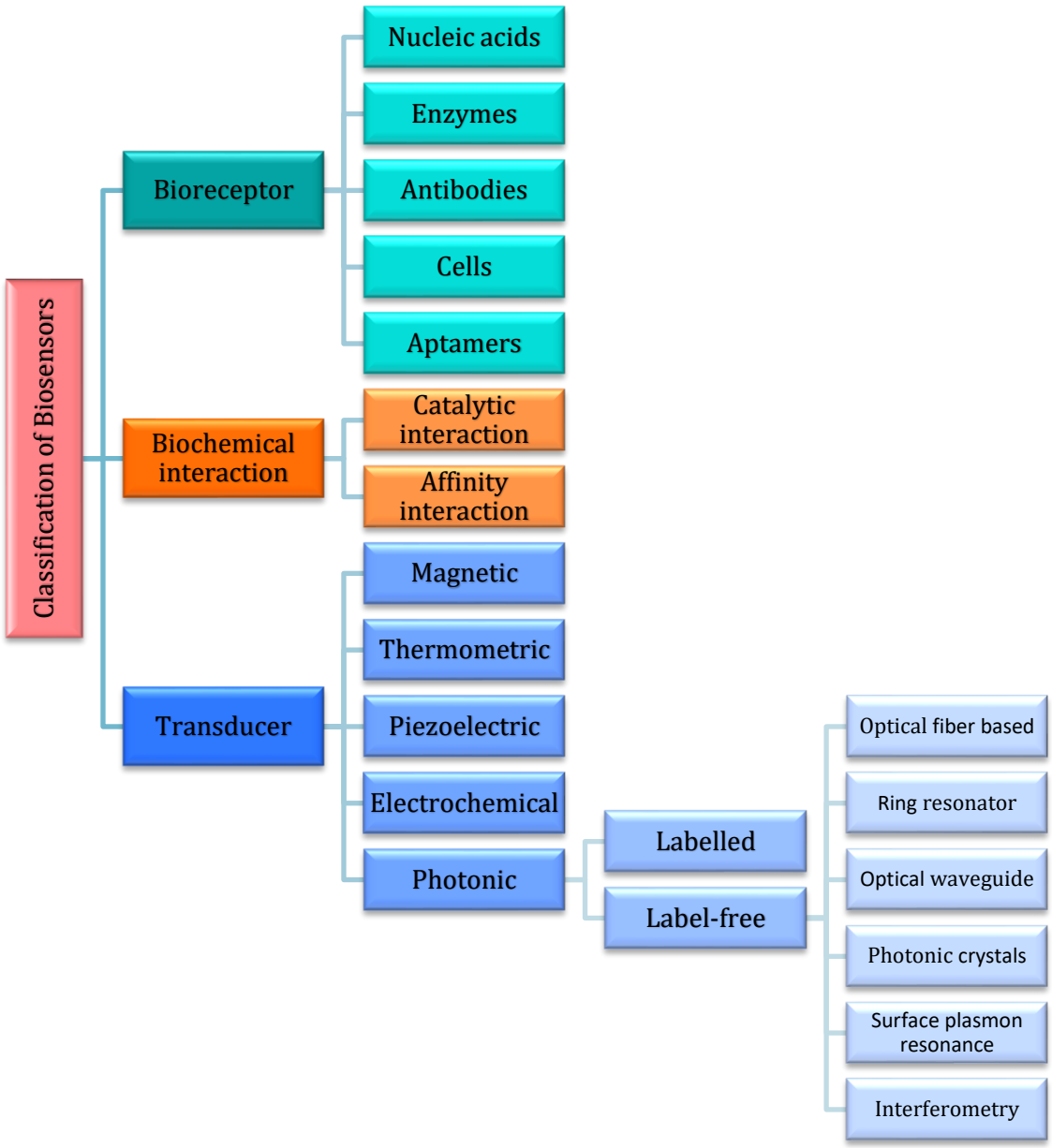

Figure 2. Biosensors classification.

2.1.2.1. *Classification based on bioreceptor used*

Biosensors depend on bioreceptors, crucial for providing selectivity by specifically binding to targeted molecules for detection. These bioreceptors can be different biomolecules, among which the most commonly used are (Ronkainen et al., 2010; Scheller et al., 2001):

- **Nucleic acids**: These biosensors rely on the phenomenon of hybridization occurring between the Deoxyribonucleic Acid (DNA) strand acting as a probe within the biosensor and the complementary strand, which serves as the target to be detected. This results in high specificity due to the exceptionally strong affinity between DNA strands.
- **Enzymes**: These biomolecules can catalyze reactions with a substrate, producing a product that can be measured by the transducer. In this scenario, numerous different enzymes can be employed, each highly specific to its substrate.
- **Abs**: Also known as Immunoglobulins (Igs), Abs exhibit high specificity as each type recognizes a specific epitope of a particular protein. Moreover, there's a wide variety of Abs capable of recognizing diverse protein types.
- **Cells**: In this case, the entire cell acts as the bioreceptor, enabling the achievement of very low detection limits.
- **Aptamers**: These are sequences of single-stranded oligonucleotides (DNA or RNA) artificially synthesized, capable of recognizing a wide range of molecules with high affinity and specificity.

2.1.2.2. *Classification based on the type of biochemical interaction*

Another viewpoint for classification is based on the interaction occurring between the bioreceptor and the target analyte. Based on this interaction, it can be divided into two subclasses:

- **Catalytic interaction**: In this scenario, a biocatalyst such as an enzyme is employed. When it interacts with the analyte (in this case, the enzyme's substrate), it triggers a chemical reaction, resulting in a detectable and measurable substance (Kwong, 2000).
- **Affinity interaction**: Detection occurs directly due to the interaction between the bioreceptor and the analyte (Rogers & Mulchandani, 2011).

In both cases, the biosensor may or may not require the presence of a marker to be measurable or to amplify the signal, distinguishing between direct detection systems and indirect detection systems (Thévenot et al., 2001).

2.1.2.3. *Classification based on the type of transducer.*

The transducer is a device capable of converting a physical magnitude (mechanical, thermal, electrical, optical, etc.) into a measurable signal. It is crucial, and depending on the type of transducer employed, they can be classified as follows:

- **Magnetic**: These biosensors use micro or NPs coated with a molecular recognition element responsible for capturing the target analyte. Subsequently, another element (matrix, gel, etc.) selectively traps only those magnetic particles where the molecular recognition reaction occurred on their surface. Finally, a magnetic technique or sensor (usually the Hall effect or variations of magnetoresistance or magneto-impedance) detects the number of magnetic particles with the analyte on their surface, with the magnetic signal being proportional to this number (Llandro et al., 2010; Marrows, 2007).
- **Thermometric**: Thermometric transducers detect the heat generated in exothermic enzymatic reactions, which can be correlated with the analyte's concentration. These temperature changes are typically determined by thermistors at the device's entry and exit points where the enzymes are immobilized. An inconvenience here could be heating losses due to radiation, conduction, or convection (González Rumayor et al., 2005).
- **Piezoelectric**: Biosensors of this type use piezoelectric materials that resonate under the influence of an external alternating electric field. These crystals are coated with the recognition element, often based on bioaffinity (such as Abs, lectins, etc.), and are exposed to the sample containing the analyte to be detected (Ivnitski et al., 1999). The oscillation frequency is determined by the crystal's mass, which varies upon the interaction between the recognition element and the analyte, resulting in a change in the oscillation frequency.
- **Electrochemical**: Electrochemical transducers convert the signal produced by the interaction between the recognition system and the analyte into an electrical signal. They provide specific quantitative or semi-quantitative analytical information. The biological recognition element and the transduction element must be in contact. Four types of electrochemical biosensors exist: **conductometric, potentiometric, amperometric, and impedimetric**, detecting changes in conductivity, potential, generated current, or impedance, respectively (Grieshaber et al., 2008; Ronkainen et al., 2010).
- **Photonic**: Optical transducers measure variations in light properties due to physical or chemical interactions between the target analyte and the biosensor's biological recognition element. These sensors rely on changes in **absorption, fluorescence, luminescence, scattering, or RI** when light interacts with recognition surfaces. The basic measurement system consists of a light source, the sensor element (where the receptor molecules would be located), and the detector. They differentiate between direct detection methods, which do not require labeling, and indirect detection methods where labeling is necessary (Damborský et al., 2016; Ligler & Taitt, 2008).

2.1.3. Optical biosensors

Optical biosensors today offer substantial advantages over conventional analytical techniques, providing **direct**, **real-time detection** that can even be **label-free**. Additionally, they boast **high specificity and sensitivity**.

These biosensors measure the interaction between the bioreceptor and the target analyte using light, assessing changes in light properties resulting from this interaction. The optical response obtained is contingent upon the transducer's characteristics, which can manifest as alterations in RI, absorption, and dispersion, among other factors (Lakshmipriya & Gopinath, 2019).

As depicted in Figure 2, optical biosensors can be categorized into labeled or label-free types. In label-free detection, the signal emerges directly from the interaction between the target analyte and the transducer, utilizing various optical structures (such as optical fibers, resonant rings, optical waveguides, photonic crystals, Surface Plasmon Resonance (SPR), and interferometric systems). Conversely, labeled detection often generates signals via colorimetric or fluorescent methods (Damborský et al., 2016).

Label-free optical biosensors are further classified as optical fibers, resonant rings, optical waveguides, photonic crystals, SPR, and interferometric systems (Singh et al., 2023).

2.1.3.1. *Optical fiber-based biosensors*

Optical fibers consist of a core and a cladding, where the Silica (Si) core is typically doped with another material (like germanium), creating a difference in RI between the core and cladding. This difference, with the core having a higher RI than the cladding, enables the propagation of light through Total Internal Reflection (TIR) (Leung et al., 2007). Bioreceptors are immobilized within the fiber core and interact with the target analyte.

This type of optical biosensor has found extensive use, for instance, in detecting *Escherichia coli* (Maas et al., 2018) or measuring glucose and hemoglobin levels (Hirsch et al., 2017). Its widespread application is attributed to its compact size, robustness, cost-effectiveness, and capability for high-volume production with finely tuned optical properties (Singh et al., 2023).

2.1.3.2. *Ring resonator-based biosensors*

A resonator ring consists of one or multiple silicon waveguides positioned on an oxide substrate, where light traveling through the resonator ring is coupled. Typically, a tunable laser light is directed into the waveguide, partially coupling to the resonator ring, creating resonance peaks (Singh et al., 2023; Steglich et al., 2019).

The surface of the resonator ring is biofunctionalized with the bioreceptor. Consequently, if the target analyte interacts with the bioreceptor, it results in a shift in the resonance wavelength (Steglich et al., 2019).

This type of biosensor is cost-effective with a very rapid response time. It has increasingly been employed in detecting various diseases, such as cancer (L. Ali et al., 2020).

2.1.3.3. *Optical waveguide based-biosensors*

Waveguides can be primarily classified into multimode and single-mode. Multimode waveguides are usually thicker than the excitation light's wavelength and are commonly made of glass or Si, making them cost-effective and easy to manufacture. In contrast, single-mode waveguides consist of a very thin layer, smaller than the excitation light's wavelength (Mukundan et al., 2009).

These have been extensively used in various biodetection applications because they can exhibit high sensitivity due to the action of the evanescent field. Commercial systems based on waveguides are employed for cell signaling (Fang et al., 2006).

2.1.3.4. *Photonic crystals-based biosensors*

Photonic crystals are periodic structures that can exist in one, two, or even three dimensions. This geometric arrangement causes destructive light interference, resulting in a range of frequencies known as the photonic bandgap (Benmerkhi et al., 2020).

The structures forming photonic crystals can vary significantly, often incorporating a defect deliberately introduced to break the network's periodicity. This defect makes the structure more sensitive to any changes in the RI near it, making it easier to monitor. The defect might involve altering the size of the periodic structure or removing one of the network's elements, directly affecting light transmission and therefore is directly related to the analyte concentration under determination (Divya et al., 2018; Gavela et al., 2016).

Biosensors based on photonic crystals have very small sizes and are easily integrable, making them widely employed in medical applications (Inan et al., 2017).

2.1.3.5. *SPR-based biosensors*

SPR is an optical phenomenon enabling real-time measurement of the binding between the analyte of interest and the bioreceptor (Kumar Singh et al., 2023). These biosensors detect minimal changes in the RI on the detection surface. This detection is highly sensitive and relies on exciting electrons in a metallic film, leading to total light absorption at a specific angle of incidence dependent on RIs (Mittal et al., 2021).

SPR-based biosensors present a remarkable alternative for clinical diagnostics due to their high sensitivity, real-time monitoring capability allowing rapid results, and capacity for parallel measurements (Kumar Singh et al., 2023). Moreover, their versatility has been extensively demonstrated in literature for detecting numerous analytes associated with various diseases (Mandala et al., 2021; Toma et al., 2022; Wittekindt et al., 2000).

2.1.3.6. *Interferometry-based biosensors*

Within label-free optical biosensors, interferometry-based ones are considered a great choice for various diagnostics due to their **small size, allowing for easy large-scale production**. They boast excellent **reproducibility and sensitivity** (Fan et al., 2008). Their operation relies on the interference of two polarized electromagnetic waves originating from the same monochromatic light source but traveling through different pathways. One pathway is biofunctionalized with the bioreceptor, interacting with the sample ($_S$), while the other acts as a reference ($_R$), remaining unchanged and possibly pretreated to prevent undesired nonspecific bindings. This process creates an interference pattern between the two light beams, enabling the **measurement of differences in the RI of both pathways** (González-Guerrero et al., 2016; Ramirez et al., 2022). When recognition occurs between the analyte and the bioreceptor in pathway $_S$, it induces a disturbance in the light, altering its phase ($\Delta\emptyset$). The resulting interference pattern (I, *Equation (Eq.) 1*) combines the intensity of both beams (I_R and I_S) based on the phase variation (Kumar Singh et al., 2023)(Damborský et al., 2016; Nguyen et al., 2015).

$$I = I_R + I_S + 2\sqrt{I_R I_s}cos(\Delta\emptyset) \qquad Eq.\ 1$$

Great sensitivity is based on this principle, as it measures the evanescent field sensitive to changes in the RI. It is also responsive to the length of the path where the interaction occurs (Ramirez et al., 2022). Currently, various types of interferometry-based biosensors can be found, including the Mach-Zehnder Interferometer (MZI) (Heideman et al., 1991), where light entering one arm is split into two different paths (measurement and reference) that later converge at a certain distance. Subsequently, the Young Interferometer (YI) was proposed, similar to the MZI, but without both paths rejoining (Brandenburg & Henninger, 1994). More recently, Bimodal Waveguides (BiMW) have been developed where light does not split into two different paths but follows a common trajectory (Torrijos-Morán et al., 2022). Additionally, the literature describes the Hartman Interferometer (HI) and the Dual-Polarization Interferometer (DPI) (González-Guerrero et al., 2016). Within this type of interferometer-based biosensors, there are those based on cavities, characterized by their resonant peak, which shifts depending on the concentration of the analyte detected by the bioreceptor. Additionally, this subgroup can also utilize evanescent field interaction. There are various cavity-based biosensors, and one of them is the **Fabry-Perot Interferometer (FPI)** (Figure 3), which forms the basis of the biosensor used for this thesis and will be detailed in the following subsection.

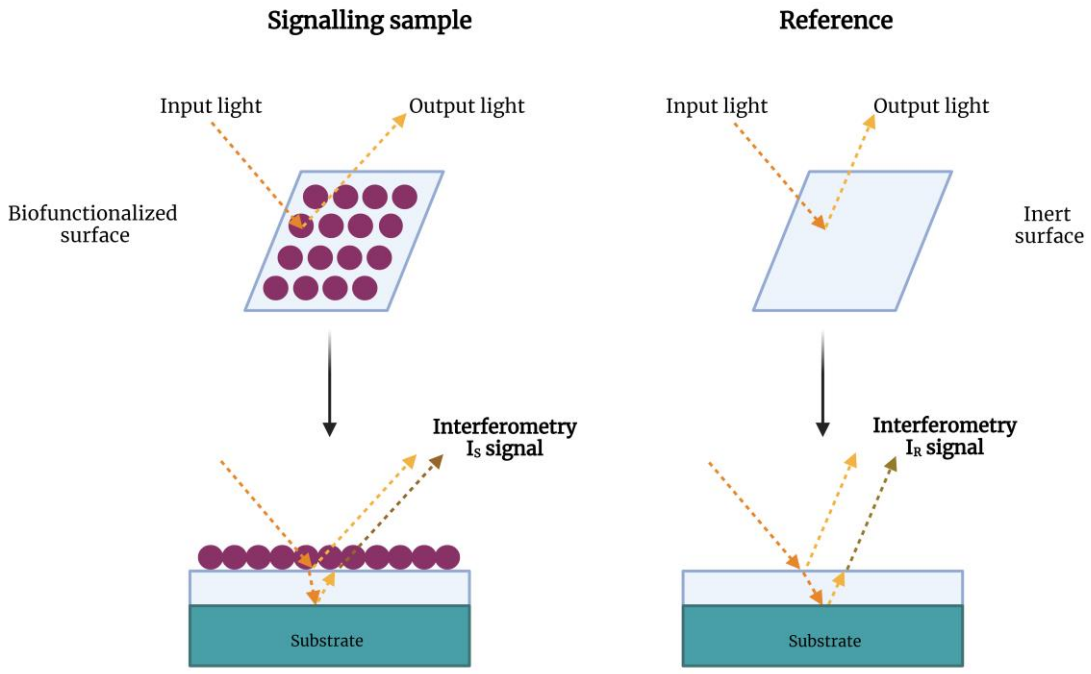

Figure 3. Representation of an FPI. On the left is depicted the interaction of the incident light with the surface when a biomolecule is anchored, while on the right is the behavior of the light on the reference surface. Created with BioRender.com.

2.1.3.6.1 Fabry-Perot-based biosensors

FPIs have been extensively used since they were described by Charles Fabry and Alfred Perot (Islam et al., 2014). They rely on two highly reflective surfaces, or one highly reflective and another semi-reflective, placed in a parallel configuration, creating a cavity with both surfaces separated by a distance *d*. This setup causes the light beam to recur within the system.

The light beam, originating from a source (*S*) and featuring a narrow angle of incidence θt, undergoes successive reflections between the reflective surfaces. The transmitted set of beams eventually converges at a photodetector, as depicted in Figure 4. Additionally, part of the light is transmitted each time it reaches the second reflective surface, and these transmitted beams interfere with each other, resulting in either a maximum or minimum depending on the path between them. The convergence of these beams is determined by the optical path difference (Δ) between them, where *n* represents the RI of the cavity medium, as shown in *Eq. 2* (Born & Wolf, 1999):

$$\Delta = 2n_f d \cos \theta_t \qquad Eq.\ 2$$

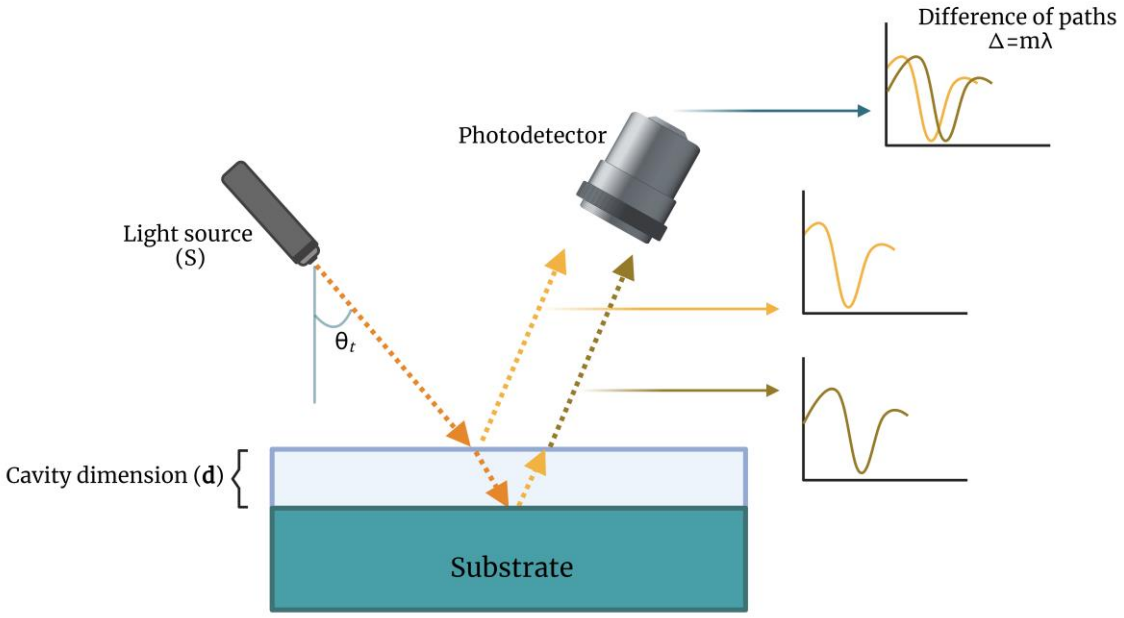

Figure 4. Description of the principle of the technique used. Created with BioRender.com.

Within the ways to modulate the behavior of this interferometer, **one can alter the cavity dimensions (*d*), the speed of light in the medium (*c*) related to the material, its RI, and the frequency of the incoming light (*ν*).** When the reflective surfaces are separated by a distance *d*, the phase shift δ experienced by the electromagnetic wave in a complete path relates to the wave vector *k*, as shown in *Eq. 3*, where *k* represents the number of waves per unit distance. This, in turn, is related to the angular frequency ω and the propagation speed in the medium *c*, expressed in *Eq. 4.*

Considering the relationship $k = \frac{2\pi}{\lambda} = \frac{2\pi\nu}{c}$ (where ν is the frequency, λ is the wavelength, and *c* is the speed of light in the medium), the displacement of the electromagnetic wave in a complete path can also be expressed as described in *Eq. 5*.

$$\delta = 2kd \qquad \textit{Eq. 3}$$

$$k = |\,\boldsymbol{k}\,| = \frac{\omega}{c} \qquad \textit{Eq. 4}$$

$$\delta = \frac{4\pi\nu d}{c} \qquad \textit{Eq. 5}$$

δ_m can also be expressed as shown in *Eq. 6* when the transmittance is at its maximum and the values of the incoming light fulfill the condition ($d = \frac{m\lambda}{2}$; *m=0, 1, 2…*). This leads to resonant frequencies within the cavity, and considering that the space within the cavity is not air and thus the RI is not 1, it would be reflected as in *Eq. 7*:

$$\delta_m = \frac{4\pi \nu_m d}{c} = 2m\pi \quad m = 0, 1, 2 \ldots \qquad \textit{Eq. 6}$$

$$\nu_m = \frac{mc}{2d} = \frac{mc_0}{2nd} \rightarrow \lambda_m = \frac{2d}{m}; \quad m = 0, 1, 2 \ldots \qquad \textit{Eq. 7}$$

Considering this, the behavior of this biosensor can be modulated by changing the cavity distance (d) and setting the resonant peaks. However, any biological material within the cavity also alters the response of the FPI, leading to a different RI correlated with the concentration of that material. Therefore, for this thesis, all parameters that could modify the FPI's response were fixed to maximize the signal to **study the response related to the RI change once recognition between the bioreceptor and the analyte of interest occurred on the surface of the FPI**.

2.1.3.6.2 Biophotonic Sensing Cells (BICELLs)

The biosensor utilized in this thesis is based on the development of **BICELLs,** engineered within the Group of Optics, Photonics, and Biophotonics (GOFB) at Universidad Politécnica de Madrid (UPM), under the leadership of Dr. Holgado (Holgado et al., 2010). These BICELLs can be vertically interrogated, avoiding light coupling, and constitute the area that encompasses the photonic structure. Moreover, they can be wafer-level fabricated, facilitating their scalability and reducing manufacturing time and cost (Casquel et al., 2020).

Initially, the BICELLs contained photonic structures based on a multilayer system that, through various fabrication techniques, could form micro and nanopillar resonant structures to enhance sensitivity by combining Fabry-Perot resonator technology with photonic crystals. Additionally, SU-8 resist was introduced onto the SiO_2/Si substrate, conducting various immunoassays such as immobilizing Bovine Serum Albumin (BSA) protein and recognizing it with the anti-BSA (αBSA) Ab, monitoring the entire process (Casquel et al., 2020; Holgado et al., 2010; López-Romero et al., 2010).

Due to the results obtained using SU-8 resist, simpler photonic structures began to be manufactured, yielding **FPI-based structures consisting of multiple-layer thin films**, significantly easing the manufacturing process. These FPI-based BICELLs rely on a resonant cavity, where the wavelength is modulated by the cavity's thickness and material, the nature of the biological material deposited on the surface, and the wavelength and angle of incidence (Figure 5). Thus, the GOFB advancements focused on enhancing and standardizing the manufacturing and biofunctionalization processes of this type of biosensor (Holgado et al., 2016; Santamaría et al., 2017).

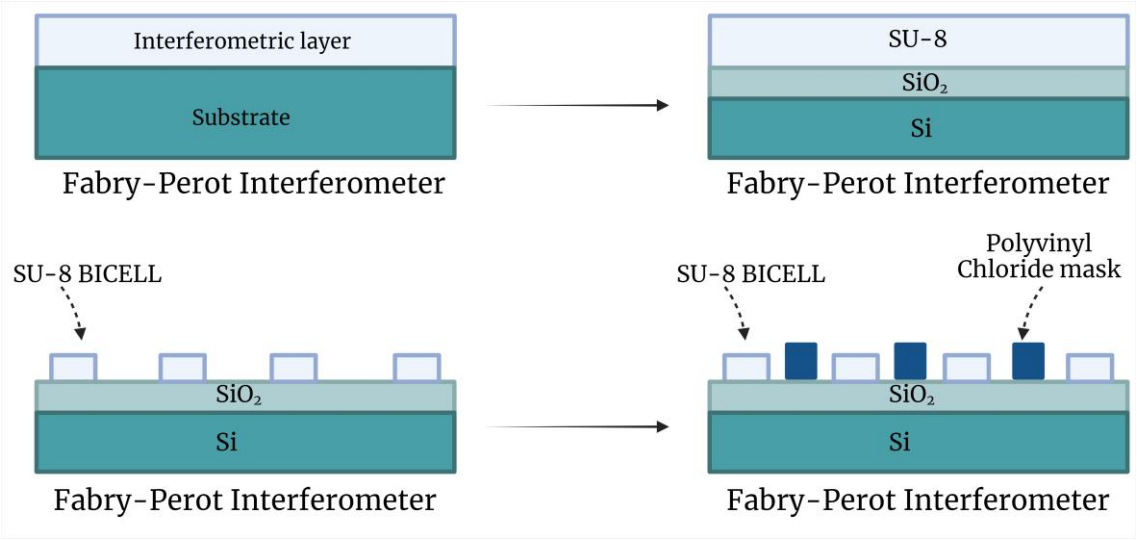

Figure 5. Composition of the BICELLs used during the thesis. Created with BioRender.com.

2.1.3.6.2.1 *BICELLs manufacturing*

To carry out the manufacturing of BICELLs, first, a Si wafer serves as the primary substrate, which has a SiO_2 film on its surface acting as an anti-reflective layer, optimizing the optical signal of the interferometer by increasing the cavity thickness. Additionally, this SiO_2 film aids the measurement device in distinguishing between the areas where the BICELLs are located and the rest of the wafer (Del Campo & Greiner, 2007; J. B. Lee et al., 2015).

Secondly, a negative polymer, SU-8, is deposited using a spinner. This biocompatible and inert resist crosslinks its components after exposure to a specific wavelength (350-400 nm) near Ultraviolet (UV) light. Therefore, negative photolithography masks with the desired geometry are used. This way, the unexposed material remains unpolymerized and can be removed, while the material exposed to UV light undergoes curing. This process involves an initial light exposure to open the epoxy groups followed by a thermal treatment to complete the process (Anhoj et al., 2006; J. Zhang et al., 2001). Subsequently, a piranha solution is used to eliminate any unpolymerized resist, leaving the desired structures imprinted on the wafer (Sanza, 2015). These structures imprinted on the wafer using photolithography techniques can vary in shape and size based on the assay requirements.

Finally, to prepare the **biosensor for use in the laboratory, the wafers are sectioned into pieces with the desired number of structures, referred to as "chips".** Each of these cut sections contains a certain number of necessary sensor surfaces, customized according to the needs, and is mounted onto a glass slide for easy handling and to fit into the measurement platform called **KIT** (Figure 6). For this assembly, a mounting apparatus determines the precise position of the "chip" and secures it to the glass slide using commercial adhesive. After a drying period, they are ready for use.

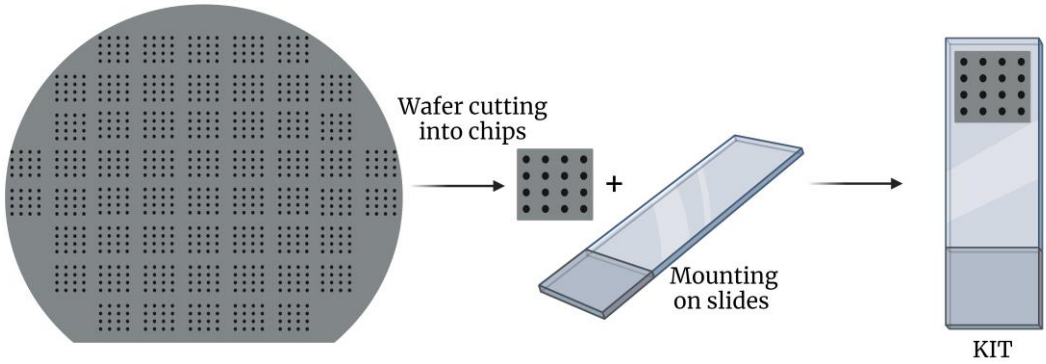

Figure 6. KITs implemented during the thesis. On the right side of the image, the Si wafer is represented, which after cutting it, the "chips" are obtained. On the left of the figure a KIT is illustrated, when the chips are mounted on the slides. Created with BioRender.com.

For this thesis, **two different types of KITs** have been used:

- **16-BICELLs KITs**: These contain 16 sensor cells, each 200 μm in diameter, made of SU-8 using the process described earlier. To confine the sensor cells for conducting assays, a Polyvinyl Chloride (PVC) mask is placed over the chip. This chip configuration with 16 cells allows for rapid tests with an n=4 typically and has been used throughout this thesis to conduct dose-response curves, reagent specificity tests, and to establish protocols (incubation times, concentrations, temperature). Subsequently, this served as a basis for scaling up to chips with a higher number of sensor cells. Additionally, they have demonstrated highly robust data with very low standard deviations among cells and chips, requiring minimal effort and time, thus facilitating working with a larger number of them (Figure 7).

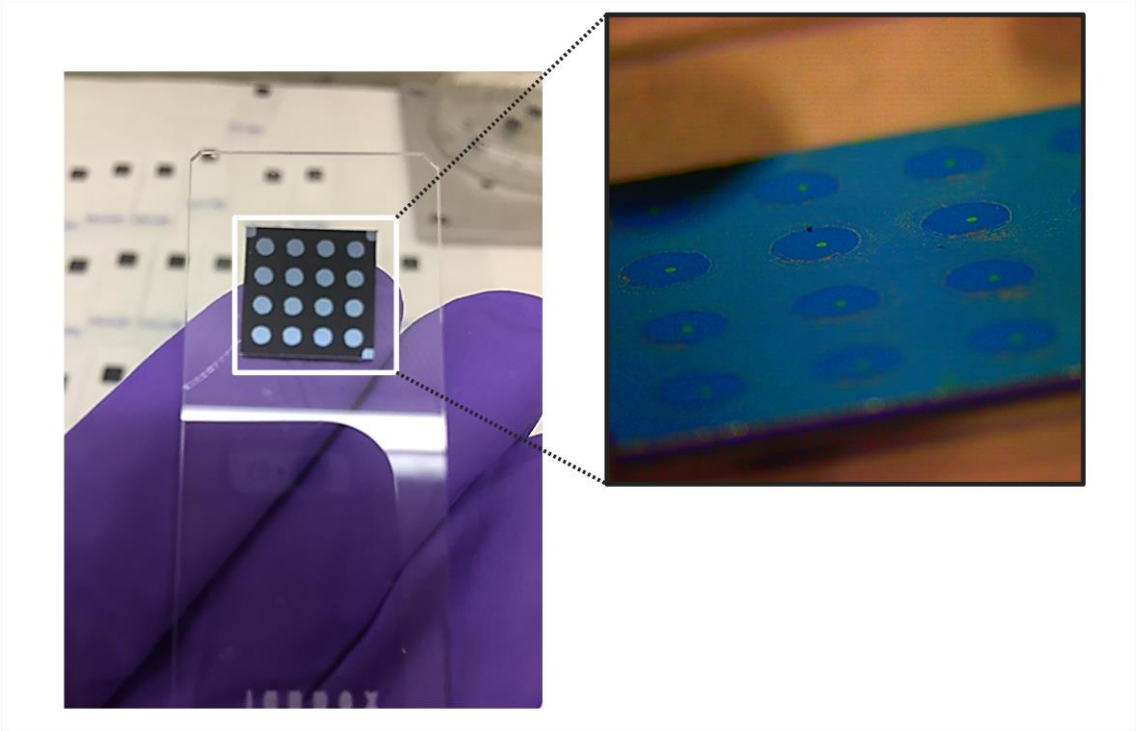

Figure 7. 16-BICELL KITs used during the experiments of this thesis. Created with BioRender.com.

- **65-BICELLs KITs**: These chips have 65 sensor cells, each 200 µm in diameter, made of SU-8 following the procedure described earlier. Similar to the 16 BICELLs chips, it's also necessary to place a PVC mask to conduct incubations during the experiments. These masks need to be changed after each incubation step in both cases. This type of chip allows for **multiplex assays** due to a large number of sensor cells, enabling the measurement of different markers for the same sample or several samples (as in the detection of specific Abs against SARS-CoV-2 in serum), or for instance measuring a marker for a high number of samples (as in the measurement of specific Immunoglobulin A (sIgA) Ab against SARS-CoV-2 in saliva). This facilitates screening a large number of samples in a short time (Figure 8).

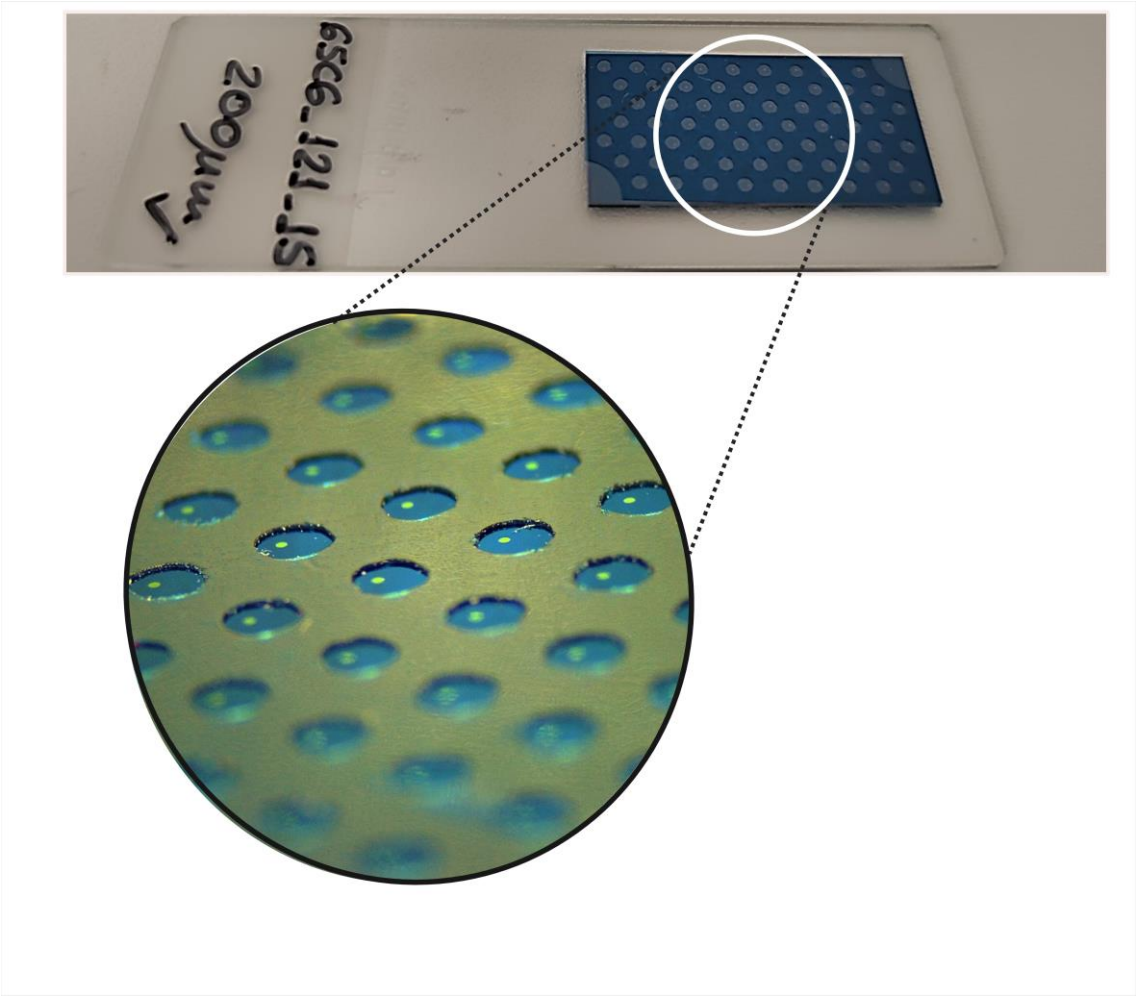

Figure 8. 65-BICELL KITs used throughout the experiments of this thesis. Created with BioRender.com.

2.1.3.6.3 Interferometric Optical Detection Method (IODM)

All the experiments presented in this thesis have been conducted using a reading platform based on the **IODM**, an innovative vertical interrogation method developed by the GOFB. This method is supported and protected by patent number EP2693164A1 (Holgado et al., 2012).

This methodology relies on **data collected from two interferometers, providing two different interferometric signals:** a reference signal (I_{ref}) and a measurement signal (I_{sig}). The interferometer generating the reference signal remains inactive, whereas the measurement interferometer is equipped with anchored bioreceptors and is used for determining the target analyte. As a result, the signal from this interferometer shifts due to recognition, while the reference signal remains unchanged.

Both interferometric signals have a mathematical correlation, resulting in the detection variable obtained through the Transfer Function (f_{trans}) represented in *Eq. 8:*

$$f_{trans} = \frac{I_{sig}}{I_{ref}} \qquad Eq.\ 8$$

This allows measurements to be carried out without the need for complex devices or as high costs as those found in the market. This principle is illustrated in Figure 9.

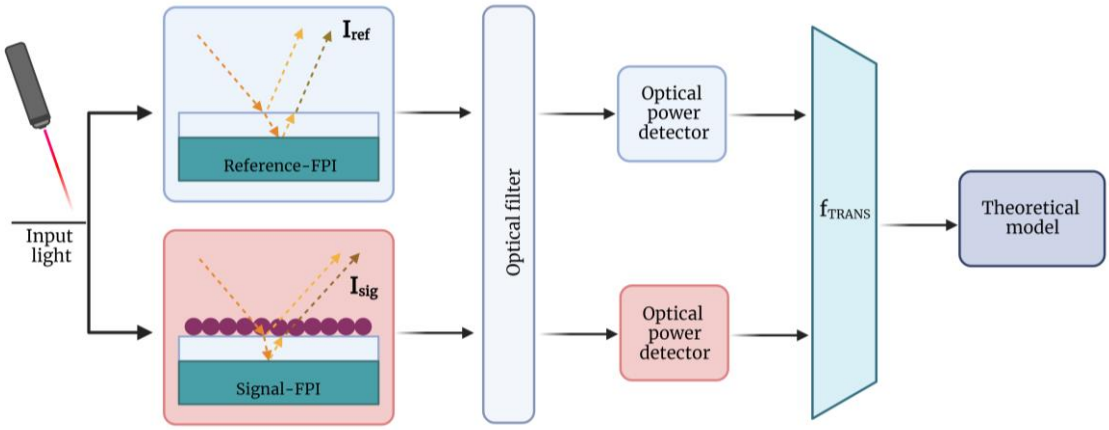

Figure 9. IODM working principle. The input light generates two signals, the I_{ref} and the I_{sig}. Both are detected and thanks to the f_{trans} we obtain the Increased Relative Optical Power (IROP) (%) value. Created with BioRender.com.

The light impacts both interferometers (**reference and measurement**), and the optical power of each of them is collected by the optical power detectors. This f_{trans} can be established considering the optical power (*OP*) for a wavelength in both signals as $f_{trans} = \frac{OP_{sig}}{OP_{ref}}$. Therefore, this *OP* would be calculated as the integral of the signal collected in a specific spectral region between [*λ1, λ2*], known as the optical interrogation band (*Eq. 9*), and is directly related to the thickness of the immobilized material layer on the interferometer.

$$OP[\lambda_1, \lambda_2] = \int_{\lambda 1}^{\lambda 2} I(\lambda) d\lambda \qquad Eq.\ 9$$

This means the **signal being detected corresponds to the area below the reference and measurement signals within that optical interrogation band** (Holgado et al., 2014; Lavín, 2016). This region provides higher sensitivity and a lower LoD along with a broader dynamic range. It occurs where the minimum of the *OP* from the reference interferometer (blue line in Figure 10) aligns with the midpoint of the positive slope of the interference signal from the measurement interferometer (red line in Figure 10).

So, initially, the difference between these signals is maximized. However, it's crucial to note that the I_{sig} will shift to the right as the interferometer undergoes biofunctionalization or recognition stages due to an increase in thickness, while the I_{ref} remains unchanged. Consequently, the measurement signal will gradually move closer to the reference signal (green line in Figure 10). This shift enables the determination of whether an interaction has occurred between the bioreceptor and the analyte of interest.

The sensor's dynamic range is achieved when I_{ref}=I_{sig}. The difference between the I_{ref} and the I_{sig} due to the thickness of the deposited biolayer is described as Increased Relative Optical Power (IROP) (Holgado et al., 2012; Laguna et al., 2014), defined as shown in ***Eq. 10***.

$$IROP(\%) = (f_{trans} - 1) \cdot 100 = \left(\frac{I_{sig}[\lambda_1, \lambda_2] - I_{ref}[\lambda_1, \lambda_2]}{I_{ref}[\lambda_1, \lambda_2]}\right) \cdot 100 \qquad Eq.\ 10$$

Considering this equation, as the thickness of the layer increases, the signal shifts to the right, resulting in a lower IROP (%) level. Thus, the value of IROP (%) for each measurement in the process is expressed in *Eqs. 11* and *12*, and the difference between both (ΔIROP (%)) is represented in *Eq. 13*.

$$\text{IROP}_{thickness\ 0\ (0nm)}(\%) = (f^0_{trans} - 1) \cdot 100 = \left(\frac{I^0_{sig}}{I_{ref}} - 1\right) \cdot 100 \qquad Eq.\ 11$$

$$\text{IROP}_{thickness\ 1\ (X\ nm)}(\%) = (f^1_{trans} - 1) \cdot 100 = \left(\frac{I^1_{sig}}{I_{ref}} - 1\right) \cdot 100 \qquad Eq.\ 12$$

$$\begin{aligned} \Delta IROP(\%) &= \text{IROP}_{th\ 1\ (X\ nm)}(\%) - \text{IROP}_{th\ 0\ (0nm)}(\%) \\ &= \left(\frac{I^1_{sig} - I^0_{sig}}{I_{ref}}\right) \cdot 100 \end{aligned} \qquad Eq.\ 13$$

So, following *Eq. 13*, with $\text{IROP}_{th\ 0\ (0nm)}(\%)$ as the measure corresponding to the initial value of the signal and $\text{IROP}_{th\ 1\ (X\ nm)}(\%)$ as the signal obtained at each step of the assay, the resulting value of ΔIROP (%)—defined as the increase in the signal between two measurements—allows us to monitor each step of the experiment and confirm the bio-recognition. Additionally, **this measure also enables us to determine the concentration of the analyte of interest.**

This technology, coupled with transducer design, maximizes the biosensor's sensitivity for *in-vitro* diagnostics by detecting minimal variations in thickness and thus very low concentrations. Moreover, this reading system enables integration into a Point-of-Care (PoC) device, facilitating swift, cost-effective, and user-friendly diagnostics.

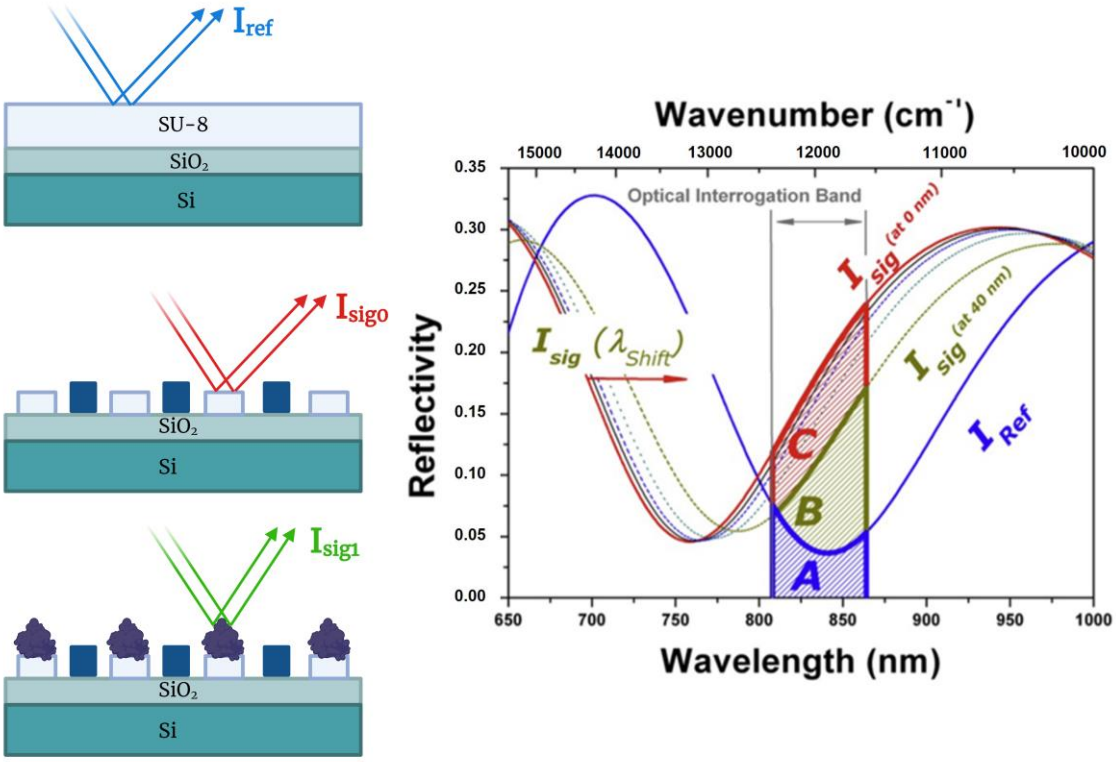

Figure 10. Principle of operation of the IODM. The red line in the image corresponds to the first measurement of the sensing surface. The green line represents the signal obtained once a bioreceptor has been immobilized on the surface. Finally, the blue line belongs to the reference KIT which is not modified during the whole experiment. The area represented by "A" is proportional to the OP of I_{ref}. The area represented by "C" is proportional to the OP of I_{sig0} when the surface has not been coated. Finally, the area represented by "B" is proportional to the OP of I_{sig1} when a molecule is anchored to the surface. Thus, as the thickness on the surface increases, the I_{sig} pattern is closer to I_{ref}, with the IROP signal becoming lower Created with BioRender.com. Figure adapted from (Holgado et al., 2016).

2.1.3.6.4 Reading platform

To carry out measurements of the transducers using vertical interrogation, **the IODM was incorporated into a PoC device.** This reading platform was designed for conducting measurements and was developed by the company Bio Optical Detection S.L. (BIOD S. L.). The technology of this device evolved during the course of this thesis, alongside the evolution of the biosensors. The optimization of the PoC device was a collaborative effort between GOFB and BIOD.

Two different devices were utilized during the thesis development, both based on the IODM methodology, explained below. **The second platform employed represents an enhanced, faster, and more precise version**.

2.1.3.6.4.1 *PoC*

The first PoC device is based on the IODM methodology and was used briefly at the beginning of this thesis. This device comprises two measurement channels: one for the biosensor used in the assay I_{sig} and another for I_{ref}. Both channels are integrated within the same optical head design, but only the measurement channel has access to the experiment's biosensor.

The light sources are based on semiconductor laser diodes emitting light at a wavelength of approximately 851 nm. Additionally, the housing is designed to ensure optical isolation.

Regarding its mechanical components, the device includes a support KIT constructed from a metal piece aimed at maintaining stability and preventing undesired movements during measurements. It features a motorized XY axis that positions the support, providing stability for the measurement, and includes anti-vibration mounts. All these mechanical elements are designed to prevent potential instabilities in the measurement and ensure accuracy. Lastly, the device is operated through a user interface that issues commands during experiments. In this case, the platform was capable of measuring the 65-BICELLs KITs in approximately two hours (Figure 11).

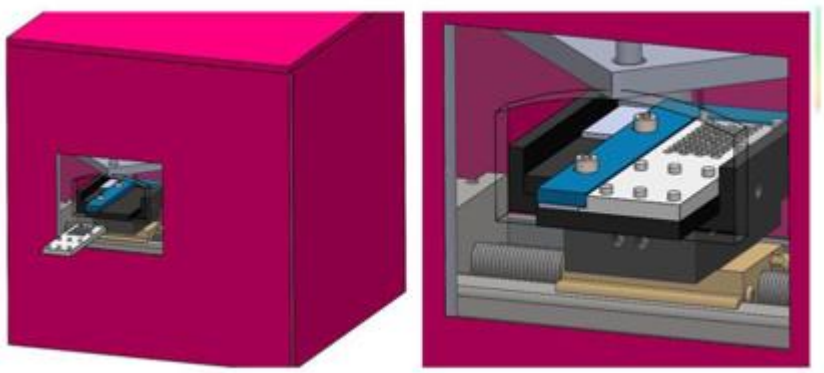

Figure 11. PoC device. On the left is the representation of the device and on the right is the detail of where the KIT is positioned for the measurement reading.

2.1.3.6.4.2 *MOX*

The latest platform version named MOX has successfully addressed most of the limitations and issues detected in the PoC. It's practically a new platform that has **improved reliability, usability, measurement robustness, and exterior design**. Figure 12 shows an image of the MOX device.

Among the most significant enhancements implemented in this measurement platform is **the speed**. Modifications were made in mechanics, optics, and electronics to reduce measurement times for KITs. The most significant change was observed in the 65-BICELLs KIT, **reducing measurement time from two hours to twelve minutes.** The software was also upgraded, achieving a user-friendly yet powerful interface. This new version includes XY axes capable of operating at nearly thirty times the previous speed. The KIT supports were optimized by introducing tabs that expanded the glass slide tolerance, solving many issues encountered with the previous platform. This adjustment ensured perfect positioning and alignment of all KITs, irrespective of glass slide size, to prevent measurement discrepancies. Laser integration with temperature stabilization was incorporated to avoid environmental climate interferences.

Finally, one of the most significant novelties of this device is the inclusion of a reference chip inside, enabling correlation and validation of the device's status just before each measurement, without causing any delay in the measurement time.

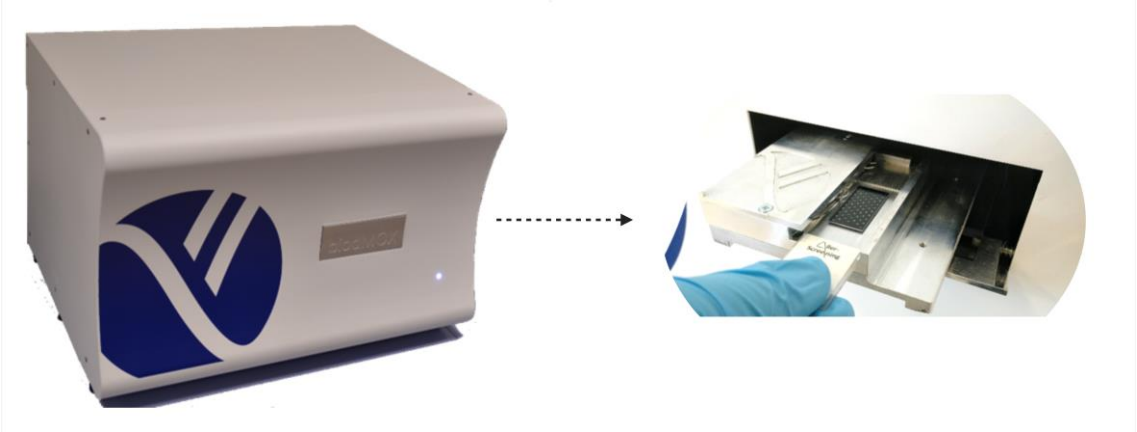

Figure 12. MOX device. The left side of the figure shows the image of the device and the right side illustrates how the KIT is placed in the holder of the device for subsequent reading.

2.1.3.6.5 Signal amplification method based on NPs

So far, *in-vitro* detection systems with high sensitivity available in the market for detecting analytes or target molecules rely on systems with chemical amplifiers or some form of detection (usually enzymatic), such as the Enzyme-Linked ImmunoSorbent Assay (ELISA). This is because there is a growing demand for systems that offer high sensitivity and deliver reliable and fast results when working with real samples.

This becomes challenging since, in certain pathologies or diagnoses, the analyte of interest is found in very low concentrations alongside numerous other elements in the sample that may interfere with the measurement.

These issues had to be considered during the completion of this thesis because the technique employed relies on changes in the RI. When dealing with **low concentrations of the target molecule** or molecules of low molecular weight, this **change in the RI becomes significantly smaller**, affecting sensitivity and the LoD. Therefore, to enhance sensitivity and specificity in such situations and achieve a LoD competitive enough with other techniques, a system is needed to address the limitations of these interference-based optical biosensors.

To overcome these limitations, a method was proposed in patent no. ES 2750374 B2, based on the use of **Nps to amplify the signal due to changes in the RI** and the potential scattering produced by these NPs, which depends on their nature and size (Holgado et al., 2020). This method allows for **qualitative and/or quantitative** detection of the target analyte in real samples **with highly complex matrices**.

To perform this method, several stages are involved, illustrated in Figure 13 and summarized as follows:

- **Stage 1: Reference signal measurement**

-First of all, it is necessary to **measure the biosensor's reference signal** once its surface is coated with the specific bioreceptor against the target analyte or with the molecule itself (Figure 13A).

- **Stage 2: Preparation of the conjugate**

-The next step involves **incubating the NPs at the desired concentration with the target analyte present in the sample**. To achieve this, the NPs must have previously undergone biofunctionalization with the specific bioreceptor, resulting in the NP-bioreceptor complex, allowing them to bind to the analyte. This incubation process should occur between 2 and 37°C. Upon completion, the **NP-bioreceptor-analyte conjugates will be obtained** (Figure 13B3b).

- **Stage 3: Conjugate separation**

-Once the analyte has been recognized by the NP-bioreceptor, these complexes need to be separated from the other components of the sample as they will be used for incubation on the biosensor. In this case, we will obtain both **NP-bioreceptor conjugates and NP-bioreceptor-analyte complexes,** depending on the concentration of the molecule being determined. The method for separating these conjugates depends on the nature of the NPs; it could involve the use of a magnet for magnetic particles or centrifugation for other types of NPs.

- **Stage 4: Recognition on the biosensor surface**

-The previously separated conjugates will be brought into contact with the biosensor surface that had been immobilized earlier with the specific bioreceptor or the target molecule (depending on the type of assay performed). At this stage of the process, the **NP-bioreceptor and NP-bioreceptor-analyte conjugates will interact with the biomolecules immobilized on the transducer** (Figure 13C).

- **Stage 5: Signal reading**

-Finally, the **signal will be read on the device**. This interference signal will be affected once the NPs conjugates have attached to the surface, thereby altering the interference pattern due to changes in the IR linked to the phenomenon of light dispersion (Figure 13C2).

Optically, this signal change, involving intensity and/or interference pattern variation, occurs because the NP conjugates, once they have recognized and adhered to the biosensor's surface, alter the optical thickness, causing a variation in the real part of the RI. Additionally, the complex part of the RI is also altered, leading to a variation in optical intensity due to the dispersion phenomenon.

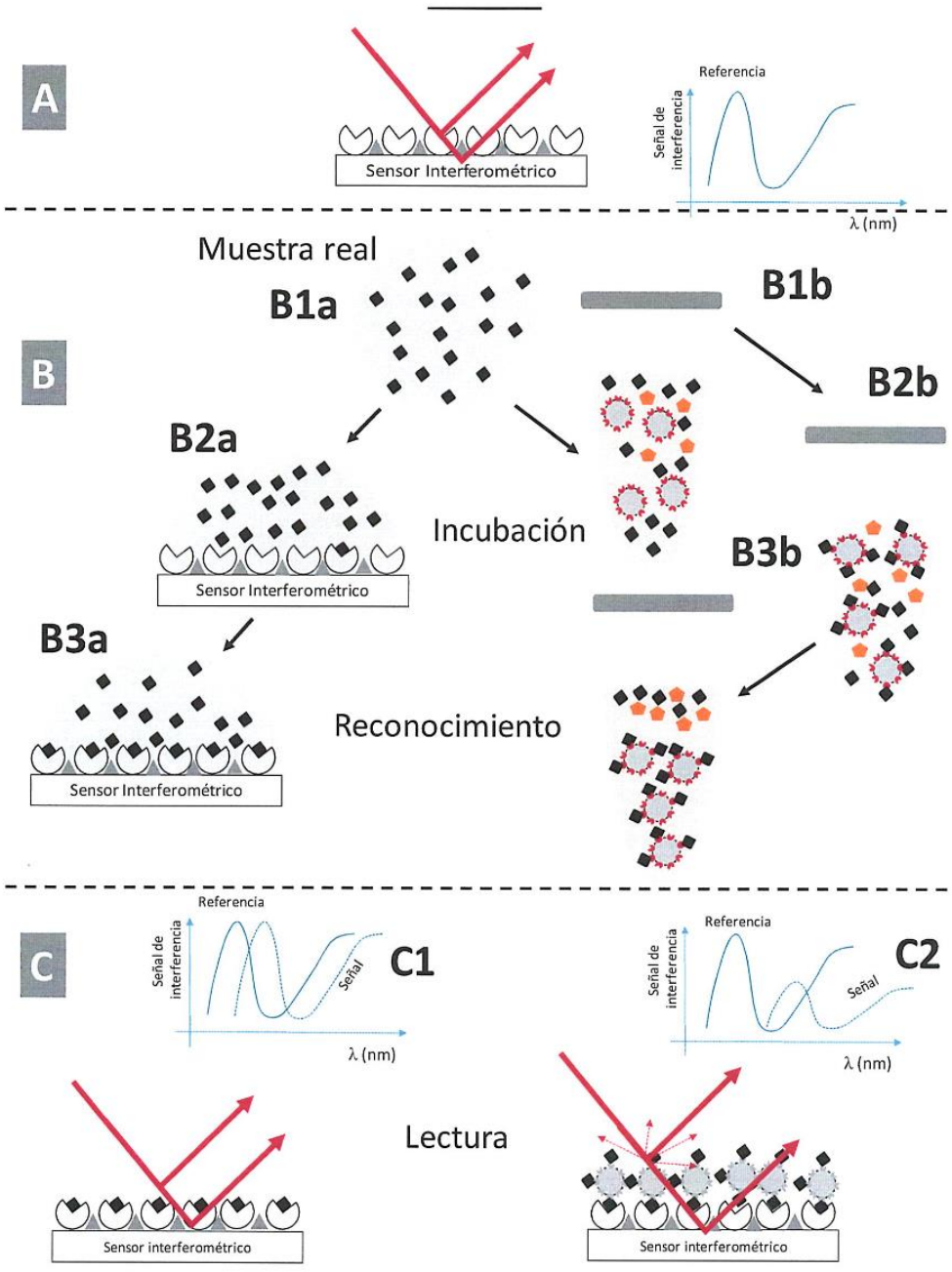

Figure 13. Signal amplification method based on NPs. A. Readout of the signal once the recognition biomolecule has been immobilized on the sensing surface. **B.** On the right shows the assay without the use of NPs. On the left is an example of the incubation of the NPs with the sample for the formation of the NP-bioreceptor-analyte conjugates. **C.** On the right, we obtain the signal that would be obtained with the assay without NPs. On the left depicts the amplification of the signal in the IODM due to the NPs (Holgado et al., 2020).

2.1.3.6.5.1 *NPs biofunctionalization techniques*

Over the last few years, the importance of nanomaterials has been increasing due to their significant role in science and technology, along with the new advancements in nanotechnology. When working with nanomaterials, it's crucial to consider different factors such as size, shape, charge, RI, and the surrounding medium, among others, as these can influence their physical and chemical characteristics (Avvakumova et al., 2014; Conde et al., 2014).

Within these nanomaterials, for example, **are NPs, which can have different sizes (ranging from 1 to 100 nm**). Thanks to the advances in NPs synthesis, a considerable interest has emerged in various fields of biomedicine and engineering. Moreover, currently, NPs of very diverse materials can be synthesized, each with varying properties, such as gold (Au), silver, magnetic, or Si NPs (Subbiah et al., 2010).

Among these, **Si NPs are of great interest due to being easily synthesizable, possessing high stability and dispersibility in water, biocompatibility, and simple surface modification capabilities** (Q. Zhang et al., 2009). Their synthesis was developed by Werner Stober (Jung et al., 2012), and since then, research based on these NPs has been on the rise. With this type of NPs, precise control over size and porosity is achievable depending on the application (Liberman et al., 2014). Additionally, the silanol groups found on the surface (Si-OH) can be modified to obtain different functional groups (Jung et al., 2012).

The techniques based on NPs are becoming increasingly important due to their multiple biomedical applications, such as detection systems, high-throughput screening, in the field of biosensors, and for *in-vivo* and *in-vitro* diagnosis in tissues and cells (Bagwe et al., 2006). However, achieving these applications requires highly optimized NPs design involving various factors in their synthesis, such as size, surface charge, and shape (Avvakumova et al., 2014).

Another process that requires significant optimization is the surface modification of NPs. **This process, where functional groups are added to the NPs's surface, is known as biofunctionalization** (Subbiah et al., 2010). The primary objective of this process is to cover the NPs's surface with the desired molecule depending on the application, altering the surface properties of the NPs (Subbiah et al., 2010). The strategy for achieving biofunctionalization depends on the NPs's surface chemistry, size, the functional groups to be added, as well as the molecules to be anchored to the NP, making these crucial points to consider (Conde et al., 2014).

These NPs are highly efficient due to their high surface to volume ratio, which allows a large number of molecules to be attached to their surface through biofunctionalization processes (Avvakumova et al., 2014). One of the benefits of this process is the ability to modify them, thereby adapting them to various applications (Subbiah et al., 2010).

The main molecules employed for the biofunctionalization of NPs are peptides, enzymes, oligonucleotides, lipids, aptamers, and Abs (Avvakumova et al., 2014). Once these biomolecules have bound, it's crucial that the NPs continue to function despite any changes in their physicochemical properties (Subbiah et al., 2010). One of the major challenges in these processes is ensuring that the **NPs remain stable in solution without aggregating,** as they often

precipitate during the process due to the loss of balance between attractive and repulsive forces (Conde et al., 2014).

Within the techniques of NPs biofunctionalization, there are different methods that can be classified depending on the steps taken to obtain the final functional group (direct functionalization and post-functionalization) or based on the type of bonding (non-covalent or covalent) (Avvakumova et al., 2014; Conde et al., 2014; Subbiah et al., 2010)(Figure 14).

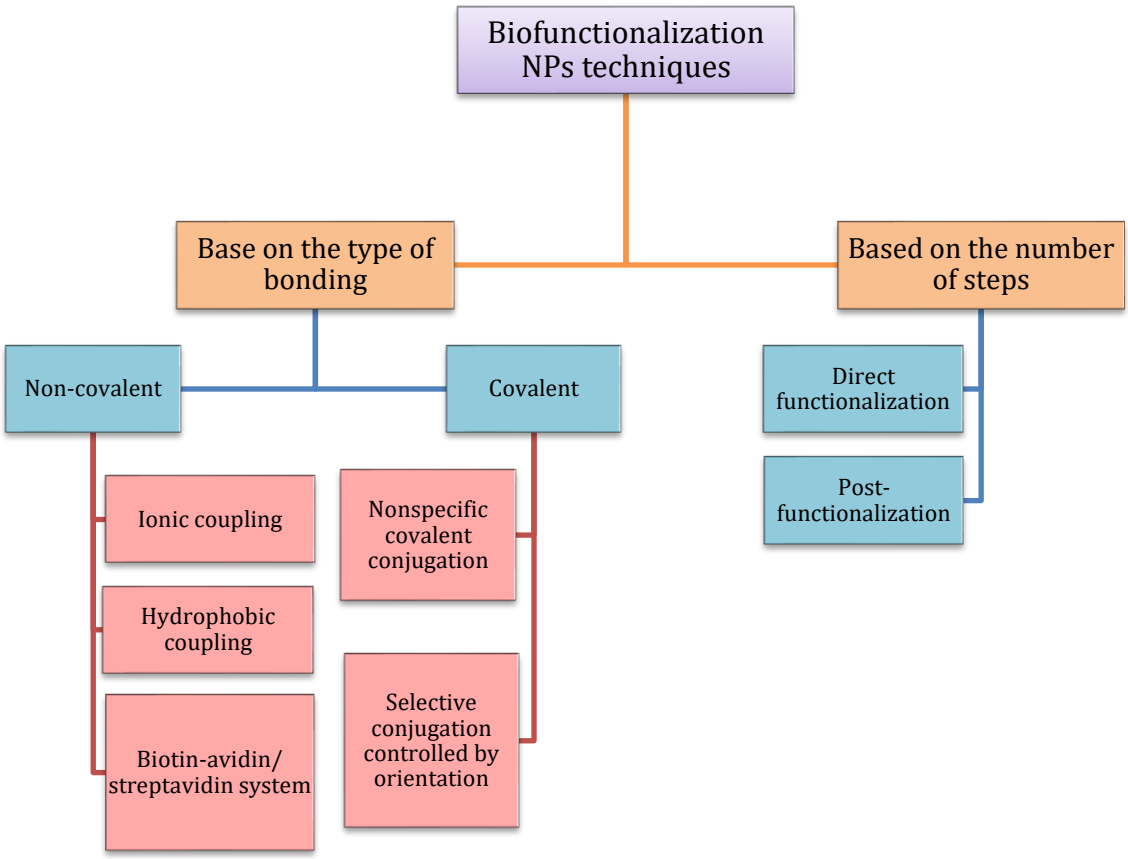

Figure 14. Classification of NPs biofunctionalization techniques.

- Based on the number of steps:
  - **Direct functionalization**: in this case, a single organic compound is used that is bifunctional, where one of the reactive groups in this compound binds to the NP, while the other group modifies the surface. **Only one conjugation step is employed in this case**. Special attention must be paid to ensure that the modifying group does not interact with the NPs's surface. Thiol or phosphine oxide groups are used in these cases (Subbiah et al., 2010)(Figure 15A).
  - **Post-functionalization**: In this process, similarly, there's an initial step of adding a bifunctional organic compound, but subsequently, **another compound is added to introduce the desired functional group** onto the NPs's surface. An example widely used in such cases is silanization (Subbiah et al., 2010)(Figure 15B).

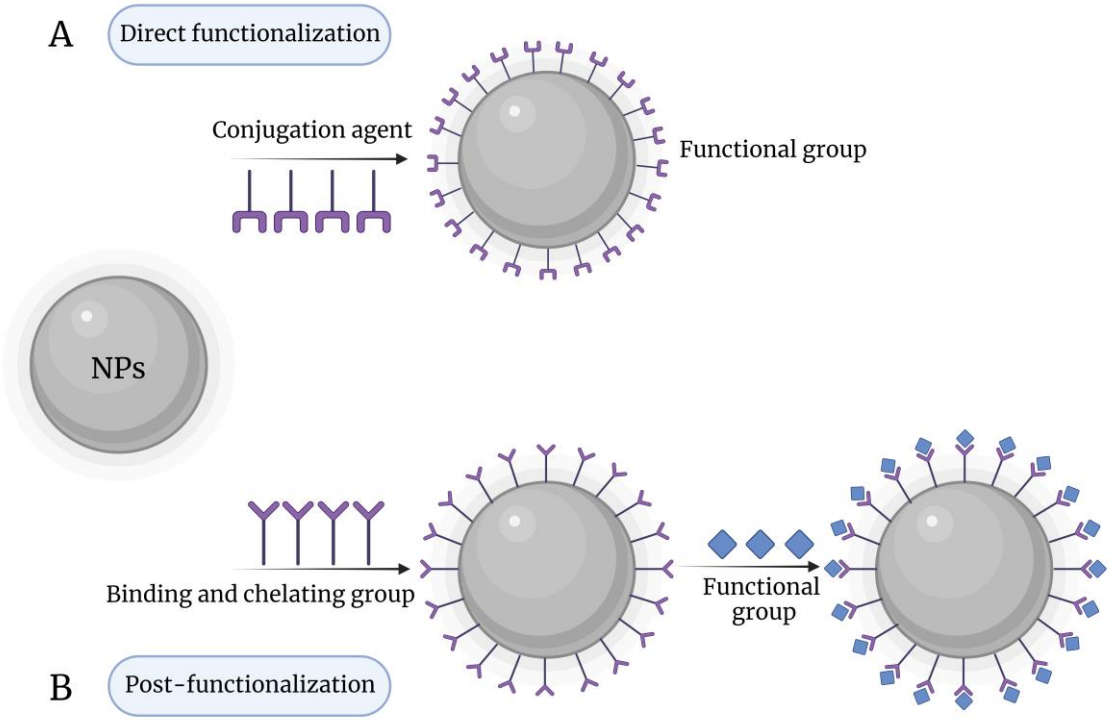

Figure 15. Biofunctionalization techniques based on the number of steps. A. Direct functionalization in which the conjugating agent provides the functional group for the following steps. **B.** In the case of post-functionalization, there is a first step in which a chelating group is added for a second step to add the functional group. Created with BioRender.com.

- Based on the type of bonding:
  - **Non-covalent**: these rely on electrostatic, hydrophobic, and affinity interactions. Biofunctionalization protocols in these cases are much simpler, but the bond is less stable and reproducible.
    - **Ionic coupling**: This can be achieved when the agent intended to be coupled to the NPs has an opposite charge to it. When attaching complex molecules like Abs, it's essential to consider the isoelectric point to control their net charge. In this scenario, the agent's attachment might lose its biological activity after conjugation because its protein structure could be affected (Conde et al., 2014)(Figure 16A).
    - **Hydrophobic coupling**: Hydrophobic molecules like fluorophores can be directly attached to NPs. However, similar to the previous method, there's a concern because hydrophobic forces also play a role in stabilizing protein structures. Additionally, these forces are more likely to destabilize proteins (Avvakumova et al., 2014)(Figure 16B).

- **Biotin-avidin/streptavidin system**: In this case, NPs are biofunctionalized with the protein avidin or Streptavidin (STV), while the molecule intended to be attached to the NPs is biotinylated. This is feasible because biotin can be synthesized with various functional groups, enabling its attachment to the molecule of interest (Conde et al., 2014)(Figure 16C).

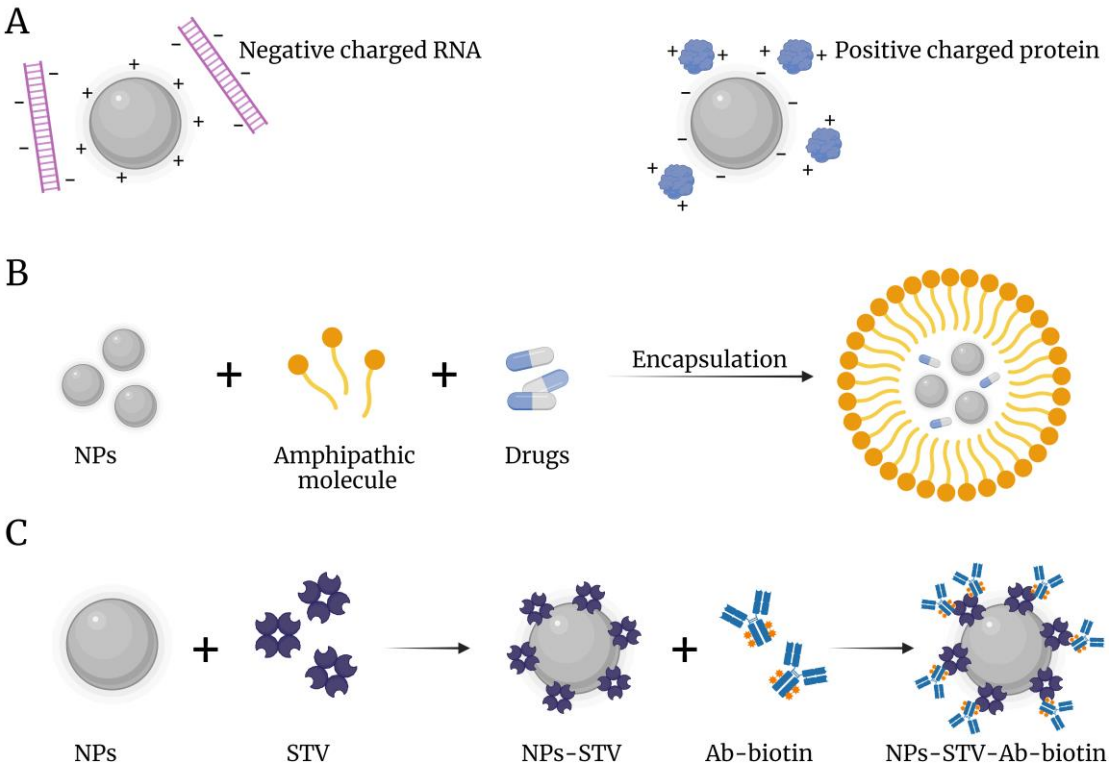

Figure 16. Non-covalent biofunctionalization techniques. A. Ionic coupling due to the charge difference between the surface of the NPs and the molecule to be anchored. **B.** Hydrophobic coupling in which the drugs are trapped in the vesicles formed around the NPs. **C.** Biotin-avidin/STV system relies on STV binding on the surface to couple biotinylated Abs on the surface. Created with BioRender.com.

- **Covalent**: The covalent bonding of molecules relies on a **stable and strong union** of the functional groups of the NPs and the molecule intended to be coupled, without causing denaturation of the protein. Within this strategy, there is nonspecific covalent conjugation and selective covalent bonding controlled by orientation (Avvakumova et al., 2014).

  - **Nonspecific covalent conjugation**: This method is used for various types of NPs like Au and Si, primarily based on carbodiimide chemistry, enabling the condensation of amino and carboxyl groups (Avvakumova et al., 2014). The most commonly used coupling reaction involves the use of Ethyl(dimethylaminopropyl) carbodiimide (EDC). **EDC is a zero-length cross-linker used to activate carboxyl groups for conjugation to primary amines**. Once EDC reacts with the carboxyl group, it forms an intermediate called an amino-reactive O-acylisourea.

This intermediate can directly react with primary amines to form a stable amide bond. Due to the instability of the intermediate, N-Hydroxysuccinimide (NHS) or sulfo-NHS is typically added to produce a stable ester-NHS that interacts with primary amines. One of its main advantages is water solubility, eliminating the need for organic solvents. Parameters to consider when using this strategy include controlling the **reaction pH**, as it significantly influences the unstable intermediate's hydrolysis, the **amount of EDC used** (as excessive EDC can cause NP aggregation by neutralizing electrostatic repulsion forces), and finally, **the EDC/NHS ratio** (Conde et al., 2014)(Figure 17A).

- **Selective conjugation controlled by orientation**: This biofunctionalization aims to achieve a controlled orientation of the biomolecule. Within these systems, there's **thiol chemistry**, **click chemistry reactions**, those mediated by **enzymes**, and those based on the production of **recombinant proteins** that integrate specific binding sites into their sequence (Avvakumova et al., 2014)(Figure 17B).

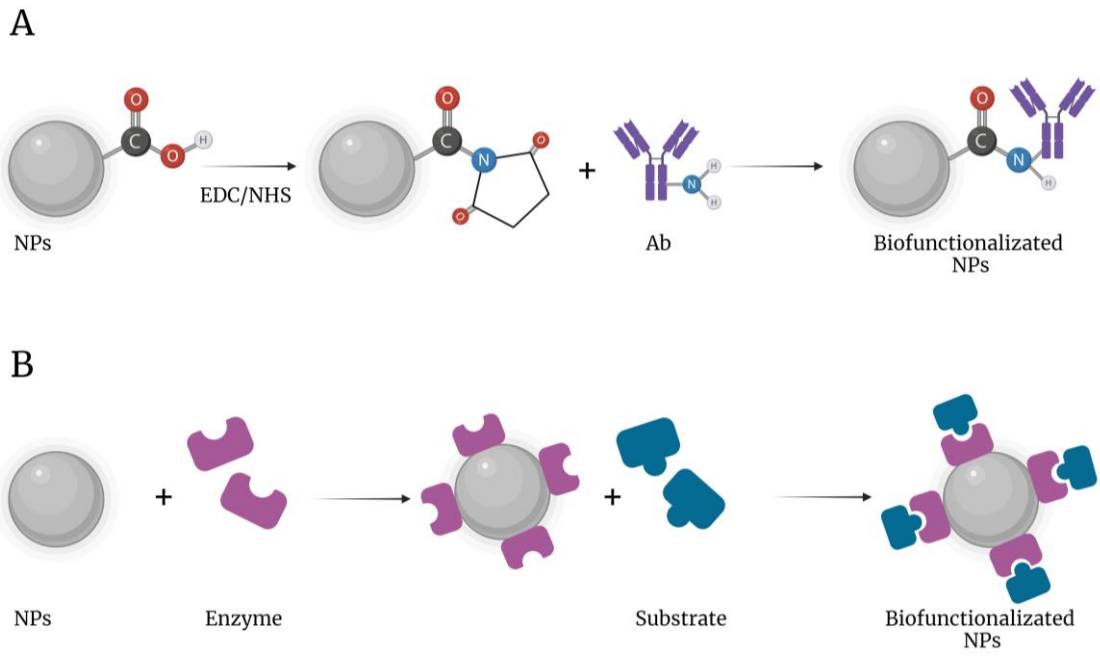

Figure 17. Covalent biofunctionalization techniques. A. Coupling by EDC/NHS chemical reaction. **B.** Example of a site-directed coupling due to the use of an enzyme that is substrate specific. Created with BioRender.com.

During this thesis work, various NPs biofunctionalization protocols have been explored. Among them, we utilized silanization combined with EDC/NHS chemistry and the biotin-STV system.

2.1.3.6.5.2 *NPs characterization techniques*

During the NPs biofunctionalization process, it's crucial to maintain control at every step. This ensures the proper implementation of biofunctionalization. Parameters typically studied include **shape and size**, **distribution of various sizes**, **surface charge**, **degree of aggregation**, and even **surface chemistry** (Mourdikoudis et al., 2018).

To characterize, various techniques can be employed, including those based on X-rays, Fourier-Transform Infrared Spectroscopy (FTIR), mass spectrometry, different microscopy techniques like Scanning Electron Microscopy (SEM) or Transmission Electron Microscopy (TEM), Atomic Force Microscopy (AFM), Nanoparticle Tracking Analysis (NTA), and Dynamic Light Scattering (DLS) (Butler et al., 1992; Mourdikoudis et al., 2018).

Depending on the specific physical property being measured, different techniques are employed, and sometimes multiple techniques can serve the same purpose. For instance, **to measure NP size, techniques such as DLS, NTA, and SEM can be used**, among others. Additionally, DLS can also be employed to obtain the surface charge of NPs (E. J. Cho et al., 2013; Modena et al., 2019).

In the following subsections, we will explain in more detail the two techniques that have been used for the characterization of the NP biofunctionalization process, through which the size, distribution, Zeta Potential (ζ-potential), concentration, and degree of aggregation have been measured.

2.1.3.6.5.2.1 DLS

It is a widely used technique **to measure the size of NPs** when they are in suspension. This technique is based on the Brownian motion of particles in solution when dispersed, determining the coefficient of free diffusion of the particles in suspension. Thus, DLS measures the dispersion of light over time, also combining the Stokes-Einstein equation (*Eq. 14*) to deduce the Hydrodynamic Diameter (D_h) of NPs (E. J. Cho et al., 2013; Modena et al., 2019).

$$D_h = \frac{K_b T}{3\pi\eta D_t} \qquad Eq.\ 14$$

In this equation, D_t represents the diffusion coefficient, K_b is the Boltzmann constant, T refers to the temperature at which the analysis is conducted, η indicates the solvent's viscosity, and $\boldsymbol{D_h}$ **is the Hydrodynamic Diameter of the particle** (Modena et al., 2019). D_h refers to the diameter of the NPs along with the surrounding solvent that diffuses at the same speed (Mourdikoudis et al., 2018)(Figure 18).

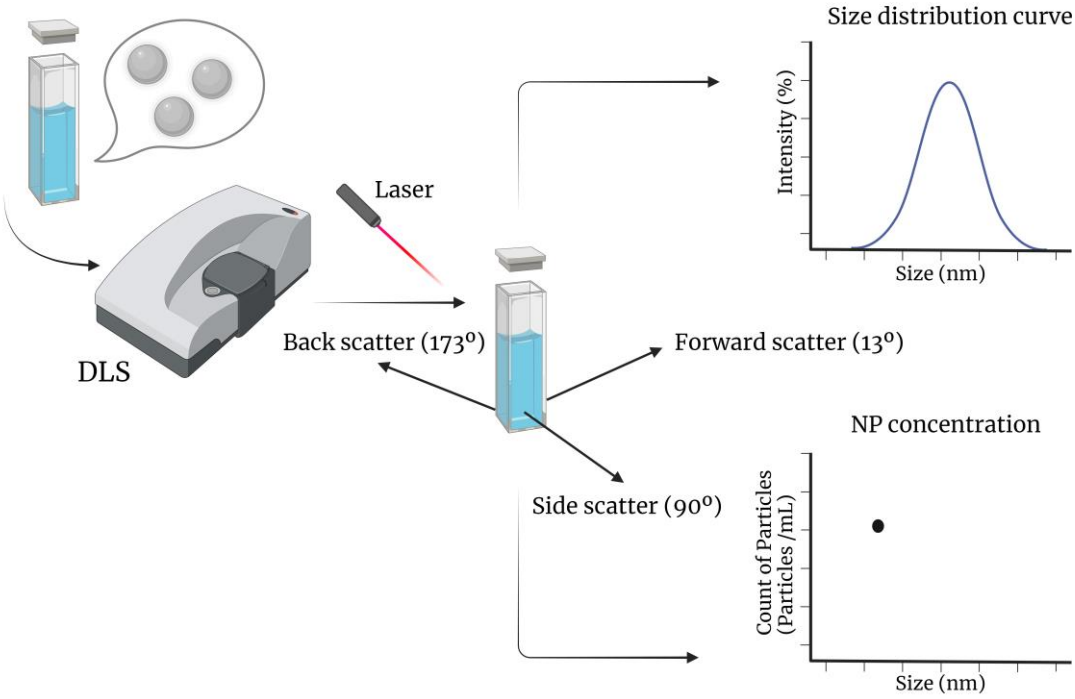

Figure 18. DLS technique. Schematic representation of DLS operation and data obtained (size and concentration). Created with BioRender.com.

The result obtained provides the average particle size and the uniformity of the size distribution. The uniformity is indicated by the Polydispersity Index (PDI). If this value falls between 0.1 and 0.25, it indicates a narrow size distribution, whereas if it's above 0.5, the distribution is broader (E. J. Cho et al., 2013). This data also informs us about potential NPs aggregation and how dispersed they are in the solution.

It's essential to consider that, during measurements, the NPs concentration cannot be too high; otherwise, an undesirable multiple scattering effect could occur. Factors such as this, solution stability, and NPs surface modifications influence the obtained value (Mourdikoudis et al., 2018). Another crucial factor is the solution's pH; if it's far from the NPs's isoelectric point, electrostatic repulsion forces dominate. However, if the pH is near the isoelectric point, repulsive forces decrease, leading to an increase in the hydrodynamic size (E. J. Cho et al., 2013).

Another value obtainable through this technique is the ζ-potential. It's defined as the difference in electrical potential between the stationary layer of charges surrounding the particle and the potential of the solution they are in (Modena et al., 2019). The surface charge of particles is an important factor as it affects their behavior, especially in terms of aggregation, where electrostatic repulsion between particles plays a key role in stability. This occurs because mobile charges in the solution are attracted to the static charges on the particle surface, potentially leading to their aggregation (Modena et al., 2019).

Several parameters affect the ζ-potential, such as the ionic strength of the solvent and the solution's pH. **NPs might aggregate if they are at a pH where their surface charge is zero** (Modena et al., 2019). To prevent this, it's important to ensure the pH is away from the isoelectric point (Mourdikoudis et al., 2018).

In general, particles with a ζ-potential more positive than +30mV or more negative than -30mV maintain stability due to electrostatic repulsions (E. J. Cho et al., 2013; Mourdikoudis et al., 2018).

Finally, **another crucial piece of information attainable through the DLS technique is the concentration of NPs.** The principle behind this measurement involves transforming the particle size distribution into the intensity of the absolute concentration distribution using the derivative of the scattered count rate and the optical properties of the dispersant and material. The measurement involves separately recording scattering data in three angular positions: backscatter, side scatter, and forward scatter (Austin et al., 2020).

Due to the low sample quantity required for these determinations, the short measurement time, the diversity of solvents usable for measurement, and the wide range of sizes it can determine, DLS proves to be a highly useful technique for routine and rapid analysis.

2.1.3.6.5.2.2 SEM

SEM **provides surface images** by directing an electron beam onto the sample and detecting the emitted secondary electrons (Mourdikoudis et al., 2018)(Figure 19).

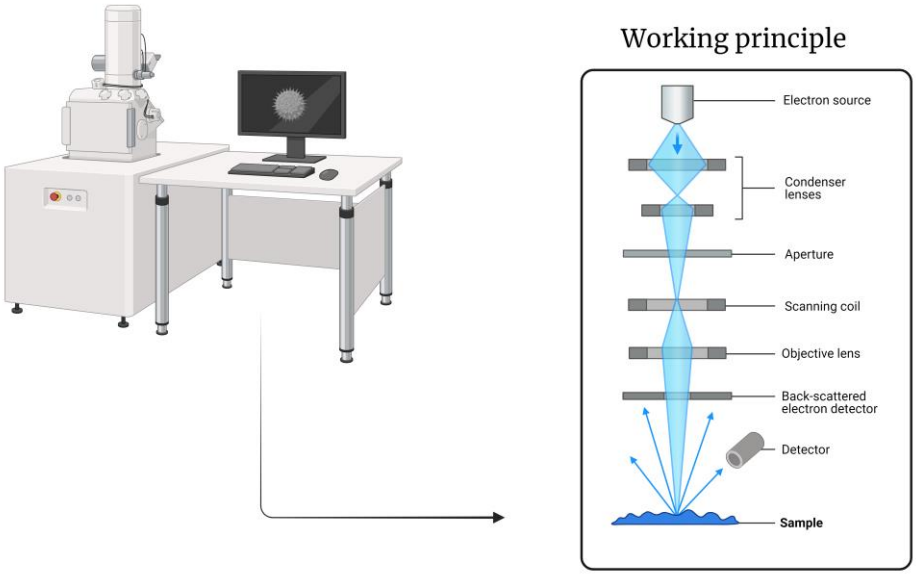

Figure 19. SEM technique. Schematic diagram of the internal workings of the SEM. Created with BioRender.com.

Due to the moderate energy used, its resolution is limited to a minimum of 2-3 nm, significantly reducing the risk of sample damage. To capture high-resolution images, a conductive substrate is required. For non-conductive samples, a metalization process can be used, adding a thin metallic layer. It's important to note that this process alters the NPs size and structure (Modena et al., 2019).

SEM images also offer information on NPs size and dispersion. However, it's crucial to note that the size measured by SEM and, for instance, DLS varies because each measurement occurs in different environments (dry and in solution). Sizes measured in SEM tend to be smaller due to the loss of the hydration layer (E. J. Cho et al., 2013).

2.1.3.6.5.3 *Methodology advantages*

Once the patented methodology used in this thesis has been explained, the advantages of using NPs alongside the described and employed optical biosensor will be specified below.

Firstly, **this method is independent of the molecular weight of the analyte to be determined**. As previously mentioned, this type of biosensor, relying on changes in the RI for detection, faces greater difficulty in detecting molecules with low molecular weights as they cause very slight variations in the RI once on the biosensor surface. However, by using NPs, this problem is resolved, allowing the quantification of these low molecular weight molecules.

Secondly, **it allows the detection and quantification of these target analytes in real samples** with highly complex matrices without requiring any prior treatment. Using NPs, unspecific bindings to the sensor surface can be greatly reduced or eliminated, as the NP-bioreceptor-analyte conjugates have been separated from the sample and all other interfering components have been removed. This step also streamlines the assay protocols, potentially eliminating blocking steps and reducing washing times.

Moreover, **NPs are a crucial tool for modifying the dynamic range of the biosensor**. Depending on the size, material, and concentration of the NPs, lower LoD can be achieved due to increased sensitivity, enabling the detection of a wider range of concentrations of the target analyte. Thus, these NPs parameters can be adjusted to custom assays to specific requirements.

Lastly, the system's versatility stands out in its use with different biological samples (serum, tears, saliva, etc.), for water quality studies, or in the food industry. Furthermore, this versatility extends to its application in various types of different optical biosensors based on interference, aside from the one described in this thesis.

2.1.3.6.5.4 *Application of the method in disease diagnosis*

This thesis focuses on the **development of an *in-vitro* diagnostic system for various pathologies**. One of these, and the case study here, is **AD**, which falls within **NDD**, specifically tauopathies (Rawat et al., 2022). In this context, **the protein of interest to be determined is tau protein**, although, throughout this thesis, assessments of other implicated markers such as **lactoferrin** were conducted.

The specificities of detecting tau protein, such as low concentration and the need for measurement in complex matrices, demand a highly sensitive and specific detection system, making the use of NPs almost obligatory.

Tau protein is primarily found in the brain, functioning as it should, but its levels start to rise as the disease progresses. Currently, determining tau protein concentration is done using CSF samples, which involve an invasive and costly extraction system, making patient monitoring and diagnosis challenging (Anoop et al., 2010). Thus, **this thesis proposes an alternative: assessing tau protein levels in serum samples.** However, serum samples have significantly lower concentrations compared to CSF, making the use of NPs essential to achieve much lower LoD necessary for this diagnostic purpose.

Additionally, employing NPs and achieving such low LoD offers a significant opportunity to screen relatives of individuals with AD, detecting this condition before symptoms arise, as these molecular changes begin years before symptoms manifest (Raskin et al., 2015).

Moreover, while transitioning to serum samples, the complexity of the matrix remains, so using NPs in serum aids in eliminating the matrix effect by separating the conjugates from the sample, thereby reducing nonspecific bindings on the sensor surface. However, during the incubation of NPs with samples, some issues arose due to the corona effect described previously in the literature (Monopoli et al., 2011; Tenzer et al., 2013; Vidaurre-Agut et al., 2019).

This system was also employed to **determine tau protein in serum samples from a Syrian hamster tauopathy model** (*Mesocricetus auratus*) and **P301S transgenic mice, which express human tau**. Here, the use of NPs was crucial due to the very low amount of serum obtained from these animals.

Finally, during this thesis, NPs were used to assess lactoferrin concentrations in saliva samples, where their use similarly aided in minimizing the matrix effect characteristic of such samples.

This demonstrates the **application and versatility of NPs** in measuring different markers across various sample types, establishing suitable protocols and optimal conditions for each application.

2.2. Introduction to the Immune System

Immunology is an experimental branch of health and life sciences that studies the mechanisms by which higher organisms molecularly **recognize what is self from what is foreign,** developing tolerance to avoid attacking their tissues (Chaplin, 2006).

Specifically, the immune system refers to the mechanisms (discriminatory of self from non-self) that higher organisms possess for **defense against pathogens**. It consists of a set of cells and molecules responsible for immunity (capable of generating a response).

This **immune response is a comprehensive and coordinated reaction** in the event of an attack by foreign agents. However, not only external pathogens like viruses, bacteria, or parasites trigger an immune response, but also various agents such as cancer cells, toxins, pollen, etc., can elicit this response (Varella, 2001).

Apart from immunology itself, there are other involved sciences, such as applied immunology, which deals with studying issues related to autoimmunity, hypersensitivity, immunodeficiencies, etc. On the other hand, there's molecular and cellular biology, which focuses on studying immune system cells, implicated genes, signaling pathways, etc.

2.2.1. General introduction

Throughout history, immunology has been closely linked to microbiology as it focused on studying prevention against microorganisms. Not all pathogens elicit the same response; it depends on their structure, size, method, and route of infection (Nicholson, 2016).

The immune system protects against **four types of pathogens** (Table 2):

- **Extracellular bacteria, parasites, and fungi**.
- **Intracellular bacteria**.
- **Viruses**.
- **Parasitic nematodes (extracellular).**

Table 2. Types of pathogens that trigger an immune response (Nicholson, 2016).

Pathogen type	Pathogen example	Diseases
Extracellular bacteria, parasites, and fungi	*Streptococcus pneumoniae* *Clostridium tetani* *Trypanosoma brucei*	Pneumonia Tetanus Sleeping sickness
Intracellular bacteria	*Mycobacterium leprae* *Leishmania donovani* *Plasmodium falciparum*	Leprosy Leishmaniasis Malaria
Viruses	Smallpox Influenza Chickenpox	Smallpox Influenza Chickenpox
Parasitic nematodes (extracellular)	Ascaris Schistosoma	Ascariasis Schistosomiasis

The size of the pathogen is very relevant because it will allow it to enter in one way or another, and depending on this invasion method, it will enable it to evade the immune system's response in a better or worse way.

Pathogens can be intracellular or extracellular. In the case of extracellular ones, they are more easily combated by the immune system as they are more accessible.

Similarly, the immune system protects us against any type of normal or pathological cells, for example:

- **Aging cells**: due to their deterioration, they express markers that identify them as target cells for destruction (P. Song et al., 2020).
- **Neoplastic (tumor) cells**: they express tumor markers on their surface that are not expressed in normal cells and are therefore recognized as foreign (Varella, 2001).
- **Allogeneic cells**: they express markers that are not native to the individual and therefore are also recognized as foreign cells (Michniacki et al., 2022).

To initiate a response, immune system cells do not recognize the entire pathogen as such, but they identify **specific foreign molecules**. **These alien substances that trigger specific immune responses recognized by immune system cells and their components are termed Antigens (Ags)**. Therefore, the term Ag could be defined as any substance that induces Ab production because the immune system recognizes it as a risk (Delves & Roitt, 2000).

All immune system cells possess specific receptors capable of recognizing different types of Ags such as sugars, lipids, proteins, nucleic acids, etc., or they can recognize conserved molecular patterns present in pathogenic microorganisms called Pathogen-Associated Molecular Patterns (PAMPs) (McComb et al., 2019).

The immune system's objectives focus on two main aspects: first, **discriminating between self and non-self,** and second, **generating tolerance or a response**. Maintaining a balance in the immune system is crucial since there are foreign Ags that are harmless and shouldn't trigger a response, just as self-Ags should be tolerated. Meanwhile, harmful foreign Ags should always provoke a response (Varella, 2001).

2.2.2. Immune system cells

The formation of all blood cells, including those belonging to the immune system, occurs during the embryonic phase through the process of **hematopoiesis**. This process takes place in the blood islands of the yolk sac initially, and this function later transitions to the liver and spleen after birth, finally occurring in the bone marrow during adulthood. For an efficient immune response, immune cells are specialized in very specific functions, distributed throughout the body via the blood and lymphatic system (Sugiyama & Nagasawa, 2012).

From the pluripotent hematopoietic stem cell, two lineages emerge: **myeloid** (Figure 20) **and lymphoid** (Figure 21).

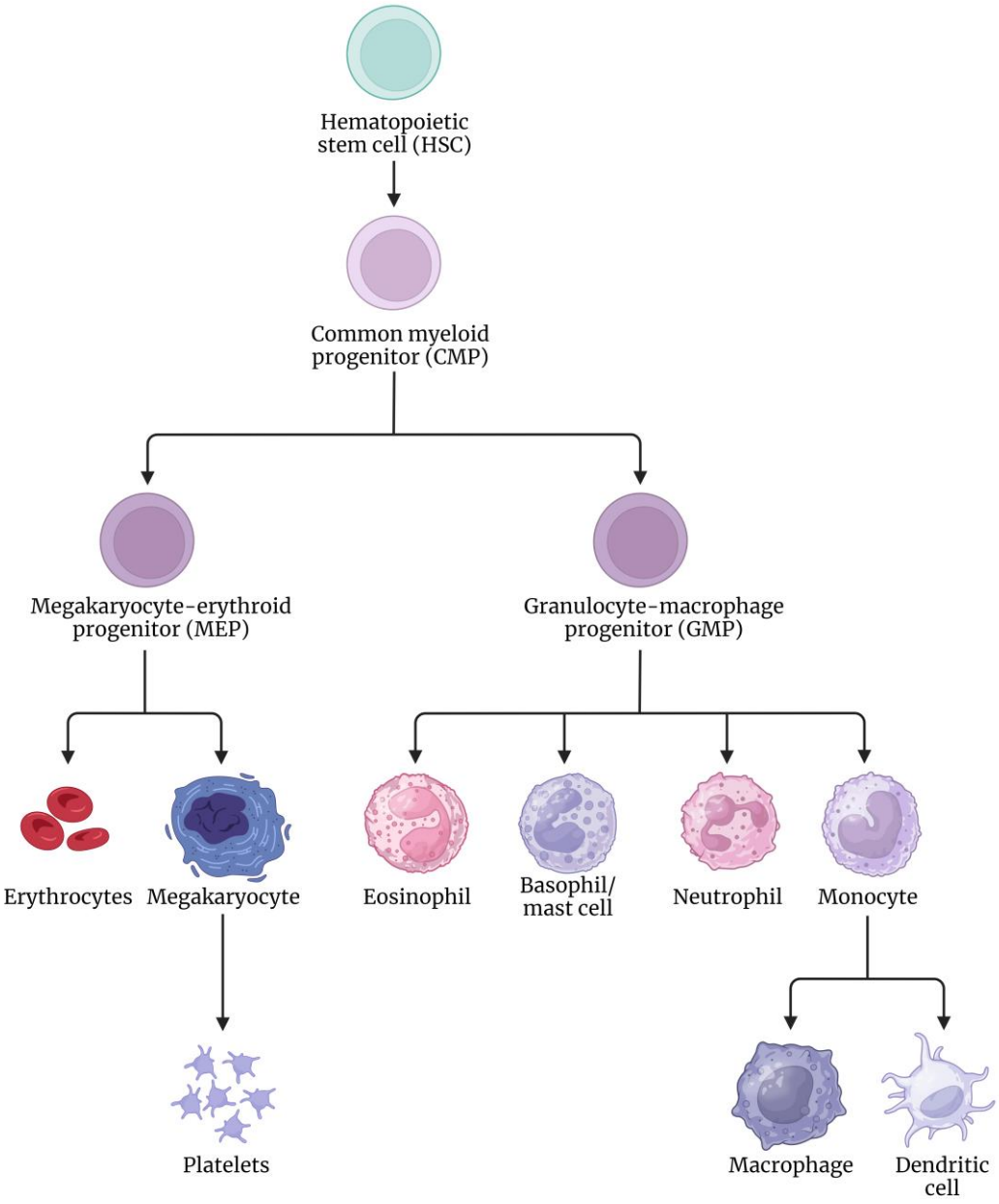

Figure 20. Differentiation of hematopoietic stem cells: myeloid lineage. Created with BioRender.com.

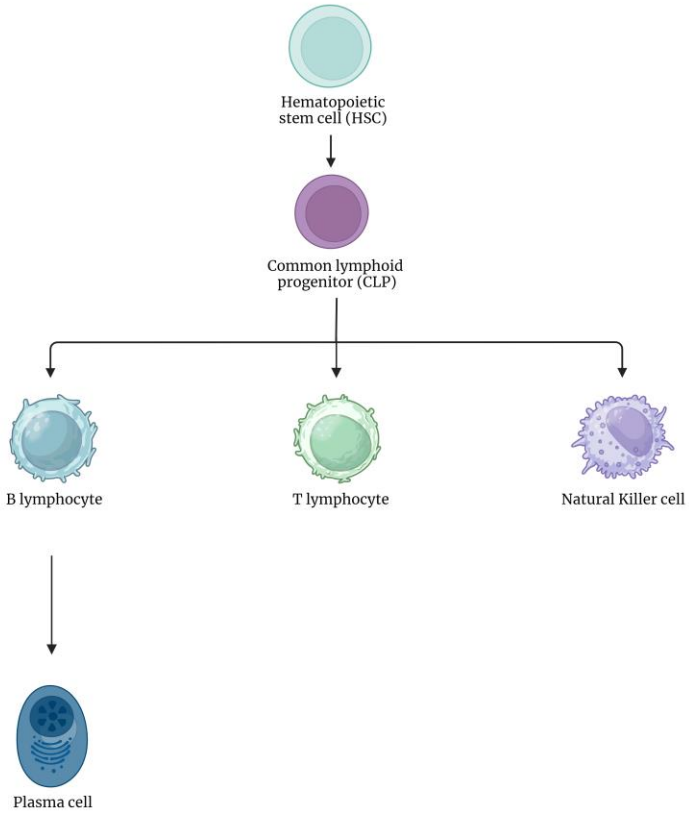

Figure 21. Differentiation of hematopoietic stem cells: lymphoid lineage. Created with BioRender.com.

Initially, cells were classified by size; later, classification was based on morphology and size, but primarily on surface markers. The expression of these membrane molecules varies depending on the cell type, differentiation stage, and activation state. Understanding the differentiation stage through the differential expression of membrane molecules is crucial for diagnosing pathologies. These surface markers are called Cluster of Differentiation (CD) followed by a number (Cruse et al., 2004).

2.2.2.1. *Myeloid lineage*

From the pluripotent hematopoietic stem cell arises the Common Myeloid Progenitor (CMP), from which all cells of this lineage derive. Within this lineage, we can find **mononuclear phagocytes, polymorphonuclear phagocytes, mast cells, erythrocytes, and megakaryocytes** (Doulatov et al., 2012).

2.2.2.1.1 Mononuclear phagocytes

These originate from monocytes found in the blood and differentiate into macrophages and myeloid Dendritic Cells (DCs) like Langerhans cells when they enter tissues. They **play a significant role in both innate and adaptive immunity**, carrying out functions such as **Ag presentation, immunomodulation, and phagocytosis** (Dale et al., 2008; Guilliams et al., 2018).

- **Macrophages**: Their main functions include removing dead cells, Ag presentation, phagocytosis, and participation in the inflammatory process. They play a key role in homeostasis. These cells invade areas of infection and phagocytose bacteria, dead cells, and foreign agents. Macrophages are present in different tissues depending on their markers, and they have different names in each tissue (Figure 22). They regulate both the adaptive and innate immune responses by recruiting various cell types (Epelman et al., 2014).

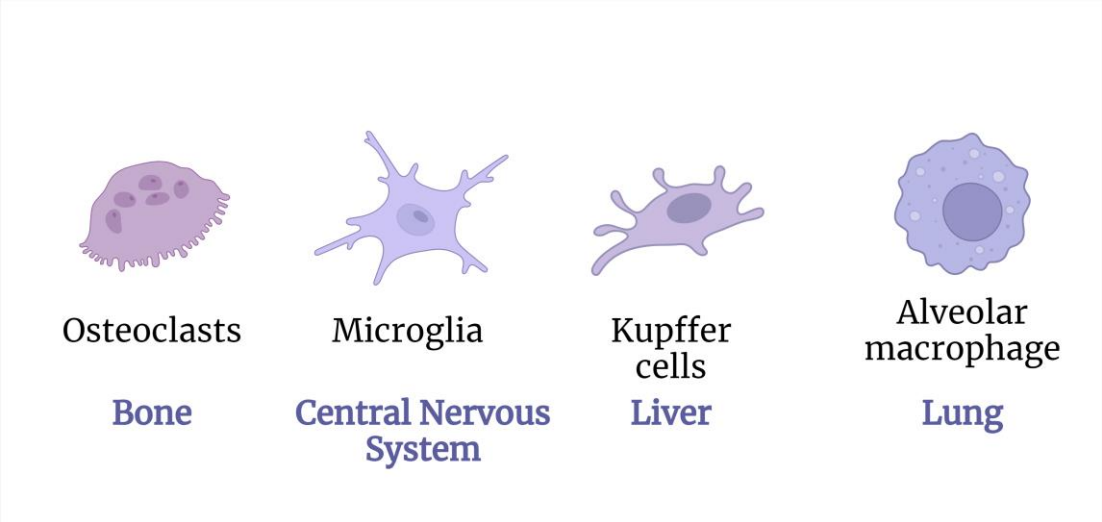

Figure 22. Macrophage types depend on the tissue in which they carry out their function. Created with BioRender.com.

Considering different pathogens, the generated microenvironment, or cellular damage, macrophages can differentiate into two distinct subpopulations. These subpopulations are called M1 and M2 (Figure 23).

- **M1 macrophages** are activated by Interferon-gamma (IFNγ) and participate in responses mediated by Th1 lymphocytes (proinflammatory). They produce proinflammatory molecules such as Interleukin-6 (IL-6). They play a crucial role in responses against viruses, intracellular bacteria, or tumors (Barros et al., 2013; K. Y. Lee, 2019).
- **M2 macrophages** are important in tissue repair processes and also function in chronic infections (regulatory functions). They are stimulated by Interleukin-4 (IL-4) and participate in responses mediated by Th2 lymphocytes (Barros et al., 2013; K. Y. Lee, 2019).

Given that these cells are involved in both types of responses and are responsible for homeostasis, in addition to their high plasticity, they open the possibility of therapies based on macrophages (Gordon & Martinez-Pomares, 2017).

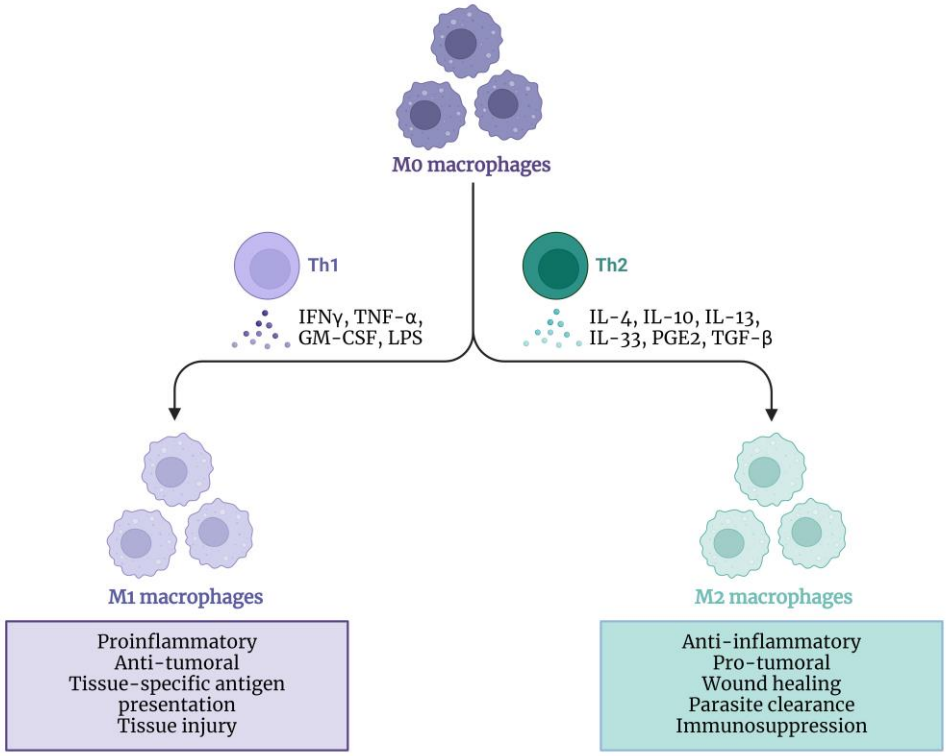

Figure 23. Macrophage polarization in M1 and M2. Created with BioRender.com.

- **DCs**: These cells are also responsible for phagocytosis and are professional Antigen-presenting Cells (APCs). They capture Ags in tissues and present them to lymphocytes in lymph nodes. They act as mediator cells in immunity and tolerance (K. Liu & Nussenzweig, 2010). DCs also have different names depending on the tissue they are in and are a highly heterogeneous group, including monocyte-derived DCs, plasmacytoid DCs, and conventional DCs (Bošnjak et al., 2022).

2.2.2.1.2 Polymorphonuclear phagocytes

Those are cell types that **contain enzymatic granules released during infectious processes, asthma, and allergic reactions**. Within this group, you can find neutrophils, basophils, and eosinophils.

- **Neutrophils**: this cell type remains in the blood for a short time as they constitute the first line of defense in the innate immune system and are the first to arrive at the site of infection. Their production is stimulated in bacterial infections, and they are responsible for destroying and phagocytizing them. They also undergo extravasation in inflammatory situations and have roles in modulating the adaptive immune response (Burn et al., 2021; Dale et al., 2008).

- **Basophils**: These cells have a more controversial immune function. They contain cytolytic enzymes to destroy pathogens during phagocytosis. They are a minority cell type and participate in allergic processes, inflammation, and defense against parasites (Ito et al., 2011; Nakashima et al., 2018).
- **Eosinophils**: They are involved in inflammation, phagocytosis, and elimination of parasites, being the first effector against these. They contain cytolytic enzymes that they secrete upon contact with the pathogen. They are also involved in tissue damage and allergic reactions. Recently, other functions within innate immunity have been investigated, linking both innate and adaptive responses for tissue remodeling (Germic et al., 2019; Shamri et al., 2011).

2.2.2.1.3 Mast cells

Mastocytes are cells that participate in both innate and adaptive immune responses and are involved in **allergic reactions and defense against parasites**. They play a key role in responses that involve Immunoglobulin E (IgE). They have the ability to quickly respond by releasing granules from their interior (histamine and heparin) when facing an infection (Kalesnikoff & Galli, 2008; McComb et al., 2019).

2.2.2.1.4 Erythrocyte

Erythrocytes are anucleated cells found in the blood with a lifespan of around 120 days. Their primary function is gas exchange; however, they have been associated with immune system functions as they are targeted by various infections. These cells can **produce cytokines or signaling molecules**. Furthermore, hemoglobin serves as a source of bioactive peptides involved in innate immune responses due to their bactericidal effects (El Bishlawy, 1999; Morera & Mackenzie, 2011).

2.2.2.1.5 Megakaryocytes

Megakaryocytes are large, multinucleated cells responsible for producing platelets, which form by shedding their cytoplasm. Due to the abundance of immunological receptors and inflammatory molecules, **they can contribute to both types of immunity (innate and adaptive)**, although megakaryocytes are not typically considered immune cells (Cunin & Nigrovic, 2019).

During adaptive immunity, platelets secrete substances that enhance the action of DCs in Ag presentation. Additionally, they promote the recruitment of lymphocytes to the site of infection and interact with them and with neutrophils (Marcoux et al., 2021). On the other hand, in terms of innate immunity, they participate in complement activation and pathogen recognition through their membrane receptors (Koupenova et al., 2022).

Moreover, megakaryocytes possess molecules necessary for Ag presentation, suggesting they may have that function. They promote the activation of Th1 and Th17 lymphocytes and regulate pluripotent stem cells to remain in quiescence or proliferation (Marcoux et al., 2021).

2.2.2.2. *Lymphoid lineage*

Lymphocytes are the primary cells of adaptive immunity. Unlike cells involved in the innate immune system, lymphocytes express Ag receptors on their surface distributed in a clonal manner and with high specificity (Anaya et al., 2013).

Once cloned, a lymphocyte will only produce one type of specificity (clonal distribution). They possess memory because, during an infection, different lymphocytes and clones are generated. The most active ones are selected against a second infection, resulting in a faster and more effective response. They are the only cells in the body capable of recognizing different antigenic determinants. Originating in the bone marrow, they differentiate based on their membrane markers, the cytokines they secrete, and the function they perform (Varella, 2001).

Among their functions are:

- They assist in **phagocytosis** and defend the body **against infections**, adding specificity to the defense.
- They have the ability to **produce Abs** against foreign agents and the capacity to generate memory against them.
- They are involved in the process of **opsonization**.

There are two different types of lymphocytes: **B cells and T cells**. Additionally, within this lymphoid lineage and sharing the same common lymphoid progenitor, we also have Natural Killer (NK) cells (Doulatov et al., 2012).

2.2.2.2.1 B cells

B cells are produced and mature in the bone marrow. During their differentiation process, they undergo gene recombination at the genes encoding for the light and heavy chains, resulting in the vast diversity of Abs with different specificities in each clone. **They can recognize more than 5 x 10^{13} different Ags** (Anaya et al., 2013).

On their membrane, they possess the B Cell Receptor (BCR) to non-covalently recognize Ags, leading to their activation, and triggering various pathways. Upon activation, they transform into plasma cells specialized in Ab production. These cells have eccentric nuclei and secrete large amounts of Abs but do not express Igs on the membrane, unlike B cells. They undergo minimal divisions and are found in the bone marrow and lymphoid tissues (Kurosaki et al., 2015; Varella, 2001).

Mature B cells can be classified into different types based on the markers they express, the pathways they activate, Ag specificity, and their location (Anaya et al., 2013). Primarily, we have **effector B cells or plasma cells** that, after an initial immune response, some of them transition into **memory B cells**. These memory B cells persist long-term and participate in quicker and more potent secondary immune responses (Knox et al., 2019). These two types of responses (primary and secondary) generate two distinct groups of plasma cells that migrate to the bone marrow, where they can persist without the need for self-renewal (Manz et al., 2002) (Figure 24).

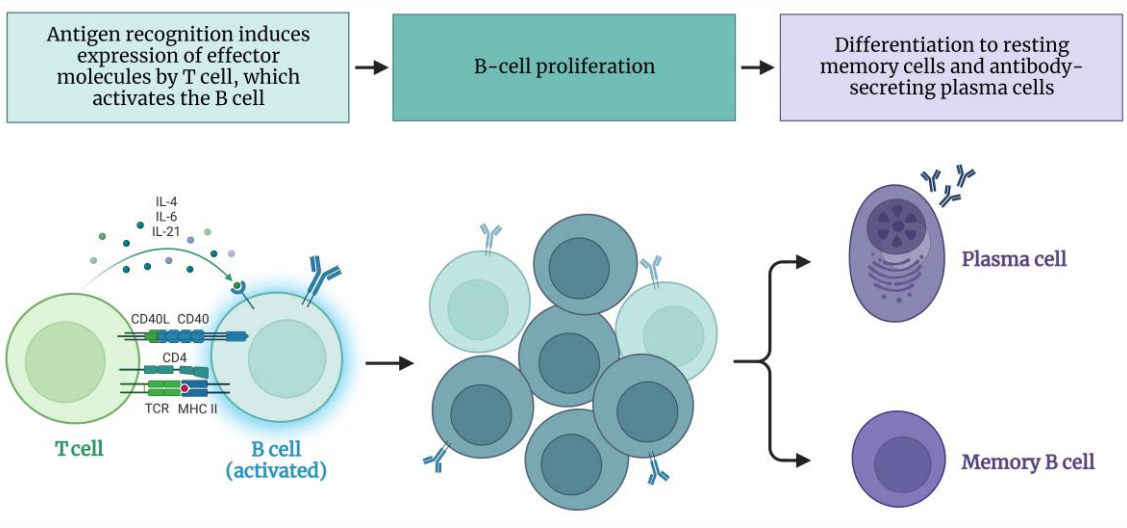

Figure 24. B cell differentiation steps. Created with BioRender.com.

Apart from their primary function of Ab production, B cells also have other roles such as regulating homeostasis. They are also necessary to initiate adaptive immune responses mediated by T cells (Lebien & Tedder, 2008).

2.2.2.2.2 T cells

T cells are produced in the bone marrow like all other cellular types, but they subsequently migrate to the thymus for maturation. Once they leave the thymus, they are considered "naïve" T cells as they have not yet encountered any pathogens. These mature cells express the T Cell Receptor (TCR) on their surface, through which they recognize Ags. Unlike B cells, **T cells require the Ag to be presented in the context of the Major Histocompatibility Complex (MHC) to recognize it** (Andersen et al., 2006). They participate in the adaptive immune response and orchestrate immune responses through signaling or by directly eliminating pathogenic agents, depending on the type of T cell (Fabbri et al., 2003).

T cells divide into different types such as helper, cytotoxic, regulatory, and memory T lymphocytes.

- **Helper T cell (Th):** characterized by the CD4+ membrane marker, their function upon activation is to mediate the body's immune responses by secreting cytokines. They activate cells involved in the innate immune response, cytotoxic T cells, and B cells. They recognize Ags presented in MHC class II (Luckheeram et al., 2012). Within helper T cells, there are various types (Figure 25):
  - **Th1:** These lymphocytes differentiate into Th1 due to Interleukin-12 (IL-12) and INFγ. Their function involves eliminating intracellular pathogens and amplifying phagocytic activity (Kidd, 2003; Luckheeram et al., 2012).

- **Th2**: Their differentiation into Th2 depends on Interleukin-2 (IL-2) and IL-4. Their function involves responding to extracellular parasites such as helminths and they are also implicated in allergic processes (Kidd, 2003; Luckheeram et al., 2012).
- **Th17**: IL-6, Interleukin-21 (IL-21), Interleukin-23 (IL-23), and Transforming Growth Factor-beta (TGF-β) are involved in their differentiation into Th17. Their function involves responding to extracellular fungi and bacteria, especially in defending mucosal and epithelial surfaces. They play a significant role in autoimmune diseases (Burgler et al., 2009; Veerdonk et al., 2009).
- **Regulatory T cells (Treg)**: These lymphocytes control the immune response at different points and through different mechanisms. Among their functions are regulating tolerance to the body's own Ags and to the flora, as well as to food. On the other hand, they limit and control immune system responses, so they don't become excessive. There are also other lymphocytes that can act as regulators of the immune response, such as CD8+ suppressor T cells (González-Amaro & Marazuela, 2016; Shevyrev & Tereshchenko, 2020).

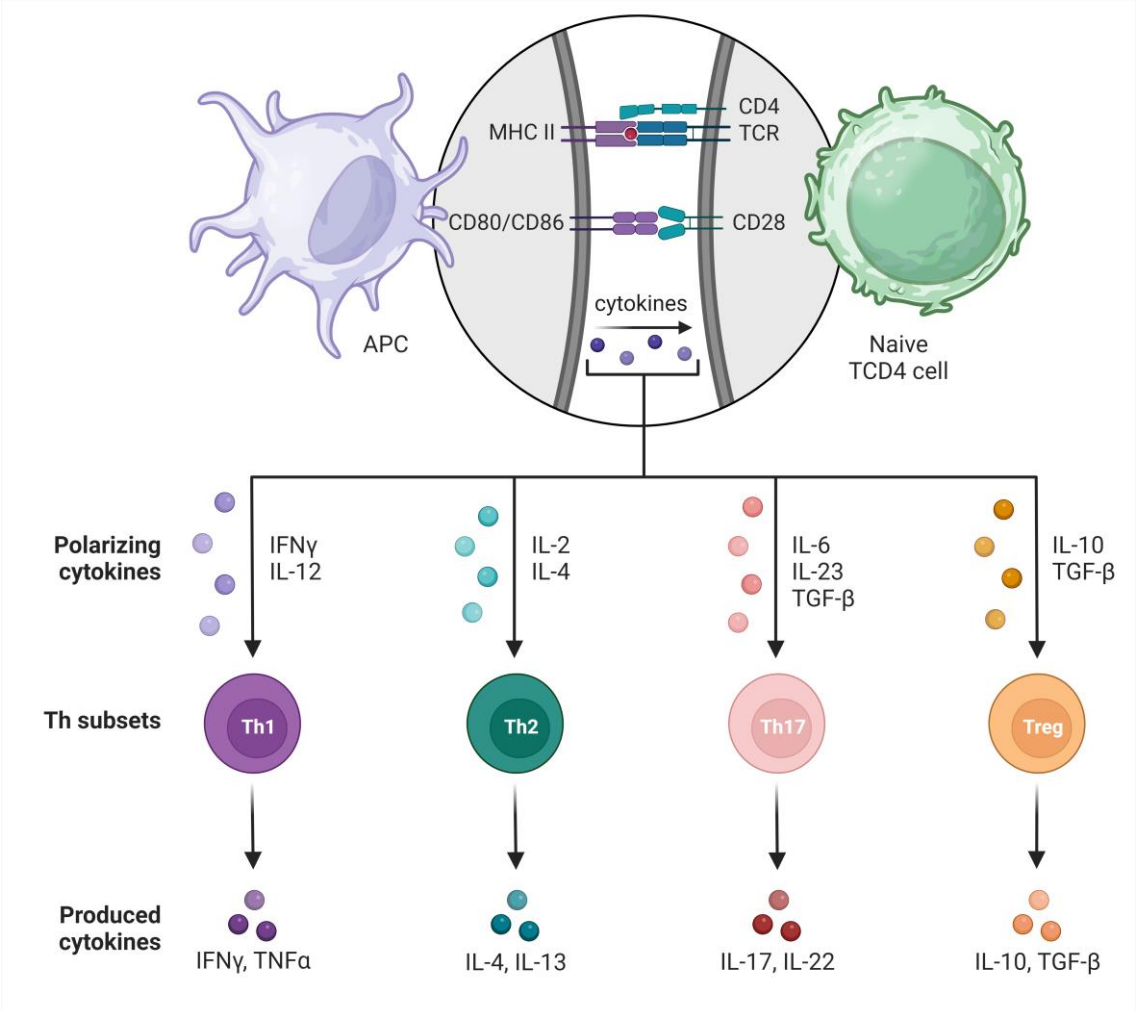

Figure 25. T cell CD4+ differentiation. Created with BioRender.com.

- **Cytotoxic T cells (CTLs):** Characterized by the CD8+ membrane marker, their function involves destroying cells deemed a threat, such as virus-infected cells. They also eliminate tumor cells as they can differentiate them from non-malignant cells in the body (Boon & Van der Bruggen, 1996). The death of these cells can occur through procedures requiring cell-to-cell contact or can be mediated by cytokines like INFγ. This type of lymphocyte recognizes Ags presented in MHC class I (Andersen et al., 2006).
- **Memory T cells**: this is a highly heterogeneous group of cells, differing in function and phenotype. Essentially, they are T cells that have responded to an Ag and are maintained long-term. Consequently, they are primed to proliferate immediately upon a second encounter with the Ag (Martin & Badovinac, 2018).

2.2.2.2.3 NK cells

NK cells have specialized in Ab-mediated cytotoxicity, as they recognize opsonized pathogens through Fraction Crystallizable (Fc) receptors. They contain cytolytic granules within and **identify cells infected by viruses or tumor cells.** Furthermore, they activate macrophages by producing IFNγ. They are found in both lymphoid and non-lymphoid tissues and have a lifespan in the blood of 12 days (Vivier et al., 2008). Various studies have demonstrated that this cell type can exhibit functions associated with conventional immunological memory (Cooper et al., 2009; O'Sullivan et al., 2015).

2.2.3. Immunity types

The immune system has two types of immunity: passive immunity and active immunity (Figure 26):

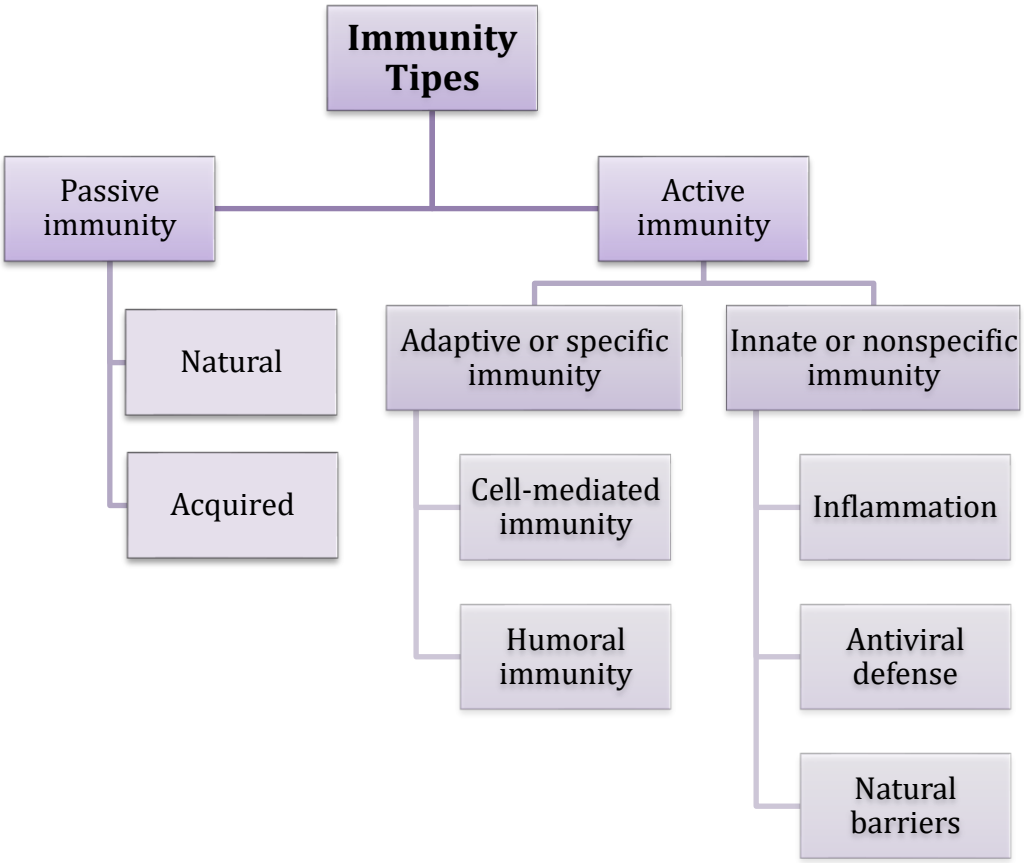

Figure 26. Classification of immunity types.

- **Passive immunity**: it is a short-term immunity, also known as temporary immunity. It is conferred through the adoptive transfer of Abs or lymphocytes. For example, the immunity transmitted by the mother during the breastfeeding period (natural) or through immunotherapy treatments (acquired) (Baxter, 2007).
- **Active immunity**: conferred through an individual's response to a pathogen. This can be natural or acquired. In the case of natural active response, it occurs when a pathogen infects us and we recover from the infection. Conversely, acquired active response would be obtained through vaccination (Baxter, 2007).

Within active immunity, we find innate or nonspecific immunity and adaptive immunity (Table 3):

- **Innate or nonspecific immunity**: it constitutes the body's second line of defense. It acts against any substance or foreign agent that manages to penetrate the body; therefore, it is nonspecific. In the response produced by this system, two main reactions occur (Weber, 2008):
  - **Inflammation**: it is the recruitment of immune cells and plasma proteins to the infection sites. Cells such as phagocytes or NK cells are involved, along with soluble molecules like complement components, cytokines, etc.

- **Antiviral defense**: mediated by soluble factors (cytokines). They confer resistance and activate cells that will destroy the infected cells.

❖ **Adaptive or specific immunity**: it constitutes the organism's third line of defense, the actual immune system, and only acts against the Ag that has stimulated it. Lymphocytes, Abs, cytokines, etc., are involved in this response (Bonilla & Oettgen, 2010).

Table 3. Differences between innate and adaptive immune response (Bonilla & Oettgen, 2010; Weber, 2008).

	Innate	***Adaptive***
Response time	Hours	Days
Specificity	Limited and fixed	Diverse and improved
Immunological memory	No	Yes
Response to repeated infections	Identical to the first one	Faster than the first one
Blood soluble components	Complement system, antimicrobial peptides, cytokines	Cytokines and antibodies
Cells involved	Phagocytes	B and T lymphocytes
Recognition	Patterns	Antigens

2.2.3.1. *Innate immunity*

The innate immunity is present from birth and serves to provide an **immediate response to a pathogen.** It's not as efficient as the adaptive immune system and consists of nonspecific mechanisms for Ag recognition. Its main functions are phagocytosis, Ag processing for presentation, and in the inflammatory response (Delves & Roitt, 2000).

Within innate immunity, there's a set of defense barriers aimed at preventing the entry of pathogens or other disease-causing agents (Chaplin, 2006). These defenses can be divided into external and internal ones (Anaya et al., 2013) (Figure 27).

- **External barriers**: these can be physical, such as the skin and mucous membranes; chemicals, like sweat glands, tear ducts, or saliva; or microbiological, through the body's own bacterial flora (Delves & Roitt, 2000).
- **Internal barriers**: in this case, an internal barrier would be fever as a protective response against infection and injury (Delves & Roitt, 2000).

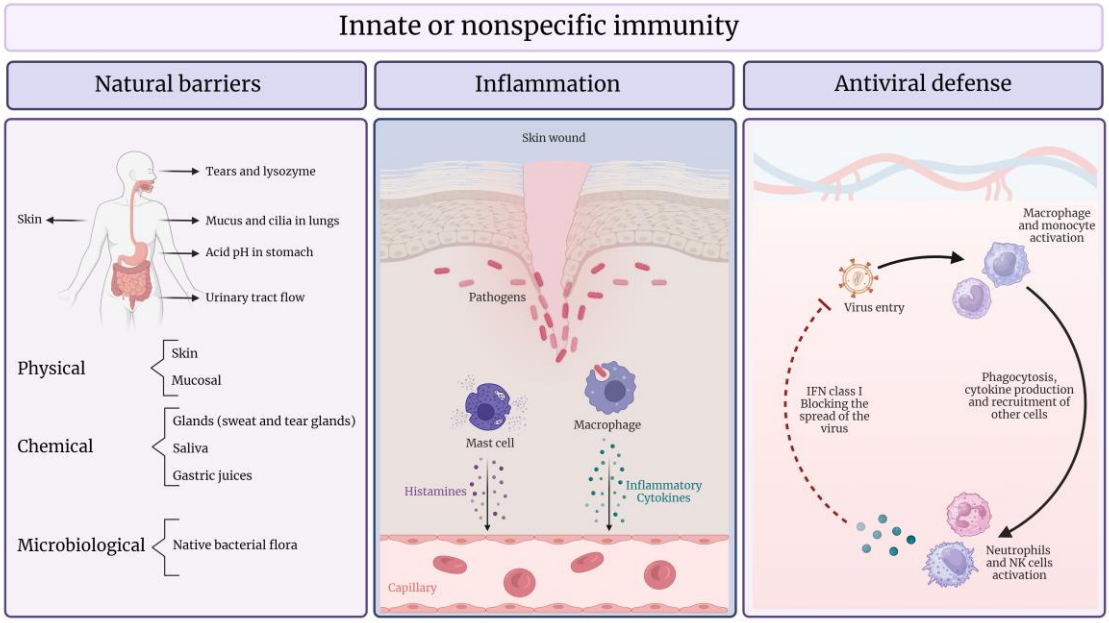

Figure 27. Innate immune responses. Created with BioRender.com.

Moreover, the innate immune system also comprises cellular components such as phagocytes responsible for pathogen phagocytosis and Ag presentation (macrophages and DCs). Neutrophils, eosinophils, and basophils are also part of this immunity (McComb et al., 2019).

Finally, various soluble mediators also participate, circulating molecules in the bloodstream and lymph that recognize and tag pathogens. This allows the immune system's effector cells to carry out a faster and more efficient response. These mediators can include natural Abs, the complement system, cytokines, and opsonins (Fabbri et al., 2003).

In summary, **innate immunity acts immediately without the need for prior sensitization**, it has a broad specificity as it recognizes PAMPs, and it does **not develop immunological memory** (McComb et al., 2019).

2.2.3.2. *Adaptive immunity*

Following the innate response, there's the response mediated by B cells responsible for Ab synthesis and secretion into the bloodstream (humoral immunity), and T cells (cellular immunity). This type of immunity is characterized using receptors that are specific to the Ag (Parkin & Cohen, 2001).

2.2.3.2.1 Cell-mediated immunity

In cell-mediated immunity, a crucial function is **defense against intracellular pathogens, particularly viruses**. Lymphocytes responsible for this are the T cells. For this type of response to occur, T cells need to be activated, but to recognize the Ag, they require presentation within the context of MHC (I or II). Once the MHC interacts with the TCR, T cells additionally require co-stimulatory signals from APCs (via membrane receptors and cytokine production). When all

signals are present, T cells activate and proliferate (Wing & Remington, 1977).

If this activation occurs in CD4+ T cells, it leads to the synthesis of proinflammatory cytokines like IL-6, immunoregulatory cytokines like IFNγ, and chemotactic properties like Interleukin-8 (IL-8). Additionally, Th2 lymphocytes interact with B cells to activate them in the case of T-dependent Ags, initiating the humoral immune response (Varella, 2001).

Moreover, CD8+ T cells are also activated (upon recognizing peptides in the context of MHC I) and secrete perforins and granzymes, creating holes in infected cells, destroying them, and facilitating granzyme entry to induce apoptosis in the cell. In this response, the first cells to respond are NK cells, which recognize virus-infected cells and can destroy them (Varella, 2001) (Figure 28).

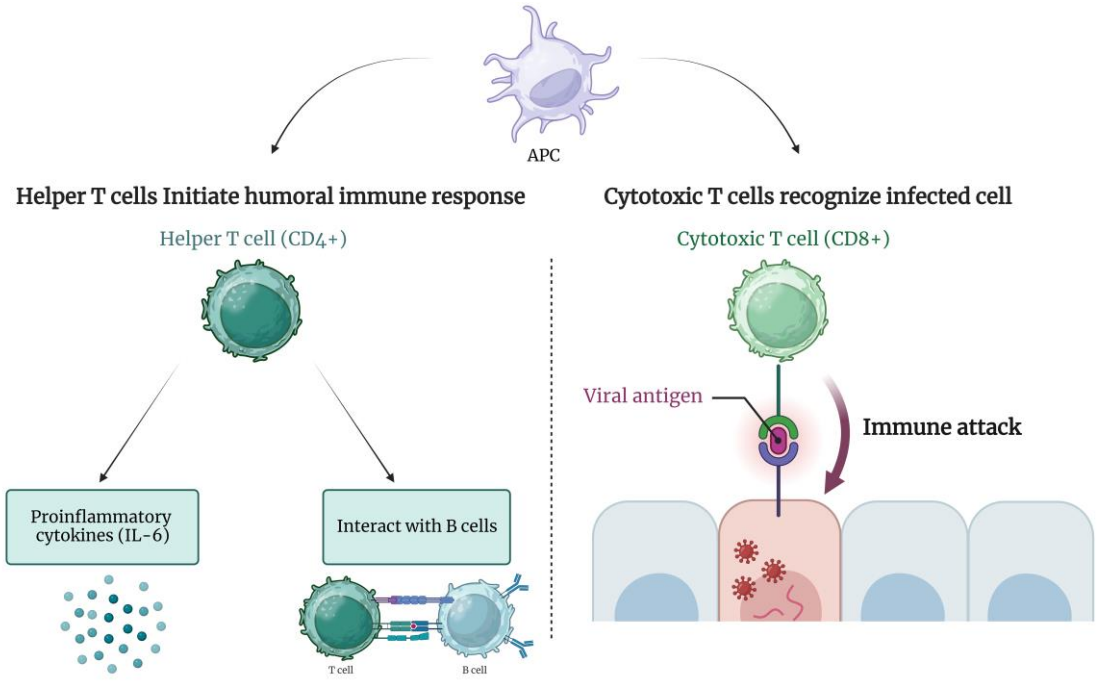

Figure 28. Cell-mediated immunity. The CD4+ T-cell mediated response is shown on the right and CD8+ T-cell mediated response on the left. Created with BioRender.com.

Finally, some of these T cells become memory cells capable of recognizing the Ag in a subsequent infection (Wing & Remington, 1977).

2.2.3.2.2 Humoral immunity

B cells and plasma cells are the main actors in this type of response. When an Ag enters the body, B cells are activated (aided by multiple signals, including those produced by Th2 cells). Recognition of the Ag is more efficient when carried out by an APC (Bonilla & Oettgen, 2010).

Once all necessary signals are received, the clonal proliferation of different types of lymphocytes begins, as typically, **the production of these Abs is polyclonal, targeting different epitopes of the Ag.** Hence, there's always a window of time until the Abs are detectable in serum (Varella, 2001).

The majority of these B cells become Ab-producing plasma cells, while some become memory B cells during the primary response. In this **primary response, the first type of Ab produced is Immunoglobulin M (IgM); subsequently, Immunoglobulin G (IgG) Abs become predominant over IgM**. IgGs reach a peak until they start to decline due to negative feedback, coupled with Ag elimination and suppressor cell-mediated activity (Bonilla & Oettgen, 2010; Elgueta et al., 2010).

Subsequently, if there were a re-exposure to the same Ag, a much faster and more efficient secondary response to eliminate that pathogen would occur. This secondary response requires a smaller amount of Ag; the window of time also decreases, and the concentration of Abs increases much more rapidly and to much higher titers. Since memory cells express IgG, this Ab type predominates in the secondary response (Varella, 2001).

This humoral response **also occurs in mucous membranes, where the primary Ab is secretory Immunoglobulin A (IgA)**. One of its attributed functions is preventing the binding of microorganisms to the mucous membranes (Varella, 2001) (Figure 29).

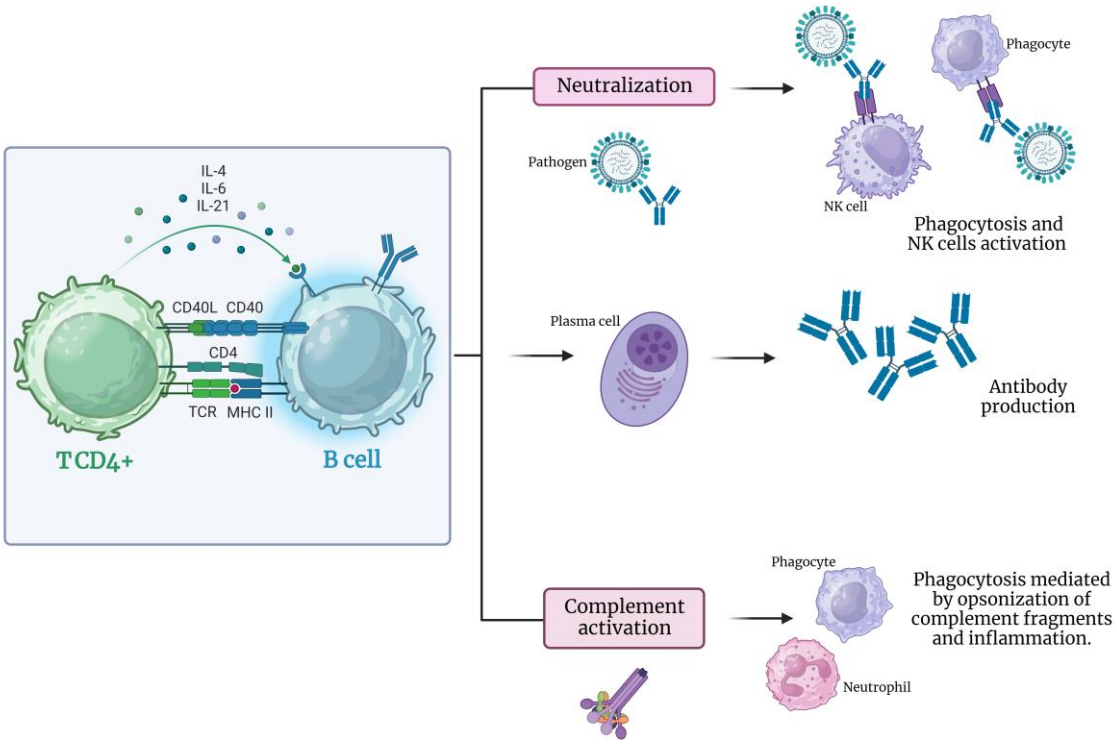

Figure 29. Humoral immunity. When activated, B cells become Ab-producing plasma cells that act in the neutralization of pathogens and in the activation of the Ab-dependent complement pathway. Created with BioRender.com.

2.2.3.2.2.1 *Immunoglobulins*

All Igs share the same basic structural characteristics but exhibit great variability in the Ag recognition region.

Igs, also known as Abs, have a symmetrical basic structure **composed of two identical light chains and two identical heavy chains** (four polypeptide chains). A light chain is covalently bound to a heavy chain through an interchain disulfide bridge, and the two heavy chains are, in turn, linked to each other via disulfide bonds. Both heavy and light chains consist of Variable (V) amino-terminal regions involved in Ag recognition and carboxy-terminal Constant (C) regions (Varella, 2001).

In the heavy chains, the V region consists of an Ig domain where the sequence has significant variation, and the C region comprises three or four Ig domains with identical sequences in all of them, at least within the same isotype. **The V region of the heavy chain associates with the V region of a light chain, forming the Ag-binding site**. On the other hand, light chains have a V region and a C region. These light chains can be of the Kappa type (60%) or the Lambda type (40%) (Schroeder & Cavacini, 2010).

The V region, in turn, has three zones or hypervariable segments, also known as Complementarity-Determining Regions (CDRs), which determine the specificity of an Ab to an Ag. They are called CDR1, CDR2, and CDR3, with CDR3 being the most variable for both light and heavy chains (Chiu et al., 2019) (Figure 30).

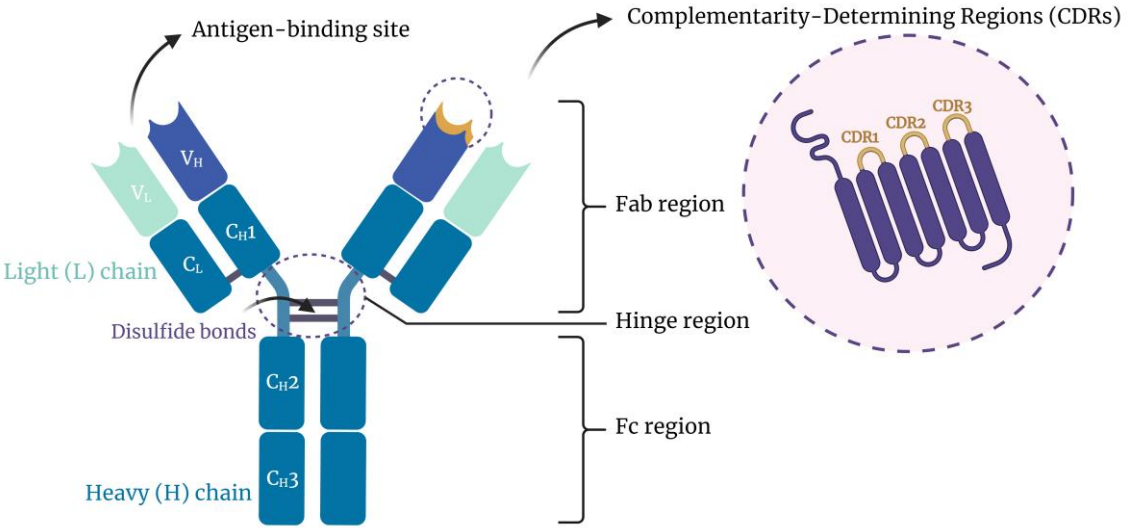

Figure 30. Ig structure. Created with BioRender.com.

Each Ab has two Ag-binding sites and can bind when they are close together or when they are apart because they possess a region called a hinge located between the C domains of the first and second heavy chains, allowing independent movement of Ag recognition sites relative to the rest of the molecule.

These chains can be cleaved by enzymes like papain and pepsin. Papain digestion separates the two Ag-binding sites (Fab') from the portion of the Ig molecule that binds to complement and Fc receptors, while pepsin digestion generates a single bivalent Ag-binding fragment F(ab')2 (Varella, 2001) (Figure 31).

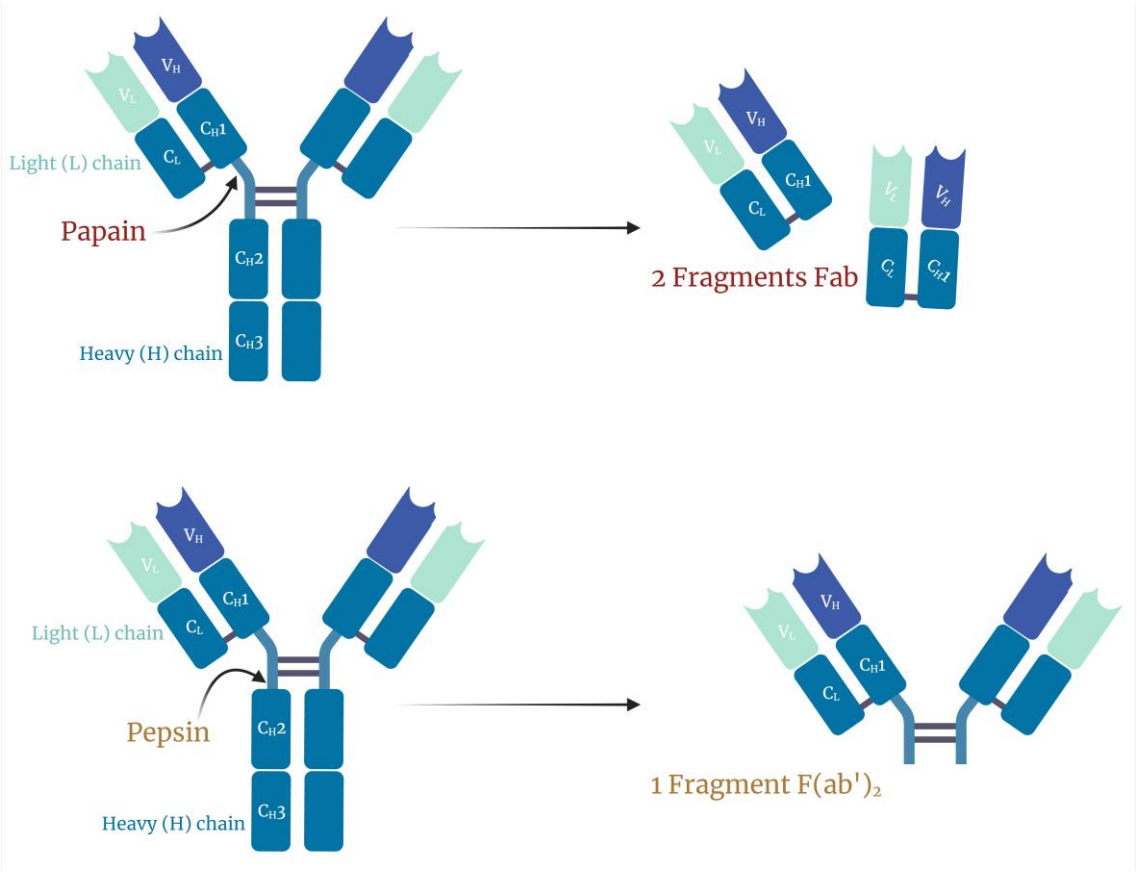

Figure 31. Ig fragments produced by enzymatic digestion of papain and pepsin. Created with BioRender.com.

Abs can exist in two forms in the body: secreted in body fluids or anchored to the membrane, for instance, as BCR. Moreover, **Abs can be distinguished by isotopic, allotypic, and idiotypic differences.** Idiotype differentiates one Ab from another, as they have different antigenic specificities, residing in the hypervariable region of the Ig. Isotypes of Igs differ in the amino acid (aa) sequence of the C regions. Lastly, allotypic variations occur within the same species due to allelic variation (Schroeder & Cavacini, 2010).

In mammals, **five different isotypes of Igs are found: IgG, Immunoglobulin D (IgD), IgE, IgM, and IgA**. The first three form monomers, while IgM and IgA, although they can also form monomers, in their secreted form, IgM forms pentamers, and IgA forms dimers. Each of these isotypes differs in the number of C regions, with IgE and IgM having four C domains and IgG, IgD, and IgA having three C domains (Figure 32):

- **IgA**: it is expressed in large quantities in human serum and has a half-life of six days. It can be found as a monomer, but predominantly as a dimer. In its secretory form, it plays a fundamental role in antimicrobial defense in the mucosa, where it acts as a neutralizing Ab (Woof & Ken, 2006).
- **IgD**: it is only expressed in B cells, not secreted, and is expressed on the surface membrane of immature B cells. It is not detected in serum and has a half-life of three days. Its function is as an Ag receptor (InvivoGen, 2012).
- **IgE**: it is found in very low concentrations in serum and has a half-life of two days, existing as monomers. It plays a crucial role in hypersensitivity reactions. It also plays an important role in controlling endothelial barrier function and consequently in the development of inflammatory processes, as it activates mast cells. Additionally, it is involved in immunity against helminths and in allergy and anaphylaxis phenomena (Janeway et al., 2001).
- **IgG**: it is the most abundant of all existing isotypes. There are four types, and its half-life is twenty-three days. They are involved in opsonization (the process by which a pathogen is marked for destruction by phagocytes), complement activation, Ab-mediated cytotoxicity, etc. They represent the first line of defense for newborns as it is the only Ig capable of crossing the placenta (Janeway et al., 2001).
- **IgM**: it can be secreted in a pentameric form and has a half-life of five days. It participates in complement activation. It also plays a central role in defense mechanisms developed in the vascular compartment (Janeway et al., 2001).

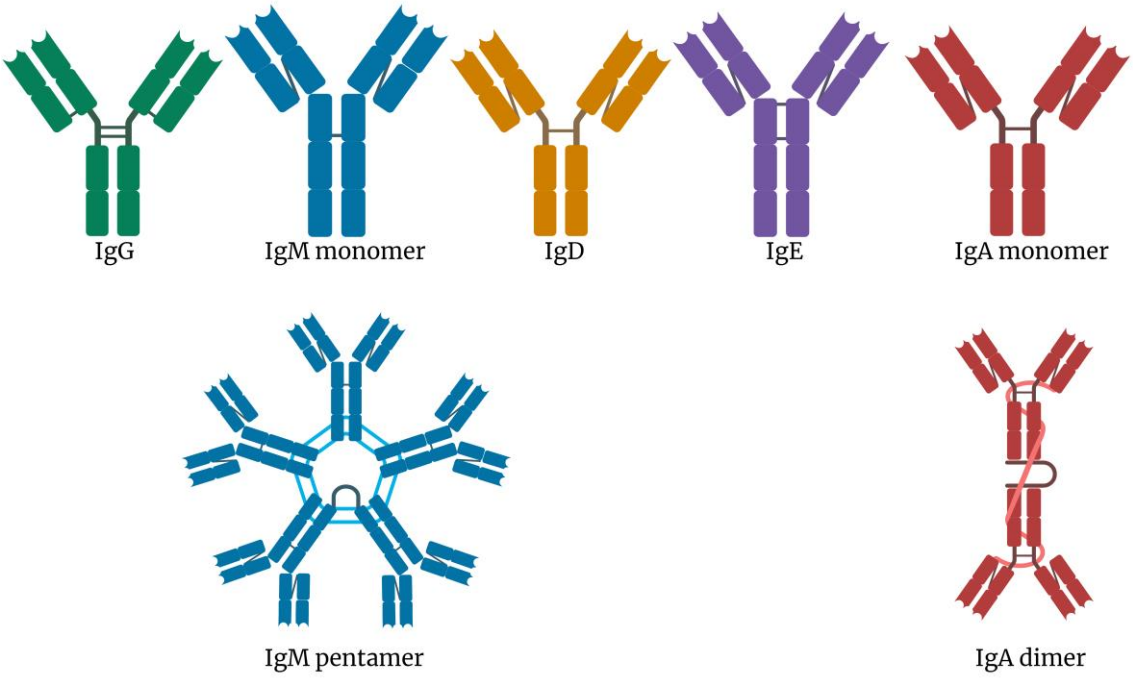

Figure 32. Ig isotypes. Created with BioRender.com.

The Abs have two main roles. On one hand, **they bind to the epitope of Ags through the Fab region**, and as biological effectors, they **activate NK cells, the classical complement pathway, and phagocytosis** (Lipman et al., 2005). Additionally, another characteristic to consider about Abs is whether they are polyclonal or monoclonal (Table 4).

- **Polyclonal Abs**: these are generated when the host (rabbit, goat, mouse, etc.) has been immunized against a specific Ag, resulting in the production of Abs against different epitopes of this Ag by various B cell clones (Ritter, 2000).
- **Monoclonal Abs**: the technique for producing monoclonal Abs was described by Köhler and Milstein and involves the growth of a single B cell clone and the purification of the Ab produced by this clone. This is achieved by creating a hybridoma between this specific B cell and a myeloma cell, so that the generated Abs only have specificity for a single epitope (Ritter, 2000).

Table 4. Differences between monoclonal and polyclonal Abs (Ritter, 2000)**.**

Polyclonal	Monoclonal
Heterogeneous population of Abs with differing paratopes for an Ag	Homogenous population of a specific Ab with one paratope
Not epitope specific	Epitope specific
Increased likelihood for cross-reactivity with similar Ags	Low cross-reactivity
Increased likelihood for background noise	Low background noise
Lot variability	Identical lots
Inexpensive to develop	Expensive to develop
Quick to produce (approx. 3 months)	Slow to produce (approx. 6 months)
Many host species options	Few host species options

2.2.3.2.2.2 *Ag-Ab reaction*

The Ag-Ab binding is of **a non-covalent nature, mediated by electrostatic forces, hydrogen bonds, hydrophobic interactions, and Van der Waals forces**. Therefore, this union is reversible, and dissociation can be achieved with significant pH changes (Varella, 2001).

The Ag area that interacts with the Ab (recognition site) is termed an epitope. Consequently, a single Ag may contain different epitopes and be recognized by different Abs. These regions usually consist of approximately 15-22 aa (Varella, 2001).

Two fundamental concepts to consider in this type of reaction are affinity and avidity.

- **Affinity**: defines the strength with which a single Ag-binding site of an Ab attaches to the epitope of that Ag. This affinity is measured by a Dissociation Constant (K_d). Lower K_d values indicate a greater interaction affinity of that complex.

- **Avidity**: defines the cumulative capacity of an Ab to bind to the Ag. Avidity is higher than affinity since an Ab has at least two Ag-binding sites. It also refers to the binding strength of multiple Abs produced in response to that Ag, which presents different epitopes (Lipman et al., 2005).

So, regarding the valence of the interaction (monovalent, bivalent, or multivalent) and the avidity of these interactions, monovalent Ags interact with a single binding site of an Ab molecule, so even if the affinity of this interaction is high, its avidity is low. When repeated epitopes are found on a cell surface, it can lead to a bivalent interaction with higher avidity. For example, IgM molecules have ten Ag-binding sites, allowing them to simultaneously bind to ten Ags, resulting in multivalent interactions with very high avidity.

Another characteristic to consider in these types of interactions is **cross-reactivity, which occurs when an Ab recognizes an epitope for which it is not specific due to having a very similar sequence or conformation** (Varella, 2001).

2.2.4. Immune response against viruses

For a virus to enter cells and cause infection, it must first breach barriers like the skin and mucous membranes. In some cases, the virus needs to reach the target organ to replicate (Mueller & Rouse, 2008).

When this happens, the **innate immune system acts as the first line of defense**, attempting to block or inhibit the infection (Mueller & Rouse, 2008). Upon a virus penetrating a cell, Pattern Recognition Receptors (PRRs) like Toll-Like Receptors (TLRs) found in endosomes recognize the virus's RNA or DNA and viral proteins, **resulting in the production of type I interferons and cytokines in infected cells or other immune cells, activating the antiviral response.** Additionally, recognition via TLR on the cell surface activates the inflammatory response (Koyama et al., 2008). PRRs also include Retinoic acid-Inducible Gene I (RIG-I)-like receptors (RLRs) following the type I interferon pathway and NOD-Like Receptors (NLRs) regulating Interleukin-1 beta (IL-1β) production (Takeuchi & Akira, 2009).

These receptors trigger signaling cascades within cells aimed at inducing apoptosis in infected cells or conferring resistance to uninfected ones. Furthermore, the produced cytokines aid in recruiting more cells involved in innate and adaptive immunity (Takeuchi & Akira, 2009). One of the primary pathways activated by type I interferons is the activation of NK cells that produce IL-12 and IFNγ, recruited to the site of infection and capable of killing infected cells. Additionally, antiviral defense involves complement activation (Brandstadter & Yang, 2011; Mueller & Rouse, 2008).

This initial innate immune response is crucial for mounting an adaptive response to viral infection. On one hand, within humoral immunity, Abs are produced, neutralizing viral particles before they can enter cells due to the activation of B cells by APCs. These Abs also play a preventive role against a secondary infection, especially in mucosal areas, and some of these B cells become memory cells (Takeuchi & Akira, 2009).

The cellular response is characterized by the activation of CD8+ T cells responsible for eliminating virus-infected cells by inducing apoptosis through cytotoxic granules and the production of Tumor Necrosis Factor alpha (TNF-α) and IFNγ. This occurs through the recognition of these cells by the interaction of the TCR on the surface of the T cell with MHC class I on the infected cells (Blattman et al., 2000; Huber et al., 2014). Consequently, when the virus has penetrated the cell, some viral proteins are degraded to be presented on MHC I on the cell surface and recognized by the specific CD8+ T cell for that Ag. CD4+ T cells are also activated through MHC II, co-stimulating the activation of CD8+ T cells (Huber et al., 2014).

Following this initial infection, within 3-4 weeks after the expansion peak, 90% of T cells die by apoptosis, and the remaining become memory T cells that will have a quicker and more effective response in a second exposure to that virus (Wherry & Ahmed, 2004) (Figure 33).

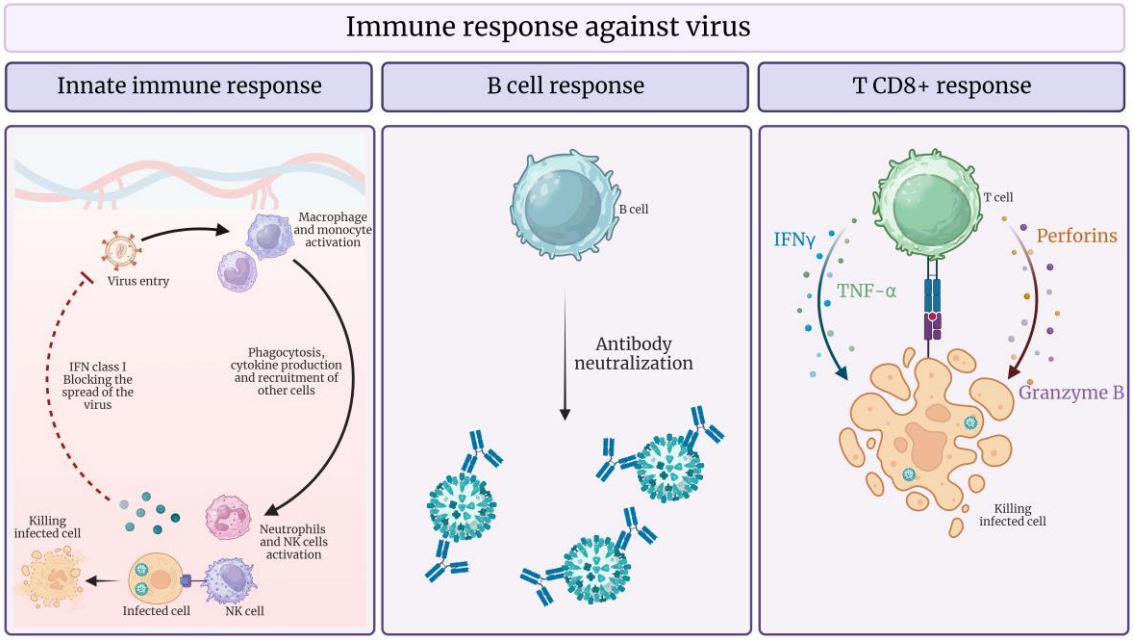

Figure 33. Immune response against the virus. The immune system reacts innately by blocking the virus and activating NK cell-mediated cytotoxicity. On the other hand, in an adaptive response, it neutralizes the viral particles with Abs and activates CD8+ T cell-mediated cytotoxicity. Created with BioRender.com.

Viral infections can be classified as acute, when the virus is eliminated, or chronic when the infection persists (latent or persistent) (Wherry & Ahmed, 2004), as viruses can also evade the immune system's response through various mechanisms (Mueller & Rouse, 2008).

2.2.5. Immunoassays

An immunoassay is a test that **employs Ag-Ab complexes as a means to generate a detectable result**. Such a complex is also known as an immune complex (Findlay et al., 2000).

Immunoassays stand out from other laboratory tests due to their specific reaction, facilitated by the presence of specific Abs against each Ag. They find broad utility in clinical settings, allowing for qualitative or quantitative measurement of either the Ag or the Ab (Wild, 2013).

2.2.5.1. *Types of immunoassays*

Immunoassays can be classified in different ways; **they can be competitive or non-competitive, and heterogeneous or homogeneous**. In all these classic immunoassays, which are based on primary interactions between the Ag and the Ab, the use of **labeled material is necessary, adding another classification**. A label is a molecule that reacts, causing a change in the signal that can be measured. Some examples of these labels are radioactive compounds, enzymes, or compounds that produce light (Hsieh & Rao, 2023).

2.2.5.1.1 Competitive immunoassay

In competitive immunoassays, **the unlabeled analyte (usually the Ag) in the sample is measured for its ability to compete with a labeled antigen (Ag*).** The unlabeled Ag blocks the ability of Ag* to bind, as the Ab recognition sites are already occupied (Slagle & Ghosn, 1996).

Therefore, in this type of assay, **a decrease in the signal produced by Ag* indicates a higher quantity of the Ag** being determined in the patient's sample. Hence, the Ag concentration in the sample is inversely proportional to the measured signal.

Competitive immunoassays can be:

- **Single-step**: In this case, both the Ag* and the unlabeled analyte from the sample compete for a limited amount of Ab (H. R. Kim et al., 2022) (Figure 34A).
- **Two-step**: In this type of competitive assay, the concentration of Ab is in excess compared to the Ag concentration. First, the excess Ab is incubated with the sample, and in a second step, the Ag* is added. This process enhances sensitivity (Huang et al., 2022) (Figure 34B).

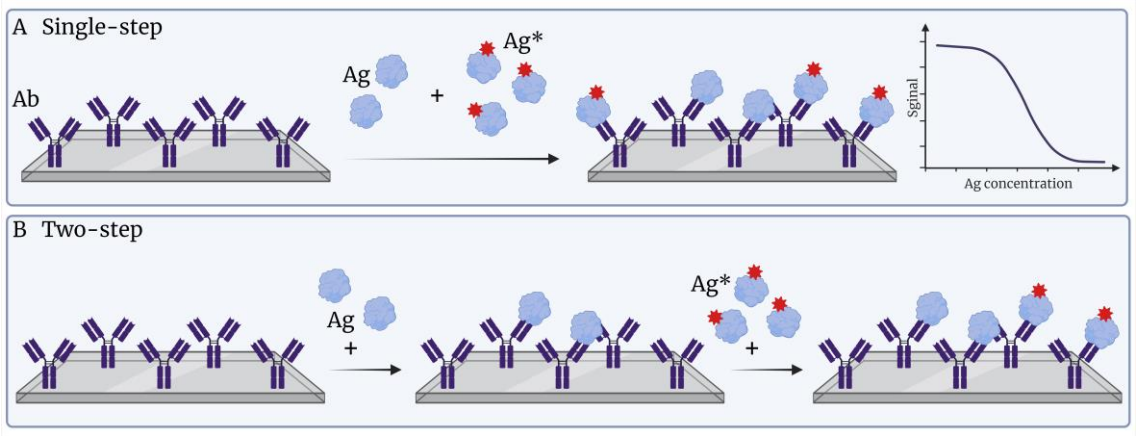

Figure 34. Competitive immunoassay. A. One-step, in which labeled and unlabeled Ag are incubated at the same time and compete for binding sites. **B.** Two-step, in which there is first an incubation of the sample and then the Ag*. In both cases, the relationship between concentration and signal is inversely proportional. Created with BioRender.com.

2.2.5.1.2 Non-Competitive immunoassay

In this type of immunoassay, **there's no competition between the analyte of interest and the labeled substance**, so the concentration of **the analyte is directly proportional to the amount of signal obtained**. These immunoassays are also referred to as sandwich assays.

- **Sandwich assays**: These typically yield the highest levels of sensitivity and specificity and are used for measuring critical analytes. They are termed as such because the analyte to be determined is sandwiched between two specific Abs targeting it. To determine Ags, a specific Ab against it is immobilized on the solid support, usually a plate, and after incubating the sample, another specific Ab is added and labeled. These assays can also be one or two-step processes. In the case of two steps, there are washing stages to remove unbound labeled reagents and interfering substances (Schwickart et al., 2014)(Figure 35).

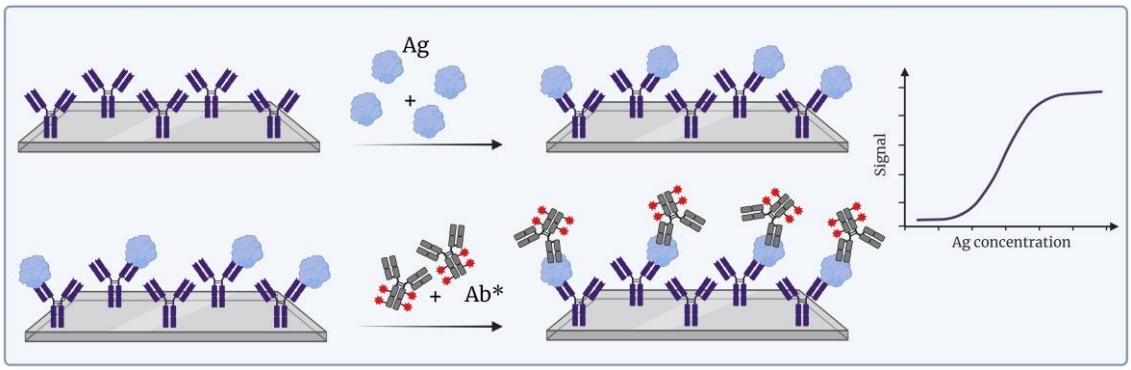

Figure 35. Non-competitive immunoassay. In the case of non-competitive assays, the Ag concentration is directly proportional to the detected signal. Created with BioRender.com.

2.2.5.1.3 Heterogeneous immunoassay

They are techniques that require the separation of the immune complex from the unconjugated molecules. That is, **it requires the separation of the Ag-Ab complex** and generally uses a solid-phase. There are different methods for separating the bound and free fractions, which sometimes involve immobilizing one of the components (Ag or Ab) on a solid system such as a microplate or NPs. This allows the fractions to be separated through washing. Additionally, this method helps eliminate all serum components that could interfere with the measurement (O'Beirne & Cooper, 1979).

2.2.5.1.4 Homogeneous immunoassays

In these cases, **the separation of the complex is not required**. These techniques are usually used to measure small analytes such as drugs of abuse and therapeutics. They are easier and quicker to perform. They take place in a solution rather than on a solid support.

The physical and chemical differences (such as size or conformational changes) between the free Ag and the Ag bound to the Ab characterize the signal response. Not separating the fractions could impact sensitivity by facilitating interference, making them less sensitive compared to heterogeneous assays (Wild, 2013).

2.2.5.1.5 Immunolabeled assays

Depending on the type of labeling molecule used in the immunoassay, these can be classified as follows (Ahsan, 2022; Rizzo, 2022):

- **Fluoroimmunoassay (FIA):** This detection system is based on Ags or Abs labeled with lanthanide chelates, which are fluorescence emitters called fluorochromes.
- **Chemiluminescence immunoassay (CLIA):** It's a variation of the standard ELISA method. An enzyme transforms the substrate into a product that emits photons instead of a visible color.
- **Radioimmunoassay (RIA)**: In this case, Ag or Abs labeled with radioactive isotopes such as iodine-125 or iodine-131 are used.
- **Enzyme Immuno Assay (EIA)**: This method is based on the high specificity of the Ab to the Ag and amplification through chemical reactions carried out by enzymes acting on substrates that generate colored products (indicator reaction). Commonly used enzymes include alkaline phosphatase, peroxidase, and β-galactosidase, although they can also be amplified by the biotin-avidin/STV system. Within this type of immunoassay is the ELISA technique, which will be explained in more detail, as it is one of the methods used in this thesis.

2.2.5.1.5.1 *ELISA*

ELISA procedures are generally more sensitive in heterogeneous formats compared to homogeneous ones. ELISA is performed on a solid phase (such as polystyrene plates or similar). It's a heterogeneous EIA, with detection preferably done through spectrometry. **Most ELISAs are non-competitive**, with a variety performed on nitrocellulose paper known as an immunoblot. It's widely used in clinical laboratories for detecting and measuring various markers.

The principle behind ELISA involves using Ags or Abs labeled with an enzyme. As a result, the resulting conjugates exhibit both immunological and enzymatic activity. One of the components marked with the enzyme is easily revealed by adding a specific substrate. The enzyme action yields a color visible to the naked eye or quantifiable using a spectrophotometer or colorimeter. There are different types of ELISA (Gan & Patel, 2013; Hidayat & Patricia Wulandari, 2021):

- **Direct ELISA**: Used for Ag detection, where the sample is incubated in the plate, immobilizing the Ags. It's then revealed with an enzyme-labeled Ab that shows the reaction after adding the substrate, without the need for a secondary Ab (Figure 36A).
- **Indirect ELISA**: Used for detecting Abs in the sample. Specific Ags against the Ab of interest are immobilized, and the sample is incubated, allowing the Abs to react with the immobilized Ag. Subsequently, an enzyme-labeled anti-Ab (αAb) is added, reacting with the Fc of the sample Ab, and then revealed in the same way. In this case we have a primary Ab and a secondary Ab. (Figure 36B).

- **Sandwich or capture ELISA**: Involves two types:
  - **Double Ab Sandwich (DAS):** The specific Ab against the Ag to be determined in the sample is immobilized on the plate. After incubating the sample and allowing the reaction, a second specific Ab against the Ag but against another epitope is incubated, marked with the enzyme. Finally, it is revealed by adding the specific substrate for the enzyme (Figure 36C).
  - **Heterologous Antiglobulin Double Ab Sandwich (HADAS)**: Similarly, the specific Ab against the Ag is immobilized on the plate. After incubating the sample and the second specific Ab against another epitope of the Ag, there's an additional step where an enzyme-labeled αAb reacts with the Fc of the second Ab. It has the same final revelation step (Figure 36D).
- **Competitive ELISA**: In this type, plates are coated with specific Ag or Ab against the molecule to be detected. A known concentration of a mixture of Ags specific to the used Ab, labeled with the enzyme, along with unknown Ags from the sample, is added. Both Ags compete for binding sites on the Ab fixed on the plate.

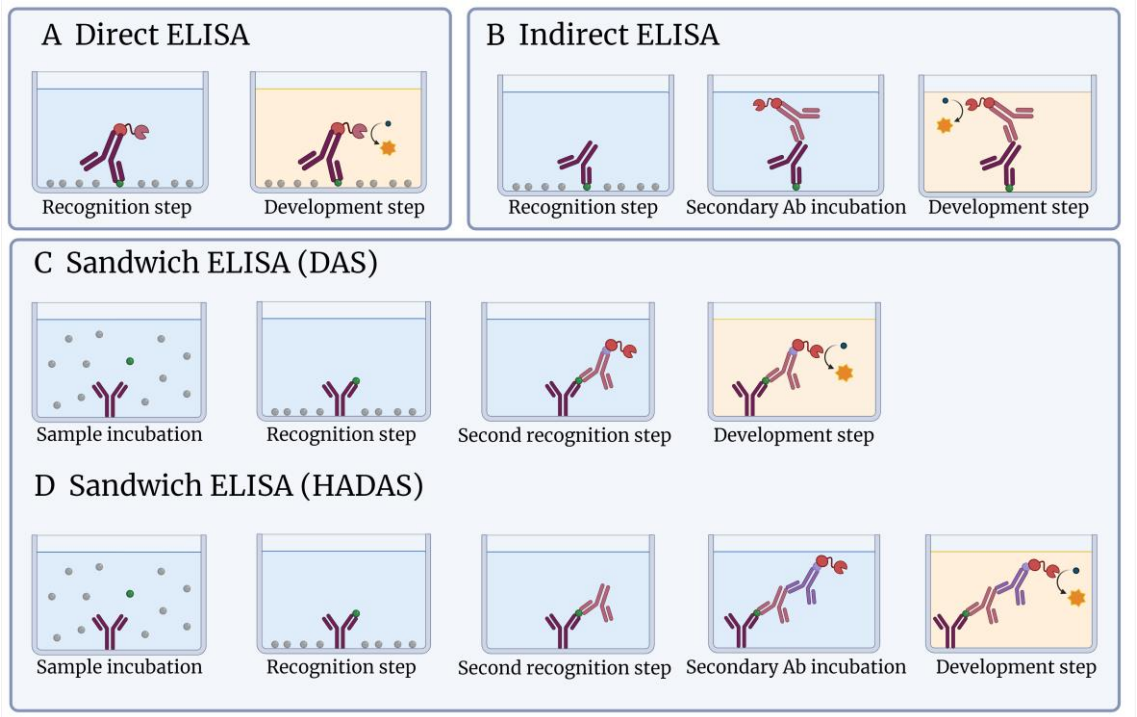

Figure 36. ELISA types. A. ELISA of direct Ag recognition. **B.** Indirect ELISA in which a secondary Ab is necessary. **C.** DAS sandwich ELISA, in which the Ab of the second recognition is labeled with an enzyme. **D.** HADAS sandwich ELISA in which a second enzyme-labeled αAb is used. Created with BioRender.com.

To quantify the Ag, known concentration standards are used simultaneously with the samples to create a reference curve. The absorbance obtained correlates with the amount of the analyte present in the standards and samples. Thus, absorbance readings are converted into concentration units (Sasaki & Mitchell, 2001).

Quantifying Abs isn't as straightforward in converting absorbances to concentration units, as appropriate standards aren't always available. It's more common to work with relative or arbitrary units. **Ab quantity can be estimated through titration curves with serial dilutions of the sample**, presented as titers. Alternatively, the Optical Density (OD) of samples can be compared to that of a standard or control serum, to which arbitrary units have been assigned.

- Characteristics of ELISAs include (Hidayat & Patricia Wulandari, 2021):
  - High sensitivity and specificity, reproducibility, and adaptability.
  - Utilization of a solid phase allows easy separation between bound and free fractions (heterogeneous immunoassays).
  - Enable quantification of hormones, drugs, metabolites, inflammation mediators, proteins, etc.

2.2.5.2. *Immunological assays in biosensors*

The nomenclature used for traditional immunoassays differs from that employed in the context of this thesis for immunoassays conducted in biosensors. To prevent confusion, the classification will now be explained, considering the immunoassay design:

- **Non-competitive immunoassays**: This type of immunoassay is conducted when the concentrations of the analyte to be determined are sufficiently high. These are divided into three different types:
  - **Direct immunoassay**: It is called so when the analyte to be determined in the sample is the Ag, thus immobilizing the specific Ab against the Ag that we want to recognize on the biosensor surface (Figure 37A).
  - **Indirect immunoassay**: Conversely, in this case, the molecule to be recognized is the Ab in the sample, so the sensor surface will have the Ag immobilized (Figure 37B).
  - **Sandwich immunoassay**: This type of immunoassay is more sensitive than the previous two. For this, monoclonal Abs are immobilized on the surface, which are specific to an epitope of the Ag to be determined. Once this interaction has occurred, in a final step, an Ab that can be either monoclonal against another epitope of the Ag or a polyclonal Ab is incubated (Figure 37C).

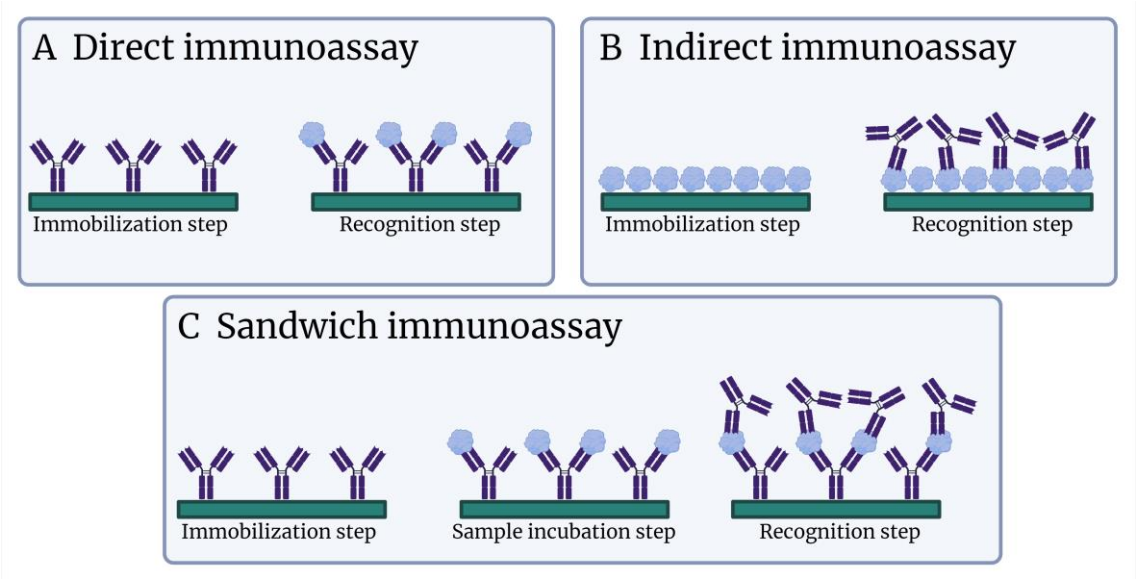

Figure 37. Biosensor immunoassay types. A. Direct type assay for recognition of Ags. **B.** Indirect type assay for detection of Abs. **C.** Sandwich assay for detection of Ags. Created with BioRender.com.

- **Competitive immunoassay**: It is performed to determine Ags present in low concentrations in the sample. For this, the biosensor's surface is coated with the known specific Ag, which is the same as the one to be determined in the sample. On the other hand, the suitable bioreceptor, in this case, a specific Ab against this Ag, is incubated in the sample, which will also be specific to the Ag immobilized on the biosensor. Once this Ag-Ab complex is formed in the sample, it is incubated on the biosensor's surface. Only the free Abs will bind, so, with a higher concentration in the sample, fewer binding sites will be free, resulting in a lower signal on the biosensor. There is an inversely proportional relationship between the concentration and the signal (Figure 38).

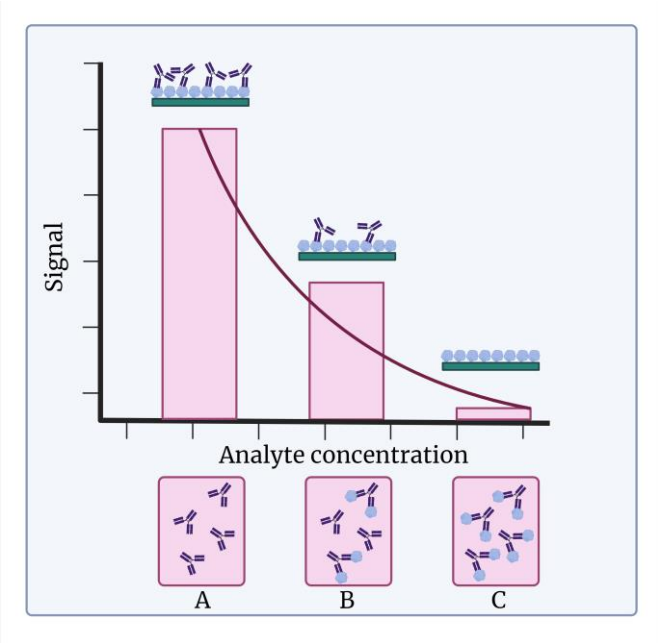

Figure 38. Competitive immunoassay. A. In the sample, there is no analyte of interest and all Abs bind to the surface having maximum signal. **B.** In this case, the concentration of the analyte is medium and there will be only a portion of free Abs binding to the surface. **C.** When the analyte concentration is very high, there will be no free Abs binding, having the minimum signal. So, in this case, the signal is inversely proportional to the concentration of the analyte. Created with BioRender.com.

Furthermore, in reference to **classification by labeling**, immunoassays include:

- **Label:** In this case a molecule is necessary to reveal the result. For example, a fluorochrome that emits light.
- **Label-free:** In label-free biosensors, no chemical labeling is necessary, so that the signal is obtained directly, eliminating the development steps. The biosensor used during the development of this thesis was label-free.

Throughout this thesis, non-competitive immunoassays of both direct and indirect types, as well as competitive immunoassays, have been conducted using NPs to form the NP-Ab-Ag complexes in the sample. In the case of competitive immunoassays, NPs have been employed to create complexes in the sample, which are then incubated on the sensor surface with the immobilized Ag.

The advantages these methods offer over conventional immunoassays include:

- **Monitoring**: Each step of the immunoassay can be monitored due to the signal change in ΔIROP (%). This allows for tracking the assay's progress, ensuring proper immobilization and recognition.
- **Blocking stage**: When working with very small surfaces, depending on the assay type, it's possible to eliminate the blocking stage, reducing the time needed to perform the immunoassay.

- **Multiplexing**: Biosensors can be designed to determine various biomarkers in one or two samples simultaneously, or alternatively, a single marker can be measured across a larger number of samples. Depending on the analysis required, the most suitable markers for each condition can be chosen.
- **Sample**: Compared to traditional methods, much lower sample volumes are used (1-2 µL per cell). This enables the measurement of many more markers when sample quantities are limited.

3. Case I. Development of an *in-vitro* optical diagnostic system for the detection of specific Abs against SARS-CoV-2

3.1. Introduction

There are numerous diseases that attack our bodies, challenging our immune system. Among the agents capable of causing infections are viruses, which overcome the natural barriers of our bodies to create diseases while evading the immune system. **The development of these infections is determined by the established relationship between the virus and the host, as well as the host's response to the infection**. The immune system's ability to control the infection will define the severity and duration of the illness. **Most symptoms that develop originate from the inflammatory response triggered by the viral infection**. Additionally, we must consider the host's susceptibility, which relies significantly on different factors (Baron, 1996):

- Exposure site and the infection mechanism.
- Intrinsic factors such as age, health condition, genetic predisposition, or the state of the immune system.
- Virus-dependent factors, such as the strain type causing the infection.

Furthermore, the nature and severity of these symptoms are also related to the specific affected organ. However, there are infections that can progress without symptoms because the infection may have been controlled before the target organ is infected. In such cases, these infections are a significant source of contagion and transmission (Baron, 1996).

Viruses can cause hundreds of thousands of deaths per year, leading to a significant transformation in diagnostic methods (Figure 39). Currently, there are several sensitive and accurate options available. These include cellular cultures, the detection of viral Ags or their genome, and cytological techniques (James H. & Ellen G., 2020).

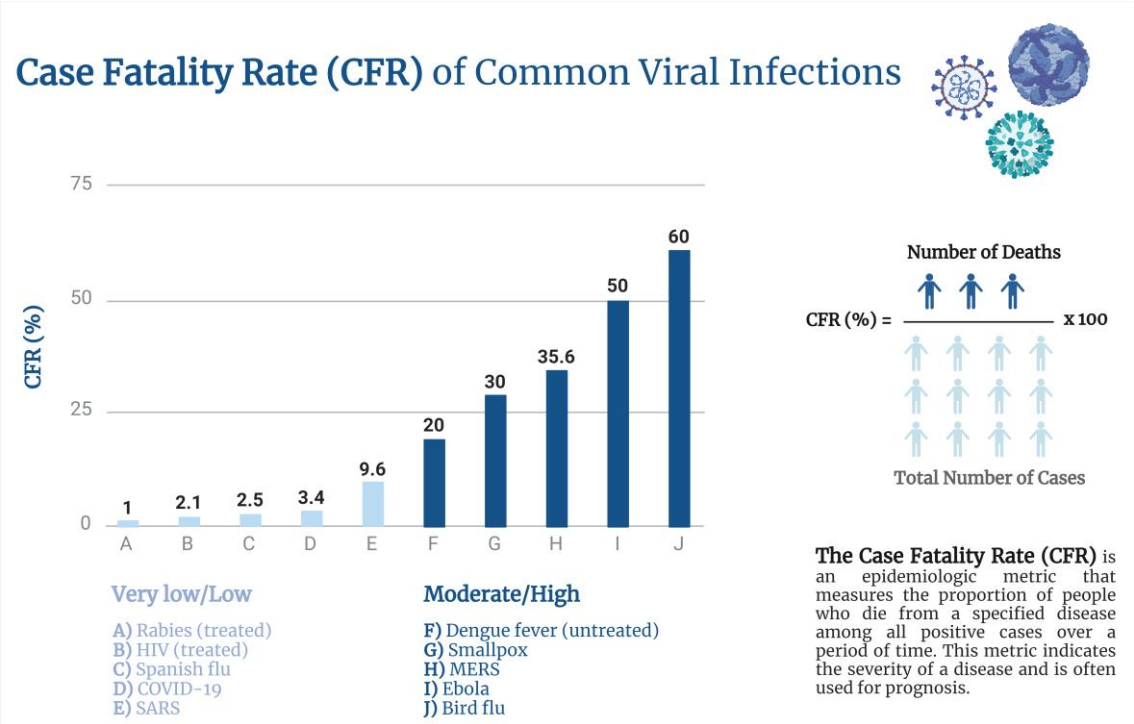

Figure 39. Case Fatality Rate (CFR) of common viral infections (WHO, 2024)**.** Created with BioRender.com.

In recent years, there **has been significant progress in the development of biosensors for the detection and identification of viral particles**. These biosensors can have diverse designs and significantly reduce sample analysis times, achieving high sensitivity and specificity.

Currently, biosensors have been developed for the detection of the Human Immunodeficiency Virus (HIV) (Babamiri et al., 2018), hepatitis B (Yao & Fu, 2014), and Dengue (Lim et al., 2018), among many others.

During the beginning of the development of this doctoral thesis a pandemic due to SARS-CoV-2 hit the world population, causing a massive collapse of the health care systems due to the high number of admissions, in addition to all the deaths that occurred. This combined with the great progress that has been taking place in the field of biosensors were the motivation to develop an *in-vitro* optical detection system for the detection of specific Abs against SARS-CoV-2 in both serum and saliva, as well as the detection of different markers involved in the progression of the infection with the aim of establishing a severity prediction model for the disease.

3.2. Viruses

Viruses are submicroscopic infectious agents defined as obligate intracellular parasites, as they require the cell's machinery to carry out the replication of their genome and utilize its metabolism.

Their basic structural unit is the virion, and they can replicate in animal, plant, or bacterial cells (Chappell & Dermody, 2015; Wang-Shick, 2017a).

They consist of two main components: firstly, coiled genetic material, which can be either DNA or RNA (single or double-stranded), found inside a protein coat called a capsid (they lack organelles). Additionally, some viruses may have a lipid envelope derived from the host cell they have infected, facilitating the infection of other cells belonging to the same cellular lineage (Wang-Shick, 2017a) (Figure 40).

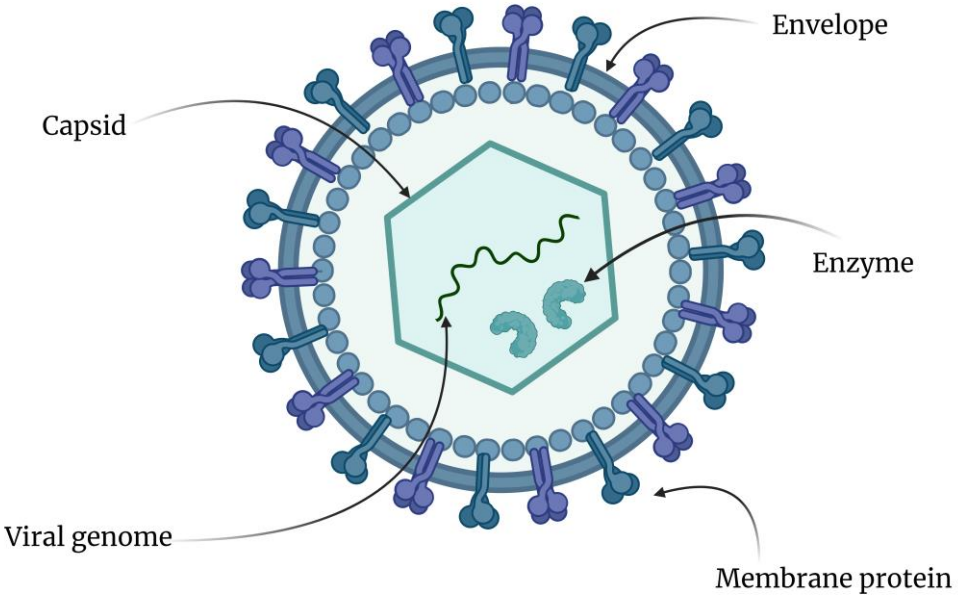

Figure 40. Generic viral structure. Created with BioRender.com.

Viruses can enter cells through different mechanisms depending on whether they have a lipid envelope. Generally, they interact with proteins on the cell surface, triggering internalization mechanisms and evading the destruction process typically carried out by the cell. **Generally, the virus infection process involves the following steps** (Cohen, 2016; Dimitrov, 2004; Wang-Shick, 2017b)(Figure 41):

1. Interaction with the cell.
2. Internalization and entry into the cell.
3. Use of the infected cell's machinery to transcribe viral genes into messenger RNA (mRNA).
4. Translation of transcribed mRNA into viral proteins.
5. Packaging of the replicated genome and assembly with translated proteins to form virions.
6. Release of these virions from the infected cell to infect other cells in the organism.

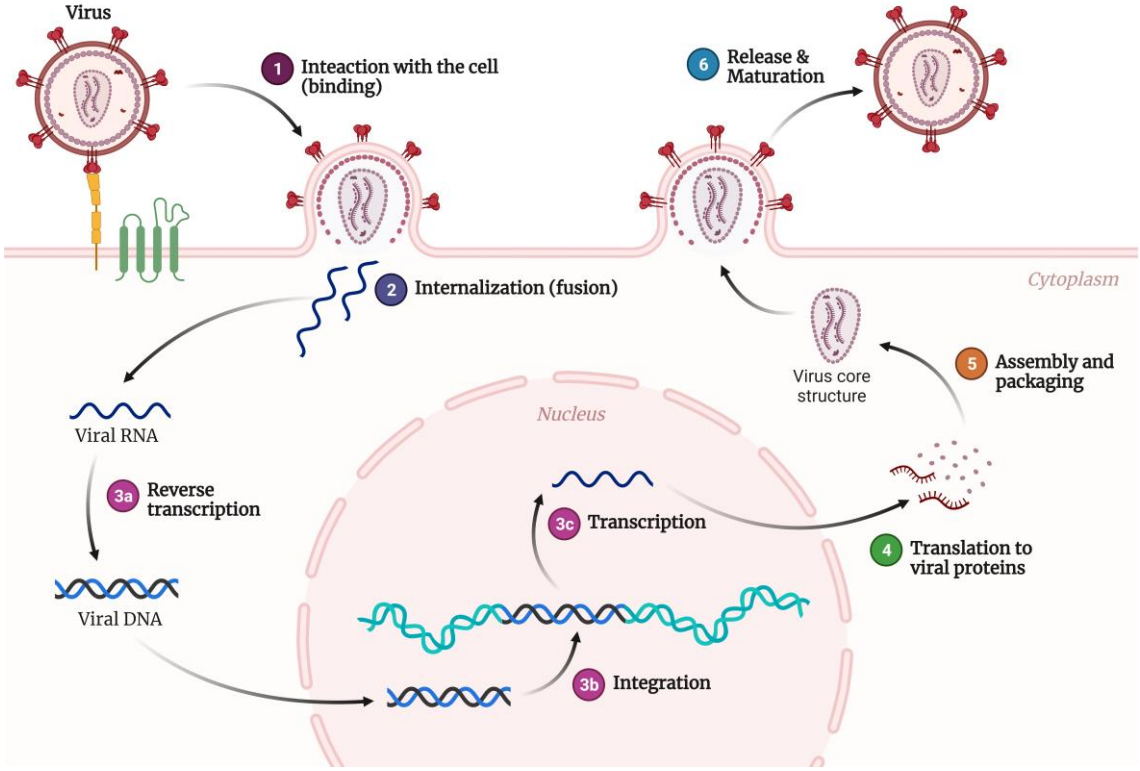

Figure 41. Virus replication cycle. Created with BioRender.com.

They can exit the cell through cell lysis, either directly or through budding (taking part of the cell's lipid membrane). On the other hand, it's possible for the virus to remain latent within cells without exiting or causing cell death, or for the cell to trigger apoptosis before virions are produced.

3.2.1. Classification

The classification of viruses can be done according to different criteria. One of the most established methods is the **Baltimore Classification (BC)**, which considers the type and structure of the virus's nucleic acid and the method of mRNA transcription (Koonin et al., 2021)(Table 5).

Table 5. Baltimore Classification (Koonin et al., 2021).

BC	***Viral nucleic acid***	***Genome structure kb***	***Genome size***	***Host range***
I	dsDNA	Mostly linear	5-2.500	Bacteria, archaea, protists, and animals
II	ssDNA	Mostly circular	1.7-25	Bacteria, rare in archaea and most eukaryotes
III	dsRNA	Linear	4-30	Protists, animals, and plants
IV	(+) RNA	Linear	3.5-40	All eukaryotes and bacteria
V	(-) RNA	Mostly linear	1.7-20	Animals and plants
VI	(+) RNA, RT	Linear	5-13	All eukaryotes
VII	dsDNA, RT	Circular	3-10	Animals and plants

Other types of classifications are based on the virus capsid structure (helical or icosahedral) (Louten, 2016), the type of cell they infect (animal, plant, bacteria) (Ackermann, 2005; Chappell & Dermody, 2015; Wang-Shick, 2017a), or whether they have a lipid envelope or not (Lucas & Knipe, 2002).

3.2.2. Coronavirus

The Orthocoronavirinae viruses, commonly known as **coronaviruses**, belong to a virus subfamily characterized by a single-stranded positive-sense RNA genome ranging from 27 to 32 Kb and a size ranging from 60 to 200 nm. They are part of the Coronaviridae family and are identified by their crown-like appearance under electron microscopy. These viruses are capable of infecting birds and mammals (Weiss & Leibowitz, 2011).

Their genome encodes for **four types of proteins** (Yoshimoto, 2020)(Figure 42):

- Spike protein (S)
- Envelope protein (E)
- Membrane protein (M)
- Nucleocapsid protein (N)

Within the envelope of these viruses, at least three protein structures are found: the M protein, the E protein involved in viral assembly, and the S protein (glycoprotein), which binds to host cell receptors, causing membrane fusion and allowing the virus to enter the cell.

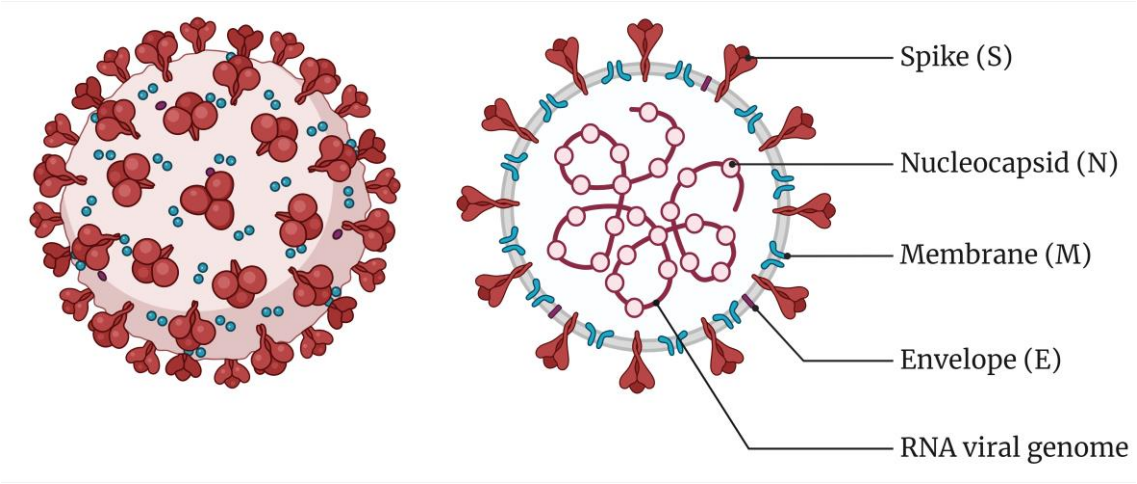

Figure 42. Coronavirus structure. Created with BioRender.com.

Human Coronaviruses (HCoV) were first described in the 1960s in patients with the common cold. Currently, **coronaviruses account for about one-third of all cases of the common cold.** However, they can also cause more severe respiratory diseases such as bronchitis or pneumonia, particularly in high-risk patients, including immunocompromised individuals and the elderly. They have also been associated with diseases affecting the intestines or the nervous system (Kahn & McIntosh, 2005; Mahase, 2020).

Currently, seven strains causing respiratory illnesses in humans have been identified and registered (Table 6) (Kahn & McIntosh, 2005; Santacroce et al., 2021).

Table 6. Coronavirus strains are described as pathogenic to humans (Santacroce et al., 2021).

Strain	***Genus/subgenus***	***Infect***
Severe Acute Respiratory Syndrome Coronavirus infection (SARS-CoV)	Betacoronavirus/ Sarbecovirus	Humans and mammals
Severe Acute Respiratory Syndrome Coronavirus 2 (SARS-CoV-2)	Betacoronavirus/ Sarbecovirus	Humans and animals
Human Coronavirus HKU1 (HCoV-HKU1)	Betacoronavirus/ Embecovirus	Humans, mice
Human Coronavirus 229E (HCoV-229E)	Alphacoronavirus/ Duvinacovirus	Humans, bats
Human Coronavirus NL63 (HCoV-NL63)	Alphacoronavirus/ Setracovirus	Humans
Human Coronavirus OC43 (HCoV-OC43)	Betacoronavirus/ Embecovirus	Humans, cattle

3.2.2.1. *Coronavirus diseases*

Each of the previously mentioned types of coronaviruses causes diseases in humans at varying levels (Santacroce et al., 2021):

- **HCoV-229E**: This strain is one of the causes of the common cold and can lead to bronchitis or pneumonia (D. X. Liu et al., 2020).
- **HCoV-OC43**: Also responsible for the common cold and can lead to pneumonia in high-risk patients (D. X. Liu et al., 2020).
- **SARS-CoV**: Responsible for the major epidemic of 2002-2004 originating in China, causing the death of at least 10-15% of those infected. It resulted in pneumonia, hypoxia, and high fevers. No severe cases have been recorded since 2005 (Pandurangan et al., 2004).
- **HCoV-NL63**: Associated with a mild respiratory syndrome similar to the flu (Van Der Hoek et al., 2006).
- **HCoV-HKU1**: Causes clinically mild infections, but deaths due to pneumonia have been reported (Woo et al., 2009).
- **MERS-CoV**: From 2012 to 2017, it was attributed to a 30% mortality rate among infected individuals. It is considered a zoonotic disease, and symptoms can vary from fever, and gastrointestinal and respiratory problems to progressing to pneumonia and Acute Respiratory Distress Syndrome (ARDS) (Drosten et al., 2013).
- **SARS-CoV-2**: Causes **COVID-19** and also originated as a zoonotic disease. Symptoms include pneumonia, ARDS, and persistent COVID-19. It had a mortality rate between 3-5% (Gorbalenya et al., 2020).

3.2.2.2. *SARS-CoV-2 and COVID-19*

On March 11, 2020, the WHO declared a global pandemic caused by the SARS-CoV-2 (WHO, 2020). **SARS-CoV-2 is an RNA virus from the coronavirus family that infects both humans and animals, causing COVID-19**. It originated around December 2019 in the city of Wuhan, Hubei Province, Central China, where a large number of pneumonia cases of unknown cause were reported. The sequencing of the virus genome led to the identification and description of SARS-CoV-2 (H. Li et al., 2020).

The most supported evidence suggests that SARS-CoV-2 is a virus originating from bats and, through an unknown intermediary, managed to infect humans, **becoming a zoonotic disease** (L. Zhang & Guo, 2020).

SARS-CoV-2 is **composed of five proteins with different functions** (Table 7). These include the S protein, the N protein, the E protein, the M protein, and the Hemagglutinin-Esterase dimer (HE) (Ravi et al., 2020).

Table 7. Function of SARS-CoV-2 proteins (Ravi et al., 2020).

Virus protein	*Binding site*	*Function*
Spike protein (S)	It uses the n-terminal fragment to access the endoplasmic reticulum	Facilitates virus binding to the host cell receptor
Nucleocapsid protein (N)	Binds the viral genome	Binds the viral genome to the replicase-transcriptase complex and encapsulates the genome into viral particles
Envelope protein (E)	It is a transmembrane protein that has ion channel activity	Significant role in the assembly and release of the virus
Membrane protein (M)	It binds to the nucleocapsid	Holds the curvature of the membrane and the attachment to the nucleocapsid
Hemagglutinin- esterase dimer protein (HE)	Binds to sialic acids of surface glycoproteins	It promotes the entry of the virus into the host cell and its propagation

The most studied protein is the **S protein, as it's the one the virus uses to interact with the host organism's cell and infect it** (L. Zhang & Guo, 2020). It's a transmembrane glycoprotein consisting of 1273 aa and a high rate of glycosylation (Jun Zhang et al., 2021). It's divided into two subunits (S1 and S2). S1 is involved in the recognition and binding of the virus to the cell, while S2 is implicated in the fusion of the two membranes. S1 consists of two distinct structural domains: the N-Terminal galectin-like Domain (S-NTD) as a stabilizer of S2, and two C-Terminal Domains (CTD1 and CTD2) used as the Receptor-Binding Domain (RBD). On the other hand, S2 has four different regions, including a transmembrane region, a Fusion Peptide (FP), and two Heptad Domains (H1 and H2) (Arya et al., 2021; Jackson et al., 2022)(Figure 43).

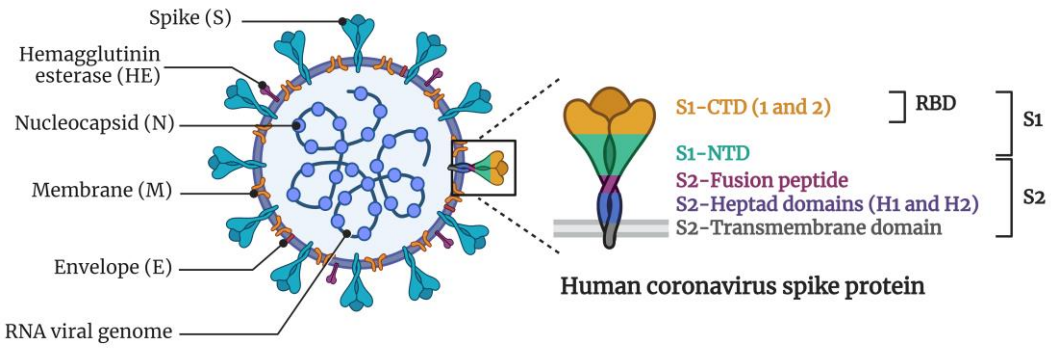

Figure 43. S protein structure. Created with BioRender.com.

To initiate infection, virus cells first interact with healthy host cells using the S protein (RBD), binding to the Angiotensin-Converting Enzyme 2 (ACE2) receptor (L. Zhang & Guo, 2020). This leads to the fusion of membranes, allowing the virus's genome to enter the host cell, enabling it to utilize the host's replication machinery and form new viral particles (Jackson et al., 2022)(Figure 44).

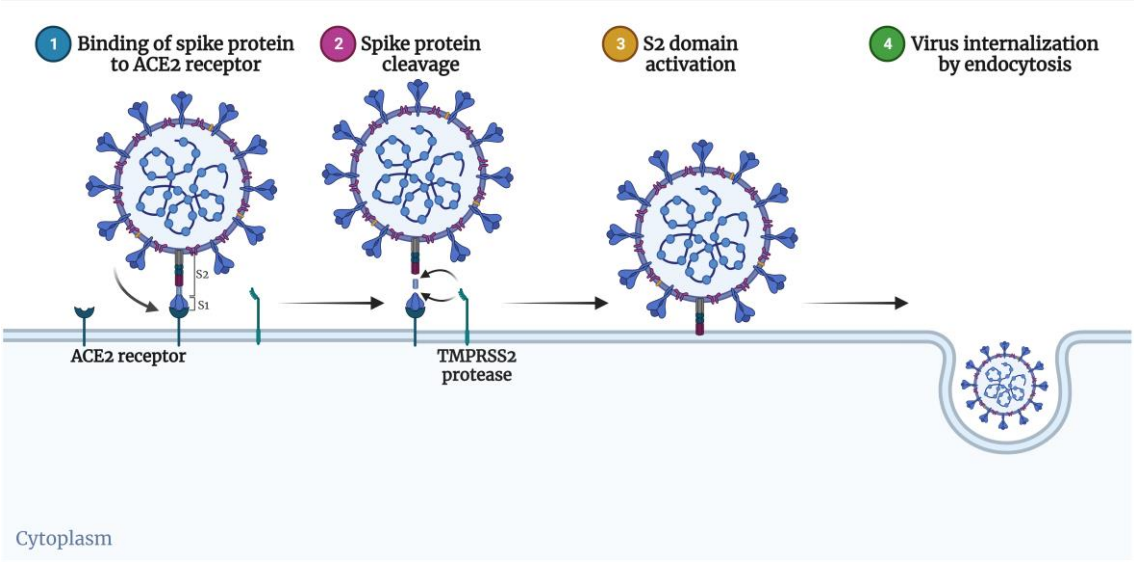

Figure 44. Mechanism of SARS-CoV-2 entry. Created with BioRender.com.

The expression of the ACE2 receptor is predominantly found in type II alveolar cells in the lower region of the lungs and in ciliated cells of the bronchial and nasal epithelium. Hence, the infection primarily targets nasal epithelial cells, progressing from there. Additionally, many other cell types express this receptor, such as those in the kidney, intestine, and brain. This indicates that there's increasing evidence suggesting it's a disease that can affect multiple organs (Jackson et al., 2022; Lamers & Haagmans, 2022).

Due to this, symptoms caused by **SARS-CoV-2 affect different systems and organs, being nonspecific with a large number of asymptomatic cases**. The most common symptoms are fever and cough, significantly affecting the respiratory tract, leading to breathing difficulties, lack of O_2, and pneumonia, which can result in death (Wu et al., 2020). Additionally, there are neurological symptoms such as loss of smell and taste, muscle pain, headaches, and dizziness. Complications of these symptoms can trigger cerebrovascular diseases (Harapan & Yoo, 2021). Other less common but found symptoms include diarrhea and hemoptysis. All these symptoms can result in a range of disease severity from mild to moderate or severe. Severity also depends on whether hospitalization or Intensive Care Unit (ICU) admission is required (Wu et al., 2020).

During the early stages of the pandemic, treatment primarily involved rest, the use of pain relievers such as ibuprofen, antiviral therapies, respiratory support, and O_2 supplementation, among other measures (Adedeji et al., 2021; Wu et al., 2020).

By that time, the disease had already spread to numerous countries, resulting in a total of 7,042,222 deaths and 775,132,086 infections reported up to today in 2024 (WHO, 2024). Given the severity of the global situation, the entire scientific community dedicated itself to numerous studies, focusing on analyzing the virus and its genome, exploring treatments, developing vaccines, and creating multiple rapid and reliable diagnostic systems.

3.2.2.2.1 Biomarkers and samples used for the diagnosis

Due to the high contagion rate and the significant mortality caused by the virus infection, it became crucial to rapidly establish biomarkers that could inform us about the infection and prognosis, as well as identify the types of samples where these markers could be measured (Semiz, 2022). **Biomarkers are defined as any objective measure serving as an indicator of a biological process, whether pathological or normal or an indicator of treatment response** (L. Zhang & Guo, 2020). Additionally, identifying the best markers allowed for the classification of patients into mild, moderate, and severe categories (Kermali et al., 2020). This knowledge is vital as it aids in the development of new medications and vaccines (L. Zhang & Guo, 2020).

These biomarkers can be classified based on the degree of disease involvement, their originating system, or clinical symptoms. Among the markers associated with COVID-19 and its severity are **increased levels of C-Reactive Protein (CRP) and the activity of Aspartate AminoTransferase (AST) and Alanine AminoTransferase (ALT) enzymes** (Semiz, 2022). Other authors also link disease severity with increased white blood cells, neutrophil counts, and D-dimer levels. Additionally, various interleukins **(IL-6, IL-4, and IL-8)** show elevated levels (Kermali et al., 2020).

The markers **most associated with mortality** have been D-dimer, IL-6, and creatinine, which are elevated in these cases, as well **as Ferritin (FTH1)** (Semiz, 2022). In the following table, they are also ordered depending on the part of the body where damage is occurring and clinical implications (Table 8) (Battaglini et al., 2022).

Table 8. Impaired organ function, a biomarker of that alteration, and its clinical significance (Battaglini et al., 2022).

Impaired function	*Biomarker*	*Clinical significance*
Pulmonary	Amino Transferase	Mortality at admission
	Ferritin	Survival at extubation
	D-dimer	Survival at extubation
Cardiovascular	Troponins	Cardiovascular disease, inflammation, mortality
	D-dimer	Prognosis
Neurological	C-Reactive Protein	Ischemic stroke
Kidney and liver	Creatinine	Acute kidney injury, mortality
Coagulation and hemostasis	Fibrinogen	Hyperinflammation, severity

The most crucial biomarker to directly determine if the virus infection has occurred is its RNA. Additionally, viral proteins are also a significant alternative for diagnosing COVID-19 (L. Zhang & Guo, 2020).

To detect all these markers, different types of samples have been used, such as serum or plasma, nasopharyngeal swabs, sputum, bronchoalveolar lavage, saliva, feces, or urine (Martinez, 2020; L. Zhang & Guo, 2020).

3.2.2.2.2 Diagnostic systems against COVID-19

The first thing to consider is that, thanks to the advancements available today, the virus could be characterized more rapidly. However, due to supply issues, the use of necessary diagnostic tests was delayed worldwide (Jayamohan et al., 2021). Initially, the strategy for developing diagnostic methods **focused on detecting the virus's RNA**, which later diversified to detect different viral proteins and Abs produced during the infection (Jalandra et al., 2020).

Among the most established and used diagnostic tests are the **Polymerase Chain Reaction (PCR),** using the virus genome, and detection using the **ELISA technique** for different biomarkers (Figure 45) (Jayamohan et al., 2021). Additionally, biosensors are a powerful tool for diagnosis, capable of performing rapid analysis with high sensitivity, stability, and cost-effectiveness. Their performance has improved over the years, making them a highly valid and suitable instrument for diagnosis (Saylan et al., 2019).

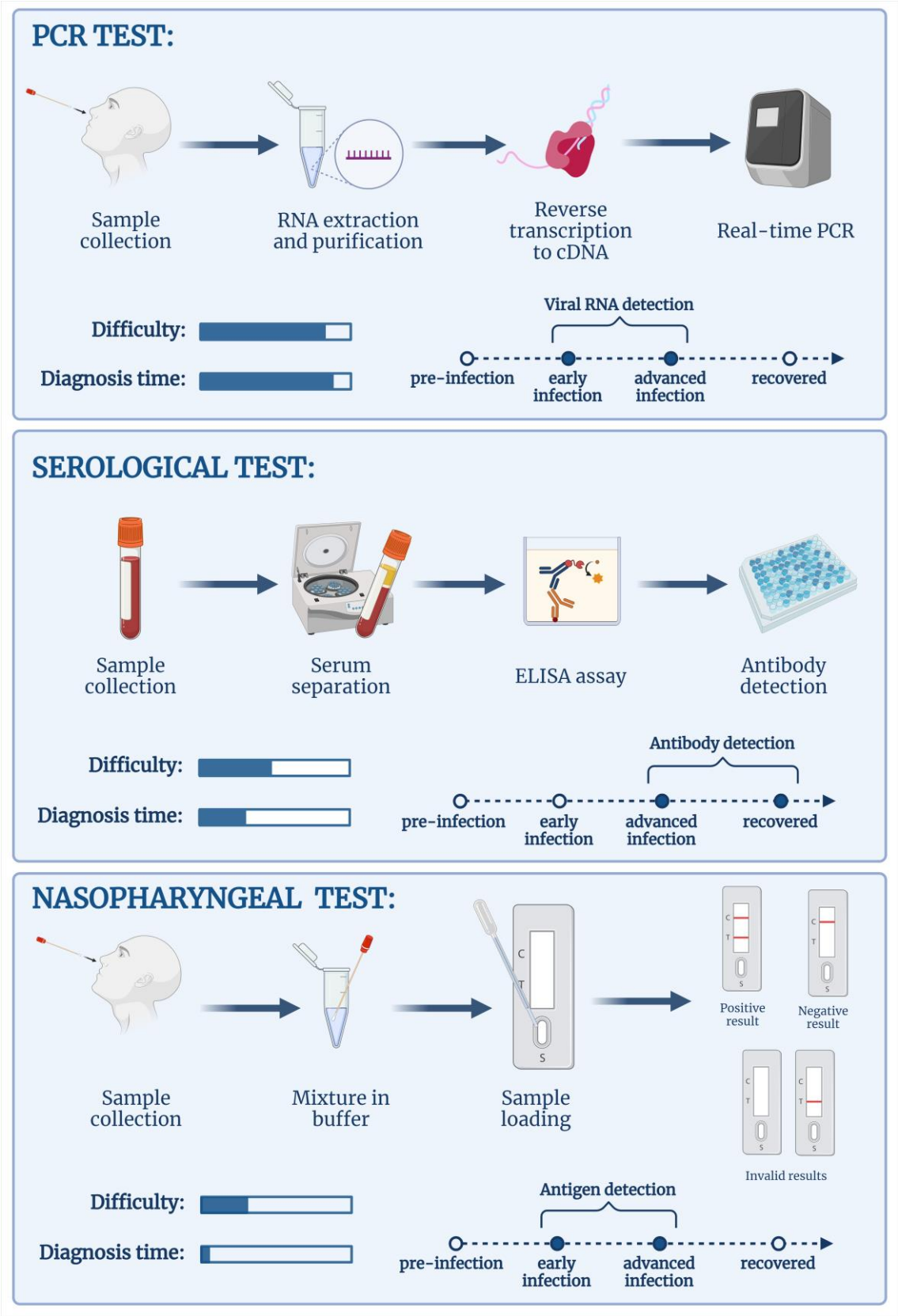

Figure 45. Detection methods for SARS-CoV-2 infection. Created with BioRender.com.

Here is a general classification of different diagnostic techniques for SARS-CoV-2:

- **Molecular diagnostic tools**:
  - Methods based on amplification of the virus's nucleic acid: the most commonly used technique is Real Time-PCR (RT-PCR) (Ravi et al., 2020).
  - Reverse Transcription Loop-Mediated Isothermal Amplification (RT-LAMP) (Eftekhari et al., 2021).
  - Clustered Regularly Interspaced Short Palindromic Repeats (CRISPR) technique (Jalandra et al., 2020).
  - Next-Generation Sequencing (NGS) (Jayamohan et al., 2021).
  - Nucleic acid hybridization of the virus on microarrays (Eftekhari et al., 2021).
  - Ag detection: typically, these are immunoassays based on the detection of viral proteins (Jayamohan et al., 2021).
- **Tools based on serological diagnosis**:
  - Ab detection: specific Abs against the virus are detected using techniques such as ELISA or CLIA (Ravi et al., 2020).
- **Cell culture tools**:
  - Virus cultivation from nasopharyngeal samples to study the cytopathic effect of the virus (Mathuria et al., 2020).
- **Tools based on nanotechnology and nanomaterials**:
  - They rely on the use of very small particles for protein detection, such as Au NPs (Eftekhari et al., 2021; Moitra et al., 2020).
- **Tools based on biosensors and point-of-care devices**:
  - Biosensors to measure inflammation markers like CRP (Boonkaew et al., 2019), IL-6 (M. A. Khan & Mujahid, 2020), or FTH1 (Boonkaew et al., 2020).
  - Biosensors to measure viral proteins like RBD (Akib et al., 2021), S protein (Rahmati et al., 2021), or N protein (Murugan et al., 2020).
  - Biosensors to measure specific Abs against SARS-CoV-2 (M. A. Ali et al., 2021; Kontou et al., 2020).
  - Biosensors to measure the virus's nucleic acid (Falasca et al., 2020; Kashefi-Kheyrabadi et al., 2022).

In summary, all these systems provide the necessary data to understand the progression of the disease and establish necessary treatments. However, each technique has its advantages and limitations, so clinical units continue constant research and development of new tests to address these limitations.

During the development of this thesis, a biosensor was developed as a diagnostic system capable of measuring both specific Abs against the virus and inflammation markers present in serum due to the infection. Among the advantages of this biosensor is the low amount of sample used for the determinations, thus allowing the screening of a greater number of markers per sample in a short time. It also allows customized design for use against different specific biomarkers.

3.3. Materials and Methods

3.3.1. Case I. I. Development of an *in-vitro* optical diagnostic system for the detection of specific Abs against SARS-CoV-2 in serum

Here are the steps followed during this doctoral thesis for the development of an *in-vitro* diagnostic system based on a previously described optical interferometric biosensor. For this purpose, a multiplexed KIT was designed, in which specific Abs against SARS-CoV-2 and biomarkers related to the disease were measured in serum samples to establish a severity prediction model for the illness.

3.3.1.1. *Production of recombinant S protein from the virus using Pichia pastoris*

The first step was to produce the virus protein through recombinant methods by Araceli Díaz Perales's group at the Centro de Biotecnología y Genómica de Plantas (CBGP-UPM). Isabel Solá from the Consejo Superior de Investigaciones Científicas-Centro Nacional de Biotecnología (CSIC-CNB), donated the complementary DNA (cDNA) of SARS-CoV-2. The S gene's truncated region was then amplified using PCR. After cloning into the pPICZalpha plasmid vector, the cells of *P. pastoris* Bg11 were electro-transformed. As previously described, two fragments were produced: one corresponding to the larger epitope and another to the smaller one (Murillo et al., 2021).

The SARS-CoV-2 recombinant S proteins (rS1 and rS2) were purified from yeast culture media supernatants and isolated through chromatography. The supernatants were then dialyzed against 0.1 M ammonium acetate (pH 6.8) for 8 hours at 4˚C using a Spectrum Labs Spectra/6–8 kD Molecular Weight Cut-Off (MWCO) RC Dry dialysis membrane (Fisher Scientific, Waltham, MA, USA). The supernatants were then lyophilized and fractionated using size exclusion chromatography. The Sephacryl S-200 High Resolution system (GE Healthcare in Chicago, IL, USA) was used with 0.1 M ammonium acetate at a flow rate of 1 mL/min, resulting in 5 mL fractions (Murillo et al., 2021).

The fractions were quantified using the Bicinchoninic Acid Test (BCA) (Thermo Scientific, Waltham, MA, USA). Coomassie staining and immunoassays were used to analyze the fractions with specific Abs against the recombinant proteins produced from SARS-CoV-2 (Invitrogen, Thermo Fisher, Carlsbad, CA, USA).

The protein's quality was assessed using Matrix-Assisted Laser Desorption/Ionization Time-Of-Flight (MALDI-TOF) mass spectrometry. The identity was confirmed using peptide mass fingerprinting analysis. An Ultraflex workstation (Bruker Daltonics, Bremen, Germany) equipped with a 337 nm nitrogen laser was used, following standard methods. Sample analysis and analytical method parameter control were carried out using FlexControl Software version 2.4 (Bruker Daltonics).

3.3.1.2. *ELISA of recombinant protein activity assays*

To prepare the plates, 96-well plates (Costar 3590) (Corning, NY, USA) were coated with 50 µL of purified virus rS1 protein at a concentration of 5 µg/mL. The plates were incubated for 2 hours at 37˚C. Next, block the plates with 1x casein hydrolysate (Sigma-Aldrich, St. Louis, MO, USA) for 1 hour at Room Temperature (RT). After blocking, the plates were washed three times with Phosphate Buffer Saline-Tween 0.05% (PBS-T) (200 µL/well) (Sigma-Aldrich). Finally, the plates were incubated with saliva samples at a dilution of 1:10 Overnight (ON) at 4˚C. To detect the presence of specific IgA (sIgA) Abs, the plates were incubated with polyclonal anti-Human-IgA (αHuman-IgA) secondary Ab conjugated with Horseradish Peroxidase (HRP) (αHuman-IgA-HRP) (Sigma-Aldrich) for 1 hour at RT. The plates were washed again, and the recognition was revealed using 50 µL of 3,3',5,5' Tetrametilbenzidina (TMB) (Thermo Scientific). After 30 minutes (min), the reaction was stopped with 50 µL of 2 N HCl, and the OD was measured at 450 nm (Figure 46)(Murillo et al., 2021).

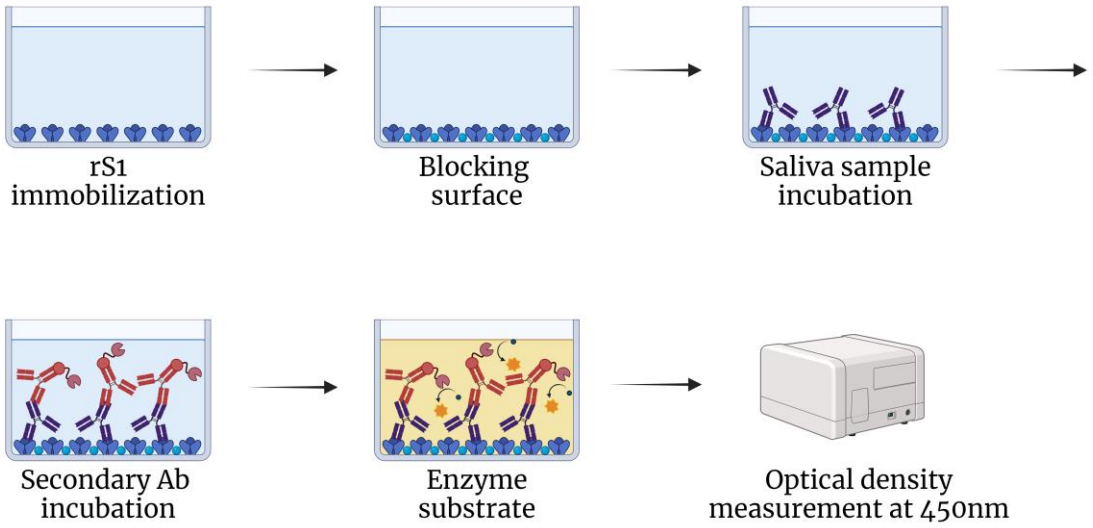

Figure 46. Diagram followed for the detection of SARS-CoV-2 sIgA in saliva. Created with BioRender.com.

A Negative Control (NC) was performed by coating the wells with 50 µL of 1x casein hydrolysate. In none of the cases, signals greater than 0.1 absorbance units were obtained. The represented data are the values obtained after subtracting the NC value. Measurements were performed in triplicates.

3.3.1.3. *Human serum samples*

The serum samples were provided by the Biobank of the Institute of Health Research, belonging to the Hospital Clínico San Carlos in Madrid (B.0000725; PT17/0015/0040; ISCIII-FEDER). The clinical studies were approved by the local ethics committee of the Hospital Clínico San Carlos (20/404-E_COVID). A total of 74 samples confirmed by PCR for SARS-CoV-2 infection and 20

blood donors from February 2020 were provided. These samples were classified according to clinical diagnostic criteria as moderate, severe, or mild cases. Age, sex, radiological findings (alveolar infiltrates), and blood group information were also recorded following legal ethical regulations with the collaboration of the Instituto de Medicina de Laboratorio (IML) and the innovation unit of the Hospital Clínico San Carlos (Murillo et al., 2021).

Upon receiving the serum samples, they were thawed and treated at 56°C to inactivate the complement and reduce potential risks from any viral residues. The presence of the virus infection in these patients was confirmed by PCR.

3.3.1.4. *Immobilization of the virus proteins on the sensor surface (dose-response curves)*

The next step performed was the incubation of the virus proteins to establish the immobilization signal obtained. The analyzed proteins were named rS1 and rS2. These were incubated in 16-BICELLs KITs of 200 µm at different concentrations (2.5 µL at 100, 50, and 25 µg/mL) and left for 1 hour and 30 min at 37°C in a humid chamber. Then they were washed with an H_2O MiliQ (H_2OmQ) syringe, agitated in H_2OmQ for 45 seconds (s), and dried with filtered compressed air. In this way, we have the dose-response curve of the two proteins. Additionally, the same test was also performed following the same protocol, but with an incubation period of 2 hours to see if we obtained a higher signal and better surface coating (Table 9). All measurements were performed in four replicates.

Table 9. Conditions applied for the dose-response curve.

Protein	*Incubation time (min)*	*Concentration (µg/mL)*	*Volume (µL)*	*Temperature (°C)*
rS1	90	100, 50, 25	2.5	37
	120	100, 50, 25	2.5	37
rS2	90	100, 50, 25	2.5	37
	120	100, 50, 25	2.5	37

3.3.1.5. *Recognition tests in KITs using positive serum sample against rS1 and rS2 proteins*

Immobilized KITs with both viral proteins (rS1 and rS2) under two conditions (1 hour and 30 min and 2 hours) were blocked with 1x casein hydrolysate for 1 hour with agitation. Then, they were washed in the same manner as described earlier for the immobilization stage, and the positive control (PC) serum was incubated at a 1:20 dilution (2.5 µL) on the sensor surface with the immobilized viral protein and on a NC protein (tau) (Sigma-Aldrich). Serum samples were incubated for 3 hours at 37°C in a humid chamber.

Afterward, the KITs were washed with a 20 mL syringe of H_2OmQ, agitated for 10 min with Phosphate Buffer Saline (PBS) (Sigma-Aldrich), and washed again with two 20 mL syringes of H_2OmQ. They were dried with compressed filtered air, and the ΔIROP (%) recognition values

were read. Finally, secondary Abs were incubated against human specific IgG (sIgG) and specific IgM (sIgM), using anti-Human-IgG (αHuman-IgG) (1:1500) and anti-Human-IgM (αHuman-IgM) (1:5000) respectively (Sigma-Aldrich), incubating 2.5 µL for 1 hour at 37°C in a humid chamber. Finally, the KITs were washed with 40 mL of PBS-T 0.05% and 40 mL of H_2OmQ, dried with compressed filtered air, and the recognition values for each of the secondary Abs were read (Table 10).

Table 10. Conditions for the first test in KITs.

Incubation step	*Incubation time (min)*	*Dilution*	*Volume (µL)*	*Temperature (°C)*
Blocking	60	1	20000	RT
PC serum	180	1:20	2.5	37
αHuman-IgG	60	1:1500	2.5	37
αHuman-IgM	60	1:5000	2.5	37

In a second instance, the experiment was repeated, modifying certain conditions. The KITs were incubated with proteins rS1 and rS2 (2.5 µL at 100 µg/mL) for 3 hours at 37°C in a humid chamber. Tau protein (2.5 µL at 50 µg/mL) was used as the control protein. After immobilizing the protein and carrying out the washes as described earlier, the KITs were blocked with casein hydrolysate 1x for 1 hour with agitation. Following wash step, 2.5 µL of serum per well was incubated at a 1:10 dilution for 3 hours at 37°C in a humid chamber. In addition to testing the PC serum, a NC serum was also used (both tested via ELISA and PCR). The same washing steps were repeated, and the secondary Abs αHuman-IgG (1:1500), αHuman-IgM (1:5000), and αHuman-IgA (1:2000) were incubated under the same conditions described earlier to recognize the specific Igs against the viral protein. Afterward, the same wash with PBS-T 0.05% and H_2OmQ was performed, the KITs were dried, and the ΔIROP (%) signal was measured (Table 11).

Table 11. Conditions used in the second experiment.

Incubation step	*Incubation time (min)*	*Concentration (µg/mL) and Dilution*	*Volume (µL)*	*Temperature (°C)*
rS1 and rS2	180	100	2.5	37
Blocking	60	1	20000	RT
PC serum	180	1:10	2.5	37
NC serum	180	1:10	2.5	37
αHuman-IgG	60	1:1500	2.5	37
αHuman-IgM	60	1:5000	2.5	37
αHuman-IgA	60	1:2000	2.5	37

For the subsequent tests involving changes in washing and increased concentration of secondary Abs, KITs with 16-BICELLs of 200 µm were immobilized with protein rS1 at 100 µg/mL (2.5 µL) for 3 hours at 37°C in a humid chamber. They were washed following the same procedure described earlier for the immobilization stage. As a NC, tau protein (2.5 µL at 50 µg/mL) was incubated in the same KITs. Then, they were blocked with 1x casein hydrolysate for 1 hour at RT with agitation. The washing and drying process remained the same as previously mentioned.

Next, in the recognition stage, two PC sera called Positive Control 1 (PC1) and Positive Control 2 (PC2), as well as a NC serum, were incubated. The same dilution and incubation time procedure was followed, and then they were washed with a 20 mL syringe of H_2OmQ, soaked in PBS for 10 min with agitation, and rinsed with 40 mL of H_2OmQ. Finally, they were dried with filtered compressed air.

Finally, in the development step, the secondary Abs against sIgG and sIgM were incubated, increasing their concentration (αHuman-IgG at 1:250, αHuman-IgM at 1:500), maintaining the volume but changing the incubation time to 2 hours under the same conditions as the previous assays. Similarly, they were washed and dried as described earlier. After each immobilization, recognition, and development stage, the ΔIROP (%) signals were read (Table 12). All measurements were performed in four replicates.

Table 12. Conditions used in the third experiment.

Incubation step	*Incubation time (min)*	*Concentration (µg/mL) and Dilution*	*Volume (µL)*	*Temperature (°C)*
rS1 and rS2	180	100	2.5	37
Blocking	60	1	20000	RT
PC1 serum	180	1:10	2.5	37
PC2 serum	180	1:10	2.5	37
NC serum	180	1:10	2.5	37
αHuman-IgG	120	1:250	2.5	37
αHuman-IgM	120	1:500	2.5	37

In Table 13, a summary of the wash selected for each step of the experiment is shown.

Table 13. Summary of selected washes in each incubation step.

Incubation step	*Rinsing*	*Washing*	*Rinsing*	*Drying*
Immobilization	20 mL H_2OmQ	45 s in H_2OmQ agitation	-	Compressed air
Blocking	20 mL H_2OmQ	45 s in H_2OmQ agitation	-	Compressed air
Serum	20 mL H_2OmQ	10 min in PBS agitation	40 mL H_2OmQ	Compressed air
Secondary Abs	40 mL PBS-T	-	40 mL H_2OmQ	Compressed air

To automate the process, tests were started using the automated liquid dispensing platform, BioDot AD1520TM. Different immobilization concentrations (100, 50, and 25 µg/mL) and volumes (2.5-1.5-1 µL) were tested. Once the drops were dispensed using the platform, the KITs were left to incubate for 3 hours at 37°C in a humid chamber. The washing and drying procedure for the KITs is the same as described earlier for immobilization. Later on, experiments were conducted by reducing the incubation volume to 1 µL at concentrations of 300-200-100 and 50 µg/mL. All measurements were performed in five replicates.

3.3.1.6. *Recognition tests in KITs using positive and negative serum samples against rRBD*

To establish the immobilization concentration of the recombinant RBD protein (rRBD) (provided by the company BiOD S.L.), a dose-response curve was performed by fixing the incubation volume at 2.5 µL and varying the protein concentration (100-50-25 and 12.5 µg/mL). The incubation was carried out at 37°C for 3 hours in a humid chamber.

After the washing step established for immobilization, the ΔIROP (%) values were read.

Following, the KITs were incubated with the rRBD protein at a concentration of 50 µg/mL (2.5 µL) for 3 hours at 37°C. Subsequently, they were blocked for 1 hour at RT with 1x casein hydrolysate under agitation. After washing, 2.5 µL of serum samples were incubated at a 1:10 dilution for 3 hours at 37°C in a humid chamber. After the incubation period, the KITs were washed with H_2OmQ using a syringe, followed by a 10 min agitation in PBS, and then rinsed with 2 syringes of H_2OmQ. Finally, the ΔIROP (%) values were read after drying the KITs with filtered compressed air.

As a NC, BSA (Sigma-Aldrich) was incubated at 50 µg/mL under the same conditions as described for the rRBD protein. Lastly, the secondary Ab against αHuman-IgG was incubated at a concentration of 1:125 for 2 hours at 37°C in a humid chamber. The KITs were washed and dried following the same procedure as described previously for the secondary Ab recognition step. All measurements were performed in four replicates.

3.3.1.7. *Study of different proteins as NCs*

The KITs were immobilized with both proteins (tau and BSA) (2.5 µL at 50 µg/mL) for 3 hours at 37°C in a humid chamber. Then, the KITs were washed according to the established procedure for the immobilization step, and the PC and NC sera (2.5 µL at a 1:10 dilution) were incubated for 3 hours at 37°C in a humid chamber. All measurements were performed in four replicates.

3.3.1.8. *Measurements of two biomarkers related to SARS-CoV-2 infection: FTH1 and CRP*

KITs with 16-BICELLs of 200 µm were immobilized with 1.5 µL of different concentrations of anti-Human-FTH1 (αHuman-FTH1) and anti-CRP (αHuman-CRP) Abs (Sigma-Aldrich) (100-50-20 and 10 µg/mL) for 1 hour and 30 min and 3 hours at 37˚C in a humid chamber. After that, the KITs were washed and dried using the same procedure described previously for immobilizations. Finally, the ΔIROP (%) values were read.

To measure the protein levels, 1.5 µL of PC and NC serum at a 1:10 dilution was incubated for 3 hours in a humid chamber at 37˚C, and the same washing procedure as described for the recognition step of specific Abs against the virus protein was performed. Once washed and dried, the ΔIROP (%) of the KITs was read. All measurements were performed in four replicates.

3.3.1.9. *Correlation between ELISA technique and IODM*

ELISA plates were coated with 50 µL/well of rS1 protein at 5 µg/mL for 2 hours at 37˚C. After that, plates were washed 4 times with PBS-T 0.05% (200 µL/well) and blocked with 1x casein hydrolysate for 1 hour at RT. Following the blocking step, the plates were washed again, and the sera (50 µL/well) were incubated at a 1:40 dilution in blocking buffer: PBS at a 1:4 dilution and left ON at 4 ˚C.

After repeating the washes, secondary Abs were incubated to detect sIgG, sIgM, and sIgA. In this case, polyclonal Abs labeled with HRP were used at different dilutions (αHuman-IgG-HRP, 1:25000; αHuman-IgM-HRP, 1:20000; αHuman-IgA-HRP, 1:10000) (Sigma-Aldrich) in blocking buffer: PBS at a 1:4 dilution with 50 µL/well for 1 hour at RT. Four washes were performed with PBS-T 0.05%, and then the reaction was revealed with the peroxidase substrate TMB. The reaction was stopped with 50 µL of 2 N HCl, and the OD was measured at 450 nm. PBS with 1% BSA was coated on the surface as a NC. All assay measurements were taken in triplicates.

KITs were immobilized with 1 µL of rS1 (300 µL/mL) and BSA as a NC protein (50 µg/mL) for 3 hours at 37°C in a humid chamber. Subsequently, a wash was performed with 20 mL of H_2OmQ, 45 s of agitation with H_2OmQ, and drying with compressed filtered air. For the recognition stage, serum samples were incubated (1.5 µL at a 1:10 dilution) for 3 hours at 37°C in a humid chamber. After washing with 20 mL of H_2OmQ, 10 min of agitation in PBS, and 40 mL of H_2OmQ for rinsing, 1.5 µL of secondary Abs αHuman-IgG (1:125), αHuman-IgM (1:250), and αHuman-IgA (1:250) were incubated for 3 hours at 37°C. The final wash was performed, and the ΔIROP signal (%) was read, as well as after each incubation stage. Each measurement was carried out in five replicates (Figure 47).

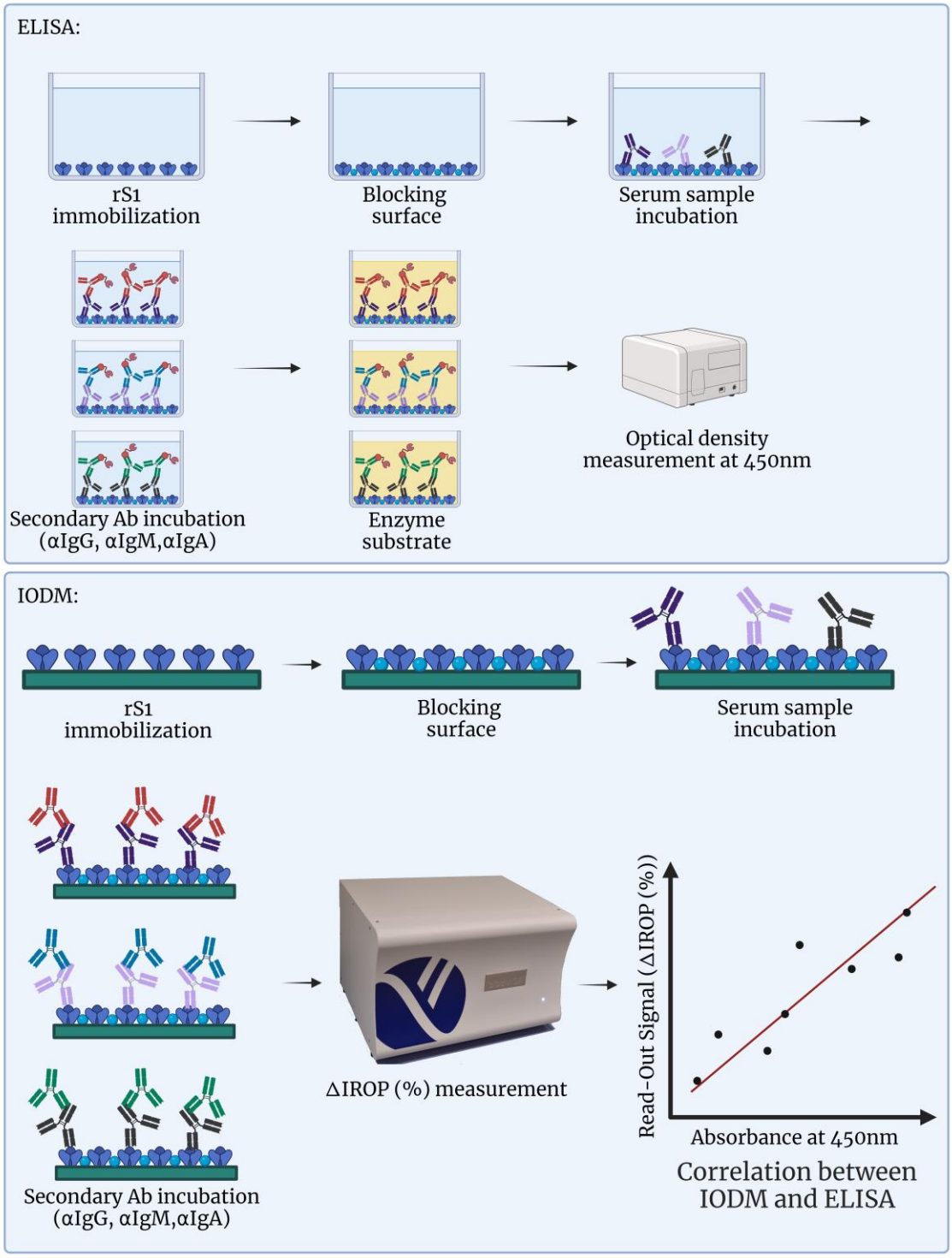

Figure 47. Correlation between ELISA and IODM. A schematic of the ELISA assay is shown above, and the steps followed for the IODM are shown below. Created with BioRender.com.

3.3.1.10. *Evaluation of COVID-19 biomarkers in serum*

65-BICELLs KITs were biofunctionalized using O_2 plasma to covalently attach specific bioreceptors, rS1, αHuman-FTH1, and αHuman-CRP. For this purpose, 1 µL of rS1 at 300 µg/mL, 1 µL of αHuman-FTH1 at 100 µg/mL, and 1 µL of αHuman-CRP at 100 µg/mL were incubated using the BioDot AD1520TM automatic dispensing platform. As a NC, BSA (1 µL at 50 µg/mL) was incubated. The proteins were incubated at 37°C in a humid chamber.

Afterward, the KITs were washed with H_2OmQ and dried with filtered compressed air. They were then blocked for 1 hour at RT with 1x casein hydrolysate under agitation to prevent nonspecific binding.

Once blocked, specific Abs against SARS-CoV-2 were measured. Serum samples were incubated at a 1:10 dilution to measure Total Specific Immunoglobulins (sIgT), FTH1, and CRP directly in a single step. Igs and markers (FTH1 and CRP) measurements were taken for two patients, along with their PC (confirmed by PCR), on each KIT. After the washing step, measurements of FTH1, CRP, and sIgT were obtained directly.

The titers of sIgs (IgG, IgM, and IgA) were determined by incubating secondary Abs (αHuman-IgG at 1:250, αHuman-IgM at 1:20, and αHuman-IgA at 1:10) for 3 hours at 37°C in a humid chamber. After washing the KITs, the values for each of the sIgs were obtained (Figures 48 and 49) (Murillo et al., 2022).

After each incubation step, the ΔIROP (%) values were read. All measurements were performed in four replicates.

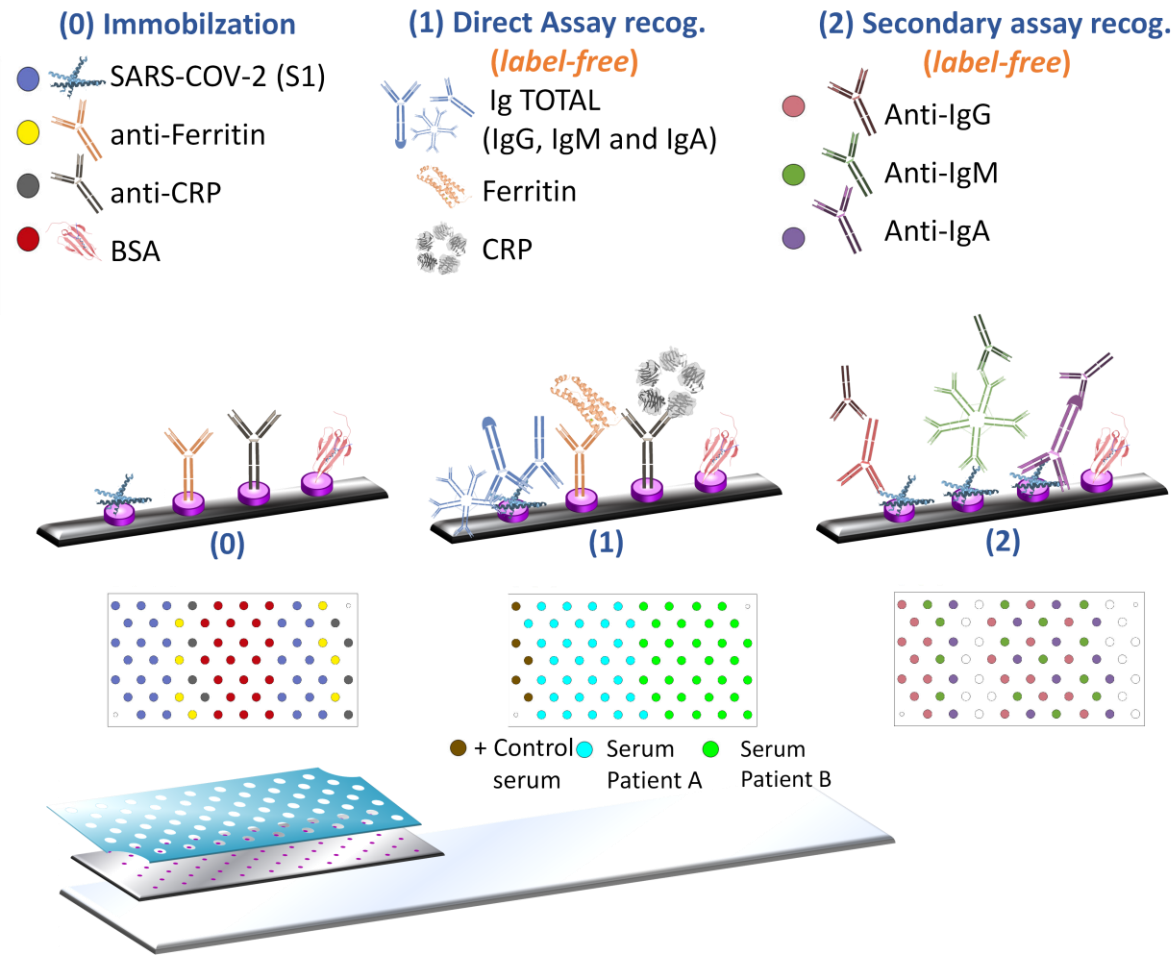

Figure 48. Depiction of the assay carried out for the detection of specific Abs against SARS-CoV-2. In the first step (0) there is the immobilization, then the recognition of sIgT together with the markers FTH1 and CRP(1), and finally (2) with the incubation of the secondary Abs, the recognition of the different isotypes of specific Abs against SARS-CoV-2 (sIgG, sIgM, and sIgA) (Murillo et al., 2022).

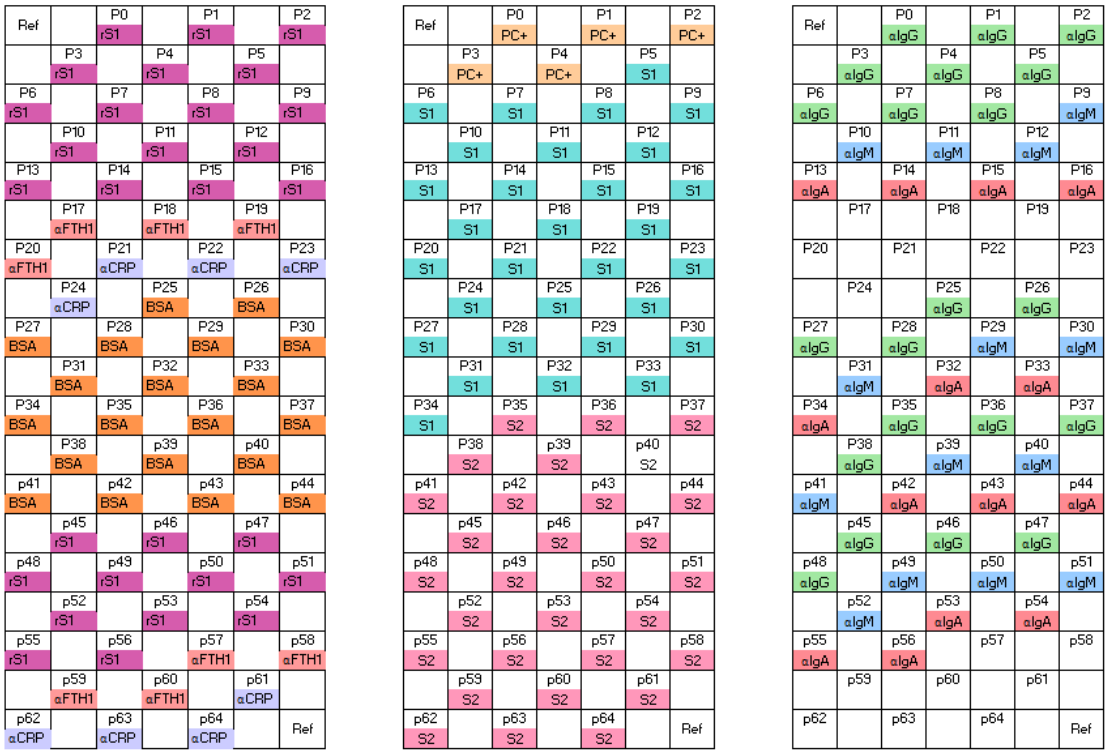

Figure 49. Organization of the 65-BICELL KITs. The figure represents by colors the organization of the KIT used in the different incubation stages (immobilization, first recognition (S1 and S2 are two different patient samples), and second recognition).

3.3.1.11. *Severity model*

The study aimed to analyze whether the severity level (categorized as severe, moderate, and mild according to the hospital's classification) was a significant factor for the response variable sIgT (the total concentration of sIgs against SARS-CoV-2). A Multiple Linear Regression Model (MLRM) was employed to assess the titers of sIgG, sIgM, and sIgA, as well as FTH1 and CRP, and how they correlated with sIgT.

Firstly, the correlation matrix between all quantitative variables (sIgT, sIgG, sIgM, sIgA, FTH1, and CRP) was obtained. Secondly, simple regression models of sIgT against sIgG, sIgM, sIgA, FTH1, and CRP were computed to verify the significance of the variables (see Table 14). Ultimately, all variables were evaluated in the model, and it was observed that the CRP variable was not significant, with a p-value of 0.472, which was much higher than the statistically significant threshold of 0.05. Consequently, the CRP variable was removed from the MLRM, resulting in a goodness of fit of 70.29% (Adjusted R-squared) (Murillo et al., 2022). Subsequently, the qualitative variable of severity (severe, moderate, and mild) was included in the MLRM, leading to a goodness of fit of 73.01% (Adjusted R-squared). All models exhibited satisfactory statistical diagnostics.

Table 14. Significance levels of the model variables (Murillo et al., 2022).

	sIgG	**sIgM**	**sIgA**	**FTH1**	**CRP**
sIgT	1.59×10^{-6}	1.22×10^{-4}	3.62×10^{-3}	1.17×10^{-6}	3.62×10^{-3}

3.3.2. Case I. II. Development of an *in-vitro* optical diagnostic system for the detection of specific Abs against SARS-CoV-2 in saliva

This section summarizes the points followed during the work of this doctoral thesis in order to develop an *in-vitro* system for the detection of SARS-CoV-2 sIgA in saliva samples based on interferometric optical biosensors. In this case, the measurement of a single marker (plus experimental controls) was carried out for a larger number of samples compared to serum markers.

3.3.2.1. *Recognition assay of sIgA in saliva samples*

The 16-BICELLs KITs, each with a size of 200 µm, were immobilized with the virus protein rS1 at a concentration of 300 µg/mL (1 µL using the BioDot AD1520TM automatic dispensing platform) and incubated for 3 hours at 37˚C. They were washed with 20 mL of H_2OmQ and agitated for 45 s in H_2OmQ. Next, they were blocked with 1x casein hydrolysate for 1 hour at RT with agitation. Saliva samples (2.5 µL) were then incubated at a 1:5 dilution in 0.1 % casein hydrolysate for 2 hours and 30 min at 37˚C in a humid chamber. Afterward, the KITs were washed with 20 mL of H_2OmQ, agitated for 10 min in PBS, rinsed with 20 mL of H_2OmQ, and dried with compressed filtered air.

In the recognition stage, the αHuman-IgA Ab (2.5 µL at 1:250 dilution) was incubated for 2 hours at 37˚C in a humid chamber. The KITs were washed with 20 mL of H_2OmQ and agitated for 2 min in H_2OmQ. The ΔIROP (%) signal was read after each washing and drying step. For these assays, 3 PC saliva samples were used (Positive Control 1 (PC1), Positive Control 2 (PC2) and Positive Control 3 (PC3) (Table 15). All measurements were performed in four replicates.

Table 15. Conditions of the first test in KITs.

Incubation step	***Incubation time (min)***	***Concentration (µg/mL) and Dilution***	***Volume (µL)***	***Temperature (°C)***
rS1	180	300	1	37
Blocking	60	1	20000	RT
PC1 saliva	150	1:5	2.5	37
PC2 saliva	150	1:5	2.5	37
PC3 saliva	150	1:5	2.5	37
αHuman-IgA	120	1:250	2.5	37

Next, the 16-BICELLs KITs with a size of 200 µm are immobilized with the virus protein using the same conditions described earlier, including the washes, and blocking step. In the recognition stage, saliva samples (2.5µL) were incubated both at a 1:5 dilution in 0.01% casein hydrolysate and undiluted. This step was carried out at 4˚C in a humid chamber ON. Subsequent steps of washing and secondary Ab incubation were performed in the same manner as defined in the

previous assay. This same assay was also conducted on the protein rRBD and the BSA protein as a NC, to compare the ΔIROP (%) signals among proteins (Table 16). All measurements were performed in four replicates. The same experiment with the same steps were followed, but two different detection Abs against sIgA (Sigma-Aldrich) were used.

Table 16. Second experiment conditions.

Incubation step	*Incubation time (min)*	*Concentration (µg/mL) and Dilution*	*Volume (µL)*	*Temperature (°C)*
rS1	180	300	1	37
Blocking	60	1	20000	RT
PC1 saliva	ON	1 / 1:5	2.5	4
PC2 saliva	ON	1 / 1:5	2.5	4
PC3 saliva	ON	1 / 1:5	2.5	4
αHuman-IgA	120	1:250	2.5	37

3.3.2.2. *Study of different incubation times of saliva samples*

KITs were incubated with the rS1 protein and BSA as a NC as previously described. After the washing step, undiluted saliva (2 µL) was incubated for different times at 37˚C in a humid chamber (1, 3, and 6 hours), and as a control, it was also left ON at 4˚C. Finally, after the washes, the αHuman-IgA Ab (2 µL at 1:10 dilution) was incubated for 3 hours at 37˚C in a humid chamber. The KITs were washed and dried, and the ΔIROP (%) signals were measured (Table 17). All measurements were performed in four replicates.

Table 17. Conditions of the study of the incubation time of saliva samples.

Incubation step	*Incubation time (min)*	*Concentration (µg/mL) and Dilution*	*Volume (µL)*	*Temperature (°C)*
rS1	180	300	1	37
Blocking	60	1	20000	RT
PC1 saliva	60, 180, 360, and ON	1	2	37 / 4
PC2 saliva	60, 180, 360, and ON	1	2	37 / 4
PC3 saliva	60, 180, 360, and ON	1	2	37 / 4
αHuman-IgA	180	1:10	2	37

3.3.2.3. *Study of different protein concentrations for immobilization*

16-BICELLs KITs with different rS1 protein concentrations (100-250 and 500 µg/mL) were incubated, with 1.5 µL per cell, for 3 hours at 37˚C in a humid chamber. After washing and blocking for 1hour, undiluted PC3 (2 µL) was incubated ON at 4˚C. The KITs were washed and the αHuman-IgA (2 µL at 1:10 dilution) was incubated for 3 hours at 37˚C in a humid chamber. Finally, the KITs were washed and dried with compressed filtered air, and the ΔIROP (%) signals were measured. All measurements were performed in four replicates.

3.3.2.4. *Recognition against the rN protein*

A dose-response curve was performed to determine the immobilization concentration required to coat the sensor surface. For this purpose, 1.5 µL of the recombinant N protein (rN) (Agrenvec, Madrid, Spain) was incubated at different concentrations (25-50 and 100 µg/mL) for 3 hours at 37˚C in a humid chamber. After washing with H_2OmQ, they were blocked with 1x casein hydrolysate for 1 hour at RT with agitation. The same washing process was repeated, and then PC3 was incubated under the same conditions as described above, on the immobilized rN protein, rRBD, and also on the rS1 and proteins as PC for the experiment, and on the BSA protein as a NC. In this case, a NC saliva was also incubated. The αHuman-IgA secondary Ab was incubated after washing the KITs following the same protocol as before. Finally, they were washed with H_2OmQ and PBS and dried with compressed filtered air. The ΔIROP (%) signals were read after each step of the protocol. All measurements were performed in four replicates.

3.3.2.5. *ELISA assays of the PC and NC samples*

The ELISA plates were coated with the virus protein rS1 at 5 µg/mL (50 µL/well) for 2 hours at 37˚C. Three washes were performed with PBS-T 0.05%, and then they were blocked with 1x casein hydrolysate for 1 hour at RT. After three washes with PBS-T 0.05% (200 µL/well), the saliva samples (positive and negative controls) were incubated at a 1:5 dilution in blocking buffer: PBS (1:4) ON at 4˚C. The plates were washed 5 times with PBS-T 0.05%, and the αHuman-IgA-HRP secondary Ab was incubated at 1:10000 dilution for 1 hour at RT. After 5 washes as described above, 50 µL of the peroxidase substrate TMB was added, and the plates were left in the dark and uncovered. The reaction was stopped with 50 µL/well of 2 N HCl, and the OD was read at 450nm. As a NC, PBS with 1% BSA was used. The measurements were performed in triplicates.

3.3.2.6. *Human saliva samples*

The saliva samples were collected in the Área Clínica of the Centro de Tecnologia Biomédica (CTB) during a voluntary and experimental pilot study with the aim of studying early detection, surveillance, and control of the disease caused by SARS-CoV-2 infection.

The saliva samples of the 196 volunteers were collected every 12 days, a total of 6 times (a total of 855 measurements), with the objective of studying the variation and evolution of sIgA against the virus over three months.

This collection was carried out following the procedure described in Annex I. The volunteers were provided with a test tube in which they deposited the saliva sample (1mL). Once collected, the samples were centrifuged at 15000 revolutions per minute (rpm) for 10 min, and the supernatants were collected and stored at -20˚C.

3.3.2.7. *ELISA assays of the saliva samples and their correlation with IODM*

The ELISA plates were coated with 5 µg/mL of the rS1 protein (50 µL/well) for 2 hours at 37˚C. After blocking with 1x casein hydrolysate for 1 hour at RT, three washes were performed with PBS-T 0.05%. Positive and negative saliva samples were then incubated at a 1:10 dilution in blocking buffer: PBS 1:4 ON at 4˚C. The washes were repeated five times, and the secondary Ab αHuman-IgA-HRP was incubated at a 1:2000 dilution in blocking buffer: PBS 1:4 (50 µL/well) for 1 hour at RT. After washing the Ab, it was developed with the peroxidase substrate TMB (50 µL/well), and the reaction was stopped after 10 minutes. The absorbance was measured at 450nm (Murillo et al., 2021).

As a NC, wells were coated with the blocking buffer instead of the protein. The obtained signals represent the average of triplicates, minus the signal obtained from the blank.

To measure sIgA in the KITs, the protocol described in the following section was followed (3.3.2.8).

3.3.2.8. *Measurements of sIgA against SARS-CoV-2 in the saliva pilot study*

The KITs were coated with 300 µg/mL (1 µL) of the rS1 protein and 50 µg/mL of BSA as a NC using an automated liquid dispensing platform, the Biodot AD1520TM. The KITs were washed for 45 s in agitated H_2OmQ and then blocked with 1x casein hydrolysate at RT for 1 hour with agitation. After washing, 2 µL of saliva samples from the volunteers (7 volunteers per KIT), along with PC and NC saliva samples (confirmed by PCR and ELISA), were incubated ON at 4˚C. They were then washed with 20 mL of H_2OmQ and agitated for 45 s in H_2OmQ to obtain the signal of sIgT.

Next, the αHuman-IgA Ab was incubated at a 1:10 dilution (2 µL) for 3 hours at 37˚C in a humid chamber. The KITs were washed with 30 mL of H_2OmQ and agitated for 2 min in H_2OmQ. The ΔIROP (%) signal was measured after drying them with compressed air (Figure 50).

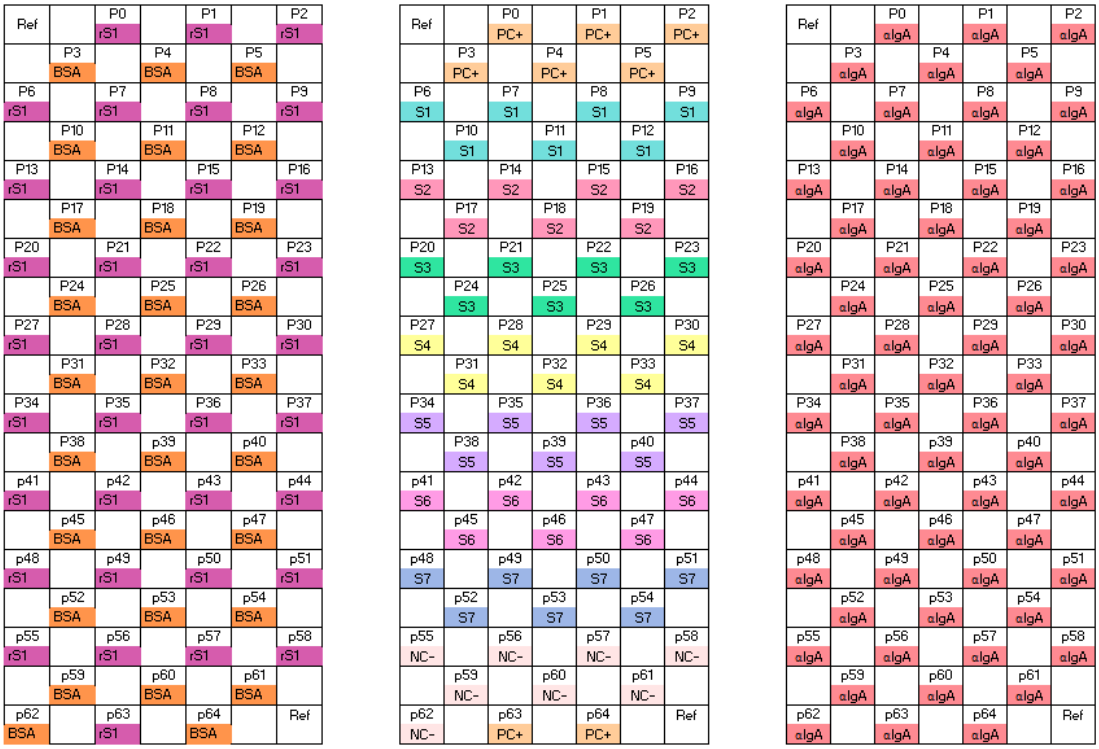

Figure 50. Schematic of the 65-BICELL KIT for determination of SARS-CoV-2 sIgA in saliva. Color description of the different stages of incubation. First the immobilization, then the incubation of the saliva samples (7 per KIT), and finally the development of the sIgA.

3.4. Results

3.4.1. Case I. I. Development of an *in-vitro* optical diagnostic system for the detection of specific Abs against SARS-CoV-2 in serum

3.4.1.1. *Production of recombinant S protein from the virus using Pichia pastoris*

The S protein domain of SARS-CoV-2 (rS1) was expressed as a recombinant protein and purified from the culture media using size exclusion chromatography on a Sephacryl S-200 High Resolution system. Subsequently, it was analyzed using sodium dodecyl sulfate-polyacrylamide gel electrophoresis (5 μg of purified protein extract) (Figure 51A-C). To assess the purity and identity of the protein, two different mass spectrometry analyses were conducted. MALDI-TOF analysis of the **protein's molecular weight revealed a single peak representing a mass of 14.322 kDa** (Figure 51D), while the mass peptide fingerprint verified the protein's identity (Figure 51E).

3.4.1.2. *ELISA of recombinant protein activity assays*

After confirming the purity and nature of the protein, its activity was evaluated using saliva samples obtained from volunteers who tested positive in PCR (Figure 51F). The specificity of recognition was assessed using ELISA. The results showed that sIgA Abs against the virus protein was only present in patients who tested positive for SARS-CoV-2 in PCR (Group 2), capable of recognizing the rS1 protein.

In the study of recombinant protein activity, **98% of patients (n = 54) who tested positive for SARS-CoV-2 in PCR between March and June 2020 exhibited positive titers**. Conversely, the **test results for patients (n = 14) who had not been in contact with the virus were negative**. Although the percentage similarity between the activity of the natural protein and the recombinant fragment remains unknown, the results confirm that the recombinant protein is a reliable bioreceptor for detecting anti-SARS-CoV-2 (αSARS-CoV-2) Abs.

3.4.1.3. *Human serum samples*

Once the serum samples were received, they were heated at 56˚C for 30 min to inactivate the complement. Afterward, all the samples were aliquoted and stored at -80˚C.

All the samples were assigned an internal code, and a database list was designed, including the hospital code, patient number, internal code, severity level, and the markers measured in each sample.

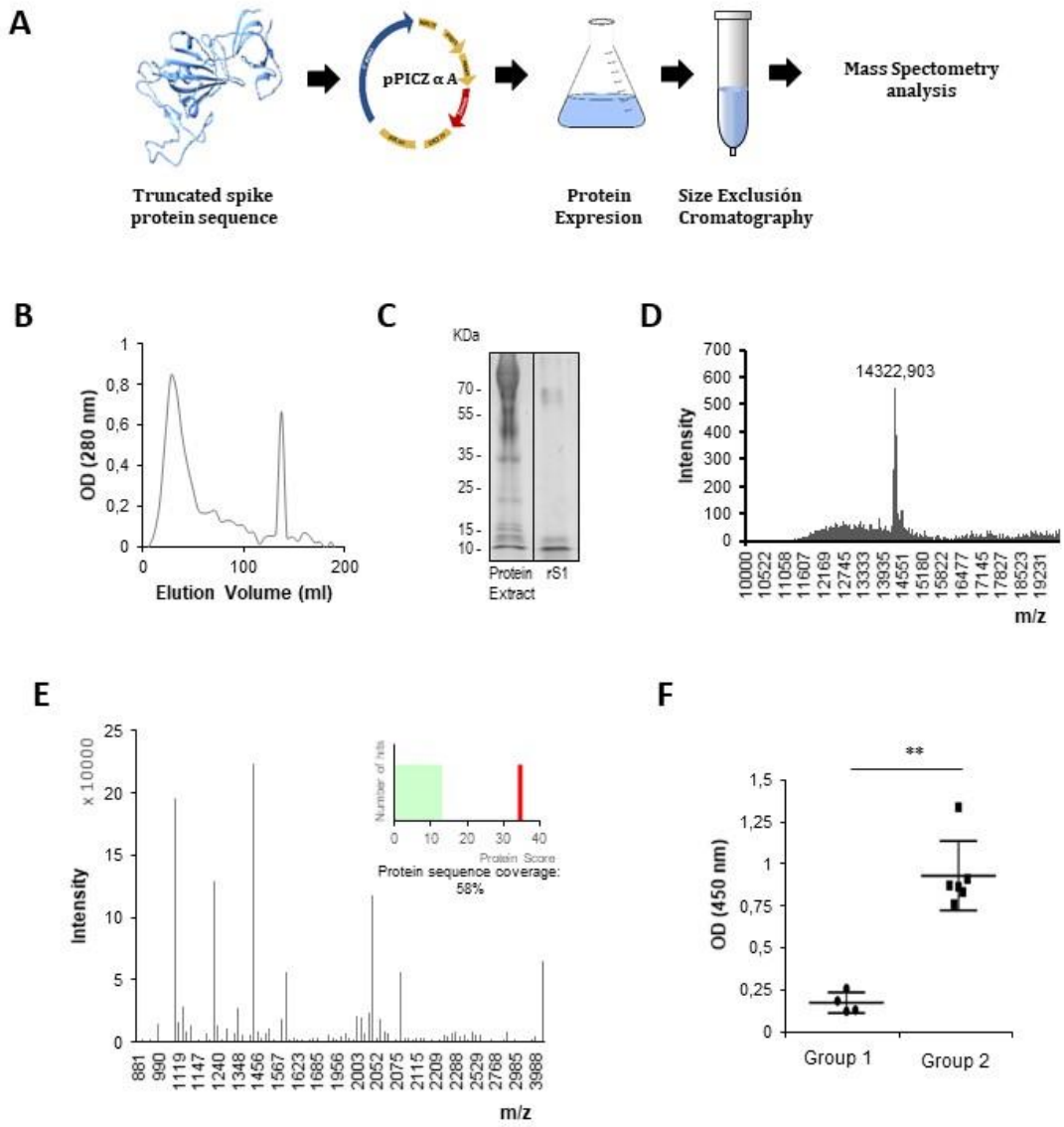

Figure 51. Description of the production process of the recombinant virus protein. A. Protocol conducted for the expression and purification of the recombinant protein rS1. **B.** Protein extract fractionation detected at 280 nm. **C.** Analysis by sodium dodecyl sulfate polyacrylamide gel electrophoresis and Coomassie staining of the purified protein extract. **D.** Molecular weight determination by MALDI-TOF. Measurements were performed in the linear positive mode, operating in the range of m/z = 4000–60000. **E.** Peptide mass fingerprinting spectrum and Mascot scores ($p < 0.05$) of the purified viral protein. **F.** Activity assay to analyze the binding of the viral protein with sIgA in the volunteer's saliva samples. Group 1: volunteers who tested negative for SARS-CoV-2 by PCR and serological tests. Group 2: volunteers who tested positive for SARS-CoV-2 by PCR and serological tests. Statistical significance (**$p < 0.01$) determined by the Mann-Whitney test for unpaired samples (n = 6) (Murillo et al., 2022).

3.4.1.4. *Immobilization of the virus proteins on the sensor surface (dose-response curves)*

Based on the results we obtained, it was observed that protein rS1 showed a higher ΔIROP (%) signal than protein rS2 under both incubation conditions (1 hour and 30 min (Figure 52A) and 2 hours (Figure 52B)). Although one protein yielded a higher signal than the other, we continued conducting experiments with both proteins because even if the immobilization values were lower, we were looking for the protein that the Abs in the serum recognized better. **The immobilization concentration of both proteins was established at 100 µg/mL.** Additionally, it is observed that increasing the incubation time resulted in an increase in the signals of both proteins for all concentrations, so **an incubation time of 2 hours was established for further experiments.**

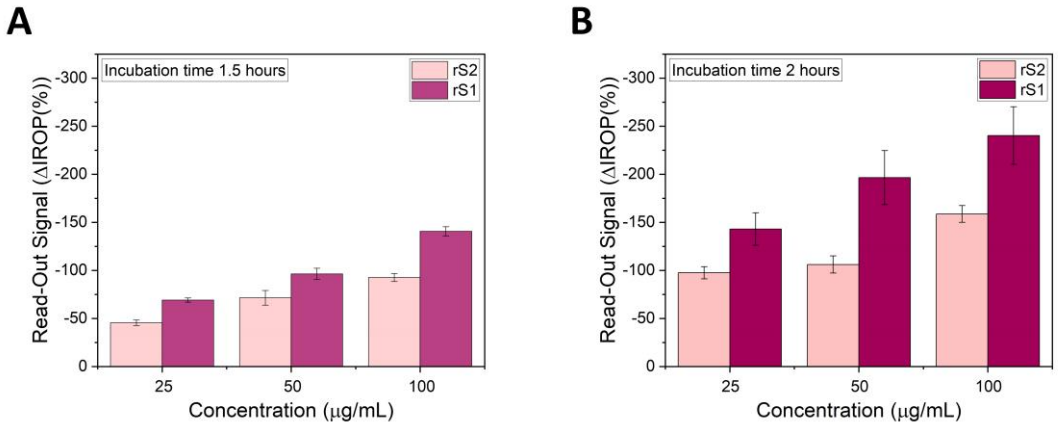

Figure 52. **Dose-response curve of rS1 and rS2 proteins. A.** Representation of the ΔIROP (%) signal based on the concentration of rS1 and rS2 proteins after 1 hour and 30 min of incubation. **B.** ΔIROP (%) signal curve based on the concentration of rS1 and rS2 proteins after 2 hours of incubation.

3.4.1.5. *Recognition tests in KITs using positive serum sample against rS1 and rS2 proteins*

Thanks to the ELISAs carried out in the activity assays, we know that specific Abs against SARS-CoV-2 are capable of recognizing the viral protein, but we have to investigate if this same recognition is happening in our system.. For this purpose, immobilized KITs with two proteins (rS1 and rS2) under two conditions (1 hour and 30 min and 2 hours) were used to incubate the serum from a PC and see if we obtained a signal from the binding of Abs to the immobilized protein on the biosensor.

As seen in Figure 53A, in the case of protein rS1 incubated for 1 hour and 30 min, we can observe that the serum produces a ΔIROP (%) signal that cannot be distinguished between the immobilized surface with the specific protein and the NC. Additionally, the obtained uncertainties are very high. On the other hand, the signals generated by the secondary Abs for sIgG and sIgM against the viral protein were very low, and even in the NC, we obtained a signal. If we compare these results with those obtained on the protein immobilized for 2 hours (Figure 53B), we can see that the signals are very different. Firstly, the signal from the serum on the NC protein is much lower than in the previous case, and the uncertainties are also lower. Secondly, the ΔIROP (%) of

the Abs is higher, which would make sense since in this case, there is more protein available on the sensor surface for the Abs to bind to. However, the signals obtained on the NC need to be improved in order to better distinguish between the levels of Igs in the serum.

For the case of protein rS2 (Figures 53C and 53D), we observe the same phenomenon as in the case of protein rS1, obtaining better signals in the KITs where the protein was incubated for 2 hours.

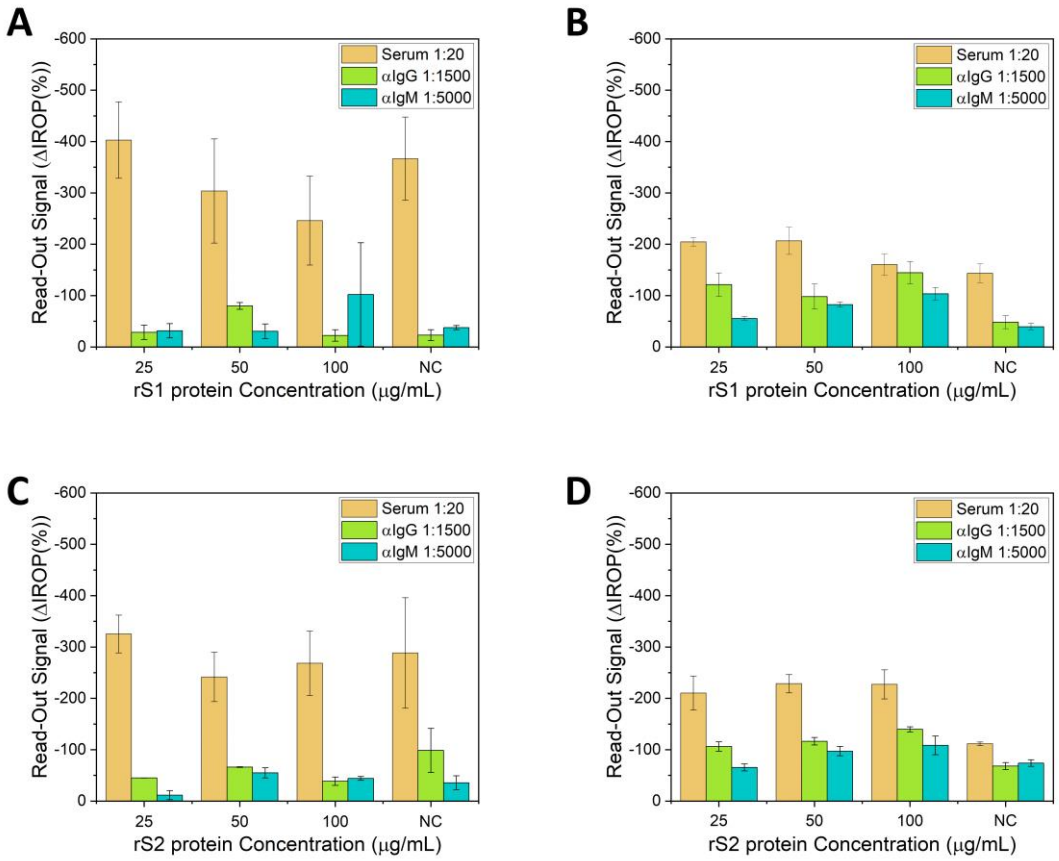

Figure 53. ΔIROP (%) signals obtained after incubation of PC serum on rS1 and rS2 proteins. A. PC serum incubated on immobilized rS1 protein for 1 hour and 30 min. **B.** PC serum incubated on immobilized rS1 protein for 2 hours. **C.** PC serum incubated on immobilized rS2 protein for 1 hour and 30 min. **D.** PC serum incubated on immobilized rS2 protein for 2 hours.

Therefore, further improvements in the experiments are necessary in order to reduce the background signal from the serum. To achieve this, **the next step was to dilute the serum at a 1:10 dilution instead of 1:20 in addition to incubating the virus protein for 3 hours.**

Once the PC and NC sera were incubated, it was observed that higher signals were obtained when we incubated the less diluted serum over the protein that had been immobilized for 3 hours. It can be observed that **the highest signal is obtained for protein rS1 in comparison with rS2** (Figures 54A and 54C), although we also obtain a signal for protein rS2, and the least signal is observed for the NC protein (tau) (Figures 54E and 54F), as expected. On the other hand, although we have a signal from the positive serum for both tested proteins, we only obtained an IgG signal

for protein rS1, while there was no signal for IgM and IgA for either of the proteins. Additionally, there is no signal from any of the specific Abs for SARS-CoV-2 on tau.

In comparison, the NC serum gave much lower signals in the case of the two viral proteins (Figure 54B y 54D). If we look at protein rS1, we can see that the NC serum gave a lower signal for IgG compared to the PC serum. However, it did show a signal for IgM and a slight signal for IgA. For protein rS2, a similar situation occurred, as we obtained a low signal for IgG and IgA, while the PC serum did not show any signal. The same pattern is observed for tau, but with lower signals. However, it is important to note that these signals from the NC should be considered very low, and they cannot be considered positive as they would correspond to non-specific binding and serum matrix effects. **The next step was to increase the concentration of the secondary Abs** because, although we were able to see the signal from the serum and differentiate it from the NC, we did not observe a significant signal from the specific Abs. Additionally, **the incubation time was increased, and the serum washing step was changed.**

Based on the latest experiments, **all subsequent assays were conducted only with protein rS1**, as it yielded better immobilization and recognition signals. Moreover, this approach helped reduce the expense of using both proteins for all tests.

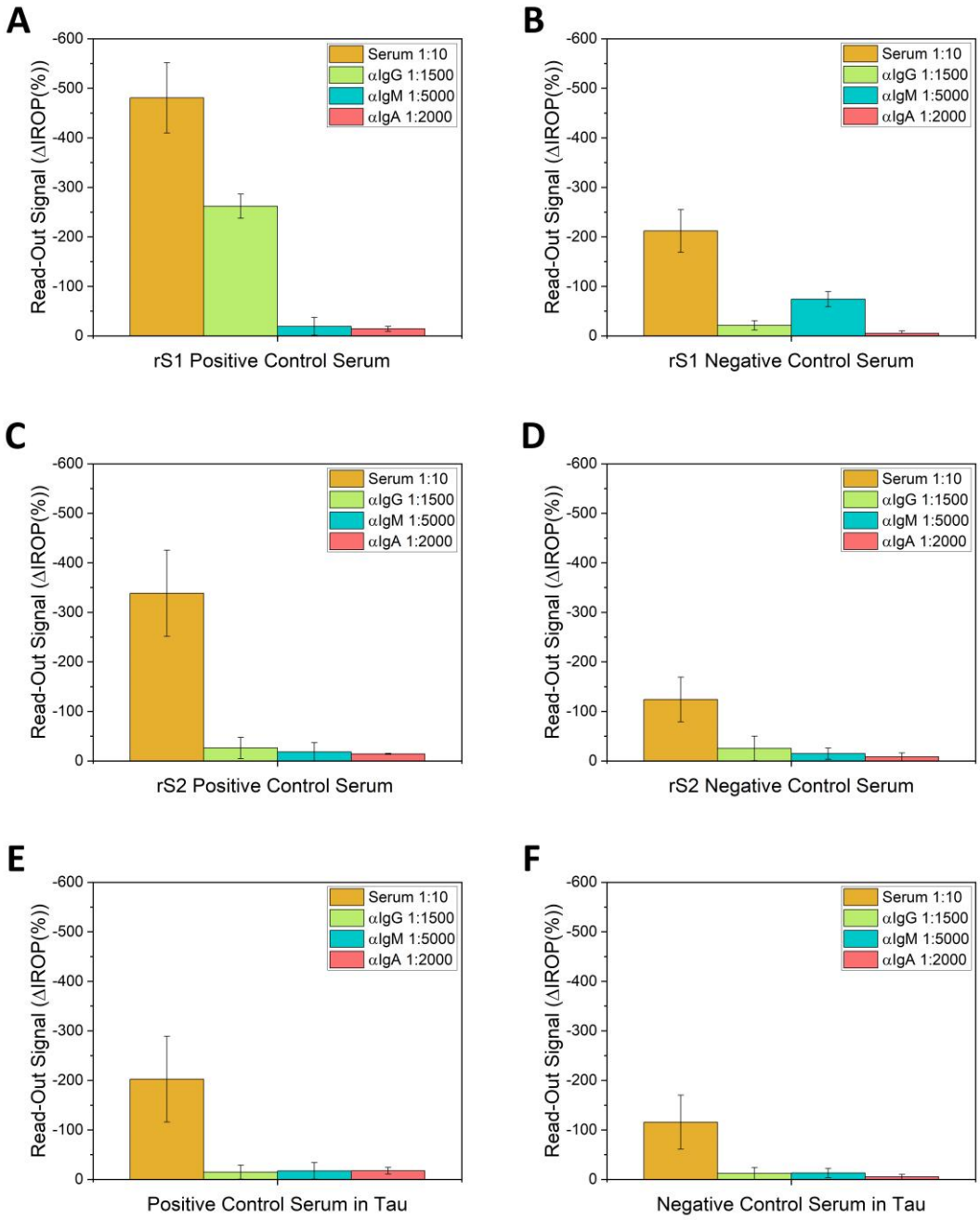

Figure 54. ΔIROP (%) signals obtained after incubation of PC and NC serum on rS1, rS2, and tau proteins and development of αHuman-IgG, αHuman-IgM, and αHuman-IgA secondary Abs. A. ΔIROP (%) signal of PC serum on rS1 protein and sIgG, sIgM and sIgA Abs. **B.** ΔIROP (%) signal of NC serum and sIgG, sIgM, and sIgA Abs after incubation on rS1 protein. **C.** ΔIROP (%) signal of PC serum and sIgG, sIgM, and sIgA Abs upon incubation on rS2 protein. **D.** ΔIROP (%) signal of NC serum on rS2 protein and sIgG, sIgM and sIgA Abs. **E.** ΔIROP (%) values obtained for PC serum and secondary Abs on NC protein. **F.** ΔIROP (%) values obtained for the NC serum and the secondary Abs when incubated on the NC protein.

As shown in Figure 55A, a serum signal was obtained for both PC that was comparable and distinguishable from the NC. Additionally, longer incubation and higher concentration of secondary Abs provided sIgG and sIgM signals for the PC while there was no signal for the NC. On the other hand, as seen in Figure 55B, the incubated serum (positive and negative) on tau protein yielded the same ΔIROP (%) signal corresponding to the background of the sample. In this case, as well, the secondary Abs did not detect sIgG and sIgM.

However, the signals obtained for the specific Abs against the viral protein are somewhat low. Therefore, **the next step in adjusting the protocol is to increase the concentration of the secondary Abs** once again while maintaining all the other protocol conditions described earlier. To verify this, a PC serum and a NC serum are incubated on the immobilized rS1 protein in the KITs, and finally, the secondary Abs (αHuman-IgG at 1:125, αHuman-IgM at 1:250) are incubated.

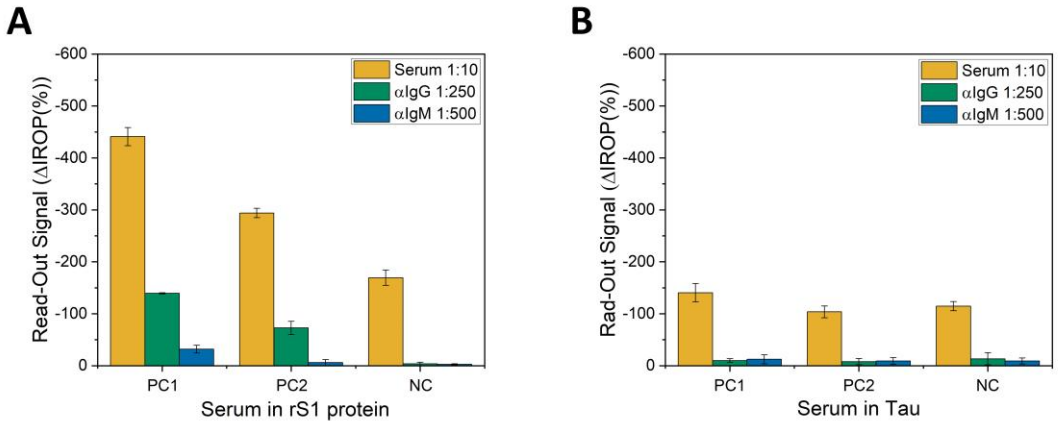

Figure 55. ΔIROP (%) values obtained after incubation of PC1, PC2, and NC sera on rS1 and tau proteins. A. ΔIROP (%) signal of PC and NC sera and their corresponding Abs after modification of incubation conditions. **B.** ΔIROP (%) signal on the NC protein of the incubated PC and NC sera and sIgG and sIgM Abs after changing conditions in the experiment.

When repeating these experiments but increasing the concentration of the secondary Abs, it was observed in Figure 56A, that the **positive serum yields a higher signal than the NC serum**, as in previous assays. However, thanks to the increased concentration of the secondary Abs, we can appreciate a greater difference between the levels of sIgs against the viral protein by comparing the ΔIROP (%) signals of the two control sera. Furthermore, this difference is also appreciated when comparing the PC serum incubated with the virus protein and with the tau protein (Figure 56B).

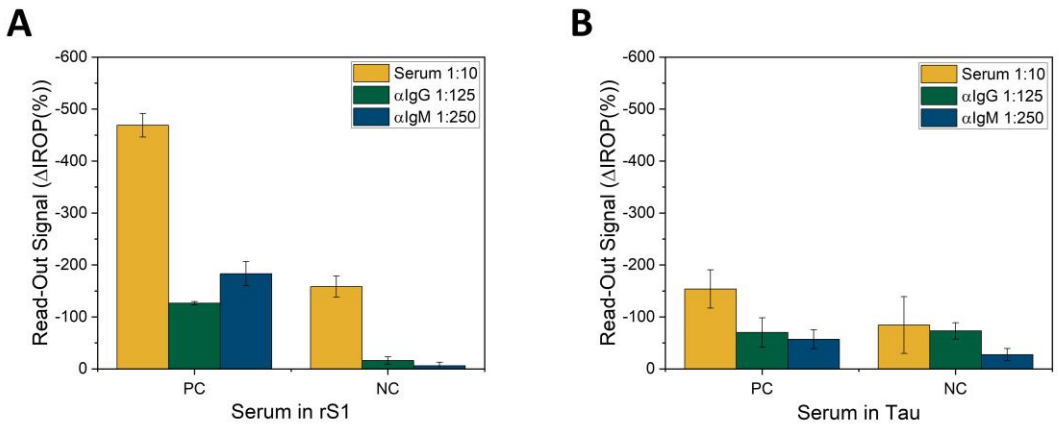

Figure 56. ΔIROP (%) values obtained after incubation of PC and NC sera on rS1 and tau proteins. A. ΔIROP (%) values obtained for PC and NC sera and virus-specific Abs with increasing concentration of secondary Abs. **B.** ΔIROP (%) signal of PC and NC sera on the NC protein and Abs revealed after increasing the concentration of secondary Abs in the assay.

In summary, rS1 protein was selected for experimental progression at the concentration of 100 µg/mL with a 3 hour incubation. The dilution of the serum samples was stipulated at 1:10 with an incubation time of 3 hours. Finally, the secondary Abs were set at a 2 hour incubation time at 1:125 for αHuman-IgG and 1:250 for αHuman-IgM.

Considering that the objective of all these experiments is to develop a diagnostic system to detect specific Abs against SARS-CoV-2, it is necessary to find a way to automate most of the process and reduce protein consumption in order to immobilize a larger number of KITs. Hence, assays were conducted to automate the dispensing step of the virus protein for immobilization, allowing for the efficient coating of more KITs in the shortest possible time.

The immobilization step began to be performed using the automated liquid dispensing platform, BioDot AD1520TM. Firstly, various concentrations at different volumes were tested (Figure 57), and it was observed that there were no significant differences in the ΔIROP (%) values within those volume and concentration variations. Consequently, the same experiment was repeated, **fixing the volume at 1 µL** and testing different concentrations (Figure 58).

After the incubation and washing of the KITs, the ΔIROP (%) values obtained are shown in Figure 58. Based on this data, the concentration of the **virus protein rS1 was established as 300 µg/mL for the immobilization** of the KITs. Similarly, after each induction and purification of the protein, dose-response curves were performed to ensure that the correct immobilization values were achieved based on the concentration.

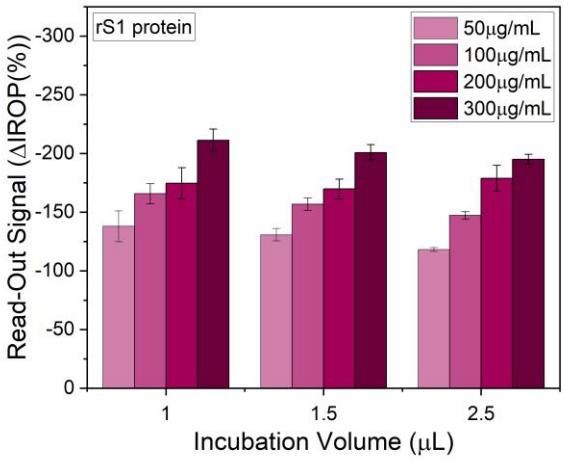

Figure 57. Dose-response curve of rS1 protein using the automated liquid dispensing platform, BioDot AD1520TM. The signal is plotted for each concentration depending on the volume selected for immobilization.

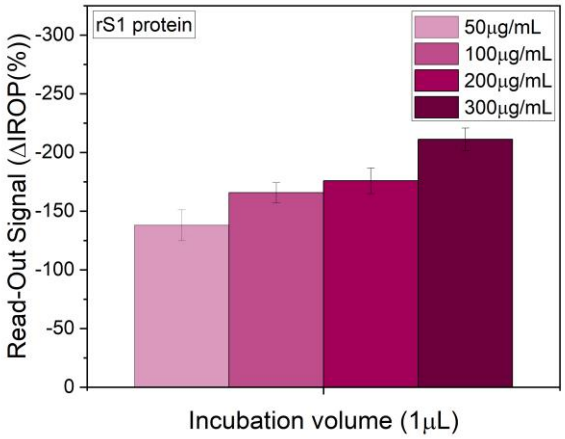

Figure 58. Dose-response curve of the rS1 protein by setting the volume with the automated liquid dispensing platform, BioDot AD1520TM. In this case, the volume was set to 1µL and the rS1 protein was incubated at different concentrations.

An automated immobilization protocol was established with the liquid dispensing platform, BioDot AD1520TM. Thus, KITs were immobilized with 1 µL at the concentration of 300 µg/mL for rS1 protein.

3.4.1.6. *Recognition tests in KITs using positive and negative serum samples against rRBD*

In addition to using the virus protein (rS1) corresponding to the spike of SARS-CoV-2, another protein corresponding to the RBD domain of the virus, named rRBD, was employed. This allowed the development of a multiplexed KIT to diagnose Abs against different virus proteins. The first step was performing a dose-response curve of the rRBD protein to select the concentration that yielded the best immobilization signal.

For the rRBD protein, **a concentration of 50 µg/mL was established for immobilization**, as shown in Figure 59. At this concentration, the sensor surface reaches saturation, and the signal plateaus. Even when doubling the concentration (100 µg/mL), no significant increase in signal is observed. Therefore, 50 µg/mL was deemed the optimal concentration for immobilization, providing the most effective signal response.

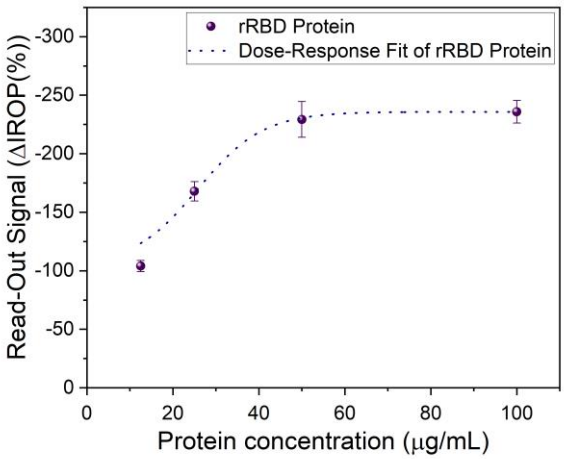

Figure 59. Dose-response curve of rRBD protein. The ΔIROP (%) signal is represented as a function of concentration. The sigmoidal fit of dose-response curves is depicted.

Once the concentration for immobilizing the KITs was determined, the next step involved incubating the PC and NC sera on the surface that had been immobilized with the rRBD protein.

As represented in Figure 60A, we observe a higher signal from the PC serum on the biosensor surface coated with the virus protein compared to the surface coated with BSA. Additionally, this signal is also greater compared to the signal obtained with the NC serum on the virus protein (Figure 60B). Regarding the αIgG signal, there is also a difference in signal from the PC serum when incubated on rRBD or BSA, with a higher signal observed on the virus protein. On the other hand, the NC serum does not produce any signal on either of the two coated sensor surfaces.

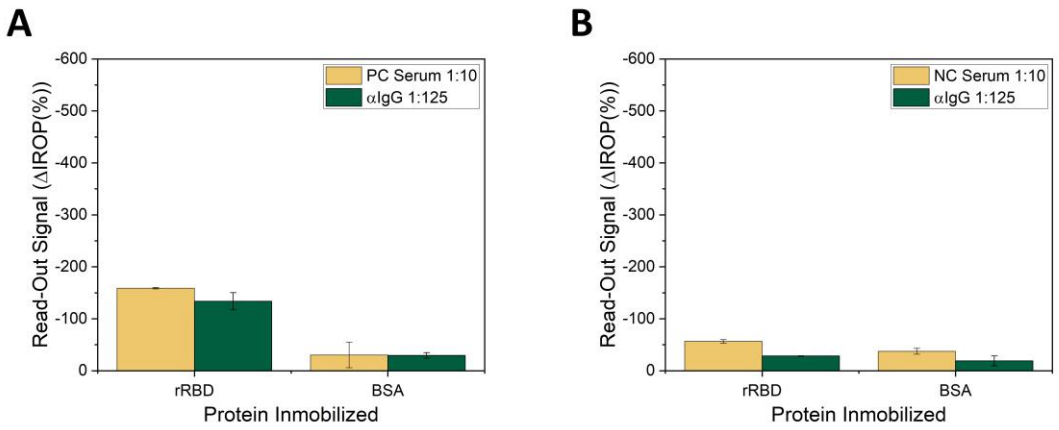

Figure 60. Incubation of PC and NC sera on rRBD protein and BSA. A. ΔIROP (%) value obtained after incubation of PC serum on rRBD and BSA proteins and development with αIgG Ab. **B.** ΔIROP (%) signal of NC serum on rRBD and BSA NC protein and revealed with the secondary Ab.

The rRBD protein immobilization concentration was set at 50 µg/mL and an incubation time of 3 hours. After incubation of the serum samples, specific Ab (sIgG) against the rRBD virus protein were detected.

3.4.1.7. *Study of different proteins as NCs*

It's essential to consider that the purpose of all these experiments is to develop a diagnostic system to detect specific Abs against SARS-CoV-2, which involves numerous parameters and details to consider. **Scalability and cost of reagents are among the factors to consider**. Up until this point, all assays were being conducted using the tau protein as the NC to incubate the serum and compare to obtain the signal's specificity. However, tau protein is highly specialized for another application and comes with a high cost. Therefore, there was a need to establish a more affordable NC protein that is less focused on a specific application. To address this, experiments were carried out using **BSA as an alternative** to the tau protein, and a comparison was made between the two to determine their suitability as NC proteins.

After incubating the 1:10 serum on the surfaces coated with both proteins (tau and BSA), Figure 61 represents the ΔIROP (%) of both control sera (positive and negative). In both cases, **there are no significant differences in the signal**, as the same signals are obtained for both proteins. Consequently, for all subsequent assays conducted from this point onward, BSA was used as the NC protein at a concentration of 50 µg/mL for coating the sensor surface.

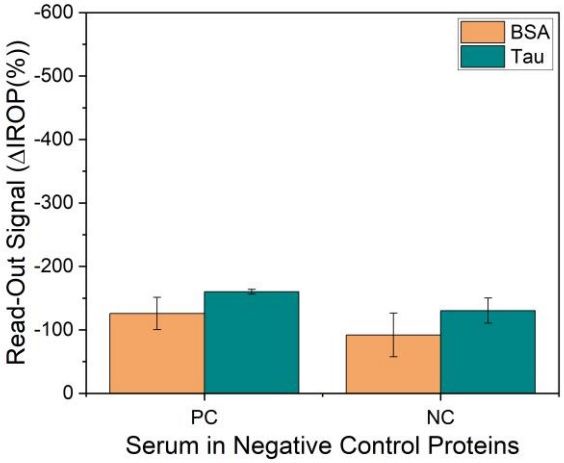

Figure 61. Study of tau proteins and BSA as a NC. The signal of the PC and NC sera on the two negative surfaces is represented.

BSA protein was established as a NC protein to coat the sensor surface at the concentration of 50 µg/mL.

3.4.1.8. *Measurements of two biomarkers related to SARS-CoV-2 infection: FTH1 and CRP*

The purpose of all these experiments is to develop a diagnostic system for SARS-CoV-2 and measure the Abs generated by the immune system in individuals who have had the disease. Additionally, **the employed technology allows for the measurement of multiple biomarkers**, as the KIT can be multiplexed. This enables the measurement of sIgs (sIgG, sIgM, and sIgA) against the virus protein and other markers that may be altered during the progression of the disease. In this case, we selected two additional markers, **FTH1 and CRP,** which are known to increase during SARS-CoV-2 infection.

To measure these biomarkers, we had to immobilize the specific Abs against them, αHuman-FTH1, and αHuman-CRP, respectively, to determine their presence or absence. The first step was to determine the immobilization concentration of the Abs on the sensor surface through a dose-response curve.

Once the Abs were immobilized at different concentrations on the sensor surface, we can observe in Figures 62A and B that there is minimal difference in the signals obtained between the 1 hour and 30 min of incubation and the 3 hours incubation for both Abs. Thus, such an extended incubation time is not necessary for these specific Abs. Additionally, **the chosen concentration for coating the sensor was 100 µg/mL in both cases**.

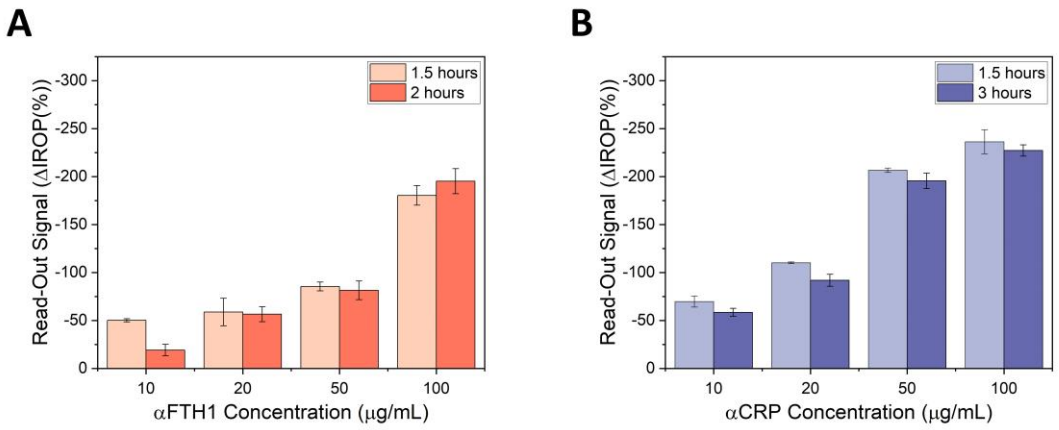

Figure 62. Dose-response curve of αHuman-FTH1 and αHuman-CRP Abs. Both Abs were incubated at different concentrations for 1 hour 30 min and for 2 hours.

Next, the PC and NC sera were measured on the KITs immobilized with the Abs to study whether we could observe differences between these controls for the two proteins of interest.

After immobilizing the Abs against FTH1 and CRP proteins and incubating the control sera, it was determined that **measurable signals were obtained for both markers in the PC**, while the signal obtained in the NC was very low (Figure 63). Therefore, through this experiment, we were able to successfully measure both proteins and distinguish between the PC and NC.

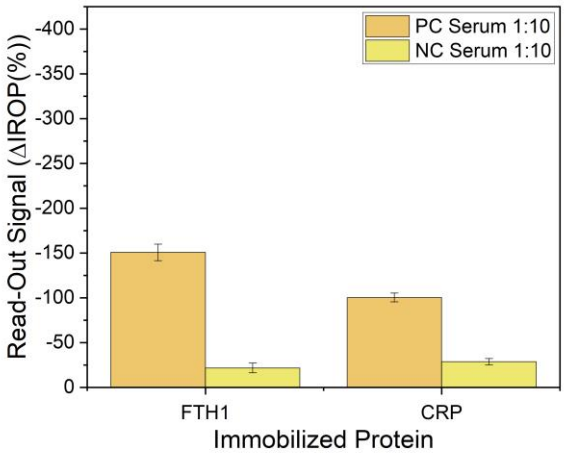

Figure 63. Analysis of FTH1 and CRP. Signals were obtained for both markers after incubation of PC and NC sera.

An incubation concentration of 100 μg/mL was established for the αFTH1 and αCRP Abs for 1 hour and 30 min. In addition, FTH1 and CRP proteins were measured in serum samples.

Once all the markers to be included in the multiplexed diagnostic KIT were measured, a summary of the PC and NC was presented. Figure 64A shows the measurement of sIgT against the virus proteins (rS1 and rRBD) and the NC protein (BSA). Figures 64B and 64C represent the values of these sIgs (sIgG, sIgM, and sIgA) for both control sera (positive and negative). Lastly, Figure 64D displays the selected biomarkers (FTH1 and CRP) for both cases as well. After conducting these experiments, it was decided to discard the measurement of Abs in serum against the rRBD protein. Multiple repetitions comparing the signals against rS1 showed that the signals were lower for the Abs against rRBD, and the background signal for the NC was higher, leading to less reproducible measurements overall.

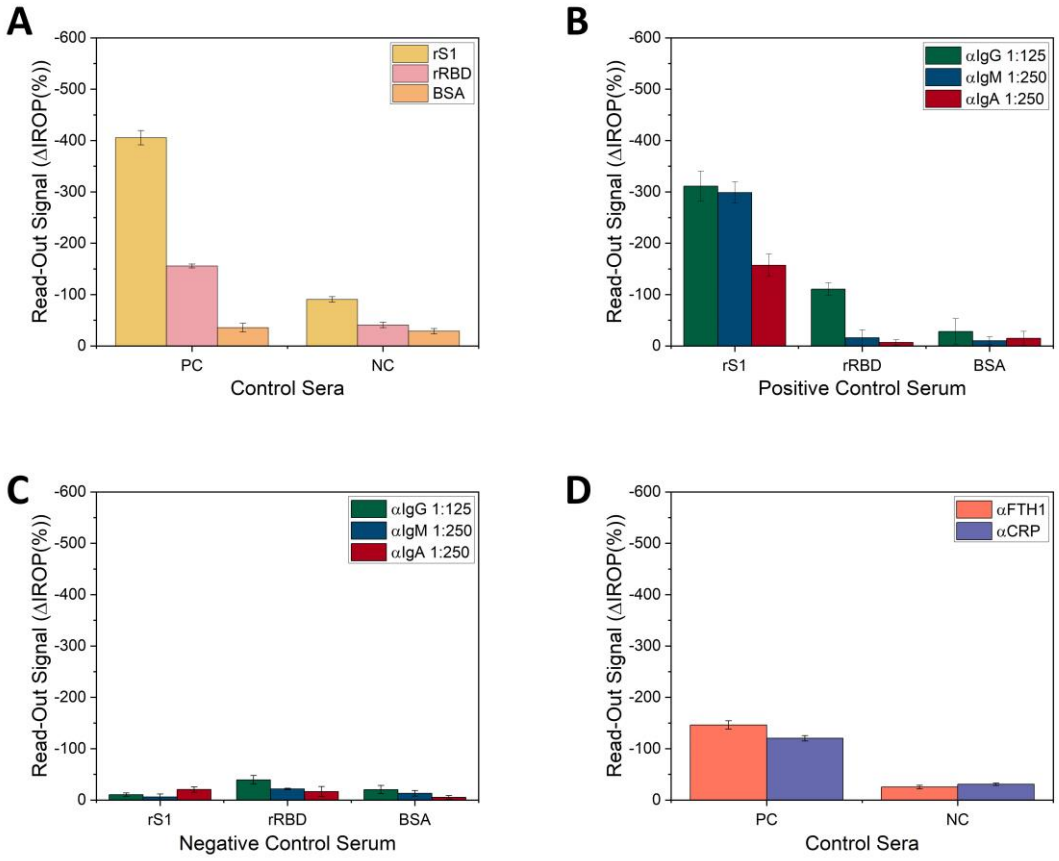

Figure 64. Results overview. A. Value of ΔIROP (%) for PC and NC sera on rS1, rRBD, and BSA proteins. **B.** Revealed sIgG, sIgM, and sIgA Abs on the three proteins for serum PC. **C.** NC values for sIgG, sIgM, and sIgA Abs after incubation on the three proteins. **D.** Results obtained for FTH1 and CRP markers in PC and NC sera.

3.4.1.9. *Correlation between ELISA technique and IODM*

After selecting the markers, establishing the protocols to measure them, and having the PC and NC samples, ELISA tests were performed to correlate and validate the results obtained through the IODM technology. Multiple patient samples (severe and moderate cases) were chosen along with the control sera for this purpose.

To correlate the two employed techniques (ELISA and IODM), detection assays were conducted for specific Abs against the virus protein rS1 (sIgG, sIgM, and sIgA) using both systems. Abs from 3 severe patients, 3 moderate patients, 1 PC, and 1 NC were detected. The titers of these Abs for severe cases (Figure 65A-C) and moderate cases (Figure 65D-F) were similar for all measurements in both techniques.

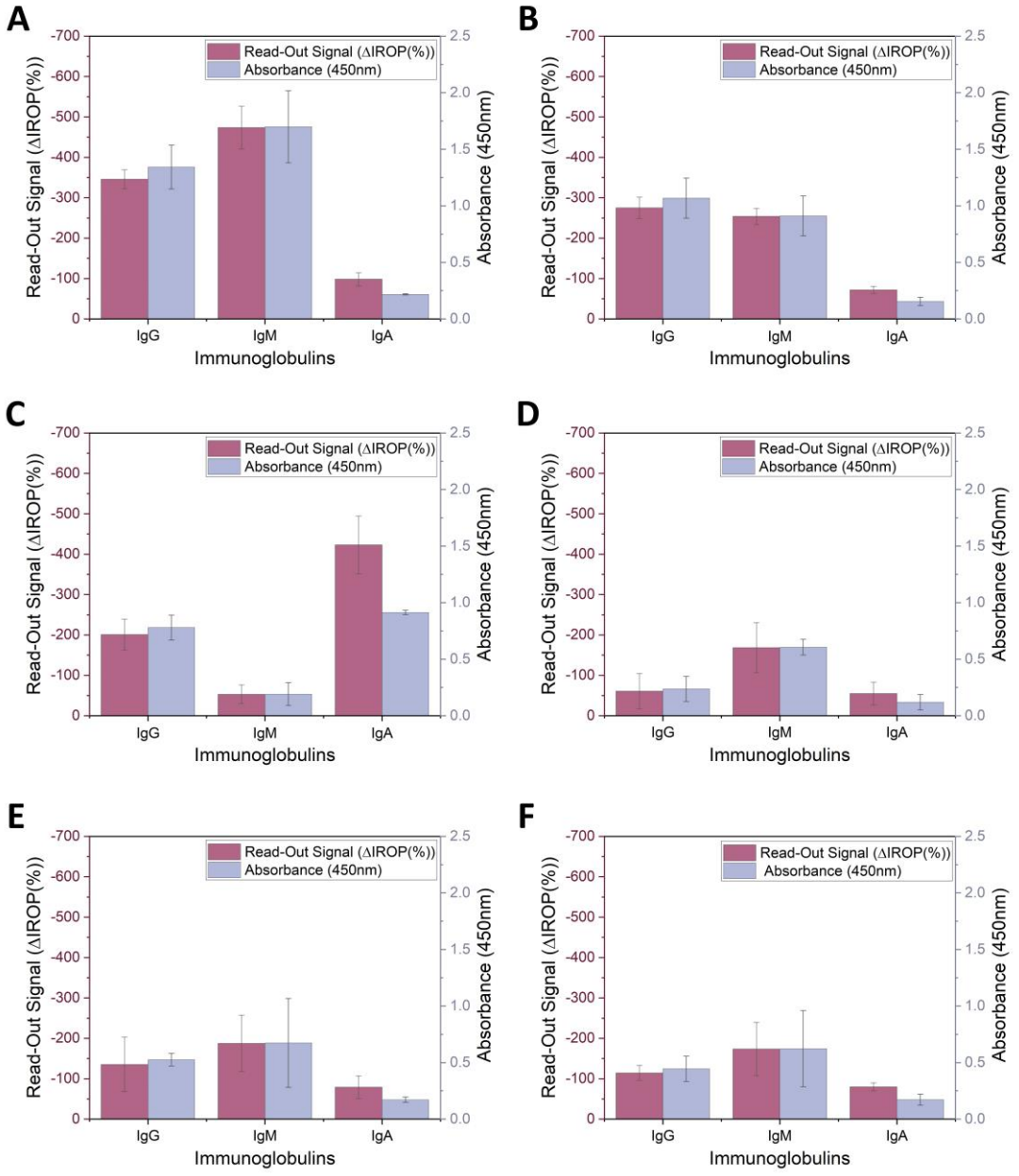

Figure 65. Correlation between ELISA and IODM. A-C. ΔIROP (%) and absorbance values at 450nm for sIgG, sIgM, and sIgA from three severe patients. **D-F.** Signals obtained by both techniques for sIgG, sIgM, and sIgA Abs from moderate cases (figure adapted from Murillo et al., 2021).

Similarly, for the PC (Figure 66A) and the NC (Figure 66B), the same results were observed. Finally, a linear fit was performed with the results obtained, correlating the measurements obtained from the IODM-based BICELLs with the ELISA technique. As shown in Figure 67, **a good correlation between the measurements was observed.**

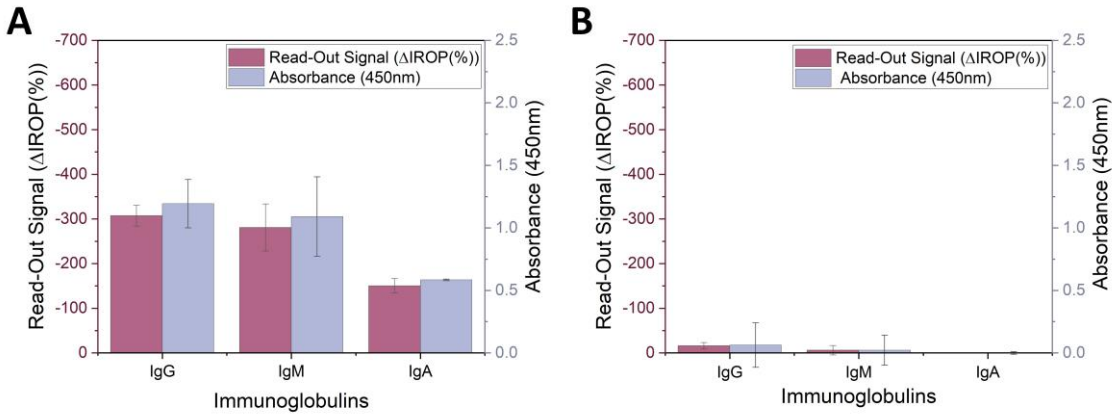

Figure 66. Correlation between ELISA and IODM. A. Values obtained in both techniques for PC serum. **B.** NC signals in ELISA and IODM on virus protein (figure adapted from Murillo et al., 2021).

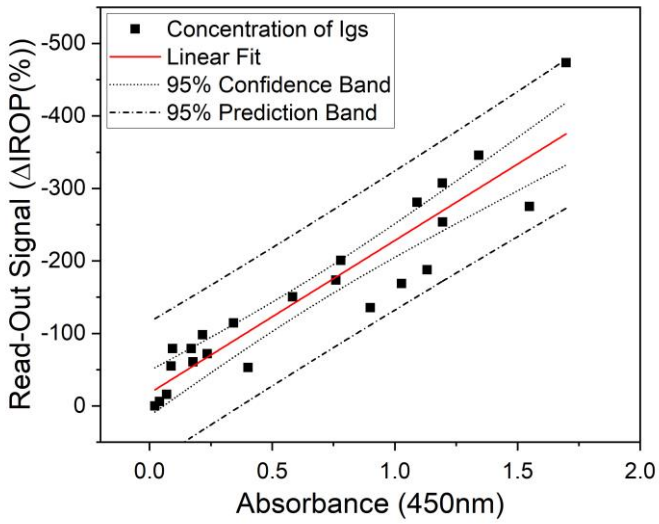

Figure 67. Linear fit between the ELISA technique and the IODM. Linear fit between the ΔIROP (%) signal obtained and the absorbance measured at 450 nm for the detected Igs (Murillo et al., 2021).

A correlation between the ELISA technique and the IODM was performed, obtaining a linear fit of the SARS-CoV-2 specific Abs (sIgG, sIgM and sIgA).

3.4.1.10. *Evaluation of COVID-19 biomarkers in serum.*

To evaluate the different biomarkers, four different bioreceptors (αHuman-FTH1, αHuman-CRP, rS1), as well as BSA as a NC protein, were immobilized in the KITs. After incubating the samples and performing the washes, the levels of sIgT, FTH1, and CRP were determined in a first step. After subsequent incubation with secondary Abs, the signal of SARS-CoV-2 specific IgG, IgM, and IgA Abs was determined. These levels of the different biomarkers measured were analyzed for each Level of Severity of COVID-19 (LSC).

To obtain the specific signal of each of the biomarkers, the difference between the signal of the serum sample of each patient on the BSA protein and the signal on the specific biomarker was calculated. In this way, the background signal of the nonspecific binding that could occur in each sample was eliminated. The levels for each biomarker of the NC were established by subtracting the signal of a clinically healthy patient sample tested on BSA from the signal obtained on each biomarker, and adding the standard deviation. This procedure was carried out in the same way to establish the PC with a sample from a clinically diagnosed patient. Both signals were used as quality control of the measurements during the experiments.

The results obtained for sIgT and for each type of Ab (sIgG, sIgM, and sIgA) in the serum samples of all patients were classified based on severity into severe (Figure 68), moderate (Figure 69), and mild (Figure 70) cases. Similarly, the results obtained for FTH1 and CRP were also represented divided into severe (Figure 71), moderate (Figure 72), and mild cases (Figure 73).

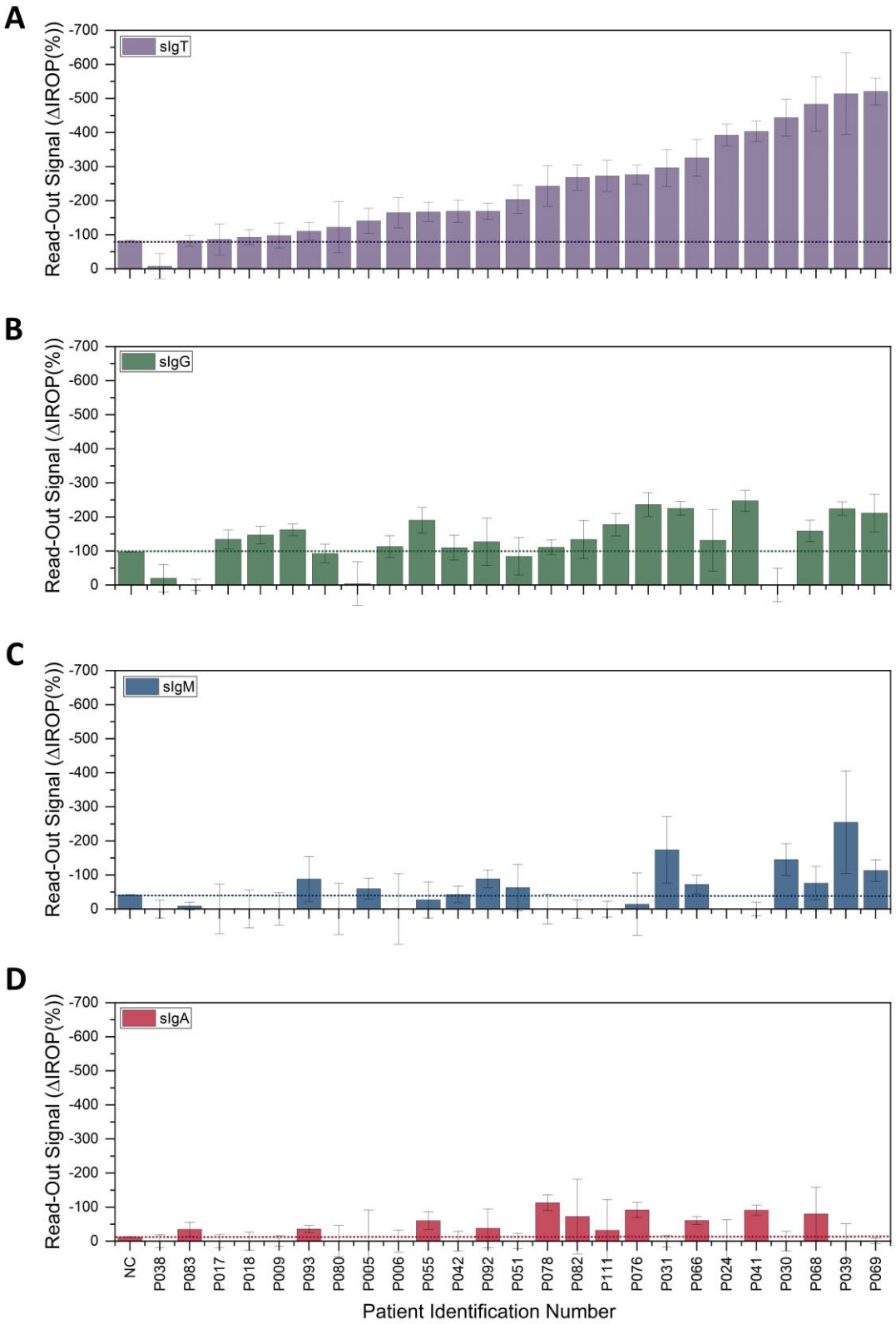

Figure 68. Detection of specific Abs against SARS-CoV-2 for severe patients. A dashed line represents the cut-off for each biomarker. **A.** sIgT signal. **B.** sIgG signal. **C.** sIgM signal. **D.** sIgA signal (figure adapted from Murillo et al., 2022).

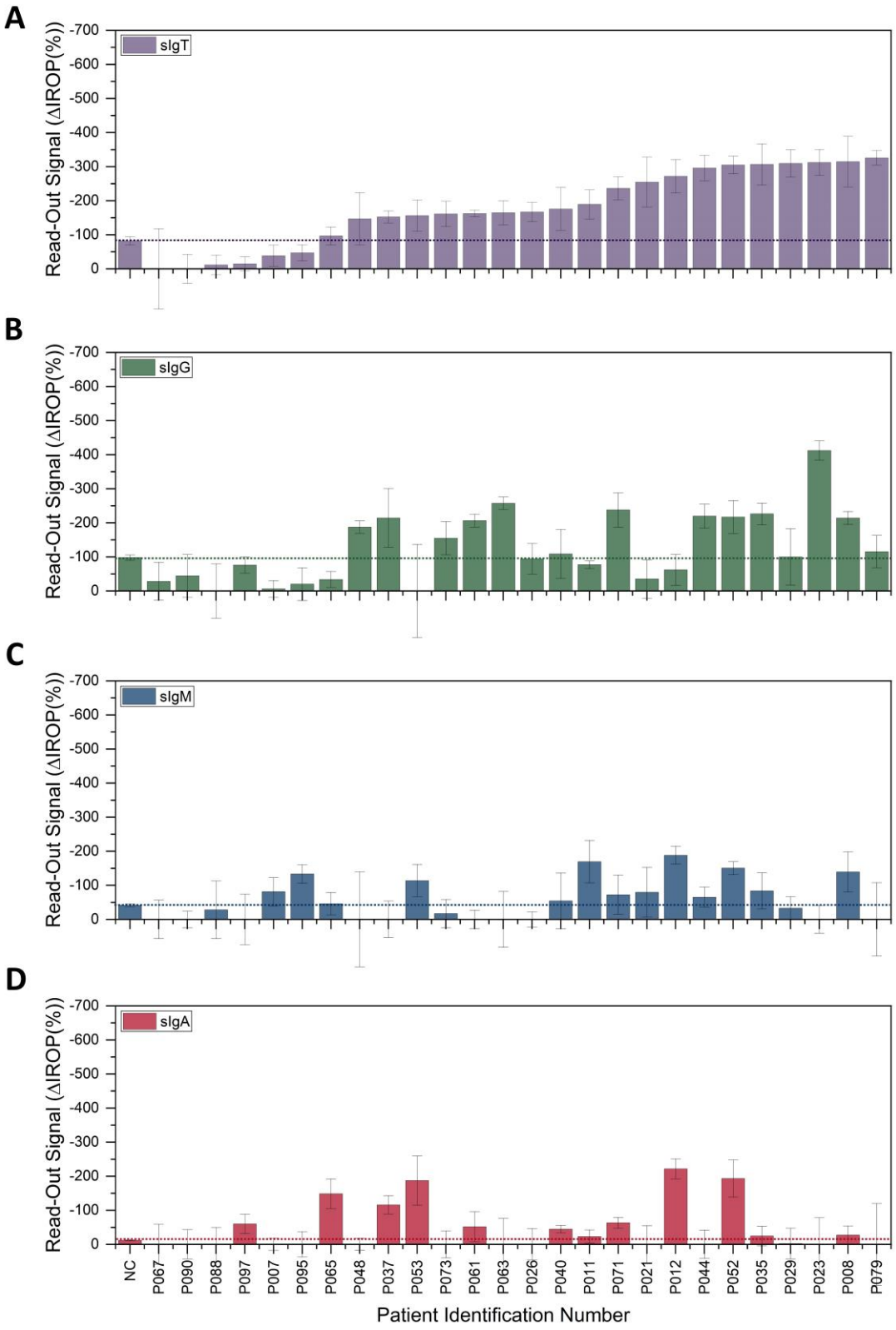

Figure 69. Detection of specific Abs against SARS-CoV-2 for moderate patients. A dashed line represents the cut-off for each biomarker. **A.** sIgT signal. **B.** sIgG signal. **C.** sIgM signal. **D.** sIgA signal (figure adapted from Murillo et al., 2022).

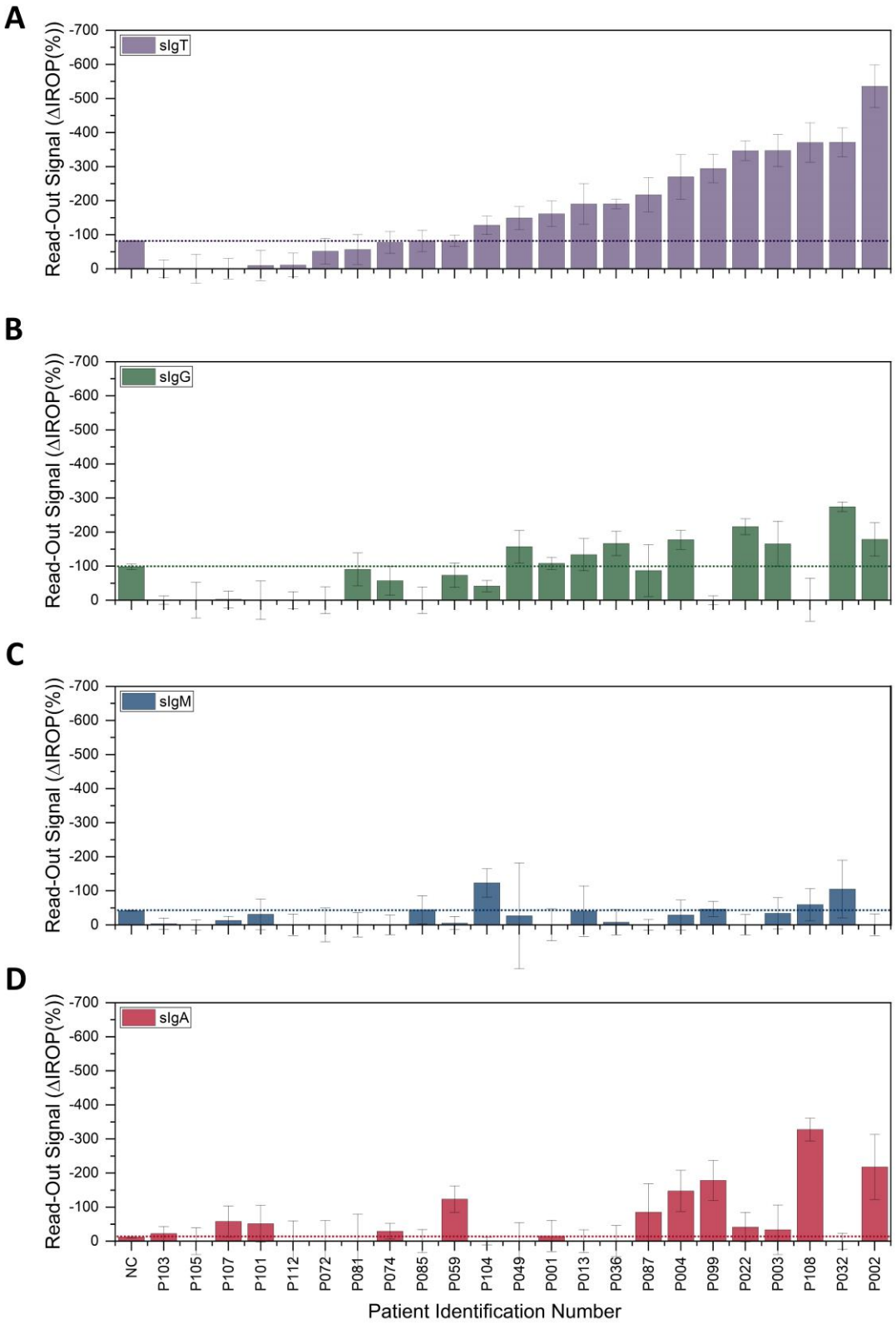

Figure 70. Detection of specific Abs against SARS-CoV-2 for mild patients. A dashed line represents the cut-off for each biomarker. **A.** sIgT signal. **B.** sIgG signal. **C.** sIgM signal. **D.** sIgA signal (figure adapted from Murillo et al., 2022).

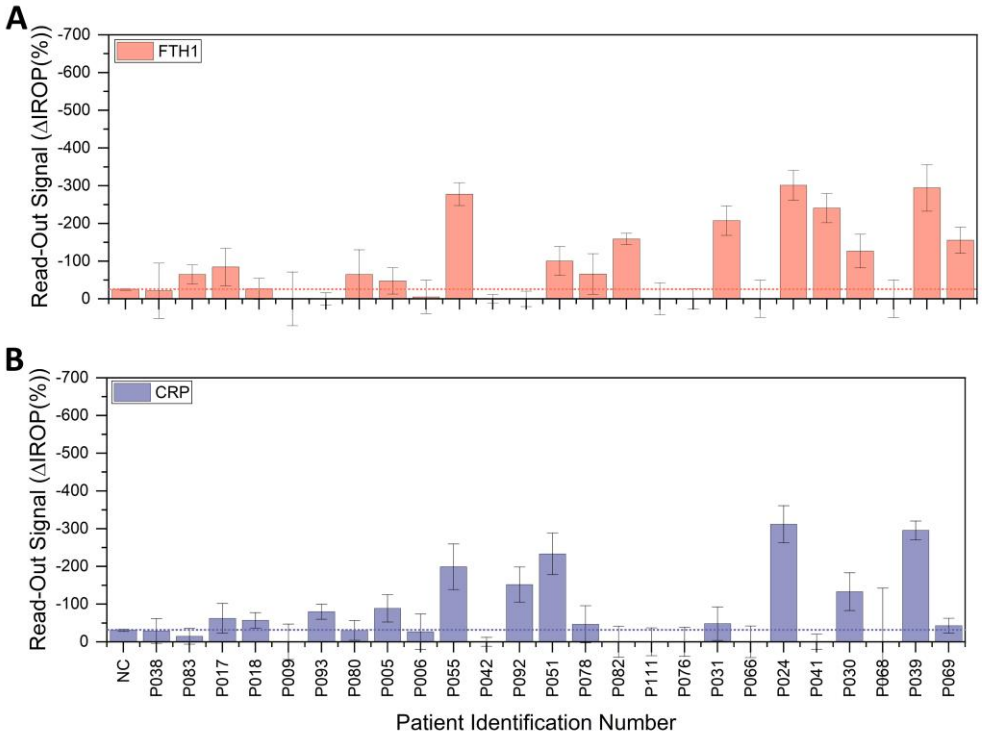

Figure 71. Detection of FTH1 and CRP markers for severe patients. A dashed line represents the cut-off for each biomarker. **A.** FTH1 signal. **B.** CRP signal (figure adapted from Murillo et al., 2022).

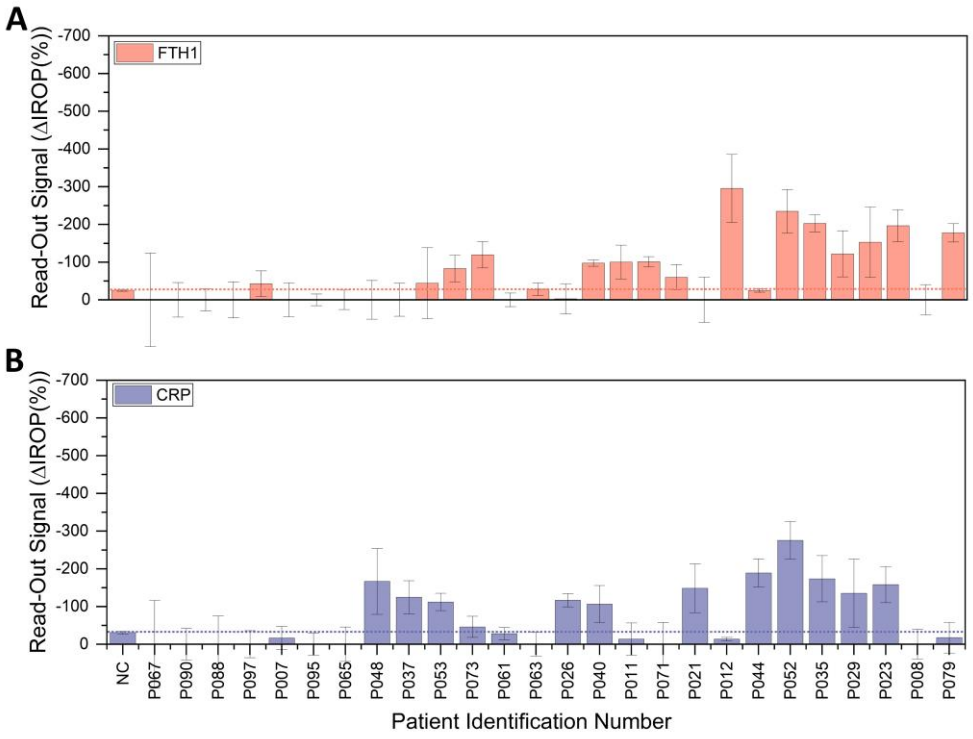

Figure 72. Detection of FTH1 and CRP markers for moderate patients. A dashed line represents the cut-off for each biomarker. **A.** FTH1 signal. **B.** CRP signal (figure adapted from Murillo et al., 2022).

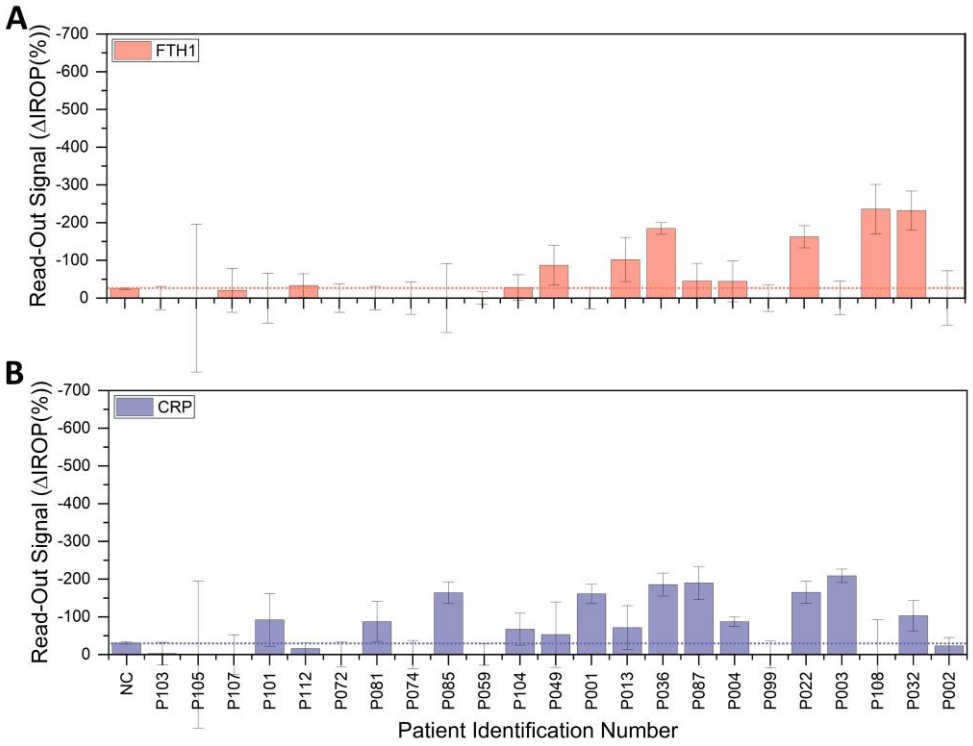

Figure 73. Detection of FTH1 and CRP markers for mild patients. A dashed line represents the cut-off for each biomarker. **A.** FTH1 signal. **B.** CRP signal (figure adapted from Murillo et al., 2022).

The results presented in Figures 74 and 75 compare the percentage of patients positive for each LSC considering the six biomarkers measured (sIgT, sIgG, sIgM, sIgA, FTH1 and CRP).

Comparing the three levels of severity, it was observed that **96% of severe patients were positive for sIgT signal**, while moderate patients showed only 77% positive and 65% in the case of mild patients. Within sIgT, for each of the measured Abs, it could be observed that **severe patients had a higher percentage of positives for sIgG (with more than 72%) in addition to a high percentage of sIgM (with more than 48%),** compared to moderate and mild patients.

In the case of **sIgA, a higher percentage of positives was observed in mild patients at 57%** compared to severe (44%) and moderate (38%) patients.

Performing this same comparison with the two biomarkers of inflammation measured, **more than 60% of severe patients presented positive levels for FTH1** compared to moderate patients (58%) and mild patients (43%). However, for the other measured marker, **CRP, no differences were observed** between the three LSC categories.

Considering this comparison between the different categories, it was observed that **the positivity for each of the biomarkers was dependent on the severity of the disease**, producing higher levels of Ab titers in the case of severe patients, especially in sIgT and sIgG, while sIgA titers were lower. Similarly, the percentage of patients positive for FTH1 is higher in severe patients, while these differences were not observable for CRP.

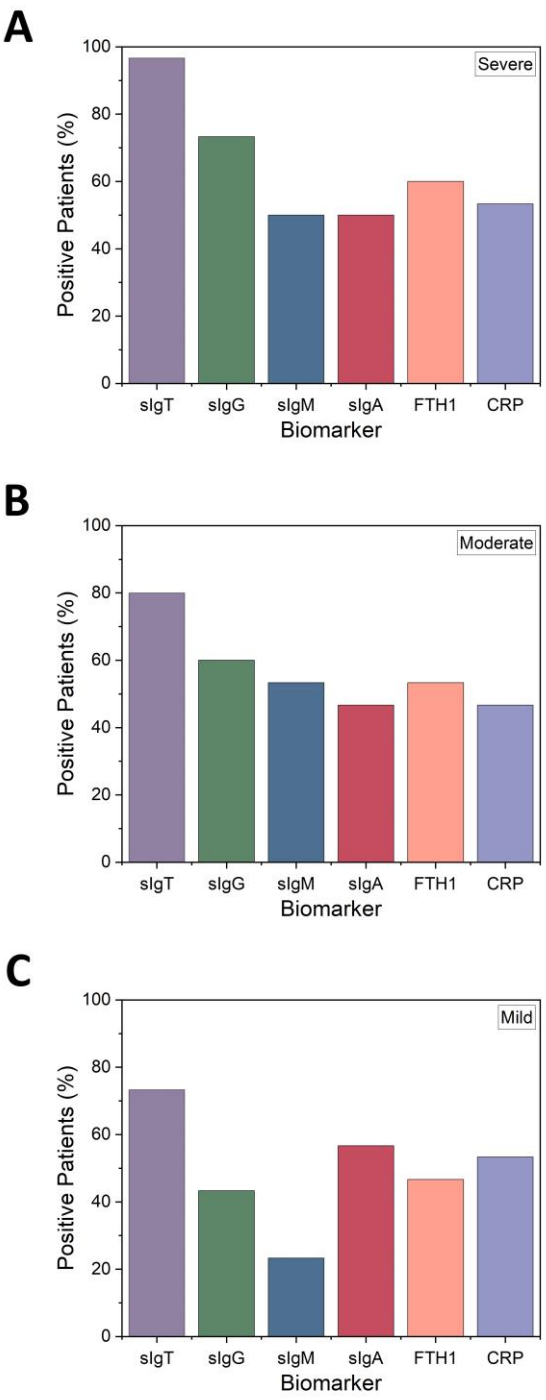

Figure 74. Percentage of positive patients for each biomarker based on LSC. A. Percentages for each biomarker in severe patients. **B.** Percentages for each biomarker of moderate patients. **C.** Percentages for each biomarker of mild patients (figure adapted from Murillo et al., 2022).

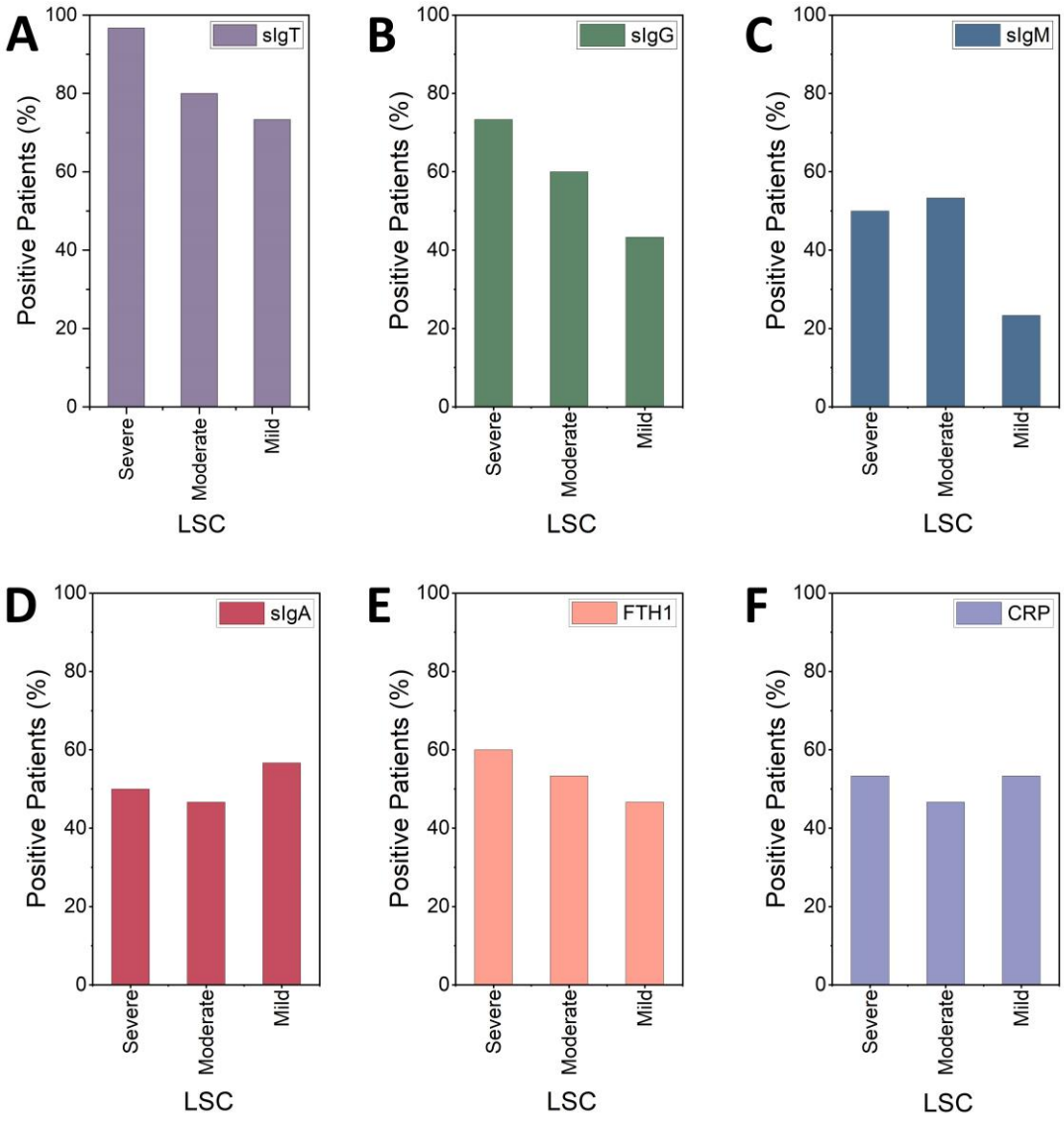

Figure 75. Percentage of patients positive for each biomarker according to LSC. A. % sIgT-positive patients. **B.** % sIgG-positive patients. **C.** % sIgM-positive patients. **D.** % sIgA-positive patients. **E.** % FTH1 positive patients. **F.** % CRP positive patients (figure adapted from Murillo et al., 2022).

In summary, it was observed that the positivity of the biomarkers measured was dependent on the degree of disease severity. Patients with severe LSC showed a higher level of sIgT, sIgG and FTH1 compared to moderate and mild patients. For the biomarker CRP no differences were observed between the LSC groups.

In these experiments, 20 samples of blood donors from the end of February 2020 from the Hospital Clínico San Carlos were analyzed in order to study cases that could have been asymptomatic. Once all markers were determined, **it was observed that some blood donors had high titers for SARS-CoV-2 specific Abs (Figure 76) and high values of FTH1 and CRP** (Figure 77).

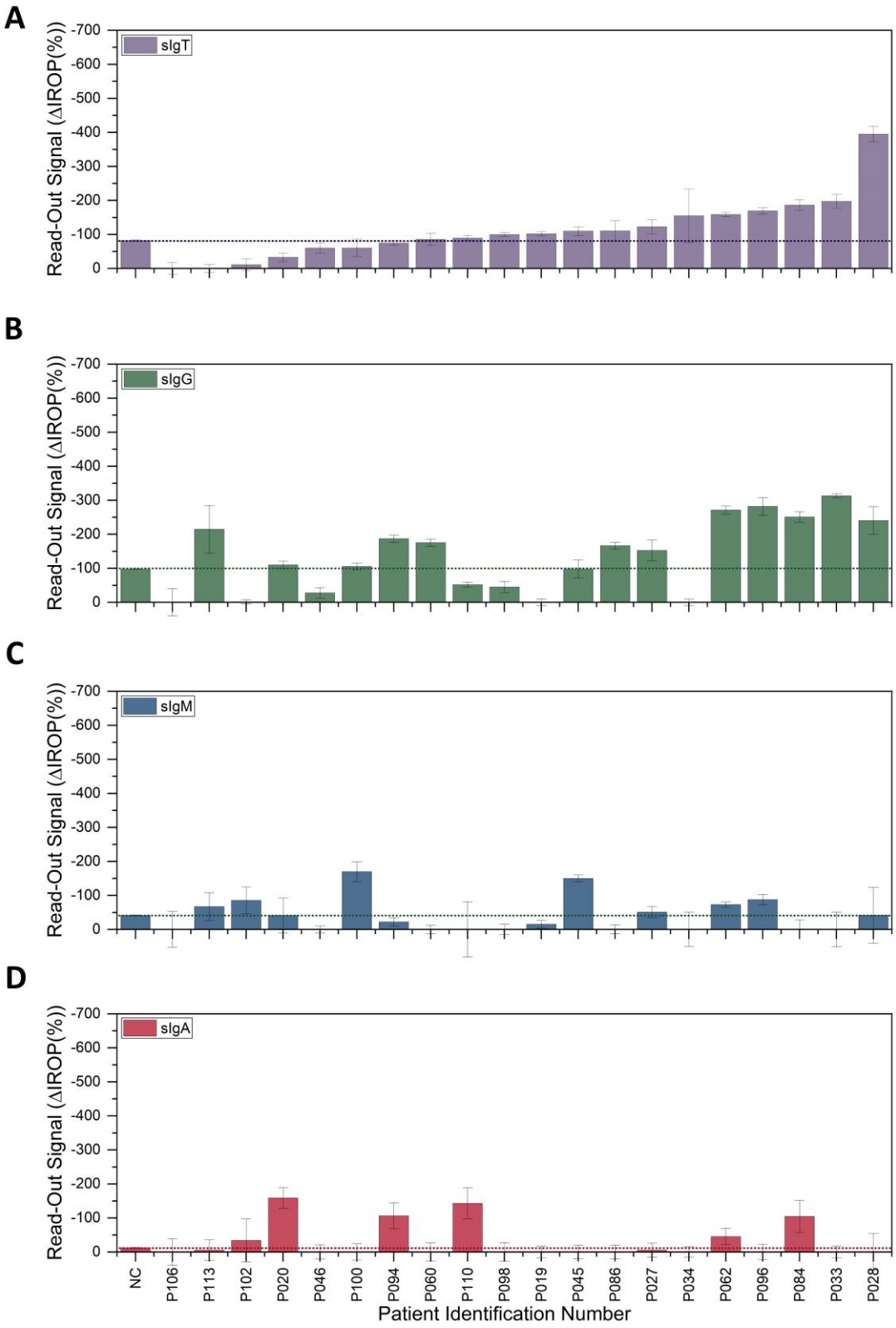

Figure 76. Detection of specific Abs to SARS-CoV-2 for blood donors. A dashed line represents the cut-off for each biomarker. **A.** sIgT signal. **B.** sIgG signal. **C.** sIgM signal. **D.** sIgA signal (figure adapted from Murillo et al., 2022).

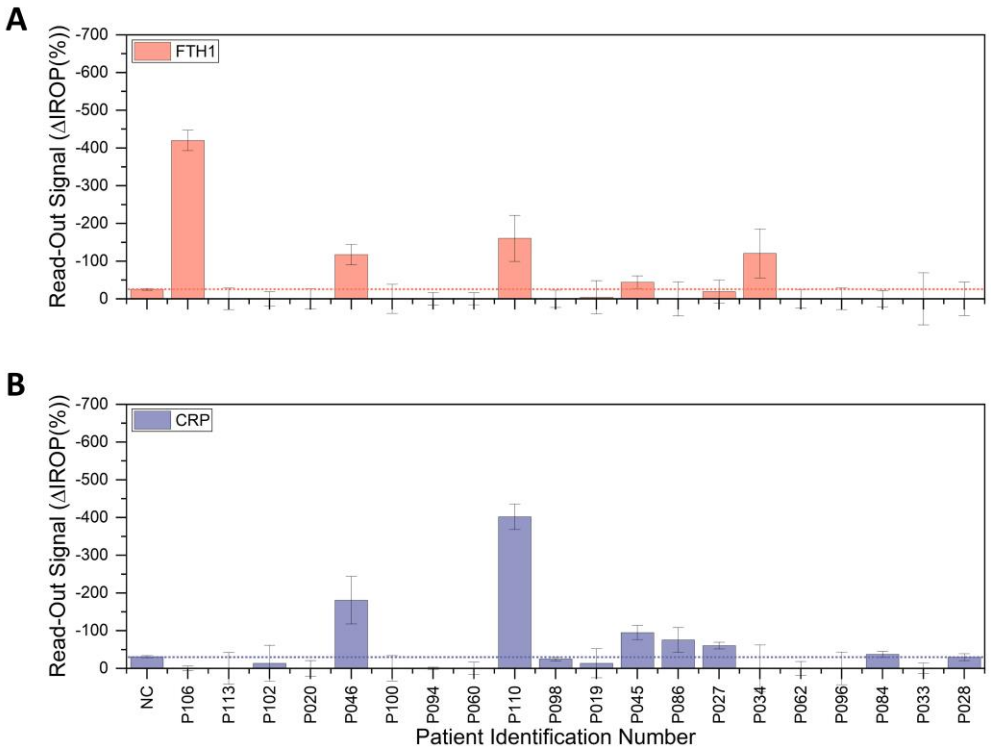

Figure 77. Detection of FTH1 and CRP markers for blood donors. A dashed line represents the cut-off for each biomarker. **A.** FTH1 signal. **B.** CRP signal (figure adapted from Murillo et al., 2022).

3.4.1.11. *Severity model*

Finally, for each of the biomarkers measured, the degree of correlation of each biomarker was analyzed against the total amount of SARS-CoV-2 specific Abs (sIgT) (Figure 78). In this model, it was observed that **the most significant biomarkers were sIgG, sIgM, and FTH1, compared to sIgA and CRP**. Based on this, it could be assumed that sIgA would not provide more information than that already obtained by sIgG and sIgM. On the other hand, CRP might not be significant in the model as it is a nonspecific marker of inflammation (Hirsch et al., 2017).

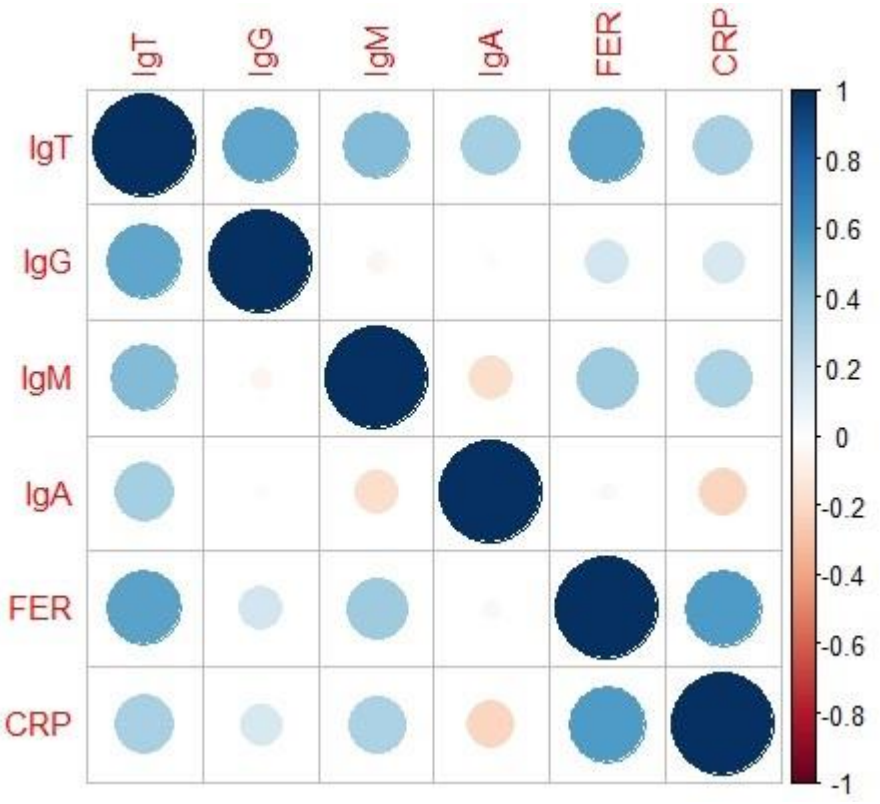

Figure 78. Correlation matrix. The size and color of the circles refer to the level of correlation represented in the bar on the right (Murillo et al., 2022).

Once the individual correlation was analyzed for each biomarker, a MLRM was designed to correlate the value of sIgT with all the biomarkers measured sIgG, sIgM, sIgA, FTH1 and CRP, with the p-values for each biomarker being represented in Table 14.

Using the model, **CRP was found to be a non-significant variable**, confirming the results obtained in the previous analysis. In fact, the p-value obtained (0.47) is far from the level considered statistically significant (0.05). Therefore, the exclusion of this variable in the model does not modify the results.

Eliminating CRP from the multiple regression model, **it was observed that the variables sIgG (p-value = 1.5×10^{-10}), sIgM (p-value = 6.08×10^{-8}), sIgA (p-value = 7.09×10^{-8}), and FTH1 (p-value = 1.7×10^{-4}) were highly significant**. Therefore, considering these variables, the coefficients of each of them were calculated to explain sIgT. The model obtained is represented by the following *Eq.* 15 (Murillo et al., 2022):

$$\widehat{IgT} = -0.20 + 0.76\,[IgG] + 1.02\,[IgM] + 1.91\,[IgA] + 0.43\,[FTH1] \qquad Eq.\ 15$$

The model indicates that the level of sIgT increases with increasing sIgG, sIgM, sIgA, and FTH1 with **a goodness of fit of 70.29%** (Adjusted R-squared) for the model.

Finally, we considered studying the relationship of the qualitative variable of severity (severe, moderate and mild) in the multiple regression model.

This model is represented in *Eq. 16* and **explains sIgT versus SARS-CoV-2 with a goodness of fit of 73.01%** (Adjusted R-squared) (Murillo et al., 2022).

$$\widehat{IgT} = 22.72 + 0.78\,[IgG] + 1.05\,[IgM] + 0.88\,[IgA] + 0.41\,[FTH1] \qquad Eq.\ 16$$
$$-58.92\,[Mild] - 14.78\,[Moderate]$$

In this model, with a coefficient of 22.72, it corresponds to the intercept. Furthermore, it shows that moderate and mild patients have lower sIgT levels than severe patients, suggesting also that **the severity of COVID-19 is related to sIgT (sIgG, sIgM, and sIgA) and FTH1 values.**

Finally, after the measurements of all biomarkers in all serum samples, a severity model was performed. In this model, first, the significance of each of the variables was analyzed against sIgT and then LSC was added improving the model fit to 73.01%. This suggested that COVID-19 severity is related to sIgT and FTH1 levels.

3.4.2. Case I. II. Development of an *in-vitro* optical diagnostic system for the detection of specific Abs against SARS-CoV-2 in saliva

On the other hand, due to the high incidence and prevalence of the disease caused by the SARS-CoV-2 virus in the population, it was necessary to have a diagnostic system to monitor and conduct a study on the population's immunity. To facilitate a much simpler monitoring of this acquired immunity, **a much less invasive and easier-to-obtain sample for all age groups, such as saliva**, was used.

Therefore, it was necessary to develop an *in-vitro* diagnostic system for specific Abs against SARS-CoV-2 in saliva, specifically for the detection of sIgA.

3.4.2.1. *Recognition assay of sIgA in saliva samples*

The first step was the immobilization of the virus protein used for detecting Abs in serum, rS1, under the same conditions as described for the serum diagnostic KIT. The washing step after the coating process of the KITs remained the same as described before.

After incubating the PC saliva on the surface coated with the virus protein rS1 and the BSA protein, it can be observed in Figure 79A that **there is a difference in signal between the specific surface and the NC surface,** although it is not very high. Once the KITs were developed with the secondary Ab for determining saliva sIgA, **we only obtained a signal in one of the saliva samples on the virus protein surface** (Figure 79B). Similarly, we observed that there was no signal on the surface coated with the NC protein. Based on these results, different steps of the protocol were modified, such as the incubation time of the saliva and its dilution in the recognition step.

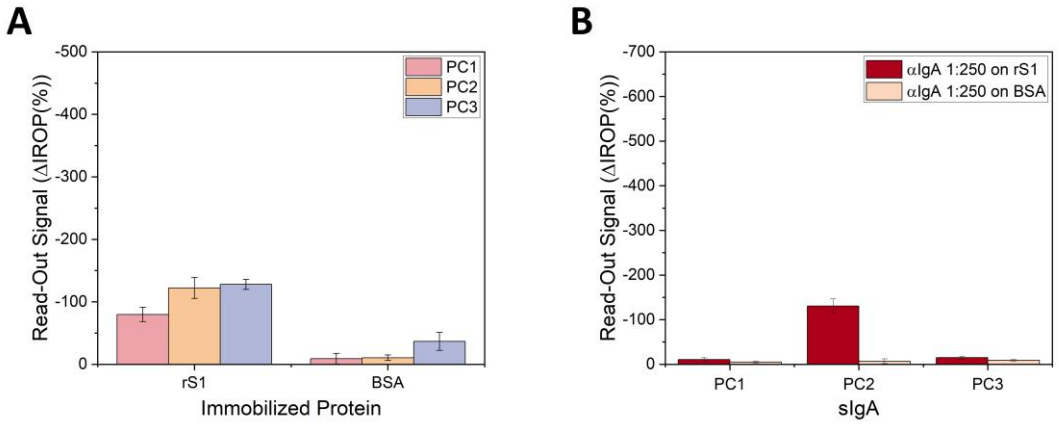

Figure 79. SARS-CoV-2 positive saliva on rS1 and BSA and sIgA Ab development. A. ΔIROP (%) values on rS1 and BSA of the three incubated PC saliva. **B.** Revealing αHuman-IgA Ab in the three samples on rS1 and BSA.

After incubating the PC saliva ON, both diluted 1:5 and undiluted, on the rS1 protein surface, it was observed that **a higher signal was obtained when the saliva was directly incubated undiluted** (Figure 80A) compared to the diluted saliva. Additionally, in this case, no signal was obtained for the diluted saliva samples, contrary to the results obtained in the previous assay. As seen in Figure 80C, **for the rRBD domain, only one of the PC saliva samples showed a signal**, while the others did not exhibit any recognition. Finally, in Figure 80E, the signal obtained on the surface coated with the NC protein, BSA, is represented. When comparing the signal from the diluted and undiluted saliva, it was noticed that undiluted saliva may lead to more background and non-specific signals compared to diluted saliva. Additionally, when comparing this signal with the signal represented in Figure 80A, it was lower in the latter case.

After obtaining the recognition signals of the saliva on the two virus proteins and the NC protein, the secondary Ab was incubated for the revelation of the sIgA bound. For the rS1 protein, although the saliva samples showed signals on the virus protein surface in contrast to the negative surface, **there was no sIgA signal in the development step** (Figure 80B). On the other hand, **for the rRBD domain, a small signal was obtained for the PC saliva 1** (Figure 80D). However, this signal was very low, and in this case, no signal had been obtained during the recognition for the rRBD protein, indicating non-specificity. Finally, when revealing the recognition of the saliva on the BSA protein surface, no signal was obtained for any of the samples (Figure 80F).

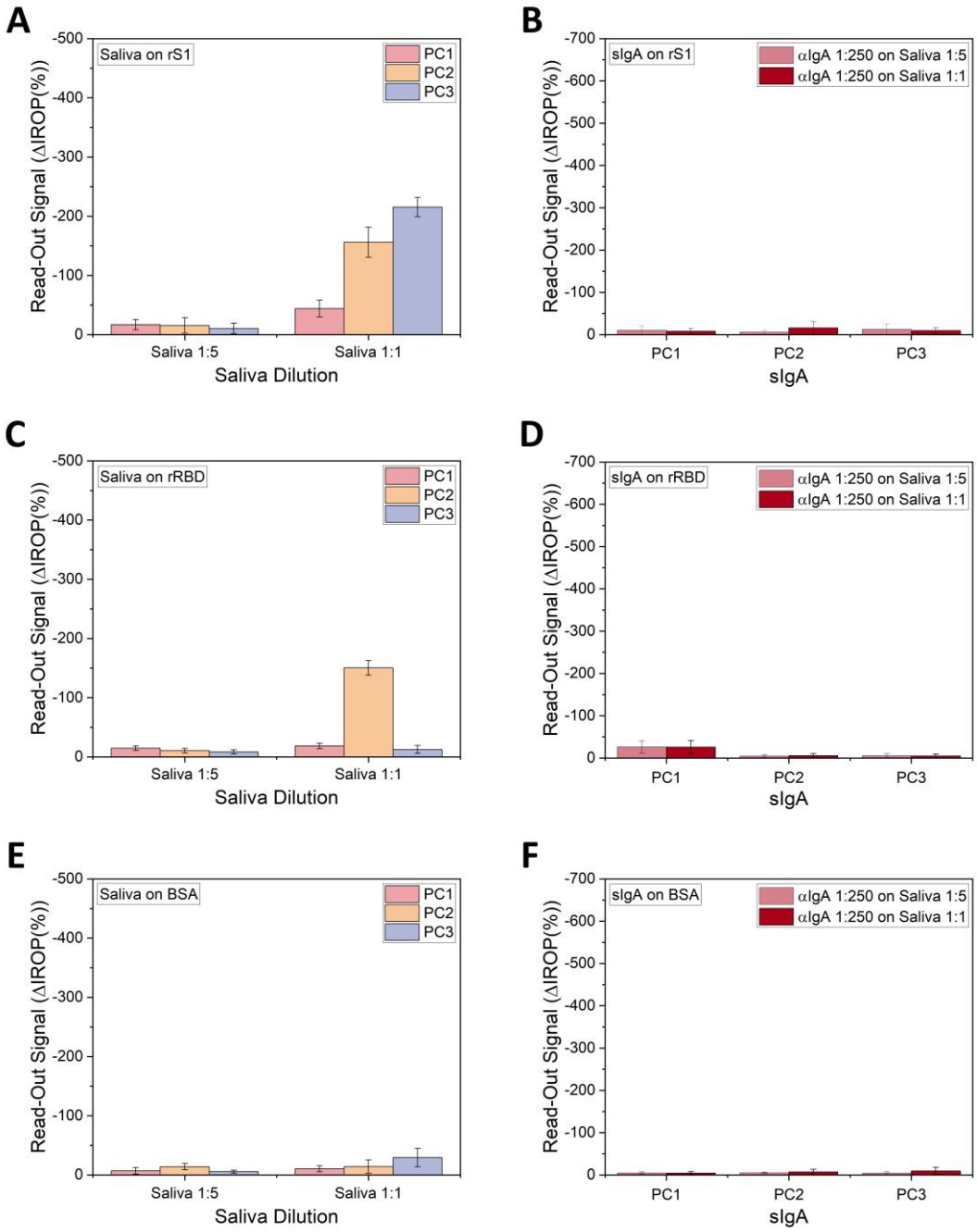

Figure 80. Positive saliva samples on rS1, rRBD and BSA. A. Incubation of 1:5 diluted and undiluted ON saliva on rS1 protein. **B.** Revealed sIgA Ab in the three diluted and undiluted positive samples incubated on rS1. **C.** Incubation on rRBD protein of the 1:5 diluted and undiluted PC saliva. **D.** sIgA Ab development on the positive samples incubated on rRBD. **E.** Incubation of PC saliva on NC BSA protein at 1:5 dilution and undiluted. **F.** sIgA Ab development of positive saliva incubated on BSA.

Considering the results obtained, it was thought that the issue could be related to the secondary Ab. Therefore, another αHuman-IgA Ab was purchased, and both Abs were tested following the latest protocol described. The undiluted saliva samples were incubated ON using the two different Abs. In this case, the PC saliva samples were also incubated on the rRBD protein and the BSA protein as a NC.

Upon incubating the saliva samples on the two virus proteins and the negative surface, it can be observed in Figure 81A that all three PC saliva samples show a signal for both viral proteins, while there is no signal for the BSA, confirming the specific recognition of the Abs present in the sample. Additionally, it can be noticed that there are more Abs against the rS1 protein compared to the rRBD protein.

In the second step of the experiment, when incubating the two αHuman-IgA Abs (the one initially used and the newly purchased one), it is clearly demonstrated in Figure 80B that the first Ab being used was not functioning properly or might have undergone some degradation, as it does not provide any signal. However, with the newly purchased Ab, we **obtain a signal for all three PC samples when they have been incubated on the rS1 protein**. Furthermore, **signals were also observed with this second Ab in cells where the rRBD protein was being recognized**, although these signals were much weaker, consistent with the signals obtained from the saliva (Figure 81C). The signals were lower for this protein compared to rS1.

Lastly, the signals obtained by incubating the secondary Ab on the samples against BSA were very low, corresponding to some non-specific bindings (Figure 81D).

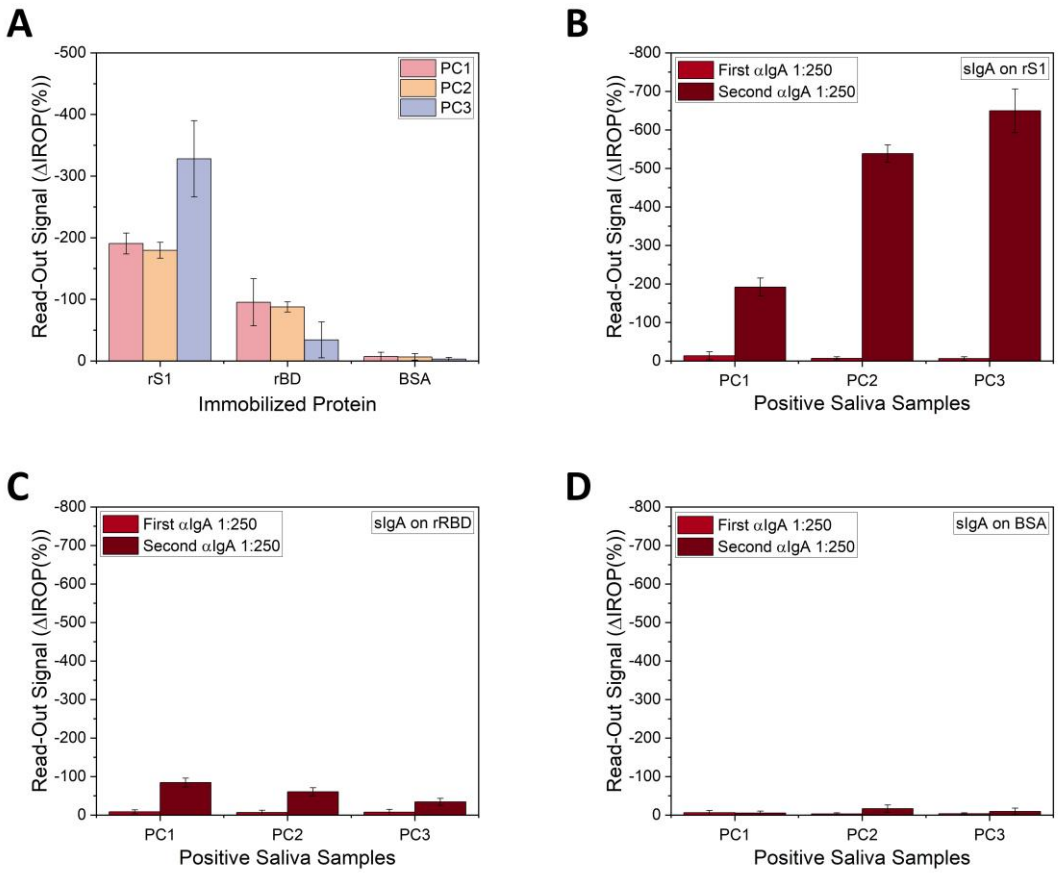

Figure 81. Comparison between the two αIgA Abs used. A. Signals obtained from ΔIROP (%) upon incubation of PC saliva on rS1, rRBD and BSA. **B.** Development of the sIgA Ab with two different αHuman-IgA Abs on the positive saliva samples incubated on rS1. **C.** Disclosed sIgA Ab with two different αHuman-IgA Abs on the positive saliva samples incubated on rRBD. **D.** sIgA Ab developed with two different αHuman-IgA Abs on the positive saliva samples incubated on BSA.

After the experiments, saliva samples were established to incubate undiluted ON and after the Ab change, sIgA signals were obtained for all samples on rS1 and rRDB virus proteins.

Due to the problems arising during the pandemic, the αHuman-IgA Ab that was purchased and used for the last experiments went out of stock. Consequently, another Ab had to be purchased, and the experiments were repeated using this new Ab. **The concentration of use for the new Ab was fixed at 1:10**, which was used for all subsequent experiments.

In order to obtain results more rapidly, incubation tests of the saliva samples were conducted at different times. This likely involved testing different incubation durations to optimize the detection of sIgA in the samples.

These adjustments were necessary to ensure the continuity of the research despite the challenges posed by the changing availability of reagents during the pandemic. The researchers adapted their methods to continue their investigation on the detection and recognition of sIgA in the saliva samples for studying the immune response against SARS-CoV-2.

3.4.2.2. *Study of different incubation times of saliva samples*

After incubating the saliva samples at different times to test if the incubation time could be shortened, the results in Figure 82A show that as the incubation time increases, the signal obtained also increases, with **the highest signal observed when the samples are incubated ON**. Additionally, it is in this case that fewer specific bindings are observed, which may be attributed to the temperature.

The secondary Ab was incubated on these samples to determine the levels of sIgA, and similarly, more signal was obtained in samples that had been incubated for a longer time (Figure 82B), corresponding to the previous averages of the saliva.

Based on these results, **it was decided to continue incubating the saliva samples ON at 4°C**.

The decision to continue with ON incubation at 4°C was likely made to ensure the most robust and reliable results, as longer incubation times appeared to yield higher signals and potentially reduce non-specific bindings that might occur at higher temperatures. This optimized incubation protocol allowed for better detection and quantification of sIgA in the saliva samples for studying the immune response against SARS-CoV-2.

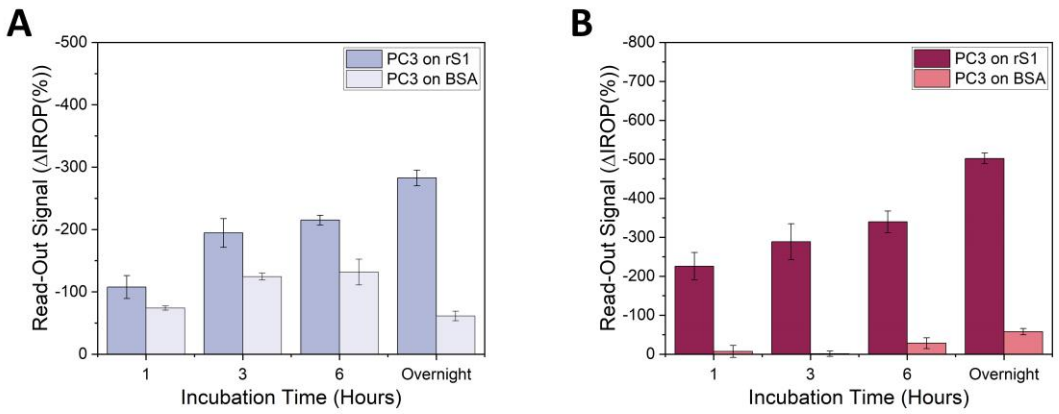

Figure 82. Incubation time study of the saliva sample. A. Representation of the signal collected from PC3 saliva incubated at different times on rS1 and BSA. **B.** Revealed sIgA Ab over all conditions.

3.4.2.3. *Study of different protein concentration for immobilization*

In an attempt to lower the concentration of the rS1 protein used for coating the KITs, they were incubated with different concentrations of the rS1 protein. These coated KITs were then recognized using the PC3 saliva, and the results are represented in Figure 83. It can be observed that as the concentration of immobilized rS1 protein on the sensor surface increases, the signal obtained upon incubating the sample also increases. However, **when revealing with the secondary Ab, the difference in signal is not as significant**, indicating that **KITs can be immobilized with a concentration of 100 µg/mL**.

On the other hand, on the NC protein surface, no signal was obtained in both the recognition and the revelation steps. **This confirms the specificity of the assay**, as the NC surface did not show any non-specific binding or signal, supporting the validity of the experimental results.

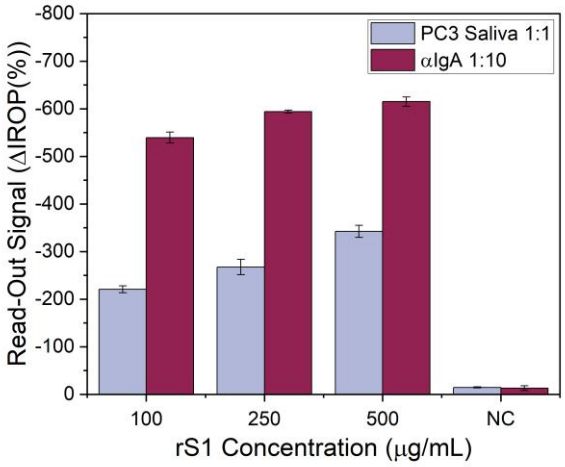

Figure 83. Test of rS1 protein concentration in the immobilization step.

In summary, the concentration of rS1 virus protein was set at 100 µg/mL. The saliva was further incubated undiluted ON at 4°C and the αHuman IgA development was determined at a 1:10 dilution.

3.4.2.4. *Recognition against the rN protein*

Later on, specific Abs against another recombinant viral protein corresponding to the nucleocapsid, called rN, were also tested. The rN protein was immobilized on the sensor surface at different concentrations (Figure 84), and **the concentration of 100 µg/mL was selected to coat the biosensor cells.**

In the KITs coated with the rN protein at this concentration, the PC and NC saliva samples were incubated, along with KITs coated with the rS1, rRBD, and BSA proteins. This assay **confirmed the specific recognition in the positive saliva sample, as indicated by the difference in signal compared to the NC saliva for all the viral proteins, with the most significant difference observed for the rS1 protein** (Figure 85A). This was further confirmed with the incubation of the secondary Ab for the development step. It was found that the signal was only obtained with the secondary Ab when incubated with the PC saliva. Furthermore, it was observed that, **for the same positive sample, the quantity of Abs against the different viral proteins varied, with the majority of Abs being specific to the rS1 protein** (Figure 85B).

These results demonstrate that the assay was able to successfully detect specific Abs against the rN protein as well, further validating its ability to identify immune responses to different components of the SARS-CoV-2 virus. Additionally, the findings showed that the level of Abs against different viral proteins varied, with a higher Ab titer against the rS1 protein.

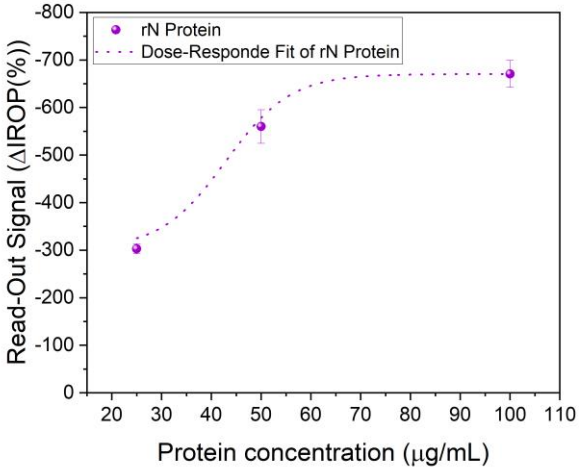

Figure 84. rN protein dose-response curve. The sigmoidal fit of dose-response curves is depicted.

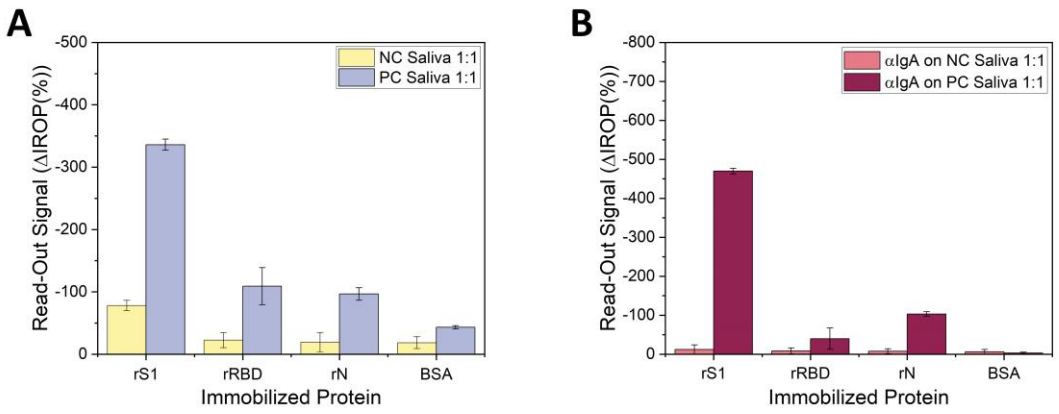

Figure 85. Ab detection against rS1, rRBD, rN, and BSA. A. Representation of PC and NC saliva signals on the three virus proteins (rS1, rN and rRBD) and the NC protein BSA. **B.** Revealed sIgA Ab for each of the proteins tested.

Finally, specific Abs (sIgA) against different virus proteins (rS1, rRBD, rN) were detected in saliva. Differences in Abs levels against the different proteins were observed.

3.4.2.5. *ELISA assays of the PC and NC samples*

To validate the established protocol for determining sIgA in saliva samples, ELISAs were conducted against the rS1 protein of both the negative and PC saliva samples. In order to validate the assays being performed and the employed method, confirmation ELISAs were conducted by incubating the control saliva samples on the surface of a plate coated with the virus protein, and on a NC surface.

The levels of sIgA against SARS-CoV-2 were measured, and **the Ab titers were found to be significantly different between the two samples**, confirming the results obtained previously using the IODM method (Figure 86). To reduce the background signal from the NC, subsequent ELISAs were conducted by varying the sample concentration to be incubated.

By performing these validation assays, the researchers ensured the reliability and accuracy of the ELISA method for detecting sIgA in saliva samples. The significant difference in Ab titers between the negative and PC samples further confirmed the specificity of the assay in identifying the presence of SARS-CoV-2 specific Abs in the PC sample. The adjustments made to reduce the background signal from the NC contributed to improving the accuracy of the ELISA results.

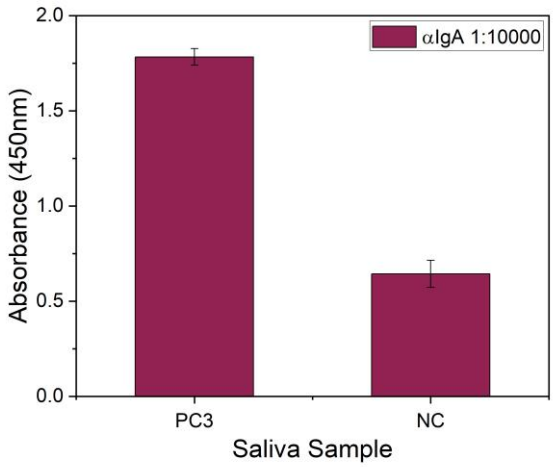

Figure 86. ELISA of saliva samples PC3 and NC.

3.4.2.6. *Human saliva samples*

Saliva samples used for the experiments came from SARS-CoV-2 positive and negative volunteers. Samples once collected were centrifuged for 10 min at 15000 rpm. The supernatants were then collected and stored at -20°C.

3.4.2.7. *ELISA assays of the saliva samples and their correlation with IODM*

ELISAs were performed on the samples obtained from the different volunteers to correlate the measurements being performed by IODM.

Figure 87A shows the results of three sIgA-positive volunteers against SARS-CoV-2, while Figure 87B shows the results of the negative volunteers. As can be seen in the two figures, **there is a correlation between the absorbance values obtained by ELISA and the ΔIROP (%) values measured by IODM**. The experiments carried out with both techniques were performed with a positive and NC saliva tested by PCR.

This correlation was then analyzed with 50 volunteer samples, performing a linear fit between the ΔIROP (%) value represented in % of the sIgT measurement and the absorbance obtained by ELISA (Figure 87C), while on the other hand the ΔIROP (%) signal represented in % of the sIgA measurement was plotted against the absorbance at 450nm (Figure 87D). In both cases a good linear fit between both techniques was observed.

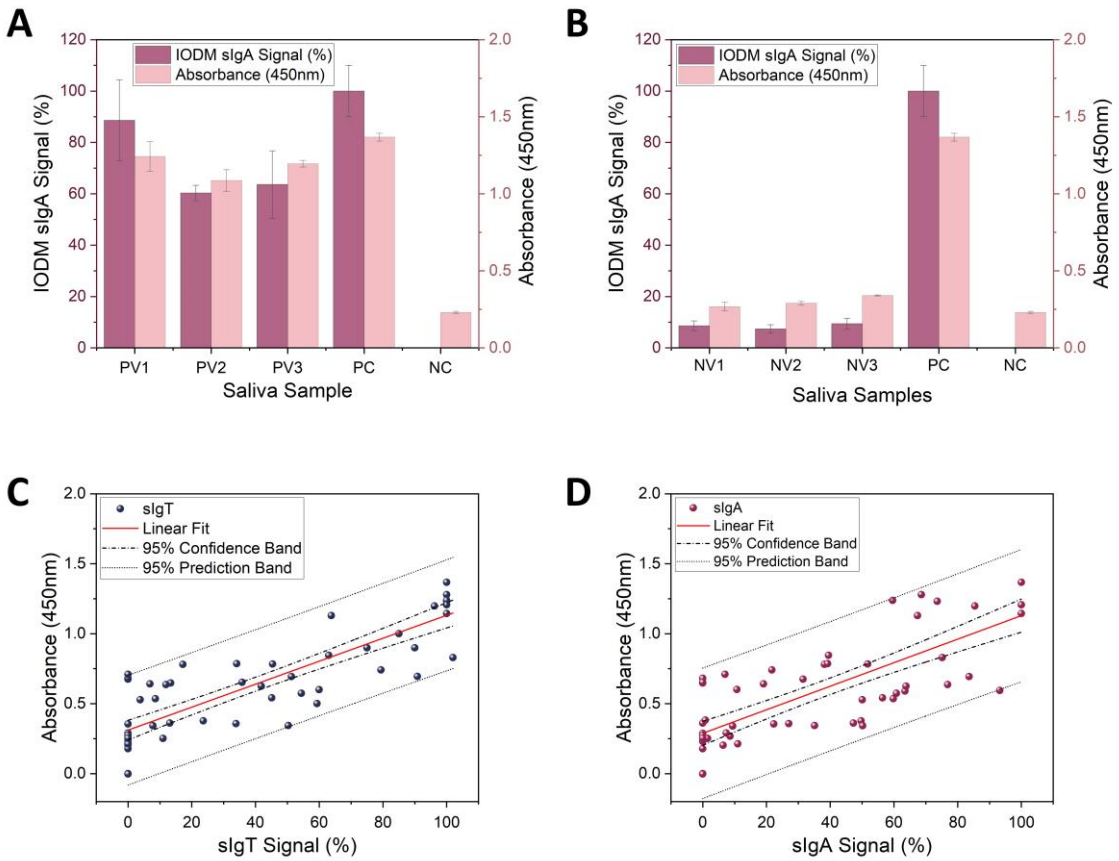

Figure 87. Correlation between ELISA and IODM. A. ΔIROP (%) signals and absorbance at 450nm for saliva samples from volunteers and positive and NC. **B.** Signals from both techniques for negative volunteers as well as controls are plotted. **C.** Correlation between ΔIROP (%) and absorbance at 450 nm of sIgT from 50 volunteers. **D.** Correlation between ΔIROP (%) and absorbance at 450 nm of the sIgA measurement of the 50 volunteers (figure adapted from A. M.M. Murillo et al., 2021).

3.4.2.8. *Measurements of sIgA against SARS-CoV-2 in the saliva pilot study*

The sIgA measurements against SARS-CoV-2 were carried out on 196 volunteers every 12 days, with a total of 6 samples per volunteer, followed up for more than two months. In this way it was possible to analyze those volunteers who remained negative during the entire analysis, those who were always positive or those who varied from negative to positive and vice versa. These results were summarized at the end of the pilot study in individual documents that were sent to each of the participants (Annex II), in which it is noted for each sample collected whether it is positive or not in sIgA against SARS-CoV-2 or if it has not been possible to determine whether it is positive or not.

A validation was performed by measuring sIgA in 50 saliva samples by ELISA and IODM, obtaining a linear fit. This validated the established protocol used in the pilot study carried out at the UPM in which the progression of sIgA in 196 volunteers was analyzed for more than two months.

3.5. Conclusions

3.5.1. Case I. I. Development of an *in-vitro* optical diagnostic system for the detection of specific Abs against SARS-CoV-2 in serum

The most important conclusions obtained during the "*Case I. I Development of an in-vitro optical diagnostic system for the detection of specific Abs against SARS-CoV-2 in serum*" experiments are summarized below:

- It was possible to produce recombinant SARS-CoV-2 proteins called rS1 and rS2. Both, once tested, were shown by ELISA to be valid for determining specific Abs against the virus since 98% of the PCR-positive samples tested by ELISA were positive.

- All the parameters necessary to establish a protocol for the determination of different biomarkers for the diagnosis of COVID-19 were evaluated. This protocol is summarized in Table 18:

Table 18. Protocol followed for the detection of sIgT, sIgG, sIgM, sIgA, FTH1 and CRP in serum samples.

Incubation step	*Protein name*	*Incubation time (min)*	*Concentration (µg/mL) and Dilution*	*Volume (µL)*	*Temperature (°C)*
Immobilization	rS1	180	300	1	37
	αHuman-FTH1	180	100	1	37
	αHuman-CRP	180	100	1	37
	BSA	180	50	1	37
Blocking	Casein hydrolysate	60	1x	20000	RT
Recognition	Serum samples	180	1:10	2.5	37
Development	αHuman-IgG	120	1:250	2.5	37
	αHuman-IgM	120	1:20	2.5	37
	αHuman-IgA	120	1:10	2.5	37

- A washing protocol was established after each of the incubation steps and is summarized in Table 19:

Table 19. Washing protocol.

Incubation step	*Rinsing*	*Washing*	*Rinsing*	*Drying*
Immobilization	20 mL H_2OmQ	45 s in H_2OmQ agitation	-	Compressed air
Blocking	20 mL H_2OmQ	45 s in H_2OmQ agitation	-	Compressed air
Recognition	20 mL H_2OmQ	10 min in PBS agitation	40 mL H_2OmQ	Compressed air
Development	40 mL PBS-T	-	40 mL H_2OmQ	Compressed air

- The correlation of the IODM with the ELISA technique was carried out, obtaining a high correlation between both techniques for the samples measured, in addition to the negative and PC for the sIgG, sIgM, and sIgA markers.

- *In vitro* detection of sIgT against SARS-CoV-2 was carried out directly without any type of developer, in addition to the markers FTH1 and CRP.

- In a second recognition step, the different types of sIg (sIgG, sIgM, and sIgA) were determined using a secondary Ab.

- It was observed that the signals obtained for sIgT were higher in severe patients compared to moderate and mild patients, as well as sIgG also followed the same behavior. This occurred similarly for sIgM, but however, sIgA was higher in mild patients.

- In the case of inflammatory markers, FTH1 was also higher in severe patients, while for CRP no differences were observed.

- In addition, it is interesting to mention, that at the end of February 2020, there were blood donors who had already been in contact with the virus.

- A MLRM was performed to analyze the influence of the markers measured. In conclusion, the model explained the influence of the markers sIgG, sIgM, sIgA, and FTH1 on sIgT with a goodness of fit of 73.01%, with the level of sIgT increasing with the increase of these markers. It is also relevant to note that CRP was a variable that did not influence the model, which could be related to the fact that it is a nonspecific marker of inflammation.

- Finally, it is also important to highlight that when the degree of severity of the disease was introduced in the model, the severe degree of the patients corresponded with the high levels of sIgT, suggesting that the severity of COVID-19 is related to the amount of sIgT and FTH1.

Therefore, this *in vitro* detection system is a promising alternative to detect SARS-CoV-2 infection, being a low-cost screening possibility. Moreover, it is a system that allows the determination of different biomarkers at the same time, being a fast, cost-effective, affordable, and reliable multiplexed diagnostic method.

3.5.2. Case I. II. Development of an *in-vitro* optical diagnostic system for the detection of specific Abs against SARS-CoV-2 in saliva

The most important conclusions obtained during the "*Case I. II. Development of an in-vitro optical diagnostic system for the detection of specific Abs against SARS-CoV-2 in saliva*" experiments are summarized below:

- It was possible to establish a protocol to determine sIgA in saliva samples against SARS-CoV-2 by means of an *in vitro* optical detection system (Table 20).

Table 20. Summary of the protocol followed to detect sIgA in saliva samples.

Incubation step	*Protein name*	*Incubation time (min)*	*Concentration (µg/mL) and Dilution*	*Volume (µL)*	*Temperature (°C)*
Immobilization	rS1	180	300	1	37
	BSA	180	50	1	37
Blocking	Casein hydrolysate	60	1x	20000	RT
Recognition	Saliva samples	ON	1	2	4
Development	αHuman-IgA	180	1:10	2	37

- In addition, sIgA was also detected in saliva against other viral proteins such as rRBD and rN, although in lower amounts than against rS1.
- ELISA and IODM techniques were correlated using positive and negative saliva samples tested by PCR and corroborated with the samples collected from the volunteers for the pilot study.

From this study, data on the prevalence of sIgA against SARS-CoV-2 were obtained from measurements that were carried out for more than two months. This demonstrates the validity of this technique for screening populations, as the sample to be analyzed is much less invasive and can be obtained more often and more easily.

4. Case II. Development of an *in-vitro* optical diagnostic system for neurodegenerative diseases

4.1. Introduction

Neurodegenerative diseases (NDD) are a diverse group of neurological disorders that cause a gradual loss of neurons in the central or peripheral nervous system. This loss of neurons affects the functionality of the networks they form, resulting in cognitive and memory impairment, changes in behavior, and sensory and/or motor deficits (Wilson et al., 2023).

Millions of people worldwide are affected by NDDs, with Alzheimer's Disease (AD) and Parkinson's disease being the most common. These disorders are heavily influenced by age and genetics, as well as other environmental factors. NDDs typically progress without remission, and treatments aim to slow the process or alleviate symptoms (Lamptey et al., 2022).

Common features of NDDs include (Wilson et al., 2023)(Figure 88):

- Dysfunction of neuronal and synaptic networks.
- Pathological protein aggregation.
- Cytoskeletal abnormalities.
- RNA and DNA defects.
- Neuronal death.
- Inflammation.
- Alterations in homeostasis.
- Dysregulation of the proteome.

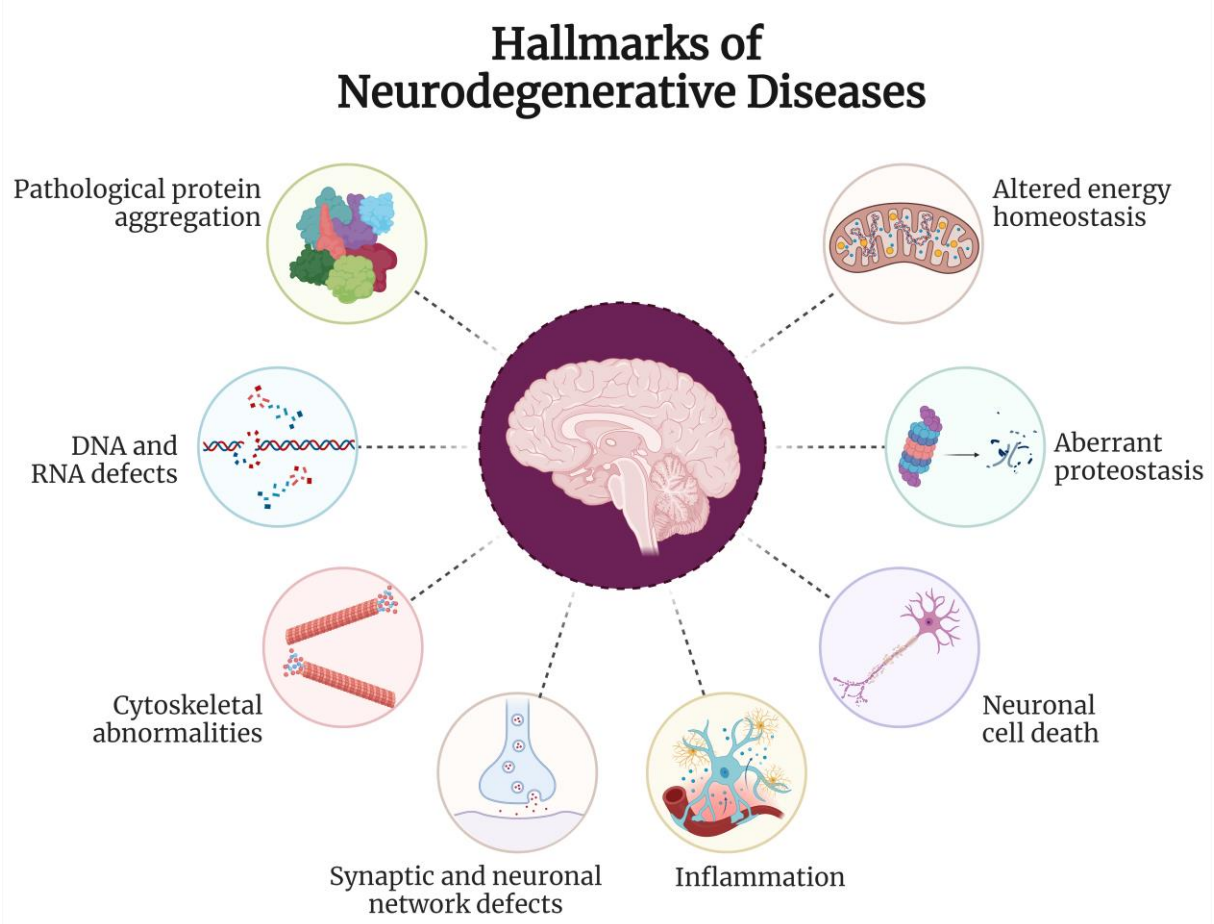

Figure 88. Hallmarks of NDD. Created with BioRender.com.

Among the NDDs are the tauopathies, also a heterogeneous group of diseases characterized by **deposits of tau protein in the brain** and clinically associated with dementia (Kovacs, 2018). AD is one of them.

Research for effective treatment of NDD is one of the major problems. Many of these diseases were described more than a hundred years ago, and **there is still no cure**. This is because the triggers and the process by which neurodegeneration progresses are unknown (Prince et al., 2013).

4.2. Alzheimer's Disease

AD is a neurodegenerative disorder named after it was described by Alois Alzheimer in 1907 (Stelzmann et al., 1995). **It is a progressive disease and the most common form of dementia, accounting for 60% to 80% of cases**. AD is one of the diseases that causes more deaths every day, and it is estimated that the number of people affected will increase from 25 million to 107 million by 2050 (Prince et al., 2013).

Characteristically, histologically there are **two main structures associated with AD**, on the one hand we have the **Senile Plaques (SPs) formed by extracellular deposition of Amyloid-beta (Aβ) peptide** and on the other hand the **Neurofibrillary Tangles (NFTs) due to intracellular**

accumulation of hyperphosphorylated tau protein (Stelzmann et al., 1995).

AD mainly affects older people (over 65 years of age), but there are cases that develop earlier. The form that affects people over 65 is called **late-onset and is the most common form**, while the form that affects younger people (aged 30-65 years) is called early-onset or familial and has a genetic component, as mutations occur in the genes encoding Amyloid Precursor Protein (APP) and components of gamma secretase (involved in APP processing) (Abeysinghe et al., 2020).

In the case of the late-onset form, the causes are completely unknown, but several risk factors, such as age, sex, hypertension, and the presence of the Apolipoprotein E4 (APOE4) gene allele, have been described that may increase the risk of developing the disease (Abeysinghe et al., 2020). There are also other risk factors related to metabolism, such as obesity or diabetes mellitus (Knopman et al., 2021) (Figure 89).

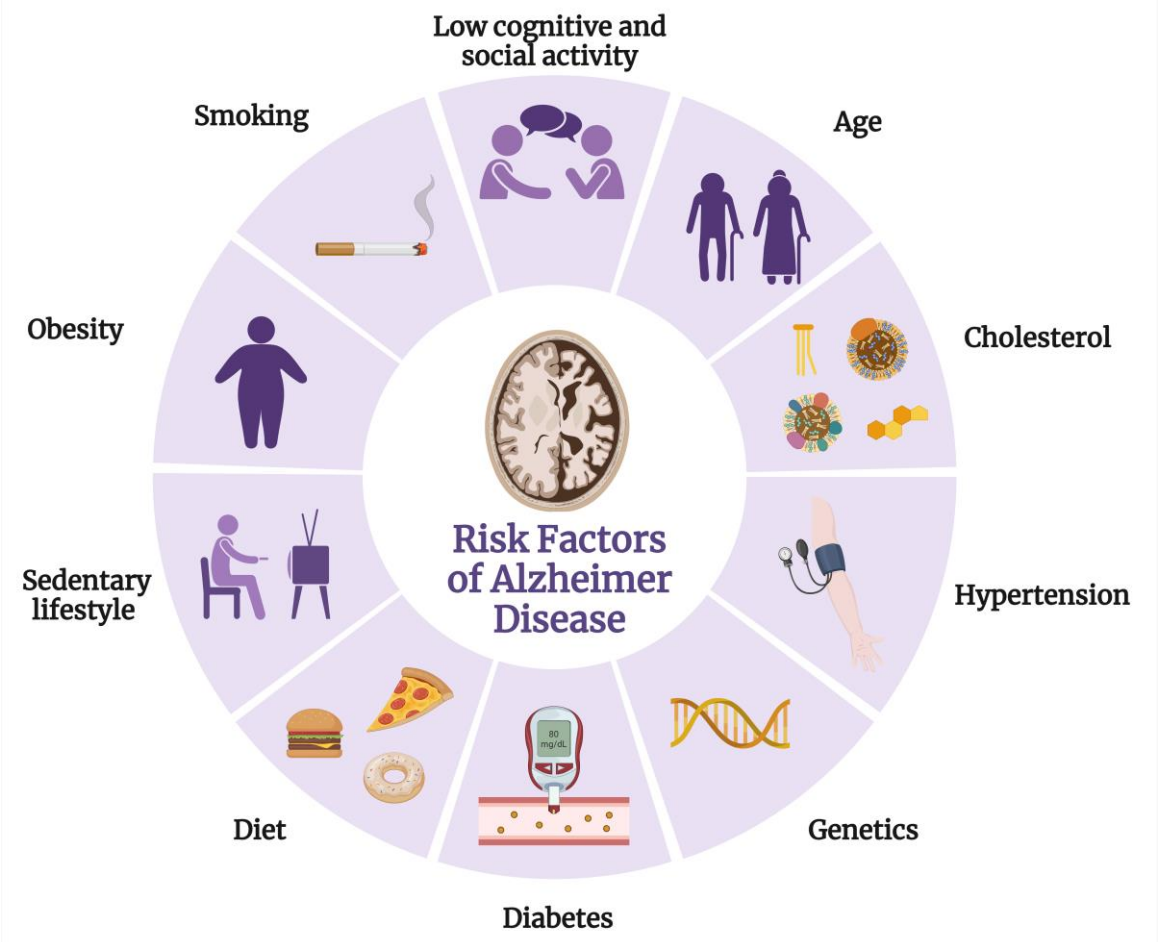

Figure 89. Risk factors of AD. Created with BioRender.com.

Polymorphism in the APOE gene is one of the most important determinants of risk factors. Among the allelic variants of the gene (E2, E3 and E4), the variant most associated with AD is **APOE4**, while the E2 allele is associated with a lower risk. This is a glycoprotein that is expressed in the brain and plays an essential role in the distribution of cholesterol and lipids to neurons. It is strongly associated with increased Aβ peptide deposition (Yamazaki et al., 2019) (Figure 90).

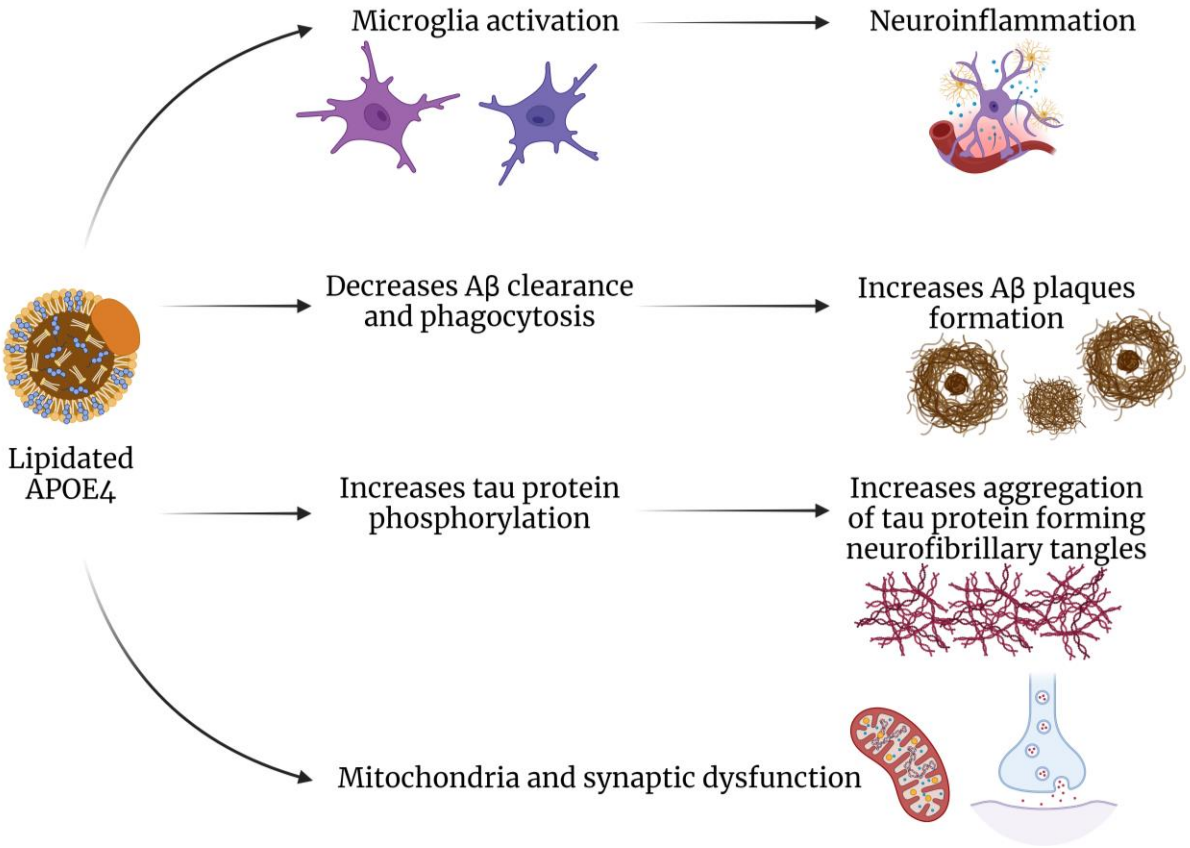

Figure 90. Role of APOE in AD pathophysiology. Created with BioRender.com.

In addition to the APOE gene, other risk factor genes related to the immune response and microglia have been implicated. Neuroinflammation is an innate immune response that occurs in the Central Nervous System (CNS) when astrocytes and microglia are activated by protein accumulation in the brain (Griciuc & Tanzi, 2021).

Clinically, AD can be classified into five different stages based on cognitive impairment: preclinical, Mild Cognitive Impairment (MCI), mild, moderate, and severe dementia (Calabrò et al., 2021).

- **Preclinical**: At this stage, the disease is usually not diagnosed because the symptoms are not very obvious, there is mild memory loss that does not interfere with daily activities, and the cognitive impairment is mild.
- **MCI**: It is a transitional stage that occurs between cognitive health and dementia. It begins to have a deterioration of memory not very severe and sometimes in language. Although the symptoms are appreciated by the sufferer and family members, it does not affect the ability to perform daily actions.
- **Mild**: At this stage, the memory loss becomes more noticeable as there begins to be an inability to generate new memories. Personality changes begin to occur and there are periods of disorientation. At this stage, the deterioration already reaches the area of the cerebral cortex.

- **Moderate**: At this stage, the damage has already spread to the areas responsible for speech and reasoning, so that speech problems begin to appear. In this stage, they also begin not to recognize family members. The symptoms of the mild stage and behavioral problems are exacerbated.
- **Severe**: By this time, individuals lose their independence to perform any activity. Systemic symptoms such as difficulty performing movements (motor activity) or changes in sleep cycles appear.

All of these cognitive impairments **are due to neurodegeneration and thus loss of synaptic connections**, coupled with low levels of neurotransmitters in the brain (Abeysinghe et al., 2020) (Figure 91).

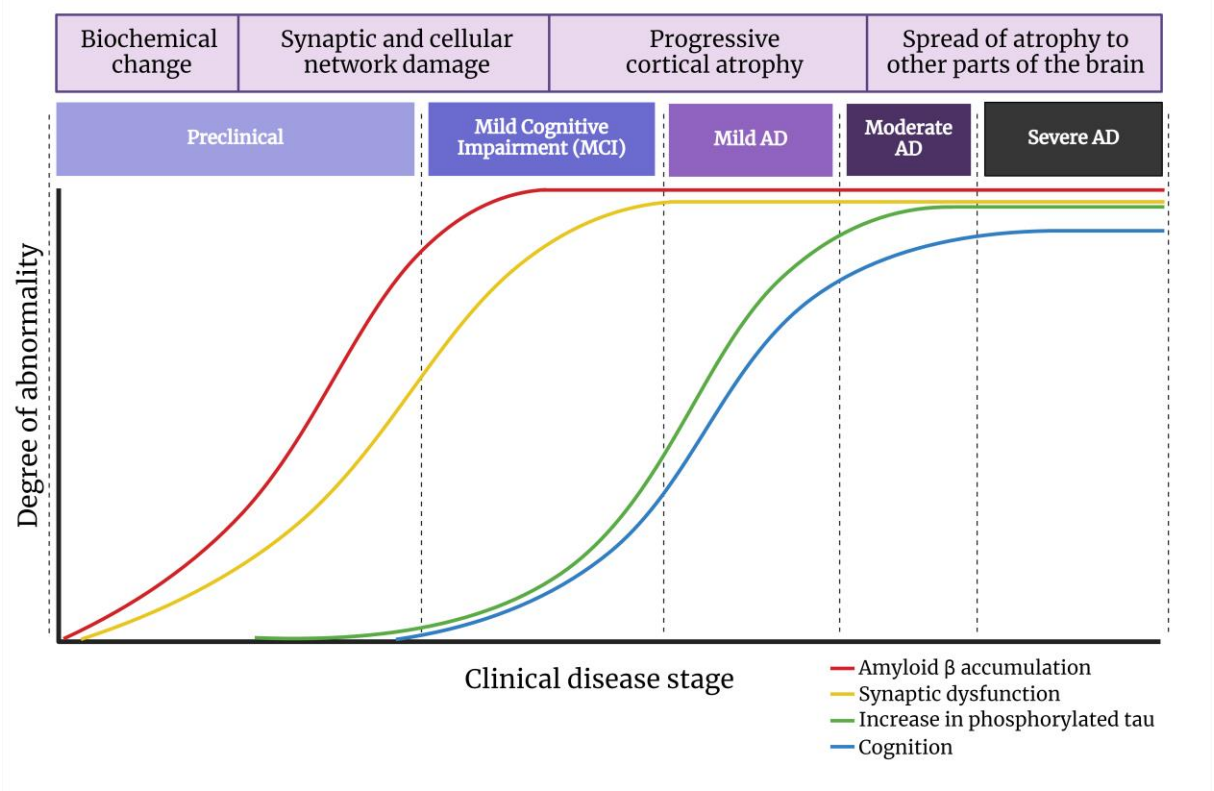

Figure 91. Stages of AD and biomarker patron expression. Created with BioRender.com.

The symptoms and severity of the disease can vary widely among patients, but the common findings in the CNS at autopsy are: **loss of synaptic connections, accumulation of abnormal plaques (SPs), and the presence of NFTs** (Calabrò et al., 2021).

Currently there are different animal models for the study of AD. One of them are the P301S transgenic mice also known as PS19, which are a model of pure tauopathy and tau protein aggregation. These mice have an overexpression of the human tau protein with a mutation in proline 301, being this overexpression of the human transgenic tau protein five times higher than the endogenous tau protein of the mice. This mutation is located on chromosome 17 and is associated with frontotemporal dementia.

In addition, these individuals begin to develop neurodegeneration and a hyperphosphorylation of the tau protein that begins to form aggregates, having a high resemblance to the NFTs that occur in AD (Iba et al., 2013; Yang et al., 2016)(Figure 92A).

On the other hand, one of the models that has also become very important is the Syriam hamster (*M. auratus*). The reason for their interest is that these animals enter a period of hibernation in conditions of low temperature and darkness. During this period, also known as torpor, their brain undergoes metabolic and structural changes, and one of these changes is the hyperphosphorylation of the tau protein, especially in serines and threonines, generating phosphorylation patterns typical of NFTs. However, in these mammals this phosphorylation is reversible very quickly when they come out of hibernation (arousal) and this is the most interesting point, since the aim is to mimic this mechanism of dephosphorylation of the tau protein that occurs naturally in these animals, as a treatment for AD (Arendt et al., 2003; Arendt & Bullmann, 2013; Härtig et al., 2007)(Figure 92B).

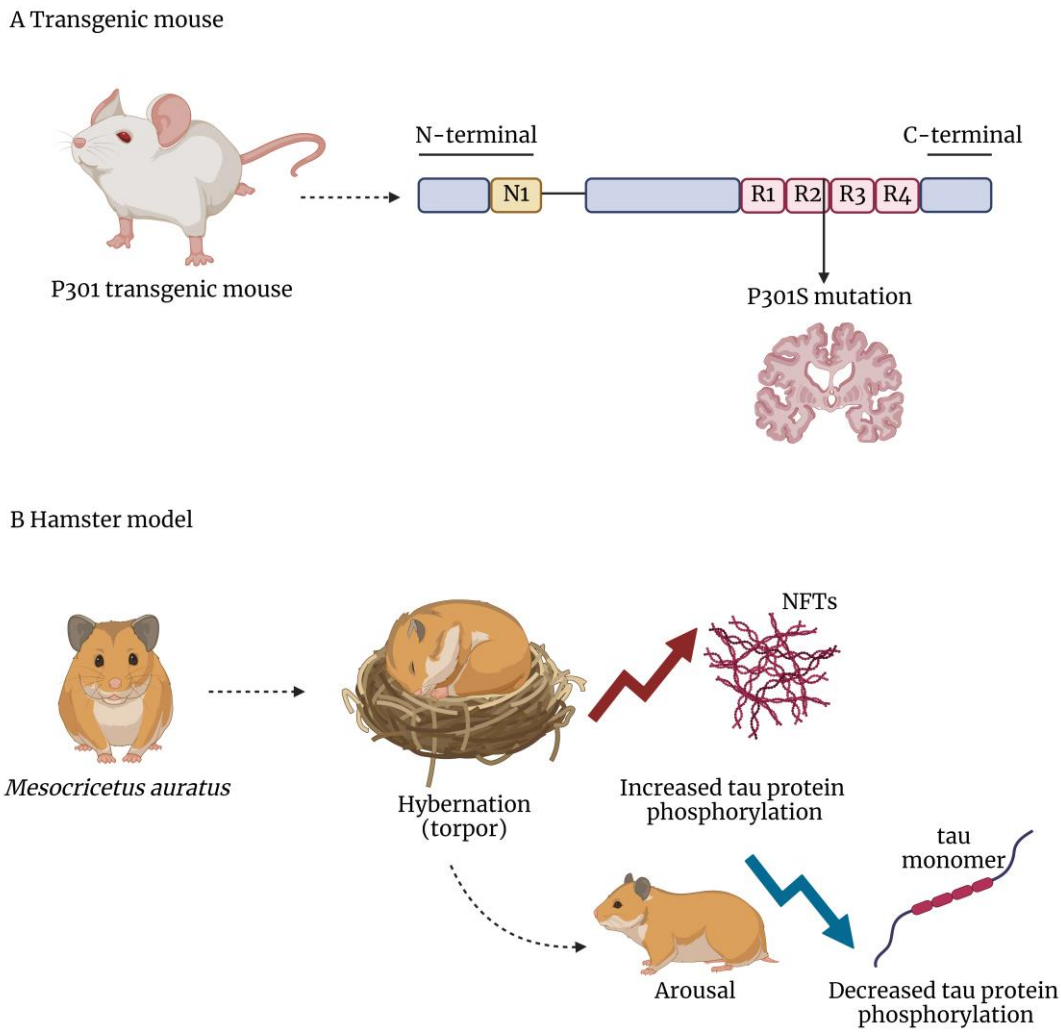

Figure 92. AD research models. A. P301S transgenic mouse. **B.** Syrian hamster model of hibernation. Created with BioRender.com.

4.2.1. Diagnostic

First of all, it is important to accurately and quickly identify the first symptoms associated with the disease and to be able to distinguish them from those of other diseases. Subsequently, a **mental evaluation and a blood test** should be performed to rule out other possible pathologies, and even **APOE4 genotyping** should be requested along with other evaluations (behavioral, functional, cognitive)(Porsteinsson et al., 2021).

Currently, diagnosis is largely based on Positron Emission Tomography (PET) and analysis of CSF **biomarkers, including threonine-phosphorylated tau protein 181 (pTau181), total tau, and $A\beta_{42}$ peptide** (S. Khan et al., 2020). Unfortunately, the use of PET to detect Aβ plaques is a very expensive technique, and measuring biomarkers in CSF requires a very invasive procedure to obtain the sample (Weller & Budson, 2018).

The National Institute on Aging-Alzheimer's Association (NIA-AA) in 2011 also included the use of serum samples, which are less invasive and are under development (Weller & Budson, 2018).

There is a serious problem with the diagnosis of the disease, which is that it is performed when the disease is already very advanced (in the symptomatic stages). Therefore, it is necessary to make progress in these diagnostic systems, especially in the study of markers that undergo changes long before (Porsteinsson et al., 2021).

4.2.2. Biomarkers and samples used

A variety of biomarkers and sample types are available for the biochemical diagnosis of AD.

- **CSF biomarkers**: In this type of sample, markers related to the formation of SPs in the brain are measured, including the concentration of $A\beta_{42}$ (decreased in the disease) and the $A\beta_{42}/A\beta_{40}$ ratio. Other markers are the concentration of total tau and phosphorylated tau (mainly from phosphorylation at position Thr181) (both markers are increased in the disease) (Blennow, 2004; Budelier & Bateman, 2020).
- **Serum and plasma biomarkers**: In addition to the markers described for CSF, which can also be measured in serum and plasma, other markers have been described, such as neurofilament light chains together with glial fibrillary acidic protein, which are increased in sporadic AD (Teunissen et al., 2022). Various disease-related micro RNAs (miRNAs) can also be examined in this type of sample (Ausó et al., 2020).
- **Biomarkers in saliva**: Some of the markers proposed to be measured in saliva as a tool for early diagnosis are the concentration of $A\beta_{42}$ peptide, which increases in saliva, as well as the increase in the ratio of total tau to phosphorylated tau (Schepici et al., 2020). Several metabolites have also been described, such as spinganine-1-phosphate and ornithine, which have higher levels in AD patients, and lactoferrin, whose levels decrease in pathology (Bouftas, 2021).

- **Tear biomarkers**: Several studies have been conducted to find tear biomarkers that can be used to diagnose AD, including the presence of $A\beta_{42}$ peptide (absent in healthy controls), as well as elevated miRNAs (Król-Grzymała et al., 2022) and total tau concentration (Kaštelan et al., 2023).
- **Urine Markers**: Several metabolites have been described that can be measured in urine as early diagnostic markers in AD, including 8,12-iso-iPF(2alpha)-VI isoprostane, 1-methyladenosine, or N2-dimethylguanosine. Another promising marker described in urine is neuronal filament protein (Ausó et al., 2020).

It must be considered that all these studies are necessary because the type of sample used today to carry out the determinations is the CSF, which is a very invasive sample to obtain and makes the diagnosis and follow-up of patients very difficult. For this reason, we have not stopped looking for other types of samples where the diagnosis is just as effective and precise, but less invasive, and with this in mind, different specific biomarkers have been studied for each type of sample and their relationship with the disease.

4.2.2.1. *Aβ peptide*

The APP family consists of the APP protein itself and Amyloid Precursor-like Proteins 1 and 2 (APLP1 and APLP2). They are membrane proteins with an extracellular N-terminal domain and a cytoplasmic C-terminal domain. They are highly expressed in the brain, which is the exclusive site of APLP1 expression (Zheng & Koo, 2011). Although the function of APP is not fully understood, **it is involved in neurotransmitter pathways, dendritic spine remodeling, and synaptic homeostasis** (Hampel et al., 2021).

APP protein can be digested by enzymes called alpha, beta, and gamma secretase, resulting in soluble peptides (non-amyloidogenic pathway), but when beta and gamma secretase act together, **an insoluble peptide called Aβ (amyloidogenic pathway) is produced** (Hampel et al., 2021) (Figure 93).

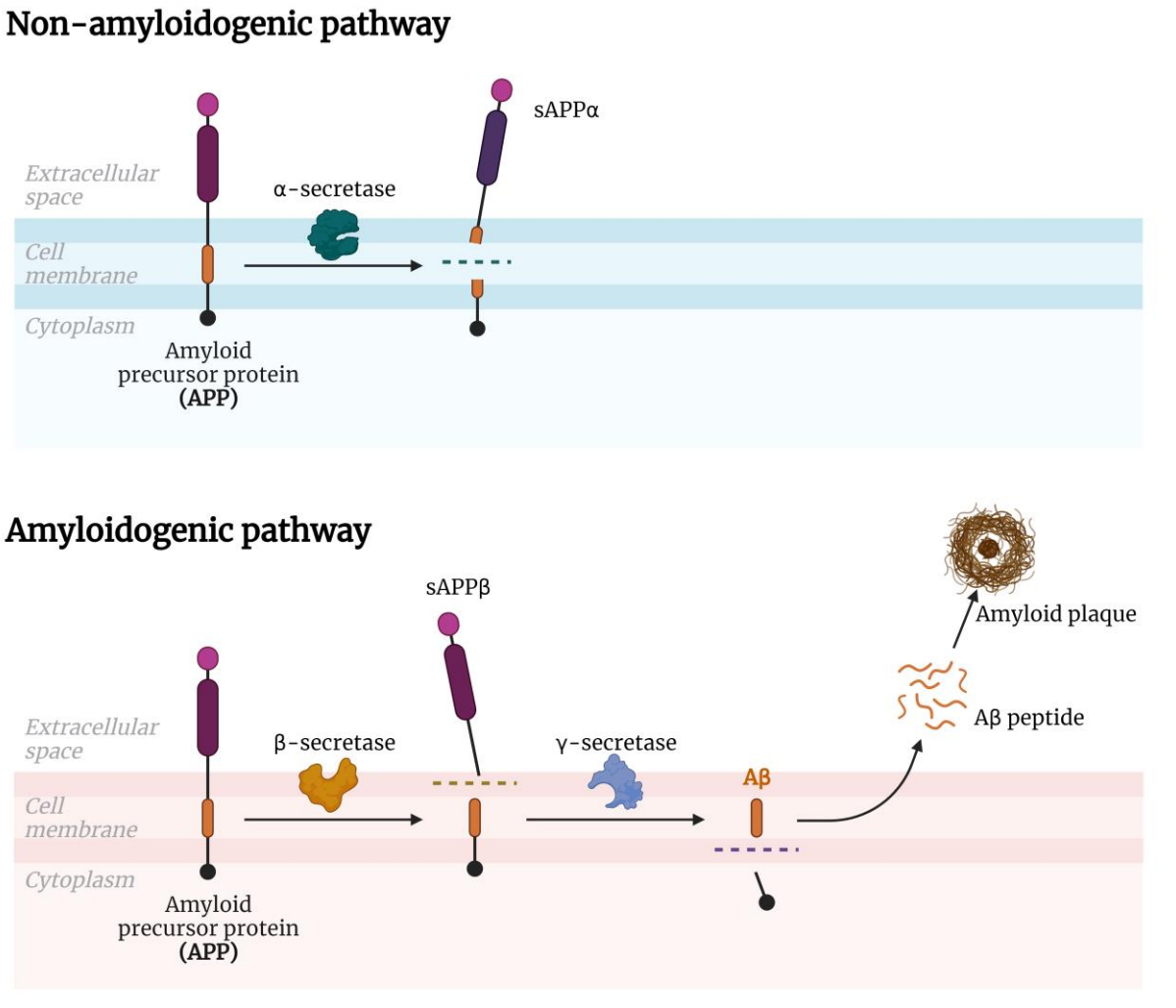

Figure 93. Non-amyloidogenic and amyloidogenic pathways of APP processing. Created with BioRender.com.

The Aβ peptide can have 37-49 aa, although 40 and 42 aa predominate (G. F. Chen et al., 2017), and has a molecular weight of 4 kDa (Hampel et al., 2021). **The Aβ monomers aggregate to form amyloid oligomers and fibrils, which ultimately form amyloid plaques** (G. F. Chen et al., 2017).

These structures disrupt signaling between neurons, causing the brain to lose some of its functions. In addition, an immune-mediated inflammatory response is triggered that damages nearby neurons. If these structures are located in blood vessels, this can lead to angiopathy and hemorrhage from ruptured blood vessels (Ashrafian et al., 2021).

4.2.2.2. *Tau protein*

Tau protein is one of the major proteins involved in AD. It was described in 1975 and named by Marc Kirschner (Weingarten et al., 1975). It is encoded on chromosome 17q21 and has different names depending on the presence or absence of N-terminal domains and repeats at the carboxy-terminal end, with six different isoforms apart from the one considered to be the large

(full) tau protein (Table 21)(Mandelkow & Mandelkow, 2012). It is mainly expressed in the axons of neurons and in glial cells, although at lower concentrations (Xia et al., 2021).

Table 21. Tau protein isoforms (Mandelkow & Mandelkow, 2012).

Clone	*Inserts/repeats*	*Number of aminoacids (aa)*	*MW (KDa)*
htau40	2N4R	441	45.9
htau39	2N3R	410	42.6
htau34	1N4R	412	43.0
htau37	1N3R	381	39.7
htau24	0N4R	383	40.0
htau23	0N3R	352	36.7
Complete tau	2N4R + exon 4a	695	72.7

This is also called Microtubule-Associated Protein Tau (MAPT) because its direct function is to **promote microtubule binding, stabilization, and interaction with the cytoskeleton** through the carboxy-terminal domains, thereby affecting axonal transport and neuronal plasticity (Sündermann et al., 2016). But it also has other indirect functions that require the N-terminal domains, such as **inhibiting microtubule-dependent transport** (Mandelkow & Mandelkow, 2012).

In the brain, there are other proteins belonging to the MAP family, but the interest in the tau protein is due to its involvement in various diseases within the known tauopathies (such as AD). **Tauopathies are NDD characterized by abnormal deposits of tau protein in the brain** (Kovacs, 2018).

In the case of AD, there is still debate as to whether tau protein can be the cause or the product of the disease, as there are studies claiming that changes in tau are seen as a consequence of prior pathology in Aβ peptide (Haass & Selkoe, 2007) and others suggesting that tau is necessary for the induction of toxicity by Aβ peptide (Roberson et al., 2007).

The function of tau protein is regulated by various post-translational modifications, including phosphorylation, as it has multiple phosphorylations in healthy neurons, mainly in the microtubule-binding domain (Wegmann et al., 2021). This has been described as one of the major components that give rise to **NFTs, considered a pathological structure in AD due to the accumulation of tau protein due to the high degree of phosphorylation,** although there are studies showing that these phosphorylations can also be found in the functional protein in a soluble form (Gong et al., 2005; Horie et al., 2020)(Figure 94).

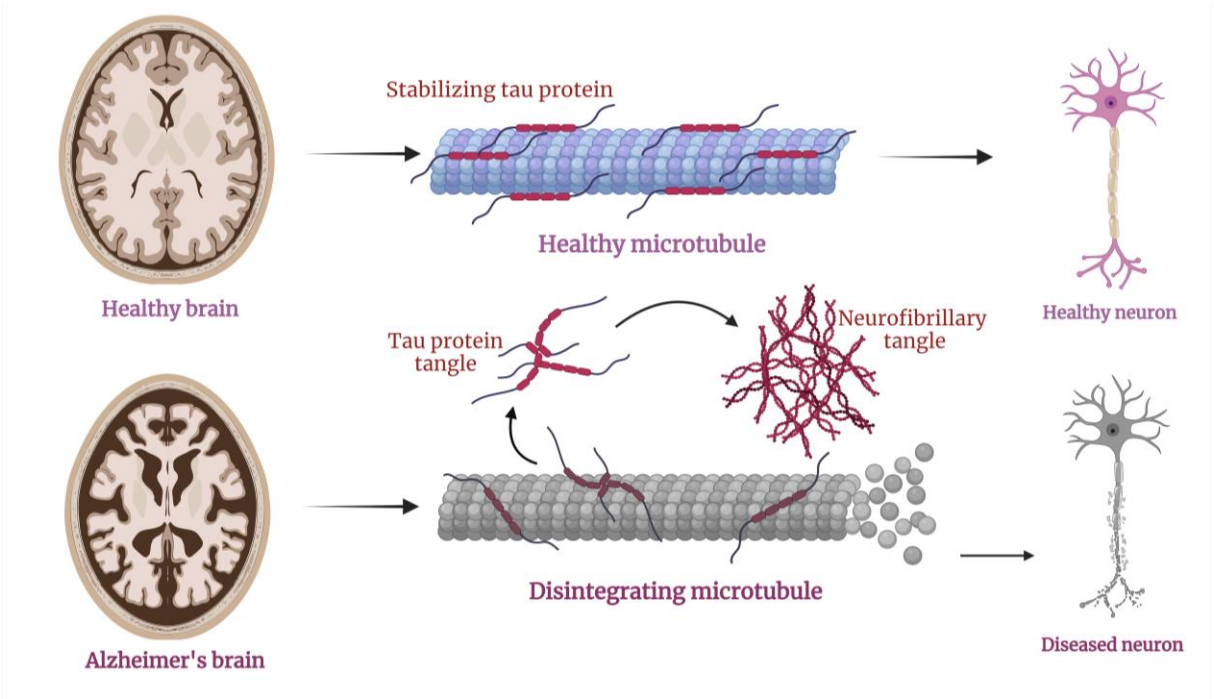

Figure 94. Tau protein pathology in AD. Created with BioRender.com.

In its full-length form, it has 85 potential phosphorylation sites on threonine, tyrosine, or serine residues. These phosphorylations result in the addition of negative charges to the microtubule-binding domain, reducing the binding between microtubules and tau protein (Xia et al., 2021). For example, studies have shown that phosphorylation at sites such as Ser231 or Ser262 can directly inhibit tau binding to microtubules; however, when this phosphorylation occurs at Ser208, tau binding to microtubules is increased. Other such phosphorylations affect the ability of the protein to stabilize microtubules (Xia et al., 2021).

In AD, **hyperphosphorylation of the tau protein has been observed, causing it to stop binding to microtubules and to form aggregates with helical filaments, resulting in NFTs** (Drummond et al., 2020). This results in loss of axonal transport and destabilization of microtubules, which act as neurotoxins and cause cognitive deficits (Muralidar et al., 2020).

Although it is a cytosolic protein, its concentration increases in the CSF in AD and therefore it has become very important as a biomarker in the study and diagnosis of this disease (Mandelkow & Mandelkow, 2012). Therefore, during the development of this thesis, several experiments were performed to develop a diagnostic system capable of detecting total tau protein and phosphorylated tau protein (at different positions) as well as phosphorylation at Thr181 in serum samples from a Syrian hamster model of AD and P301 transgenic mice.

4.2.2.3. *Lactoferrin protein*

The protein lactoferrin was first described in cow's milk in 1940 (Sorensen & Sorensen, 1940) and isolated and purified from human milk in 1960 (Groves, 1960). It is a glycoprotein of the transferrin group (capable of binding and transferring iron ions) and **is the major iron-binding**

protein in human milk (Bukowska-Ośko et al., 2022). It has a molecular weight of 78 kDa with 691 aa forming a globular structure (Wang et al., 2019). In addition, it is involved in various functions such as antioxidant, anti-inflammatory, antimicrobial and antiviral activities, although recently it has also been implicated as a marker for various diseases such as AD or dry eye disease (Bukowska-Ośko et al., 2022).

It also acts as a transcription factor, controlling the expression of several genes involved in the immune response and metabolism, and plays a critical role in protecting DNA from damage (Bukowska-Ośko et al., 2022). It has also been suggested to have anticancer properties (Pan et al., 2021).

It is highly abundant in respiratory, digestive, and genitourinary tissues. It is present in various secretions including saliva, milk, tears, and plasma. Its presence has also been demonstrated in intestinal mucus and genital secretions (Hao et al., 2018).

Several studies are currently underway to clarify **the role of lactoferrin in the brain, as it has been associated with several diseases of the CNS**. This association is related to the fact that these diseases typically involve inflammatory and oxidative stress components. As a result, lactoferrin levels are elevated in inflamed tissues. In AD, inflammation is accompanied by abnormal iron deposition. Thus, **lactoferrin levels are significantly elevated in the brains of AD patients**, where it is deposited in areas such as NTs and SPs as a defensive response of the brain (Y. Q. Li & Guo, 2021) (Figure 95).

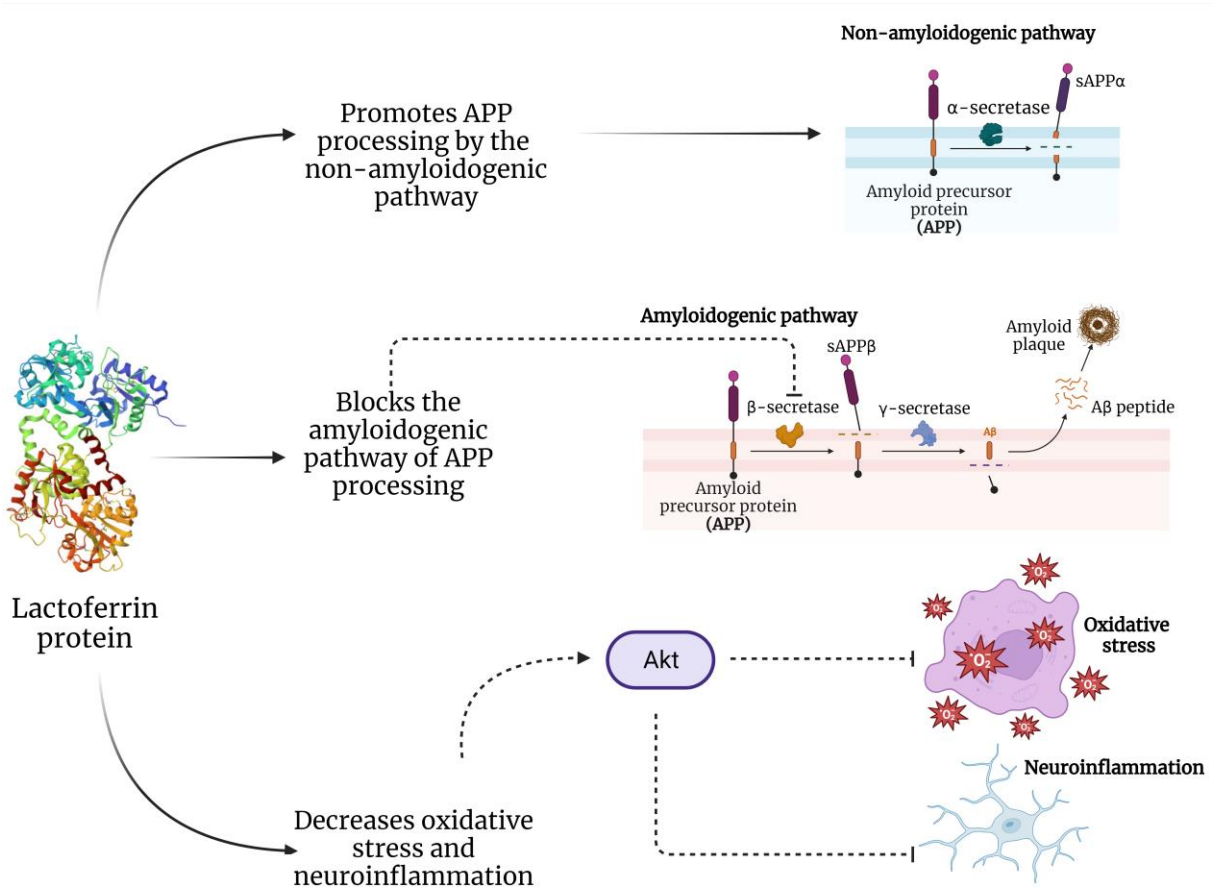

Figure 95. Protective role of lactoferrin in brain. Created with BioRender.com.

Because of **its presence in readily accessible body fluids such as saliva, salivary lactoferrin has been proposed as a potential biomarker for AD** (Liang & Lu, 2019). Several studies have linked bacterial and viral infections to the disease, and lactoferrin acts as a first line of defense in saliva (Budelier & Bateman, 2020). To date, only studies by the Carro group have linked a decrease in salivary lactoferrin concentration to the disease in MCI (Bermejo-Pareja et al., 2020; González-Sánchez et al., 2020).

In this work, lactoferrin protein levels were measured, along with other related markers, in saliva samples from a cohort of relatives of individuals with AD and NC. These relatives were also genotyped for the APOE genotype, and an attempt was made to correlate all the information obtained.

4.2.3. Treatment

Currently available treatments do not cure the disease but are used to slow the symptoms and try to improve the quality of life of patients. On the one hand, **behavioral and psychosocial therapy** is crucial and forms one of the pillars in the treatment of people with AD. These therapies begin after diagnosis and are periodically re-evaluated. They involve the patient, family members, and caregivers, and include exercise and maintaining a healthy diet (Gerald G. & Amanda Vaughn,

2010). It's also a good idea to simplify your environment and establish regular routines (Yiannopoulou & Papageorgiou, 2020).

On the other hand, there are several pharmacological treatments approved by the Food and Drug Administration (FDA), such as those based on **acetylcholinesterase inhibitors and memantine**.

Acetylcholinesterase inhibitors include donepezil, galantamine, and rivastigmine, which inhibit the action of the enzyme to increase levels of the neurotransmitter acetylcholine, thereby maintaining postsynaptic stimulation (Massoud & Léger, 2011). Although these inhibitors show some efficacy in slowing the progression of the disease (Gerald G. & Amanda Vaughn, 2010). **Memantine**, on the other hand, acts as an antagonist of N-methyl-D-aspartic acid (NMDA) receptors that affect glutamate transmission, which has been shown to be beneficial. Moreover, these benefits are enhanced when used in combination with donepezil (Massoud & Léger, 2011; Yiannopoulou & Papageorgiou, 2020) (Figure 96).

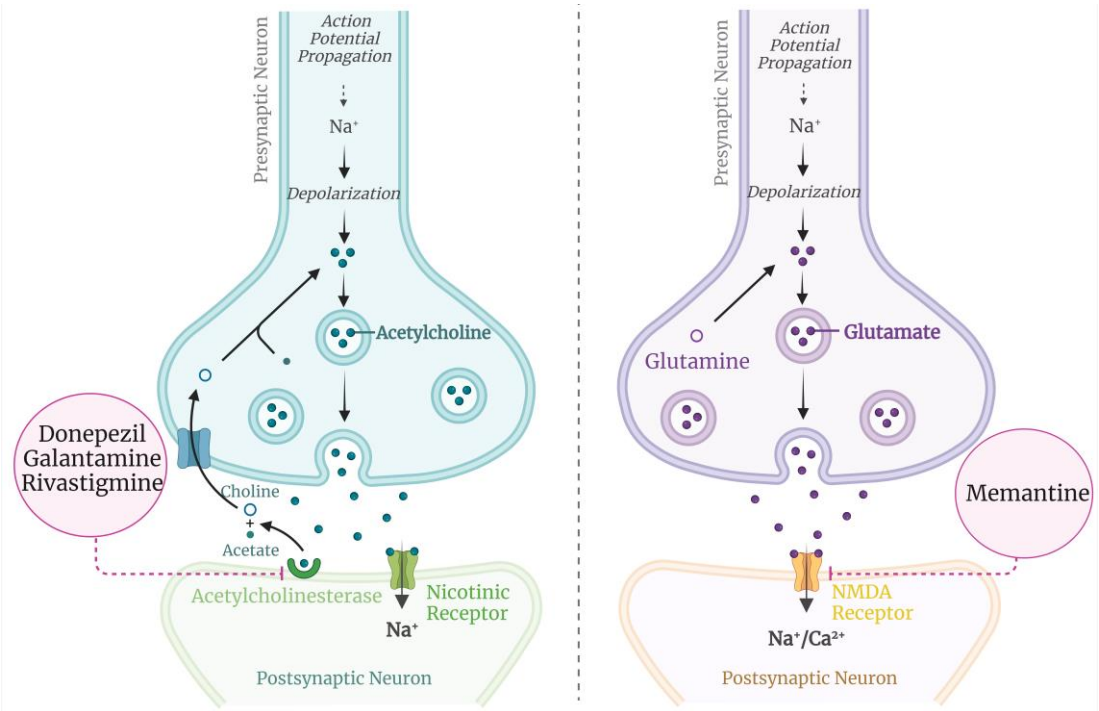

Figure 96. Current treatments against AD. Created with BioRender.com.

No new treatment has been approved by the FDA since 2003 (Yiannopoulou & Papageorgiou, 2020), and more than 50 drugs have failed phase 3 clinical trials since 2007 (Marasco, 2020). Efforts are underway to develop new drugs aimed at reducing $A\beta_{42}$ peptide production and plaque formation, stabilizing microtubules, immunotherapy against $A\beta_{42}$ peptide and tau protein, and anti-inflammatory agents (Marasco, 2020; Massoud & Léger, 2011; Yiannopoulou & Papageorgiou, 2020).

Nevertheless, there are still many uncertainties surrounding AD today, and it is believed that treatment failures occur because drugs are administered too late. Therefore, there is an urgent need for early diagnosis of the disease.

4.3. Materials and methods

4.3.1. Case II. I. Total tau detection system

4.3.1.1. *Comparison between O_2 plasma activation and acid catalysis in sensing surface*

Initially, two different protocols were implemented to activate the surface of the SU-8 resist. This pre-activation step involved an oxidation treatment, which is essential to generate available functional groups capable of forming bonds with the protein groups intended for immobilization.

In the acid catalysis approach, sulfuric acid (H_2SO_4) (Panreac, Barcelona, Spain) was used as a strong oxidizing agent for surface activation. The KITs were immersed in the H_2SO_4 solution for 20 s, then were thoroughly rinsed using four 20 mL syringes of H_2OmQ to ensure removal of any residual acid. Finally, they were carefully dried with compressed and filtered air (Figure 97A).

Alternatively, O_2 plasma treatment induces a surface modification that makes it hydrophilic by activating the SU-8 resist groups (Anbumani et al., 2021). Figure 97 shows a schematic of how the O_2 plasma chamber works. The KIT is positioned inside the chamber to create a vacuum, followed by the introduction of the required O_2 flow to activate the surface (Grimaldi et al., 2016). This treatment not only activates the surface, but also ensures surface homogenization for subsequent immobilization procedures. In this case, the KITs underwent a 40 w plasma treatment for a duration of 45 s (Figure 97B).

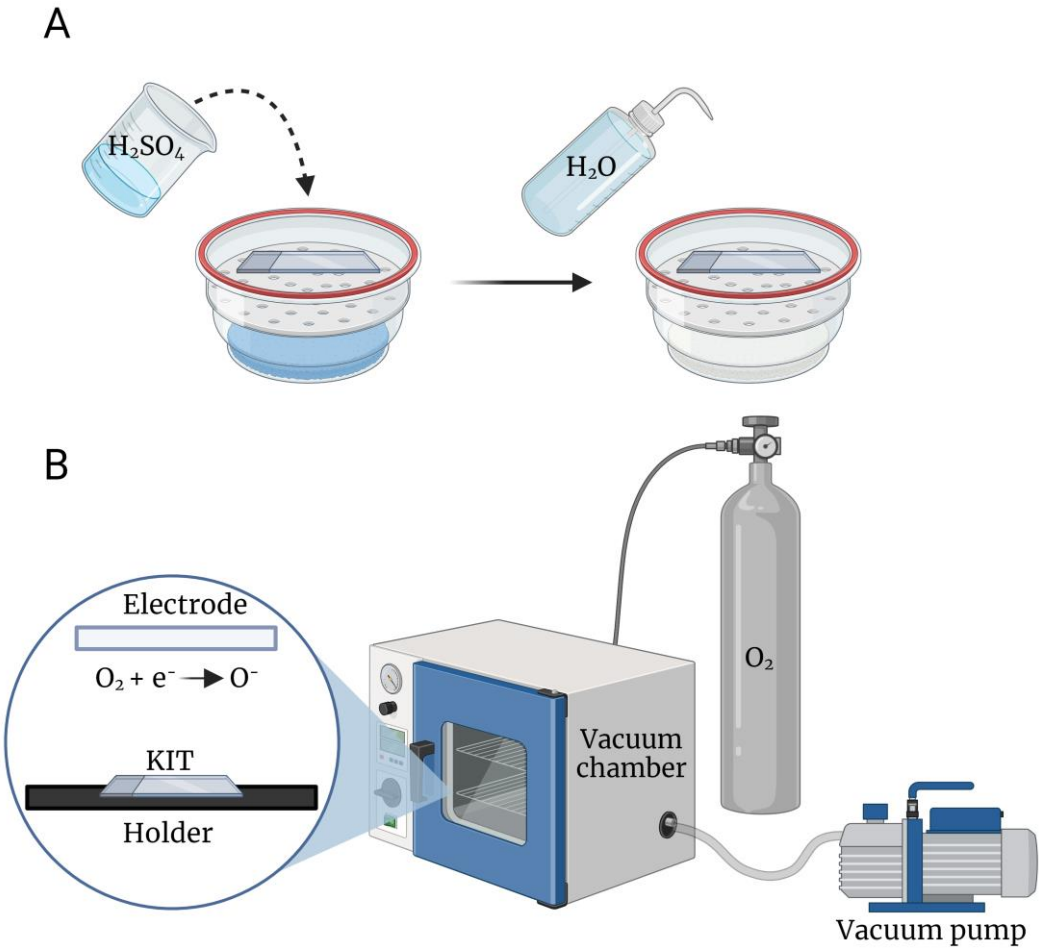

Figure 97. SU-8 surface activation. A. Activation using H_2SO_4. **B.** Activation by O_2 plasma. Created with BioRender.com.

Both methods aim to establish a covalent bond between the activated surface groups and the proteins to be immobilized.

Surface activation was followed by immobilization of tau (Sigma-Aldrich) and p24 (Abcam, Cambridge, UK) proteins. Each KIT cell received 4 µL at 50 µg/mL of the respective protein and the cells were incubated for 1 hour at 37°C in a humid chamber. The KITs were then thoroughly washed with H_2OmQ for 2 min and dried with compressed filtered air. The surface was then treated with 2 µL of 0.1 M diethanolamine (DEA) (Sigma-Aldrich) per cell and blocked for another hour at 37°C in a humidity chamber. At the end of this phase, the KITs underwent the same washing and drying steps used previously. After immobilization, the KITs were read in the MOX and the resulting data were recorded. All measurements were performed in four replicates.

4.3.1.2. *Incubation volume adjustment*

For this experiment, 16-BICELLs KITs of 200 µm each were used. After O_2 plasma treatment and initial data acquisition, tau and p24 proteins were incubated at a concentration of 50 µg/mL using

volumes of 4 µL, 3 µL, 2 µL, and 1.37 µL (each with four replicates per measurement) for 1 hour at 37°C in a humid chamber. After incubation, the KITs were washed with a 20 mL syringe filled with H_2OmQ, followed by agitation in H_2OmQ for 2 min, and then dried with filtered compressed air. Finally, the ΔIROP (%) values corresponding to immobilization were recorded.

4.3.1.3. *Stability studies of immobilization*

Four KITs, each containing 16-BICELLs measuring 200 µm, were incubated with the tau protein (2.5 µL at a concentration of 50 µg/mL) for 1 hour at 37°C in a humid chamber. After immobilization, two of the KITs were blocked with DEA, while the remaining KIT was refrigerated and covered with a glass slide under pressure. For blocking, 2.5 µL of 0.1 M DEA was incubated for 1 hour at 37°C in a humid chamber. All KITs were then washed with a 20 mL syringe filled with H_2OmQ, agitated in H_2OmQ for 2 min, and dried with filtered compressed air. Blocked KITs were stored in the same manner under refrigeration and read at 24 and 48 hours to assess the stability of the immobilized protein. All measurements were performed in four replicates.

4.3.1.4. *Evaluation of blocking step*

Four KITs with 16-BICELLs of 200 µm were immobilized with tau and p24 proteins under the same conditions described earlier. The same washing and drying protocol were followed, but two of the KITs were blocked with 1x casein hydrolysate for 1 hour with agitation at RT. Subsequently, the corresponding Abs (anti-Tau (αTau) and anti-p24 (αp24)) (Sigma-Aldrich) (Abcam) were incubated on their specific protein, while the opposite protein was used as a NC for the experiment. All measurements were conducted in four replicates.

4.3.1.5. *Dose-response curve of tau protein immobilization*

KITs of 16-BICELLs of 200 µm were immobilized with tau protein at various concentrations (from 50 µg/mL to 3.13 µg/mL in 1:2 dilutions), 2.5 µL per cell was added, and incubated for 1 hour and 30 min at 37°C in a humidity chamber.

After incubation, the KITs were washed with 20 mL H_2OmQ, agitated for 2 min in H_2OmQ, and dried with filtered compressed air. Finally, the ΔIROP (%) values were read. All measurements were carried out in four replicates.

4.3.1.6. *Protein-Ab pair specificity test*

KITs of 16-BICELLs of 200 µm cells were coated with tau protein at a concentration of 50 µg/mL using 2.5 µL per cell and with BSA protein under the same conditions. They were incubated for 1 hour and 30 min at 37°C in a humidity chamber. They were washed with 20 mL H_2OmQ, shaken in H_2OmQ for 2 min and dried with filtered compressed air.

After reading the immobilization values, the αTau Ab was incubated at different concentrations (from 100 µg/mL to 6.25 µg/mL in 1:2 dilutions) on the surface coated with tau protein and at the maximum concentration on BSA protein. On the other hand, the αBSA Ab was incubated at 50 µg/mL, dispensing 2.5 µL on the cells on which its specific protein was immobilized and also on

the other protein to test the cross-reactivity. Detection was performed for 2 hours at 37°C in a humid chamber, followed by the same wash as for immobilization, and finally the ΔIROP (%) signal was read. All measurements were performed in four replicates.

4.3.1.7. *Biofunctionalization of SiO_2 NPs*

80 nm SiO_2 NPs (Superior Silica, Chandler, AZ, USA) in ethanol were used for the biofunctionalization protocol. First, three washes were performed with 1 mL of H_2OmQ to remove all ethanol by centrifugation at 7500 rpm for 20 min. In the last wash, they were resuspended in 5 mM sodium carbonate buffer (Na_2CO_3) (Sigma-Aldrich) and carboxyethylsilanetriol sodium salt 25% in water (Fluorochem, UK) was added and kept under agitation for 1 hour at RT (Figure 98A). The same wash was then performed with H_2OmQ, and in the final wash they were resuspended in 2-Morpholinoethanesulphonic acid (MES) buffer at pH 5.5 for the addition of EDC and NHS (Sigma-Aldrich). The reaction was allowed to stand for 1 hour at RT with agitation. After the washes, G- protein (Sigma-Aldrich) was added at 500 µg/mL in H_2OmQ and left at 4°C with agitation. The next day, 0.1 M DEA was added as a blocker and allowed to react for 1 hour at RT with agitation. The washes were repeated and αTau Ab was added at 50 µg/mL and this incubation was left ON at 4°C. Final washes were performed and the NPs were resuspended in PBS and stored at 4°C (Figure 98B)(Murillo et al., 2023).

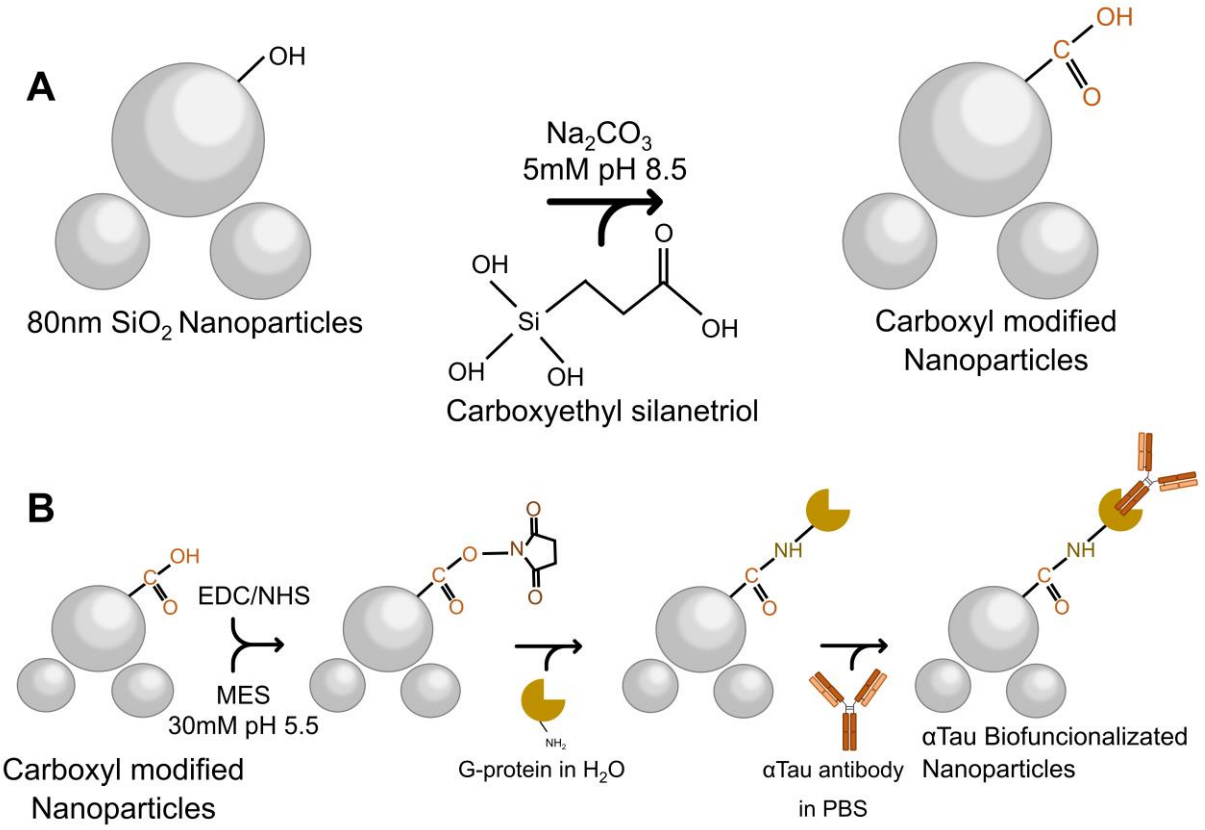

Figure 98. Protocol for SiO_2 NPs biofunctionalization. A. Silanization process to modify the surface and add carboxyl groups. **B.** Biofunctionalization after activation of carboxyl groups and addition of G-protein and αTau Ab (Murillo et al., 2023).

During the biofunctionalization process, DLS measurements of D_h, NPs concentration and ζ-potential were performed. For this purpose, at each step of the biofunctionalization process, 1 µL of NPs was taken and a 1:10000 dilution was performed for measurement in the DLS.

To determine the final biofunctionalization protocol, many parameters were modified, such as centrifugation time and rpm, as well as temperature. In addition, the concentrations of the reagents were gradually adjusted until the most appropriate concentrations were obtained.

4.3.1.8. *NPs concentration curves*

KITs with 16-BICELLs of 200 µm were immobilized with tau protein at 50 µg/mL for 3 hours at 37°C in a humid chamber. After washes, NPs were incubated at the initial concentration and at two successive dilutions (1:10 and 1:100). In addition, they were incubated on the surface coated with the NC protein, BSA. After 2 hours of incubation, the KITs were washed and ΔIROP (%) values were read (Murillo et al., 2023). All determinations were measured in four replicates.

4.3.1.9. *KITs washing tests*

After the incubation of the NPs on the KITs, different washes were tested by varying the time, temperature and washing buffer to determine the most appropriate one and to eliminate unspecific binding. All measurements were carried out in four replicates.

4.3.1.10. *Incubation time and specifity tests*

To characterize the specificity of the NPs, they were incubated on KITs coated with BSA protein at 50 µg/mL and tau protein at 50 µg/mL at a concentration of 1 x 10^7 NPs/µL. This incubation was left for 1 and 2 hours at 37°C in a humid chamber to also determine the appropriate incubation time. After incubation, the KITs were washed and the ΔIROP (%) values were read (Murillo et al., 2023). All determinations were conducted in four replicates.

4.3.1.11. *Competitive assay for tau protein determination in PBS and serum*

KITs with 65-BICELLs of 200 µm (Figure 99A) were used to immobilize tau proteins and BSA at 50 µg/mL (Figure 99B). On the other hand, biofunctionalized NPs with αTau Ab were incubated at the concentration of 1 x 10^8 NPs/µL with different concentrations of tau protein (from 100 µg/mL to 1 x 10^{-5} µg/mL) in PBS. They were left to incubate 1 hour at RT under shaking and after washes were resuspended in PBS to leave them at the concentration of 1 x 10^7 NPs/µL (Figure 99C). Finally, they were incubated on the KITs coated with tau protein and on the NC surface coated with BSA. After this incubation, the KITs were washed and the ΔIROP (%) signals were read (Figure 99D). This process was performed the same with the serum samples varying the incubation time, since the NPs were left ON at 4°C incubating with the serum samples (Murillo et al., 2023). All measurements were performed in five replicates.

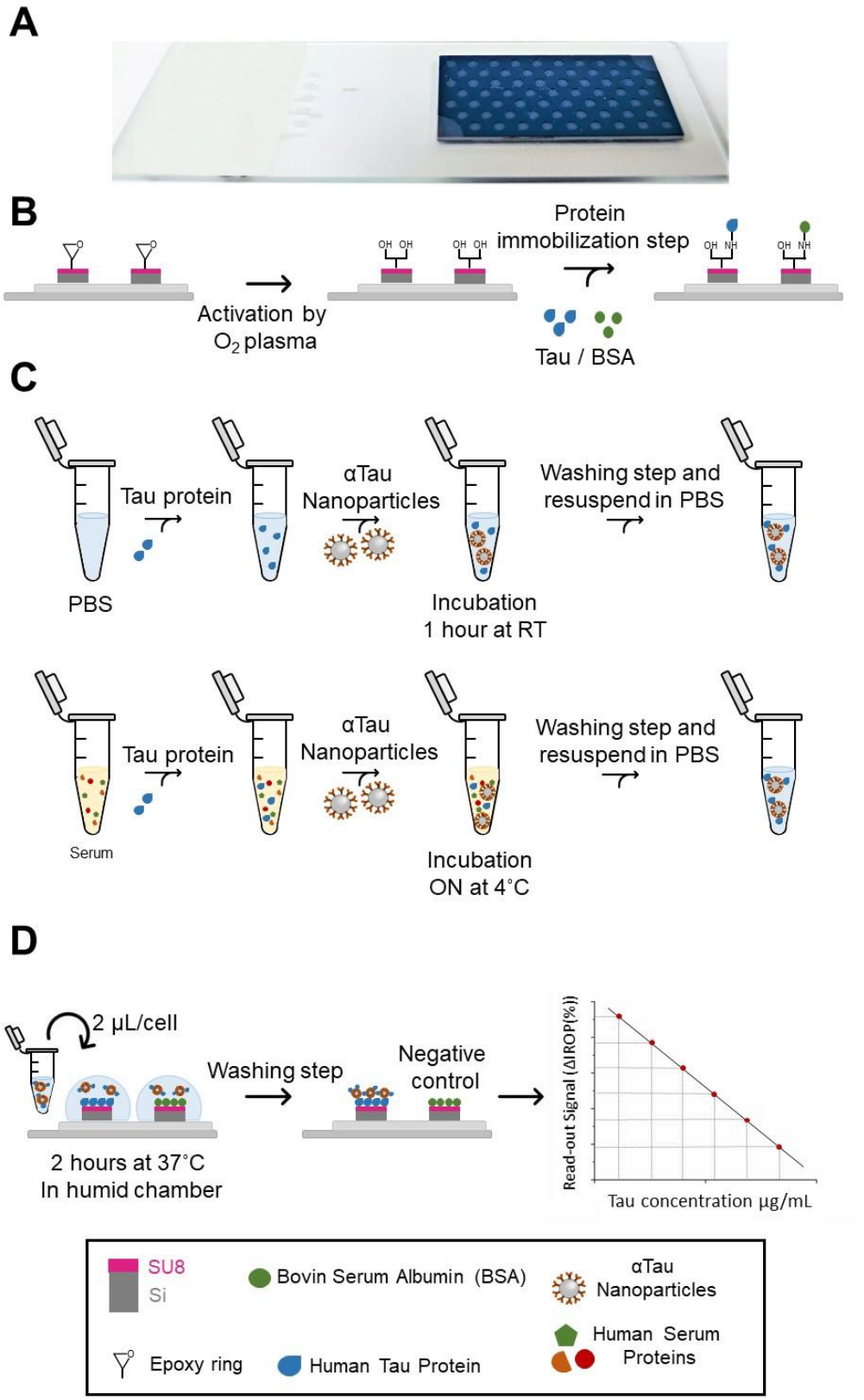

Figure 99. Competitive assay protocol for the detection of tau protein. A. KIT of 65-BICELLs used during the assays. **B.** Surface activation process using O_2 plasma for immobilization of tau and BSA proteins. **C.** Incubation of NPs with PBS and serum doped with tau protein. **D.** Incubation of the NPs-αTau-tau protein complexes on the sensor surface (Murillo et al., 2023).

4.3.1.12. *Protein-Ab pair specificity test with the new αTau Ab*

KITs with 16-BICELLs of 200 µm were immobilized with the tau and BSA proteins at 50 µg/mL by depositing 1.5 µL and incubated at 37°C for 2 hours. The KITs were washed as described above and then in the recognition step, 1.5 µL per cell of new αTau Ab (Sigma-Aldrich) at 50 µg/mL was applied to the tau and BSA proteins. The previous Ab was used as a PC. All determinations were conducted in four replicates.

4.3.1.13. *Biofunctionalization of SiO_2 NPs with the new Ab*

In the case of NPs biofunctionalization, the same protocol described above was performed, but the Ab was changed for the new αTau without changing any other variable.

4.3.1.14. *NPs concentration curves with the new Ab*

Similarly, once the NPs were biofunctionalized, a concentration curve was performed to determine the concentration of NPs for subsequent assays. KITs of 200 µm 16-BICELLs cells were immobilized with tau protein at 50 µg/mL and after washes the NPs were incubated at a concentration of 1 x 10^7 NPs/µL and at 1:10 and 1:100 dilutions. As a NC the NPs were incubated at 1 x 10^7 NPs/µL on the BSA. All measurements were conducted in four replicates.

4.3.1.15. *SEM images*

For SEM imaging, slides were cut with a diamond tip and placed in the holder, holding them in place with a conductive tape (Figure 100).

Images were taken using SEM with a working distance of ≈10 mm, a high voltage of 5 kW, a probe current of 800 pA, and at normal incidence (Murillo et al., 2023).

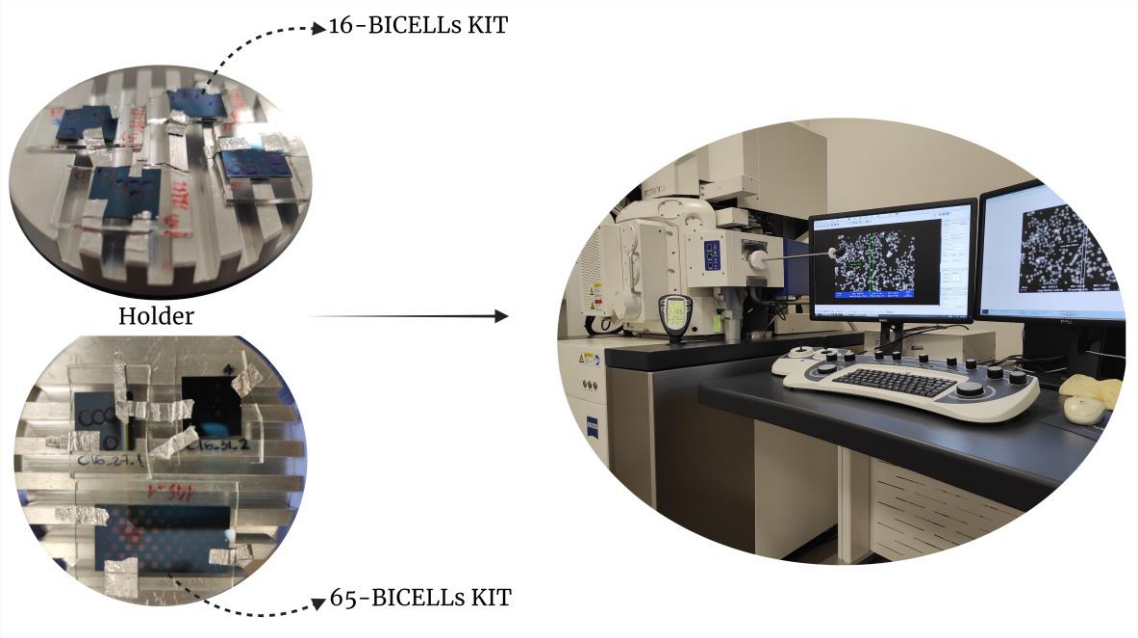

Figure 100. Sample preparation for SEM.

4.3.2. Case II. II. Triphosphorylated tau detection system

4.3.2.1. *Validation of reagents using the ELISA technique*

ELISA plates were coated with 100 µL/well of the 3-phosphotylated-Tau (3P-Tau) peptide (Lincbiotech, Galicia, Spain) at different concentrations (ranging from 1 µg/mL to 0.000064 µg/mL in 1:5 dilutions) and incubated ON at 4°C. The plates were then blocked with 1x casein hydrolysate (200 µL/well) for 1 hour at RT with agitation. After washing the plates three times with PBS-T 0.05%, the B6-biotin Ab (LincBiotech) was incubated at a concentration of 1:1000 diluted in blocking buffer:PBS 1:4 (100 µL/well) with agitation for 1 hour at RT. Subsequently, the plates were washed again with PBS-T 0.05%, and STV-HRP was added at a concentration of 0.2 µg/mL (100 µL/well) for 1 hour at RT with agitation. After repeating the washes, the peroxidase substrate (TMB) was added (50 µL/well) and incubated in darkness. The reaction was stopped with 50 µL/well of 2 N HCl, and the absorbance was read at 450nm (Figure 101A).

Other plates were immobilized with the same concentrations of the 3P-Tau peptide, and after blocking and washing, the B6 Ab (Lincbiotech) without biotin was incubated at a concentration of 1:2000 in blocking buffer:PBS 1:4 (100 µL/well) for 1 hour at RT with agitation. After washing the plates, the secondary anti-Mouse-IgG Ab labeled with HRP (αMouse-IgG-HRP) produced in rabbit was added at 1:5000 in the same buffer as the primary Ab (50 µL/well) and incubated for 1 hour at RT with agitation. The plates were washed, and 50 µL/well of the enzyme substrate was added and left in darkness. After 15 minutes, the reaction was stopped with 50 µL/well of 2 N HCl, and the absorbance was read at 450nm (Figure 101B). All measurements were performed in triplicates.

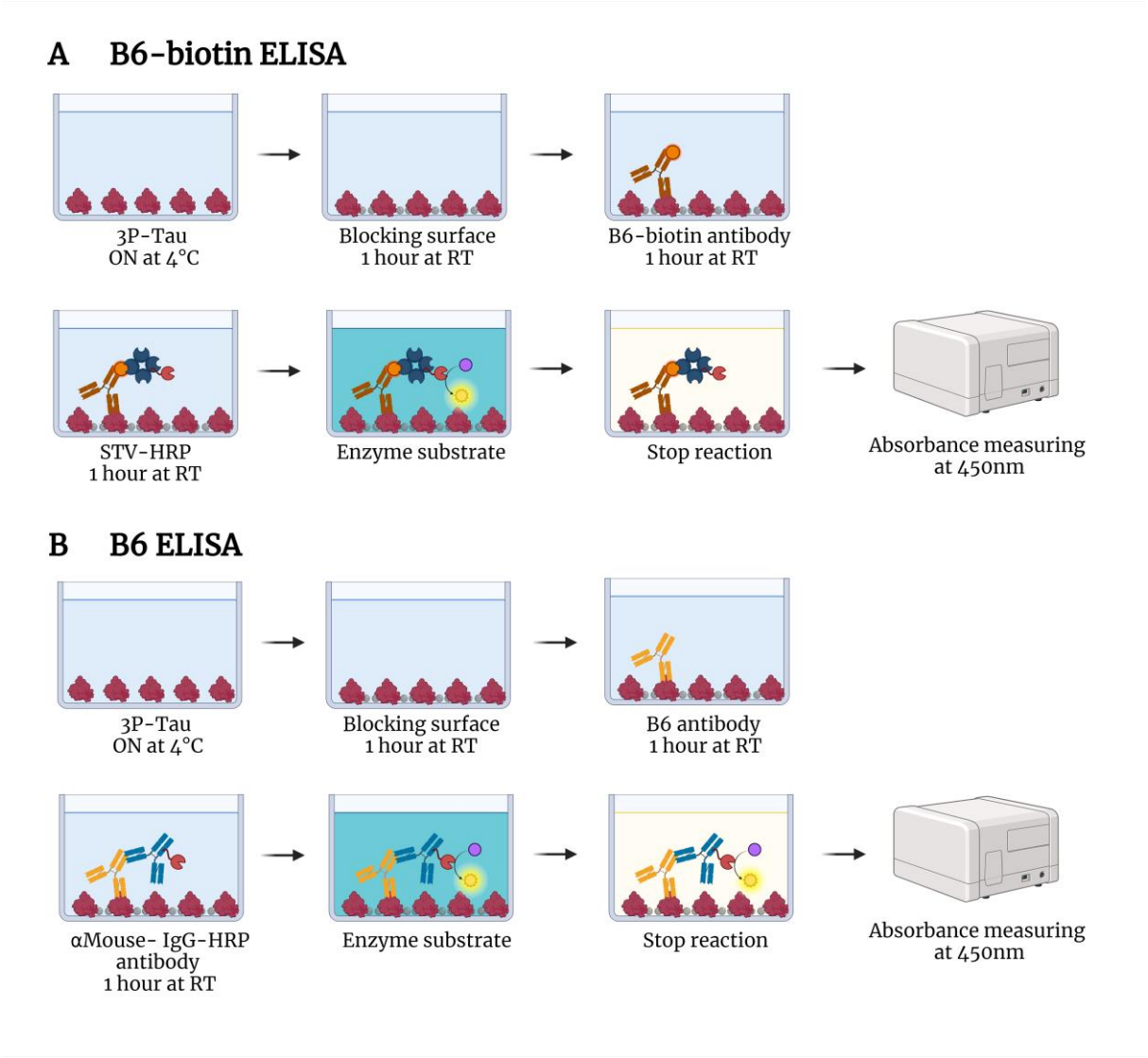

Figure 101. ELISAs for reagent testing. A. In this case the B6-biotin Ab is used and revealed with STV-HRP. **B.** In the second case, the non-biotin B6 Ab is used and revealed with an αMouse-IgG-HRP Ab. Created with BioRender.com.

Measurements for each concentration were performed in triplicates. As a NC, wells were coated with 1x casein hydrolysate, and the final signal represented is after subtracting the signal of the NC.

4.3.2.2. *Immobilization of the 3P-Tau peptide and the B6 Ab on the sensor surface (dose-response curves)*

65-BICELLs of 200 µm KITs were immobilized with the 3P-Tau peptide at different concentrations (300, 100, 50 and 20 µg/mL), depositing 1.5 µL in each cell. They were left to incubate in a humid chamber, some KITs ON at 4°C and others for 3 hours at 37°C. Subsequently, they were washed with 20 mL of H_2OmQ, agitated for 2 min in H_2OmQ, and dried with compressed air to measure ΔIROP (%) values.

The B6 Ab was also immobilized at different concentrations (1000, 200 and 50 µg/mL), using the same volume as the peptide and the same conditions (ON at 4°C and 3 hours at 37°C). The same washing procedure was carried out, and the ΔIROP (%) signal was measured.

As a PC for immobilization, the tau protein at 50 µg/mL (1.5 µL/cell) was used. All measurements were performed in five replicates.

4.3.2.3. *Recognition assays on KITs*

For the recognition assays, 65-BICELLs KITs of 200 µm were immobilized with the 3P-Tau peptide at different concentrations (20, 50, 100 and 300 µg/mL) using 1.5 µL for 3 hours at 37°C in a humid chamber. The KITs were washed, and the B6 Ab was recognized on each immobilization concentration at two different concentrations (1000 and 200 µg/mL), using 1.5 µL under two different conditions, ON at 4°C and 3 hours at 37°C. They were washed with 20 mL of H_2OmQ and agitated for 2 min in H_2OmQ. After drying with filtered compressed air, the ΔIROP (%) values were measured.

Furthermore, KITs were coated with the B6 Ab at 50, 200, and 1000 µg/mL for 3 hours at 37°C in a humid chamber. After washing, the 3P-Tau peptide was incubated at a concentration of 300 µg/mL under two different conditions, ON at 4°C and 3 hours at 37°C in a humid chamber. Finally, the KITs were washed, and the ΔIROP (%) signal was measured.

As a PC, cells were coated with the tau protein at 50 µg/mL and recognized with the αTau Ab at 50 µg/mL. As a NC, the B6 and αTau Abs were incubated on BSA-coated cells at 50 µg/mL. All measurements were repeated in five replicates.

4.3.2.4. *Blocking assays*

The 65-BICELLs KITs of 200 µm immobilized with the B6 Ab at 50 and 200 µg/mL for 3 hours at 37°C in a humid chamber were blocked with 10 µg/mL of Polivinilpirrolidona (PVP) (Sigma-Aldrich) using 1.5 µL/cell for 1 hour at 37°C. Subsequently, they were washed with 20 mL of H_2OmQ and agitated for 2 min in H_2OmQ, then dried with filtered compressed air. Other KITs were left unblocked. In both types of KITs (blocked and unblocked), the 3P-Tau peptide was incubated at two different concentrations (50 and 300 µg/mL) for 3 hours at 37°C. Finally, the KITs were washed, and the ΔIROP (%) values were read. All determinations were measured in five replicates.

4.3.2.5. *Recognition assays on KITs biofunctionalized with STV*

65-BICELLs KITs of 200 µm were immobilized with STV at a concentration of 500 µg/mL using 1.5 µL and left to incubate for 3 hours at 37°C. After this initial incubation, they were further incubated ON at 4°C. Following this, they were washed using a 20 mL syringe filled with H_2OmQ and agitated for 2 min in H_2OmQ before being dried using filtered compressed air. The B6-biotin Ab was then incubated on the STV-coated surface at a concentration of 1000 µg/mL (1.5 µL/cell) for 3 hours at 37°C. The same washing process was repeated, and the surface of half of the KITs was blocked with 10 µg/mL PVP. Finally, the 3P-Tau peptide was incubated at concentrations of

50, 100, and 300 µg/mL (1.5 µL/cell) for 3 hours at 37°C.

As a NC, the B6 Ab without biotin was incubated on the STV-coated surface. The PC for the experiment and the performance of the KITs was the tau-αTau Ab pair. All measurements were repeated in five replicates.

4.3.2.6. *Recognition of the 3P-Tau peptide in different matrixes in BICELLs with and without STV*

65-BICELLs 200 µm KITs were immobilized with the B6 Ab at a concentration of 1000 µg/mL (1.5 µL/cell) for 3 hours at 37°C in a humid chamber. After washing the KITs, half of them were blocked with 10 µg/mL PVP (1.5 µL/cell) for 1 hour at 37°C in a humid chamber. After another round of washing, the different matrices in which recognition would be tested were incubated on both the blocked and unblocked KITs. The matrices tested included serum, PBS, artificial Cerebrospinal Fluid (aCSF) (Gelest, Morrisville, PA, USA), and H_2OmQ. These matrices were incubated both undoped and doped with the 3P-Tau peptide at 300 µg/mL for 3 hours at 37°C in a humid chamber. The washing step was repeated, and the ΔIROP (%) signal was read after drying (Figure 102A).

The same experiment was conducted by immobilizing STV on the sensor surface at a concentration of 500 µg/mL (1.5 µL/cell), followed by incubation with the B6-biotin Ab under the same conditions described above. Half of the biofunctionalized KITs were blocked with PVP, and the different matrices were tested following the same protocol described for the non-biotinylated B6 AB (Figure 102B). All measurements were performed in five replicates.

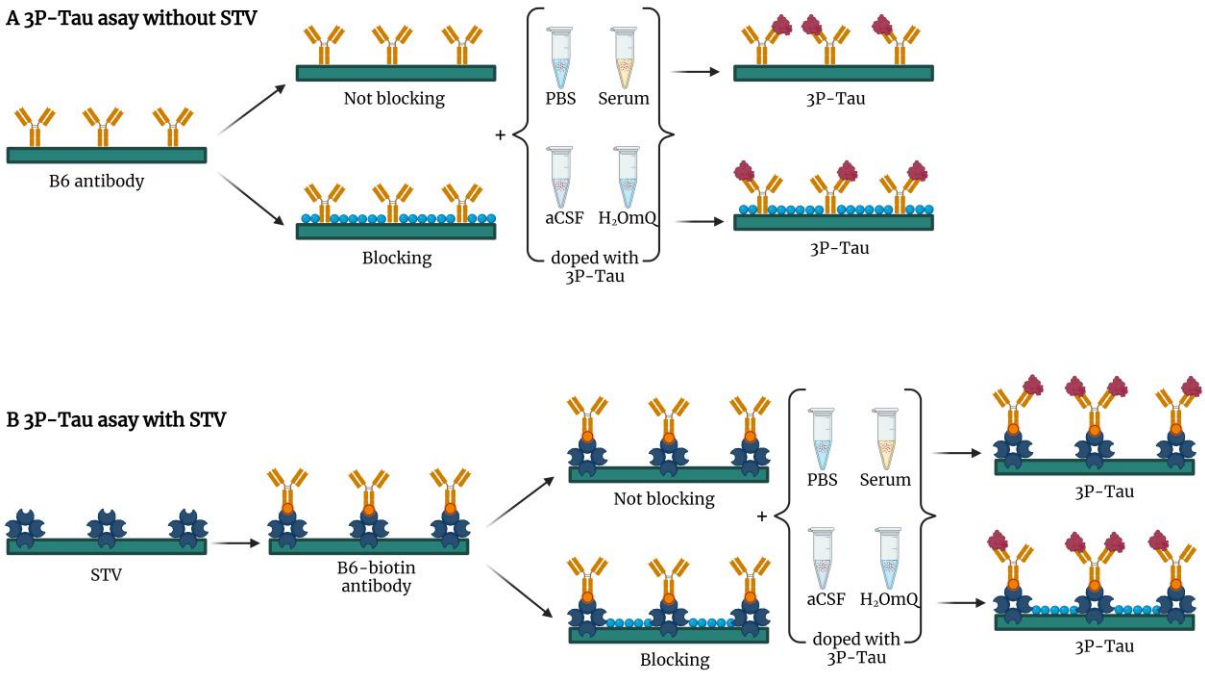

Figure 102. 3P-Tau peptide detection assay in KITs in different matrices. A. Assay by immobilizing the B6 Ab directly on the sensor surface. **B.** Assay by coating the surface with STV and then adding the B6-biotin Ab. Created with BioRender.com.

4.3.2.7. *Specificity assays by ELISA and IODM*

The ELISA plates were immobilized with the tau protein (100 µL/well) at different concentrations (from 25 µg/mL to 0.00032 µg/mL in 1:5 dilutions) ON at 4°C. They were then blocked with 1x casein hydrolysate for 1 hour at RT. After three washes with PBS-T 0.05%, the αTau Ab was incubated at a concentration of 1:1000 (100 µL/well) for 1 hour with agitation. Following additional washes, a secondary anti-Rabbit-IgG labeled with HRP (αRabbit-IgG-HRP) Ab (Sigma-Aldrich) was added at a concentration of 1:12000 (100 µL/well) and incubated for 1 hour at RT with agitation. After washing the plates, 75 µL/well of TMB was added, and the reaction was stopped with 75 µL of 2 N HCl. The results were read at 450nm.

Additionally, the BSA protein was immobilized under the same conditions as the tau protein. After blocking and washing the plates, the αBSA Ab was incubated at a concentration of 1:1500 (100 µL/well) for 1 hour at RT with agitation. Finally, the same secondary Ab (αRabbit-IgG-HRP) was used at the same concentration, and the signal was revealed following the same protocol as described for the tau protein.

Furthermore, ELISA plates were immobilized with the 3P-Tau peptide using the protocol described in section 4.3.2.1. In the recognition stage, the Abs were cross-incubated on the three immobilized proteins for specificity studies (Figure 103A). All measurements were repeated in triplicates.

The IODM assay was performed on 16-BICELLs 200 µm KITs, immobilizing the 3P-Tau peptide at a concentration of 300 µg/mL and the tau protein at 50 µg/mL for 3 hours at 37°C in a humid chamber. The KITs were washed and blocked with PVP at a concentration of 10 µg/mL for 1 hour at 37°C in a humid chamber. In the recognition step, the B6 Ab (200 µg/mL) and αTau Ab (50 µg/mL) were incubated for 3 hours at 37°C in a humid chamber. Cross-recognition was also performed to study specificity.

This experiment was repeated using the B6-biotin Ab. In the final revelation step, a secondary αRabbit-IgG Ab (1:50) (Sigma-Aldrich) was incubated in cells where the αTau Ab had been applied; a secondary αMouse-IgG Ab (1:20) (Sigma-Aldrich) was applied in cells where the B6 Ab had been incubated, and STV-HRP (0.2 µg/mL) was applied in cells where the B6-biotin had been incubated to ensure recognition. This incubation was carried out for 3 hours at 37°C in a humid chamber, followed by agitation, drying with filtered compressed air, and reading the ΔIROP (%) signal (Figure 103B). All measurements were conducted in four replicates.

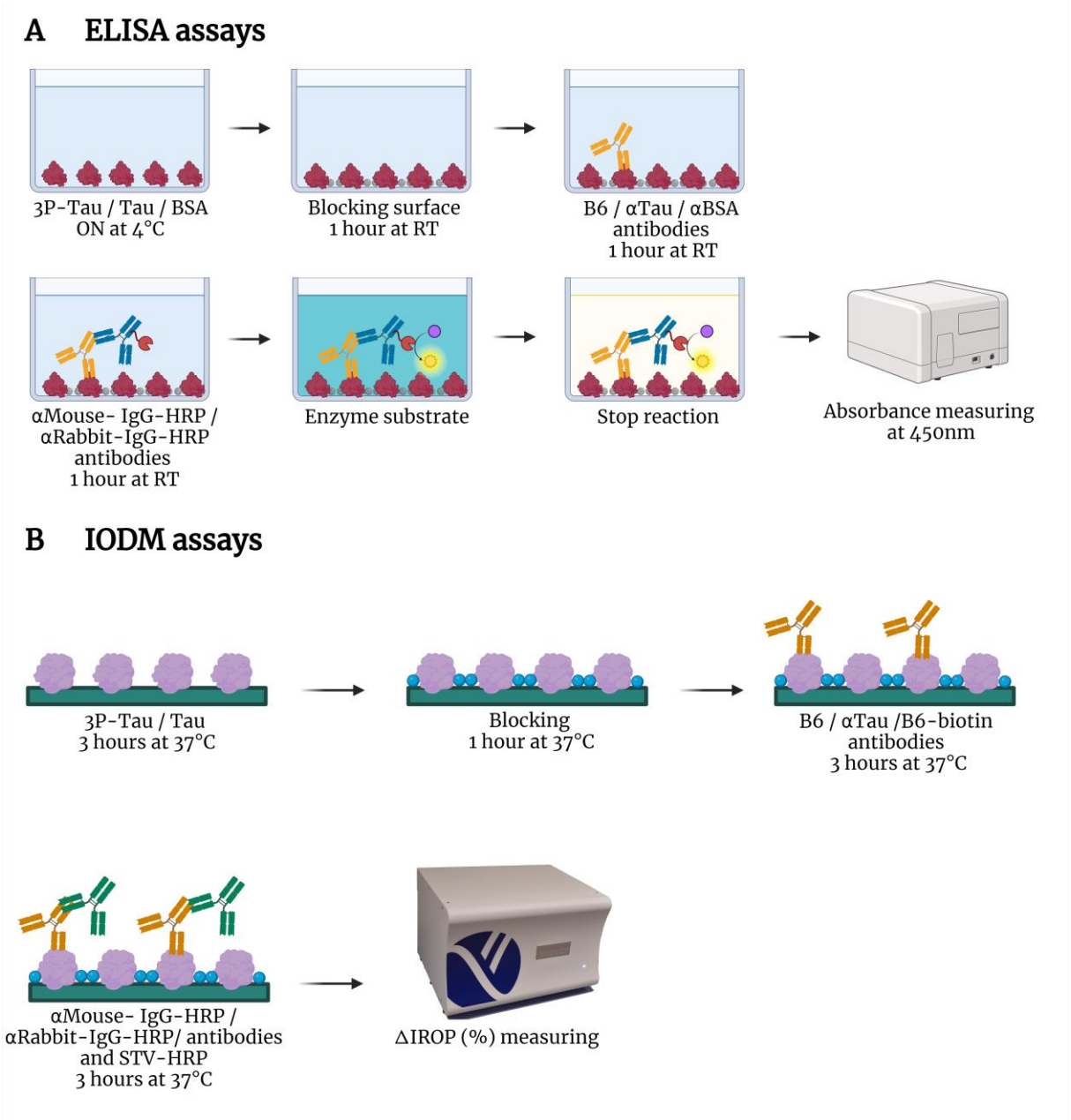

Figure 103. Specificity assays in ELISA and IODM. A. Scheme of the ELISAs performed. **B.** Protocol followed in the KITs for the IODM. Created with BioRender.com.

4.3.2.8. *Biofunctionalization of SiO_2 NPs with the B6 Ab*

80nm SiO_2 NPs were used for the biofunctionalization process. Firstly, they underwent 3 washes with H_2OmQ to remove ethanol, followed by centrifugation at 7500 rpm for 20 min. After the washes, the NPs were resuspended in 5 mM Na_2CO_3, and carboxyethylsilanetriol sodium salt at 25 % in water was added. The mixture was then incubated for 1 hour at RT with agitation. The same H_2OmQ wash steps were repeated, and in the final wash, the NPs were resuspended in 30 mM MES buffer. EDC and NHS were added, and the mixture was left to incubate for 1 hour at RT with agitation. After washing, the NPs were resuspended in H_2OmQ and G-protein (500 µg/mL) was

added, followed by ON incubation at 4°C with agitation. The next day, 0.1 M DEA was added for blocking and left for 1 hour at RT with agitation. After washing, the B6 Ab was added at a concentration of 200 µg/mL and left ON at 4°C. Following another round of washes with H_2OmQ, the NPs were resuspended in PBS.

In addition, commercially available 100 nm SiO_2 NPs that were pre-biofunctionalized with STV were used (Creative Diagnostics, NY, USA). To these NPs, B6-biotin Ab was added at a concentration of 200 µg/mL and left ON at 4°C. After washing with H_2OmQ, they were also resuspended in PBS (Figure 104).

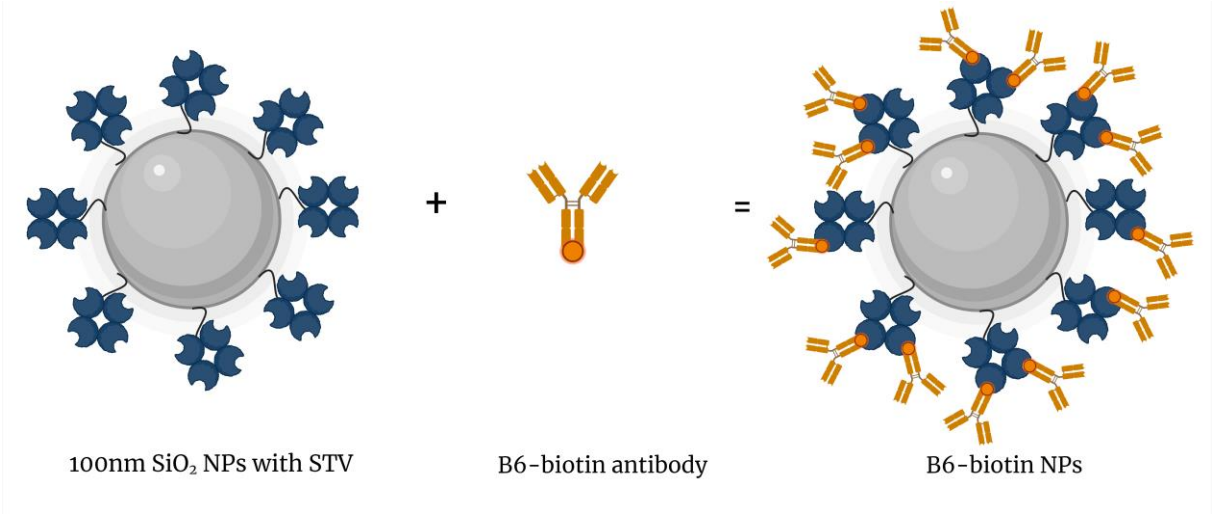

Figure 104. Biofunctionalization protocol of commercial 100 nm SiO_2 NPs with STV. Created with BioRender.com.

At each step of the biofunctionalization process, a portion of NPs was separated to measure the size and NPs concentration by DLS.

4.3.2.9. *Concentration curve of α3P-Tau SiO_2 NPs*

KITs with 16-BICELLs of 200 µm were coated with the 3P-Tau peptide at a concentration of 300 µg/mL for 3 hours at 37°C in a humid chamber. After washing, α3P-Tau NPs were incubated at different concentrations in 1:10 dilutions on the coated surface with the 3P-Tau peptide and with BSA at 50 µg/mL as a NC. Two concentration curves were generated, one using the silanized NPs and the other using commercial NPs. All measurements were performed with four replicates.

4.3.2.10. *Immobilization and recognition assays at different pH levels*

KITs with 16-BICELLs of 200 µm were immobilized with the 3P-Tau peptide at different concentrations (75, 150, and 300 µg/mL) in H_2OmQ. Additionally, the 3P-Tau peptide was immobilized at 300 µg/mL in different buffers (PBS-HCl, carbonate buffer, PBS, MES, and H_2OmQ), covering a pH range from 4 to 10. All these KITs were immobilized with a volume of 1.5 µL for 3 hours at 37°C in a humid chamber. After washing with 20 mL of H_2OmQ, they were agitated for 45 s in H_2OmQ. They were recognized with the B6 Ab and revealed with the αRabbit-IgG Ab (1:50).

Finally, they were dried with filtered compressed air, and the ΔIROP (%) signal was read.

In parallel, KITs with the surface coated with STV were used, on which the Abs B6-biotin (1000 µg/mL), anti-Lactoferrin (αLactoferrin) (100 µg/mL), and αBSA (100 µg/mL) were incubated, with the latter two serving as controls for the experiment. After washing the KITs, the 3P-Tau peptide was incubated at 300 µg/mL in different buffers (H_2OmQ, carbonate buffer, PBS, and MES) on the surface coated with B6-biotin Ab. For αLactoferrin, lactoferrin protein was incubated at 25, 50, and 100 µg/mL, and similarly for the BSA protein.

4.3.3. Case II. III. Detection of pTau181 in the Syrian hamster model

4.3.3.1. *Hamster model*

We used 16 male 3-month-old Syrian hamsters (*M. auratus*) purchased from Janvier Labs (Le Genest-Saint-Isle, France). All experimental procedures were performed in the animal facility of the CTB of the UPM. The procedures were approved by the Institutional Animal Experimentation Ethics Committee (PROEX_203-4-21). Animals had free access to food and water and were maintained at 23°C with an 8:16 h light/dark cycle.

After the acclimatization period (4 weeks), 11 of the 16 animals were transferred to a special chamber to artificially induce hibernation and to obtain torpor and arousal experimental groups (temperature and lighting were controlled, while the hamsters could be monitored by measuring their locomotor activity). To induce torpor, the temperature and light were gradually reduced until total darkness and 4°C were reached.

Torpor was considered to have begun after 24 hours of inactivity. We considered animals to be torpid only if they had completed three full periods of torpor (3-4 days of inactivity) before sacrifice. We sacrificed torpid animals on day 2 after the onset of torpor to ensure that the animals were in deep torpor. The awakening experimental group was obtained by removing the torpid animals from the hibernation chamber and awakening them 1 hour before sacrifice. The temperatures of the animals were checked with an infrared thermometer prior to perfusion to ensure that they were in deep torpor (n = 6) or arousal (n = 5). Control animals (n=5) were kept under normal temperature conditions (not transferred to the hibernation chamber) for the same period of time as the torpor and arousal groups until sacrifice (Figure 105A).

In addition, we used adult P301 transgenic mice as a control for pTau T181 detection (n=4). The animals were obtained from The Jackson Laboratory (B6;C3-Tg, Prnp-MAPT*P301S, PS19Vle/J strain #008169) and express the human tau protein P301S mutation (1N4R isoform) under the control of the mouse prion protein promoter. All experimental procedures were performed at the animal facility of the University of San Pablo CEU (SVA-CEU.USP, ES 280220000015), previously approved by the Ethics Committee for Animal Experimentation of the Community of Madrid (PROEX 165.6/21), according to international guidelines and Spanish law by Royal Decree (RD 53/2013). All animals were maintained on a 12-hour light/dark schedule with ad libitum access to food and water (Figure 105B).

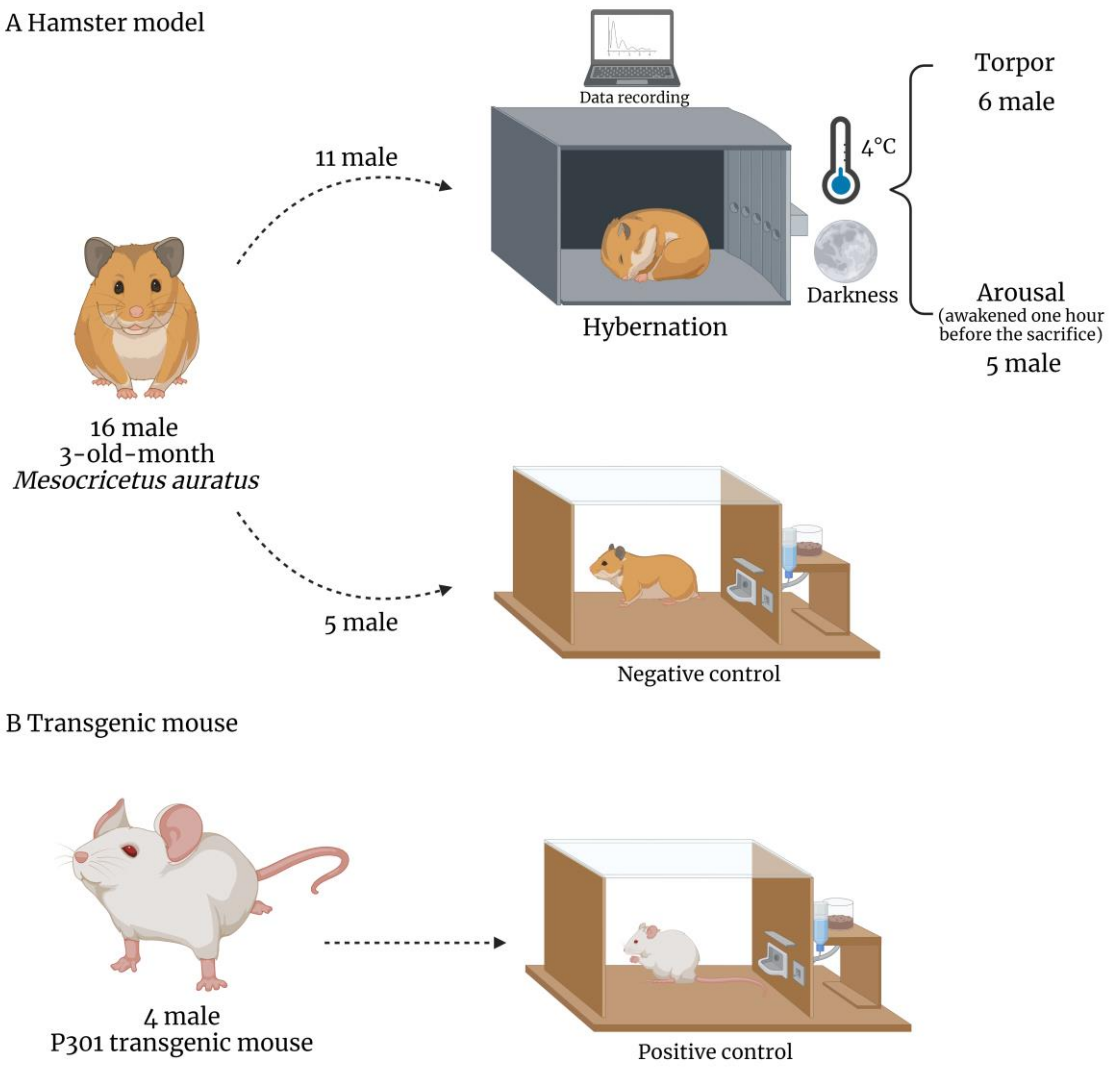

Figure 105. Model followed for the experiment. A. Torpor, arousal and control hamster conditions. **B.** Conditions of human tau protein-producing transgenic mice. Created with BioRender.com.

All animals were killed by lethal intraperitoneal injection of pentobarbital sodium (200 mg/kg). Plasma samples were obtained by drawing blood directly from the heart of the anesthetized animal and the volume obtained was transferred to an Eppendorf tube. After 4 hours at RT samples were centrifuged at 2000 rpm for 10 min and the supernatant was collected for serum assays.

4.3.3.2. *Biofunctionalization of αpTau181 SiO_2 NPs*

To biofunctionalize the NPs with αpTau181 (Abcam), the protocol described above for the αTau Ab was followed. G-protein silanized 80 nm SiO_2 NPs were used to which the αpTau181 Ab was added (15 µL at 500 µg/mL).

At each step of the biofunctionalization process, a portion of NPs was separated to measure the size and concentration of the NPs using DLS.

4.3.3.3. *αpTau181 NPs concentration curve*

KITs of 16-BICELLs were immobilized with pTau181 protein (Abcam) at 50 µL/mL for 3 hours in a 37°C humidity chamber. Tau protein at 50 µg/mL was also incubated as a control. They were washed with 20 mL H_2OmQ and shaken in H_2OmQ for 45 s. After drying with compressed air, the immobilization values were read.

The biofunctionalized NPs were then incubated at a concentration of 1 x 10^{10} NPs/µL and at a dilutions of 1:10 on the KIT coated with pTau181. They were kept in a humid chamber at 37°C for 2 hours. They were then washed with 20 mL H_2OmQ, kept in shaking PBS for 10 min, and rinsed with 40 mL H_2OmQ. Finally, after drying, ΔIROP (%) values were read. All points were measured in four replicates.

4.3.3.4. *Competitive assay on hamster serum samples*

KITs of 65-BICELLs were immobilized with pTau181 protein at 50 µg/mL (1.5 µL/cell) for 3 hours at 37°C in a humid chamber. Tau was immobilized at 50 µg/mL as a NC protein.

NPs biofunctionalized with αpTau181 Ab at a concentration of 1 x 10^8 NPs/µL in PBS were doped with different concentrations of pTau181 protein (from 100 µg/mL to 0.00001 µg/mL in 1:10 dilutions) for 1 hour at RT with shaking. After washes, they were incubated in the KIT (1.5 µL/cell) for 2 hours in a humidity chamber at 37°C. Finally, they were washed with 20 mL H_2OmQ, kept in PBS with agitation for 10 min, and then rinsed with 40 mL H_2OmQ.

These NPs were incubated with the hamster serum samples at 1:10 dilution for 1 hour at RT with agitation. The KITs were washed and incubated in the same manner as the concentration standard curve.

In addition, as a PC, the biofunctionalized NPs were incubated with samples from transgenic mice producing phosphorylated human tau protein diluted 1:10. All measurements were performed in five replicates (Figure 106).

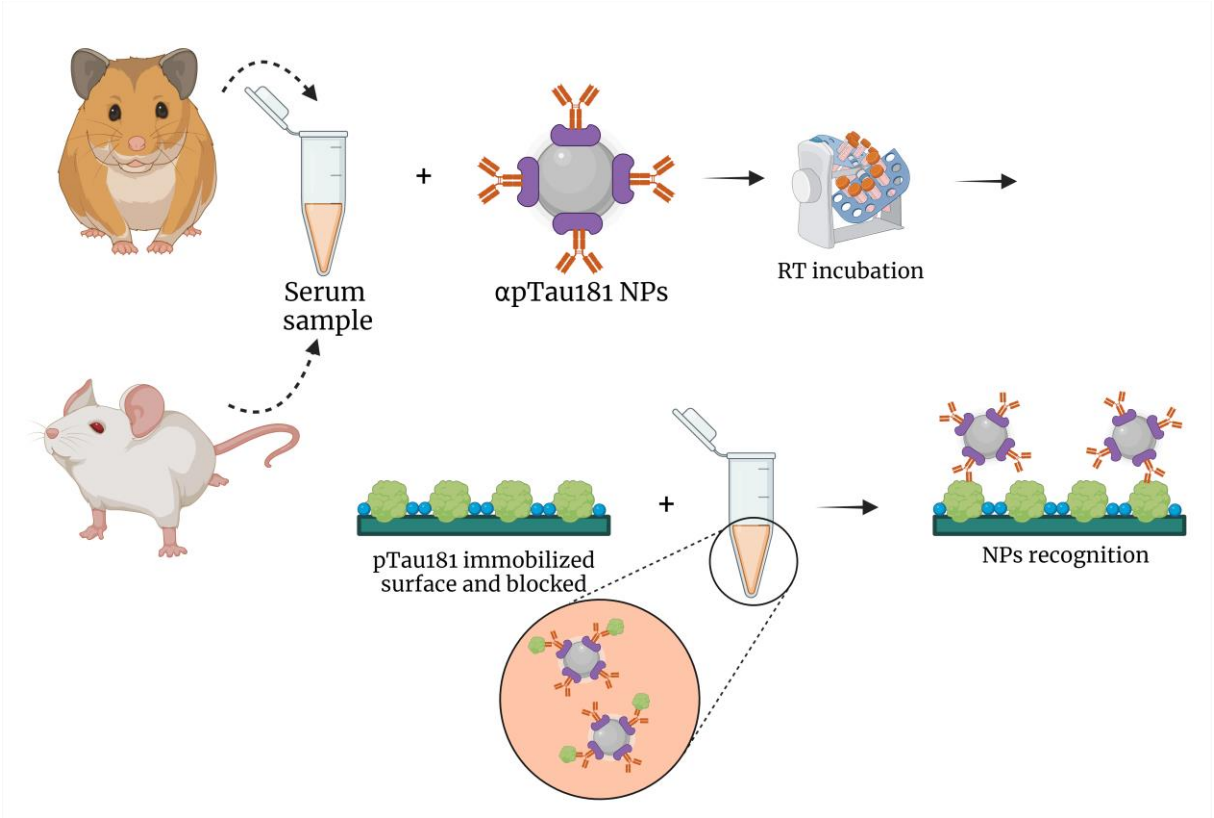

Figure 106. Schematic of the steps followed to perform the competitive assay for pTau181 detection. Created with BioRender.com.

4.3.4. Case II. IV. Lactoferrin detection system in saliva samples

4.3.4.1. *Human saliva samples*

The saliva samples used were kindly donated by Dr. Fernando Maestu. The samples used belonged to relatives of patients who had suffered AD and relatives with no history of the disease. These samples were centrifuged at 15000 rpm for 10 min and the supernatant was collected and stored at -80°C.

4.3.4.2. *Biofunctionalization of αLactoferrin SiO_2 NPs*

Different protocols for the biofunctionalization of NPs were performed. On the one hand, 1 x 10^{10} NPs/µL of 80 nm SiO_2 NPs were biofunctionalized following the previously described protocol of silanization with G-protein, with the addition of αLactoferrin Ab (15 µL at 500 µg/mL) (Bio-rad, CA, USA) in the last step (Figure 107A). In addition, the same protocol described above was carried out in parallel with the addition of the STV protein instead of the G-protein. This was added at the same concentration and all other steps were performed in the same manner. The Ab used in this case was the αLactoferrin-biotin Ab (Figure 107B).

Finally, commercial 100 nm SiO_2 NPs with STV attached to the surface were used at a concentration of 1 x 10^{10} NPs/µL. These were then incubated with the αLactoferrin-biotin Ab (15 µL at 500 µg/mL) (Figure 107C).

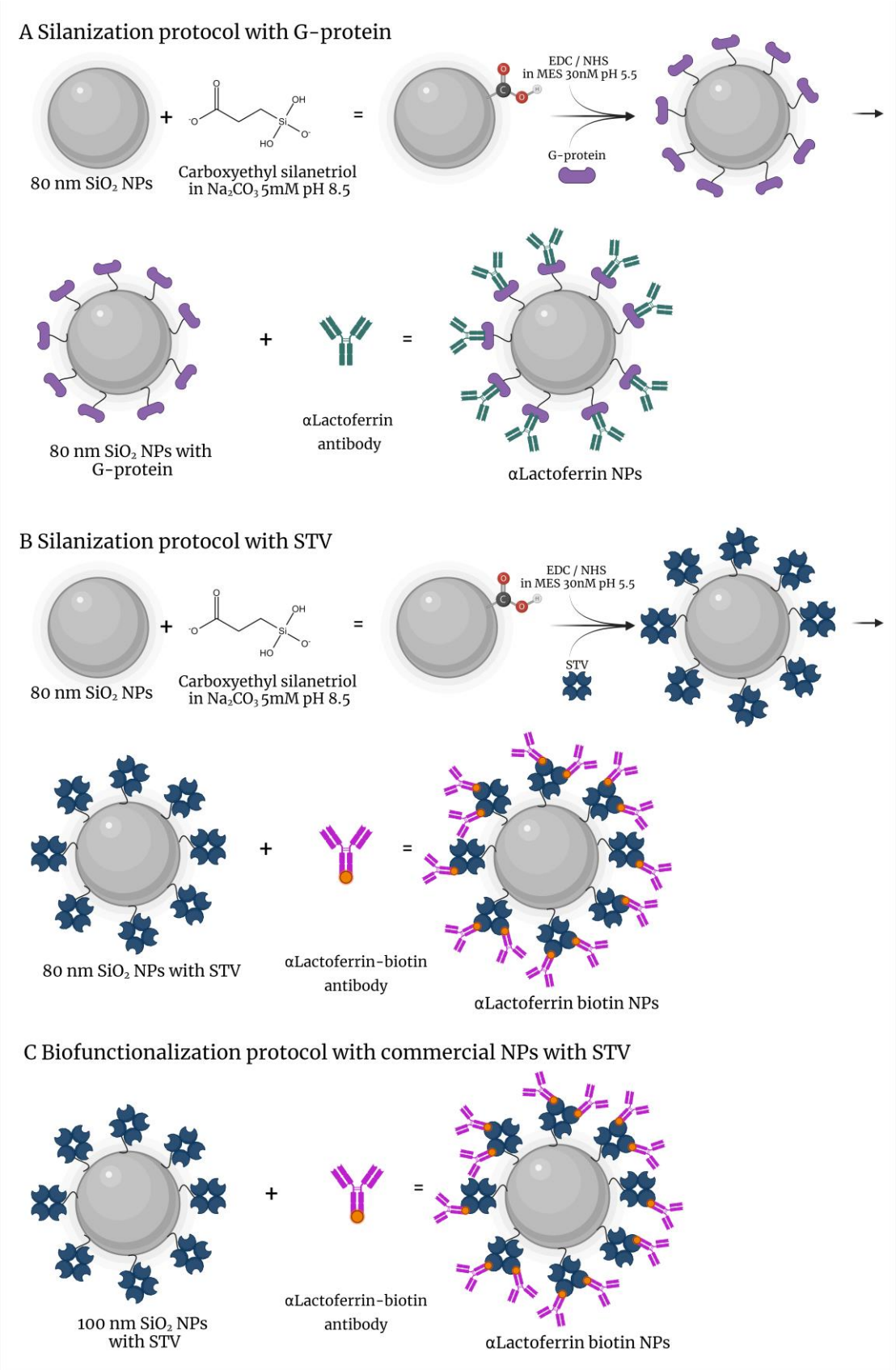

Figure 107. Protocols for biofunctionalization of NPs with αLactoferrin Ab. A. Silanization of 80nm SiO_2 NPs to surface coat with G-protein and then add the αLactoferrin Ab **B.** Silanization of 80nm SiO_2 NPs to surface coat with STV and then add the αLactoferrin-biotin Ab. **C.** Addition of αLactoferrin-biotin Ab to 100nm commercial NPs with STV. Created with BioRender.com.

At each step of the biofunctionalization process, a portion of NPs was separated to measure the size and concentration of the NPs using DLS.

4.3.4.3. *αLactoferrin NPs concentration curves*

16-BICELLs KITs of 200 µm were immobilized with lactoferrin protein at 100 µL/mL (Bio-rad) for 3 hours in a humid chamber at 37°C. BSA protein at 50 µg/mL was also incubated as a NC. They were washed with 20 mL H_2OmQ and agitated in H_2OmQ for 45 s. KITs were blocked with 1x casein hydrolysate 1 hour at RT under agitation. Then the same washing was performed as for the immobilization step. After drying with compressed air, the ΔIROP (%) values were read.

The biofunctionalized NPs with the αLactoferrin Ab using the three methods described above were incubated over the KIT surface coated with lactoferrin and BSA proteins. The silanized NPs were incubated at a concentration of 1 x 10^7 NPs/µL and at a dilutions of 1:10, while the commercial NPs were incubated at a concentration of 1 x 10^9 NPs/µL and at a dilutions of 1:10. They were kept in a humid chamber at 37°C for 2 hours. They were then washed with 20 mL H_2OmQ, kept in shaking PBS for 10 min and rinsed with 40 mL H_2OmQ. Finally, after drying, ΔIROP (%) values were read. All points were measured in four replicates.

4.3.4.4. *Competitive assay in saliva*

65-BICELLs KITs of 200 µm were immobilized with lactoferrin protein at 100 µL/mL for 3 hours in a humid chamber at 37°C. As a NC, BSA protein was incubated under the same conditions as described above.

On the other hand, commercial NPs biofunctionalized with the αLactoferrin-biotin Ab at a concentration of 1 x 10^9 NPs/µL were doped in PBS with different concentrations of lactoferrin protein (from 100 µg/mL to 0.00001 µg/mL in 1:10 dilutions) for 1 hour at RT with shaking. After the washes, they were incubated on the KIT (1.5 µL/cell) for 2 hours in a humidity chamber at 37°C. Finally, they were washed with 20 mL H_2OmQ, kept in PBS for 10 min with agitation, and rinsed with 40 mL H_2OmQ.

In addition, the NPs were incubated with the saliva samples at 1:10 dilution at the same concentration and under the same time and temperature conditions. The procedure was the same for both concentration standards and samples. All measurements were performed in five replicates (Figure 108).

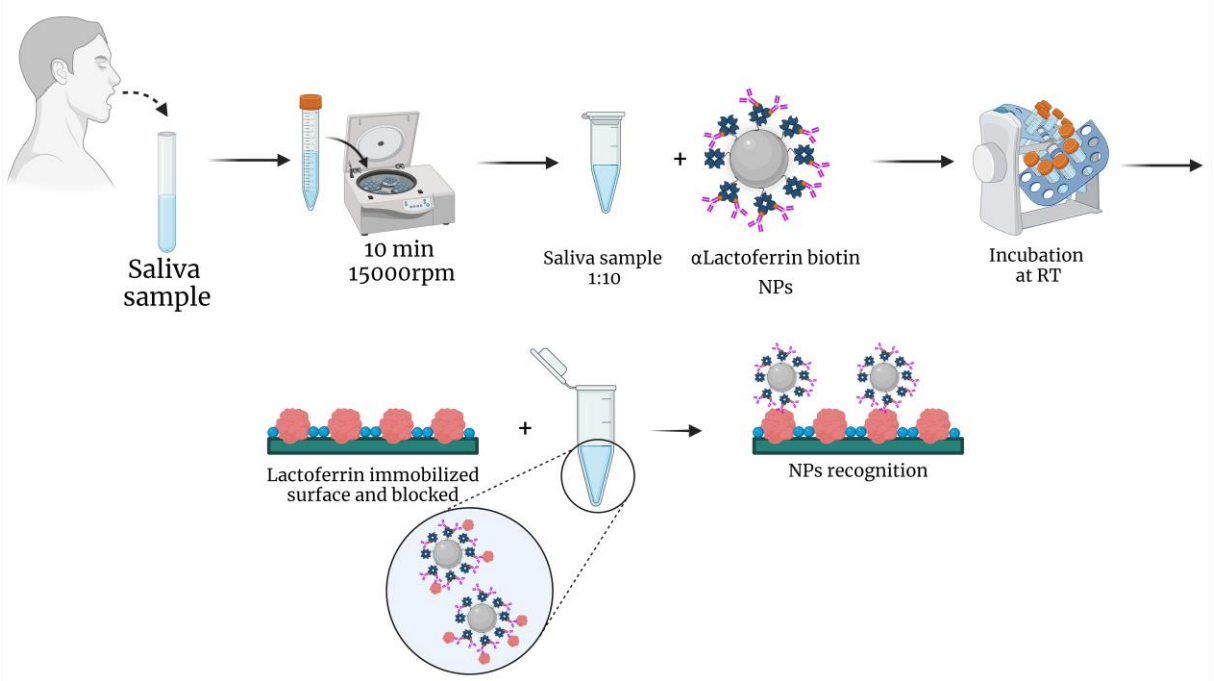

Figure 108. Diagram of the protocol performed for the detection of lactoferrin in saliva samples by competitive assay. Created with BioRender.com.

4.4. Results

4.4.1. Case II. I. Total tau detection system

4.4.1.1. *Comparison between O_2 plasma activation and acid catalysis in sensing surface*

In order to immobilize proteins on the sensor surface, it is necessary to activate the surface and different protocols can be used for this purpose. On the one hand, we have the activation by O_2 plasma, which introduces oxygenated functional groups on the surface, generally, hydroxyl (-OH), while on the other hand, acid catalysis (with H_2SO_4) can protonate groups on the surface, generating charged active sites (acids) that promote specific chemical reactions. Both methods are valid for our application, so we wanted to compare them in order to select the most suitable one.

For this purpose, two different proteins were immobilized by both methods and the signals obtained were compared.

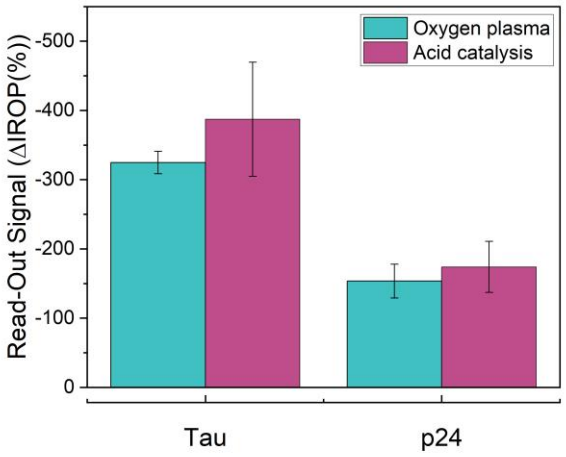

Figure 109. Immobilization after activation with H_2SO_4 and O_2 plasma.

As shown in Figure 109, **both methods achieved protein immobilization on the sensor surface.** Moreover, the signal difference between O_2 plasma activation and acid catalysis was not very high. On the other hand, in addition to obtaining similar signals, when **using O_2 plasma, the results were more reproducible** and we obtained a smaller error between immobilizations, whereas this step was more heterogeneous when using acid catalysis.

4.4.1.2. *Incubation volume adjustment*

Another factor to consider was the incubation volume to be used, as this was compromised by the distance between the cells, as they could not be joined together. To determine this volume, the concentration of the proteins to be incubated was set at 50 µg/mL and only the volume to be deposited on the surface was changed.

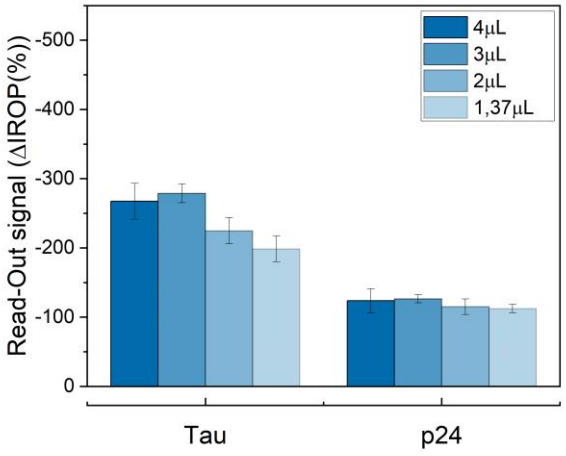

Figure 110. Incubation volume set-up in the KITs.

Looking at Figure 110, for p24 protein there is very little difference in ΔIROP (%) values for all volumes tested. However, in the case of tau protein, some difference can be seen between the lowest volume (1.37 µL) and 3-4 µL. Based on these signals and considering the trade-off between volume, reagent concentration, and signal obtained, **the volume of 2.5 µL was selected for dispensing on KIT cells.**

4.4.1.3. *Stability studies of immobilization*

Another parameter to be known is the stability of the immobilization, i.e. once the surface is covered, how stable the proteins remain over time in order to perform the experiments. For this purpose, the KITs were immobilized with tau protein and the IROP (%) values were read and also after blocking with DEA (for those blocked). The KITs were then stored in the refrigerator and read again at 24 and 48 hours to examine signal differences.

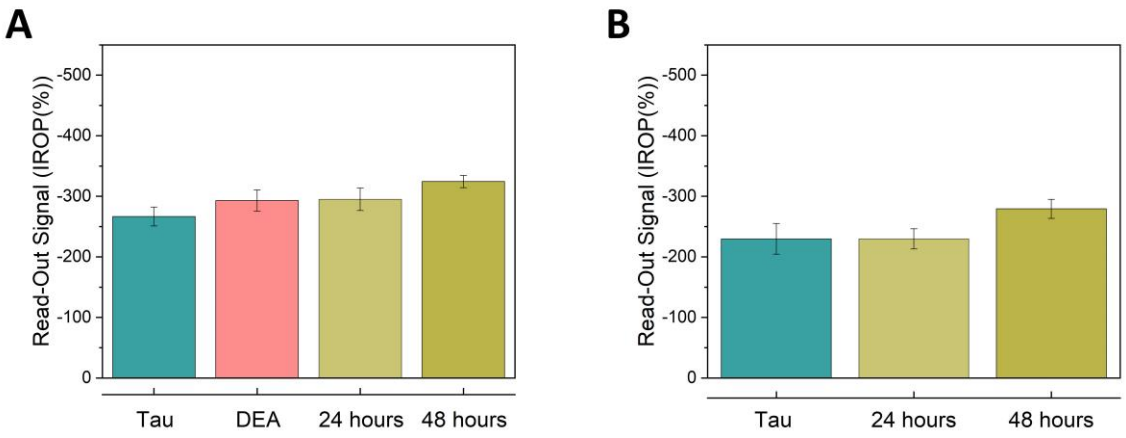

Figure 111. Stability studies in KITs. A. IROP (%) value at 24 and 48 hours after immobilization in KITs that have been stored after blocking. **B.** IROP (%) signals after immobilization and at 24 and 48 hours in unblocked KITs.

Figures 111A and 111B show the IROP (%) of the measurements, i.e. the IROP (%) signal at 24 and 48 hours was measured in both cases. In the case of tau-immobilized and **blocked KITs, no variation of the immobilization signal was observed at 24 hours, and there was a very small variation at 48 hours** (Figure 111A). For the **unblocked KITs, there were also no signal differences at 24 hours, and these were slightly higher at 48 hours when stored at 4°C** (Figure 111B).

4.4.1.4. *Evaluation of blocking step*

The next step was to verify the need for surface blocking since the sensor cells have a very small area. The goal is to cover the entire surface with the protein and prevent the need for blocking while ensuring that specificity in recognition is not compromised.

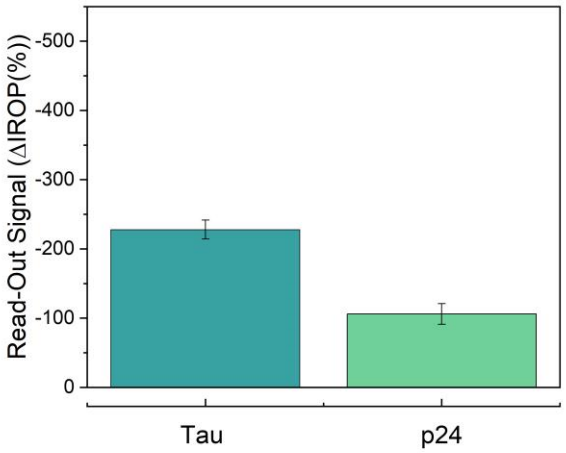

Figure 112. ΔIROP (%) signal of immobilization of tau and p24 proteins.

Figure 112 represents the ΔIROP (%) signal of the immobilization of the KITs used in the experiment, confirming that the immobilization has occurred correctly. Furthermore, as observed in Figure 113, we have the Ab recognition signal on its specific protein with and without surface blocking, and we did not obtain significant differences in the signal. **This indicates that the surface is fully covered during immobilization**. On the other hand, we also measure the signal of the Ab on a non-specific protein without surface blocking, which indicates that the Ab is not binding non-specifically to the sensor surface, **confirming specific recognition without the need for surface** blocking.

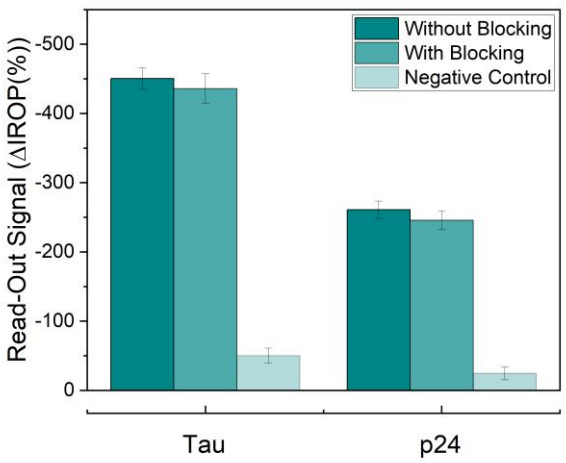

Figure 113. ΔIROP (%) signal of Ab recognition. Recognition was performed on the immobilized surface with its specific protein blocking and non-blocking surface. As a NC, recognition was performed on the surface immobilized with the non-specific protein.

Furthermore, to confirm these data, in Figure 114, we can see that there is hardly any difference in signal between the immobilization of the protein and the signal obtained after blocking, further supporting the assumption that **the surface is fully covered after immobilization**.

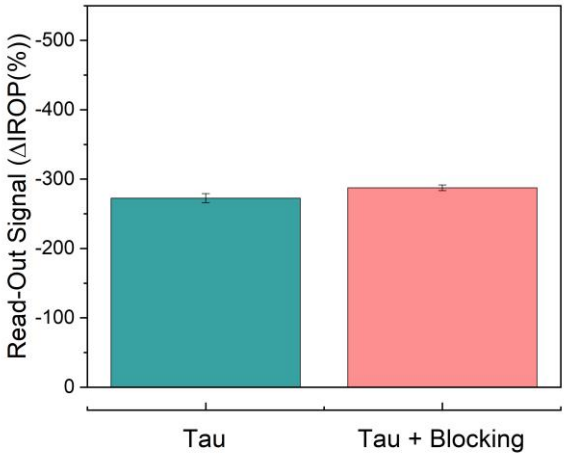

Figure 114. IROP (%) signal of immobilization of tau without and with blocking.

Thanks to these assays, the general conditions for all subsequent experiments were established, optimizing the necessary conditions (temperature, time, concentration, etc.) for each specific case.

In summary, immobilization of proteins in KITs using O_2 plasma and a volume of 2.5 µL was selected. This immobilization step was found to be stable for at least 48 hours. Finally, it was observed that the blocking step was not necessary for this application.

4.4.1.5. *Dose-response curve of tau protein immobilization*

To establish the immobilization concentration of the tau protein in the KITs, it was incubated on the sensor surface at different concentrations and after the washes the ΔIROP (%) signal was read.

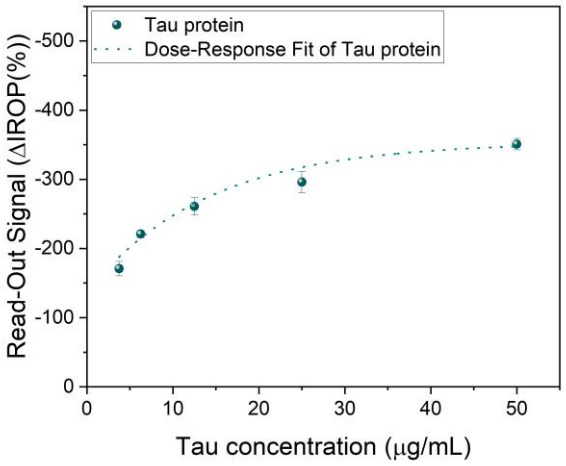

Figure 115. Dose-response curve of tau protein. The sigmoidal fit of dose-response curves is depicted.

As we increased the concentration of the protein, an increase in the signal was obtained, being at **50 µg/mL** the highest obtained (Figure 115). Therefore, **in all subsequent experiments the tau protein was immobilized at this concentration**.

4.4.1.6. *Protein-Ab pair specificity test*

To test the specificity of the αTau Ab that will be used during all the experiments, KITs were coated with tau protein and BSA protein and then the Ab was incubated at different concentrations on both proteins.

Figure 116 shows the signal of the αTau Ab on the surface covered with tau, so that as we increase the concentration of Ab, we have an increase in the signal. Considering the signals obtained, **a concentration of 50 µg/mL was stipulated for the use of the αTau Ab**.

In addition, αTau was incubated at a concentration of 50 µg/mL on BSA protein, on which no signal was obtained. The αBSA Ab was incubated on BSA and tau protein to study if there was cross-reactivity and no signal was obtained on tau protein.

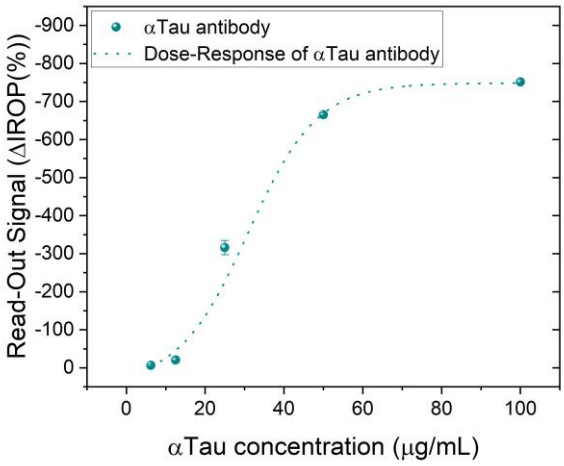

Figure 116. αTau Ab dose-response curve. The sigmoidal fit of dose-response curves is depicted.

4.4.1.7. *Biofunctionalization of SiO_2 NPs*

To verify each step of the biofunctionalization protocol, the size and ζ-potential were measured by DLS. In addition, the concentration of the NPs was measured to know the final concentration at which we had them for the following experiments.

In this case, **we observed an increase in size after each biofunctionalization step** (Figure 117) (Table 22) confirming the addition to the NPs surface of molecules such as G-protein and Ab. In addition, the PDI confirms that we have a homogeneous population (Table 22).

On the other hand, we have the ζ-potential value (Table 22), which initially indicates a negative ζ-potential in the range of -50 to -56 mV, which is consistent with a SiO_2 surface. After the addition of G-protein, the ζ -potential increases to a value of -40 ± 2.5 mV, due to the positive charges of the amino groups of the protein. Finally, **the ζ-potential decreases again to -35 ± 0.4 mV, confirming that we have a stable NPs solution**. So finally, we obtain a stable and dispersed NPs solution in the solution. Finally, in terms of concentration we obtain a final NPs concentration lower than the starting concentration.

Table 22. DLS measurements of size, concentration, ζ-potential and PDI during the biofunctionalization process of the NPs (Murillo et al., 2023)**.**

	Initial	***G-Protein***	***αTau***
Size (nm)	79.21 ± 2.70	95.11 ± 1.30	114.10 ± 2.80
Concentration (NPs/µL)	2.99 x 10^{10}	7.44 x 10^{10}	6.80 x 10^{7}
ζ-Potential (mV)	-50.71 ± 4.38	-40.16 ± 2.50	-35.62 ± 0.40
PDI	0.11 ± 0.05	0.13 ± 0.04	0.16 ± 0.06

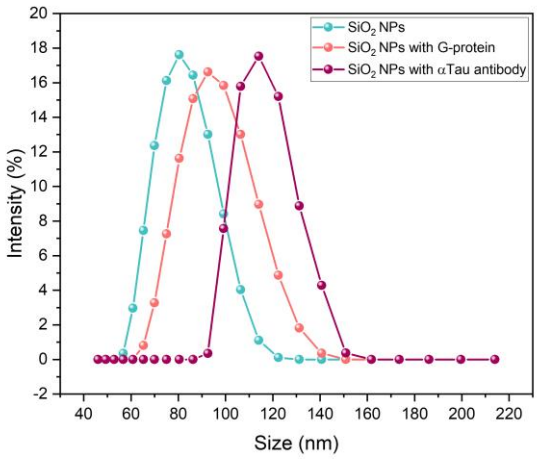

Figure 117. NPs size after each biofunctionalization step measured by DLS (Murillo et al., 2023)**.**

4.4.1.8. *NPs concentration curves*

After biofunctionalization of the NPs, they were incubated at different concentrations (1 x 10^{7} to 1 x 10^{4} NPs/µL) on KITs coated with tau protein.

This curve was used **to determine the concentration of NPs to be used in the subsequent assays (1 x 10^{7} NPs/µL)** (Figure 118), since it is the one with which we obtained the highest signal on the sensor.

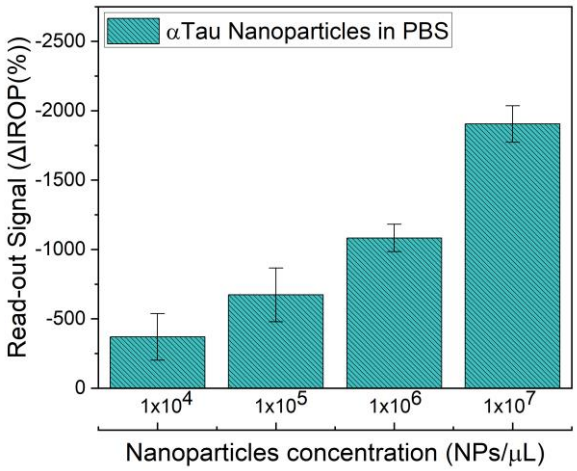

Figure 118. NPs concentration curve (Murillo et al., 2023).

4.4.1.9. *KITs washing tests*

To establish the best washing of the NPs after incubation on the KITs, different strategies described in the Table 23 below were tested.

After testing all types of washing and studying the signals, **strategy number 9 was chosen for all subsequent NPs assays as it provided the best signal with the highest specificity**. In addition, all these washing strategies were tested in KITs in which the NPs were incubated for 1, 2 and 24 hours.

Table 23. Washing strategies of the NPs after incubation in the KIT.

	Rinse	***Wash***	***Rinse***	***Drying***
Strategy 1	20 mL of H_2OmQ	1 min in agitation on a plate with H_2OmQ	10 mL of H_2OmQ	Oven at 65°C
Strategy 2	20 mL of H_2OmQ	1 min in agitation on a plate with H_2OmQ	10 mL of H_2OmQ	Hot plate at 70°C
Strategy 3	10 mL of H_2OmQ	2 min in PBS under agitation	10 mL of H_2OmQ	Hot plate at 70°C
Strategy 4	10 mL of H_2OmQ	-	-	Hot plate at 70°C
Strategy 5	10 mL of H_2OmQ	5 min in PBS under agitation	10 mL of H_2OmQ	Hot plate at 70°C
Strategy 6	10 mL of H_2OmQ	10 mL of PBS	10 mL of H_2OmQ	Hot plate at 70°C
Strategy 7	KIT immersion upside down in H_2OmQ	-	-	Hot plate at 70°C
Strategy 8	KIT immersion upside down in H_2OmQ	15 min in PBS-T 0.05 % under agitation	KIT immersion upside down in H_2OmQ	Compressed air
Strategy 9	20 mL of H_2OmQ	10 min in PBS under agitation	20 mL of H_2OmQ	Compressed air

4.4.1.10. *Incubation time and specifity tests*

In order to determine the optimal incubation time of the NPs, they were incubated on KITs biofunctionalized with tau protein for 1 and 2 hours. In addition, to test their specificity after biofunctionalization, they were also incubated on BSA protein under the same conditions at a concentration of 1×10^7 NPs/µL.

In this way **it could be determined that the most optimal incubation time was 2 hours** (Figure 119) since the signal was much higher compared to incubation at 1 hour. In addition, the specificity of the signal was demonstrated since a great difference was observed at 2 hours of the signal on the tau protein compared to that obtained on BSA.

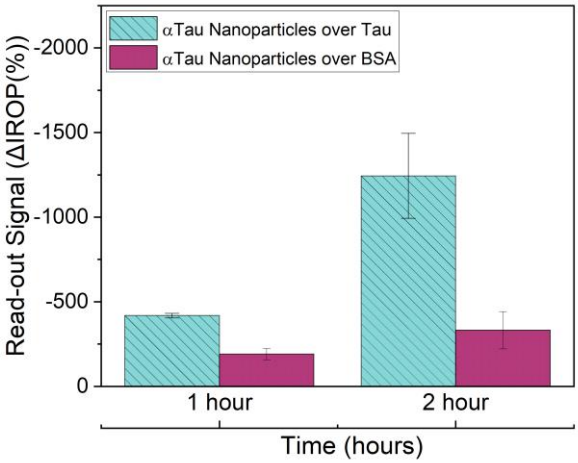

Figure 119. Incubation time test of NPs and their specificity (Murillo et al., 2023).

After the different tests, a protocol was established to biofunctionalize the NPs. This biofunctionalization was verified by DLS measurements, which confirmed each step of the biofunctionalization. The best concentration for the biosensor was tested, establishing the concentration of 1 x 10^7 NPs/µL. An incubation time of 2 hours at 37°C and washing strategy 9 were selected.

4.4.1.11. *Competitive assay for tau determination in PBS and serum*

The competitive assay was performed in PBS in order to determine the range of tau protein concentrations that we were able to determine. For this purpose, NPs at a concentration of 1 x 10^7 NPs/µL were incubated with different concentrations of tau protein (from 100 µg/mL to 0.01 µg/mL) and then deposited on the sensor surface previously coated with tau protein.

The lower the concentration of tau in the solution, more Abs will be free on the surface of the NPs, so they will bind more to the surface of the sensor, obtaining a higher signal, while as the concentration increases, fewer Abs will be free, resulting in a decrease in the signal. In this way we obtain a calibration curve of the tau concentration based on the ΔIROP (%) signal (Figure 120A).

Similarly, for the serum, the same experiment was performed, only in this case the **NPs were left incubating with the doped serum ON at 4°C due to the Vroman effect already mentioned**, since the low molecular weight proteins of the serum adhere on the surface of the NPs and with

time are displaced by those that have more specificity but less mobility (Monge Argilés et al., 2014). As a result, we obtain a calibration curve with similar values (Figure 120B). The data represented in the figure are the mean of the repeated experiments and the uncertainty is considered as the standard deviation.

However, if we compare both curves, we observe a difference in the signal (around 300 ΔIROP (%), as we cannot be sure that the serum is free of a basal tau concentration and that the matrix effect of the serum is not playing an important role in this difference.

Thus, **we are able to detect concentrations of 10 pg/mL in both matrices.** A table comparing the LoD of this system with others reported in the literature can be found **in Annex III.**

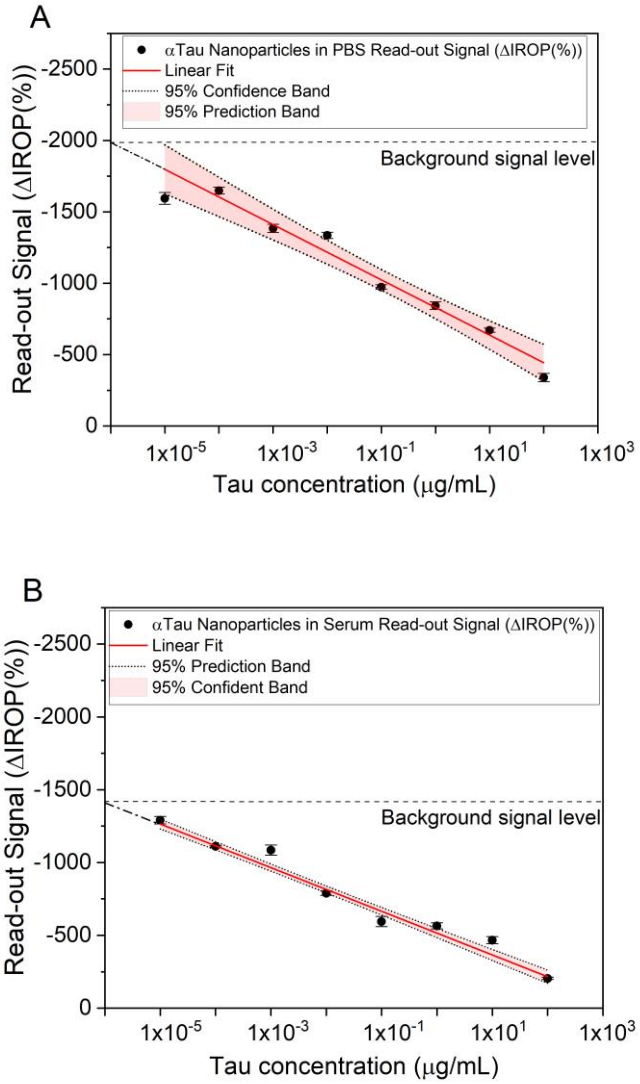

Figure 120. Competitive assay for total tau determination. A. Assay performed in PBS. **B.** Assay performed in serum (Murillo et al., 2023).

A competitive assay for the determination of tau protein in both PBS and serum was achieved, reaching a LoD of 10 pg/mL.

4.4.1.12. *Protein-Ab pair specificity test with the new αTau Ab*

Due to the decataloging of the Ab used during the first batches of experiments, the specificity of the new Ab against the protein we were using had to be checked. For this purpose, the same procedure was followed as with the previous Ab.

After performing the experiment, **it was observed that the new Ab was specific for tau** due to the difference in signal obtained on the surface coated with tau to that coated with BSA (Figure 121), although the signal of this Ab was somewhat lower in terms of ΔIROP (%) compared to the previous Ab we were using.

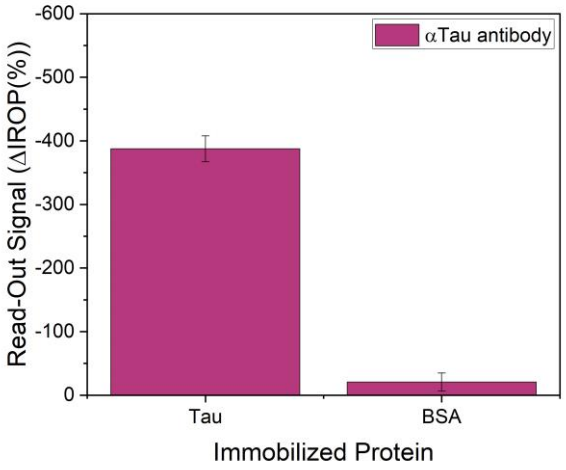

Figure 121. Specificity test of the new αTau Ab.

4.4.1.13. *Biofunctionalization of SiO_2 NPs with the new Ab*

During the process of biofunctionalization of the NPs with the new αTau Ab, **the protocol steps were corroborated by measuring the size and the PDI**. In addition, the concentration was also measured (Table 24).

Table 24. DLS measurements of concentration, size and PDI collected during the NPs biofunctionalization protocol.

	Initial	***G-Protein***	***αTau***
Size (nm)	84.64 ± 0.80	96.54 ± 7.34	142.10 ± 2.87
Concentration (NPs/µL)	3.55×10^{10}	7.10×10^{9}	8.32×10^{7}
PDI	0.10 ± 0.02	0.13 ± 0.03	0.18 ± 0.05

As shown in Figure 122 and Table 24, the NPs are increasing in diameter after each biofunctionalization step, **confirming the addition of the molecules on their surface**. However, in this case, the number of final NPs has greatly decreased during the process.

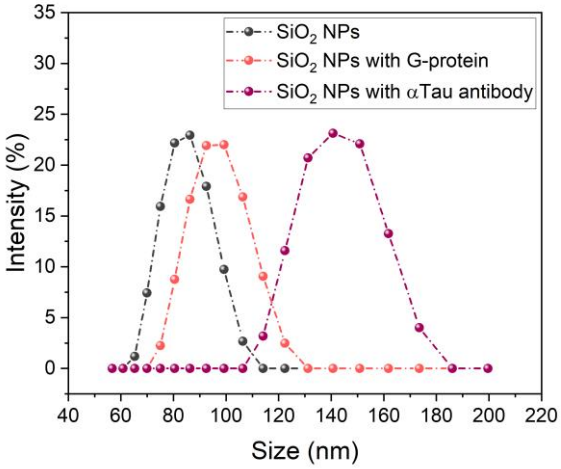

Figure 122. Measurements collected by DLS during the NPs biofunctionalization protocol.

4.4.1.14. *NPs concentration curves with the new Ab*

Similarly, after the biofunctionalization process, a concentration curve of NPs with the new αTau was performed. For this purpose, NPs were incubated on the KITs immobilized with the tau protein at different concentrations, starting from 1 x 10^7 NPs/µL and at 1:10, 1:100 and 1:1000 dilutions. They were also incubated at the highest concentration on BSA protein as a negative specificity control.

When performing the curve (Figure 123), we observed an increase in signal with concentration, although this signal is lower compared to the NPs biofunctionalized with the old Ab for the same concentration. Similarly, **the concentration of 1 x 10^7 NPs/µL continued to be selected** as the signal was still high enough.

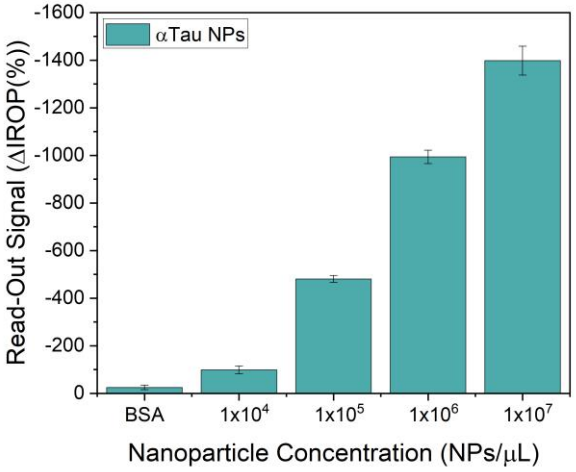

Figure 123. Concentration curve of biofunctionalized NPs with the new αTau Ab.

Following the replacement of the αTau Ab in use, all the same tests were performed with the new Ab to test specificity. In this way, the experiments could be continued.

4.4.1.15. *SEM images*

In the different tests of the biofunctionalization protocol of the NPs, **SEM images were taken to study the dispersion of the NPs on the cells**. As observed in the two images at the top of Figure 124, during the first trials and tests of the biofunctionalization protocol, **the NPs appear agglomerated on the surface and create multilayers**. However, if we look at the two images at the bottom, **we can see how the NPs are dispersed and covering the surface in the form of a monolayer**. This is thanks to the changes that were made to the protocol, such as the centrifugation temperature, which was changed from RT to 4°C, as well as the centrifuge speed, which was lowered to 7500 rpm. Finally, we also changed the concentrations of the reagents, such as EDC/NHS and G-protein (increasing their concentration in the incubations).

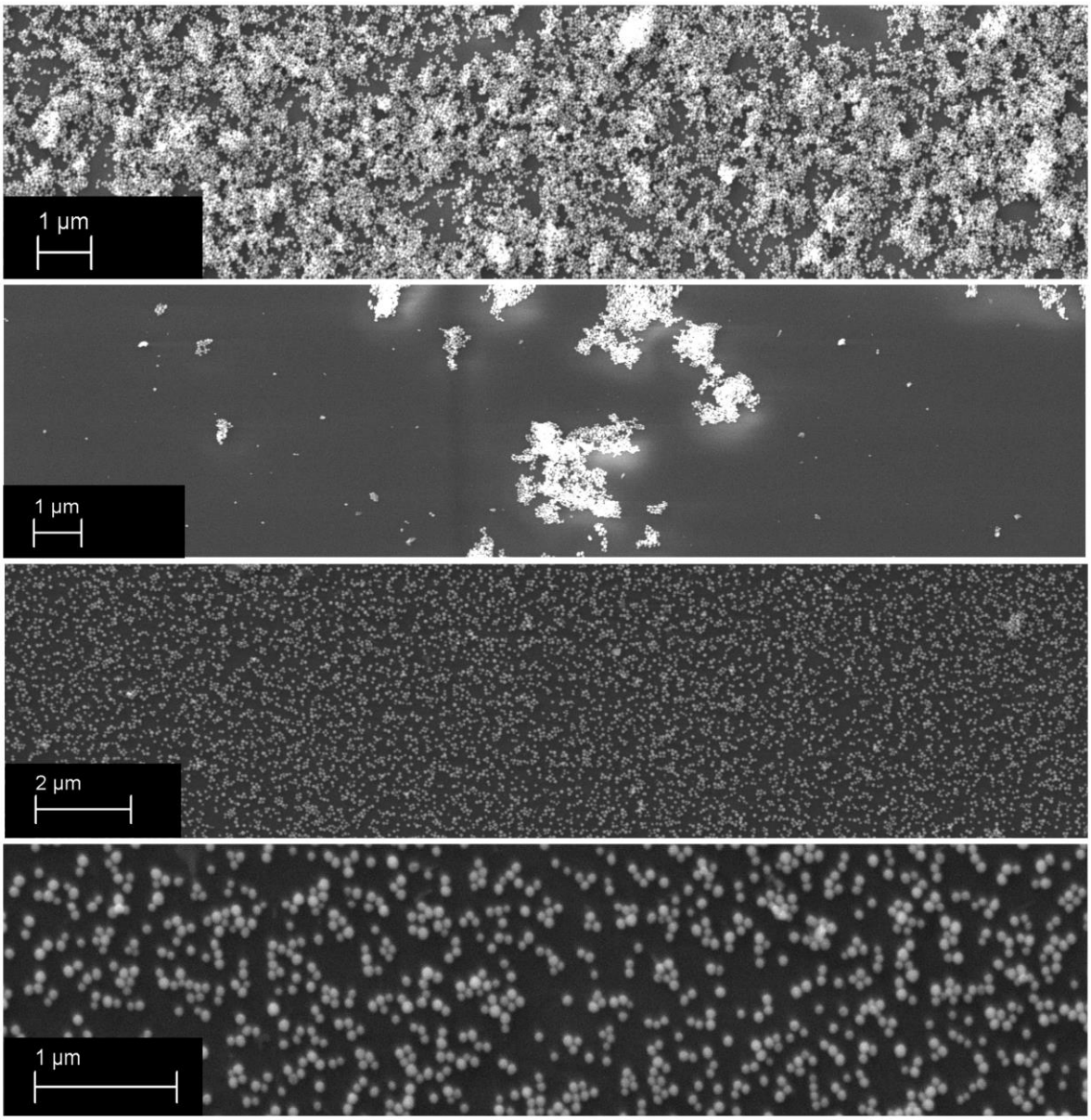

Figure 124. SEM images of the NPs on the sensor surface. In the first two images are the NPs from the first tests of the protocol. In the two lower images the NPs can be appreciated after the changes and improvements of the protocol.

In addition, it was possible to measure the size of the NPs by SEM as shown in Figure 125.

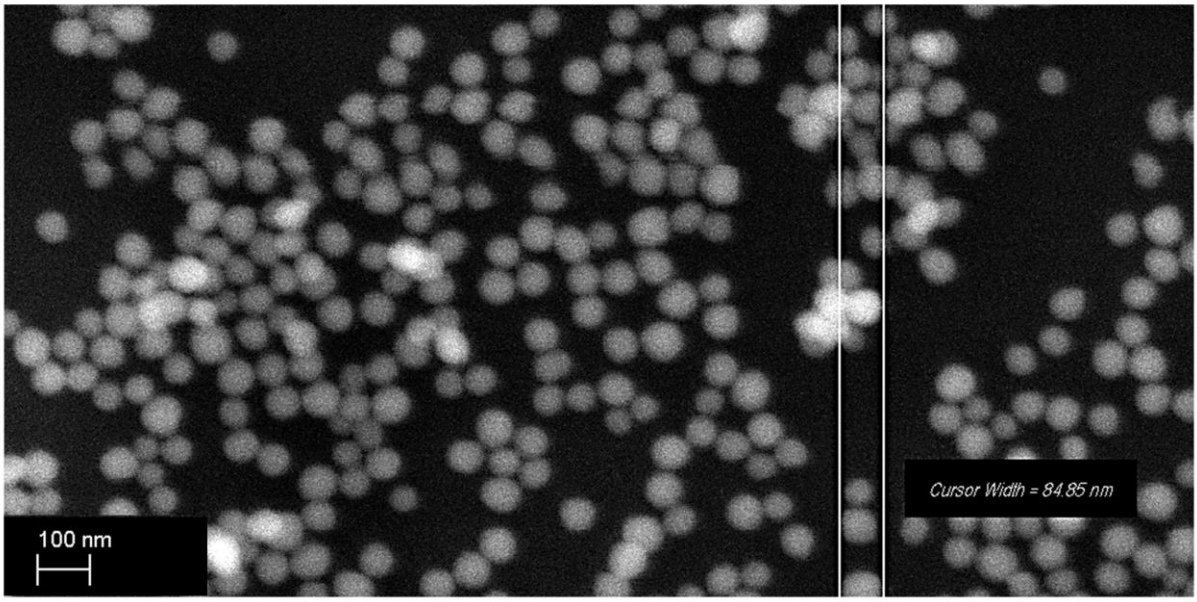

Figure 125. NPs size measurement with SEM.

Below in Figure 126 is a summary of images from different assays, where on the left is the KIT cell and on the right is a detail of the sensing surface on which the NPs are recognizing the immobilized protein.

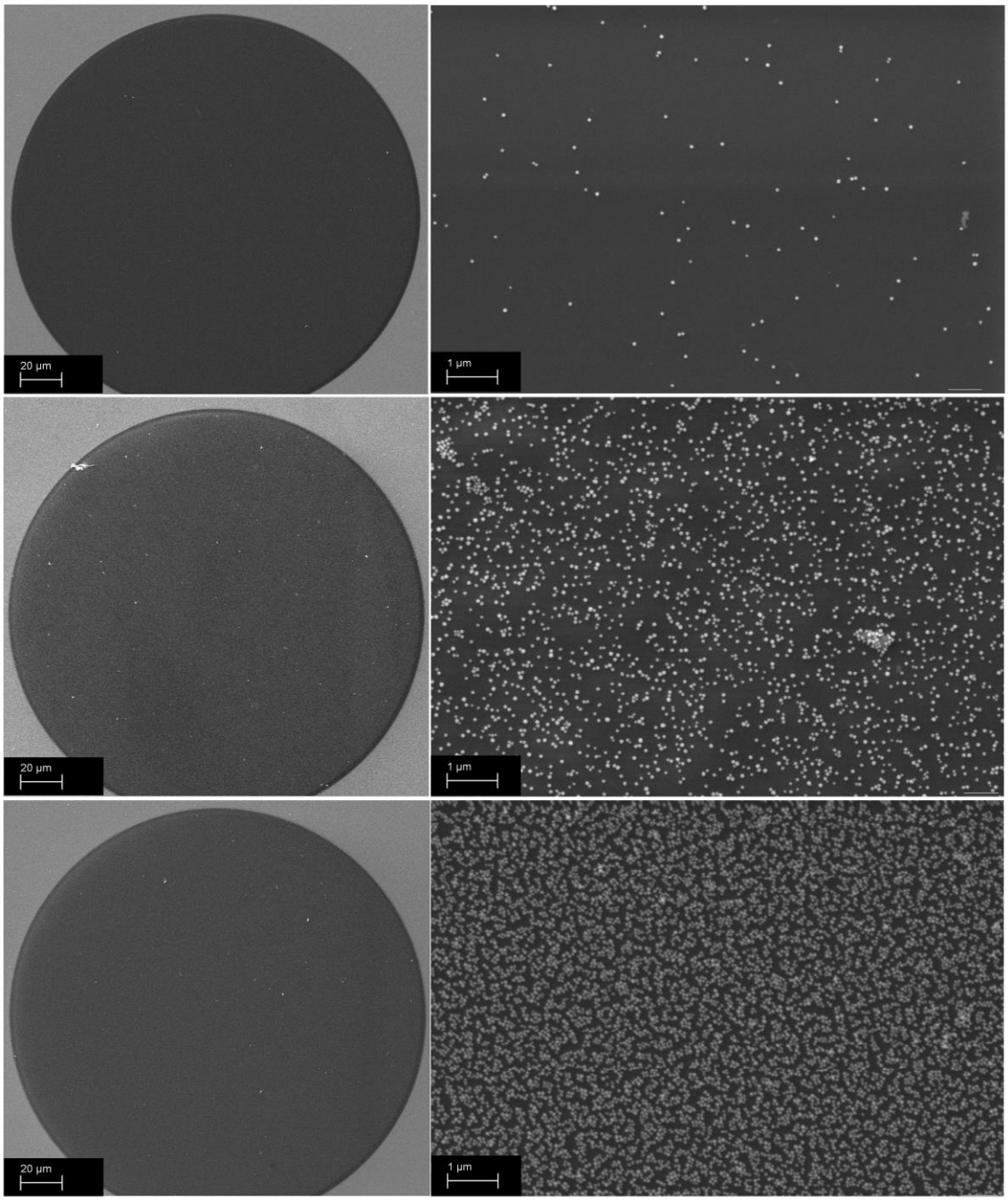

Figure 126. SEM images of the NPs recognizing on the sensor surface.

Finally, during the competitive assay, SEM images were taken of the NPs on the KIT after being incubated in PBS with different concentrations of tau protein.

On the one hand, images were taken of the **NPs that had been incubated with the highest concentration of tau protein (100 µg/mL)** (Figure 127A-B), which gave low ΔIROP (%) signal and as observed in the image **few NPs are found on the surface**. **By decreasing the concentration of tau protein (1 x 10^{-2} µg/mL) more NPs are observed on the surface** (Figure 127C-D), consistent with an increase in the signal.

Finally, **images were taken with the lowest amount of tau protein (1 x 10^{-5} µg/mL), in which the signal on the sensor is maximal and the surface is covered with NPs** (Figure 127E-F). In addition, these images help us to verify that the **NPs are not agglomerated and are dispersed and stable in the solution.**

Through SEM imaging, it was possible to ensure the size of the NPs, that they were not aggregated, and that recognition was occurring on the sensing surface.

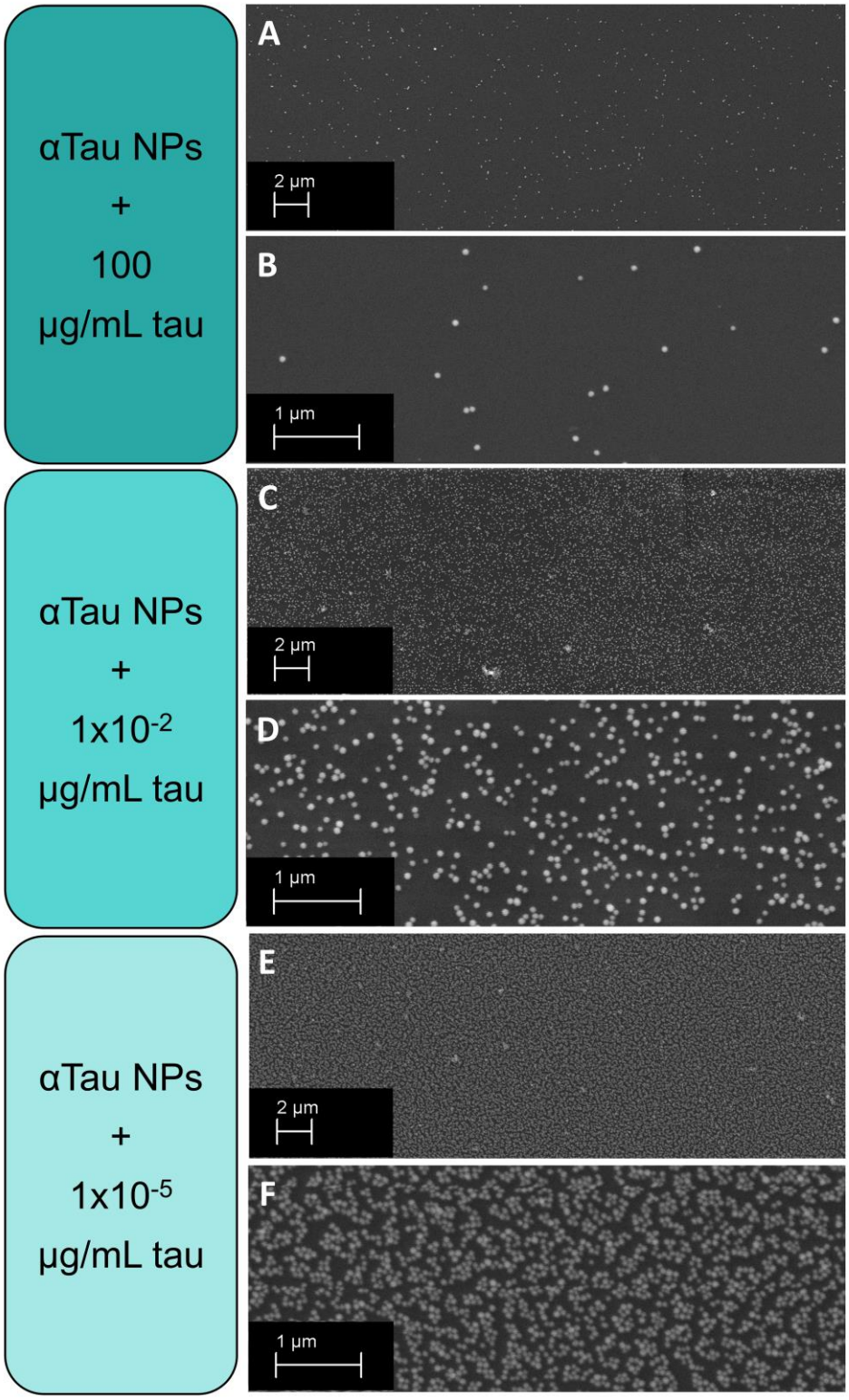

Figure 127. SEM images of the competitive assay for the determination of tau protein in PBS. A-B. NPs on the surface after being incubated with a high concentration of tau protein. **C-D.** NPs recognizing on the sensor surface after being incubated with a medium concentration of tau protein. **E-F.** Surface covered with NPs in the recognition stage after being incubated with a minimum concentration of tau protein (adapted from Murillo et al., 2023).

4.4.2. Case II. II. Triphosphorylated tau detection system

4.4.2.1. *Reagents validation using the ELISA technique*

To validate the performance of the reagents received by LyncBiotech, ELISAs were conducted to verify the recognition of the 3P-Tau peptide by the B6 Ab and the B6-biotin Ab. For this purpose, ELISA plates were immobilized with the 3P-Tau peptide at different concentrations ranging from 1µg/mL to 6.4 x 10^{-5} µg/mL in 1:5 dilutions. Recognition was carried out using the B6-biotin Ab at a 1:1000 dilution and the B6 Ab without biotin at a 1:2000 dilution, following the company's instructions.

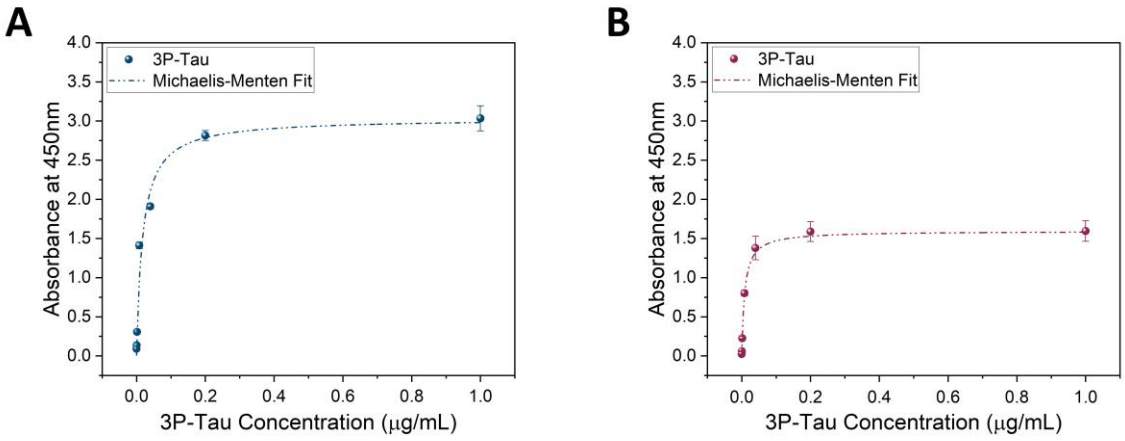

Figure 128. ELISAs for reagent validation. A. ELISA performed with the B6-biotin Ab for recognition. **B.** ELISA carried out using the B6 Ab without biotin.

In Figure 128A, the result of the ELISA performed with the B6-biotin Ab is depicted, and in Figure 128B, for the case of the B6 Ab without biotin, **we obtained a positive result for both Abs**. This confirmed that there was recognition by the Abs against the peptide. Furthermore, **no signal was obtained in the NC**, indicating that **the signal is specific** to the recognition and not background signal from the Ab.

4.4.2.2. *Immobilization of the 3P-Tau peptide and the B6 Ab on the sensor surface (dose-response curves)*

Once the reagents were validated, dose-response curves were generated to select the concentration and incubation time for immobilizing the peptide and the Ab. To do this, they were deposited on the sensor surface at different concentrations while varying the incubation conditions (3 hours at 37°C and ON at 4°C).

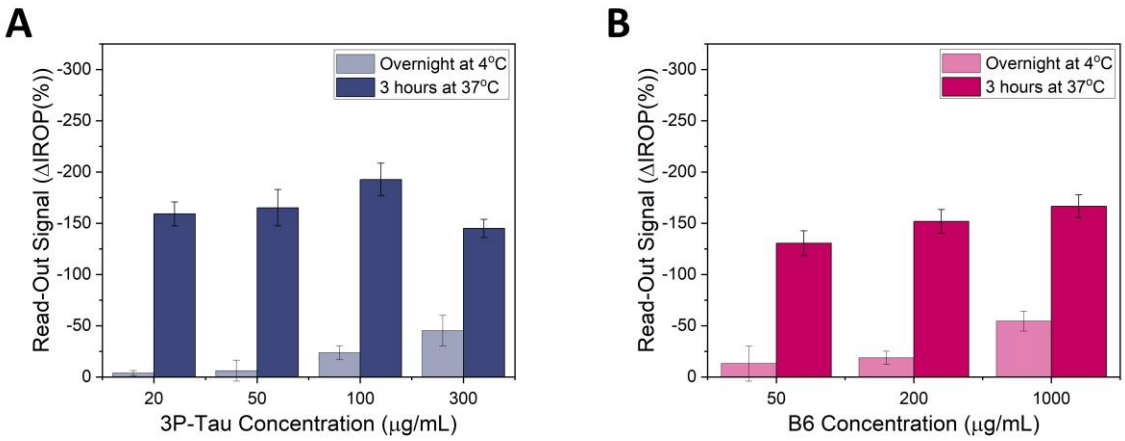

Figure 129. Dose-response curve of 3P-Tau peptide and B6 Ab. A. ΔIROP (%) signals of 3P-Tau peptide immobilization at different concentrations under two different incubation conditions (ON at 4°C and 3 hours at 37°C). **B.** ΔIROP (%) signals of B6 Ab immobilization at different concentrations under two different incubation conditions (ON at 4°C and 3 hours at 37°C).

As observed in Figure 129A, **for the 3P-Tau peptide, better immobilization signals were obtained when incubation was carried out at 37°C for 3 hours instead of ON at 4°C**. This signal increased as the concentration was increased. Therefore, **a concentration of 300 µg/mL was selected** to coat the entire surface of the KIT cell, with an incubation time of 3 hours at 37°C in a humid chamber. This concentration was determined because in repeated experiments it was observed that at 100 µg/mL or less concentration we did not always obtain the same signal, so incubation at 300 µg/mL was more consistent.

Similarly, the same trend was observed **for the B6 Ab** (Figure 129B), as higher signals were obtained with **incubation at 37°C for 3 hours**, and this signal also increased with higher concentrations. Consequently, a concentration of 1000 µg/mL was selected for the B6 Ab for subsequent experiments.

4.4.2.3. *Recognition assays on KITs*

Once the concentrations for immobilization were established, it was necessary to confirm recognition in the KITs and establish the assay conditions. To do this, on one hand, the KITs were immobilized with the peptide at different concentrations and recognized with the B6 Ab at two different concentrations and under two different conditions (3 hours at 37°C and ON at 4°C). On the other hand, other KITs were incubated with the B6 AB at different concentrations and then incubated with the peptide under different conditions (3 hours at 37°C and ON at 4°C).

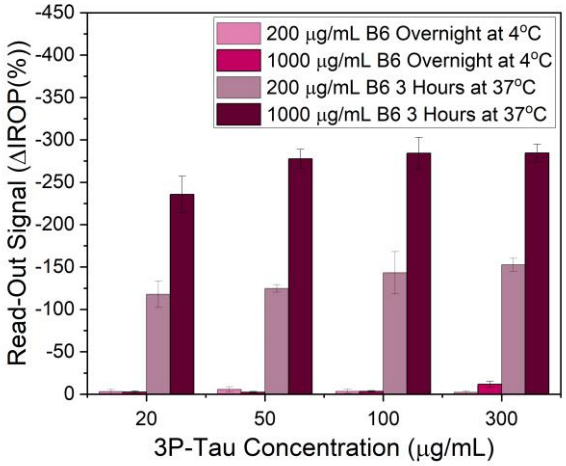

Figure 130. ΔIROP (%) signals of B6 Ab recognition on the 3P-Tau peptide surface.

As seen in Figure 130, regardless of the concentration of the immobilized peptide, **the best recognition occurs when incubation is carried out at 37°C for 3 hours**, and the **concentration of the Ab is 1000 µg/mL**. Therefore, these recognition conditions were established for the B6 Ab.

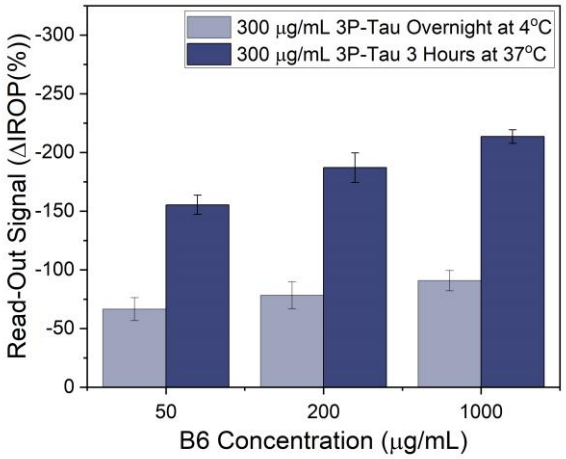

Figure 131. Recognition of the 3P-Tau peptide on the surface immobilized with the B6 Ab.

Conversely, when the Ab is immobilized at different concentrations on the sensor, it is observed that **the highest signal is obtained when the peptide is incubated at 300 µg/mL for 3 hours at 37°C** compared to ON incubation. Furthermore, it is evident that this signal increases with higher concentrations of immobilized Ab (Figure 131).

After verification of the correct functioning of the reagents received, a concentration of 300 µg/mL for peptide immobilization and 1000 µg/mL for Ab B6 was established at 37°C for 3 hours. For the recognition step, the same concentrations, time, and incubation temperature were determined.

4.4.2.4. *Blocking assays*

To determine the necessity of surface blocking and potentially save time by avoiding this incubation step, the same recognition assays were conducted, but in half of the KITs, the blocking phase with PVP was added for 1 hour at 37°C.

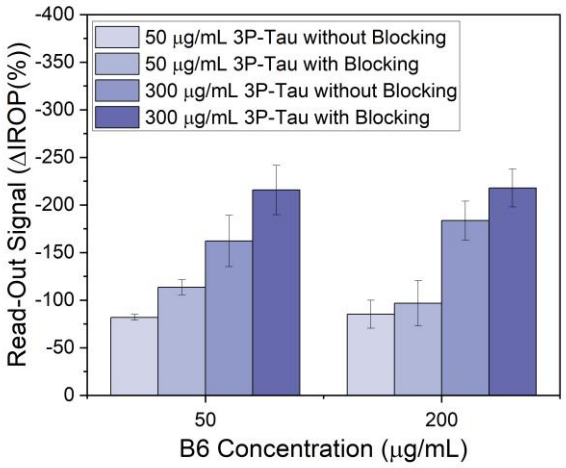

Figure 132. Recognition of the 3P-Tau peptide on the surface immobilized with the B6 Ab with and without blocking.

Comparing the signals obtained with and without blocking, it is evident that differences are observed for both concentrations of the 3P-Tau peptide and the two concentrations of immobilized Ab (Figure 132). In all cases, **the signal is higher when the surface is blocked**, which makes sense because in that case, all the peptide would be fully available to bind to the immobilized Ab rather than staying on the surface due to its small size.

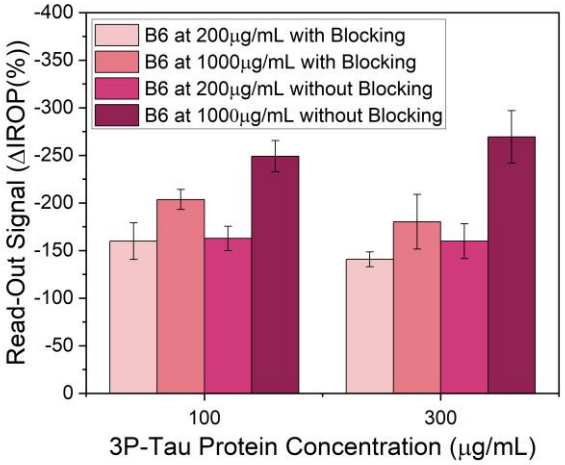

Figure 133. Recognition of the B6 Ab on the surface capped with 3P-Tau peptide with and without blocking.

In the case of Ab recognition on the surface coated with the peptide, when the Ab is incubated at a lower concentration, there are fewer differences between the blocked and unblocked surfaces for both concentrations of immobilized peptide. However, when the Ab concentration is increased to 1000 μg/mL, a significant difference in signal is observed, **which increases when the surface is unblocked**. This may be due to increased nonspecific binding on the sensor surface without blocking (Figure 133). Therefore, it is confirmed that for these experiments, the blocking step is necessary.

4.4.2.5. *Recognition assays on KITs biofunctionalized with STV*

To test for enhanced peptide recognition, KITs were immobilized with STV and then incubated with the B6-biotin Ab to recognize the 3P-Tau peptide. This experiment was carried out in parallel by blocking and not blocking the KITs after Ab incubation.

In this case, **we observed that there is no difference in peptide recognition between the two situations** (with and without blocking) (Figure 134). This may be because the surface is already fully upholstered with the STV and even if we then add the blocking, it does not improve the recognition. In addition, it was found that the peptide concentration at which the best recognition signal is obtained is at 300 μg/mL and that when it decreases to 100 μg/mL, there is a very drastic reduction in the signal.

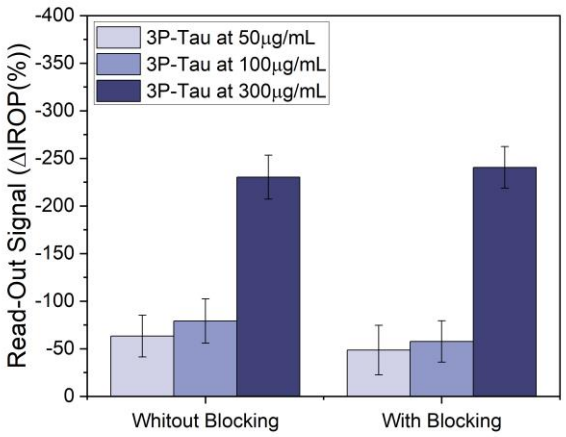

Figure 134. Recognition of the 3P-Tau peptide on the surface with STV. KITs immobilized with STV were incubated with the B6-biotin Ab and then part of them were blocked before incubating the 3P-Tau peptide at different concentrations.

After recognition tests with and without surface blocking, a blocking with PVP was established for 1 hour at 37°C. However, when the tests were performed by covering the entire surface with STV, it was observed that the blocking step could be eliminated.

4.4.2.6. *Recognition of the 3P-Tau peptide in different matrixes in BICELLs with and without STV*

In order to conduct competitive recognition assays for the peptide in real samples, it's necessary to determine if the peptide remains stable in different matrices that might be used for concentration determination. Recognition assays for the peptide were therefore performed in various matrices that were of interest for subsequent experiments, such as PBS, serum, and aCSF. These experiments were conducted both with and without coating the surface with STV to assess if sensitivity could be improved, and the surface was blocked or left unblocked as well.

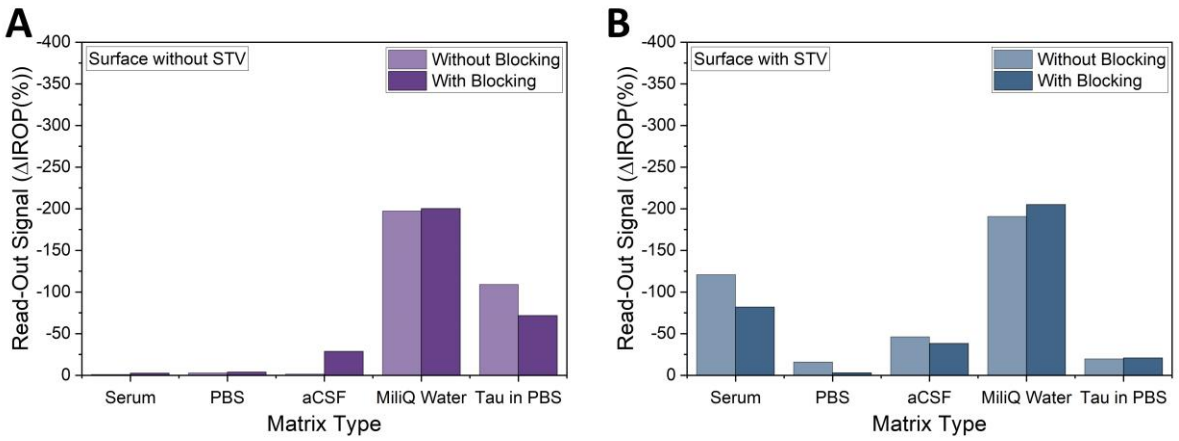

Figure 135. Assay of 3P-Tau peptide recognition in different matrices. A. Assay performed by immobilizing the B6 Ab on the surface and then the 3P-Tau peptide (blocking and non-blocking the surface). **B.** Assay carried out after immobilizing STV on the surface of the KIT and then the B6-biotin Ab to recognize the 3P-Tau peptide (blocking and not blocking the surface). The signal represented is the difference between the ΔIROP (%) signal of the undoped matrix on the Ab and the ΔIROP (%) signal of the doped matrix on the Ab.

In the case of recognition assays without STV (Figure 135A), no signal is obtained for serum and PBS matrices, regardless of surface blocking or not. There is also very low signal for aCSF when the surface is blocked, compared to the signals obtained in the PC with H_2OmQ. Additionally, there is some signal observed in the experiment control with tau protein.

On the other hand, **when the experiment was conducted with the surface coated with STV (Figure 135B), signals were obtained for serum and aCSF matrices, and minimal signal was observed for the peptide in PBS**. However, the signals are much lower than those obtained for the peptide in H_2OmQ. In this case, tau protein served as a NC since the αTau Ab was not biotinylated, so it did not bind to the STV-coated surface, and the signal observed is background noise.

Peptide recognition signals were achieved in serum and aCSF, although lower than having it in H_2OmQ, only when the surface is coated with STV.

4.4.2.7. *Specificity assays by ELISA and IODM*

First, to test the specificity of reagent recognition and that we would have cross-recognition with the unphosphorylated tau protein and BSA used as a NC, ELISAs were performed by immobilizing the three proteins and cross-recognizing the Abs.

The B6, the αTau, and the αBSA Abs were incubated on the ELISA surface covered with the 3P-Tau peptide. After development, it was observed that we only had absorbance values in those wells in which the 3P-Tau peptide had been immobilized and was being recognized with the B6

Ab (Figure 136A). Similarly, on the ELISA surface covered with tau protein, the three Abs were incubated, obtaining a signal only in those in which tau was being recognized by the αTau Ab (Figure 136B), confirming the specificity of both Abs.

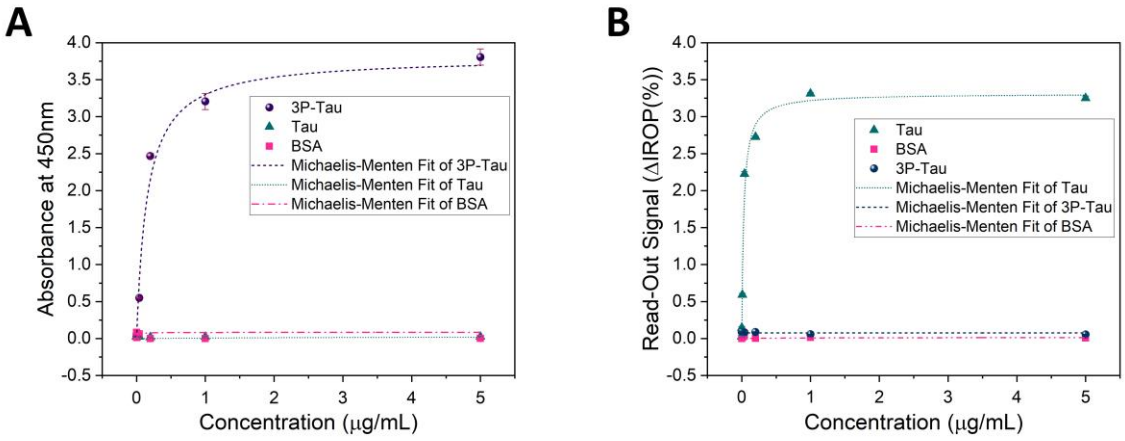

Figure 136. ELISAs of 3P-Tau peptide and tau protein to test specificity. A. 3P-Tau peptide recognition ELISA. **B.** ELISA for tau protein recognition. In both, Abs were cross-linked to test specificity, and a Michaelis-Menten adjustment was performed.

Due to some recognition issues and to ensure that in subsequent assays when measuring in real samples, **there was no cross-reactivity the unphosphorylated tau protein**, specificity tests were conducted by crossing the B6 and αTau Abs.

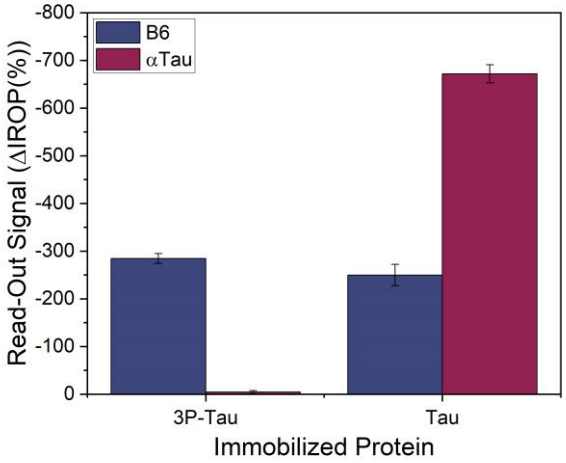

Figure 137. B6 and αTau Ab specificity test in KITs.

In this case, it was observed that the αTau Ab was very specific to unphosphorylated tau protein, while the B6 Ab recognized both the triphosphorylated peptide and the unphosphorylated form of the protein, **indicating cross-reactivity** (Figure 137).

To verify these results, specificity tests were repeated in 16-BICELLs KITs to check if there was an issue with the batch of PVC of the 65-BICELLs KITs, as there were suspicions of potential leaks. Additionally, in this case, a detection step was included to confirm the results.

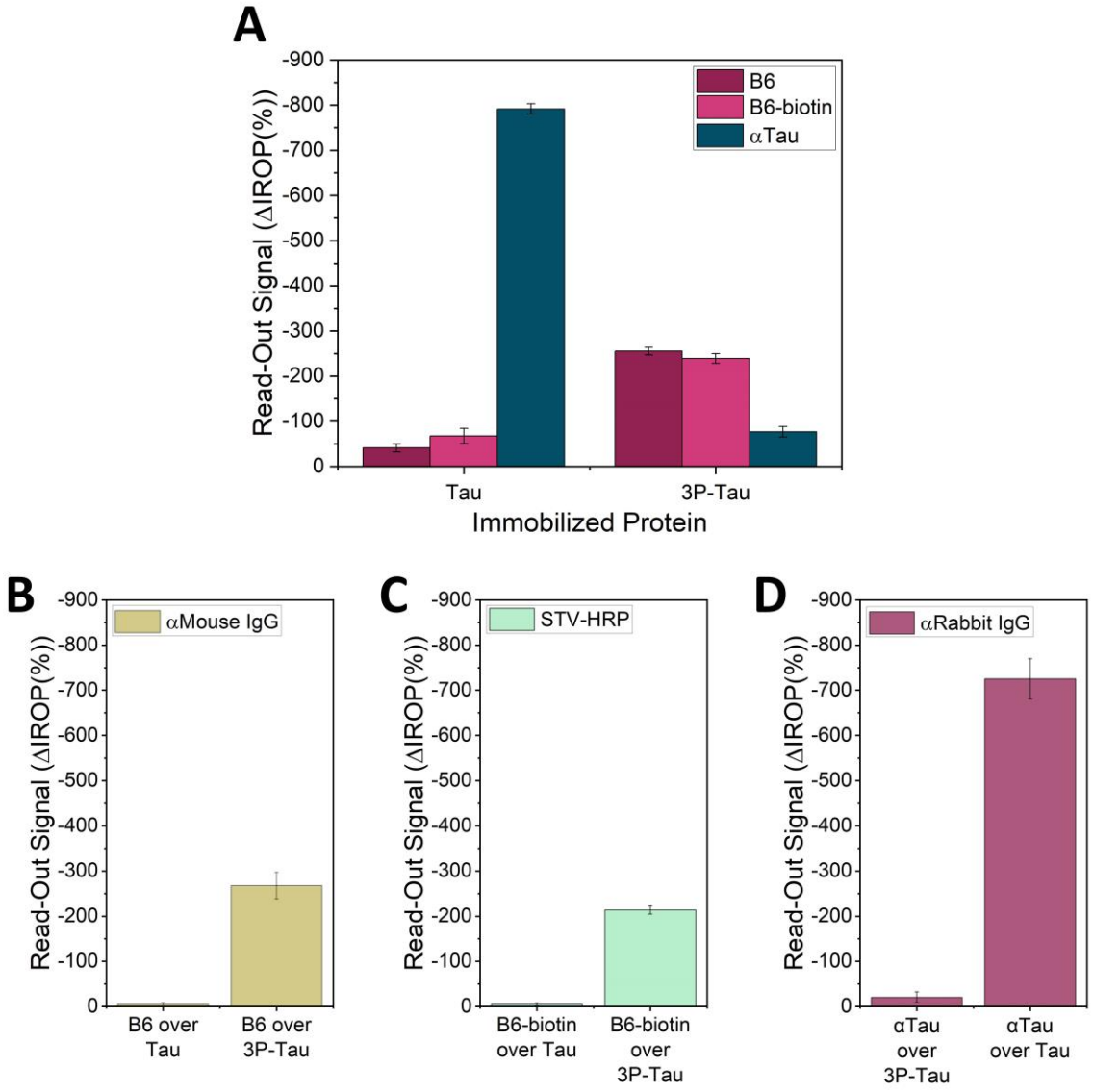

Figure 138. Specificity test for B6 and αTau Abs in KITs and revealed with secondary Abs. A. Recognition of surface immobilized 3P-Tau peptide and tau protein by B6, B6-biotin and αTau Abs. **B.** Revealing of cells incubated with B6 Ab with αMouse-IgG secondary Ab. **C.** Development of cells incubated with B6-biotin Ab with STV-HRP. **D.** Revealed cells incubated with αTau Ab with αRabbit-IgG secondary Ab.

After repeating the assays, in Figure 138A, it can be observed that the αTau Ab behaved in the same way as before. However, **the B6 and B6-biotin Abs in these experiments exhibited specific recognition, showing a difference in signal between the two proteins**. To confirm this result, the cells incubated with the B6 Ab were subsequently detected with the αMouse-IgG Ab (Figure 138B), confirming the presence of the Ab only in the cells where the triphosphorylated peptide had been immobilized. Similarly, in the cells where the B6-biotin Ab was deposited, they were detected with STV-HRP, and signal was only obtained in the cells where recognition was

specific (Figure 138C). Lastly, the αTau Ab was detected with an αRabbit-IgG Ab, demonstrating specificity (Figure 138D). **This confirmed that the PVC used in the previous assays was not in good condition and that the B6 Ab recognition is specific to the phosphorylations of the peptide.**

Due to cross-recognition problems in the KITs, different assays were performed to test specificity, and it was determined that it was a problem with the PVC being used.

4.4.2.8. *Biofunctionalization of SiO_2 NPs with the B6 Ab*

To achieve the necessary sensitivity for detecting the 3P-Tau peptide at very low concentrations in different matrices, NPs are used to capture the peptide from the sample of interest, followed by a competitive assay. Therefore, the biofunctionalization step of the NPs with the specific B6 Ab is crucial. To ensure the process is proceeding correctly, the protocol is followed meticulously, and at each step of the biofunctionalization process, the concentration and D_h of the NPs are measured.

In each step of the protocol, after washing, 1 µL was taken and diluted to 10 µL, and from these 10 µL, one was taken and diluted to 1 mL (the necessary amount for measurements using DLS). This careful approach helps ensure the accuracy and success of the biofunctionalization process.

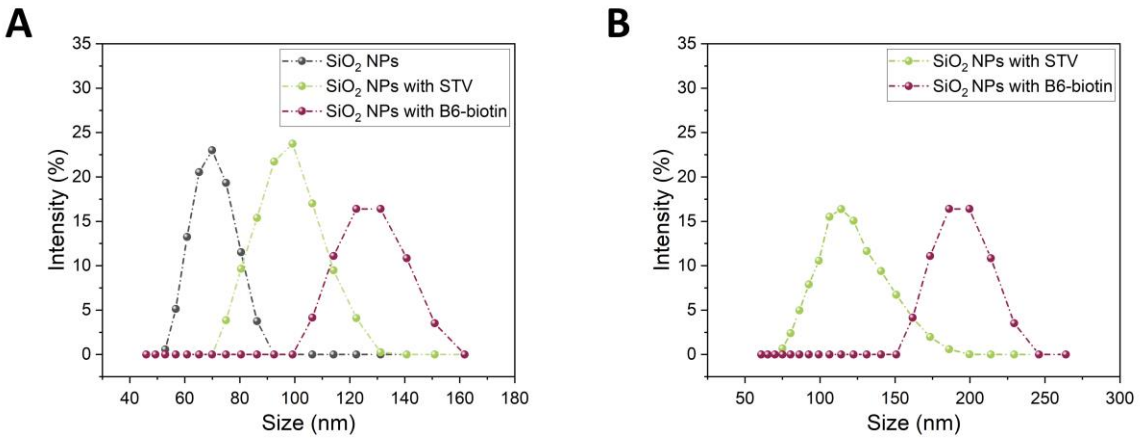

Figure 139. Size measurements obtained with DLS of the NPs in the biofunctionalization process. A. DLS measurements of silanized NPs to which STV and B6-biotin Ab were added. **B.** Measurements of the DLS of commercial NPs with STV that were biofunctionalized with the B6-biotin Ab.

Through the biofunctionalization protocol, **there is an increase in the D_h for the NPs in the case of those that have been biofunctionalized using the silanization protocol** (Figure 139A) **and similarly for the commercial NPs** (Figure 139B). For the silanized SiO_2 NPs, the diameter increased at each step of the protocol, both when STV was added and when they were incubated with the Ab (Table 25). For the commercial NPs, there is only one step in the protocol with the addition of the Ab, as they already contain STV. All these changes in the D_h are reflected in Table 26.

Table 25. DLS measurements of size, concentration and PDI during the silanization-based biofunctionalization protocol.

	Initial	*STV*	*B6-biotin*
Size (nm)	69.95 ± 5.58	97.67 ± 3.08	131.20 ± 2.63
Concentration (NPs/µL)	4.35 x 10^{11}	2.31 x 10^{10}	2.45 x 10^{8}
PDI	0.15 ± 0.03	0.17 ± 0.05	0.21 ± 0.3

Table 26. DLS measurements of size, concentration and PDI during biofunctionalization protocol with commercial NPs.

	Initial	*B6-biotin*
Size (nm)	119.19 ± 1.82	193.34 ± 3.67
Concentration (NPs/µL)	8.06 x 10^{10}	6.31 x 10^{8}
PDI	0.20 ± 0.04	0.21 ± 0.03

In both cases we observe that the size of the NPs increases after the incubation steps, so the surface area of the NP is changing and that it is a homogeneous population as indicated by the value of the PDI. Similarly, in both cases we see a very large decrease in the concentration of NPs as the incubation steps in the protocol pass.

4.4.2.9. *Concentration curve of α3P-Tau SiO_2 NPs*

Once the biofunctionalization protocol was completed, and the entire process was monitored, it was necessary to verify if the NPs could recognize the 3P-Tau peptide immobilized on the surface of the KITs. To do this, the KITs were immobilized with the peptide, and the NPs were incubated in 1:10 dilutions starting from concentration 1 x 10^{8} NPs/µL. Depending on the signal of ΔIROP (%) obtained, the initial starting concentration for subsequent experiments could also be selected.

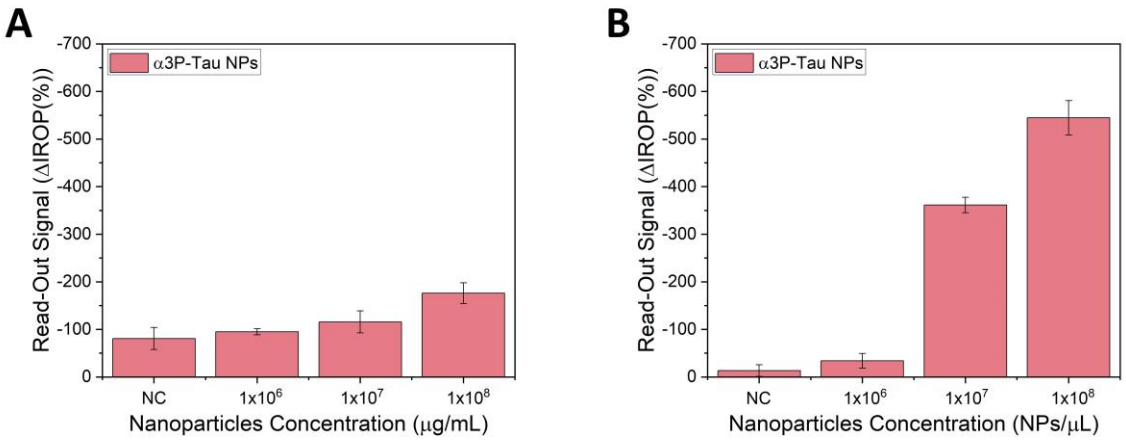

Figure 140. NPs concentration curve. A. Curve of the NPs silanized and modified with STV. **B.** Concentration curve of commercial STV NPs.

In the recognition stage on the KITs, both types of NPs used in the biofunctionalization process were employed. On one hand, the **NPs biofunctionalized using the silanization protocol did not yield good results** (Figure 140A) as the signals were very low compared to what was expected. On the other hand, **the commercial NPs** (Figure 140B) **provided better results** with higher signals, but they were still lower than expected for that concentration.

For the first type of NPs, the low performance could be due to an attempt to replicate the silanization protocol for G-protein with STV. Considering the results, **the protocol may need optimization and testing for this new application.**

For the commercial NPs, it could be that they require a higher concentration of Ab to achieve complete biofunctionalization of the surface. Additionally, it's important to consider that the affinity and specificity of Abs can vary, so increasing the incubation time of the NPs on the sensor could also be explored.

Further experimentation and optimization may be necessary to improve the recognition efficiency of the NPs in this context.

The NPs were biofunctionalized with Ab B6 although the expected signals were not achieved when performing the concentration curve on the peptide-covered surface. Although better signals were obtained with the commercial NPs.

4.4.2.10. *Immobilization and recognition assays at different pH levels*

In subsequent experiments, we encountered issues with peptide immobilization and recognition. To address this problem, tests for immobilization and recognition were carried out at different pH levels.

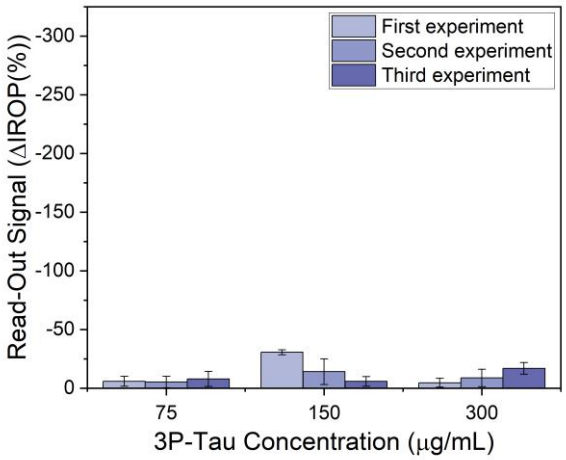

Figure 141. Repeated 3P-Tau peptide dose-response curves.

Firstly, the immobilization assays were repeated multiple times, and in Figure 141, it can be seen that in none of these repetitions, regardless of the concentration, **immobilization values were obtained that matched expectations or were consistent with previous assays**.

Therefore, attempts were made to perform immobilizations in various buffer solutions, including PBS-HCl (pH 4.5), carbonate buffer (pH 9.6), PBS (pH 7.4), MES (pH 3.5), and H_2OmQ as a PC for comparison of values.

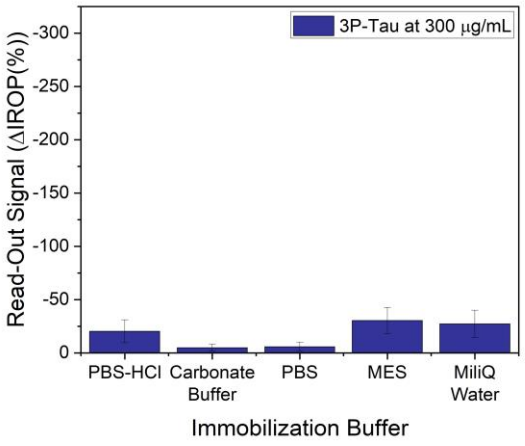

Figure 142. 3P-Tau peptide immobilization at different pH on KITs.

After reading the ΔIROP (%) signals, the same problem persisted. **Regardless of the buffer used, the signals were too low** and did not align with the initial results. **Similarly, the PC in H_2OmQ did not yield the expected signal** (Figure 142).

In this case, the immobilization of the tau protein was carried out as a PC for the experiment, and its values were within the standardized range for this protein, confirming that the KITs and the entire incubation process, along with O_2 plasma activation, were carried out correctly.

For recognition, the STV system was used to enhance sensitivity. The B6-biotin Ab was incubated on the STV-coated surface, followed by the peptide deposition in the different buffers, all at the same pH except for PBS-HCl.

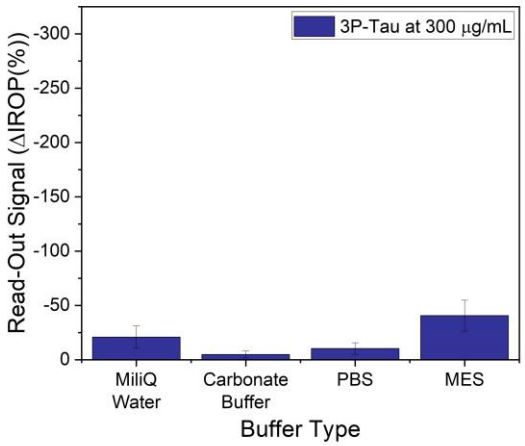

Figure 143. Recognition of 3P-Tau peptide at different pHs in KITs coated with STV and incubated with B6-biotin Ab.

Similarly, none of the buffers tested in the assay yielded acceptable values for recognition (Figure 143). Although there was a slightly higher signal with the MES buffer in this case, it still did not compare to the results obtained in the initial experiments.

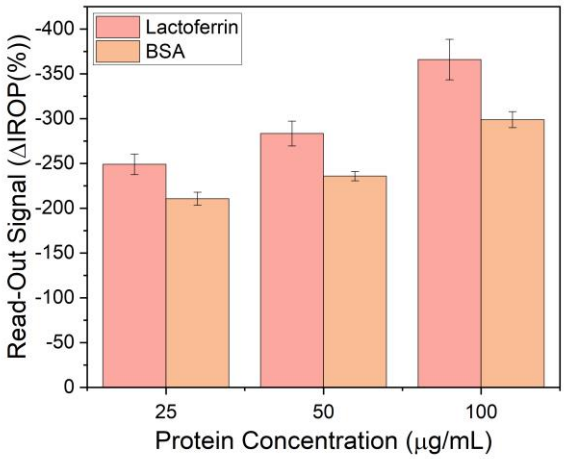

Figure 144. Recognition of lactoferrin and BSA proteins in KITs coated with STV and incubated with αBSA y αLactoferrin Ab.

In this case, as a PC, two biotinylated Abs, αLactoferrin and αBSA, were incubated, followed by their specific proteins, and the obtained signals were as expected and appropriate (Figure 144). Therefore, in these experiments, the KITs used and the incubation and washing processes throughout the procedure were correct. This led to the assumption that the issue was likely related to the peptide.

Upon receipt of the new peptide synthesis, problems with immobilization and recognition were encountered, so the peptide was tested in solutions with different pHs. After many attempts, it was not possible to achieve the values previously obtained, so no further progress could be made.

4.4.3. Case II. III. Detection of pTau181 in the Syrian hamster model

4.4.3.1. *Hamster and mouse models*

16 serum samples were extracted from 16 hamsters (5 controls, 5 arousal and 6 torpor). In addition, 4 serum samples from human tau protein-producing transgenic mice were used as PCs (Figure 145).

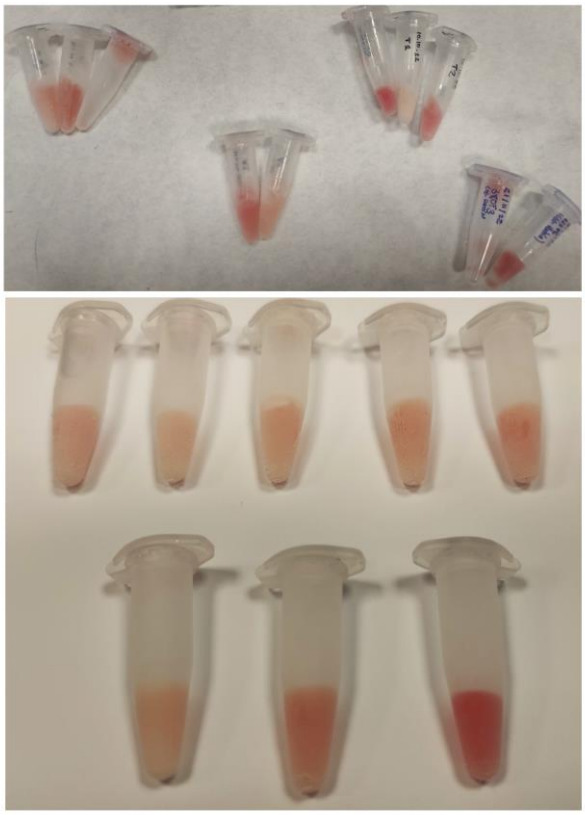

Figure 145. Samples used for the competitive assay for the determination of pTau181 protein.

4.4.3.2. *Biofunctionalization of αpTau181 SiO_2 NPs*

80 nm SiO_2 NPs were biofunctionalized with the αpTau181 Ab using the silanization protocol and G-protein. During this process, each step was verified by DLS to measure the concentration and size of the NPs.

Table 27 shows the size of the NPs and how it increases as we progress in the biofunctionalization protocol (Figure 146). We also have the concentration of the NPs after each step and what is the final working concentration of the NPs once they are biofunctionalized.

Table 27. NPs concentrations, size and PDI during the biofunctionalization process.

	Initial	*G-Protein*	*αpTau181*
Size (nm)	78.81 ± 3.35	101.30 ± 4.50	141.60 ± 2.88
Concentration (NPs/µL)	4.33×10^{10}	2.16×10^{10}	5.42×10^{9}
PDI	0.15 ± 0.06	0.11 ± 0.08	0.15 ± 0.04

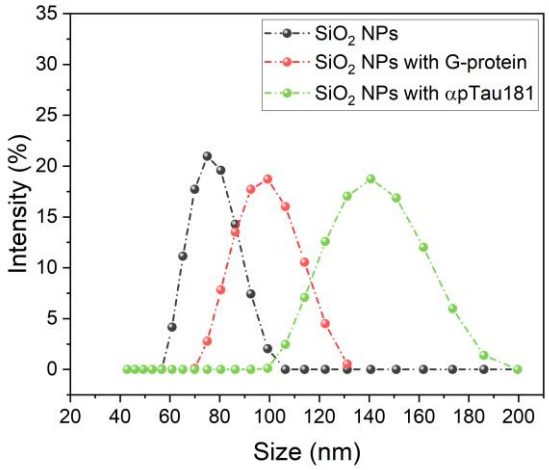

Figure 146. DLS measurements of the hydrodynamic diameter of the NPs during the biofunctionalization protocol.

4.4.3.3. *αpTau181 NPs concentration curve*

Following the biofunctionalization protocol, the NPs were incubated on the biofunctionalized KITs with pTau181 protein and BSA at the concentration of 5.42×10^{9} and at 1:10 and 1:100 dilutions (1.5 µL/cell).

After incubation, the KITs were washed and the ΔIROP (%) signals were read (Figure 147), obtaining a curve in which the signal decreases as the concentration of NPs decreases. In addition, **it is observed that they have specificity on the surface covered with pTau181 protein** since a very low background signal is obtained on the BSA protein.

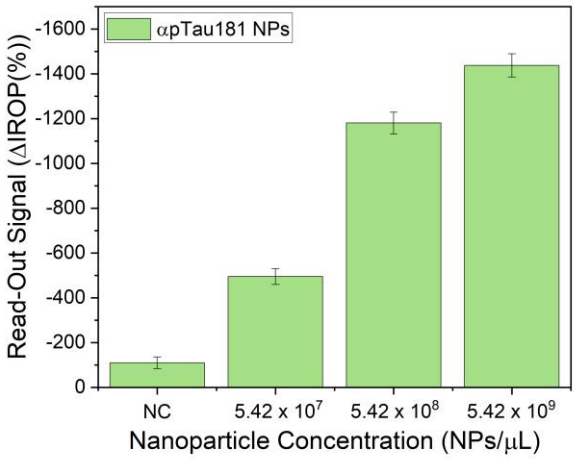

Figure 147. Concentration curve of NPs biofunctionalized with αpTau181.

The NPs were successfully biofunctionalized with the αpTau181 Ab, confirmed by DLS measurements. Subsequently, their specificity was tested, and the concentration of use was set at 1 x 10^9 NPs/µL.

4.4.3.4. *Competitive assay on hamster serum samples*

After testing the functionality of the NPs, the competitive assay was performed. For this purpose, the **NPs were incubated at a concentration of 1 x 10^9 NPs/µL with different concentrations of pTau181 protein (from 100 µg/mL to 0.00001 µg/mL in 1:10 dilutions)** and left at a final concentration of 1 x 10^8 NPs/µL. After the incubation time, they were applied to the sensor surface coated with pTau181 and left to incubate for the calibration curve.

At the same time, **hamster serum samples at 1:10 dilution were incubated with the NPs at a final concentration of 1 x 10^8 NPs/µL** and the same procedure as for the calibration curve was followed. Sera from transgenic mice were incubated with the NPs as a PC.

Once the ΔIROP (%) signals of the NPs were read, the calibration curve was obtained (Figure 148), in which the signals obtained from the samples were extrapolated to determine the concentration of pTau181 protein in the sera of hamster (Table 28) and transgenic mice (Table 29).

Considering the results, **we can see that there are differences between the control samples, having levels between 3-16 µg/mL with the samples obtained from torpor hamsters that have a concentration of pTau181 between 35-100 µg/mL**. On the other hand, the arousal hamsters have concentrations similar to the controls, which would make sense since when they stop hibernating, they would start the tau protein dephosphorylation machinery that they have active during hibernation.

On the other hand, the PCs of the transgenic mice also present high concentrations of pTau181 protein (140-200 µg/mL). This would correspond to what is expected, since this type of mouse is a model of tauopathies with a 5-fold increased expression of human tau protein.

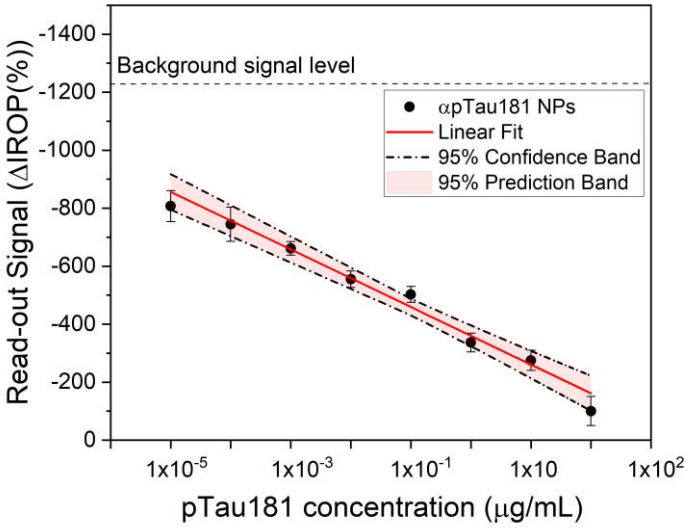

Figure 148. Calibration curve of the competitive assay to determine pTau181.

Table 28. Data of p181Tau protein concentration in hamster sera once extrapolated on the calibration curve.

Serum sample	*Concentration (µg/mL)*	*Serum sample*	*Concentration (µg/mL)*
Control 1	8.65	***Arousal 4***	8.22
Control 2	16.45	***Arousal 5***	7.03
Control 3	11.28	***Torpor 1***	41.00
Control 4	5.70	***Torpor 2***	102.78
Control 5	3.08	***Torpor 3***	34.75
Arousal 1	2.19	***Torpor 4***	44.68
Arousal 2	1.24	***Torpor 5***	50.51
Arousal 3	1.91	***Torpor 6***	80.56

Table 29. Data of p181Tau protein concentration in transgenic mice sera once extrapolated on the calibration curve.

Serum sample	*Concentration (µg/mL)*	*Serum sample*	*Concentration (µg/mL)*
Transgenic mouse 1	137.79	***Transgenic mouse 3***	148.38
Transgenic mouse 2	214.20	***Transgenic mouse 4***	143.42

Figure 149 shows the box plot obtained after performing the One-Way ANOVA statistical analysis with a Tukey's comparison of means and a Levene's test of homogeneity of variance with a significance level of $p<0.01$. As shown, there are significant differences in the concentration of pTau181 protein between control and torpor hamsters, as well as between torpor and arousal hamsters.

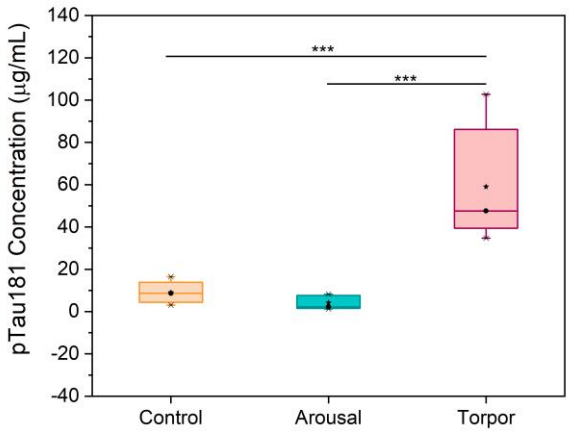

Figure 149. Comparison of pTau181 protein concentration in control, torpor, and arousal hamsters. ***p<0.01. In the graph the median is represented by "▪" and the mean by "*".

We were able to perform a competitive assay on serum samples from mice and hamsters and were able to determine concentrations between 1 to 214 µg/mL of pTau181 protein and significant differences were obtained between torpor and control hamsters and between torpor and arousal hamsters.

4.4.4. Case II. IV. Lactoferrin detection system in saliva samples

4.4.4.1. *Human saliva samples*

The concentration of lactoferrin protein was measured in **9 saliva samples from relatives of patients diagnosed with AD and relatives with no history of the disease**. The samples were centrifuged for 10 min at 15000 rpm and did not undergo any pretreatment prior to the assay.

4.4.4.2. *Biofunctionalization of αLactoferrin SiO_2 NPs*

First, three different protocols for biofunctionalization of the NPs were carried out. On the one hand, 80 nm SiO_2 NPs were silanized and G-protein was added to anchor the αLactoferrin Ab. After each biofunctionalization step, NPs concentration and NPs size were measured (Table 30). In this case, **it was seen that at each step, the size of the NPs was increasing, confirming the biofunctionalization** process (Figure 150). However, the concentration of the NPs is getting smaller and smaller due to the multitude of steps and washes.

Table 30. Size, concentration and PDI of NPs in each biofunctionalization step with G-protein.

	Initial	***G-Protein***	***αLactoferrin***
Size (nm)	74.06 ± 6.23	97.96 ± 2.75	146.4 ± 2.67
Concentration (NPs/µL)	6.70 x 10^{10}	3.92 x 10^{10}	2.57 x 10^{7}
PDI	0.19 ± 0.04	0.22 ± 0.03	0.25 ± 0.03

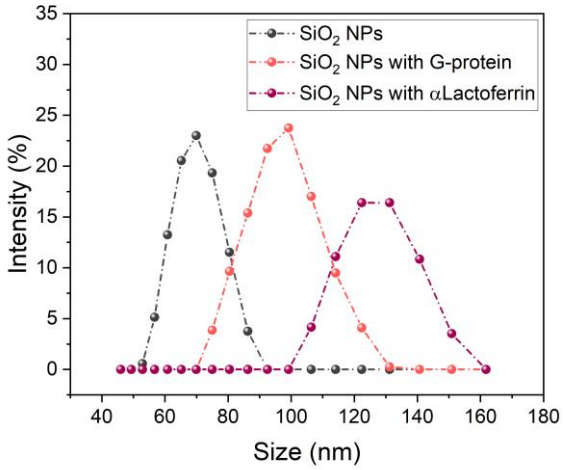

Figure 150. DLS measurements obtained during the biofunctionalization process of the nanoparticles.

On the other hand, these same NPs were silanized to biofunctionalized them with the STV protein and anchor the αLactoferrin-biotin Ab. The concentration and D_h were also measured. As shown in Table 31, **the NPs undergo a larger increase in size when STV is added than when G-protein is added, due to the fact that STV has a higher molecular weight**. Finally, we also see this increase in size when the Ab is added (Figure 151). With the concentration of NPs, we have the same disadvantage, since the concentration at each step is lower.

Table 31. Size, concentration and PDI of NPs in each biofunctionalization step with STV.

	Initial	***STV***	***αLactoferrin-biotin***
Size (nm)	76.42 ± 4.92	108.80 ± 11.85	161.8 ± 6.58
Concentration (NPs/µL)	4.87×10^{10}	3.97×10^{10}	6.57×10^{7}
PDI	0.21 ± 0.04	0.23 ± 0.03	0.22 ± 0.05

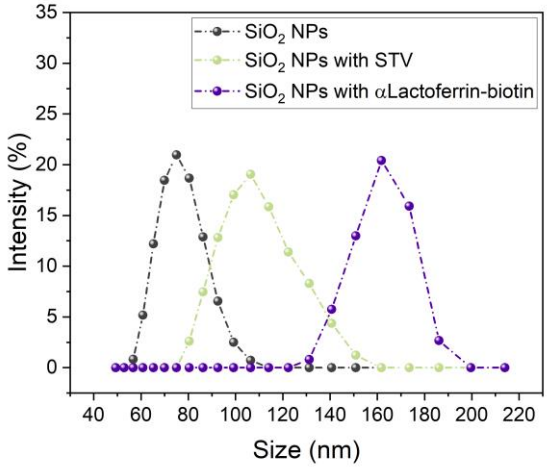

Figure 151. Measurements taken by DLS during the biofunctionalization process of NPs with STV and αLactoferrin-biotin Ab.

Finally, 100 nm SiO_2 commercial NPs already biofunctionalized with the STV protein were used to anchor the αLactoferrin-biotin Ab directly. These NPs were measured only before addition of the Ab and after incubation of the Ab to know the concentration and size after the single step of the protocol (Table 32). **In this case, the increase in the diameter of the NPs was also observed when the Ab was added** and in the case of the concentration, since there was only one washing step after adding the Ab (Figure 152), **the final concentration of NPs is much higher than in the two previous cases** (Tables 30 and 31).

Table 32. Size, concentration and PDI of commercial NPs in each biofunctionalization step.

	Initial	*αLactoferrin-biotin*
Size (nm)	119.10 ± 1.812	171.8 ± 2.36
Concentration (NPs/µL)	8.06 x 10^{10}	3.57 x 10^{9}
PDI	0.22 ± 0.02	0.17 ± 0.05

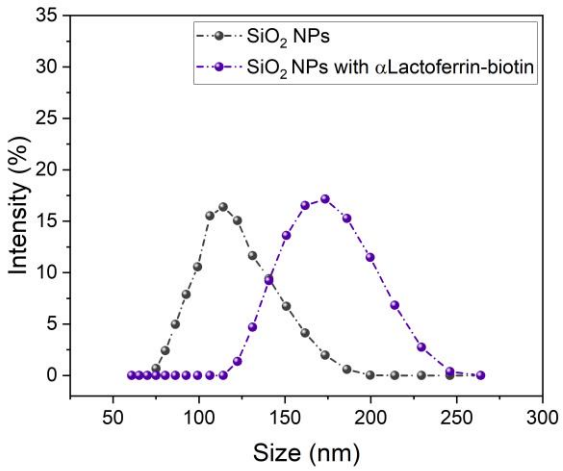

Figure 152. Measurements acquired by DLS of the biofunctionalization process of commercial-STV NPs.

4.4.4.3. *αLactoferrin NPs concentration curves*

To know the concentration of the NPs necessary to obtain the maximum signal in the KITs, after the DLS measurements, the biofunctionalized NPs were incubated at different concentrations on the KITs coated with lactoferrin and BSA proteins.

On the one hand, 80nm SiO_2 NPs silanized and biofunctionalized with G-protein and αlactoferrin were incubated at the concentration of 2.57 x 10^{7} NPs/µL (1.5 µL/cell) on lactoferrin and tau proteins. In addition, 1:10 and 1:100 dilution were also incubated on lactoferrin coated surface (Figure 153). For the NPs that were biofunctionalized with STV and the αlactoferrin-biotin Ab, the same procedure was carried out, but starting from a NPs concentration of 6.57 x 10^{7} NPs/µL (Figure 154). As for the commercial NPs, we started from a concentration of 3.57 x 10^{9} NPs/µL (Figure 155).

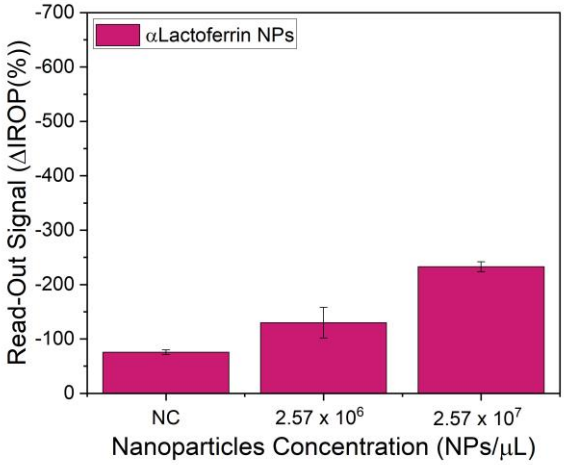

Figure 153. Concentration curve of NPs silanized with G-protein and αLactoferrin Ab.

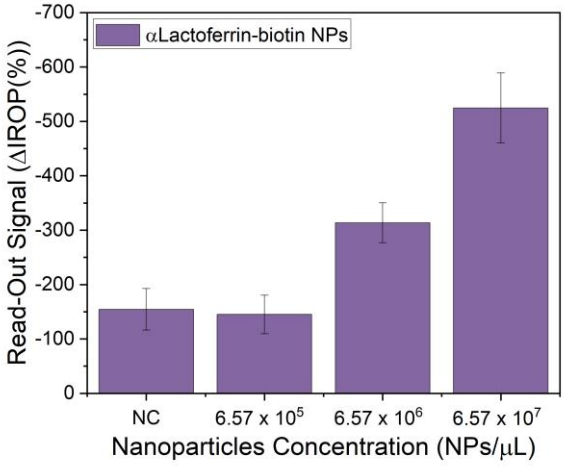

Figure 154. Concentration curve of NPs silanized with STV and αLactoferrin-biotin Ab.

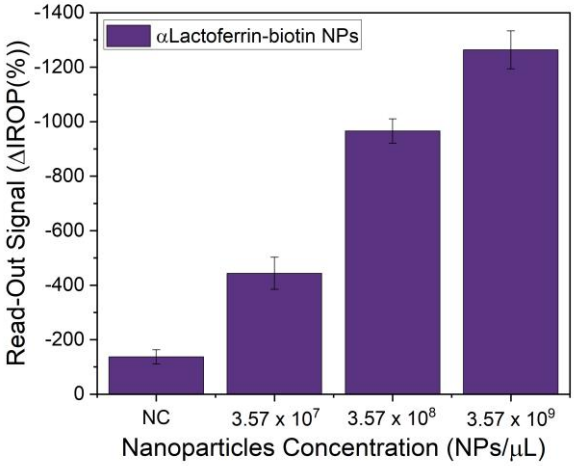

Figure 155. Concentration curve of commercial-STV NPs with αLactoferrin-biotin Ab.

As we can see in Figure 153, **the signal obtained at the highest concentration of NPs on the surface (2.57 x 10^7 NPs/µL) is too low**, so there would be few NPs recognizing on the surface. If we compare this signal with that obtained from NPs silanized with STV (Figure 154), we see that in this case it is higher, reaching -500 ΔIROP (%). This would make sense since the starting concentration in this second case is higher (6.57 x 10^7 NPs/µL), although the signal is still a bit low. Finally, when compared to the biofunctionalized commercial NPs, we observe that we obtain a signal around -1200 ΔIROP (%) when we incubate them at the concentration of 3.57 x 10^9 NPs/µL (Figure 155). Therefore, to carry out the following experiments, **biofunctionalized commercial NPs were used**, since we need to start from that concentration and obtain signals in that range in order to make a calibration curve with a higher detection limit.

Three different protocols were followed for the biofunctionalization of the NPs with the αLactoferrin Ab, obtaining the best recognition results on the sensor using the commercial NPs with STV and the αLactoferrin-biotin Ab. Therefore, it was chosen to use the commercial NPs at a concentration of 1 x 10^9 NPs/µL.

4.4.4.4. *Competitive assay in saliva*

To perform the competitive assay, biofunctionalized commercial NPs (1 x 10^9 NPs/µL) were incubated with lactoferrin protein at different concentrations (from 100 µg/mL to 0.00001 µg/mL in 1:10 dilutions), leaving the NPs at a concentration of 1 x 10^8 NPs/µL. After incubation, they were incubated on the sensor surface coated with lactoferrin and the maximum concentration was also incubated on the NC protein BSA.

On the other hand, the saliva samples used were incubated with the NPs also at the concentration of 1 x 10^9 NPs/µL leaving them at a final concentration of 1 x 10^8 NPs/µL. Similarly, after the incubation time, the NPs were deposited on the surface of the sensor.

Once the incubation was completed, the KITs were washed and the ΔIROP (%) signals of the calibration curve and the samples were read. In this way, the signal of the samples was extrapolated on the calibration curve (Figure 156) obtaining the concentration of lactoferrin in the saliva samples. Furthermore, these data were compared with the concentration of lactoferrin that had been measured by the ELISA technique for these same samples (Table 33).

As can be seen in Table 33, **the results of lactoferrin protein concentration obtained by the IODM technique are very similar to those obtained by the ELISA technique**, thus validating the results and the protocol performed. Figure 157 shows the correlation between the values obtained with the ELISA technique and the IODM.

A competitive assay was performed on saliva samples and lactoferrin protein was determined from almost 0 to 16 µg/mL. In addition, this determination was correlated with ELISA measurements obtaining a close linear fit.

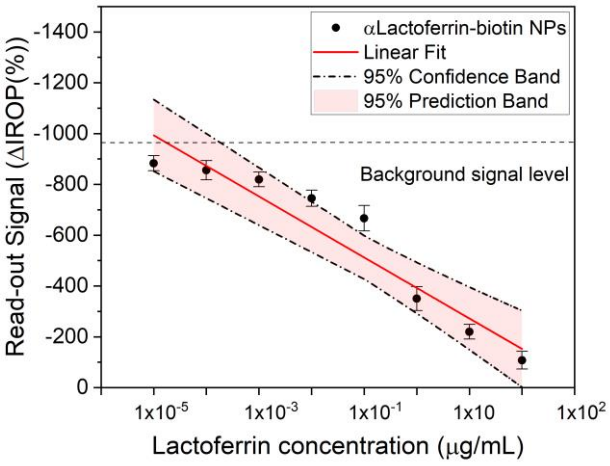

Figure 156. Calibration curve to determine the concentration of lactoferrin protein.

Table 33. Results of lactoferrin protein concentrations measured in saliva samples by IODM and ELISA.

Saliva sample	μg/mL by MOX	μg/mL by ELISA	Saliva sample	μg/mL by MOX	μg/mL by ELISA
26	5.67	4.34	**7**	1.62	0.99
40	15.48	17.29	**36**	0.52	1.03
49	6.60	7.19	**45**	6.61	6.64
54	3.21	2.71	**35**	2.40	5.57
41	4.14	3.63			

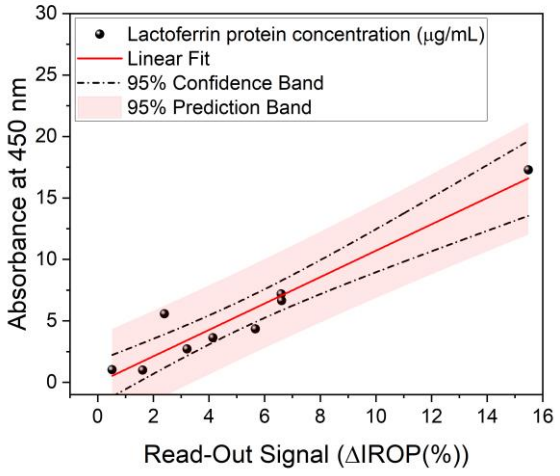

Figure 157. Linear fit between the concentration of lactoferrin protein in saliva measured by ELISA and IODM.

4.5. Conclusions

4.5.1. Case II. I. Total tau detection system

The most important conclusions obtained during the "*Case II. I. Total tau detection system*" experiments are summarized below:

- **O_2 plasma activation** of the sensor surface for protein immobilization was established as a great improvement over H_2SO_4 activation.
- **The incubation volume** on the cells was also determined at **2.5 µL** considering the compromise between droplet size and evaporation during incubation.
- **KITs stability** was achieved for at least **48 hours** stored in a refrigerator **at 4°C** covered with glass.
- Studies were carried out on the need for blocking, in order to shorten the time of the experiments, but without compromising the specificity of the system. In view of the results, **for this type of experiments when the surface is coated with tau protein and BSA it was not necessary to block** due to the high coating of the surface, so that non-specific binding was still avoided.
- Dose-response curves were made for the **tau protein immobilization**, setting it at **50 µg/mL**, and for **the αTau Ab** in the recognition stage, **50 µg/mL** was also being the concentration selected.
- **A protocol was established to coat the surface of the NPs** with the αTau Ab. This was corroborated by DLS measurements of size and ζ-potential and SEM images.
- **Recognition by the NPs was shown to be specific**, as a large signal difference was obtained between the surface coated with tau protein and the one coated with BSA.
- **An incubation time of 2 hours could be established**, since 1 hour was not enough for recognition to occur, and the best washing strategy to eliminate non-specific binding after incubation of the NPs was established, choosing **strategy 9 (20 mL H_2OmQ, 10 min in shaking plate with PBS, 20 mL H_2OmQ and drying with compressed air).**
- NPs concentration curves were made, **choosing the concentration of 1 x 10^7 NPs/µL** as the maximum signal.
- This concentration of NPs was doped in serum and PBS with different concentrations of tau protein to subsequently incubate them on the sensor and **carry out a competitive assay**, in which the lower the ΔIROP (%) signal, the higher the concentration of tau in the sample. Once this assay was performed, **it was possible to reach a LoD of 10 pg/mL in**

both matrices, considering that the incubation time of the NPs with the serum matrix has to be longer due to the Vroman effect. Thus, demonstrating the possibility of using this type of assay and technology to determine proteins in serum at low concentrations for diagnostic purposes.

- SEM images were taken of the NPs on the sensing surface, showing differences between the cells based on the concentration of tau in the doped PBS matrix. **These images also demonstrated the dispersion of the NPs**.

- Finally, all these experiments were repeated **with the new αTau** in order to continue with the research due to the discontinuation of the one we were using. **These experiments confirmed that the new pair allowed us to continue.**

4.5.2. Case II. II. Triphosphorylated tau detection system

The most important conclusions obtained during the "*Case II. II. Triphosphorylated tau detection system*" experiments are summarized below:

- The initial validation of received reagents (the 3P-Tau peptide and the B6 and B6-biotin Abs) was successful using the ELISA technique. **Positive results were obtained in both ELISAs, testing both Abs, confirming their recognition of the peptide.**

- The immobilization conditions for the peptide and the Ab were determined. In both cases, the two reagents were successfully immobilized, and the best ΔIROP (%) **signals were achieved through incubation at 37°C for 3 hours compared to ON incubation at 4°C**.

- For **the peptide, the higher concentration (300 µg/mL)** was chosen for immobilization because, although there was not much difference in the initial experiments with a concentration of 100 µg/mL, subsequent recognition assays showed that a better and more reproducible signal was obtained at the higher concentration. Similarly, **for the B6 Ab, so the immobilization concentration was established at 1000 µg/mL**.

- Good recognition signals were also obtained, with the same concentrations used for immobilization applied to the recognition step, and the incubation conditions remained the same as for immobilization. **Thus, a protocol for the assay was established, confirming the sensor's ability to recognize the peptide directly and indirectly**.

- By studying the need for blocking, **it was concluded that it was necessary**, as it improved the recognition signals of the peptide in both types of assays, whether immobilizing the peptide or immobilizing the Ab. In the first case, thanks to blocking, the entire peptide is available to bind to the Ab, and in the second case, nonspecific binding of the Ab to the surface is avoided, ensuring that the entire Ab is involved in recognizing the immobilized peptide. **Therefore, a blocking step of 1 hour at 37°C with PVP at a concentration of 10 µg/mL was established.**

- To try to improve the ability to detect the peptide, **the KITs were immobilized with STV to then anchor the B6-biotinylated Ab** to the surface and perform peptide recognition. We also tested whether blocking the surface made any difference, but the recognition occurred in the same way for both conditions and at a high concentration of the peptide (300 µg/mL), since the signal decreases considerably as the concentration decreases.

- To perform experiments to determine the concentration of the peptide in real samples, **it's essential to determine if the peptide can be recognized in such samples and whether it remains stable in a different media**. This information is necessary for creating calibration curves and extrapolating concentrations accurately. In this case, **it was observed that signals obtained in other matrices were not comparable to those in water**. Although **the assay conducted on the STV-coated surface provided slightly more sensitivity and a higher signal in the serum matrix**, it may not be valid due to the

significantly lower ΔIROP (%) compared to the PC, making it challenging to determine very low concentrations. Therefore, efforts should continue to improve sensitivity and further investigate the stability of the peptide.

- During the experiments, **issues related to the specificity of the B6 Ab began to arise**, as signals were obtained that were comparable to incubating it with tau protein. This suggests a potential issue with Ab specificity that needs to be addressed.

- ELISAs were performed to confirm the specificity of the reagents and that **we would not have cross-reactivity between phosphorylated and non-phosphorylated tau** in subsequent experiments.

- After repeating the experiments with KITs in a different format, it was determined that the problem was occurring **because the PVC used in those assays was not functioning correctly**. In the first immobilization step, there were leaks, and in the wells where only the tau protein should have been immobilized, the 3P-Tau peptide was also being immobilized, leading to cross-reactivity. **After conducting experiments with a different PVC and using a revelation step, it was confirmed that the Ab was specifically recognizing the phosphorylations**.

- To perform a competitive assay and determine the low concentrations present in real samples of the phosphorylated tau protein, **the use of NPs was necessary**. In this case, **the initial biofunctionalization protocol using the silanization process did not work**. Therefore, the protocol needs optimization, and different concentrations of STV and B6-biotin Ab should be tested to achieve the desired signals. The measurements from DLS regarding the D_h confirm that biofunctionalization is taking place. Similarly, **optimization is needed for the biofunctionalization of commercial NPs,** although the results were better in this case. Adjusting the concentrations of the reagents used and extending the incubation times for the NPs could be explored. Additionally, **it's important to improve the efficiency of the process,** as a significant number of NPs are lost during the wash steps after each stage, leading to higher reagent costs and less efficiency in subsequent assays.

- Lastly, it's important to note that the peptide and Ab used in the experiments are not commercial but are in the production and improvement phase. As a result, **there were many differences in the behavior of the peptide depending on the synthesis source**. Therefore, all final experiments conducted with the peptide from a new synthesis were not the same as previous ones, and many problems arose in immobilization and, consequently, recognition. While tests were conducted to try different buffer solutions with varying pH levels to coat the sensor surface, **no improvement was achieved**. Additionally, consistent immobilization signals were not obtained in the PC with H_2OmQ.

4.5.3. Case II. III. Detection of pTau181 in the Syrian hamster model

The most important conclusions obtained during the "*Case II. III. Detection of pTau181 in the Syrian hamster model*" experiments are summarized below:

- The **concentration of pTau181 protein was determined in 20 serum samples** distributed in 4 samples of transgenic mice as PC, 5 samples of NC hamster, 5 samples of arousal hamster and 6 samples of torpor hamster.

- The biofunctionalization of the NPs was carried out using the silanization and G-protein protocol, **obtaining a final concentration for the use of 5.42 x 10^9 NPs/µL**.

- After verification of the biofunctionalization process by DLS, their specificity was tested by performing a three-point line and incubating them on a NC protein also. In this way **it was determined that they were specific against the pTau181 protein, and that the concentration of use was 1 x 10^9 NPs/µL**.

- A competitive assay was performed to determine the concentration of the samples, **being able to discern between the different stages of the hamsters**, since those in which hibernation was induced (torpor) had much higher concentrations of phosphorylated tau protein than those controls that did not hibernate, corresponding to the concentrations determined in the transgenic mice that acted in the assay as PC. In addition, the arousal hamsters had concentrations of phosphorylated tau protein similar to the controls, **demonstrating that this phosphorylation is reversible once they come out of hibernation.**

- There are significant differences in the concentration of pTau181 protein between control and torpor hamsters, as well as between torpor and arousal hamsters with a significance level of $p<0.01$.

4.5.4. Case II. IV. Lactoferrin detection system in saliva samples

The most important conclusions obtained during the "*Case II. IV. Lactoferrin detection system in saliva samples"* experiments are summarized below:

- A total of 9 saliva samples from relatives of people with AD were analyzed to determine the **concentration of lactoferrin protein in saliva**.

- SiO_2 NPs were first biofunctionalized following different protocols. All three protocols were valid since the DLS measurements corroborated the biofunctionalization process of the NPs. However, following the two processes involving silanization, a concentration of NPs was obtained at the end of the protocol due to the large number of washing steps and stages. Due to this, **commercial NPs biofunctionalized with the αLactoferrin-biotin Ab were used to perform the competitive assay**, since they had a higher concentration, which is necessary to have a wider calibration curve and a lower LoD.

- **The concentration of the NPs used to perform the competitive assay was set at 1 x 10^9 NPs/µL**, so that when doped with the different concentrations of lactoferrin they remained at a concentration of 1 x 10^8 NPs/µL. At this concentration, they were incubated on the surface of the sensor, both for the calibration curve and for the samples.

- When extrapolating the signals obtained from the samples in the calibration curve it was observed that **we can determine values up to 0.51 µg/mL since it is the sample measured with the lowest concentration of lactoferrin**, being able to measure even lower concentrations. In addition, **we were able to discern concentrations ranging from 15 µg/mL to 0.51 µg/mL**.

- Finally, **these data were validated as they could be compared with the concentrations measured for these same samples by the ELISA technique**, obtaining values with much similarity between both techniques. Therefore, it is a completely valid method for measuring lactoferrin in saliva samples, **as well as other proteins of interest**.

5. Pre-doctoral stay at the Universidade de Aveiro

5.1. Introduction

During this doctoral thesis, was carried out a pre-doctoral stay thanks to the grant provided by the UPM's Programa Propio called "**Convocatoria de ayudas dirigidas al personal investigador en formación predoctoral para realizar una estancia de investigación internacional igual o superior a tres meses**" during the academic year 2022, aiming to obtain the International Mention.

This stay took place at the **University of Aveiro, Portugal**, from September to December, lasting three months. The host department was the Department of Medical Sciences at the University of Aveiro.

The receiving group during this stay was **led by Ana Gabriela Henriques, focusing on the study of AD** and specifically researching new markers for diagnosing the disease. These markers are found in exosomes from various biological samples.

The primary objective of the thesis was the development and optimization of a label-free optical biosensor for *in-vitro* diagnosis of different pathologies, particularly emphasizing early detection of AD. This condition results in changes in concentrations of certain biomarkers, which we aim to measure.

Considering the purpose of this thesis, **the goal of this stay was to learn about the methods for isolating exosomes from different types of samples, their characterization using various techniques, and identifying potential candidate markers** according to the following organization (Table 34). Once the biomarkers are selected, **the next objective is to develop a multiplexed diagnostic KIT based on the optical biosensor used for AD during this thesis**.

Table 34. Temporal organization of the stay at Universidade de Aveiro

Tasks	1º month	2º month	3º month
Exosome isolation			
Exosome characterization			
Candidate biomarker study			
Establish the protocol for measuring the concentration of biomarkers			
Determine articles to be written and future collaborations			

5.2. Exosomes isolation

Extracellular vesicles (EVs) are an undefined and heterogeneous group of membrane-enclosed particles derived from cells (both prokaryotic and eukaryotic), which are divided into **apoptotic bodies, microvesicles, and exosomes**. EVs differ in their biogenesis, function, composition, and size (Kurian et al., 2021). Apoptotic bodies are the largest, with a size of 1000 nm; microvesicles range from 100 to 1000 nm, and finally, **exosomes are the smallest vesicles, typically ranging from 30 to 150 nm in size,** with a density of 1.10 to 1.20 g/mL (Alzhrani et al., 2021; Spitzer et al., 2019) (Figure 158).

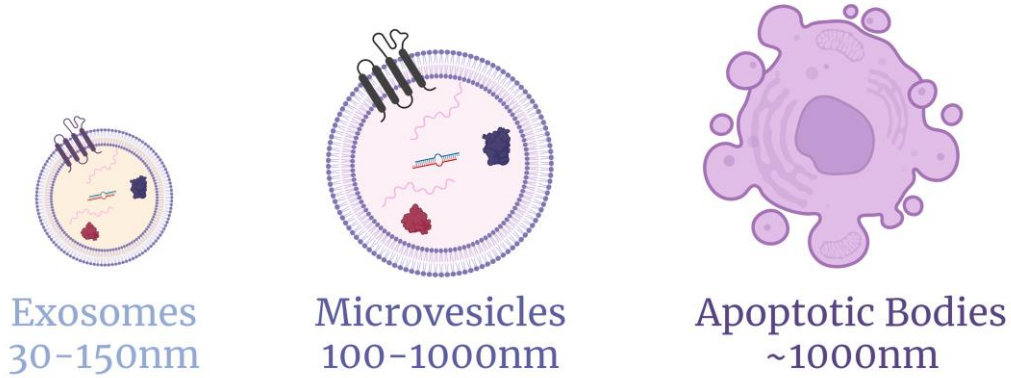

Figure 158. Extracellular vesicle types. Created with BioRender.com.

The first known report on exosomes was given by the works of C. Harding et al. and B. T. Pan and Johnstone in 1983, observing small vesicles of about 50 nm in the maturation of reticulocytes. Years later, in 1989, these small vesicles were named exosomes by (Johnstone et al., 1989).

The International Society for Extracellular Vesicles (ISEV) recommended using the term EVs to refer to particles released by cells that are surrounded by a lipid membrane but lack replication capability (Alzhrani et al., 2021). However, a**ccording to the ISEV recommendations in 2018, it was suggested that the term exosome (widely established) be replaced by small Extracellular Vesicles (sEVs)** due to the many difficulties in separation methods (Y. Zhang et al., 2020).

Among their functions are cell-to-cell communication, regulating various biological functions, and eliminating cellular waste. They are also involved in cellular signaling processes, immune responses, and tumor metastasis (Kurian et al., 2021; Zhu et al., 2020). This is due to their composition, which enables them to protect the interior and regulate processes such as angiogenesis, coagulation, and neuronal regeneration (Alzhrani et al., 2021).

Almost all cell types produce exosomes, including endothelial cells, lymphocytes (B and T), macrophages, NK cells, neurons, and glial cells (Alzhrani et al., 2021; Y. Zhang et al., 2020). These exosomes reach target cells and release their content into the cytosol either by fusing their membrane or through processes like endocytosis or phagocytosis, thereby altering the physiological state of the cell (Zhu et al., 2020).

Regarding the composition of exosomes, it depends on the cell type from which they originate, as well as their function. This composition is typically divided into two categories: firstly, **there are those components common to all exosomes** involved in the process of vesicle formation and secretion, for example, Rab, Heat Shock Protein 70 (HSP70), CD63, and CD81, or Alix, and secondly, components specific to the cell type they come from (Y. Zhang et al., 2020). On the other hand, **there are specific markers such as L1 Cell Adhesion Molecule (L1-CAM)** which was discovered in neurons (Faissner et al., 1984; Gomes & Witwer, 2022). This transmembrane protein is a member of the L1 family of adhesion proteins and has Igs domains in its N-terminal extracellular portion and its C-terminal part is involved in cell signaling. Due to its expression in the brain, it has been used in several studies for the **separation of exosomes of neuronal origin from total exosomes** (Hornung et al., 2020; Jiang et al., 2021; Mustapic et al., 2017). Additionally, their main components are lipids, enriched in cholesterol, and they can contain molecules of DNA and RNA. They also contain cytoskeletal, fusion, and transfer proteins like flotillin and annexin (Alzhrani et al., 2021). To date, approximately 600 lipids, 40,000 nucleic acids, and around 350,000 proteins have been reported in exosomes, opening doors to numerous opportunities for clinical diagnosis and treatments (J. Chen et al., 2022).

Their biogenesis begins with the invagination of the plasma membrane to produce endocytic vesicles. These vesicles merge to form early endosomes, which mature into late endosomes that encapsulate part of the cell's content into Intraluminal Vesicles (ILVs). At this stage, they are termed Multivesicular Bodies (MVBs). These MVBs fuse their membrane with the cell's plasma membrane, releasing the exosomes into the extracellular space (J. Chen et al., 2022) (Figure 159).

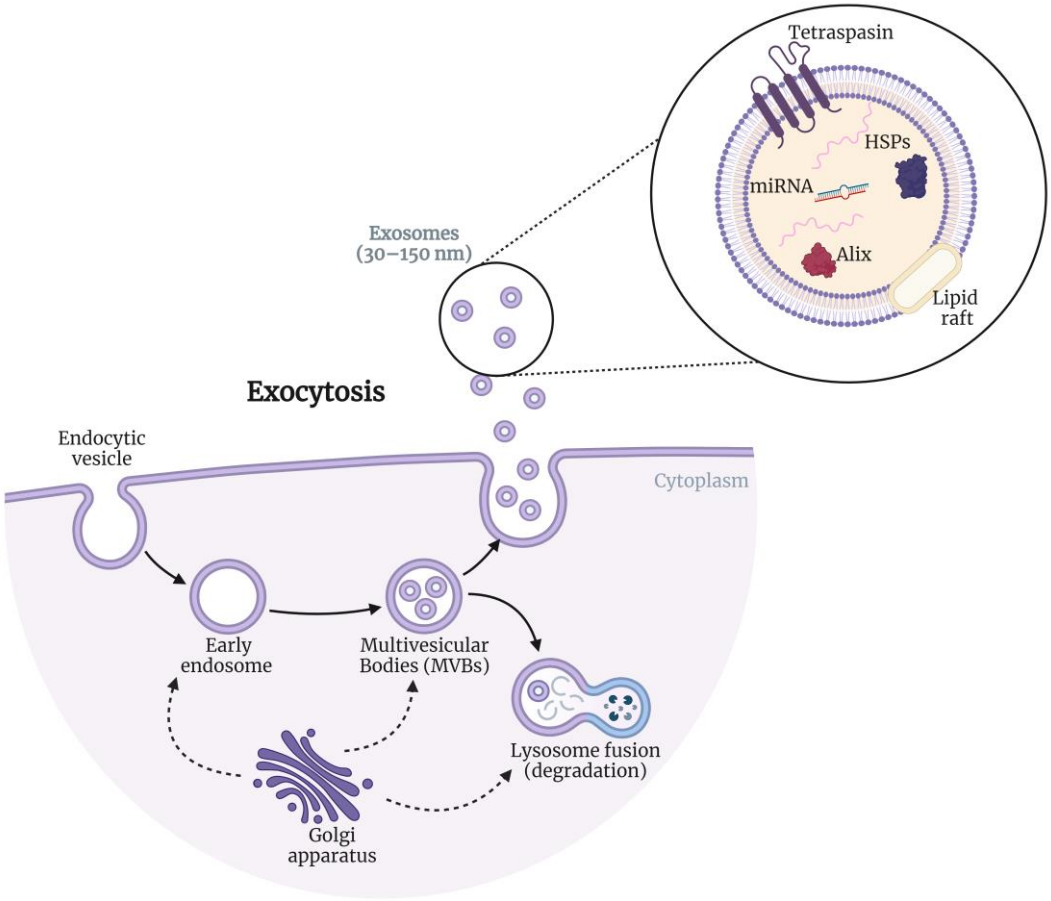

Figure 159. Exosome formation process. Created with BioRender.com.

Exosomes have been isolated from various body fluids such as saliva, serum, plasma, urine, and CSF, among others (Gurunathan et al., 2019). Their isolation from these samples makes them a powerful tool for diagnostic analysis or predicting the progression of different diseases, utilizing the proteins within them as biomarkers. They can also be used in tissue reprogramming and therapies based on their transport abilities, serving as drug carriers due to their capability to cross the blood-brain barrier, low immunogenicity, and biocompatibility (Kurian et al., 2021; Ludwig et al., 2019).

Over the years, **various techniques have been developed to isolate exosomes from different types of samples**, including ultracentrifugation, precipitation, size-based separation, immunoaffinity, and microfluidics.

- **Ultracentrifugation**: This method is widely used for isolation. It relies on consecutive centrifugation and ultracentrifugation steps, gradually increasing speed to achieve size-based separations (Alzhrani et al., 2021)(Figure 160A).
- **Precipitation**: This method alters the solubility of exosomes by exposing them to a solvent, causing them to precipitate in the solution. Various commercial kits are available for this type of isolation (Kurian et al., 2021) (Figure 160B).

- **Size-based separation**: Techniques such as ultrafiltration, affinity chromatography, and AF4 (Asymmetrical Flow Field-Flow Fractionation) can be used for size-based separation (Figure 160C).
  - **Ultrafiltration**: This method is used to concentrate exosomes using different MWCO. It involves consecutive filtrations until finally obtaining the exosomes (Zhu et al., 2020).
  - **Size exclusion chromatography**: In this case, the sample passes through a column with very small pores. Exosomes, having a larger D_h, cannot pass through and travel faster down the column (Kurian et al., 2021).
  - **AF4**: This is a relatively new technique involving a chamber with two semi-permeable membranes, with the sample between them. Two flows pass through these membranes, allowing separation based on size and molecular weight, which impart different mobilities to the exosomes (Alzhrani et al., 2021).
- **Immunoaffinity**: This technique relies on the affinity binding of proteins present in the exosome membrane to proteins anchored on a support (Zhu et al., 2020)(Figure 160D).
- **Microfluidics**: In this case, some of the previously described techniques, such as immunoaffinity or size separation, are adapted to a microfluidic system (Kurian et al., 2021).

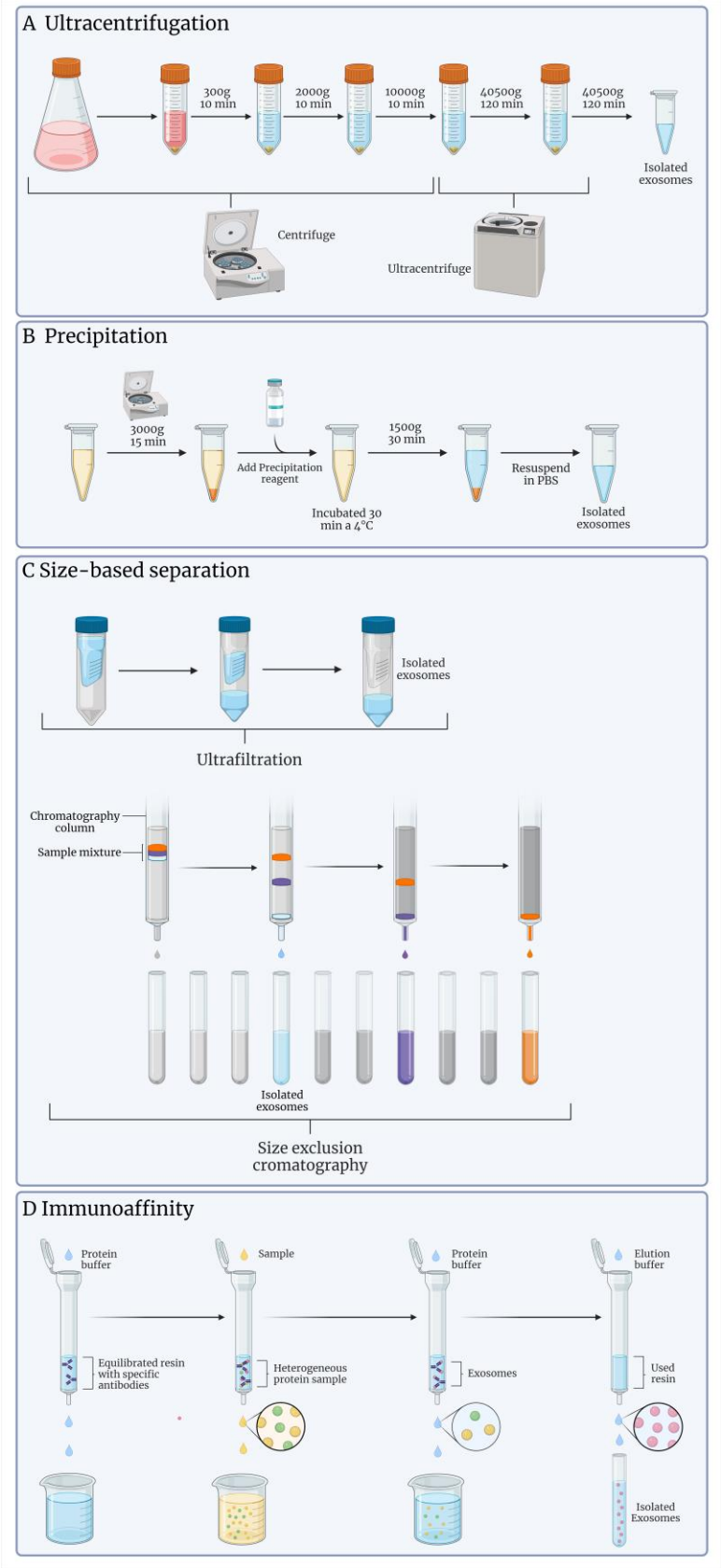

Figure 160. Exosome isolation techniques. A. Ultracentrifugation. **B.** Precipitation. **C.** Size-based separation. **D.** Immunoaffinity. Created with BioRender.com.

The methods have various advantages and disadvantages summarized in Table 35 (J. Chen et al., 2022).

Table 35. Advantages and disadvantages of the most commonly used techniques for exosome isolation (J. Chen et al., 2022).

Exosome isolation technique	*Advantages*	*Disadvantages*
Ultracentrifugation	It is the gold-standard technique, is not very expensive and allows the use of large volumes	Time-consuming, labor-intensive and can damage exosomes
Precipitation	It is simple to perform and allows the use of large volumes	May leave residues
Size-based techniques	Allows isolation of exosomes without damaging them, no special equipment is required and they are easy to perform	Loss of exosomes depending on the cut by size
Immunoaffinity	Allows for the separation of exosome subtypes	It is expensive due to the use of some Abs

Once the exosomes are isolated, **it's necessary to characterize them** to ensure that the isolated vesicles are indeed exosomes. For this purpose, different techniques are used, such as Nanoparticle Tracking Analysis (NTA), DLS, Atomic Force Microscopy (AFM), TEM, Flow Cytometry, and Western Blot (WB).

- **NTA**: This technique helps determine the size distribution of particles within a specified range (10 nm to 2 μm) and measures the concentration for each size. It's based on detecting the movement and speed of particles, analyzing the motion of each exosome through image analysis. This movement correlates with the particle size (Gurunathan et al., 2019)(Figure 161A).
- **DLS**: Widely used for determining particle size, DLS relies on the Brownian motion of particles in a solution. When an incident light beam hits the particles, it causes light scattering in all directions. Differences in the intensity of scattered light are detected by a photodetector, providing information about size and concentration (Kurian et al., 2021)(Figure 161B).
- **AFM**: Using a silicon probe, AFM scans the vesicle's surface, generating topographic images that provide data on vesicle morphology and molecular composition (Alzhrani et al., 2021)(Figure 161C).
- **TEM**: TEM is employed to characterize the structure, morphology, and size of exosomes by creating images when an electron beam passes through the sample (Gurunathan et al., 2019)(Figure 161D).

- **Flow cytometry**: This method is used to determine exosome concentration and size. However, exosomes need to be associated with other particles as their size falls outside the cytometer's size range. The light scattered by these particles with attached exosomes is detected, enabling concentration and size determination (Kurian et al., 2021)(Figure 161E).
- **WB**: For this technique, intact exosomes aren't used initially. Instead, there's a process of lysis and denaturation. WB allows the analysis of markers that identify exosomes (Alzhrani et al., 2021)(Figure 161F).

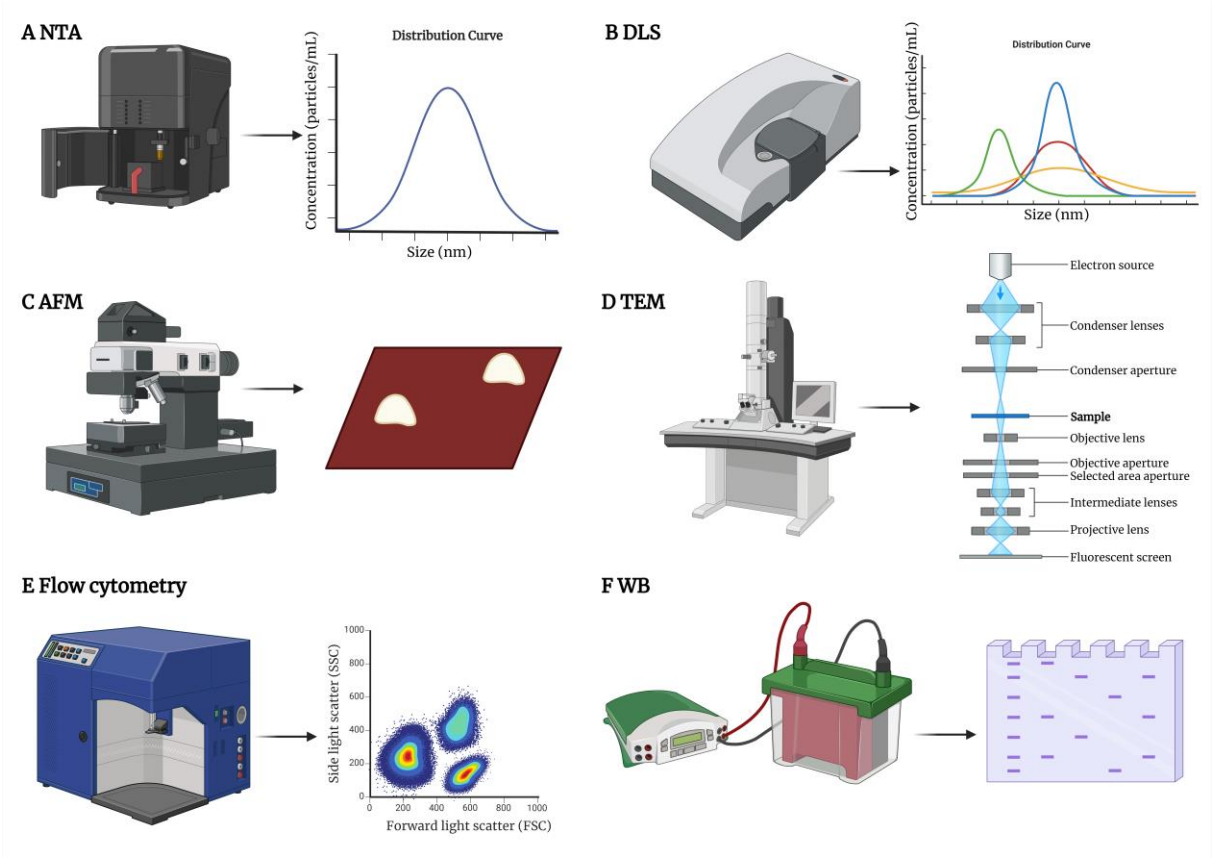

Figure 161. Exosome characterization techniques. A. NTA. **B.** DLS. **C.** AFM. **D.** TEM. **E.** Flow cytometry. **F.** WB. Created with BioRender.com.

The ISEV proposed that it was necessary to determine different proteins (presence or absence in exosomes) to confirm that the vesicles being worked with are indeed exosomes. Generally, **exosome identification is based on three levels: morphology analysis using TEM, size determination through NTA, and protein marker analysis via WB** (Y. Zhang et al., 2020).

Regarding their applications, they have been extensively studied in the biomedical field due to their significance in various pathologies, such as NDD. In this area, **there is increasing evidence that exosomes are a valuable subject of study in such diseases, like in the case of AD**, as they facilitate protein aggregation in the brain and contribute to misfolding of proteins (Alzhrani et al., 2021).

Although much about their functions in the brain remains unknown, **they play a crucial role in maintaining cerebral physiology**. For instance, in the survival of neuronal axons and their myelination. Additionally, it is believed that they are involved in the elimination of connections between neurons (Soares Martins et al., 2021).

Exosomes, **due to their capability to cross the blood-brain barrier, carry information about their environment upon release by neurons and glial cells**, reaching the peripheral blood. This highlights their importance as disease biomarkers and a potential monitoring tool in the pathological process (Alzhrani et al., 2021).

Studies have demonstrated that **exosomes derived from the brains of AD patients contain higher levels of tau protein and Aβ peptide**, acting as carriers of the Aβ peptide and APP (T. Zhang et al., 2021). Moreover, markers of exosomes like Alix and flotillin have been found around SPs formed in the brain, supporting the theory that the release of exosomes with high Aβ peptide content contributes to disease progression. Similarly, these vesicles transport hyperphosphorylated or aggregated tau protein, contributing to the formation of NFTs, especially enriched with phosphorylated tau at threonine 181. Additionally, **they play a role in neuroinflammation and consequently in neurodegeneration** (Soares Martins et al., 2021; T. Zhang et al., 2021). Furthermore, elevated levels of $A\beta_{42}$ peptide and phosphorylated tau proteins at positions 181 and 396 have been found in CSF and blood samples of AD patients (T. Zhang et al., 2021).

On the other hand, **protective roles have also been attributed to exosomes** in the disease, associated with the restoration of neuronal functions. For instance, they can be phagocytosed by microglia, aiding in the clearance of Aβ peptide in the brain. Additionally, these exosomes contain enzymes capable of degrading the peptide, representing a potential tool as vehicles to transport various drugs to the brain for different therapies (Soares Martins et al., 2021)(Figure 162).

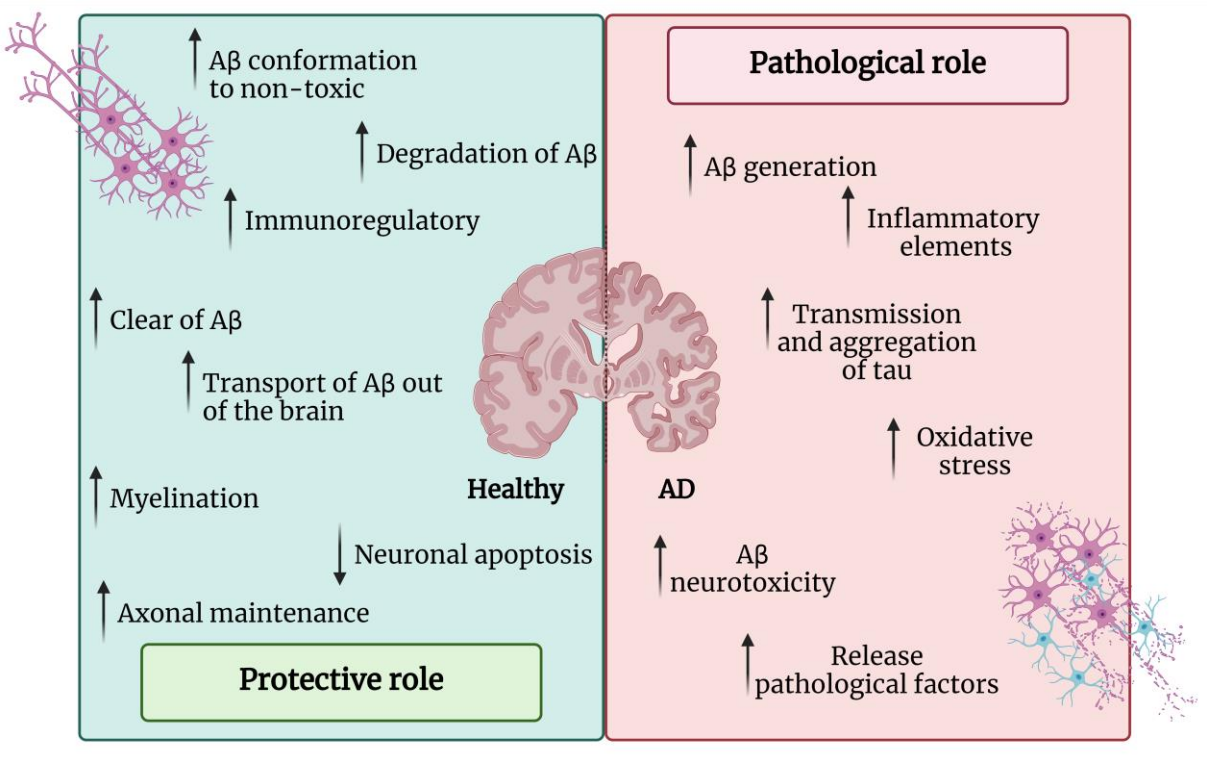

Figure 162. Role of exosomes in AD. Created with BioRender.com.

It's important to consider that in fluids like peripheral blood, when isolating exosomes, these originate from various cell types. However, among them are those derived from CNS cells capable of crossing the blood-brain barrier (K. Y. Kim et al., 2021). Hence, apart from studying the overall exosome population in peripheral blood, it's also possible to isolate those specifically originating from the brain.

5.2.1. Progress of the stay

During the initial weeks of the internship, time was dedicated to reading the group's articles to better understand the work and techniques to be implemented. Additionally, two exams were required, one on biological risks and another on good practices in handling human samples, to obtain permission to work in the clinical research laboratory at the center.

Upon passing these exams, the focus shifted to **learning the techniques used for isolating exosomes and their characterization**. Initially, work was conducted with neuronal cell cultures (N2a, mouse neuroblastoma) under control conditions and with Aβ treatment. After a specified period, the medium was removed, and the EVs secreted by the cells were isolated from this medium. **An ultracentrifugation protocol was employed** for this isolation process, allowing the separation of the desired vesicles from the medium.

The ultracentrifugation protocol involved differential centrifugations (Table 36), culminating in the collection of two aliquots: **one in PBS designated for TEM and NTA analyses, and the other in lysis buffer (RIPA) intended for WB analysis**.

Table 36. Ultracentrifugation protocol for obtaining exosomes.

Speed (rpm)	*Time (min)*	*Temperature (°C)*	*Objective*
300	10	4	Discard dead cells from the medium
2000	10	4	Discard cell membranes
10000	30	4	Discard other microvesicles
Filter media with a 0.22 µm filter			
40500	120	4	Obtaining exosomes
Clean pellet with filtered PBS			
40500	120	4	Obtaining exosomes
Remove supernatant, resuspend in PBS and freeze at -20°C.			

On the other hand, the cells are also collected after washing them with PBS, lysed using RIPA buffer, lifted from the plate using a cell scraper, and supplemented with phosphatase and protease inhibitors. Finally, they are sonicated five times, 10 s each time, and stored at -20°C. Additionally, **exosomes were also extracted from plasma samples** (NCs without disease and PCs from AD). This isolation was carried out using the commercial ExoQuickTM kit (System Biosciences, Palo Alto, CA, USA) **based on precipitation** following the protocol described below:

1. Two Eppendorf tubes containing 500 µL of plasma were used, then centrifuged at 3000 rpm for 15 min at 4°C to eliminate dead cells and lysates.
2. After this centrifugation, the supernatant was carefully collected, the reagent (126 µL into each Eppendorf tube) was added, and mixed gently.
3. It was incubated for 30 min at 4°C.
4. Centrifugation was performed at 1500 rpm for 30 min at 4°C.
5. The supernatant was discarded, and the pellet was obtained. Half of the eppendorf tubes were resuspended in 200 µL of PBS for TEM and NTA measurements. The other half was resuspended in RIPA with phosphatase and protease inhibitors for lysis to carry out WB analysis. Afterwards, they were stored at -20°C.

To perform the WB, it's first necessary to quantify the protein content of the samples because we'll need to run an electrophoresis gel, and for this, we'll load the same amount of protein onto the gel. Quantification was done using the BCA method based on the formation of protein-copper ion complexes that form the Cu-BCA chelate with an intense purple color, which absorbs at 562 nm. A BSA standard curve was prepared in a 96-well plate to extrapolate the concentrations of the samples. The samples were also incubated with the BCA reagent and left incubating for 30 min at 37°C. In this case, the samples are in RIPA to extract all the proteins contained in the exosomes.

Finally, the absorbance of the standard curve and samples at 562 nm is measured, and the concentrations are calculated.

The proteins from the exosomes were separated using electrophoresis gels and subsequently transferred to nitrocellulose membranes to reveal the characteristic exosomes markers using Abs.

The electrophoresis gel was performed under denaturing conditions with a gradient ranging from 5% to 20% acrylamide. To create the gel's resolving part (bottom portion), two recipes were followed, one for 5% acrylamide and the other for 20%. These solutions were poured into the gradient-making mechanism. Initially, the 20% acrylamide solution was allowed to flow by opening the valve until a line formed between the crystals. Then, the valve for the 5% solution was opened to mix the two solutions, creating the gradient. Once polymerized, the stacking gel was added, and the comb was placed to create the wells. Finally, after polymerizing the upper part of the gel, the comb was removed to load the samples. Meanwhile, the samples were prepared. 50 µg of protein mixed with the loading buffer were heated for 5 min at 95°C.

After 5 minutes, the samples (Table 37) were loaded into the gel wells, and electrophoresis was initiated at a constant 90 mA for 4 hours.

Table 37. Samples loaded on the acrylamide gels made for the N2a cell line and plasma samples.

Samples loaded on acrylamide gels		
Molecular weight marker	Control N2a cell lysate	N2a cell lysate Aβ treatment
Exosomes isolated from the control N2a cells	Isolated exosomes from treated N2a cells	SH-SY5Y* cell line lysate
Plasma 1:20**	Exosomes isolated from NC plasma	Exosomes isolated from PC plasma

*The cell line lysate was used in the acrylamide gels of the plasma samples as a PC to check the Ab functionality.

**Plasma diluted 1:20 was loaded onto the acrylamide gels of the plasma samples to verify that the signals obtained in the exosomes are higher than those obtained in plasma.

Once the gels are completed, it's necessary to transfer the proteins to a nitrocellulose membrane to determine the presence or absence of the target marker proteins. The assembled cassette is placed into the transfer tank containing the transfer buffer.

After connecting, set it to 90 volts and 200 milliamps and leave it ON with ice blocks.

Once the transfer is completed, the membranes are hydrated in 1x Tris-Buffered Saline (TBS) for 5 min with agitation at RT. After 5 min, they are stained with Ponceau Red for 10 minutes with agitation at RT. Ponceau Red is a quick and reversible protein staining method for membranes, enabling visualization of bands to confirm the success of the transfer. After 10 min, membranes are washed with distilled H_2O until achieving a white background with red bands.

This also helps in cutting the membrane at the desired molecular weight range for subsequent incubation with primary Abs. The membranes were cut, the first one above 50 kDa and below 37 kDa, and the second membrane below 75 kDa. Once cut, they were washed in TBS-Tween (TBS-T) 0.05% until the red color from the membrane bands disappears (5-10 minutes).

Before incubating the primary Abs on the membranes, they were blocked for 4 hours with 5% milk in TBS-T 0.05% at RT with agitation. Subsequently, they were washed three times with TBS-T 0.05% for 5 min each at RT with agitation. After the washes, the primary Abs (Table 38) were incubated for 3 hours at RT with agitation, followed by an ON incubation at 4°C with agitation, and finally, 2 hours at RT with agitation. The primary Abs were prepared in 3% milk in TBS-T 0.05%.

Table 38. Primary Abs used in the WB for the N2a cell line and plasma samples.

Name	***Host***	***Dilution***	***Function***	***Expression***
Calnexin	Rabbit	1:1000	Protein folding	Negative
Flotilin	Mouse	1:500	Plasma membrane endocytosis process	Positive
Rab11	Mouse	1:500	Fusion of multivesicular bodies	Positive
Alix	Mouse	1:500	Classification of vacuole contents	Positive
APP c-terminal	Rabbit	1:500	APP processing marker	Positive
APP 22C11	Mouse	1:250	APP processing marker	Positive
Rab27	Rabbit	1:1000	Exosome secretion process	Positive
CD63	Mouse	1:500	Tetraspanin (protein marker)	Positive

First, the membranes were probed for calnexin, flotillin, Rab11, APP22C11, and Rab27. Following the primary Ab incubation, the membranes were washed 6 times for 10 min each at RT with agitation using TBS-T 0.05%. Subsequently, the secondary Abs (Table 39) were incubated for 2 hours at RT with agitation. In this case, the secondary Abs were prepared in 5% milk in TBS-T 0.05%.

Table 39. Secondary Abs used and their dilution for membrane development.

Name	Type	Dilution
Calnexin	αRabbit-IgG-HRP	1:10000
Flotilin	αMouse-IgG-HRP	1:2000
Rab11	αMouse-IgG HRP	1:5000
Alix	αMouse-IgG-HRP	1:10000
APP c-terminal	αRabbit-IgG-HRP	1:5000
APP 22C11	αMouse-IgG-HRP	1:5000
Rab27	αRabbit-IgG-HRP	1:5000
CD63	αMouse-IgG-HRP	1:2000

After the 2-hour incubation, the same washing steps as for the primary Ab were repeated, and the membranes were kept in TBS until the revelation.

For revelation, the Amersham ECL™ reagent (GE Healthcare, UK) was used. This reagent is a chemiluminescence-based developer that emits light resulting from the oxidation reaction of luminol catalyzed by the enzyme HRP. The reagent was pipetted onto the membrane and left in the dark for 3 min. After 3 min, the reaction was read using the ChemiDoc Imaging System (Bio-Rad, USA).

To determine the other markers (Alix, APP C-terminal, and CD63), a membrane stripping procedure was necessary. The stripping process involved applying hydrogen peroxide (H_2O_2) onto Parafilm and placing the membrane face down in contact with the liquid for 15 min at 37°C. This process is used to inactivate the HRP enzyme from the secondary Abs but does not remove the Ab from the membrane. After 15 min, the membranes were washed twice with TBS-T 0.05% for 5 min with agitation at RT. They were then re-blocked for 1 hour with 5% milk in TBS-T 0.05%. Finally, the same washing process was repeated, and the primary Abs (Table 34) were incubated. The process for incubating the primary and secondary Abs and revelation is the same after the stripping process.

After the WB characterization, in the case of TEM, the exosomes need to maintain their integrity for morphological characterization, so they were not lysed. The following protocol was followed for visualizing the samples using TEM:

1. Prepare the samples (10 µL for cell samples, 5 µL for plasma). Mix 5 µL of the sample with 5 µL of 4% Paraformaldehyde (PFA).
2. Place 5 µL of the sample mixed with PFA on a Parafilm square. Using tweezers, gently position the TEM grid over the drop on the Parafilm to ensure contact.
3. Allow it to sit for 30 min at RT in darkness.
4. Prepare the contrast solution, consisting of 3% phosphotungstic acid at pH 7.

5. Wash the grids that were in contact with the sample. Using tweezers, dip the grid in a droplet of PBS (20 µL) placed on the Parafilm and then gently touch it to filter paper to remove excess liquid. Repeat this process twice.
6. Place the grid over the contrast solution, also in a droplet on the Parafilm.
7. Incubate for 10 min in darkness.
8. Carefully remove the grid and blot-dry it on filter paper. Store it in a box to complete the drying process.

Once the samples are prepared and dried, they can be observed under the TEM. Figure 163 shows an exosome from one of the human plasma samples from the PC.

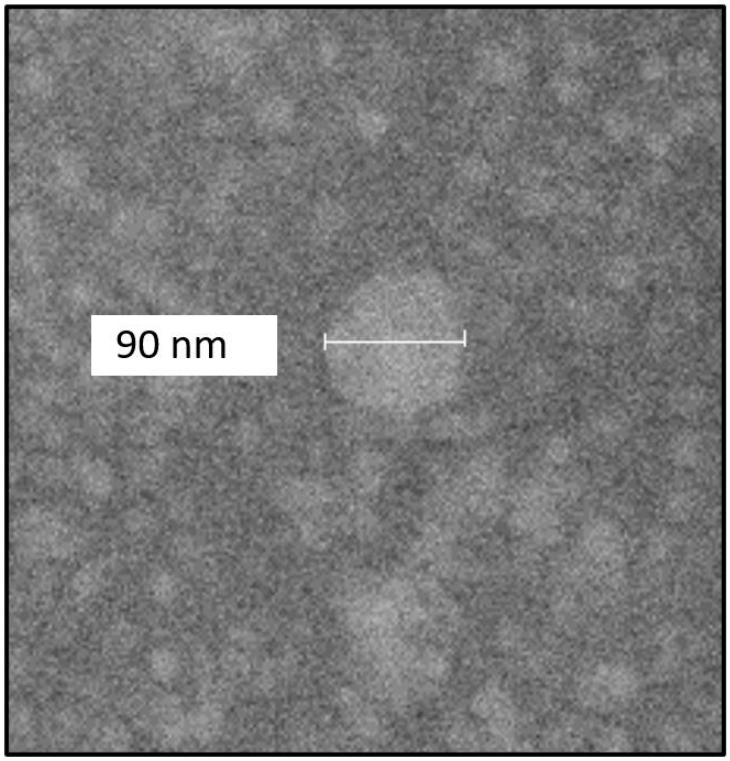

Figure 163. Image obtained by TEM of an exosomes isolated from human plasma samples.

Finally, for the quantification of exosomes using the NTA technique, they shouldn't be lysed. NTA utilizes both light scattering properties and Brownian motion of particles to determine the size distribution and concentration of EVs suspended in solution. To understand how this technique works, different samples of EVs isolated from plasma were measured. The NTA device, NTA NS300 Nanosight (Malvern Panalytical, Germany), was borrowed from the University of Coimbra for these experiments. Sample preparation was straightforward, involving mixing 2 µL of the sample with 1 mL of PBS. Next, it was injected into the microfluidic chamber and read at 488 nm with a flow rate of 30 µL/second. Additionally, 5 videos of 30 s each were recorded while the sample was being read (Figure 164).

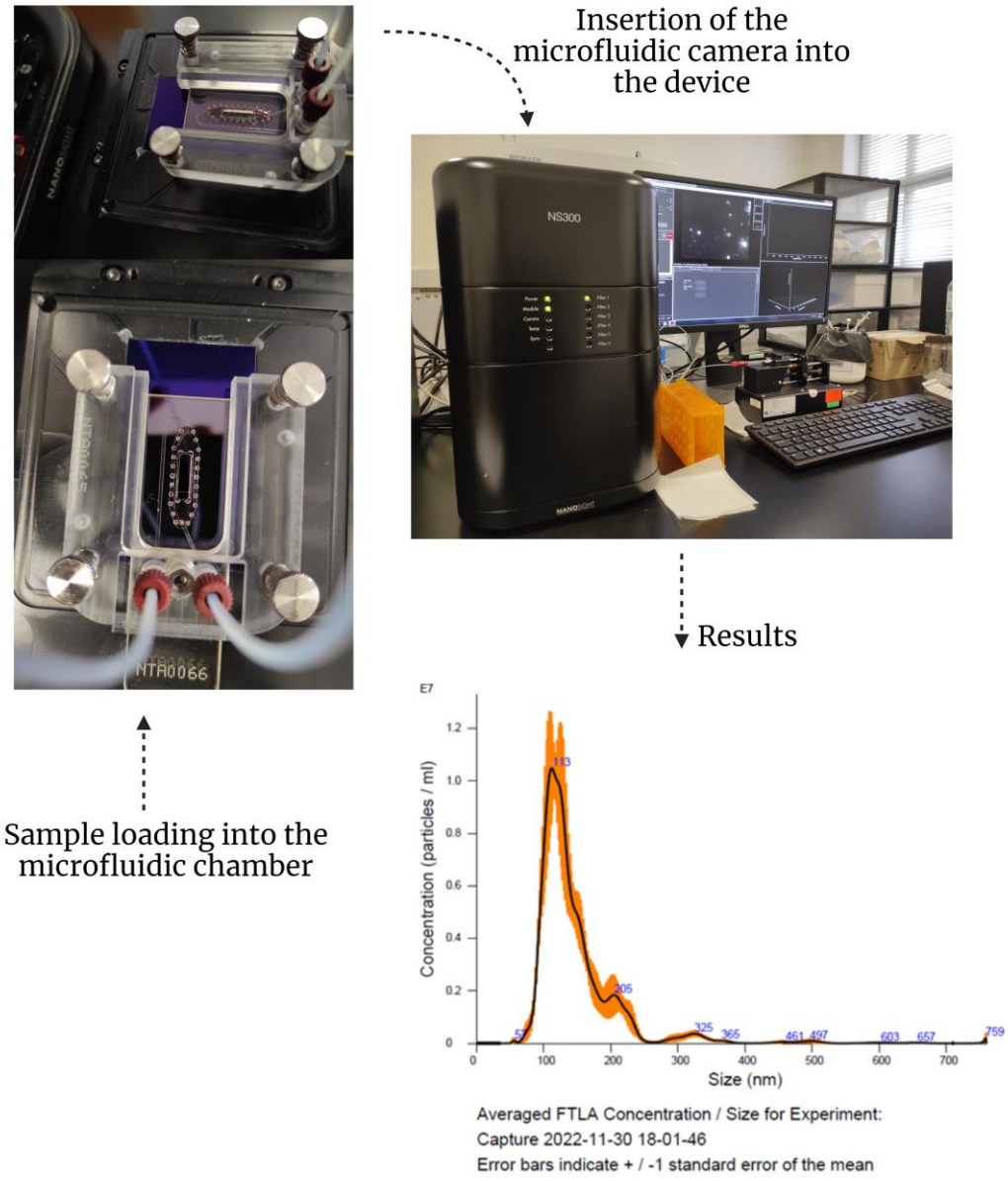

Figure 164. Size distribution of isolated EVs from human serum samples obtained by NTA. The concentration of particles per milliliter for each size population is represented. On the left of the figure is a detail of the microfluidic chamber where the sample is loaded. Created with BioRender.com.

5.2.2. Conclusions

During the stay at the Neuroscience and Signaling Group of the University of Aveiro, methodologies for the isolation and characterization of EVs from both cell lines and plasma samples were learned. Isolation of exosomes was performed in the N2a cell line and in NC and PC plasma samples from the AD. The use of the NTA technique was learned and these exosomes were also characterized by TEM and WB. Thanks to this stay, these protocols could be transferred to the research group with the aim of being able to isolate these exosomes and measure the biomarkers involved in AD using the optical biosensor described in this thesis.

5.2.3. Proof of concept for the measurement of markers in exosomes from serum samples

5.2.3.1. *Materials and methods*

After the stay at the University of Aveiro, the same protocol performed for the isolation of the exosomes learned in serum samples was replicated to subsequently test the separation of exosomes of neuronal origin by immunoprecipitation.

5.2.3.1.1 Isolation of exosomes from human serum samples

Five samples of 300 µL each of human serum were used, which were centrifuged for 15 min at 3000 rpm at 4°C. The supernatant was collected and transferred to new Eppendorf tubes. To each of these Eppendorf tubes, 75.60 µL of ExoQuickTM reagent was added. After mixing, it was allowed to incubate for 30 min at 4°C.

After incubation, the samples were centrifuged for 30 min at 1500 rpm at 4°C. The supernatant was removed and resuspended in 200 µL of PBS with 2 µL of phosphatase inhibitors (Thermo Scientific) and 20 µL of protease inhibitors (Sigma-Aldrich). From this, 10 µL (solution with isolated exosomes) were taken and mixed in a vortex with 10 µL of RIPA buffer for lysis.

After isolation, a 1:1000 dilution of a small amount of the exosomes was performed to determine their concentration and size by DLS.

5.2.3.1.2 Total protein exosome quantification

Once the total exosomes were isolated from the samples, their protein content were quantified using the BCA method. For this, 5 µL of each sample at a 1:20 dilution in RIPA buffer were incubated with the BCA reagent. It was left incubating for 30 min at 37°C. Then, the absorbance was read at 495 nm. Additionally, a BSA standard curve (ranging from 2 to 0.03125 mg/mL) was prepared to extrapolate the absorbance and determine the protein concentration of the isolated exosomes (Figure 165). All samples were measured in triplicate.

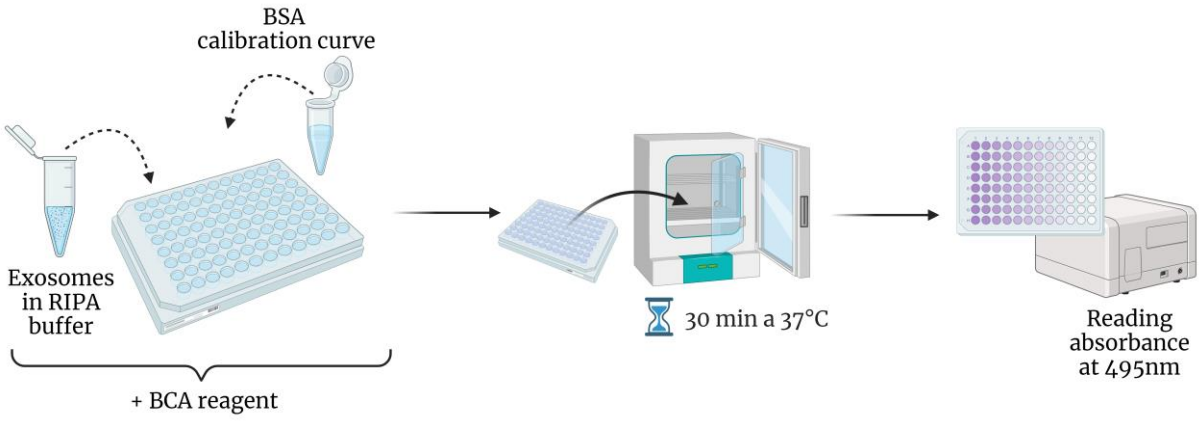

Figure 165. Procedure to carry out the BCA. Created with BioRender.com.

5.2.3.1.3 Neuronal exosome immunoprecipitation

For the immunoprecipitation, 3.5 mg of total protein is required. Knowing the concentration of each sample, the necessary volume of exosomes in PBS (without lysis) was measured to obtain 3.5 mg of each sample and adjusted to a final volume of 500 µL.

The samples were mixed with 10 µL of Protein A/G PLUS-Agarose (Santa Cruz Biotechnology, Dallas, USA) to remove nonspecific bindings. They were left incubating for 1 hour in the refrigerator at 4°C with agitation. Then, they were centrifuged at 5300 rpm for 5 min at 4°C to remove the agarose.

The supernatants were collected and transferred to new Eppendorf tubes. Phosphatase and protease inhibitors were added, followed by 4 µL of the anti- L1CAM (αL1CAM) monoclonal Ab (Sigma-Aldrich). They were incubated ON at 4°C with agitation.

After incubation, 40 µL of Protein A/G PLUS-Agarose was added and left for 2 hours with agitation at 4°C. Then, they were centrifuged for 5 min at 5300 rpm at 4°C. After this incubation, the supernatants were removed, leaving the pellet to elute the exosomes from the agarose binding.

For elution, 25 µL of glycine-HCl at pH 3 was added, and the mixture was vortexed for 40 s. Next, 5 µL of Tris-HCl at pH 7.5 was quickly added to adjust the solution's pH suitable for proteins. Subsequently, 20 µL of RIPA buffer heated to 37°C was added to lyse the exosomes.

This solution was passed through the columns to retain the agarose on the filter and collect the exosome lysate. The 50 µL of the lysate was placed in the column and centrifuged at 8000 rpm for 5 min at 4°C, thus collecting the lysate of the neuronal exosomes (Figure 166).

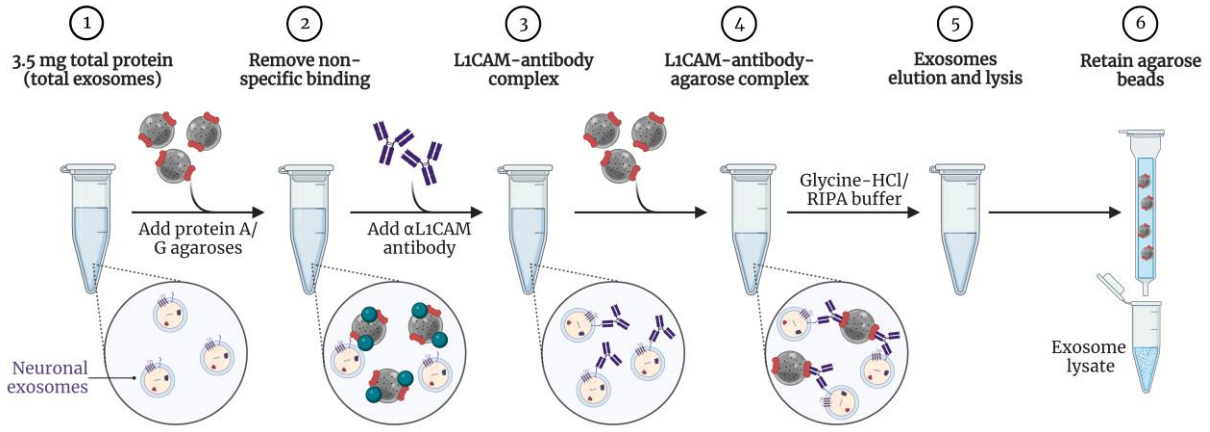

Figure 166. Neuronal exosome immunoprecipitation. Created with BioRender.com.

5.2.3.1.4 Protein quantification of neuronal exosomes

The lysate obtained from the immunoprecipitation was quantified using the BCA method. In this case, 5 µL of each sample at a 1:10 dilution was used. The procedure followed for this quantification was the same as that used to quantify the total exosomes. All samples were measured in triplicates.

5.2.3.1.5 ELISAs to determine different biomarkers in total and neuronal exosomes

ELISA plates were coated with anti-$A\beta_{42}$ Ab ($\alpha A\beta_{42}$) (Biolegend, SD, USA) at 20 µg/mL (100 µL/well) in carbonate buffer at pH 9.6 ON at 4°C. After washes with PBS-T 0.05%, they were blocked with 2% BSA in dilution buffer for 2 hours at RT. After repeated washes, the samples (total exosomes and neuronal exosomes in RIPA buffer) were incubated ON at 4°C. The plates were washed again, and anti-$A\beta_{16}$-biotin ($\alpha A\beta_{16}$-biotin) (Biolegend) Ab was incubated at 1 µg/mL (100 µL/well) in dilution buffer and allowed to incubate for 2 hours at RT. After washes, STV-HRP was incubated at 0.2 µg/mL for 1 hour at RT. Finally, the TMB substrate was incubated for 15 min at RT in the dark and the reaction was stopped with 2 N HCl. OD was read at 450nm.

To determine the $A\beta_{40}$ peptide, the same type of ELISA was performed, changing the capping Ab for anti-$A\beta_{40}$ ($\alpha A\beta_{40}$) (Biolegend). The rest of the conditions were kept the same (Figure 167).

Other plates were immobilized with the αTau Ab at 1:1000 (50 µL/well) ON at 4°C. The blocking steps were the same for all ELISAs. Samples were then incubated under the same conditions and developed with another polyclonal αTau Ab (Sigma-Aldrich) (1:1000) for 2 hours at RT. Subsequently an αRabbit-IgG-HRP was incubated at 1:5000 for 1 hour at RT. The development process with TMB was the same as described above (Figure 168).

Finally, the total and neuronal exosome samples were incubated directly on ELISA plates to determine lactoferrin. After incubation of the ON samples at 4°C and the blocking step, the αLactoferrin-biotin Ab was incubated 1:10000 (100 µl/well) for 2 hours at RT and revealed as previously described for Aβ42 (Figure 169).

All ELISAs performed were qualitative and not quantitative and the measurements were performed in triplicates.

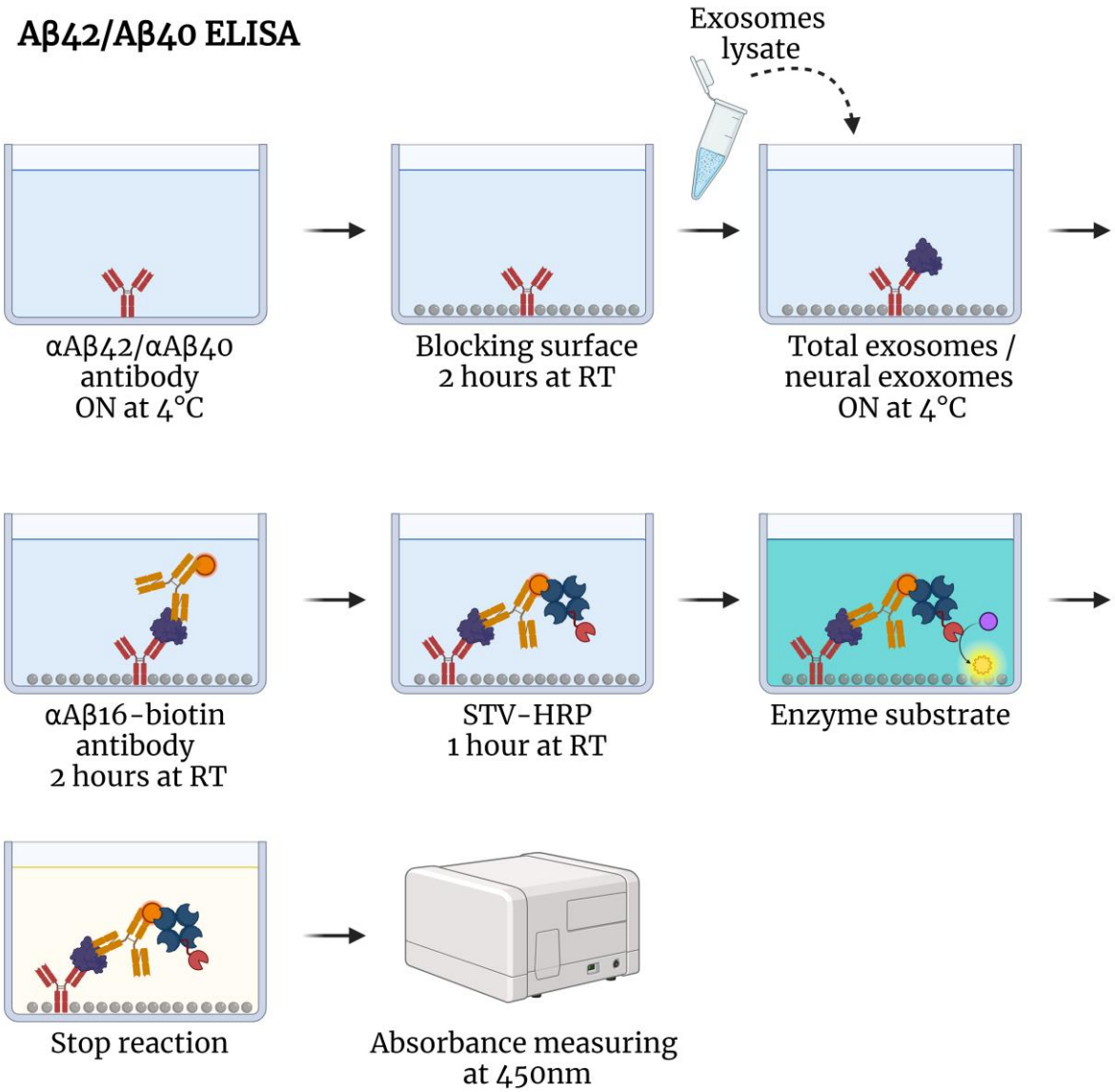

Figure 167. Protocol performed for qualitative ELISAs of markers in total and neuronal exosomes for Aβ$_{42/40}$ peptide. Created with BioRender.com.

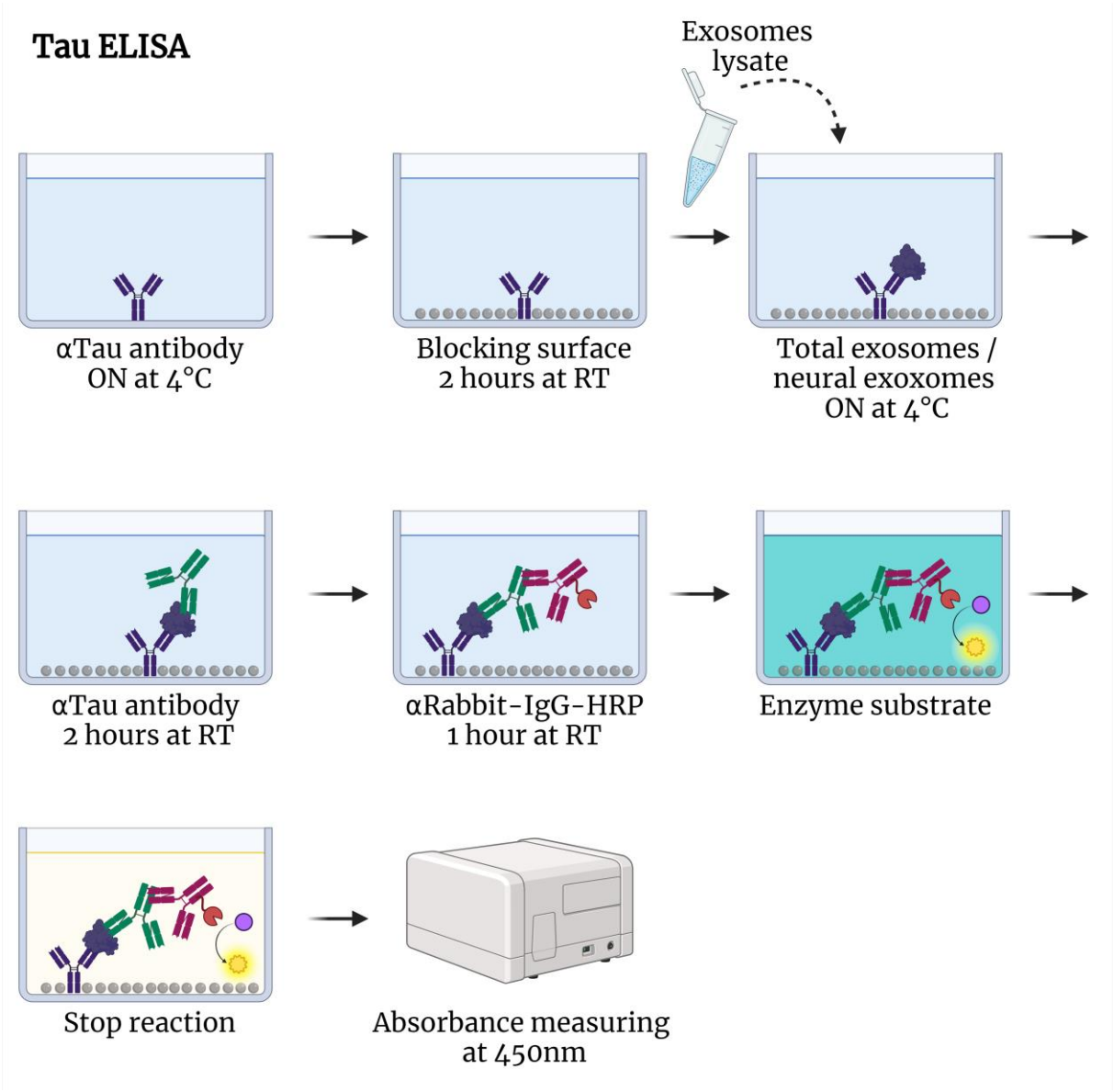

Figure 168. Protocol performed for qualitative ELISAs of markers in total and neuronal exosomes for tau protein. Created with BioRender.com.

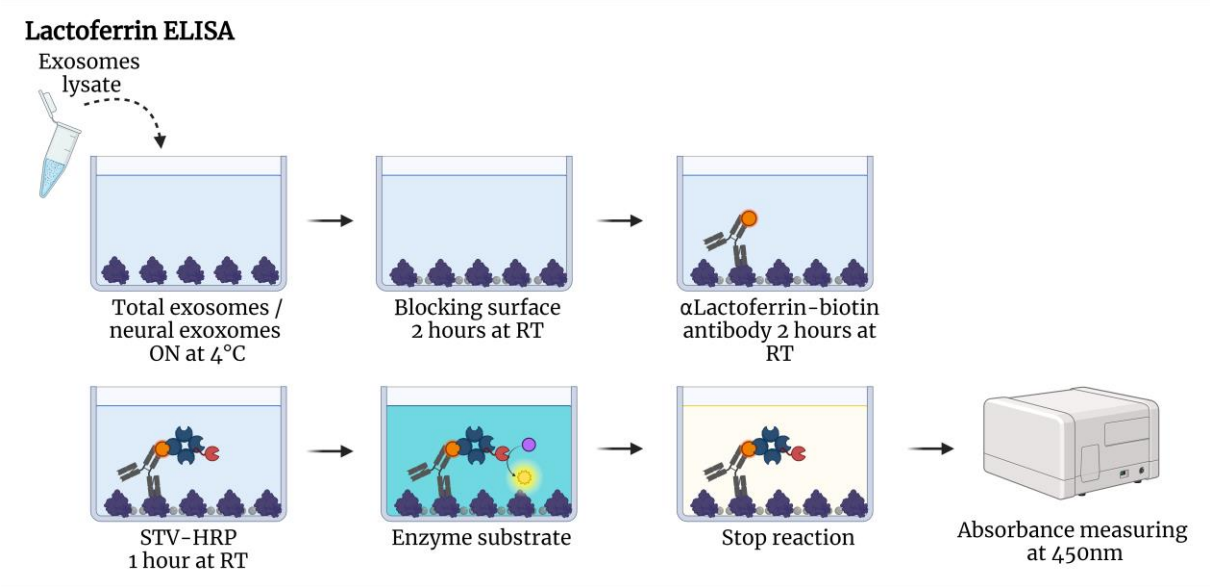

Figure 169. Protocol performed for qualitative ELISAs of markers in total and neuronal exosomes for lactoferrin protein. Created with BioRender.com.

5.2.3.2. *Results*

5.2.3.2.1 Exosomes isolation from human serum samples

Five human serum samples were used to exosomes isolation. Once isolated, a portion was separated for possible characterization analyses (such as quantification and size determination), another portion of the isolated total exosomes was diluted in RIPA buffer to release their content, and the rest were saved to separate the neuronal exosomes (Figure 170).

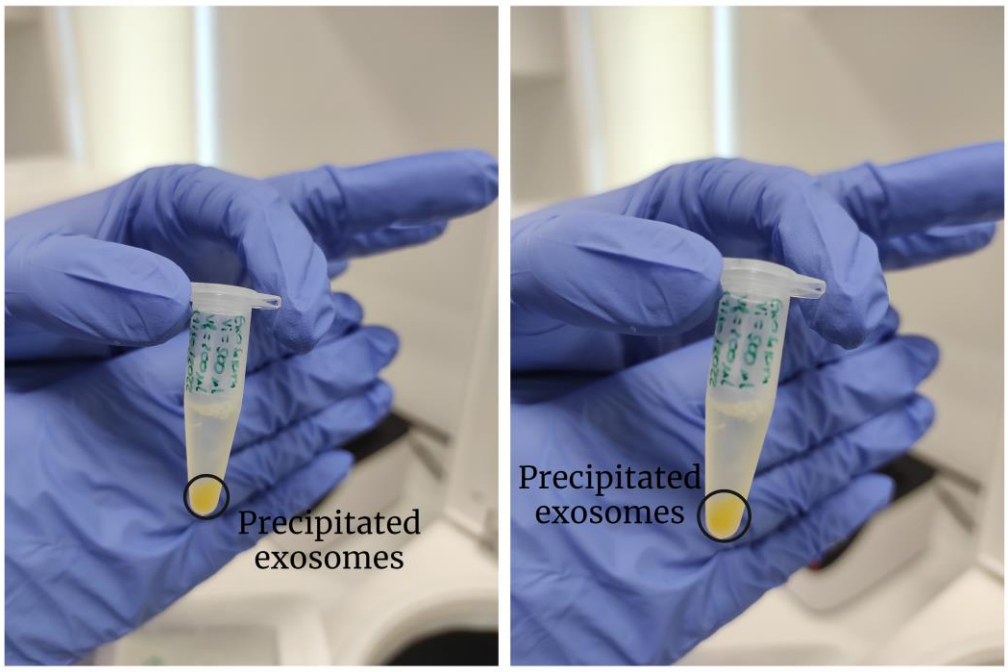

Figure 170. Exosomes precipitated from serum samples.

In addition, after isolation, a small fraction was diluted to measure their concentration in the DLS in addition to their size. The data obtained for the concentration are represented in Table 40. **The size of the isolated exosomes was found to be in the range of 35-80nm**.

Table 40. Concentration of total exosomes measured in DLS after isolation.

	Concentration (nº exosomes/mL)
Exosomes 1	4.8×10^{13}
Exosomes 2	3.58×10^{14}
Exosomes 3	3.80×10^{16}
Exosomes 4	6.67×10^{16}
Exosomes 5	2.67×10^{17}

5.2.3.2.2 Total protein exosome quantification

To determine the amount of protein content in the exosomes, they were lysed and quantified by BCA. For this purpose, a BSA standard curve was made with the aim of extrapolating the OD data on the straight line (Figure 171).

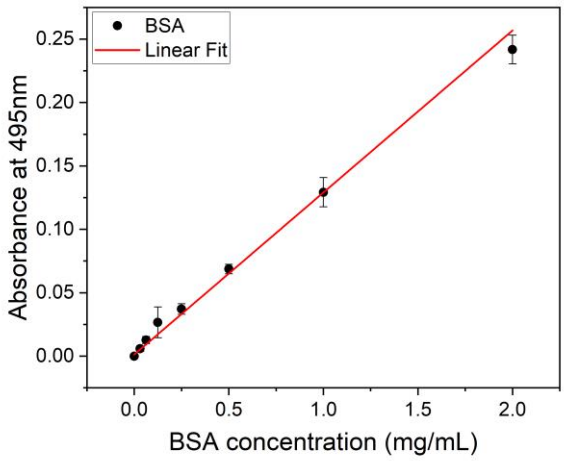

Figure 171. BSA standard curve.

After extrapolation, the protein concentration data of the isolated total exosomes are shown in Table 41.

Table 41. Total protein concentration of isolated total exosomes.

	DO at 495nm	*Protein concentration (mg/mL)*	*mg of total protein*
Exosomes 1	0.1776	28.75	5.75
Exosomes 2	0.1781	28.84	5.77
Exosomes 3	0.1397	22.45	4.49
Exosomes 4	0.1784	28.88	5.78
Exosomes 5	0.2003	32.53	6.51

Having the data on the number of total exosomes and the amount of total protein, **we can calculate the protein/exosome ratio** (Table 42). This is interesting because there is literature that suggests that there may be no difference in the number of exosomes produced in AD, but **there is a difference in the amount of protein they contain or the type of protein content.**

Table 42. Protein per exosome ratio.

	Concentration (nº exosomes/mL)	*Protein concentration (mg/mL)*	*Ratio protein concentration (mg)/ exosome*
Exosomes 1	4.8×10^{13}	28.75	5.99×10^{13}
Exosomes 2	3.58×10^{14}	28.84	8.06×10^{14}
Exosomes 3	3.80×10^{16}	22.45	5.91×10^{16}
Exosomes 4	6.67×10^{16}	28.88	4.33×10^{16}
Exosomes 5	2.67×10^{17}	32.53	1.22×10^{16}

Considering the results, **differences are observed between the samples in the amount of protein content per exosome**, which could be very interesting data to analyze by expanding the sample size, since the analyses performed gave promising results.

5.2.3.2.3 Neuronal exosome immunoprecipitation

From the total exosomes, a fraction (corresponding to 3.5 mg of total protein) was used to immunoprecipitate neuronal exosomes. This was possible thanks to the L1CAM marker, which is a transmembrane protein expressed by exosomes from the brain. **In this way it is possible to determine the concentration of the proteins of interest that really have neuronal origin** and that do not come from the exosomes of cells found in the blood coming from other organs. Although it must be considered that they are found in much lower concentration.

On the other hand, once the immunoprecipitation is performed, part of the characterization cannot be performed, since **the same protocol for separating the neuronal exosomes involves breaking them**, so that neither their concentration by DLS or the size of the exosomes can be determined.

5.2.3.2.4 Protein quantification of neuronal exosomes

After the immunoprecipitation that allowed the separation of neuronal exosomes, the protein content of this fraction of exosomes was quantified following the same procedure as for the total exosomes.

Thus, after extrapolation on the BSA curve, the concentrations of protein of neuronal origin were obtained (Table 43).

Table 43. Protein concentration from immunoprecipitated neuronal exosomes.

	DO at 495nm	*Protein concentration (mg/mL)*	*mg of total protein*
Exosomes 1	0.1776	1.491	0.119
Exosomes 2	0.1781	1.722	0.138
Exosomes 3	0.1397	1.514	0.121
Exosomes 4	0.1784	2.273	0.182
Exosomes 5	0.2003	1.070	0.086

In this case, **it was not possible to calculate the amount of protein per exosome since these cannot be quantified**, but the protein concentration calculated above for total exosomes can be related to the concentration of exosomes of neural origin (Table 44).

Table 44. Ratio of protein from neuronal exosomes to total exosomes.

	mg of total protein of total exosomes	*mg of total protein of neuronal exosomes*	*Ratio (%) protein neuronal exosomes / total exosomes*
Exosomes 1	5.75	0.119	2.073
Exosomes 2	5.77	0.138	2.388
Exosomes 3	4.49	0.121	2.698
Exosomes 4	5.78	0.182	3.147
Exosomes 5	6.51	0.086	1.315

If we analyze the results, **we also observe that there is a difference between the samples in the calculated ratio**, with the two samples with the highest ratio coinciding with those with the highest amount of protein per exosome. Moreover, as we can see, this does not correlate with the total number of exosomes obtained, or with the protein concentration of total exosomes. Therefore, this data could also be very interesting, since within the theories of the functions of the exosomes, **it is described in the literature that one of their functions could be the clearance of the Aβ peptide** in the brain and for this reason those exosomes with neuronal origin could be appearing in serum with a greater amount of protein.

The isolation of total exosomes from human serum samples, quantification of their total protein and its concentration by DLS was achieved. From total exosomes it was possible to isolate exosomes of neuronal origin by immunoprecipitation and their protein content was quantified.

5.2.3.2.5 ELISAs to determine different markers in total and neuronal exosomes

ELISAs were performed to determine different AD-related markers in isolated exosomes (total and neuronal) such as $A\beta_{40}$ peptide, $A\beta_{42}$ peptide, tau protein and lactoferrin protein.

The results of these ELISAs are presented qualitatively rather than quantitatively, although a standard line was carried on each ELISA plate. This is because the objective when they were performed was not to quantify, but to test the capacity we had to measure these markers in both types of exosomes and to know the range of concentrations in which each marker was found.

In the case of the $A\beta_{42}$ marker, we obtained detectable levels for all samples in both types of exosomes as well as for the determination of lactoferrin. For the $A\beta_{40}$ marker, some of the samples were at the detection limit, while for tau protein it could not be detected in any of the samples due to problems in the experiment (Table 45).

Table 45. Summary of detectable markers of in total and neuronal exosomes.

	Aβ42	***Aβ40***	***Tau protein***	***Lactoferrin protein***
Exosomes 1	detectable	at detection limit	undetectable	detectable
Exosomes 2	detectable	at detection limit	undetectable	detectable
Exosomes 3	detectable	detectable	undetectable	detectable
Exosomes 4	detectable	detectable	undetectable	detectable
Exosomes 5	detectable	detectable	undetectable	detectable

The results obtained were very promising to be able to observe concentration differences in the markers that could be detected.

We tested the possibility of measuring different markers of AD by ELISA in total exosomes and those of neuronal origin, obtaining detectable signals for the markers Aβ42, Aβ40, and lactoferrin protein.

5.2.4. Conclusions

The most important conclusions obtained during the experiments carried out in the proof of concept of exosome isolation are summarized as follows:

- We can highlight that **we were able to replicate the exosome isolation protocol learned during the stay**.
- Once isolated, **we were able to quantify them and know their concentration and size**. This allowed us to know the amount of protein/exosome in the samples analyzed.
- **We were able to isolate the exosomes of neuronal origin** and perform protein quantification of these and relate this amount of protein with the calculated number of total exosomes.
- Finally, **qualitative ELISAs of different markers related to AD were performed**, of which three were detectable in both types of exosomes. Based on these results, ELISA protocols for each type of marker and the range of concentrations in which they are found would have to be established in order to adequately quantify the samples. In addition, it would be necessary to perform tests for the ELISA for detection of the tau protein.

6. Sensor sensitivity enhancement system

6.1. Introduction

Immunoassays rely on the use of Abs due to their ability to specifically recognize a particular analyte. As they form the foundation of recognition systems in both conventional assays and biosensor applications, an essential step to consider is surface immobilization.

Abs, upon immobilization, **can assume four types of orientations: end-on Fab-up, end-on Fab-down, flat-on, or side-on**. Another influential factor to consider is the Ab concentration used, as excessively high concentrations can favor multilayer formation, adversely affecting the Ab's analyte recognition (Susini et al., 2023)(Figure 172).

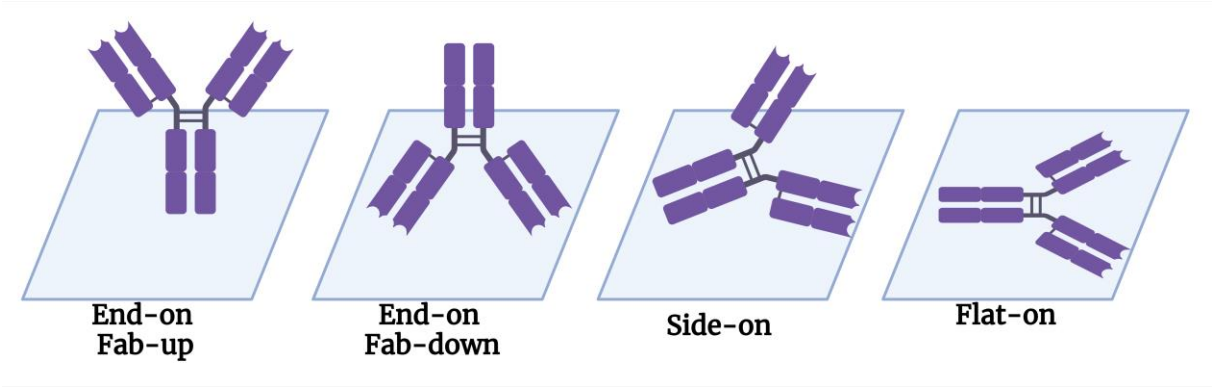

Figure 172. Possible Ab orientation in immobilization. Created with BioRender.com.

Various techniques exist for Ab immobilization. For instance, in the case of polystyrene plates, they undergo treatments to enable hydrophilic groups on the surface to interact with carbohydrates found in the Fc region of the Ab (Welch et al., 2017).

However, these surface immobilization methods still present the same problem of Ab orientation. **When Abs are positioned in the four ways described earlier, the Ab recognition function is affected**. Actually, **only 5-10% of Ag-binding sites are available when no strategy is employed to orient Ab immobilization** (Butler et al., 1992). Hence, orienting Abs to the end-on Fab-up position is crucial to enhance system sensitivity.

One of the first methods described to achieve Ab orientation is the covalent binding of carboxyl or amino groups of Abs with a chemically activated surface (Dixit et al., 2011; Lu et al., 1995)(Figure 173A). However, due to the widespread distribution of these groups throughout the Ab structure, it did not result in a well-controlled orientation (Gao et al., 2022).

Another method used for orientation involves proteins that have binding specificity against the Fc region of Abs, such as A-protein and G-protein. These proteins specifically bind to aa residues found between the two C domains of the Fc (C2 and C3) of mammalian IgGs (Deisenhofer, 1981; Sauer-eriksson et al., 1995)(Figure 173B).

Another way to achieve the best orientation is by immobilizing Abs using disulfide bridges found in the hinge region. These disulfide bridges are reduced by various agents, resulting in two monovalent Abs that are immobilized in an oriented manner on the surface, enhancing system sensitivity and reproducibility (Baniukevic et al., 2013; Ho et al., 2010)(Figure 173C).

Plasma O_2 treatments can also be employed to modify the surface and create active groups capable of interacting with Abs. Three-dimensional substrates can enhance sensitivity due to their extensive surface area. Additionally, peptides and aptamers specific to the Fc region of Abs exist and can be used for their orientation (Welch et al., 2017)(Figure 173D).

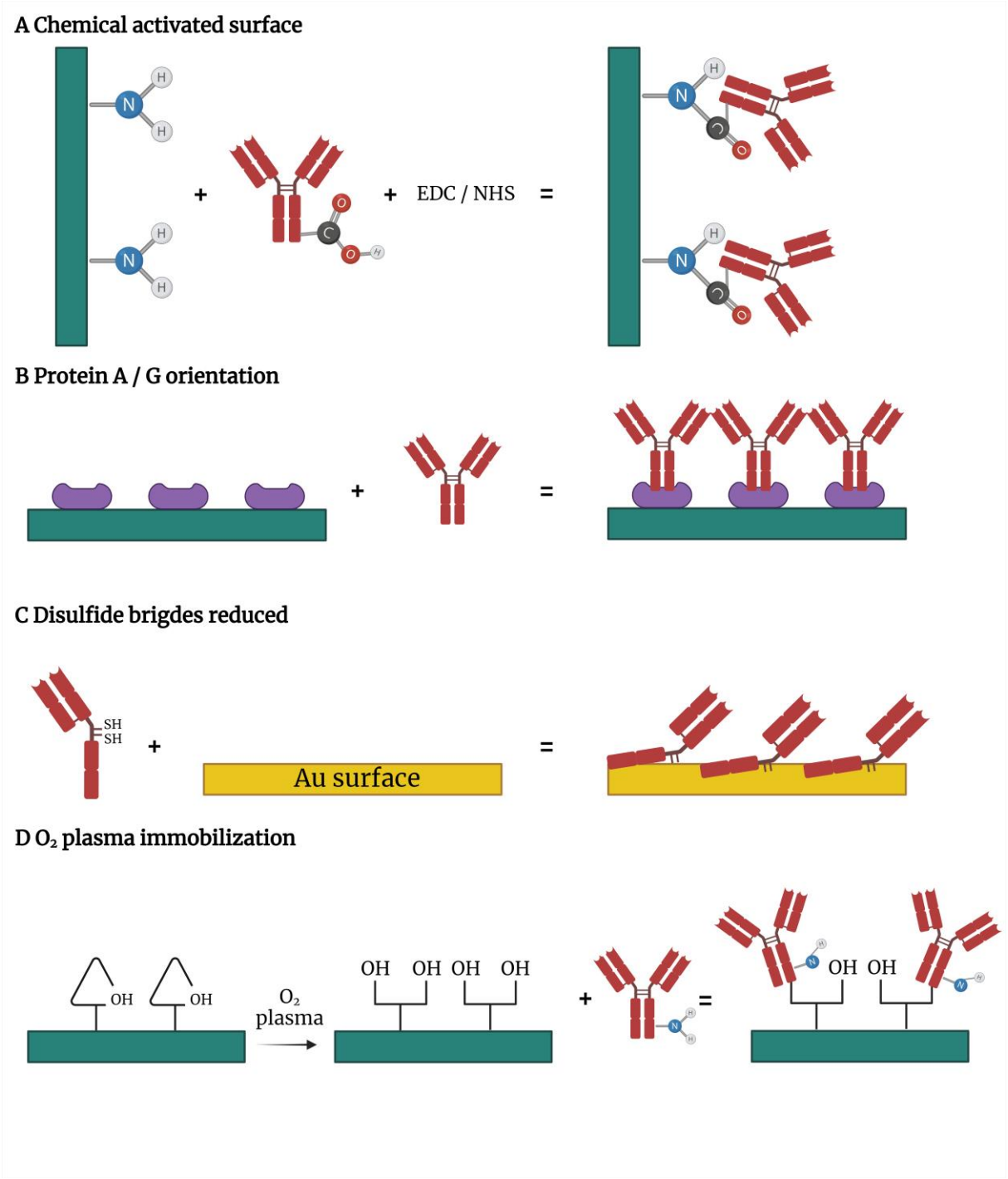

Figure 173. Ab immobilization strategies. A. By chemical activation of the surface. **B.** Use of G or A proteins by binding to the Fc of the Abs. **C.** Reduction of the disulfide bridges of the Abs for binding to the Au surface. **D.** Activation of the surface with O_2 plasma to bind the Abs. Created with BioRender.com.

Finally, there's the system based on the interaction between biotin and STV, which was employed during the development of this thesis and is detailed in the following section.

6.2. Biotin-STV system

Biosensors have been increasingly developed and have had a growing impact on society and clinical diagnostics. However, **in many applications, achieving very high sensitivity and specificity is necessary**. One of the limiting factors is the **biofunctionalization of surfaces with Abs in an oriented manner to avoid losing active Ag binding sites**, as specificity relies on the bioreceptors anchored to the surface, and sensitivity depends on how well-optimized that anchoring process is (Welch et al., 2017).

One of the systems used **to achieve this orientation relies on the interaction of biotin**, also known as vitamin B7, **with STV protein**, which originates from the bacterium *Streptomyces avidinii*. STV is a homotetrameric protein with a molecular weight of 56 g/mol, **capable of binding to four biotin molecules**, thus **enhancing system sensitivity and providing signal amplification** (Dundas et al., 2013; Wilchek & Bayer, 1990). Furthermore, STV exhibits high specificity for biotin, boasting **the highest known affinity constant among biological reactions, with $K_a = 10^{15}\ M^{-1}$** (I. H. Cho et al., 2007; Delgadillo et al., 2019; Wilchek & Bayer, 1990).

The biotin-STV binding is the strongest non-covalent interaction and **remains irreversible even under extreme pH or temperature conditions, or when using organic or denaturing solvents** (Gao et al., 2022). This enables the use of this system in diverse diagnostic applications due to its versatility and stability.

Hence, for its application, the sensor surface will be coated with STV, and the Ab will be biotinylated to bind to the surface. **It has been demonstrated in various studies that using this random biotinylation system increases the availability of Ab binding sites by up to 70%** (Morgan & Taylor, 1992; Rowe et al., 1999)(Figure 174).

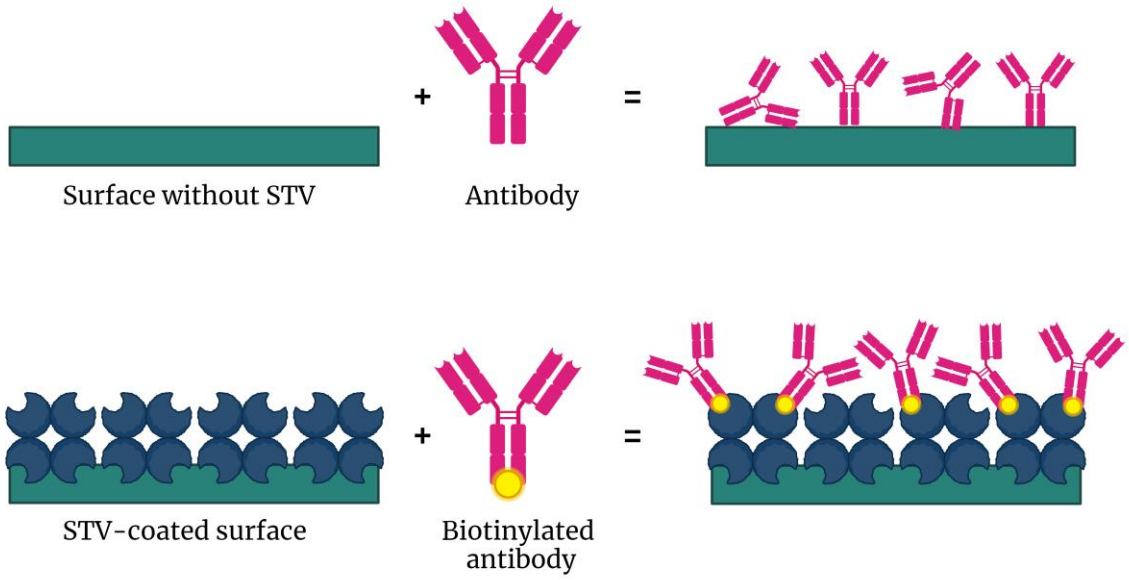

Figure 174. Comparison between immobilization without STV and with the biotin-STV system. Created with BioRender.com.

Therefore, to use this system, a preliminary step is necessary in which the Abs will be biotinylated, meaning that biotin molecules are anchored to them through processes that can be either chemical or enzymatic (Dundas et al., 2013). **The attachment of these molecules can occur with different functional groups of the Ab, such as carboxyls or amines** (I. H. Cho et al., 2007).

This process can be carried out in two ways, **either in a non-directed manner** (biotin will be added throughout the entire Ab) **or in a targeted manner,** such as to the sulfhydryl groups of the hinge region, potentially increasing the Ab's recognition capacity by up to 20 times compared to non-directed biotinylation (I. H. Cho et al., 2007). Moreover, **the binding of these molecules typically does not affect the biological activity of the biotinylated molecules or their physical characteristics** (Wilchek & Bayer, 1990).

One of the chemical methods for **biotinylating molecules is based on NHS esters of biotin**, which provides **non-directed biotinylation**. When this compound is mixed with Abs, it reacts with the primary amines of lysine residues found throughout the Ab structure, forming stable amide-type bonds (Shioya et al., 2022)(Figure 175).

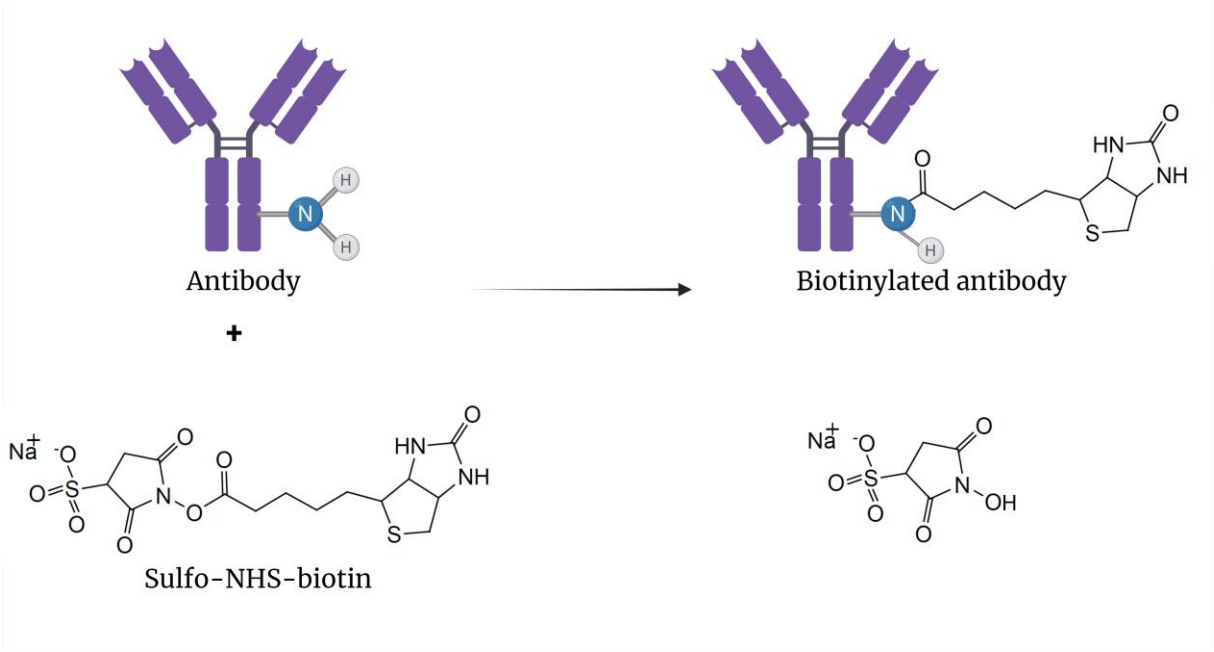

Figure 175. Biotinylation reaction using sulfo-NHS-biotin reagent. Created with BioRender.com.

Therefore, the objective addressed in this thesis **was to optimize a protocol for biotinylating Abs and studying their stability to enhance the biosensor's sensitivity used throughout the study**. Different biotinylation ratios were tested, and the biotinylation was quantified. Subsequently, the stability over time and under different conditions of this process was studied using the ELISA technique. Finally, immunoassays were performed on the biosensor to quantify the BSA protein using the biotin-STV system and without using it **to compare the detection sensitivity**.

6.3. Materials and methods

6.3.1. αBSA Ab biotinylation

The compound EZ-Link Sulfo-NHS-Biotin (Thermo Fisher) was used to perform the biotinylation of the αBSA Ab. Biotinylation was tested at ratios of 1:10, 1:20, and 1:50 to select the best Ab:biotin relationship. For this, 100 µL of αBSA at a concentration of 6.2 mg/mL was mixed with the different selected ratios, establishing the biotin concentration at 10 mM. Once mixed, they were incubated for 40 min at RT and subsequently for 1 hour at 4°C with agitation.

After the reaction is complete, it is necessary to remove all unbound biotin from the solution. For this purpose, all mixtures were passed through Zeba Spin Desalting Columns with a MWCO of 7 kDa (Thermo Fisher). This yields the biotinylated αBSA Ab at a concentration of 0.62 mg/mL.

To compare the biotinylation obtained between the different ratios used, it was quantified using the Pierce Biotin Quantitation Kit (Thermo Fisher). Ten microliters of the HABA (4´-hydroxyazobenzene-2-carboxylic acid)-Avidin reagent were mixed with 160 µL of PBS at pH 7.4, and absorbance at 500 nm was measured, denoted as A_{500} HABA/Avidin after a 15 min reaction. Then, 20 µL of αBSA-biotin Ab at different ratios (in triplicate) were added, and as a PC, biotinylated-HRP enzyme supplied by the manufacturer was added. Subsequently, absorbance was again measured at 500 nm after a 15 min reaction, denoted as A_{500} HABA/Avidin/biotin sample. Once these data were obtained, using the HABA Calculator available on the Thermo Fisher website, the number of biotins bound to the Ab was calculated (Murillo et al., 2023)(Figure 176).

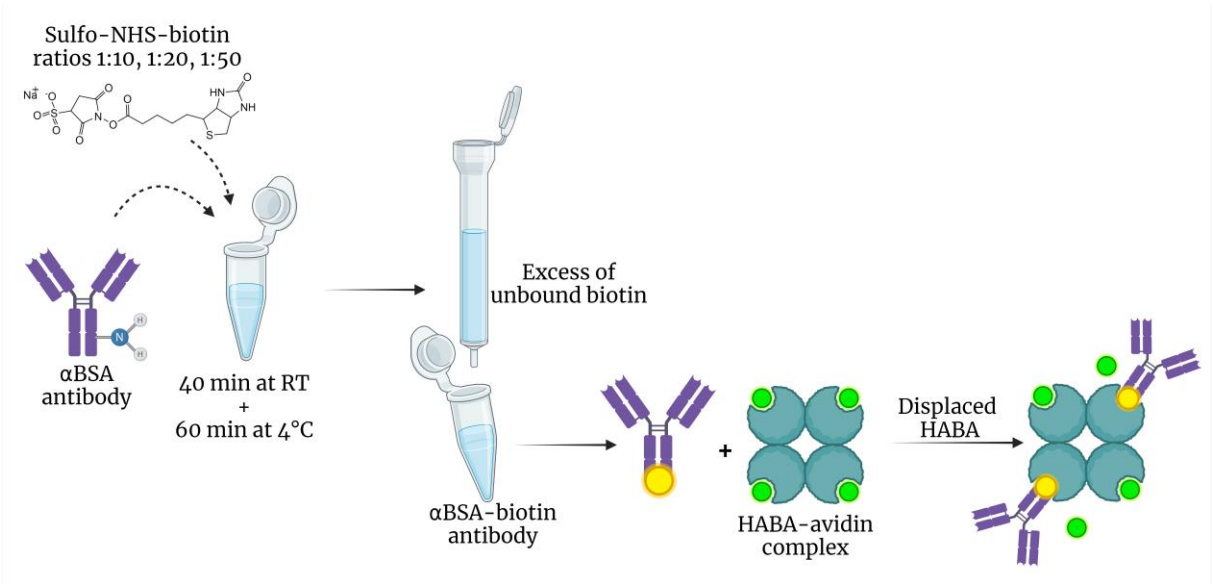

Figure 176. Biotinylation and quantification process using HABA-avidin reagent. Created with BioRender.com.

6.3.2. Control tests

To verify the biotinylation and proper functioning of the Ab post-biotinylation, ELISA plates were coated with BSA protein (50 µL/well) at various concentrations to generate a standard curve from 5 mg/mL to 0.00032 mg/mL following 1:5 dilutions in carbonate buffer at pH 9.6. Plates were left ON at 4°C and subsequently blocked with 200 µL of 1x casein hydrolysate for 1 hour at RT.

After three washes with PBS-T 0.05%, the αBSA-biotin (from the three ratios) was incubated at 1:5000 (50 µL/well) for 1 hour at RT. As a PC, a rabbit polyclonal Ab against BSA at 1:1500 was incubated under the same time and temperature conditions. Washes were repeated, and then STV-HRP at 0.2 mg/mL (50 µL/well) was added to the wells incubated with αBSA-biotin, while in the wells incubated with αBSA without biotin, an αRabbit-IgG-HRP Ab at 1:12000 was added. This incubation was completed in 1 hour at RT.

Finally, after three washes, the reaction was developed using TMB substrate by adding 75 µL/well and incubating it in darkness for 15 min. The reaction was stopped with 75 µL/well of 2 N HCl, and absorbance was read at 450 nm. All points on the curve were performed in triplicate (Murillo et al., 2023).

6.3.3. Stability tests

To study the stability of the biotinylation process over time, the αBSA-biotin Ab (1:10, 1:20, and 1:50) was stored under two different conditions. Aliquots were stored in a refrigerator at 4°C, while others were kept in the freezer at -20°C. ELISAs were conducted at 15, 30, and 90 days for both storage conditions following the procedure described in the previous section (Murillo et al., 2023).

6.3.4. Comparison tests on the biosensor

To compare the sensitivity of the sensor using and not using the biotin-STV system, 65-BICELLs KITs with a 200 µm diameter were used. Parallel assays were conducted, where arrays were coated with the αBSA Ab by depositing 1.5 µL per cell at a concentration of 0.62 µg/mL for 3 hours at 37°C in a humid chamber, followed by ON incubation at 4°C. Other arrays were incubated with the STV protein at 500 µg/mL under the same conditions.

After washing with H_2OmQ, in the KITs coated with the αBSA Ab, BSA protein was incubated in a concentration range from 1000 µg/mL to 3.9 µg/mL following 1:2 dilutions, depositing 1.5 µL/cell and incubating for 2 hours at 37°C in a humid chamber. In the arrays coated with STV, αBSA-biotin at a ratio 20 at 0.62 µg/mL was incubated under the same conditions.

Finally, the arrays incubated with αBSA-biotin at a ratio 20 were incubated with BSA protein following the same conditions and concentration range as the arrays without STV. After each of the described incubation steps, the values of ΔIROP (%) were measured (Murillo et al., 2023).

6.3.5. Correlation assays between ELISA and IODM

To compare the results obtained through IODM with the ELISA technique in terms of sensitivity, a sandwich ELISA was conducted. Plates were coated with 50 µL per well of a polyclonal αBSA Ab (Thermo Fisher) in carbonate buffer at pH 9.6 at a dilution of 1:1000 at 4°C ON. Three washes of 200 µL/well were done with PBS-T 0.05%, followed by blocking with 200 µL/well of 1x casein hydrolysate for 1 hour at RT. After washing, the BSA protein was incubated from a concentration of 15 µg/mL down to 0.03 µg/mL in 1:5 dilutions (100 µL/well) for 2 hours at RT. The washes were repeated, and αBSA-biotin at a ratio 20 was incubated at 1:1500 (50 µL/well) for 2 hours at RT. Finally, STV-HRP at 0.2 µg/mL (100 µL/well) was added and left for 1 hour at RT. The reaction was developed with 75 µL/well of TMB, and the reaction was stopped with an equal volume of 2 N HCl. Absorbance was measured at 450 nm, and all measurements were performed in triplicates (Murillo et al., 2023).

6.4. Results

6.4.1. αBSA Ab biotinylation

After carrying out the biotinylation protocol with the αBSA Ab at different tested ratios (1:10, 1:20, and 1:50), **the biotinylation was quantified to study and compare between ratios and select the most suitable one**. For this purpose, the Pierce Biotin Quantitation Kit was used. This kit is based on the HABA reagent, which allows estimating the molar ratio of biotin per protein, in this case, the Ab. This is because when the biotinylated Ab is mixed with the HABA-Avidin compound, the biotin bound to the Ab competes for binding sites on avidin with the HABA compound, displacing HABA due to the high affinity of biotin for avidin. This displacement results in a decrease in absorbance at 500 nm. Therefore, by measuring absorbance at 500 nm before and after the mixture, along with the molecular weight and concentration of the biotinylated Ab, the number of biotin molecules per Ab can be determined. Calculations were performed using the HABA Calculator and are summarized in Table 46.

Table 46. Quantification obtained through the Pierce Biotin Quantitation Kit (Murillo et al., 2023)**.**

	Positive control	***Ratio 10***	***Ratio 20***	***Ratio 50***
Initial absorbance (500nm)	0.655	0.6841	0.6419	0.6543
Final absorbance (500nm)	0.552	0.6015	0.6001	0.6159
ΔAbsorbance (500nm)	0.103	0.0826	0.0418	0.0384
Molecular weight (g/mol)	40000	150000	150000	150000
Concentration (mg/mL)	1	6.2	6.2	6.2
Biotin molecules per IgG molecule	2	1	6	5

Once the number of biotin molecules per Ab was calculated, **it was observed that using the 1:20 ratio resulted in the highest number of biotin molecules (6 per Ab).** In comparison to the 1:50 ratio, there isn't much difference, but it's important to consider that this is a signal amplification system, and that difference could have significant consequences. However, **there's a noticeable contrast with the 1:10 ratio,** where only one biotin molecule attaches per Ab. This quantification method helps establish which ratio could be best for the protocol and to verify that biotinylation is occurring correctly. These data are validated by the PC, as the obtained result for this control aligns with the manufacturer's specifications.

6.4.2. Control tests

Although the quantification assays showed that the 1:20 ratio provided a higher number of biotin molecules per Ab, all three ratios were tested to confirm their proper functioning and to determine which one yielded the best signal. To determine this, direct ELISAs were performed, and as a PC, another direct ELISA was conducted using the non-biotinylated αBSA Ab.

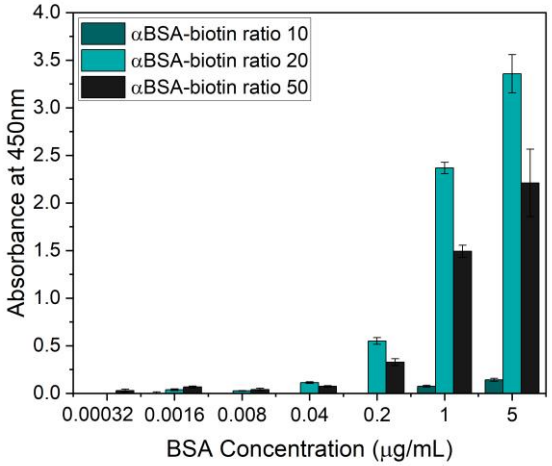

Figure 177. ELISAs using the αBSA-biotin Ab at the different ratios (Murillo et al., 2023)**.**

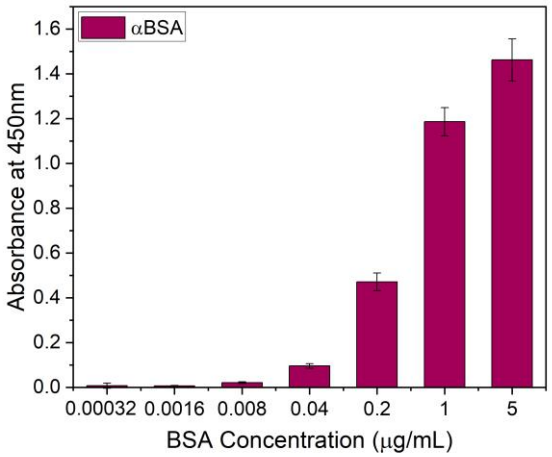

Figure 178. ELISA to determine BSA concentration using the αBSA Ab without biotinylation (Murillo et al., 2023)**.**

If we compare Figures 177 and 178, **we observe a higher absorbance signal when using biotinylated Abs,** nearly three times greater. This is due to the amplification provided by the biotin-STV system. Looking at Figure 177 and comparing the signals from different ratios, **it's noticeable that the highest absorbance signal is obtained with the biotinylated Ab at a 1:20 ratio**, which aligns with the quantification data obtained. Considering the results of these ELISAs, it was decided not to use αBSA-biotin ratio 1:10 in subsequent experiments as the signal was too low.

Biotinylation of the αBSA Ab was performed at different ratios and quantified, obtaining a better biotinylation with the 1:20 ratio. After testing these Abs by ELISA, better results were obtaining with the Ab biotinylated at 1:20.

6.4.3. Stability tests

The αBSA-biotin Ab at ratios of 1:20 and 1:50 was aliquoted and these aliquots were stored under two different conditions. Half of them were kept in the refrigerator at 4°C, while the others were stored in the freezer at -20°C. To verify the stability of the biotinylation protocol and determine the optimal storage method, direct ELISAs were conducted at 15, 30, and 90 days of storage.

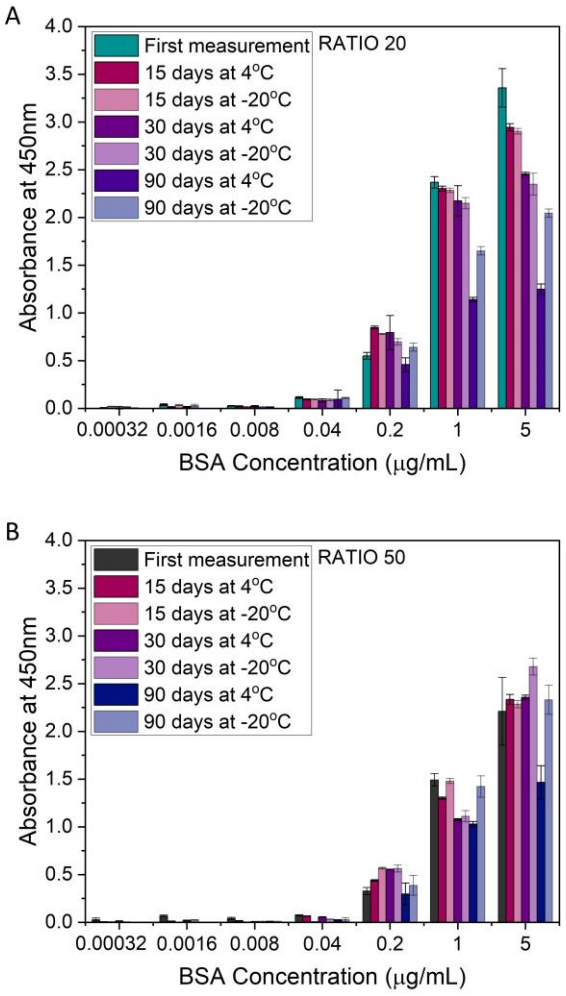

Figure 179. ELISAs to study biotinylated stability. A. ELISAs performed with the αBSA-biotin Ab Ab ratio 20. **B.** ELISAs performed αBSA-biotin Ab ratio 50 (Murillo et al., 2023).

Comparing Figures 179A and 179B, as observed in previous results, the signal remains consistently higher when revealed with the αBSA-biotin Ab at a 1:20 ratio. Additionally, for both ratios, **it's evident that the signal decreases over time under both storage conditions (4°C and -20°C), with consistently higher signal retention observed at -20°C**. Therefore, based on these results, **it can be confirmed that after 90 days, biotinylation remains relatively stable**, although some signal loss is observed. Furthermore, **the optimal way to preserve biotinylated samples appears to be at -20°C.**

Once ELISAs were performed at 15, 30 and 90 days after biotinylation, it was observed that the best way to store the biotinylated Abs were at -20°C, confirming that the 1:20 ratio gave the best results.

6.4.4. Comparison tests on the biosensor

Once the optimal biotinylation ratio was established and its functionality was tested in ELISA, assays were conducted using the kits. For this purpose, 65-BICELLs KITs were selected, with half of them coated with αBSA without biotinylation and the other half coated with the STV protein and αBSA-biotin to compare the biosensor's sensitivity. Once the surfaces were prepared with the Ab, BSA protein at various concentrations was incubated, and the ΔIROP (%) signal obtained was compared for both scenarios.

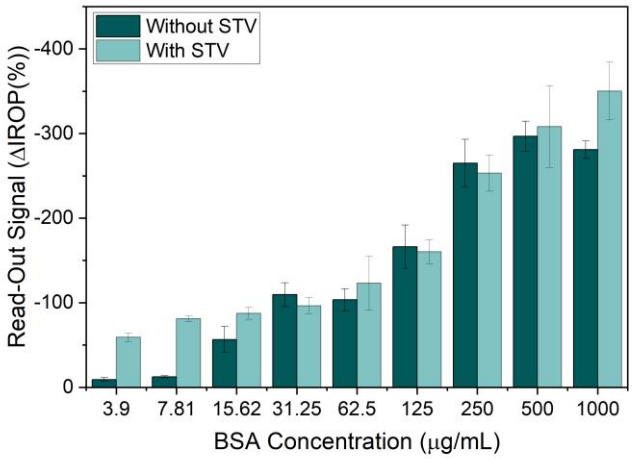

Figure 180. Comparison of the sensitivity of the sensor with and without STV surface coating for the detection of BSA protein (Murillo et al., 2023)**.**

The data in Figure 180 indicates that the ΔIROP (%) signal obtained was higher when the biosensor surface was coated with STV, particularly at lower concentrations, where measurement without this system is nearly impossible. **This enhanced sensitivity allows us to detect concentrations as low as 3.9 µg/mL of BSA (equivalent to 5.9 ng in total) compared to 15.62 µg/mL (23 ng total) without utilizing the biotin-STV system. This enhancement in detection sensitivity is at least fourfold**.

6.4.5. Correlation assays between ELISA and IODM

To compare the sensitivity achieved between IODM and the ELISA technique, sandwich ELISAs were conducted to ensure the same assay configuration. The ELISA plates were coated with the αBSA Ab to detect various concentrations of BSA (15 µg/mL to 0.03 µg/mL).

An important factor to consider when comparing the two techniques is the difference in the volume utilized **(100 µL per well in ELISA versus 1.5 µL per cell in the KIT).** To compare sensitivity, the total protein amount within these volumes was used rather than concentration. **Considering this, 100 µL at 15 µg/mL equals a total of 1.5 µg of BSA, equivalent to the initial concentration measured by the biosensor at 1.5 µL and 1000 µg/mL, amounting to 1.5 µg total BSA**.

Dilutions were then prepared from this starting concentration to establish a calibration curve.

Figure 181 represents the correlation obtained from ELISA and IODM. **Comparing both techniques, the biotin-STV system utilized in the biosensor enables detection limits comparable to the well-established ELISA technique**. However, **it's important to highlight that IODM detects concentration directly without the need for a secondary Ab**, thereby reducing the number of protocol steps, required time, reagent consumption, and sample quantity.

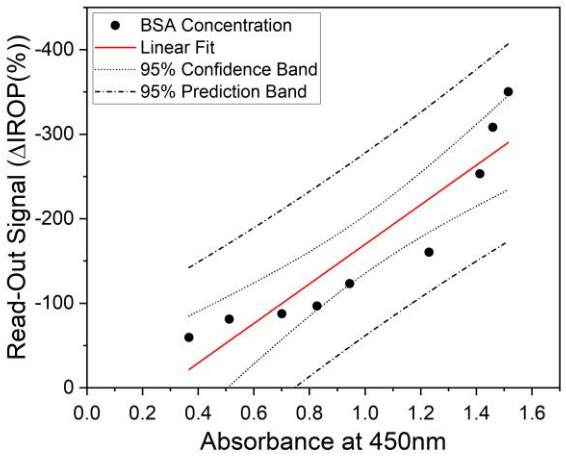

Figure 181. Correlation between ELISA and IODM measurements in KITs using the biotin-STV system (Murillo et al., 2023)**.**

Thanks to the use of the biotinylated Ab on the surface of the biosensor coated with STV, it was possible to improve the detection sensitivity up to almost 4 times, comparing this sensitivity with that obtained with the ELISA.

6.5. Conclusions

The most important conclusions obtained during the experiments carried out on the use of the biotin-STV system to obtain a higher sensitivity in the sensor are as follows:

- This work successfully **established a biotinylation protocol for Abs with the most suitable ratio for our method (1:20),** yielding the best results across all conducted experiments.

- The study on biotinylation **stability revealed its efficacy for up to 90 days**, potentially lasting longer, especially **when stored at the most favorable condition of -20°C in the freezer.**

- The research demonstrated that **the biosensor's sensitivity was enhanced through increased Ag binding sites availability due to the application of the biotin- STV system**. This led to a significantly improved sensor surface, allowing the detection of lower analyte concentrations through signal amplification. It **exhibited at least a fourfold sensitivity enhancement** compared to the assay conducted without the STV surface.

- Comparatively, when this method is juxtaposed with ELISA, **the biotin-STV system allowed us to reach ELISA's detection limits**.

- It's essential to note the advantages offered by this biosensor type, **enabling direct detection without the need for secondary Abs or chemical developers**. This results in fewer steps during the protocol, **reducing the time required to obtain results**. Additionally, it utilizes much smaller sample quantities, enabling multiplexing of the KIT and the simultaneous measurement of numerous markers with minimal sample amounts.

7. General conclusions

This section summarizes the **general and main conclusions** of this work that have been explained in each of the sections:

- Firstly, during the development of this thesis **several biological applications for a new technology have been demonstrated**, covering all the steps of the value chain, from the fabrication of the diagnostic KITs, their functionalization with O_2 plasma avoiding H_2SO_4, the measurement equipment, the biofunctionalization of the NPs and the determinations of different proteins in real samples (serum and saliva). The results obtained by IODM were verified with well-established techniques such as the ELISA technique.

- For the case study of COVID-19, **it was possible to develop a multiplexed detection system of specific Abs in serum against SARS-CoV-2**. Being one of the first research groups to start with the development of a valid system for this purpose. Thus, it was possible to measure 74 samples from people who had passed the disease with different degrees of severity (mild, moderate and severe) and to determine the levels of **sIgT and sIgG, sIgM and sIgA**, finding differences in the values of Igs for each LSC. In addition, in all these samples we also measured two markers related to COVID-19, **such as FTH1 and CRP**, **finding differences in FTH1 levels** between the different LSCs, but, however, there were no differences in CRP levels. After having all these data, a model could be made to study how each of the markers affected the severity of the disease, **the most important of which were sIgT and FTH1.** This objective is a **significant advance in advanced in-vitro diagnostics**, where automation is a very important factor that allows us to save time and errors. In addition, multiplex assays can facilitate and accelerate the diagnosis of different diseases.

- Similarly, **this system could be followed to determine sIgA in saliva against SARS-CoV-2**, thanks to which a pilot study could be carried out at the UPM on the prevalence of SARS-CoV-2 by studying the levels of sIgA in the saliva of volunteers for 3 months.

- In both cases (serum and saliva) **the signals obtained by IODM were correlated with the ELISA technique, obtaining a good linear fit for both sample types**.

- In the case of the study of AD, different advances have been achieved for the determination of biomarkers related to the disease. To this end, **we were first able to establish a protocol for biofunctionalization of SiO_2 NPs with the different Abs of interest**, in addition to using commercial NPs.

- **Thanks to the use of NPs, it was possible to detect tau protein by competitive assay in PBS and serum, reaching a LoD of 10 pg/mL**

- In addition, by using these NPs, **it was also possible to measure the marker lactoferrin in saliva and compare the concentrations obtained with those measured by ELISA**, obtaining very similar lactoferrin concentration data between both techniques used.

- Finally, **these NPs were also used to measure the pTau181 protein in sera from the hamster model and the transgenic mice**, observing differences between the different states of the model (control, arousal and torpor).

- Thus, the versatility of NPs has been demonstrated in order to measure different biomarkers and in different types of samples, despite their matrix effect. **It has also corroborated the possible use of this technology and this type of biosensor in the clinic for the diagnosis and monitoring of different diseases**.

- During the realization of this doctoral thesis, **a stay at the University of Aveiro was carried out**, **where exosome isolation and characterization techniques were learned.** This knowledge was transferred to the laboratory of the research group where the first tests were performed, and **it was determined that the protocol learned could be replicated and that from these isolated total exosomes we were also able to separate those of neuronal type**. After performing the isolation technique and its characterization by DLS, we also tested whether **AD biomarkers could be measured in both types of exosomes, obtaining positive and promising values for the markers $A\beta_{42}$, $A\beta_{40}$ and lactoferrin**.

- Finally, we studied how to improve the sensitivity of the biosensor by using the biotin-STV system. For this purpose, **Abs were biotinylated by studying their stability and the best biotinylation ratio**. After establishing these parameters, the sensitivity of the biosensor was compared by covering the sensing surface with STV and without covering to determine the concentration of BSA, with which it was observed that **the sensitivity was improved by almost four times when using the biotin-STV system, reaching the LoD of the ELISA technique without the use of NPs**.

8. Future research lines

After the research carried out during the doctoral thesis, progress has been made in several aspects, but also new areas and lines of research have been discovered such as:

- **The development of different diagnostic KITs for other diseases**. Due to the high versatility of the sensor and the technology used, many opportunities open up in the diagnostic field after testing its performance during this thesis. **In addition to further improving the diagnostic KITs already developed**.
- **The improvement and extension of NPS biofunctionalization protocols.** During this work, many changes have been made in the protocols for their optimization, but even so, for example, the number of NPs lost during the process is very high, so the technique should be further refined for higher performance. On the other hand, **it would be very interesting to try with NPs of other materials or with surfaces that have other modifications** in order to implement new biofunctionalization protocols in the research group.
- In collaboration with other research groups such as the Cajal Institute, the concentration of pTau181 protein in the sera of Syrian hamsters and transgenic mice should be determined. **It would be very important to validate and compare these data with those obtained by other techniques such as ELISA or WB**, in addition to being able **to increase the number of individuals in the study**.
- Another collaboration was with Fernando Maestu's group who gave us saliva samples for the determination of lactoferrin. This also opens the way **to study a new marker and to perform a much more complex analysis since the samples come from family members with and without a history of AD** and allows a study of the probability of suffering the disease and to know how many years before the symptoms begin to manifest the first biochemical changes. Because of this, it would also be interesting to measure different markers in the serum of these same individuals and to perform a population analysis with all these data and their genotyping of the APOE4 gene.
- **Another line of research that opens up after the tests performed is the study of exosomes**. Exosomes have proved to be a great source of information in different pathological stages. One of those addressed in this thesis is AD, **but their implication is also important in other pathologies**. Due to the lack of time, the work with exosomes has been brief so that ELISAs for determining exosomal biomarkers could be fine-tuned to be quantitative and after this, move on to measure these markers in the sensor. **This would have the ultimate goal of being able to develop a multiplexed KIT of markers of AD or other pathology found in exosomes**. In addition, characterization techniques for these could be expanded. It would also be interesting to isolate exosomes from other

types of samples such as saliva.

- To extend the study of sensitivity enhancement in the sensor. **In this thesis, two very different strategies are addressed, on the one hand the use of NPs and on the other hand the surface modification with STV to anchor biotinylated Abs**. Both techniques have been shown to improve sensitivity, but other strategies, such as targeted biotinylation or Abs reduction, among others, could be tested to compare the sensitivity between the different approaches.

9. Bibliography

9.1. Publications by the author

Murillo, A. M. M., Tomé-Amat, J., Ramírez, Y., Garrido-Arandia, M., Valle, L. G., Hernández-Ramírez, G., Tramarin, L., Herreros, P., Santamaría, B., Díaz-Perales, A., & Holgado, M. (2021). Developing an Optical Interferometric Detection Method based biosensor for detecting specific SARS-CoV-2 immunoglobulins in Serum and Saliva, and their corresponding ELISA correlation. *Sensors and Actuators, B: Chemical*, *345*. https://doi.org/10.1016/j.snb.2021.130394

Murillo, A. M. M., Valle, L. G., Ramírez, Y., Sánchez, M. J., Santamaría, B., Molina-Roldan, E., Ortega-Madueño, I., Urcelay, E., Tramarin, L., Herreros, P., Díaz-Perales, A., Garrido-Arandia, M., Tome-Amat, J., Hernández-Ramírez, G., Espinosa, R. L., Laguna, M. F., & Holgado, M. (2022). Integration of Multiple Interferometers in Highly Multiplexed Diagnostic KITs to Evaluate Several Biomarkers of COVID-19 in Serum. *Biosensors*, *12*(9). https://doi.org/10.3390/bios12090671

Tramarin, L., Casquel, R., Gil-Rostra, J., González-Martínez, M. A., Herrero-Labrador, R., Murillo, A. M. M., Laguna, M. F., Bañuls, M.J., González-Elipe, A. R., & Holgado, M. (2022). Design and Characterization of ITO-Covered Resonant Nanopillars for Dual Optical and Electrochemical Sensing. *Chemosensors*, 10*(10),*393. https://doi.org/10.3390/chemosensors10100393

Pioz, M.J., Espinosa, R.L., Laguna, M.F., Santamaria, B., Murillo, A.M.M., Hueros, Á.L., Quintero, S., Tramarin, L., Valle, L.G., Herreros, P., Bellido, A., Casquel, R., & Holgado, M. (2022). A review of Optical Point-of-Care devices to Estimate the Technology Transfer of These Cutting-Edge Technologies. *Biosensors*, *12*, 1091. https://doi.org/10.3390/bios12121091

Murillo, A. M. M., Laguna, M. F., Valle, L. G., Tramarin, L., Ramirez, Y., Lavín, Á., Santamaría, B., & Holgado, M. (2023). A New Optical Interferometric Biosensing System Enhanced with Nanoparticles for Alzheimer's Disease in Serum. *Biosensors*, *13*(7), 1–15. https://doi.org/10.3390/bios13070707

Murillo, A. M. M., Holgado, M., & Laguna, M. (2023). Reports on the sensitivity enhancement in interferometric based biosensors by biotin-streptavidin system. *Heliyon*, *9*(12), e23123. https://doi.org/10.1016/j.heliyon.2023.e23123

9.2. References

Abeysinghe, A. A. D. T., Deshapriya, R. D. U. S., & Udawatte, C. (2020). Alzheimer's disease; a review of the pathophysiological basis and therapeutic interventions. *Life Sciences*, *256*(April), 117996. https://doi.org/10.1016/j.lfs.2020.117996

Ackermann, H.-W. (2005). Bacteriophage taxonomy Ha. *Microbiology Australia*, *32*, 90–94. https://health.uni-hohenheim.de/fileadmin/einrichtungen/gesundheitswissenschaften/Downloads/Bacteriophages_Taxonomy_2011-Ackermann.pdf

Adedeji, J. B., Adaramodu, M. O., Iseoluwa, J. O., Ayodeji, E. A., Ajibola, Y. I., Babatunde, S. A., Bolaji, B. T., Gbadegesin, L. A., Akinyemi, T. O., Odoh, C. K., Umeobi, H. U., & Adeoye, A. B.-E. (2021). Therapeutic drugs for SARS-CoV-2 treatment: Current state and perspective. *International Immunopharmacology*, *90*, 1–19. https://doi.org/10.1016/j.intimp.2020.107228

Ahsan, H. (2022). Monoplex and multiplex immunoassays: approval, advancements, and alternatives. *Comparative Clinical Pathology*, *31*(2), 333–345. https://doi.org/10.1007/s00580-021-03302-4

Akib, T. B. A., Mou, S. F., Rahman, M. M., Rana, M. M., Islam, M. R., Mehedi, I. M., Parvez Mahmud, M. A., & Kouzani, A. Z. (2021). Design and numerical analysis of a graphene-coated spr biosensor for rapid detection of the novel coronavirus. *Sensors*, *21*(10), 1–21. https://doi.org/10.3390/s21103491

Akobeng, A. K. (2007). Understanding diagnostic tests 1: Sensitivity, specificity and predictive values. *Acta Paediatrica, International Journal of Paediatrics*, *96*(3), 338–341. https://doi.org/10.1111/j.1651-2227.2006.00180.x

Ali, L., Mohammed, M. U., Khan, M., Yousuf, A. H. Bin, & Chowdhury, M. H. (2020). High-Quality Optical Ring Resonator-Based Biosensor for Cancer Detection. *IEEE Sensors Journal*, *20*(4), 1867–1875. https://doi.org/10.1109/JSEN.2019.2950664

Ali, M. A., Hu, C., Jahan, S., Yuan, B., Saleh, M. S., Ju, E., Gao, S. J., & Panat, R. (2021). Sensing of COVID-19 Antibodies in Seconds via Aerosol Jet Nanoprinted Reduced-Graphene-Oxide-Coated 3D Electrodes. *Advanced Materials*, *33*(7), 1–15. https://doi.org/10.1002/adma.202006647

Alzhrani, G. N., Alanazi, S. T., Alsharif, S. Y., Albalawi, A. M., Alsharif, A. A., Abdel-Maksoud, M. S., & Elsherbiny, N. (2021). Exosomes: Isolation, characterization, and biomedical applications. *Cell Biology International*, *45*(9), 1807–1831. https://doi.org/10.1002/cbin.11620

Anaya, J.-M., Shoenfeld, Y., Rojas-Villarraga, A., Levy, R. A., & Cervera, R. (Eds.). (2013). *AUTOIMMUNITY From Bench to Bedside*. El Rosario University Press.

Andersen, M. H., Schrama, D., Straten, P. T., & Becker, J. C. (2006). Cytotoxic T cells. *Journal of Investigative Dermatology*, *126*, 32–41. https://doi.org/10.1038/sj.jid5700001

Anhoj, T. A., Jorgensen, A. M., Zauner, D. A., & Hübner, J. (2006). The effect of soft bake temperature on the polymerization of SU-8 photoresist. *Journal of Micromechanics and Microengineering*, *16*, 1819–1824. https://doi.org/10.1088/0960-1317/16/9/009

Anoop, A., Singh, P. K., Jacob, R. S., & Maji, S. K. (2010). CSF biomarkers for Alzheimer's disease diagnosis. *International Journal of Alzheimer's Disease*, *2010*, 1–13. https://doi.org/10.4061/2010/606802

Arendt, T., & Bullmann, T. (2013). Neuronal plasticity in hibernation and the proposed role of the microtubule-associated protein tau as a "master switch" regulating synaptic gain in neuronal networks. *American Journal of Physiology - Regulatory Integrative and Comparative Physiology*, *305*(5), 478–489. https://doi.org/10.1152/ajpregu.00117.2013

Arendt, T., Stieler, J., Strijkstra, A. M., Hut, R. A., Rüdiger, J., Van der Zee, E. A., Harkany, T., Holzer, M., & Härtig, W. (2003). Reversible paired helical filament-like phosphorylation of tau is an adaptive process associated with neuronal plasticity in hibernating animals. *Journal of Neuroscience*, *23*(18), 6972–6981. https://doi.org/10.1523/jneurosci.23-18-06972.2003

Arya, R., Kumari, S., Pandey, B., Mistry, H., Bihani, S. C., Das, A., Prashar, V., Gupta, G. D., Panicker, L., & Kumar, M. (2021). Structural insights into SARS-CoV-2 proteins. *Journal of Molecular Biology*, *233*(January), 1–25. https://doi.org/10.1016/j.jmb.2020.11.024

Ashrafian, H., Zadeh, E. H., & Khan, R. H. (2021). Review on Alzheimer's disease: Inhibition of amyloid beta and tau tangle formation. *International Journal of Biological Macromolecules*, *167*, 382–394. https://doi.org/10.1016/j.ijbiomac.2020.11.192

Ausó, E., Gómez-Vicente, V., & Esquiva, G. (2020). Biomarkers for alzheimer's disease early diagnosis. *Journal of Personalized Medicine*, *10*(3), 1–27. https://doi.org/10.3390/jpm10030114

Austin, J., Minelli, C., Hamilton, D., Wywijas, M., & Jones, H. J. (2020). Nanoparticle number concentration measurements by multi-angle dynamic light scattering. *Journal of Nanoparticle Research*, *22*(5). https://doi.org/10.1007/s11051-020-04840-8

Avvakumova, S., Colombo, M., Tortora, P., & Prosperi, D. (2014). Biotechnological approaches toward nanoparticle biofunctionalization. *Trends in Biotechnology*, *32*(1), 11–20. https://doi.org/10.1016/j.tibtech.2013.09.006

Babamiri, B., Salimi, A., & Hallaj, R. (2018). A molecularly imprinted electrochemiluminescence sensor for ultrasensitive HIV-1 gene detection using EuS nanocrystals as luminophore. *Biosensors and Bioelectronics*, *117*(June), 332–339. https://doi.org/10.1016/j.bios.2018.06.003

Bagwe, R. P., Hilliard, L. R., & Tan, W. (2006). Surface modification of silica nanoparticles to reduce aggregation and nonspecific binding. *Langmuir*, *22*(9), 4357–4362. https://doi.org/10.1021/la052797j

Baniukevic, J., Hakki Boyaci, I., Goktug Bozkurt, A., Tamer, U., Ramanavicius, A., & Ramanaviciene, A. (2013). Magnetic gold nanoparticles in SERS-based sandwich immunoassay for antigen detection by well oriented antibodies. *Biosensors and Bioelectronics*, *43*(1), 281–288. https://doi.org/10.1016/j.bios.2012.12.014

Baron, S. (Ed.). (1996). Viral Pathogenesis. In *Medical Microbiology*. University of Texas.

Barros, M. H. M., Hauck, F., Dreyer, J. H., Kempkes, B., & Niedobitek, G. (2013). Macrophage polarisation: An immunohistochemical approach for identifying M1 and M2 macrophages. *PLoS ONE*, *8*(11), 1–11. https://doi.org/10.1371/journal.pone.0080908

Battaglini, D., Lopes-Pacheco, M., Castro-Faria-Neto, H. C., Pelosi, P., & Rocco, P. R. M. (2022). Laboratory Biomarkers for Diagnosis and Prognosis in COVID-19. *Frontiers in Immunology*, *13*(April), 1–11. https://doi.org/10.3389/fimmu.2022.857573

Baxter, D. (2007). Active and passive immunity, vaccine types, excipients and licensing. *Occupational Medicine*, *57*(8), 552–556. https://doi.org/10.1093/occmed/kqm110

Benmerkhi, A., Bouchemat, M., & Bouchemat, T. (2020). Design of two-dimensional photonic crystal biosensor using DNA detection. *Phosphorus, Sulfur and Silicon and the Related Elements*, *195*(11), 960–964. https://doi.org/10.1080/10426507.2020.1804206

Bermejo-Pareja, F., del Ser, T., Valentí, M., de la Fuente, M., Bartolome, F., & Carro, E. (2020). Salivary lactoferrin as biomarker for Alzheimer's disease: Brain-immunity interactions. *Alzheimer's and Dementia*, *16*(8), 1196–1204. https://doi.org/10.1002/alz.12107

Bhalla, N., Jolly, P., Formisano, N., & Estrela, P. (2016). Introduction to biosensors. *Essays in Biochemistry*, *60*, 1–8. https://doi.org/10.1042/EBC20150001

Blattman, J. N., Sourdive, D. J. D., Murali-Krishna, K., Ahmed, R., & Altman, J. D. (2000). Evolution of the T Cell Repertoire During Primary, Memory, and Recall Responses to Viral Infection. *The Journal of Immunology*, *165*(11), 6081–6090. https://doi.org/10.4049/jimmunol.165.11.6081

Blennow, K. (2004). Cerebrospinal Fluid Protein Biomarkers for Alzheimer's Disease. *NeuroRx: The Journal of the American Society for Experimental NeuroTherapeutics Cerebrospinal*, *1*(2), 213–225. https://doi.org/10.1602/neurorx.1.2.213

Bonilla, F. A., & Oettgen, H. C. (2010). Adaptive immunity. *Journal of Allergy and Clinical Immunology*, *125*(2 SUPPL. 2), S33–S40. https://doi.org/10.1016/j.jaci.2009.09.017

Boon, T., & Van der Bruggen, P. (1996). Human tumor antigens recognized by T lymphocytes. *Journal of Experimental Medicine*, *183*, 725–729. https://doi.org/10.1084/jem.183.3.725

Boonkaew, S., Chaiyo, S., Jampasa, S., Rengpipat, S., Siangproh, W., & Chailapakul, O. (2019). An origami paper-based electrochemical immunoassay for the C-reactive protein using a screen-printed carbon electrode modified with graphene and gold nanoparticles. *Microchimica Acta*, *186*(3), 1–10. https://doi.org/10.1007/s00604-019-3245-8

Boonkaew, S., Teengam, P., Jampasa, S., Rengpipat, S., Siangproh, W., & Chailapakul, O. (2020). Cost-effective paper-based electrochemical immunosensor using a label-free assay for sensitive detection of ferritin. *Analyst*, *145*(14), 5019–5026. https://doi.org/10.1039/d0an00564a

Born, M., & Wolf, E. (1999). Principles of Optics: electromagnetic theory of propagation, interference and diffraction of light. In *Cambridge* (7th expand). Cambridge University Press.

Bošnjak, B., Do, K. T. H., Förster, R., & Hammerschmidt, S. I. (2022). Imaging dendritic cell functions*. *Immunological Reviews*, *306*, 137–163. https://doi.org/10.1111/imr.13050

Bouftas, M. (2021). A Systematic Review on the Feasibility of Salivary Biomarkers for Alzheimer's Disease. *Journal of Prevention of Alzheimer's Disease*, *8*(1), 84–91. https://doi.org/10.14283/jpad.2020.57

Brandenburg, A., & Henninger, R. (1994). Integrated optical Young interferometer. *Applied Optics*, *33*(25), 5941–5947. https://doi.org/10.1364/ao.33.005941

Brandstadter, J. D., & Yang, Y. (2011). Natural killer cell responses to viral infection. *Journal of Innate Immunity*, *3*(3), 274–279. https://doi.org/10.1159/000324176

Budelier, M. M., & Bateman, R. J. (2020). Biomarkers of Alzheimer Disease. *Journal of Applied Laboratory Medicine*, *5*(1), 194–208. https://doi.org/10.1373/jalm.2019.030080

Bukowska-Ośko, I., Sulejczak, D., Kaczyńska, K., Kleczkowska, P., Kramkowski, K., Popiel, M., Wietrak, E., & Kowalczyk, P. (2022). Lactoferrin as a Human Genome "Guardian"—An Overall Point of View. *International Journal of Molecular Sciences*, *23*(9), 5248. https://doi.org/10.3390/ijms23095248

Burgler, S., Ouaked, N., Bassin, C., Ing, D., Basinski, T. M., Mantel, P. Y., Siegmund, K., Meyer, N., Akdis, C. A., & Schmidt-Weber, C. B. (2009). Differentiation and functional analysis of human TH17 cells. *Journal of Allergy and Clinical Immunology*, *123*(3), 588–595. https://doi.org/10.1016/j.jaci.2008.12.017

Burn, G. L., Foti, A., Marsman, G., Patel, D. F., & Zychlinsky, A. (2021). The Neutrophil. *Immunity*, *54*, 1377–1391. https://doi.org/10.1016/j.immuni.2021.06.006

Butler, J. E., Ni, L., Nessler, R., Joshi, K. S., Suter, M., Rosenberg, B., Chang, J., Brown, W. R., & Cantarero, L. A. (1992). The physical and functional behavior of capture antibodies adsorbed on polystyrene. *Journal of Immunological Methods*, *150*(1–2), 77–90. https://doi.org/10.1016/0022-1759(92)90066-3

Calabrò, M., Rinaldi, C., Santoro, G., & Crisafulli, C. (2021). The biological pathways of Alzheimer disease: a review. *AIMS Neuroscience*, *8*(1), 86–132. https://doi.org/10.3934/Neuroscience.2021005

Carlin, N., & Martic-Milne, S. (2018). Anti-Tau Antibodies Based Electrochemical Sensor for Detection of Tau Protein Biomarkers. *Journal of The Electrochemical Society*, *165*(12), G3018–G3025. https://doi.org/10.1149/2.0041812jes

Casquel, R., Holgado, M., Laguna, M. F., Hernández, A. L., Santamaría, B., Lavín, Á., Luca Tramarin, & Herreros, P. (2020). Engineering vertically interrogated interferometric sensors for optical label-free biosensing. *Analytical and Bioanalytical Chemistry*, *412*, 3285–3297. https://doi.org/10.1007/s00216-020-02411-3

Chaplin, D. D. (2006). Overview of the human immune response. *Journal of Allergy and Clinical Immunology*, *117*(2), 430–435. https://doi.org/10.1016/j.jaci.2005.09.034

Chappell, J. D., & Dermody, T. S. (2015). Biology of Viruses and Viral Diseases. *Principles and Practice of Infectious Diseases*, 1681–1693. https://doi.org/10.1016/B978-1-4557-4801-3.00134-X

Chen, G. F., Xu, T. H., Yan, Y., Zhou, Y. R., Jiang, Y., Melcher, K., & Xu, H. E. (2017). Amyloid beta: Structure, biology and structure-based therapeutic development. *Acta Pharmacologica Sinica*, *38*(9), 1205–1235. https://doi.org/10.1038/aps.2017.28

Chen, J., Li, P., Zhang, T., Xu, Z., Huang, X., Wang, R., & Du, L. (2022). Review on Strategies and Technologies for Exosome Isolation and Purification. *Frontiers in Bioengineering and Biotechnology*, *9*(January), 1–18. https://doi.org/10.3389/fbioe.2021.811971

Chiu, M. L., Goulet, D. R., Teplyakov, A., & Gilliland, G. L. (2019). Antibody structure and function: The basis for engineering therapeutics. *Antibodies*, *8*(4). https://doi.org/10.3390/antib8040055

Cho, E. J., Holback, H., Liu, K. C., Abouelmagd, S. A., Park, J., & Yeo, Y. (2013). Nanoparticle characterization: State of the art, challenges and emerging technologies. *Molecular Pharmaceutics*, *10*(6), 2093–2110. https://doi.org/10.1021/mp300697h

Cho, I. H., Paek, E. H., Lee, H., Kang, J. Y., Kim, T. S., & Paek, S. H. (2007). Site-directed biotinylation of antibodies for controlled immobilization on solid surfaces. *Analytical Biochemistry*, *365*(1), 14–23. https://doi.org/10.1016/j.ab.2007.02.028

Cohen, F. S. (2016). How Viruses Invade Cells. *Biophysical Journal*, *110*(5), 1028–1032. https://doi.org/10.1016/j.bpj.2016.02.006

Conde, J., Dias, J. T., Grazú, V., Moros, M., Baptista, P. V., & de la Fuente, J. M. (2014). Revisiting 30 years of biofunctionalization and surface chemistry of inorganic nanoparticles for nanomedicine. *Frontiers in Chemistry*, *2*(48), 1–27. https://doi.org/10.3389/fchem.2014.00048

Cooper, M. A., Elliott, J. M., Keyel, P. A., Yang, L., Carrero, J. A., & Yokoyama, W. M. (2009). Cytokine-induced memory-like natural killer cells. *Proceedings of the National Academy of Sciences of the United States of America*, *106*(6), 1915–1919. https://doi.org/10.1073/pnas.0813192106

Cruse, J. M., Lewis, R. E., & Wang, H. (2004). Cluster of Differentiation (CD) Antigens. In J. M. Cruse, R. E. Lewis, & H. Wang (Eds.), *Immunology Guidebook*. Elsevier. https://doi.org/10.1016/B978-012198382-6/50027-3

Cunin, P., & Nigrovic, P. A. (2019). Megakaryocytes as immune cells. *Journal of Leukocyte Biology*, *105*(6), 1111–1121. https://doi.org/10.1002/JLB.MR0718-261RR

Currie, L. A. (1995). Nomenclature in evaluation of analytical methods including detection and quantification capabilities (IUPAC Recommendations 1995). *Pure and Applied Chemistry*, *67*(10), 1699–1723. https://doi.org/10.1351/pac199567101699

Dai, Y., Chiu, L. Y., Chen, Y., Qin, S., Wu, X., & Liu, C. C. (2019). Neutral Charged Immunosensor Platform for Protein-based Biomarker Analysis with Enhanced Sensitivity. *ACS Sensors*, *4*(1), 161–169. https://doi.org/10.1021/acssensors.8b01126

Dale, D. C., Boxer, L., & Conrad Liles, W. (2008). The phagocytes: Neutrophils and monocytes. *Blood*, *112*, 935–945. https://doi.org/10.1182/blood-2007-12-077917

Damborský, P., Švitel, J., & Katrlík, J. (2016). Optical biosensors. *Essays in Biochemistry*, *60*, 91–100. https://doi.org/10.1042/EBC20150010

Deisenhofer, J. (1981). Crystallographic Refinement and Atomic Models of a Human Fc Fragment and Its Complex with Fragment B of Protein A from Staphylococcus aureus at 2.9- and 2.8-Å Resolution. *Biochemistry*, *20*(9), 2361–2370. https://doi.org/10.1021/bi00512a001

Del Campo, A., & Greiner, C. (2007). SU-8: A photoresist for high-aspect-ratio and 3D submicron lithography. *Journal of Micromechanics and Microengineering*, *17*, 81–95. https://doi.org/10.1088/0960-1317/17/6/R01

Delgadillo, R. F., Mueser, T. C., Zaleta-Rivera, K., Carnes, K. A., González-Valdez, J., & Parkhurst, L. J. (2019). Detailed characterization of the solution kinetics and thermodynamics of biotin, biocytin and HABA binding to avidin and streptavidin. In *PLoS ONE* (Vol. 14, Issue 2). https://doi.org/10.1371/JOURNAL.PONE.0204194

Delves, P. J., & Roitt, I. M. (2000). The immune system. First of two parts. *The New England Journal of Medicine*, *343*(1), 37–49. https://doi.org/10.1056/NEJM200007063430107

Derkus, B., Acar Bozkurt, P., Tulu, M., Emregul, K. C., Yucesan, C., & Emregul, E. (2017). Simultaneous quantification of Myelin Basic Protein and Tau proteins in cerebrospinal fluid and serum of Multiple Sclerosis patients using nanoimmunosensor. *Biosensors and Bioelectronics*, *89*(October 2016), 781–788. https://doi.org/10.1016/j.bios.2016.10.019

Dimitrov, D. S. (2004). Virus entry: Molecular mechanisms and biomedical applications. *Nature Reviews Microbiology*, *2*(2), 109–122. https://doi.org/10.1038/nrmicro817

Divya, J., Selvendran, S., & Sivanantha Raja, A. (2018). Photonic crystal-based optical biosensor: A brief investigation. *Laser Physics*, *28*, 1–8. https://doi.org/10.1088/1555-6611/aab7d2

Dixit, C. K., Vashist, S. K., MacCraith, B. D., & O'Kennedy, R. (2011). Multisubstrate-compatible ELISA procedures for rapid and high-sensitivity immunoassays. *Nature Protocols*, *6*(4), 439–445. https://doi.org/10.1038/nprot.2011.304

Doulatov, S., Notta, F., Laurenti, E., & Dick, J. E. (2012). Hematopoiesis: A human perspective. *Cell Stem Cell*, *10*(2), 120–136. https://doi.org/10.1016/j.stem.2012.01.006

Drosten, C., Seilmaier, M., Corman, V. M., Hartmann, W., Scheible, G., Sack, S., Guggemos, W., Kallies, R., Muth, S., Junglen, S., Müller, M. A., Haas, W., Guberina, H., Röhnisch, T., Schmid-Wendtner, M., Aldabbagh, S., Dittmer, U., Gold, H., Graf, P., … Wendtner, C.-M. (2013). Clinical features and virological analysis of a case of Middle East respiratory syndrome coronavirus infection. *The Lancet. Infectious Diseases*, *13*(9), 745–751. https://doi.org/10.1016/S1473-3099(13)70154-3

Drummond, E., Pires, G., MacMurray, C., Askenazi, M., Nayak, S., Bourdon, M., Safar, J., Ueberheide, B., & Wisniewski, T. (2020). Phosphorylated tau interactome in the human Alzheimer's disease brain. *Brain*, *143*(9), 2803–2817. https://doi.org/10.1093/brain/awaa223

Dundas, C. M., Demonte, D., & Park, S. (2013). Streptavidin-biotin technology: Improvements and innovations in chemical and biological applications. *Applied Microbiology and Biotechnology*, *97*(21), 9343–9353. https://doi.org/10.1007/s00253-013-5232-z

Eftekhari, A., Alipour, M., Chodari, L., Dizaj, S. M., Ardalan, M. R., Samiei, M., Sharifi, S., Vahed, S. Z., Huseynova, I., Khalilov, R., Ahmadian, E., & Cucchiarini, M. (2021). A comprehensive review of

detection methods for SARS-CoV-2. *Microorganisms*, *9*(2), 1–18. https://doi.org/10.3390/microorganisms9020232

El Bishlawy, I. M. (1999). Red blood cells, hemoglobin and the immune system. *Medical Hypotheses*, *53*(4), 345–346. https://doi.org/10.1054/mehy.1997.0778

Elgueta, R., De Vries, V. C., & Noelle, R. J. (2010). The immortality of humoral immunity. *Immunological Reviews*, *236*(1), 139–150. https://doi.org/10.1111/j.1600-065X.2010.00924.x

Epelman, S., Lavine, K. J., & Randolph, G. J. (2014). Origin and Functions of Tissue Macrophages. *Immunity*, *41*(1), 21–35. https://doi.org/10.1016/j.immuni.2014.06.013

Fabbri, M., Smart, C., & Pardi, R. (2003). T lymphocytes. *International Journal of Biochemistry and Cell Biology*, *35*, 1004–1008. https://doi.org/10.1016/S1357-2725(03)00037-2

Faissner, A., Kruse, J., Nieke, J., & Schachner, M. (1984). Expression of neural cell adhesion molecule L1 during development, in neurological mutants and in the peripheral nervous system. *Developmental Brain Research*, *15*(1), 69–82. https://doi.org/10.1016/0165-3806(84)90141-X

Falasca, F., Sciandra, I., Di Carlo, D., Gentile, M., Deales, A., Antonelli, G., & Turriziani, O. (2020). Detection of SARS-COV N2 Gene: Very low amounts of viral RNA or false positive? *Journal of Clinical Virology*, *133*(January), 1–3. https://doi.org/10.1016/j.jcv.2020.104660

Fan, X., White, I. M., Shopova, S. I., Zhu, H., Suter, J. D., & Sun, Y. (2008). Sensitive optical biosensors for unlabeled targets: A review. In *Analytica Chimica Acta* (Vol. 620, Issues 1–2). https://doi.org/10.1016/j.aca.2008.05.022

Fang, Y., Ferrie, A. M., Fontaine, N. H., Mauro, J., & Balakrishnan, J. (2006). Resonant waveguide grating biosensor for living cell sensing. *Biophysical Journal*, *91*, 1925–1940. https://doi.org/10.1529/biophysj.105.077818

Findlay, J. W. A., Smith, W. C., Lee, J. W., Nordblom, G. D., Das, I., Desilva, B. S., Khan, M. N., & Bowsher, R. R. (2000). Validation of immunoassays for bioanalysis: A pharmaceutical industry perspective. *Journal of Pharmaceutical and Biomedical Analysis*, *21*(6), 1249–1273. https://doi.org/10.1016/S0731-7085(99)00244-7

Gan, S. D., & Patel, K. R. (2013). Enzyme immunoassay and enzyme-linked immunosorbent assay. *Journal of Investigative Dermatology*, *133*(9), 1–3. https://doi.org/10.1038/jid.2013.287

Gao, S., Guisán, J. M., & Rocha-Martin, J. (2022). Oriented immobilization of antibodies onto sensing platforms - A critical review. *Analytica Chimica Acta*, *1189*, 228907. https://doi.org/10.1016/j.aca.2021.338907

García-Chamé, M. Á., Gutiérrez-Sanz, Ó., Ercan-Herbst, E., Haustein, N., Filipiak, M. S., Ehrnhöfer, D. E., & Tarasov, A. (2020). A transistor-based label-free immunosensor for rapid detection of tau protein. *Biosensors and Bioelectronics*, *159*(November 2019), 1–6. https://doi.org/10.1016/j.bios.2020.112129

Gavela, A. F., García, D. G., Ramirez, J. C., & Lechuga, L. M. (2016). Last advances in silicon-based optical biosensors. *Sensors*, *16*, 285. https://doi.org/10.3390/s16030285

Gerald G., O., & Amanda Vaughn, S. (2010). Current Treatments for Patients With Alzheimer Disease. *Journal of the American Osteopathic Association*, *110*(9), 16–26. https://doi.org/10.7556/jaoa.2010.20042

Germic, N., Frangez, Z., Yousefi, S., & Simon, H. U. (2019). Regulation of the innate immune system by autophagy: neutrophils, eosinophils, mast cells, NK cells. *Cell Death and Differentiation*, *26*(4), 703–714. https://doi.org/10.1038/s41418-019-0295-8

Gomes, D. E., & Witwer, K. W. (2022). L1CAM-associated extracellular vesicles: A systematic review of

nomenclature, sources, separation, and characterization. *Journal of Extracellular Biology*, *1*(3), 1–30. https://doi.org/10.1002/jex2.35

Gong, C. X., Liu, F., Grundke-Iqbal, I., & Iqbal, K. (2005). Post-translational modifications of tau protein in Alzheimer's disease. *Journal of Neural Transmission*, *112*(6), 813–838. https://doi.org/10.1007/s00702-004-0221-0

González-Amaro, R., & Marazuela, M. (2016). T regulatory (Treg) and T helper 17 (Th17) lymphocytes in thyroid autoimmunity. *Endocrine*, *52*, 30–38. https://doi.org/10.1007/s12020-015-0759-7

González-Guerrero, A. B., Maldonado, J., Herranz, S., & Lechuga, L. M. (2016). Trends in photonic lab-on-chip interferometric biosensors for point-of-care diagnostics. *Analytical Methods*, *0*(1–3), 1–15. https://doi.org/10.1039/C6AY02972H

González-Sánchez, M., Bartolome, F., Antequera, D., Puertas-Martín, V., González, P., Gómez-Grande, A., Llamas-Velasco, S., Herrero-San Martín, A., Pérez-Martínez, D., Villarejo-Galende, A., Atienza, M., Palomar-Bonet, M., Cantero, J. L., Perry, G., Orive, G., Ibañez, B., Bueno, H., Fuster, V., & Carro, E. (2020). Decreased salivary lactoferrin levels are specific to Alzheimer's disease. *EBioMedicine*, *57*, 102834. https://doi.org/10.1016/j.ebiom.2020.102834

González Rumayor, V., García Iglesias, E., Ruiz Galán, O., & Gago Cabezas, L. (2005). Aplicaciones de los biosensores en la industría agroalimentaria. *Informe de Vigilancia Tecnológica. Comunidad de Madrid*, 1–119.

Gorbalenya, A. E., Baker, S. C., Baric, R. S., de Groot, R. J., Drosten, C., Gulyaeva, A. A., Haagmans, B. L., Lauber, C., Leontovich, A. M., Neuman, B. W., Penzar, D., Perlman, S., Poon, L. L. M., Samborskiy, D. V., Sidorov, I. A., Sola, I., & Ziebuhr, J. (2020). The species Severe acute respiratory syndrome-related coronavirus: classifying 2019-nCoV and naming it SARS-CoV-2. *Nature Microbiology*, *5*(4), 536–544. https://doi.org/10.1038/s41564-020-0695-z

Gordon, S., & Martinez-Pomares, L. (2017). Physiological roles of macrophages. *Pflugers Archiv European Journal of Physiology*, *469*(3), 365–374. https://doi.org/10.1007/s00424-017-1945-7

Griciuc, A., & Tanzi, R. E. (2021). The role of innate immune genes in Alzheimer's disease. *Current Opinion in Neurology*, *34*(2), 228–236. https://doi.org/10.1097/WCO.0000000000000911

Grieshaber, D., MacKenzie, R., Vörös, J., & Reimhult, E. (2008). Electrochemical biosensors - Sensor principles and architectures. *Sensors*, *8*, 1400–1458. https://doi.org/10.3390/s8031400

Groves, M. L. (1960). The Isolation of a Red Protein from Milk. *Journal of the American Chemical Society*, *82*(13), 3345–3350. https://doi.org/10.1021/ja01498a029

Guilliams, M., Mildner, A., & Yona, S. (2018). Developmental and Functional Heterogeneity of Monocytes. *Immunity*, *49*, 595–613. https://doi.org/10.1016/j.immuni.2018.10.005

Gurunathan, S., Kang, M. H., Jeyaraj, M., Qasim, M., & Kim, J. H. (2019). Review of the isolation, characterization, biological function, and multifarious therapeutic approaches of exosomes. *Cells*, *8*(4), 307. https://doi.org/10.3390/cells8040307

Haass, C., & Selkoe, D. J. (2007). Soluble protein oligomers in neurodegeneration: Lessons from the Alzheimer's amyloid β-peptide. *Nature Reviews Molecular Cell Biology*, *8*(2), 101–112. https://doi.org/10.1038/nrm2101

Hampel, H., Hardy, J., Blennow, K., Chen, C., Perry, G., Kim, S. H., Villemagne, V. L., Aisen, P., Vendruscolo, M., Iwatsubo, T., Masters, C. L., Cho, M., Lannfelt, L., Cummings, J. L., & Vergallo, A. (2021). The Amyloid-β Pathway in Alzheimer's Disease. *Molecular Psychiatry*, *26*(10), 5481–5503. https://doi.org/10.1038/s41380-021-01249-0

Hao, L., Shan, Q., Wei, J., Ma, F., & Sun, P. (2018). Lactoferrin: Major Physiological Functions and Applications. *Current Protein & Peptide Science*, *20*(2), 139–144.

https://doi.org/10.2174/1389203719666180514150921

Harapan, B. N., & Yoo, H. J. (2021). Neurological symptoms, manifestations, and complications associated with severe acute respiratory syndrome coronavirus 2 (SARS-CoV-2) and coronavirus disease 19 (COVID-19). *Journal of Neurology*, *268*(9), 3059–3071. https://doi.org/10.1007/s00415-021-10406-y

Härtig, W., Stieler, J., Boerema, A. S., Wolf, J., Schmidt, U., Weißfuß, J., Bullmann, T., Strijkstra, A. M., & Arendt, T. (2007). Hibernation model of tau phosphorylation in hamsters: Selective vulnerability of cholinergic basal forebrain neurons - Implications for Alzheimer's disease. *European Journal of Neuroscience*, *25*(1), 69–80. https://doi.org/10.1111/j.1460-9568.2006.05250.x

Heideman, R. G., Kooyman, R. P. H., & Greve, J. (1991). Development of an optical waveguide interferometric immunosensor. *Sensors and Actuators: B. Chemical*, *4*, 297–299. https://doi.org/10.1016/0925-4005(91)80126-5

Hidayat, R., & Patricia Wulandari. (2021). Enzyme Linked Immunosorbent Assay (ELISA) Technique Guideline. *Bioscientia Medicina : Journal of Biomedicine and Translational Research*, *5*(5), 447–453. https://doi.org/10.32539/bsm.v5i5.228

Hirsch, M., Majchrowicz, D., Wierzba, P., Weber, M., Bechelany, M., & Jędrzejewska-Szczerska, M. (2017). Low-coherence interferometric fiber-optic sensors with potential applications as biosensors. *Sensors*, *17*, 261. https://doi.org/10.3390/s17020261

Ho, J. an A., Hsu, W. L., Liao, W. C., Chiu, J. K., Chen, M. L., Chang, H. C., & Li, C. C. (2010). Ultrasensitive electrochemical detection of biotin using electrically addressable site-oriented antibody immobilization approach via aminophenyl boronic acid. *Biosensors and Bioelectronics*, *26*(3), 1021–1027. https://doi.org/10.1016/j.bios.2010.08.048

Holgado, M., Barrios, C. A., Ortega, F. J., Sanza, F. J., Casquel, R., Laguna, M. F., Bañuls, M. J., López-Romero, D., Puchades, R., & Maquieira, A. (2010). Label-free biosensing by means of periodic lattices of high aspect ratio SU-8 nano-pillars. *Biosensors and Bioelectronics*, *25*, 2553–2558. https://doi.org/10.1016/j.bios.2010.04.042

Holgado, M., Casquel, R., Molpeceres, C., Ocaña, J. L., Laguna, M. F., & Morales, M. (2010). *OPTICAL DETECTION SYSTEM FOR LABELLING-FREE HIGH-SENSITIVITY BIOASSAYS (57)*. https://doi.org/10.1016/j.aca.2008.05.022

Holgado, M., Diaz-Perales, A., Garrido-Arandia, M., L. Espinosa, R., Romero-Sahagun, A., Laguna, M. F., Fernández Pacios, L., Santamaría, B., Ramírez, Y., & Sanza, F. J. (2020). *Método óptico de detección de una molécula objetivo mediante amplificación en la respuesta de interferencia por índice de refracción y dispersión*. https://worldwide.espacenet.com/patent/search/family/069845641/publication/ES2750374A1?q=ES2750374A1

Holgado, M., Maigler, M. V., Santamaría, B., Hernandez, A. L., Lavín, A., Laguna, M. F., Sanza, F. J., Granados, D., Casquel, R., Portilla, J., & Riesgo, T. (2016). Towards reliable optical label-free point-of-care (PoC) biosensing devices. *Sensors and Actuators, B: Chemical*, *236*, 765–772. https://doi.org/10.1016/j.snb.2016.06.047

Holgado, M., Sanza, F. J., Laguna, M. F., Lavín, A., & Casquel, R. (2012). *Interferometric Detection Method* (Patent No. EP2693164A1).

Holgado, M., Sanza, F. J., López, A., Lavín, Á., Casquel, R., & Laguna, M. F. (2014). Description of an advantageous optical label-free biosensing interferometric read-out method to measure biological species. *Sensors*, *14*, 3675–3689. https://doi.org/10.3390/s140203675

Horie, K., Barthélemy, N. R., Mallipeddi, N., Li, Y., Franklin, E. E., Perrin, R. J., Bateman, R. J., & Sato, C.

(2020). Regional correlation of biochemical measures of amyloid and tau phosphorylation in the brain. *Acta Neuropathologica Communications*, *8*(149), 1–14. https://doi.org/10.1186/s40478-020-01019-z

Hornung, S., Dutta, S., & Bitan, G. (2020). CNS-Derived Blood Exosomes as a Promising Source of Biomarkers: Opportunities and Challenges. *Frontiers in Molecular Neuroscience*, *13*(March), 1–16. https://doi.org/10.3389/fnmol.2020.00038

Hsieh, Y.-H. P., & Rao, Q. (2023). Food Analysis. In S. S. Nielsen (Ed.), *Food Science Text Series* (Fifth). Springer, Cham. https://doi.org/10.1007/978-3-319-45776-5_27

Huang, R., Quan, J., Su, B., Cai, C., Cai, S., Chen, Y., Mou, Z., Zhou, P., Ma, D., & Cui, X. (2022). A two-step competition assay for visual, sensitive and quantitative C-reactive protein detection in low-cost microfluidic particle accumulators. *Sensors and Actuators B: Chemical*, *359*, 131583. https://doi.org/10.1016/j.snb.2022.131583

Huber, S. R., van Beek, J., de Jonge, J., Luytjes, W., & van Baarle, D. (2014). T cell responses to viral infections - opportunities for peptide vaccination. *Frontiers in Immunology*, *5*(APR), 1–12. https://doi.org/10.3389/fimmu.2014.00171

Iba, M., Guo, J. L., McBride, J. D., Zhang, B., Trojanowski, J. Q., & Lee, V. M. Y. (2013). Synthetic tau fibrils mediate transmission of neurofibrillary tangles in a transgenic mouse model of alzheimer's-like tauopathy. *Journal of Neuroscience*, *33*(3), 1024–1037. https://doi.org/10.1523/JNEUROSCI.2642-12.2013

Inan, H., Poyraz, M., Inci, F., Lifson, M. A., Baday, M., Cunningham, B. T., & Demirci, U. (2017). Photonic crystals: Emerging biosensors and their promise for point-of-care applications. *Chemical Society Reviews*, *46*(2), 366–388. https://doi.org/10.1039/c6cs00206d

InvivoGen. (2012). *InvivoGen Review | Antibody Isotypes*. *33*(0), 0–1.

Islam, R. M., Ali, M. M., Lai, M. H., Lim, K. S., & Ahmad, H. (2014). Chronology of fabry-perot interferometer fiber-optic sensors and their applications: A review. *Sensors*, *14*, 7451–7488. https://doi.org/10.3390/s140407451

Ito, Y., Satoh, T., Miyagishi, C., Walls, A. F., & Yokozeki, H. (2011). Basophil recruitment and activation in inflammatory skin diseases. *Allergy*, *66*, 1107–1113. https://doi.org/10.1111/j.1398-9995.2011.02570.x

IUPAC. (2012). Compendium of Chemical Terminology. In J. Kaiser & S. Chalk (Eds.), *International Union of Pure and Applied Chemistry*. https://doi.org/10.1351/goldbook.

Ivnitski, D., Abdel-Hamid, I., Atanasov, P., & Wilkins, E. (1999). Biosensors for detection of pathogenic bacteria. *Biosensors and Bioelectronics*, *14*, 599–624. https://doi.org/10.1016/S0956-5663(99)00039-1

Jackson, C. B., Farzan, M., Chen, B., & Choe, H. (2022). Mechanisms of SARS-CoV-2 entry into cells. *Nature Reviews Molecular Cell Biology*, *23*(1), 3–20. https://doi.org/10.1038/s41580-021-00418-x

Jalandra, R., Yadav, A. K., Verma, D., Dalal, N., Sharma, M., Singh, R., Kumar, A., & Solanki, P. R. (2020). Strategies and perspectives to develop SARS-CoV-2 detection methods and diagnostics. *Biomedicine and Pharmacotherapy*, *129*(May), 1–10. https://doi.org/10.1016/j.biopha.2020.110446

James H., S., & Ellen G., S. (2020). Overview of Viruses and Virus Infection. *Viruses and Human Disease*, *167*(1), 1–33. https://doi.org/10.1016/B978-0-12-373741-0.50004-0

Janeway, C., Travers, P., Walport, M., & Shlomchik, M. (2001). The distribution and functions of immunoglobulin isotypes. In *Immunobiology: The Immune System in Health and Disease* (5th ed.,

p. 732). Garland Science.

Jayamohan, H., Lambert, C. J., Sant, H. J., Jafek, A., Patel, D., Feng, H., Beeman, M., Mahmood, T., Nze, U., & Gale, B. K. (2021). SARS-CoV-2 pandemic: a review of molecular diagnostic tools including sample collection and commercial response with associated advantages and limitations. *Analytical and Bioanalytical Chemistry*, *413*(1), 49–71. https://doi.org/10.1007/s00216-020-02958-1

Jiang, C., Hopfner, F., Berg, D., Hu, M. T., Pilotto, A., Borroni, B., Davis, J. J., & Tofaris, G. K. (2021). Validation of α-Synuclein in L1CAM-Immunocaptured Exosomes as a Biomarker for the Stratification of Parkinsonian Syndromes. *Movement Disorders*, *36*(11), 2663–2669. https://doi.org/10.1002/mds.28591

Johnstone, R. M., Bianchini, A., & Teng, K. (1989). Reticulocyte maturation and exosome release: transferrin receptor containing exosomes shows multiple plasma membrane functions. *Blood*, *74*, 1844–1851.

Jung, H. S., Moon, D. S., & Lee, J. K. (2012). Quantitative analysis and efficient surface modification of silica nanoparticles. *Journal of Nanomaterials*, *2012*. https://doi.org/10.1155/2012/593471

Kahn, J. S., & McIntosh, K. (2005). History and Recent Advances in Coronavirus Discovery. *Pediatric Infectious Disease Journal*, *24*(11), 223–227. https://doi.org/10.1097/01.inf.0000188166.17324.60

Kalesnikoff, J., & Galli, S. J. (2008). New developments in mast cell biology. *Nature Immunology*, *9*(11), 1215–1223. https://doi.org/10.1038/ni.f.216

Karunakaran, C., Rajkumar, R., & Bhargava, K. (2015). Introduction to Biosensors. In C. Karunakaran, R. Rajkumar, & K. Bhargava (Eds.), *Biosensors and Bioelectronics*. Elsevier Inc. https://doi.org/10.1016/B978-0-12-803100-1.00001-3

Kashefi-Kheyrabadi, L., Nguyen, H. V., Go, A., Baek, C., Jang, N., Lee, J. M., Cho, N.-H., Min, J., & Lee, M.-H. (2022). Rapid, multiplexed, and nucleic acid amplification-free detection of SARS-CoV-2 RNA using an electrochemical biosensor. *Biosensors and Bioelectronics*, *195*(January), 1–9. https://doi.org/10.1016/j.bios.2021.113649

Kaštelan, S., Braš, M., Pjevač, N., Bakija, I., Tomić, Z., Pjevač Keleminić, N., & Gverović Antunica, A. (2023). Tear Biomarkers and Alzheimer's Disease. *International Journal of Molecular Sciences*, *24*(17), 1–19. https://doi.org/10.3390/ijms241713429

Kaur, H., Bhosale, A., & Shrivastav, S. (2018). Biosensors: Classification, Fundamental Characterization and New Trends: A Review. *International Journal of Health Sciences & Research*, *8*(6), 315–333. www.ijhsr.org

Kermali, M., Khalsa, R. K., Pillai, K., Ismail, Z., & Harky, A. (2020). The role of biomarkers in diagnosis of COVID-19 – A systematic review. *Life Sciences*, *254*(January), 1–12. https://doi.org/10.1016/j.lfs.2020.117788

Khan, M. A., & Mujahid, M. (2020). Recent advances in electrochemical and optical biosensors designed for detection of Interleukin 6. *Sensors*, *20*(646), 1–27. https://doi.org/10.3390/s20030646

Khan, S., Barve, K. H., & Kumar, M. S. (2020). Recent Advancements in Pathogenesis, Diagnostics and Treatment of Alzheimer's Disease. *Current Neuropharmacology*, *18*(11), 1106–1125. https://doi.org/10.2174/1570159x18666200528142429

Kidd, P. (2003). Th1/Th2 Balance: The Hypothesis, its Limitations, and Implications for Health and Disease. *Alternative Medicine Review*, *8*(3), 223–246.

Kim, H. R., Bong, J. H., Kim, T. H., Shin, S. S., Kang, M. J., Shim, W. B., Lee, D. Y., Son, D. H., & Pyun, J. C.

(2022). One-Step Homogeneous Immunoassay for the Detection of Influenza Virus Using Switching Peptide and Graphene Quencher. *Biochip Journal*, *16*(3), 334–341. https://doi.org/10.1007/s13206-022-00076-x

Kim, K. Y., Shin, K. Y., & Chang, K. A. (2021). Brain-derived exosomal proteins as effective biomarkers for alzheimer's disease: A systematic review and meta-analysis. *Biomolecules*, *11*(980), 1–16. https://doi.org/10.3390/biom11070980

Knopman, D. S., Amieva, H., Peterse, R. C., Chételat, G., Holtzman, D. M., Hyman, B. T., Nixon, R. A., & Jones, D. T. (2021). Alzheimer disease. *Nature Reviews Disease Primers*, *7*(331), 1–47. https://doi.org/10.1038/s41572-021-00269-y

Knox, J. J., Myles, A., & Cancro, M. P. (2019). T-bet+ memory B cells: Generation, function, and fate. *Immunological Reviews*, *288*(1), 149–160. https://doi.org/10.1111/imr.12736

Kontou, P. I., Braliou, G. G., Dimou, N. L., Nikolopoulos, G., & Bagos, P. G. (2020). Antibody tests in detecting SARS-CoV-2 infection: A meta-analysis. *Diagnostics*, *10*(319), 1–15. https://doi.org/10.3390/diagnostics10050319

Koonin, E. V., Krupovic, M., & Agol, V. I. (2021). The Baltimore Classification of Viruses 50 Years Later: How Does It Stand in the Light of Virus Evolution? *Microbiology and Molecular Biology Reviews*, *85*(3), 1–19. https://doi.org/10.1128/mmbr.00053-21

Koupenova, M., Livada, A. C., & Morrell, C. N. (2022). Platelet and Megakaryocyte Roles in Innate and Adaptive Immunity. *Circulation Research*, *130*(2), 288–308. https://doi.org/10.1161/CIRCRESAHA.121.319821

Kovacs, G. G. (2018). Tauopathies. *Handbook of Clinical Neurology*, *145*, 355–368. https://doi.org/10.1016/B978-0-12-802395-2.00025-0

Koyama, S., Ishii, K. J., Coban, C., & Akira, S. (2008). Innate immune response to viral infection. *Cytokine*, *43*(3), 336–341. https://doi.org/10.1016/j.cyto.2008.07.009

Król-Grzymała, A., Sienkiewicz-Szłapka, E., Fiedorowicz, E., Rozmus, D., Cieślińska, A., & Grzybowski, A. (2022). Tear Biomarkers in Alzheimer's and Parkinson's Diseases, and Multiple Sclerosis: Implications for Diagnosis (Systematic Review). *International Journal of Molecular Sciences*, *23*(17), 10123. https://doi.org/10.3390/ijms231710123

Kumar, A., Mahato, K., Purohit, B., & Chandra, P. (2022). Commercial Aspects and Market Pull of Biosensors in Diagnostic Industries. In K. Mahato & P. Chandra (Eds.), *Miniaturized Biosensing Devices: Fabrication and Applications* (First, pp. 351–368). Springer. https://doi.org/10.1007/978-981-16-9897-2_15

Kumar, J. V., N, S., Srinivas, S., Khosla, A., R, H. K., & C, M. (2022). Review on Biosensors: Fundamentals, Classifications, Characteristics, Simulations, and Potential Applications. *ECS Transactions*, *107*(1), 13005–13029. https://doi.org/10.1149/10701.13005ecst

Kumar Singh, A., Anwar, M., Pradhan, R., Ashar, M. S., Rai, N., & Dey, S. (2023). Surface plasmon resonance based-optical biosensor: Emerging diagnostic tool for early detection of diseases. *Journal of Biophotonics*, *16*(7), e202200380. https://doi.org/10.1002/jbio.202200380

Kurian, T. K., Banik, S., Gopal, D., Chakrabarti, S., & Mazumder, N. (2021). Elucidating Methods for Isolation and Quantification of Exosomes: A Review. *Molecular Biotechnology*, *63*(4), 249–266. https://doi.org/10.1007/s12033-021-00300-3

Kurosaki, T., Kometani, K., & Ise, W. (2015). Memory B cells. *Nature Reviews Immunology*, *15*(3), 149–159. https://doi.org/10.1038/nri3802

Kwong, W. K. (2000). *Catalytic biosensors: novel analitycal tools and their applications in sports, food and environment monitoring*. Hong Kong University of Science and Technology.

Laguna, M. F., Holgado, M., Sanza, F. J., Lavín, A., López, A., & Casquel, R. (2014). Optimization of dengue immunoassay by label-free interferometric optical detection method. *Sensors*, *14*, 6695–6700. https://doi.org/10.3390/s140406695

Lakshmipriya, T., & Gopinath, S. C. B. (2019). An introduction to biosensors and biomolecules. In *Nanobiosensors for Biomolecular Targeting*. Elsevier Inc. https://doi.org/10.1016/B978-0-12-813900-4.00001-4

Lamers, M. M., & Haagmans, B. L. (2022). SARS-CoV-2 pathogenesis. *Nature Reviews Microbiology*, *20*(5), 270–284. https://doi.org/10.1038/s41579-022-00713-0

Lamptey, R. N. L., Chaulagain, B., Trivedi, R., Gothwal, A., Layek, B., & Singh, J. (2022). A Review of the Common Neurodegenerative Disorders: Current Therapeutic Approaches and the Potential Role of Nanotherapeutics. *International Journal of Molecular Sciences*, *23*(3), 1851. https://doi.org/10.3390/ijms23031851

Lavín, Á. (2016). Caracterización y optimización de estructuras biofotónicas y técnicas avanzadas de interrogación para desarrollo de biosensores ópticos [Universidad Politécnica de Madrid]. In *Escuela Técnica Superior de Ingenieros Industriales*. https://doi.org/10.20868/UPM.thesis.39356.

Lavín, Á., de Vicente, J., Holgado, M., Laguna, M. F., Casquel, R., Santamaría, B., Maigler, M. V., Hernández, A. L., & Ramírez, Y. (2018). On the determination of uncertainty and limit of detection in label-free biosensors. *Sensors*, *18*, 38. https://doi.org/10.3390/s18072038

Lebien, T. W., & Tedder, T. F. (2008). B lymphocytes: How they develop and function. *Blood*, *112*(5), 1570–1580. https://doi.org/10.1182/blood-2008-02-078071

Lee, J. B., Choi, K. H., & Yoo, K. (2015). Innovative SU-8 lithography techniques and their applications. *Micromachines*, *6*, 1–18. https://doi.org/10.3390/mi6010001

Lee, K. Y. (2019). M1 and M2 polarization of macrophages: a mini-review. *Medical Biological Science and Engineering*, *2*(1), 1–5. https://doi.org/10.30579/mbse.2019.2.1.1

Leung, A., Shankar, P. M., & Mutharasan, R. (2007). A review of fiber-optic biosensors. *Sensors and Actuators, B: Chemical*, *125*, 688–703. https://doi.org/10.1016/j.snb.2007.03.010

Li, H., Liu, S., Yu, X., Tang, S., & Tang, C. (2020). Coronavirus disease 2019 (COVID-19): current status and future perspectives. *International Journal of Antimicrobial Agents*, *55*(5), 105951. https://doi.org/j.ijantimicag.2020.105951

Li, Y. Q., & Guo, C. (2021). A review on lactoferrin and central nervous system diseases. *Cells*, *10*(7), 1810. https://doi.org/10.3390/cells10071810

Liang, D., & Lu, H. (2019). Salivary biological biomarkers for Alzheimer's disease. *Archives of Oral Biology*, *105*(April), 5–12. https://doi.org/10.1016/j.archoralbio.2019.06.004

Liberman, A., Mendez, N., Trogler, W. C., & Kummel, A. C. (2014). Synthesis and surface functionalization of silica nanoparticles for nanomedicine. *Surface Science Reports*, *69*(2–3), 132–158. https://doi.org/10.1016/j.surfrep.2014.07.001

Ligler, F. S., & Taitt, C. R. (Eds.). (2008). *Optical biosensors: today and tomorrow.* (Second). Elsevier.

Lim, J. M., Kim, J. H., Ryu, M. Y., Cho, C. H., Park, T. J., & Park, J. P. (2018). An electrochemical peptide sensor for detection of dengue fever biomarker NS1. *Analytica Chimica Acta*, *1026*, 109–116. https://doi.org/10.1016/j.aca.2018.04.005

Lipman, N. S., Jackson, L. R., Trudel, L. J., & Weis-Garcia, F. (2005). Monoclonal versus polyclonal antibodies: Distinguishing characteristics, applications, and information resources. *ILAR Journal*, *46*(3), 258–267. https://doi.org/10.1093/ilar.46.3.258

Lisi, S., Scarano, S., Fedeli, S., Pascale, E., Cicchi, S., Ravelet, C., Peyrin, E., & Minunni, M. (2017). Toward

sensitive immuno-based detection of tau protein by surface plasmon resonance coupled to carbon nanostructures as signal amplifiers. *Biosensors and Bioelectronics*, *93*(June 2016), 289–292. https://doi.org/10.1016/j.bios.2016.08.078

Liu, D. X., Liang, J. Q., & Fung, T. S. (2020). Human Coronavirus-229E, -OC43, -NL63, and -HKU1 (Coronaviridae). *Encyclopedia of Virology: Volume 1-5, Fourth Edition*, *1–5*(January), 428–440. https://doi.org/10.1016/B978-0-12-809633-8.21501-X

Liu, K., & Nussenzweig, M. C. (2010). Origin and development of human dendritic cells. *Immunological Reviews*, *234*, 45–54. https://doi.org/10.1111/j.0105-2896.2009.00879.x.

Llandro, J., Palfreyman, J. J., Ionescu, A., & Barnes, C. H. W. (2010). Magnetic biosensor technologies for medical applications: A review. *Medical and Biological Engineering and Computing*, *48*, 977–998. https://doi.org/10.1007/s11517-010-0649-3

López-Romero, D., Barrios, C. A., Holgado, M., Laguna, M. F., & Casquel, R. (2010). High aspect-ratio SU-8 resist nano-pillar lattice by e-beam direct writing and its application for liquid trapping. *Microelectronic Engineering*, *87*, 663–667. https://doi.org/10.1016/j.mee.2009.09.007

Louten, J. (2016). Virus Structure and Classification. *Essential Human Virology*, *167*(1), 19–29. https://doi.org/10.1016/B978-0-12-800947-5.00002-8

Lu, B., Xie, J., Lu, C., Wei, Y., & Wu, C. (1995). Oriented Immobilization of Fab' Fragments on Silica Surfaces. *Analytical Chemistry*, *67*(1), 83–87. https://doi.org/10.1021/ac00097a014

Lucas, W., & Knipe, D. M. (2002). Viral Capsids and Envelopes: Structure and Function. *ELS*, 1–7. https://doi.org/10.1038/npg.els.0001091

Luckheeram, R. V., Zhou, R., Verma, A. D., & Xia, B. (2012). CD4 +T cells: Differentiation and functions. *Clinical and Developmental Immunology*, 925135. https://doi.org/10.1155/2012/925135

Ludwig, N., Whiteside, T. L., & Reichert, T. E. (2019). Challenges in exosome isolation and analysis in health and disease. *International Journal of Molecular Sciences*, *20*(19), 4684. https://doi.org/10.3390/ijms20194684

Maas, M. B., Maybery, G. H. C., Perold, W. J., Neveling, D. P., & Dicks, L. M. T. (2018). Borosilicate Glass Fiber-Optic Biosensor for the Detection of Escherichia coli. *Current Microbiology*, *75*, 150–155. https://doi.org/10.1007/s00284-017-1359-y

Mahase, E. (2020). Covid-19: First coronavirus was described in The BMJ in 1965. *BMJ (Clinical Research Ed.)*, *369*(April), 1547. https://doi.org/10.1136/bmj.m1547

Mandala, S. H. S., Liu, T., Chen, C., Liu, K., Januar, M., Chang, Y., Lai, C., Chang, K., & Liu, K. (2021). Enhanced Plasmonic Biosensor Utilizing Paired Antibody and Label-Free Fe3O4 Nanoparticles for Highly Sensitive and Selective Detection of Parkinson's α-Synuclein in Serum. *Biosensors*, *11*, 402. https://doi.org/10.3390/bios11100402

Mandelkow, E. M., & Mandelkow, E. (2012). Biochemistry and cell biology of Tau protein in neurofibrillary degeneration. *Cold Spring Harbor Perspectives in Biology*, *3*(10), 1–25. https://doi.org/10.1101/cshperspect.a006247

Manz, R. A., Arce, S., Cassese, G., Hauser, A. E., Hiepe, F., & Radbruch, A. (2002). Humoral immunity and long-lived plasma cells. *Current Opinion in Immunology*, *14*(4), 517–521. https://doi.org/10.1016/S0952-7915(02)00356-4

Marasco, R. A. (2020). Addressing Unmet Needs in Alzheimer Disease: Implications of Delayed Diagnosis and Examining New and Emerging Therapies. *The American Journal of Managed Care Supplement*, *26*(8), S165–S188.

Marcoux, G., Laroche, A., Espinoza Romero, J., & Boilard, E. (2021). Role of platelets and

megakaryocytes in adaptive immunity. *Platelets*, *32*(3), 340–351. https://doi.org/10.1080/09537104.2020.1786043

Marrows, C. H. (2007). Magnetic Biosensor Techniques. In R. S. Marks, D. C. Cullen, I. Karube, C. R. Lowe, & H. H. Weetall (Eds.), *Handbook of Biosensors and Biochips* (pp. 1–16). https://doi.org/10.1002/9780470061565.hbb068

Martin, M. D., & Badovinac, V. P. (2018). Defining memory CD8 T cell. *Frontiers in Immunology*, *9*, 2692. https://doi.org/10.3389/fimmu.2018.02692

Martinez, R. M. (2020). Clinical Samples for SARS-CoV-2 Detection: Review of the Early Literature. *Clinical Microbiology Newsletter*, *42*(15), 121–127. https://doi.org/10.1016/j.clinmicnews.2020.07.001

Massoud, F., & Léger, G. C. (2011). Pharmacological treatment of Alzheimer disease. *Canadian Journal of Psychiatry*, *56*(10), 579–588. https://doi.org/10.1177/070674371105601003

Mathuria, J. P., Yadav, R., & Rajkumar. (2020). Laboratory diagnosis of SARS-CoV-2 - A review of current methods. *Journal of Infection and Public Health*, *13*(7), 901–905. https://doi.org/10.1016/j.jiph.2020.06.005

McComb, S., Thiriot, A., Akache, B., Krishnan, L., & Stark, F. (2019). Introduction to the Immune System. In K. M. Fulton & S. M. Twine (Eds.), *Immunoproteomics: Methods and Protocols, Methods in Molecular Biology* (Vol. 2024, pp. 1–24). Springer Nature. https://doi.org/10.1007/978-1-4939-9597-4_1

Michniacki, T. F., Choi, S. W., & Peltier, D. C. (2022). Immune Suppression in Allogeneic Hematopoietic Stem Cell Transplantation. *Handbook of Experimental Pharmacology*, *272*, 209–243. https://doi.org/10.1007/164_2021_544

Mittal, S., Sharma, T., & Tiwari, M. (2021). Surface plasmon resonance based photonic crystal fiber biosensors: A review. *Materials Today: Proceedings*, *43*, 3071–3074. https://doi.org/10.1016/j.matpr.2021.01.405

Modena, M. M., Rühle, B., Burg, T. P., & Wuttke, S. (2019). Nanoparticle Characterization: What to Measure? *Advanced Materials*, *31*(32), 1–26. https://doi.org/10.1002/adma.201901556

Moitra, P., Alafeef, M., Alafeef, M., Alafeef, M., Dighe, K., Frieman, M. B., Pan, D., Pan, D., & Pan, D. (2020). Selective Naked-Eye Detection of SARS-CoV-2 Mediated by N Gene Targeted Antisense Oligonucleotide Capped Plasmonic Nanoparticles. *ACS Nano*, *14*(6), 7617–7627. https://doi.org/10.1021/acsnano.0c03822

Monge Argilés, J. A., Blanco Cantó, M. A., Leiva Salinas, C., Flors, L., Muñoz Ruiz, C., Sánchez Payá, J., Gasparini Berenguer, R., & Leiva Santana, C. (2014). Comparación de la capacidad diagnóstica precoz de los biomarcadores de la enfermedad de Alzheimer en resonancia magnética cerebral y líquido cefalorraquídeo. *Neurologia*, *29*(7), 397–401. https://doi.org/10.1016/j.nrl.2013.06.002

Monopoli, M. P., Walczyk, D., Campbell, A., Elia, G., Lynch, I., Bombelli, F. B., & Dawson, K. A. (2011). Physical-Chemical aspects of protein corona: Relevance to in vitro and in vivo biological impacts of nanoparticles. *Journal of the American Chemical Society*, *133*, 2525–2534. https://doi.org/10.1021/ja107583h

Monošík, R., Streďanský, M., & Šturdík, E. (2012). Biosensors - classification, characterization and new trends. *Acta Chimica Slovaca*, *5*(1), 109–120. https://doi.org/10.2478/v10188-012-0017-z

Morera, D., & Mackenzie, S. A. (2011). Is there a direct role for erythrocytes in the immune response? *Veterinary Research*, *42*, 89. https://doi.org/10.1186/1297-9716-42-89

Morgan, H., & Taylor, D. M. (1992). A surface plasmon resonance immunosensor based on the streptavidin-biotin complex. *Biosensors and Bioelectronics*, *7*(6), 405–410.

https://doi.org/10.1016/0956-5663(92)85039-D

Mourdikoudis, S., Pallares, R. M., & Thanh, N. T. K. (2018). Characterization techniques for nanoparticles: Comparison and complementarity upon studying nanoparticle properties. *Nanoscale*, *10*(27), 12871–12934. https://doi.org/10.1039/c8nr02278j

Mueller, S. N., & Rouse, B. T. (2008). Immune responses to viruses. *Clinical Immunology*, 421–431. https://doi.org/10.1016/B978-0-323-04404-2.10027-2

Mukundan, H., Anderson, A. S., Grace, W. K., Grace, K. M., Hartman, N., Martinez, J. S., & Swanson, B. I. (2009). Waveguide-based biosensors for pathogen detection. *Sensors*, *9*, 5783–5809. https://doi.org/10.3390/s90705783

Muralidar, S., Ambi, S. V., Sekaran, S., Thirumalai, D., & Palaniappan, B. (2020). Role of tau protein in Alzheimer's disease: The prime pathological player. *International Journal of Biological Macromolecules*, *163*, 1599–1617. https://doi.org/10.1016/j.ijbiomac.2020.07.327

Murillo, A. M. M., Holgado, M., & Laguna, M. (2023). Reports on the sensitivity enhancement in interferometric based biosensors by biotin-streptavidin system. *Heliyon*, *9*(12), e23123. https://doi.org/10.1016/j.heliyon.2023.e23123

Murillo, A. M. M., Laguna, M. F., Valle, L. G., Tramarin, L., Ramirez, Y., Lavín, Á., Santamaría, B., & Holgado, M. (2023). A New Optical Interferometric Biosensing System Enhanced with Nanoparticles for Alzheimer's Disease in Serum. *Biosensors*, *13*(7), 1–15. https://doi.org/10.3390/bios13070707

Murillo, A. M. M., Tomé-Amat, J., Ramírez, Y., Garrido-Arandia, M., Valle, L. G., Hernández-Ramírez, G., Tramarin, L., Herreros, P., Santamaría, B., Díaz-Perales, A., & Holgado, M. (2021). Developing an Optical Interferometric Detection Method based biosensor for detecting specific SARS-CoV-2 immunoglobulins in Serum and Saliva, and their corresponding ELISA correlation. *Sensors and Actuators, B: Chemical*, *345*. https://doi.org/10.1016/j.snb.2021.130394

Murillo, A. M. M., Valle, L. G., Ramírez, Y., Sánchez, M. J., Santamaría, B., Molina-Roldan, E., Ortega-Madueño, I., Urcelay, E., Tramarin, L., Herreros, P., Díaz-Perales, A., Garrido-Arandia, M., Tome-Amat, J., Hernández-Ramírez, G., Espinosa, R. L., Laguna, M. F., & Holgado, M. (2022). Integration of Multiple Interferometers in Highly Multiplexed Diagnostic KITs to Evaluate Several Biomarkers of COVID-19 in Serum. *Biosensors*, *12*(9). https://doi.org/10.3390/bios12090671

Murugan, D., Bhatia, H., Sai, V. V. R., & Satija, J. (2020). P-FAB: A Fiber-Optic Biosensor Device for Rapid Detection of COVID-19. *Transactions of the Indian National Academy of Engineering*, *5*(2), 211–215. https://doi.org/10.1007/s41403-020-00122-w

Mustapic, M., Eitan, E., Werner, J. K., Berkowitz, S. T., Lazaropoulos, M. P., Tran, J., Goetzl, E. J., & Kapogiannis, D. (2017). Plasma extracellular vesicles enriched for neuronal origin: A potential window into brain pathologic processes. *Frontiers in Neuroscience*, *11*(MAY), 1–12. https://doi.org/10.3389/fnins.2017.00278

Nakashima, C., Otsuka, A., & Kabashima, K. (2018). Recent advancement in the mechanism of basophil activation. *Journal of Dermatological Science*, *91*, 3–8. https://doi.org/10.1016/j.jdermsci.2018.03.007

Naresh, V., & Lee, N. (2021). A review on biosensors and recent development of nanostructured materials-enabled biosensors. *Sensors*, *21*(4), 1–35. https://doi.org/10.3390/s21041109

Nguyen, L. V., Hill, K., Warren-Smith, S., & Monro, T. (2015). Interferometric-type optical biosensor based on exposed core microstructured optical fiber. *Sensors and Actuators, B: Chemical*, *221*, 320–327. https://doi.org/10.1016/j.snb.2015.06.068

Nicholson, L. B. (2016). The immune system. *Essays in Biochemistry*, *60*(3), 275–301.

https://doi.org/10.1042/EBC20160017

O'Beirne, A. J., & Cooper, H. R. (1979). Heterogeneus Enzyme Immunoassay. *Journal of Histochemistry and Cytochemistry*, *27*(8), 1148–1162. https://doi.org/10.1177/27.8.383822

O'Sullivan, T. E., Sun, J. C., & Lanier, L. L. (2015). Natural Killer Cell Memory. *Immunity*, *43*(4), 634–645. https://doi.org/10.1016/j.immuni.2015.09.013

Pan, Y., Chua, N., Lim, K., & Ho, C. L. (2021). Engineering of Human Lactoferrin for Improved Anticancer Activity. *ACS Pharmacology and Translational Science*, *4*(5), 1476–1482. https://doi.org/10.1021/acsptsci.1c00134

Pandurangan, V., Ed, W., & Mark, W. (2004). Severe Acute Respiratory Syndrome (SARS): a review. *Clinical Medicine*, *4*(2), 152–160. https://doi.org/10.7861/clinmedicine.4-2-152

Parkin, J., & Cohen, B. (2001). An overview of the immune system. *Lancet*, *357*(9270), 1777–1789. https://doi.org/10.1016/S0140-6736(00)04904-7

Porsteinsson, A. P., Isaacson, R. S., Knox, S., Sabbagh, M. N., & Rubino, I. (2021). Diagnosis of Early Alzheimer's Disease: Clinical Practice in 2021. *Journal of Prevention of Alzheimer's Disease*, *8*(3), 371–386. https://doi.org/10.14283/jpad.2021.23

Prince, M., Bryce, R., Albanese, E., Wimo, A., Ribeiro, W., & Ferri, C. P. (2013). The global prevalence of dementia: A systematic review and metaanalysis. *Alzheimer's and Dementia*, *9*(1), 63–75. https://doi.org/10.1016/j.jalz.2012.11.007

Rahmati, Z., Roushani, M., Hosseini, H., & Choobin, H. (2021). Electrochemical immunosensor with Cu2O nanocube coating for detection of SARS-CoV-2 spike protein. *Microchimica Acta*, *188*(3), 105. https://doi.org/10.1007/s00604-021-04762-9

Ramirez, J. C., García, D. G., Maldonado, J., & Fernández-Gavela, A. (2022). Current Trends in Photonic Biosensors: Advances towards Multiplexed Integration. *Chemosensors*, *10*, 398. https://doi.org/10.3390/chemosensors10100398

Raskin, J., Cummings, J., Hardy, J., Schuh, K., & Dean, R. (2015). Neurobiology of Alzheimer's Disease: Integrated Molecular, Physiological, Anatomical, Biomarker, and Cognitive Dimensions. *Current Alzheimer Research*, *12*(8), 712–722. https://doi.org/10.2174/1567205012666150701103107

Ravi, N., Cortade, D. L., Ng, E., & Wang, S. X. (2020). Diagnostics for SARS-CoV-2 detection: A comprehensive review of the FDA-EUA COVID-19 testing landscape. *Biosensors and Bioelectronics*, *165*(April), 1–13. https://doi.org/10.1016/j.bios.2020.112454

Rawat, P., Sehar, U., Bisht, J., Selman, A., Culberson, J., & Reddy, P. H. (2022). Phosphorylated Tau in Alzheimer's Disease and Other Tauopathies. *International Journal of Molecular Sciences*, *23*(21), 1–27. https://doi.org/10.3390/ijms232112841

Ritter, M. A. (2000). *Polyclonal and Monoclonal Antibodies*. *40*, 23–34. https://doi.org/10.1385/1-59259-076-4:23

Rizzo, F. (2022). Optical Immunoassays Methods in Protein Analysis: An Overview. *Chemosensors*, *10*(326), 1–24. https://doi.org/10.3390/chemosensors10080326

Roberson, E. D., Scearce-Levie, K., Palop, J. J., Yan, F., Cheng, I. H., Wu, T., Gerstein, H., Yu, G. Q., & Mucke, L. (2007). Reducing endogenous tau ameliorates amyloid β-induced deficits in an Alzheimer's disease mouse model. *Science*, *316*(5825), 750–754. https://doi.org/10.1126/science.1141736

Rogers, K., & Mulchandani, A. (Eds.). (2011). *Affinity Biosensors: Techniques and Protocols* (First). Human Press.

Ronkainen, N. J., Halsall, H. B., & Heineman, W. R. (2010). Electrochemical biosensors. *Chemical Society*

Reviews, *39*, 1747–1763. https://doi.org/10.1039/b714449k

Rowe, C. A., Scruggs, S. B., Feldstein, M. J., Golden, J. P., & Ligler, F. S. (1999). An array immunosensor for simultaneous detection of clinical analytes. *Analytical Chemistry*, *71*(2), 433–439. https://doi.org/10.1021/ac980798t

Santacroce, L., Charitos, I. A., Carretta, D. M., De Nitto, E., & Lovero, R. (2021). The human coronaviruses (HCoVs) and the molecular mechanisms of SARS-CoV-2 infection. *Journal of Molecular Medicine*, *99*(1), 93–106. https://doi.org/10.1007/s00109-020-02012-8

Santamaría, B., Laguna, M. F., López-Romero, D., Hernandez, A. L., Sanza, F. J., Lavín, Á., Casquel, R., Maigler, M. V., Espinosa, R. L., & Holgado, M. (2017). Development towards compact nitrocellulose-based interferometric biochips for dry eye mmp9 label-free in-situ diagnosis. *Sensors*, *17*, 1158. https://doi.org/10.3390/S17051158

Sanza, F. J. (2015). *Development and fabrication of optical biosensors based on biophotonic sensing cells (BICELLs)* [Universidad Politécnica de Madrid]. http://oa.upm.es/37543/1/FRANCISCO_JAVIER_SANZA_GUTIERREZ.pdf

Sasaki, D., & Mitchell, R. A. (2001). How to Obtain Reproducible Quantitative ELISA Results. *Oxford Biomedical Research*, 1–11. https://www.oxfordbiomed.com/sites/default/files/2017-02/How to Obtain Reproducible Quantitative ELISA results.pdf

Sauer-eriksson, A. E., Kleywegt, G. J., Uhlen, M., & Jones, T. A. (1995). Crystal structure of the C2 fragment of streptococcal protein G in complex with the Fc domain of human IgG. *Structure*, *3*(3), 265–278. https://doi.org/10.1016/S0969-2126(01)00157-5

Saylan, Y., Erdem, Ö., Ünal, S., & Denizli, A. (2019). An alternative medical diagnosis method: Biosensors for virus detection. *Biosensors*, *9*(2), 1–22. https://doi.org/10.3390/bios9020065

Scheller, F. W., Wollenberger, U., Warsinke, A., & Lisdat, F. (2001). Research and development in biosensors. *Current Opinion in Biotechnology*, *12*, 35–40. https://doi.org/10.1016/S0958-1669(00)00169-5

Schepici, G., Silvestro, S., Trubiani, O., Bramanti, P., & Mazzon, E. (2020). Salivary biomarkers: Future approaches for early diagnosis of neurodegenerative diseases. *Brain Sciences*, *10*(4), 245. https://doi.org/10.3390/brainsci10040245

Schroeder, H. W., & Cavacini, L. (2010). Structure and function of immunoglobulins. *Journal of Allergy and Clinical Immunology*, *125*(2 SUPPL. 2), 41–52. https://doi.org/10.1016/j.jaci.2009.09.046

Schwickart, M., Vainshtein, I., Lee, R., Schneider, A., & Liang, M. (2014). Interference in immunoassays to support therapeutic antibody development in preclinical and clinical studies. *Bioanalysis*, *6*(14), 1939–1951. https://doi.org/10.4155/bio.14.127

Semiz, S. (2022). COVID19 biomarkers: What did we learn from systematic reviews? *Frontiers in Cellular and Infection Microbiology*, *12*(December), 1–15. https://doi.org/10.3389/fcimb.2022.1038908

Shamri, R., Xenakis, J. J., & Spencer, L. A. (2011). Eosinophils in innate immunity: An evolving story. *Cell and Tissue Research*, *343*(1), 57–83. https://doi.org/10.1007/s00441-010-1049-6

Shevyrev, D., & Tereshchenko, V. (2020). Treg Heterogeneity, Function, and Homeostasis. *Frontiers in Immunology*, *10*, 3100. https://doi.org/10.3389/fimmu.2019.03100

Shioya, R., Yamada, K., Kido, K., Takahashi, H., Nozawa, A., Kosako, H., & Sawasaki, T. (2022). A simple method for labeling proteins and antibodies with biotin using the proximity biotinylation enzyme TurboID. *Biochemical and Biophysical Research Communications*, *592*, 54–59. https://doi.org/10.1016/j.bbrc.2021.12.109

Shui, B., Tao, D., Cheng, J., Mei, Y., Jaffrezic-Renault, N., & Guo, Z. (2018). A novel electrochemical aptamer-antibody sandwich assay for the detection of tau-381 in human serum. *Analyst*, *143*(15), 3549–3554. https://doi.org/10.1039/c8an00527c

Singh, A. K., Mittal, S., Das, M., Saharia, A., & Tiwari, M. (2023). Optical biosensors: a decade in review. *Alexandria Engineering Journal*, *67*, 673–691. https://doi.org/10.1016/j.aej.2022.12.040

Slagle, K. M., & Ghosn, S. J. (1996). Immunoassays: Tools for sensitive, specific, and accurate test results. *Laboratory Medicine*, *27*(3), 177–183. https://doi.org/10.1093/labmed/27.3.177

Soares Martins, T., Trindade, D., Vaz, M., Campelo, I., Almeida, M., Trigo, G., da Cruz e Silva, O. A. B., & Henriques, A. G. (2021). Diagnostic and therapeutic potential of exosomes in Alzheimer's disease. *Journal of Neurochemistry*, *156*(2), 162–181. https://doi.org/10.1111/jnc.15112

Song, C., Deng, P., & Que, L. (2018). Rapid multiplexed detection of beta-amyloid and total-tau as biomarkers for Alzheimer's disease in cerebrospinal fluid. *Nanomedicine: Nanotechnology, Biology, and Medicine*, *14*(6), 1845–1852. https://doi.org/10.1016/j.nano.2018.05.013

Song, P., An, J., & Zou, M. H. (2020). Immune Clearance of Senescent Cells to Combat Ageing and Chronic Diseases. *Cells*, *9*(3), 671. https://doi.org/10.3390/cells9030671

Sorensen, M. G., & Sorensen, S. P. (1940). *The proteins in whey*.

Spitzer, P., Mulzer, L. M., Oberstein, T. J., Munoz, L. E., Lewczuk, P., Kornhuber, J., Herrmann, M., & Maler, J. M. (2019). Microvesicles from cerebrospinal fluid of patients with Alzheimer's disease display reduced concentrations of tau and APP protein. *Scientific Reports*, *9*(7089), 1–10. https://doi.org/10.1038/s41598-019-43607-7

Steglich, P., Hülsemann, M., Dietzel, B., & Mai, A. (2019). Optical biosensors based on silicon-on-insulator ring resonators: A review. *Molecules*, *24*, 519. https://doi.org/10.3390/molecules24030519

Stelzmann, R. A., Norman Schnitzlein, H., & Reed Murtagh, F. (1995). An english translation of alzheimer's 1907 paper, "über eine eigenartige erkankung der hirnrinde." *Clinical Anatomy*, *8*(6), 429–431. https://doi.org/10.1002/ca.980080612

Subbiah, R., Veerapandian, M., & S. Yun, K. (2010). Nanoparticles: Functionalization and Multifunctional Applications in Biomedical Sciences. *Current Medicinal Chemistry*, *17*(36), 4559–4577. https://doi.org/10.2174/092986710794183024

Sugiyama, T., & Nagasawa, T. (2012). Bone Marrow Niches for Hematopoietic Stem Cells and Immune Cells. *Inflamm Allergy Drug Targets*, *11*(3), 201–206. https://doi.org/10.2174/187152812800392689

Sündermann, F., Fernandez, M. P., & Morgan, R. O. (2016). An evolutionary roadmap to the microtubule-associated protein MAP Tau. *BMC Genomics*, *17*(264), 1–16. https://doi.org/10.1186/s12864-016-2590-9

Susini, V., Sanguinetti, C., Ursino, S., Caponi, L., & Franzini, M. (2023). Antibody-Antigen Binding Events: The Effects of Antibody Orientation and Antigen Properties on the Immunoassay Sensitivity. *Rapid Antigen Testing*. https://doi.org/10.5772/intechopen.1001374

Takeuchi, O., & Akira, S. (2009). Innate immunity to virus infection. *Immunological Reviews*, *227*(1), 75–86. https://doi.org/10.1111/j.1600-065X.2008.00737.x

Tao, D., Shui, B., Gu, Y., Cheng, J., Zhang, W., Jaffrezic-Renault, N., Song, S., & Guo, Z. (2019). Development of a label-free electrochemical aptasensor for the detection of Tau381 and its preliminary application in AD and non-AD patients' sera. *Biosensors*, *9*(3), 1–12. https://doi.org/10.3390/bios9030084

Tenzer, S., Docter, D., Kuharev, J., Musyanovych, A., Fetz, V., Hecht, R., Schlenk, F., Fischer, D., Kiouptsi, K., Reinhardt, C., Landfester, K., Schild, H., Maskos, M., Knauer, S. K., & Stauber, R. H. (2013). Rapid formation of plasma protein corona critically affects nanoparticle pathophysiology. *Nature Nanotechnology*, *8*(10), 772–781. https://doi.org/10.1038/nnano.2013.181

Teunissen, C. E., Verberk, I. M. W., Thijssen, E. H., Vermunt, L., Hansson, O., Zetterberg, H., van der Flier, W. M., Mielke, M. M., & del Campo, M. (2022). Blood-based biomarkers for Alzheimer's disease: towards clinical implementation. *The Lancet Neurology*, *21*(1), 66–77. https://doi.org/10.1016/S1474-4422(21)00361-6

Thévenot, D. R., Toth, K., Durst, R. A., & Wilson, G. S. (2001). Electrochemical biosensors: Recommended definitions and classification. *Biosensors and Bioelectronics*, *16*, 121–131. https://doi.org/10.1016/S0956-5663(01)00115-4

Toma, K., Oishi, K., Iitani, K., Arakawa, T., & Mitsubayashi, K. (2022). Surface plasmon-enhanced fluorescence immunosensor for monitoring cardiac troponin I. *Sensors and Actuators B: Chemical*, *368*, 132132. https://doi.org/10.1016/j.snb.2022.132132

Torrijos-Morán, L., Lisboa, B. D., Soler, M., Lechuga, L. M., & García-Rupérez, J. (2022). Integrated optical bimodal waveguide biosensors: Principles and applications. *Results in Optics*, *9*, 100285. https://doi.org/10.1016/j.rio.2022.100285

Van Der Hoek, L., Pyrc, K., & Berkhout, B. (2006). Human coronavirus NL63, a new respiratory virus. *FEMS Microbiology Reviews*, *30*(5), 760–773. https://doi.org/10.1111/j.1574-6976.2006.00032.x

Varella, G. (2001). Medical Immunology. In G. Virella (Ed.), *New York* (Fifth). Marcel Dekker.

Veerdonk, F. L. Van De, Gresnigt, M. S., Kullberg, B. J., Meer, J. W. M. Van Der, Joosten, L. A. B., & Netea, M. G. (2009). Th17 responses and host defense against microorganisms : an overview. *BMB Reports*, *42*(12), 776–787. https://doi.org/10.5483/bmbrep.2009.42.12.776

Vessman, J., Stefan, R. I., Van Staden, J. F., Danzer, K., Lindner, W., Burns, D. T., Fajgelj, A., & Müller, H. (2001). Selectivity in analytical chemistry. *Pure and Applied Chemistry*, *73*(8), 1381–1386. https://doi.org/10.1351/pac200173081381

Vidaurre-Agut, C., Rivero-Buceta, E., Romaní-Cubells, E., Clemments, A. M., Vera-Donoso, C. D., Landry, C. C., & Botella, P. (2019). Protein corona over mesoporous silica nanoparticles: Influence of the pore diameter on competitive adsorption and application to prostate cancer diagnostics. *ACS Omega*, *4*, 8852–8861. https://doi.org/10.1021/acsomega.9b00460

Vivier, E., Tomasello, E., Baratin, M., Walzer, T., & Ugolini, S. (2008). Functions of natural killer cells. *Nature Immunology*, *9*(5), 503–510. https://doi.org/10.1038/ni1582

Wang-Shick, R. (2017a). Discovery and Classification. *Molecular Virology of Human Pathogenic Viruses*, 3–20. https://doi.org/10.10.1016/B978-0-12-800838-6.00001-1

Wang-Shick, R. (2017b). Virus Life Cycle. *Molecular Virology of Human Pathogenic Viruses*, *10*(1), 31–45. https://doi.org/10.1016/B978-0-12-800838-6.00003-5

Wang, B., Timilsena, Y. P., Blanch, E., & Adhikari, B. (2019). Lactoferrin: Structure, function, denaturation and digestion. *Critical Reviews in Food Science and Nutrition*, *59*(4), 580–596. https://doi.org/10.1080/10408398.2017.1381583

Weber, F. (2008). Innate Immunity: Introduction. *Encyclopedia of Virology*, 111–117. https://doi.org/10.1016/B978-012374410-4.00655-5

Wegmann, S., Biernat, J., & Mandelkow, E. (2021). A current view on Tau protein phosphorylation in Alzheimer's disease. *Current Opinion in Neurobiology*, *69*, 131–138. https://doi.org/10.1016/j.conb.2021.03.003

Weingarten, M. D., Lockwood, A. H., Hwo, S. Y., & Kirschner, M. W. (1975). A protein factor essential for microtubule assembly. *Proceedings of the National Academy of Sciences of the United States of America*, *72*(5), 1858–1862. https://doi.org/10.1073/pnas.72.5.1858

Weiss, S. R., & Leibowitz, J. L. (2011). Coronavirus pathogenesis. In *Advances in Virus Research* (Vol. 81, Issue 1). https://doi.org/10.1016/B978-0-12-385885-6.00009-2

Welch, N. G., Scoble, J. A., Muir, B. W., & Pigram, P. J. (2017). Orientation and characterization of immobilized antibodies for improved immunoassays (Review). *Biointerphases*, *12*(2). https://doi.org/10.1116/1.4978435

Weller, J., & Budson, A. (2018). Current understanding of Alzheimer's disease diagnosis and treatment. *F1000Research*, *7*(0), 1–9. https://doi.org/10.12688/f1000research.14506.1

Wherry, E. J., & Ahmed, R. (2004). Memory CD8 T-Cell Differentiation during Viral Infection. *Journal of Virology*, *78*(11), 5535–5545. https://doi.org/10.1128/jvi.78.11.5535-5545.2004

WHO. (2020). *World Health Organization*.

WHO. (2024). *World Health Organization*. https://data.who.int/dashboards/covid19/cases?n=c

Wilchek, M., & Bayer, E. A. (1990). Introduction to avidin-biotin technology. *Methods in Enzymology*, *184*(C), 5–13. https://doi.org/10.1016/0076-6879(90)84256-G

Wild, D. (2013). Immunoassay for Beginners. In *The Immunoassay Handbook: Theory and Applications of Ligand Binding, ELISA and Related Techniques* (pp. 7–10). https://doi.org/10.1016/B978-0-08-097037-0.00002-6

Wilson, D. M., Cookson, M. R., Van Den Bosch, L., Zetterberg, H., Holtzman, D. M., & Dewachter, I. (2023). Hallmarks of neurodegenerative diseases. *Cell*, *186*(4), 693–714. https://doi.org/10.1016/j.cell.2022.12.032

Wing, E. J., & Remington, J. S. (1977). Cell-mediated immunity and its role in resistance to infection. *Western Journal of Medicine*, *126*(1), 14–31.

Wittekindt, C., Fleckenstein, B., Wiesmüller, K. H., Eing, B. R., & Kühn, J. E. (2000). Detection of human serum antibodies against type-specifically reactive peptides from the N-terminus of glycoprotein B of herpes simplex virus type 1 and type 2 by surface plasmon resonance. *Journal of Virological Methods*, *87*, 133–144. https://doi.org/10.1016/S0166-0934(00)00160-9

Woo, P. C. Y., Lau, S. K. P., Yip, C. C. Y., Huang, Y., & Yuen, K. Y. (2009). More and more coronaviruses: Human coronavirus HKU1. *Viruses*, *1*(1), 57–71. https://doi.org/10.3390/v1010057

Woof, J. M., & Ken, M. A. (2006). The function of immunoglobulin A in immunity. *Journal of Pathology*, *208*(2), 270–282. https://doi.org/10.1002/path.1877

Wu, D., Wu, T., Liu, Q., & Yang, Z. (2020). The SARS-CoV-2 outbreak: What we know. *International Journal of Infectious Diseases*, *94*(January), 44–48. https://doi.org/10.1016/j.ijid.2020.03.004

Xia, Y., Prokop, S., & Giasson, B. I. (2021). "Don't Phos Over Tau": recent developments in clinical biomarkers and therapies targeting tau phosphorylation in Alzheimer's disease and other tauopathies. *Molecular Neurodegeneration*, *16*(37), 1–19. https://doi.org/10.1186/s13024-021-00460-5

Yamazaki, Y., Zhao, N., Caulfield, T. R., Liu, C. C., & Bu, G. (2019). Apolipoprotein E and Alzheimer disease: pathobiology and targeting strategies. *Nature Reviews Neurology*, *15*(9), 501–518. https://doi.org/10.1038/s41582-019-0228-7

Yang, S., Kuan, W. L., & Spillantini, M. G. (2016). Progressive tauopathy in P301S tau transgenic mice is associated with a functional deficit of the olfactory system. *European Journal of Neuroscience*, *44*(6), 2396–2403. https://doi.org/10.1111/ejn.13333

Yao, C. Y., & Fu, W. L. (2014). Biosensors for hepatitis B virus detection. *World Journal of Gastroenterology*, *20*(35), 12485–12492. https://doi.org/10.3748/wjg.v20.i35.12485

Yiannopoulou, K. G., & Papageorgiou, S. G. (2020). Current and Future Treatments in Alzheimer Disease: An Update. *Journal of Central Nervous System Disease*, *12*, 1–12. https://doi.org/10.1177/1179573520907397

Yoshimoto, F. K. (2020). The Proteins of Severe Acute Respiratory Syndrome Coronavirus-2 (SARS CoV-2 or n-COV19), the Cause of COVID-19. *Protein Journal*, *39*(3), 198–216. https://doi.org/10.1007/s10930-020-09901-4

Zhang, J., Tan, K. L., & Gong, H. Q. (2001). Characterization of the polymerization of SU-8 photoresist and its applications in micro-electro-mechanical systems (MEMS). *Polymer Testing*, *20*, 693–701. https://doi.org/10.1016/S0142-9418(01)00005-8

Zhang, Jun, Xiao, T., Cai, Y., & Chen, B. (2021). Structure of SARS-CoV-2 spike protein. *Current Opinion in Virology*, *50*, 173–182. https://doi.org/10.1016/j.coviro.2021.08.010

Zhang, L., & Guo, H. (2020). Biomarkers of COVID-19 and technologies to combat SARS- CoV-2. *Advances in Biomarker Sciences and Technology*, *2*(January), 1–23. https://doi.org/10.1016/j.abst.2020.08.001

Zhang, Q., Huang, R. F., & Guo, L. H. (2009). One-step and high-density protein immobilization on epoxysilane-modified silica nanoparticles. *Chinese Science Bulletin*, *54*(15), 2620–2626. https://doi.org/10.1007/s11434-009-0210-7

Zhang, T., Ma, S., Lv, J., Wang, X., Afewerky, H. K., Li, H., & Lu, Y. (2021). The emerging role of exosomes in Alzheimer's disease. *Ageing Research Reviews*, *68*(November 2020), 101321. https://doi.org/10.1016/j.arr.2021.101321

Zhang, Y., Bi, J., Huang, J., Tang, Y., Du, S., & Li, P. (2020). Exosome: A review of its classification, isolation techniques, storage, diagnostic and targeted therapy applications. *International Journal of Nanomedicine*, *15*, 6917–6934. https://doi.org/10.2147/IJN.S264498

Zheng, H., & Koo, E. H. (2011). Biology and pathophysiology of the amyloid precursor protein. *Molecular Neurodegeneration*, *6*(1), 27. https://doi.org/10.1186/1750-1326-6-27

Zhu, L., Sun, H. T., Wang, S., Huang, S. L., Zheng, Y., Wang, C. Q., Hu, B. Y., Qin, W., Zou, T. T., Fu, Y., Shen, X. T., Zhu, W. W., Geng, Y., Lu, L., Jia, H. liang, Qin, L. X., & Dong, Q. Z. (2020). Isolation and characterization of exosomes for cancer research. *Journal of Hematology and Oncology*, *13*(152), 1–24. https://doi.org/10.1186/s13045-020-00987-y

Ziegler, C., & Göpel, W. (1998). Biosensor Development. *Current Opinion in Chemical Biology*, *2*, 585–591. https://doi.org/10.1016/S1367-5931(98)80087-2

Ziu, I., Laryea, E. T., Alashkar, F., Wu, C. G., & Martic, S. (2020). A dip-and-read optical aptasensor for detection of tau protein. *Analytical and Bioanalytical Chemistry*, *412*(5), 1193–1201. https://doi.org/10.1007/s00216-019-02350-8

Annexes

Annex I. Protocol followed to collect saliva samples and handling in the laboratory

PROTOCOLO PARA EL MANEJO Y USO DE SALIVA CON VOLUNTARIOS PARA EL PILOTO COVID-19 DENTRO DEL LABORATORIO NCB2 DEL CENTRO DE TECNOLOGÍA BIOMÉDICA PARA EL DESARROLLO DE UN NUEVO DIAGNÓSTICO

Este documento describe de manera exclusiva el protocolo que se sigue para el manejo y uso de las muestras de salivas de participantes voluntarios del ensayo "Piloto de investigación, voluntario, experimental y no vinculante para PARA DETECCIÓN PRECOZ, VIGILANCIA Y CONTROL DE COVID-19".

El protocolo que se presenta está sujeto a todas las recomendaciones establecidas en la "GUÍA DE LA RED NACIONAL DE BIOBANCOS PARA EL MANEJO DE MUESTRAS HUMANAS EN INVESTIGACIÓN BIOMÉDICA. RECOMENDACIONES ANTE LA PANDEMIA DE COVID-19" elaborada por la Red de Biobancos española, el Instituto de Salud Carlos III y el Ministerio de Ciencia e Innovación del Gobierno de España, así como a los procedimientos y recomendaciones descritas en el MANUAL DE BIOSEGURIDAD de la Unidad de Cultivos Celulares del Centro de Tecnología Biomédica (CTB) y Procedimientos Normalizados de Trabajo aprobados por el Servicio de Prevención de Riesgos Laborales de la Universidad Politécnica de Madrid.

ASPECTOS GENERALES

Según se recoge en la guía citada, "el personal que maneje muestras clínicas rutinarias (exudado nasofaríngeo preferiblemente y/o orofaríngeo, lavado broncoalveolar, esputo, aspirado endotraqueal, muestras para hemogramas y pruebas bioquímicas, muestras de orina, serología y otras pruebas diagnósticas en suero, sangre y orina) de pacientes ingresados con diagnóstico o sospecha de infección por SARS-CoV-2, o cualquier otro patógeno, deberá seguir las pautas estándar y recomendaciones generales de bioseguridad establecidas para los laboratorios de nivel de Bioseguridad 2 (NCB-2)".

Por ello, el siguiente procedimiento se llevará a cabo exclusivamente en el laboratorio certificado como NCB2 de la Unidad de Cultivos Celulares de CTB.

De forma general, se establece la obligación a todo el personal trabajando con este tipo de muestras o dentro del laboratorio donde se trabajen con éstas, el uso de bata, gafas, guantes y mascarilla de tipo FFP2.

INSTALACIONES

Nivel de Contención Biológica 2 (NCB2)

El laboratorio de la Unidad de Cultivos Celulares situado en la planta -1 es donde se procederá al almacenamiento, manejo y uso de las muestras. Estos cumplen con los requerimientos descritos en la mencionada guía para los laboratorios tipo NCB2.

RECEPCIÓN Y ALMACENAMIENTO DE MUESTRAS

Las muestras son recogidas en el área clínica por personal cualificado conforme a las siguientes medidas de seguridad.

Los voluntarios accederán al área clínica directamente a través del acceso exterior de la planta -2 del CTB. Dicho acceso permanecerá abierto durante el horario de recogida para facilitar una correcta ventilación del área.

Figure 182. De izquierda a derecha: Zona de recepción donde se recoge el recipiente y se entrega la muestra. Acceso directo a la zona clínica desde la calle. Puertas de acceso que permanecerán siempre abierta.

El encargado de recoger las muestras proporcionará, desde dentro del cubículo de recepción y con el equipo de protección adecuados (guantes, mascarilla FFP2, bata y pantalla facial), el tubo con el número de identificación del voluntario e indicará (siempre que las condiciones meteorológicas lo permitan) que rellene el tubo fuera del edificio con saliva procedente de la cavidad oral. Una vez rellenado el tubo el voluntario lo descontaminará[1] con el papel y solución hidroalcohólica dispuestos en la entrada y lo entregará al encargado. Todos los desechos de papel se depositarán en un contenedor de residuos biológicos para su posterior retirada por parte de la empresa especializada INTERLUN SL.

Las muestras serán almacenadas individualmente en un contenedor secundario y transportadas al laboratorio NCB2 situado en la planta -1 del CTB, conforme indica en la GUÍA DE LA RED

[1] Descontaminación llevada a cabo con solución hidroalcohólica de etanol al 70% mediante pulverización indirecta y un tiempo de contacto mínimo de 1 minuto.

NACIONAL DE BIOBANCOS PARA EL MANEJO DE MUESTRAS HUMANAS EN INVESTIGACIÓN BIOMÉDICA. RECOMENDACIONES ANTE LA PANDEMIA DE COVID-19, sección RECEPCIÓN Y REGISTRO DE MUESTRAS EN EL BIOBANCO página 7.

Toda la manipulación posterior de contenedores y muestras será realizada por personal autorizado para el acceso del laboratorio NCB2, siempre con guantes y dentro de la campana de bioseguridad tipo II del laboratorio NCB2 de Cultivos Celulares del CTB en la planta -1. Así mismo, se procederá a la descontaminación[1] exterior de los productos (contenedores terciarios) que se encuentren dentro.

Toda muestra recibida en el CTB contiene tres contenedores (primario, secundario y terciario, **¡Error! No se encuentra el origen de la referencia.**). El almacenamiento de éstas hasta su uso se realiza en su contenedor terciario. Las muestras recogidas se almacenan a temperatura ambiente dentro de la campana de bioseguridad tipo II hasta su uso.

Figure 183. El contenedor terciario, secundario y primario en el que se transportan las muestras desde el área clínica hasta el laboratorio NCB2 de CTB situado en la planta -1.

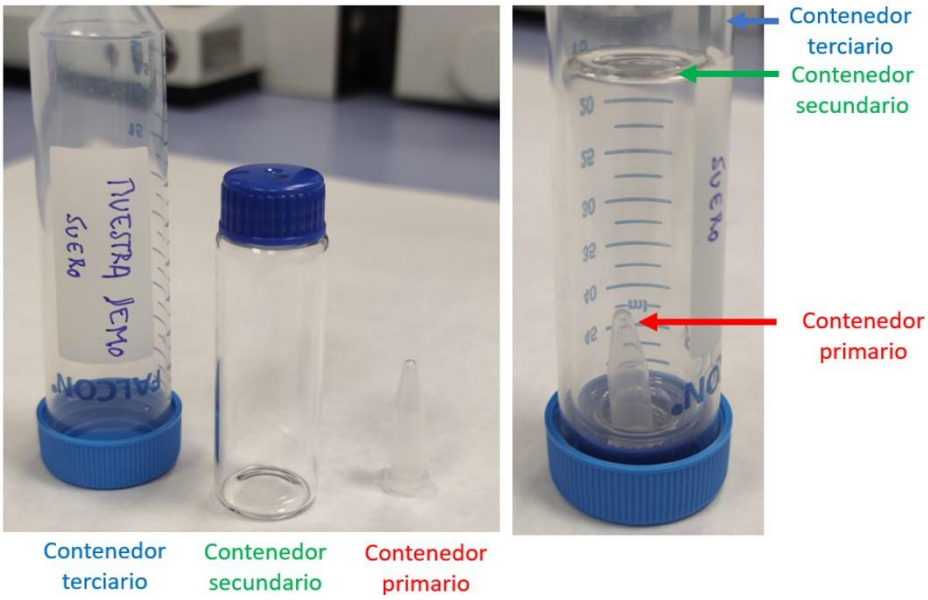

Figure 184. Otra posible configuración de los diferentes contenedores en los que se almacenan las muestras.

PROTOCOLO PARA EL MANEJO Y USO DE MUESTRAS

El manejo y uso de muestras para el desarrollo del BIOKIT se realizará SIEMPRE en el laboratorio NCB2 de la Unidad de Cultivos Celulares del CTB, dentro de las campanas de seguridad biológica tipo II, tal y como se indica a continuación.

PROCEDIMIENTO PARA LA MEDIDA EN EL BIOKIT

La muestra de saliva se incuba directamente en el biosensor desarrollado durante un tiempo habitualmente de unas 2 horas dentro de un contenedor estanco dentro de la campana de seguridad biológica tipo II. Éste, a su vez, podrá ser o no introducido en un incubador, también situado dentro de la cabina, para reducir el tiempo en el que se obtendrá la lectura del diagnóstico. Éste es debidamente descontaminado con una solución hidroalcohólica de etanol al 70% mediante pulverización indirecta y un tiempo de contacto mínimo de 1 minuto antes y después de su uso.

Pasado este tiempo el biosensor se lava sumergido en agua en un agitador de placas durante 10 min, que también se localizará en la campana de seguridad biológica. Es opcional antes de introducir el BioKit en el agitador de placas realizar un primer aclarado con jeringa sin aguja con 10 mL de agua miliQ. Con ello, aseguramos que toda sustancia contenida en la saliva (excepto los anticuerpos que se desean detectar), quedan eliminados del BioKit, **dejando a este sin capacidad infectiva.**

Los desechos que se generan a raíz de la limpieza son inactivados previo a su depósito en el contenedor de residuos destinados para estas limpiezas y situado dentro de la campana (Figura 4).

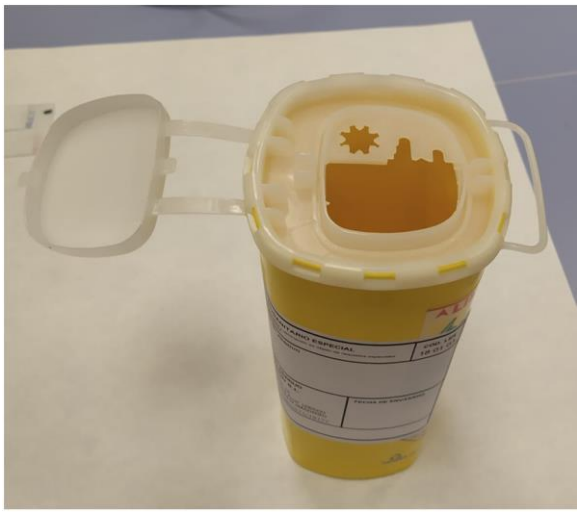

Figure 185. Contenedor de desechos previamente neutralizados.

La cuantificación las inmunoglobulinas específicas a la proteína vírica (Ig Total) que se tienen en saliva se realiza introduciendo el biosensor ya lavado y por lo tanto sin capacidad infectiva dentro del dispositivo de lectura óptica Point of Care (PoC), situado en una de las bancadas del laboratorio NCB2 de la Unidad de Cultivos Celulares.

(OPCIONAL): En caso de que la determinación anterior ser positiva, se procederá a una segunda comprobación mediante la determinación específica de la inmunoglobulina tipo IgA. Para ello se realiza una incubación de anticuerpos secundarios comerciales (anti- IgA). Se incuba durante 2 horas bajo las condiciones descritas en el punto 1: Durante un tiempo habitualmente de unas 2 horas dentro de un contenedor estanco, dentro de la campana de seguridad biológica tipo II.

Las condiciones de lavado son las mismas descritas en el punto 2: el biosensor se lava sumergido en agua en agitador de placas durante 10 min, que también se localizará en la campana de seguridad biológica.

La cuantificación de IgAs de la saliva se realiza introduciendo el biosensor ya lavado dentro del dispositivo PoC mencionado anteriormente.

LIMPIEZA Y MÉTODOS DE DESINFECCIÓN E INACTIVACIÓN DE LOS RESIDUOS

Como medidas de prevención se procederá antes y después de la jornada laboral a la limpieza de todas las superficies (mesas, suelos, estanterías) y equipos (centrífugas, pipetas, gradillas…) con alguno de los siguientes agentes desinfectantes recomendados por la OMS:

Limpieza general: disolución de etanol al 70% durante 1 minuto o hipoclorito de sodio al 0.1% durante 10 minutos.

Además, se limpiará a fondo las cabinas de seguridad biológica antes y después de su uso con alcohol al 70%. Será obligatorio tras su uso poner en marcha la luz UV de la cabina durante al menos 30 minutos con la cabina libre de objetos y contenedores.

Annex II. Document sent to the participants of the pilot trial of measurement of sIgA in saliva

Piloto de investigación, voluntario, experimental y no vinculante PARA DETECCIÓN PRECOZ, VIGILANCIA Y CONTROL DE COVID-19 mediante diagnóstico en saliva

ID Voluntario*	-
Fecha Informe	-
Tipo de Muestra	Saliva

*Los datos que se muestran están sujetos a la veracidad del ID facilitado por el voluntario a la hora de la entrega de la muestra.

MÉTODO:

Recolección de saliva y posterior detección de anticuerpos específicos al virus SARS-CoV-2, Inmunoglobulinas totales (IgT) e inmunoglobulinas IgA, mediante técnica interferométrica de interrogación óptica[1]

RESULTADO:

En las muestras analizada se han obtenido los siguientes resultados:

		IgTotal	IgA
ID 101	**Fecha Recogida**	**Resultado**	**Resultado**
Entrega 1			
Entrega 2			
Entrega 3			
Entrega 4			
Entrega 5			
Entrega 6			

POSITIVO: Un resultado positivo implica que el sistema inmune del voluntario ha generado anticuerpos expresados en mucosa específicos al virus SARS-CoV-2. Dado que el tiempo transcurrido desde la última muestra recogida supera los 15 días de tiempo incubación en la actualidad esto indica que la infección debe de estar resuelta.

NEGATIVO: Un resultado negativo puede deberse a tres causas:

1.- Que el voluntario no ha tenido contacto con la enfermedad,
2.- Que el sistema inmune del voluntario no ha expresado anticuerpos específicos al virus SARS-CoV-2
3.- Dado que la IgAs están presentes en la saliva un tiempo determinado, es posible que este tiempo ya haya transcurrido desde que el voluntario pudiera haber tenido contacto con la enfermedad.

INDETERMINADO (Ind): Un resultado indeterminado sugiere realizar nuevamente la medida de la muestra debido a un resultado no concluyente. La realización de esta nueva medida se realizará con posterioridad y aparecerá actualizada en los siguientes informes.

SIN RESULTADO: Puede ser debido a la falta de entrega de muestra o la demora en la realización del ensayo de esta.

[1] Sensors 2014, 14, 3675-3689; Sensors and Actuators B 236 (2016) 765–772

Campus Montegancedo, Crta M-40 Km 38, 28223 Pozuelo de Alarcón; informatica.cbgp@upm.es

Annex III. Comparative table of biosensors for tau protein measurement

Table 47: Comparison between biosensors for the detection of tau protein (Murillo et al., 2023)**.**

Signal transduction	*Analytical method(A)*	*Sensor platform*	*Target*	*Linear detection range*	*Limit of detection(C)*	*Sample tested*	*Label*	*Ref.*
Optical	BLI	Streptavidin interface probe sensor	Tau441	2-55 nM	6.7 nM (8.02 pM)	Buffer and FBS	Label-free	(Ziu et al., 2020)
	Spectrophotometry/ Interferometry	Nanopore sensor with integrated microfluidic network	T-Tau	15.6-2000 pg/mL	15.6 pg/mL in buffer (0.284pM)	Buffer and CSF	Label-free	(C. Song et al., 2018)
	LSPR	Resonance-based immunochip	T-Tau	10-100000 pg/mL	10 pg/mL (0.15 pM)	Buffer	Label-free	(Ramirez et al., 2022)
	SPR	Surface plasmon resonance coupled to carbon nanostructures	T-Tau	125-1000 pM	125 pM	Buffer and aCSF(D)	Label-free	(Lisi et al., 2017)
	Interferometry	**Two Fabry-Perot interferometers**	**T-Tau**	**12.5-0.0005 µg/mL in buffer 12.5 µg/mL to 10 pg/ml in serum**	**9.1 pM in buffer 0.18 pM in serum**	**Buffer and Human serum**	**Label-free**	(Murillo et al., 2023)
Electrochemical	CV and EIS	Anti-Tau antibodies on polycrystalline Au surface	Tau441	10-100 µg/mL	10 µg/mL	Buffer	Label-free	(Carlin & Martic-Milne, 2018)
	DPV	Aptamer-antibody-sandwich	Tau381	0.5-100 pM	0.42 pM in PBS (0.50 pM)	Human serum diluted 1/100	Label-free	(Shui et al., 2018)
	DPV	Neutral charged immunosensor	T-Tau	0.968-454 pM	0.968 pM	Human serum	Label-free	(Dai et al., 2019)
	CV and EIS	Aptasensor	Tau381	1-100 pM	0.7 pM	Human serum diluted 1/100	Label-free	(Tao et al., 2019)
	DVP and EIS	GO/pPG/anti-Tau nanoimmunosensor(B)	T-Tau	0.25-250 nM	150 pM	CSF and human serum	Label-free	(Derkus et al., 2017)
Potentiometric	FET	Transistor-based biosensor	T-Tau	1-10 pM	1 pM in buffer and cell culture media, 10 pM in aCSF	Buffer, cell culture and aCSF	Label-free	(García-Chamé et al., 2020)

(A) Abbreviations: BLI = Biolayer interferometry; LSPR = Localized surface plasmon resonance; SPR = Surface plasmon resonance; CV = Cyclic voltammetry; EIS = Electrochemical impedance spectroscopy; DPV = Differential pulse voltammetry; FET = Field effect transistor. (B) Abbreviations: GO = Graphene oxide; pPG = poly (propyleneglycol). (C) Conversion to molarity was carried out by assuming a mean tau molecular weight of 55KDa. (D) Abbreviation: aCSF = artificial cerebral spinal fluid.